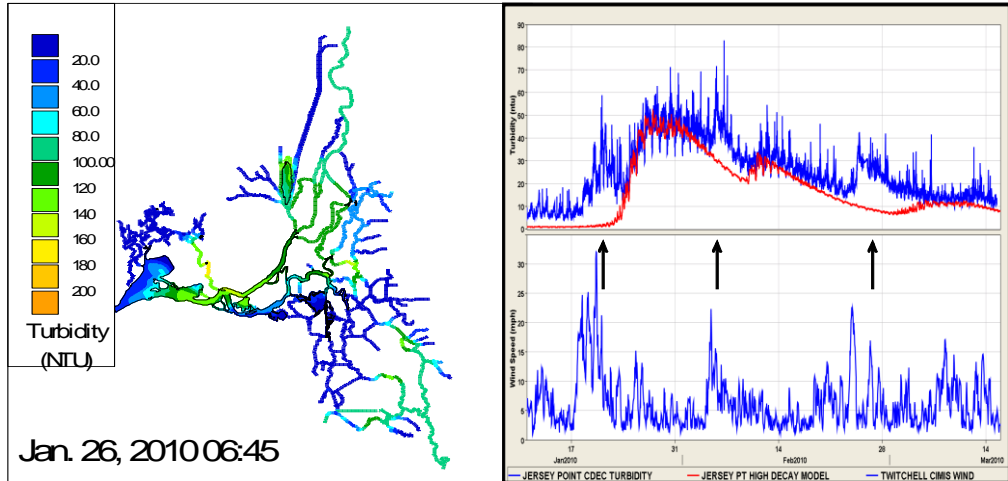


Turbidity and Adult Delta Smelt Forecasting with RMA 2-D Models: December 2009 – May 2010



Prepared For:
Metropolitan Water District of Southern California

Contact:
Dr. Paul Hutton
Authorized Technical Representative
916 – 651 – 2620

Prepared By:
Resource Management Associates
4171 Suisun Valley Road, Suite J
Fairfield, CA 94534

Contact:
John DeGeorge
707 – 864 – 2950

This Page intentionally left blank.

Table of Contents

Figures	vi
Tables	xvii
1. Executive Summary	1
2. Objectives	3
3. Background	4
3.1. Relationship between turbidity and suspended-sediment measurements	6
3.2. Previous turbidity/suspended sediment models	7
3.3. RMA Delta model configuration	8
3.3.1. RMA numerical models	8
3.3.2. Grid and bathymetry	9
3.3.3. Stage and flow boundaries	10
3.3.4. Gates and barriers	10
3.3.5. DICU (flow)	10
3.3.6. Salinity and turbidity	10
3.3.7. Grid changes for the current project	11
3.3.8. Turbidity – regional decay values for the current project	11
4. Near-Real-time modeling	14
4.1. Turbidity recalibration	14
4.1.1. Turbidity data	14
4.1.2. Meteorological data (CIMIS)	14
4.1.3. Flow data	15
4.2. Developing weekly forecasts using RMA2 and RMA11	18
4.2.1. Background	18

4.2.2.	DWR-supplied flow and EC boundary conditions	18
4.2.3.	Turbidity forecast development	19
4.2.4.	Turbidity boundary conditions	21
4.2.5.	Synthesized EC boundary conditions	21
4.2.6.	Development of initial conditions.....	22
4.2.7.	Gate and barrier operations	22
4.2.8.	Flow boundary conditions using CNRFC and USGS.....	22
4.3.	Forecast methodology	23
4.3.1.	General guidelines	23
4.3.2.	Suggested guidelines for developing turbidity forecasts at Vernalis and Freeport	24
5.	Final Turbidity Model	44
5.1.	Single-parameter model examples	44
5.2.	Results	44
5.2.1.	Effects of wind and rain; missing runoff flow.....	44
5.2.2.	Effects of velocity and potential for sediment settling	45
5.2.3.	Potential for missing flow during high flow events.....	45
5.2.4.	Turbidity model results at additional locations	46
5.2.5.	Turbidity contour plots – data and model	46
6.	Adult delta smelt particle tracking models	77
6.1.	Hypotheses behind the behavior model (ref:RMA 2009)	77
6.2.	Adult delta smelt behavior model.....	78
6.3.	Particle tracking model parameters.....	79
6.4.	Adult delta smelt modeled period and particle count.	80
6.5.	Particle observation locations	80

6.6.	Delta smelt salvage data.....	80
7.	Forecast results.....	86
7.1.	Examples of flow and turbidity forecast boundary condition methodology	86
7.1.1.	Forecast results	87
7.1.2.	February 25 th forecast	87
7.1.3.	April 14 th forecast	88
7.2.	Adult delta smelt model results	88
8.	Discussion.....	122
9.	Conclusion	122
10.	References.....	124
11.	Appendix I	125
11.1.	Background	125
11.2.	Historical turbidity locations (pre-12/2009)	127
11.3.	Setting flow boundaries	128
11.3.1.	Sacramento River at I Street – CNRFC forecast – stage to flow conversion	128
11.3.2.	CIMIS wind and precipitation data	130
11.3.3.	Additional adult delta smelt model results	134
12.	Appendix II - Detailed forecast model results for Apr. 14 th and Feb. 25 th	137
13.	Appendix III - Model results for forecasts Jan. 12 th , Feb. 11 th , Feb. 17 th , Apr. 07 th	243

Figures

Figure 3-1 Finite element model configuration of the Sacramento – San Joaquin Delta.	12
Figure 3-2 Approximate gate and barrier locations in the RMA grid.	13
Figure 3-3 Final decay values and regions used in the current turbidity model.	14
Figure 4-1 Locations of new turbidity monitoring stations.	16
Figure 4-2 The CIMIS website map with the location of the four stations whose meteorological data was downloaded on a weekly basis (red stars).	17
Figure 4-3 Information flow for developing turbidity and adult delta smelt forecasts.	30
Figure 4-4 Plot of categorization of Freeport turbidity (SSC-based) during rainy seasons 1991 – 2007.	33
Figure 4-5 Scatter plot of the high flow/rainy period data set of flow vs. suspended sediment at Freeport used to create the turbidity/flow relationships.	34
Figure 4-6 Possible values for a turbidity forecast during the highest flow event on the Sacramento in Feb. 2010.	35
Figure 4-7 Comparison of data with 50% turbidity-flow relationship at Freeport.	36
Figure 4-8 Comparison of data with 75% turbidity-flow relationship at Freeport.	37
Figure 4-9 Comparison of data with 90% turbidity-flow relationship at Freeport.	38
Figure 4-10 Turbidity peak timing vs. flow peak timing at Freeport is skewed – turbidity tends to peak before flow.	39
Figure 4-11 Categorization of Vernalis turbidity (SSC-based) during rainy seasons 1991 – 2007.	40
Figure 4-12 Comparison of data with 50% turbidity-flow relationship at Vernalis.	41
Figure 4-13 Comparison of data with 95% turbidity-flow relationship at Vernalis.	42
Figure 4-14 Time series of measured flow, and time series of turbidity (center) and salinity (bottom) synthesized as a function of flow at the RMA model Yolo-boundary.	43
Figure 5-1 Low decay (green) and high decay (red) coefficient models in comparison with data (blue) at Old River at Hwy 4.	47
Figure 5-2 Low decay (green) and high decay (red) coefficient models in comparison with data (blue) at Little Potato Slough at Terminous.	48
Figure 5-3 Low decay (green) and high decay (red) coefficient models in comparison with data (blue) at Jersey Point, with CIMIS (Twitchell) wind data (lower plot).	49
Figure 5-4 Turbidity data/model comparison with wind and precipitation data from CIMIS (Twitchell) indicates that the effects of meteorological conditions may be significant – turbidity increases near Jersey Point during wind and rain events.	50
Figure 5-5 Expanded scale of data/model comparison at Jersey Point in comparison with CIMIS (Twitchell) wind data.	51
Figure 5-6 Turbidity data/model comparison with wind and precipitation data from CIMIS (Twitchell) indicates that the effects of meteorological conditions may be significant – turbidity increases near Dutch Slough during wind and rain events.	52

Figure 5-7 Turbidity data/model comparison at Old River at Bacon (ROLD024).....	53
Figure 5-8 Turbidity data/model comparison at Old River at Bacon in comparison with CIMIS wind data.	54
Figure 5-9 Data (Upper plots) show EC dilution downstream of Mossdale after late January rain event (arrow) - modeled EC (lower plots) is good at Mossdale but too high downstream, also indicating possible dilution from local inflow sources.	55
Figure 5-10 CIMIS data at the Twitchell station shows the timing of the wind and rain events January to mid-March, 2010.....	56
Figure 5-11 Data (upper plot) show turbidity dilution downstream of Mossdale after late January rain event (arrow) - modeled turbidity (lower plots) is good at Mossdale but too high downstream, also indicating possible dilution from local inflow sources.	57
Figure 5-12 Turbidity data/model comparison at Garwood on the San Joaquin R. indicates possible evidence of missing effects of dilution.	58
Figure 5-13 Turbidity data/model comparison at Grant Line Canal indicates possible evidence of missing effects of sediment settling.	59
Figure 5-14 Turbidity data/model comparison at Little Potato Sl. at Terminous indicates possible evidence of missing effects of sediment settling.	60
Figure 5-15 Local low velocity is associated with model over-prediction of turbidity during high turbidity events at Little Potato Sl. at Terminous – this is not evidence of this at high velocity locations such as Georgiana-Sac.....	61
Figure 5-16 Local low velocity is associated with model over-prediction of turbidity during high turbidity events at Garwood on the San Joaquin R. and in Grant Line canal.....	62
Figure 5-17 Three areas were identified as having problems with missing flow – i.e., where gauged data upstream and downstream didn’t match.	63
Figure 5-18 Flow at Freeport (blue) is up to 5,000 cfs less than gauged downstream flow around the time of the late January storm – this flow difference is not accounted for in the model.	64
Figure 5-19 Flow into the Mokelumne system does not match flow out of the Mokelumne system.....	65
Figure 5-20 Gauged flow (shown here as tidally-averaged flow) at Brandt Br. (green) and at Garwood (black) does not add up on the San Joaquin R., upstream and downstream of the Calaveras R. Note that peak flows on the Calaveras include flow from Mormon Sl. (blue line).	66
Figure 5-21 Turbidity data (blue) and model results (red) at Rio Vista.....	67
Figure 5-22 Turbidity data (blue) and model results (red) at Cache-Ryer.....	68
Figure 5-23 Turbidity data (blue) and model results (red) at Middle River near Holt.	69
Figure 5-24 Turbidity data (blue) and model results (red) at Antioch.	70
Figure 5-25 Turbidity data (blue) in Clifton Court Forebay (CCFB) and model results (red) at the intake to CCFB (SWP intake).....	71
Figure 5-26 Contour plot of spatially interpolated data (left) is missing some regions (red circles) within the RMA 2-D model grid (right) due to a lack of data.....	72

Figure 5-27 Contour plots of spatially interpolated data (left) and model output (right) at 21:00 on January 21, 2010.	73
Figure 5-28 Contour plots of spatially interpolated data (left) and model output (right) at 21:00 on January 23, 2010.	74
Figure 5-29 Contour plots of spatially interpolated data (left) and model output (right) at 21:00 on January 25, 2010.	75
Figure 5-30 Contour plots of spatially interpolated data (left) and model output (right) at 21:00 on January 30, 2010. Note change in color contour scale from previous plots.	76
Figure 6-1 User interface for setting the initial location (Suisun region), timing (00:30, Jan. 01, 2010) and distribution (random distributed instantaneous vertical placement) of 40,000 particles.	81
Figure 6-2 Insertion region for the delta smelt PTM model.	82
Figure 6-3 Behavioral parameters used in the delta smelt PTM Model.	83
Figure 6-4 The fate of particles in the delta smelt PTM model is recorded in many regions including the three regions shown above. Particle fate is also recorded at the SWP and CVP export facilities.	84
Figure 6-5 Observed delta smelt salvage combined (blue) from the state (SWP, green dash-dot) and federal (CVP red dash) fish salvage facilities January to mid-April, 2010.	85
Figure 7-1 Three-week flow forecast period at Freeport February 11 – March 01, 2010.	90
Figure 7-2 Three-week flow forecast period at Freeport February 25 – March 15, 2010.	91
Figure 7-3 Three-week flow forecast period at Freeport April 12 – May 03, 2010.	92
Figure 7-4 Comparison of Freeport flow data (blue) vs. forecast, RMA (red) and DWR (green), for forecast periods starting Feb. 11 th , Feb. 25 th , and April 14 th (top to bottom).	93
Figure 7-5 Freeport turbidity 50% exceedance forecast – Feb. 11 th , 25 th (top and center plots) and 90% exceedance forecast April 14 th (bottom plot).	94
Figure 7-6 Three-week flow forecast period at Vernalis was February 11 – March 01, 2010.	95
Figure 7-7 Three-week flow forecast period at Vernalis February 25 – March 15, 2010.	96
Figure 7-8 Three-week flow forecast period at Vernalis April 12 – May 03, 2010.	97
Figure 7-9 Comparison of RMA (red) and DWR (green) Vernalis flow for forecast periods starting Feb. 11 th , Feb. 25 th , and April 14 th (top to bottom).	98
Figure 7-10 Vernalis turbidity 50% exceedance forecast Feb 11 th , 25 th and 95% exceedance estimate April 14 th (top to bottom).	99
Figure 7-11 Martinez turbidity forecast – Feb 11 th , 25 th and April 14 th (top to bottom).	100
Figure 7-12 Computed 3-day average turbidity at Holland Cut, Prisoner Point and Victoria Canal.	101
Figure 7-13 Location of turbidity monitoring stations in the Delta.	102
Figure 7-14 Turbidity data and model results for the forecast beginning Feb 25 th at Rio Vista.	103
Figure 7-15 Turbidity data and model results for the forecast beginning Feb 25 th at SJR-JP.	104
Figure 7-16 Turbidity data and model results for the forecast beginning Feb 25 th at Antioch.	105

Figure 7-17 Turbidity data and model results for the forecast beginning Feb 25 th at Middle R-Holt.....	106
Figure 7-18 Turbidity data and model results for the forecast beginning Feb 25 th at Old-R-Bacon.	107
Figure 7-19 Turbidity data and model results for the forecast beginning Feb 25 th at Grant Line.	108
Figure 7-20 Turbidity data and model results for the forecast beginning Feb 25 th at Clifton Court (data) and SWP (model).	109
Figure 7-21 Turbidity data and model results for the forecast beginning April 14 th at Rio Vista-U.....	110
Figure 7-22 Turbidity data and model results for the forecast beginning April 14 th at SJR-JP.	111
Figure 7-23 Turbidity data and model results for the forecast beginning April 14 th at Antioch.	112
Figure 7-24 Turbidity data and model results for the forecast beginning April 14 th at Middle R-Holt.....	113
Figure 7-25 Turbidity data and model results for the forecast beginning April 14 th at Old-R-Bacon.....	114
Figure 7-26 Turbidity data and model results for the forecast beginning April 14 th at Grant Line.	115
Figure 7-27 Turbidity data and model results for the forecast beginning April 14 th at Clifton Court (data) and SWP (Model).....	116
Figure 7-28 Adult delta smelt model results (top) for the RMA Feb. 11 th forecast show a small percentage of particles (of 40,000 inserted) reached the Old, Middle and Victoria regions. The lower plot shows combined delta smelt salvage count at the SWP+CVP facilities.	117
Figure 7-29 Adult delta smelt model results (top) for the RMA Feb. 25 th forecast show a small percentage of particles (of 40,000 inserted) reached the Old, Middle and Victoria regions. The lower plot shows combined delta smelt salvage count at the SWP+CVP facilities.	118
Figure 7-30 Adult delta smelt model results (top) for the RMA Apr. 14 th forecast show a small percentage of particles (of 40,000 inserted) reached the Old, Middle and Victoria regions. The lower plot shows combined delta smelt salvage count at the SWP+CVP facilities.	119
Figure 7-31 Adult delta smelt model results (top) for the RMA Apr. 14 th forecast show a small percentage of particles (of 40,000 inserted) reached the SWP+CVP exports. The lower plot shows combined delta smelt salvage count at the SWP+CVP facilities.	120
Figure 7-32 Particle tracking results using the adult delta smelt behavior model.	121
Figure 11-1 Locations of original turbidity monitoring stations in a previous grid.	127
Figure 11-2 CIMIS wind and precipitation data at Hastings Tract.....	130
Figure 11-3 CIMIS wind and precipitation data at Lodi West.	131
Figure 11-4 CIMIS wind and precipitation data at Tracy.	132
Figure 11-5 CIMIS wind and precipitation data at Twitchell.	133

Figure 11-6 Adult delta smelt model results (top) for the Feb. 17th forecast show a small number of particles (40,000 inserted) reached the Old, Middle and Victoria regions. The lower plot shows combined delta smelt salvage count at the SWP+CVP facilities. 134

Figure 11-7 Adult delta smelt model results (top) for the Apr. 7th forecast show a small number of particles (40,000 inserted) reached the SWP+CVP exports. The lower plot shows combined delta smelt salvage count at the SWP+CVP facilities..... 135

Figure 11-8 Adult delta smelt model results (top) for the Apr. 7th forecast show a small number of particles (40,000 inserted) reached the Old, Middle and Victoria regions. The lower plot shows combined delta smelt salvage count at the SWP+CVP facilities. 136

Figure 12-1 Turbidity data and model results for the RMA forecast beginning April 14th at Antioch. 138

Figure 12-2 Turbidity data and model results for the RMA forecast beginning April 14th at Cache-Ryer. 139

Figure 12-3 Turbidity data and model results for the RMA forecast beginning April 14th at Clifton Court (data) and SWP (model). 140

Figure 12-4 Turbidity data and model results for the RMA forecast beginning April 14th at Dutch SL..... 141

Figure 12-5 Turbidity data and model results for the RMA forecast beginning April 14th at Georgiana-BLW..... 142

Figure 12-6 Turbidity data and model results for the RMA forecast beginning April 14th at Georgiana-SAC..... 143

Figure 12-7 Turbidity data and model results for the RMA forecast beginning April 14th at Grant Line. 144

Figure 12-8 Turbidity data and model results for the RMA forecast beginning April 14th at Holland Cut..... 145

Figure 12-9 Turbidity data and model results for the RMA forecast beginning April 14th at LIT-POT-SL-TERM..... 146

Figure 12-10 Turbidity data and model results for the RMA forecast beginning April 14th at Middle R-Holt..... 147

Figure 12-11 Turbidity data and model results for the RMA forecast beginning April 14th at Moke-at-SJR..... 148

Figure 12-12 Turbidity data and model results for the RMA forecast beginning April 14th at Mossdale..... 149

Figure 12-13 Turbidity data and model results for the RMA forecast beginning April 14th at Old-R-Bacon..... 150

Figure 12-14 Turbidity data and model results for the RMA forecast beginning April 14th at Old-R-Hwy 4. 151

Figure 12-15 Turbidity data and model results for the RMA forecast beginning April 14th at Old-R-Quimby. 152

Figure 12-16 Turbidity data and model results for the RMA forecast beginning April 14th at Rio Vista-U.	153
Figure 12-17 Turbidity data and model results for the RMA forecast beginning April 14th at SAC AT Decker.	154
Figure 12-18 Turbidity data and model results for the RMA forecast beginning April 14th at SJR-Garwood.	155
Figure 12-19 Turbidity data and model results for the RMA forecast beginning April 14th at SJR-JP.	156
Figure 12-20 Turbidity data and model results for the RMA forecast beginning April 14th at Threemile-SJR.	157
Figure 12-21 Turbidity data and model results for the RMA forecast beginning April 14th at Turner Cut-Holt.	158
Figure 12-22 Expanded results - turbidity data and model results for the RMA forecast beginning April 14th at Antioch.	159
Figure 12-23 Expanded results - turbidity data and model results for the RMA forecast beginning April 14th at Cache-Ryer.	160
Figure 12-24 Expanded results - turbidity data and model results for the RMA forecast beginning April 14th at Clifton Court (data) and SWP (model).	161
Figure 12-25 Expanded results - turbidity data and model results for the RMA forecast beginning April 14th at Dutch SL.	162
Figure 12-26 Expanded results - turbidity data and model results for the RMA forecast beginning April 14th at Georgiana-BLW.	163
Figure 12-27 Expanded results - turbidity data and model results for the RMA forecast beginning April 14th at Georgiana-SAC.	164
Figure 12-28 Expanded results - turbidity data and model results for the RMA forecast beginning April 14th at Grant Line.	165
Figure 12-29 Expanded results - turbidity data and model results for the RMA forecast beginning April 14th at Holland Cut.	166
Figure 12-30 Expanded results - turbidity data and model results for the RMA forecast beginning April 14th at LIT-POT-SL.	167
Figure 12-31 Expanded results - turbidity data and model results for the RMA forecast beginning April 14th at Middle R-Holt.	168
Figure 12-32 Expanded results - turbidity data and model results for the RMA forecast beginning April 14th at Moke-at-SJR.	169
Figure 12-33 Expanded results - turbidity data and model results for the RMA forecast beginning April 14th at Mossdale.	170
Figure 12-34 Expanded results - turbidity data and model results for the RMA forecast beginning April 14th at Old-R-Bacon.	171

Figure 12-35 Expanded results - turbidity data and model results for the RMA forecast beginning April 14th at Old-R-Hwy 4.....	172
Figure 12-36 Expanded results - turbidity data and model results for the RMA forecast beginning April 14th at Old-R-Quinby.	173
Figure 12-37 Expanded results - turbidity data and model results for the RMA forecast beginning April 14th at Rio Vista-U.	174
Figure 12-38 Expanded results - turbidity data and model results for the RMA forecast beginning April 14th at SAC at Decker.....	175
Figure 12-39 Expanded results - turbidity data and model results for the RMA forecast beginning April 14th at SJR-Garwood.	176
Figure 12-40 Expanded results - turbidity data and model results for the RMA forecast beginning April 14th at SJR-JP.....	177
Figure 12-41 Expanded results - turbidity data and model results for the RMA forecast beginning April 14th at Threemile-SJR.....	178
Figure 12-42 Expanded results - turbidity data and model results for the RMA forecast beginning April 14th at Turner Cut-Holt.....	179
Figure 12-43 Flow data and model results for the RMA forecast beginning April 14th at Cache-Ryer.	180
Figure 12-44 Flow data and model results for the RMA forecast beginning April 14th at Georgiana-BLW.....	181
Figure 12-45 Flow data and model results for the RMA forecast beginning April 14th at LIT-POT-SL.	182
Figure 12-46 Flow data and model results for the RMA forecast beginning April 14th at Middle R-Holt.....	183
Figure 12-47 Flow data and model results for the RMA forecast beginning April 14th at Moke-at-SJR.	184
Figure 12-48 Flow data and model results for the RMA forecast beginning April 14th at Mossdale.....	185
Figure 12-49 Flow data and model results for the RMA forecast beginning April 14th at Old R Head.	186
Figure 12-50 Flow data and model results for the RMA forecast beginning April 14th at Old-R-Bacon.....	187
Figure 12-51 Flow data and model results for the RMA forecast beginning April 14th at Old-R-Hwy 4.	188
Figure 12-52 Flow data and model results for the RMA forecast beginning April 14th at Rio Vista-U.	189
Figure 12-53 Flow data and model results for the RMA forecast beginning April 14th at SAC-ABV-DCC.	190

Figure 12-54 Flow data and model results for the RMA forecast beginning April 14th at SJR Brandt BR.....	191
Figure 12-55 Flow data and model results for the RMA forecast beginning April 14th at SJR-Garwood.....	192
Figure 12-56 Flow data and model results for the RMA forecast beginning April 14th at Threemile-SJR.....	193
Figure 12-57 Expanded results - flow data and model results for the RMA forecast beginning April 14th at Cache-Ryer.....	194
Figure 12-58 Expanded results - flow data and model results for the RMA forecast beginning April 14th at Georgiana-BLW.....	195
Figure 12-59 Expanded results - flow data and model results for the RMA forecast beginning April 14th at LIT-POT-SL-TERM.....	196
Figure 12-60 Expanded results - flow data and model results for the RMA forecast beginning April 14th at Middle R-Holt.....	197
Figure 12-61 Expanded results - flow data and model results for the RMA forecast beginning April 14th at Moke-at-SJR.....	198
Figure 12-62 Expanded results - flow data and model results for the RMA forecast beginning April 14th at Mossdale.....	199
Figure 12-63 Expanded results - flow data and model results for the RMA forecast beginning April 14th at Old R Head.....	200
Figure 12-64 Expanded results - flow data and model results for the RMA forecast beginning April 14th at Old-R-Bacon.....	201
Figure 12-65 Expanded results - flow data and model results for the RMA forecast beginning April 14th at Old-R-Hwy 4.....	202
Figure 12-66 Expanded results - flow data and model results for the RMA forecast beginning April 14th at Rio Vista-U.....	203
Figure 12-67 Expanded results - flow data and model results for the RMA forecast beginning April 14th at SAC-ABV-DCC.....	204
Figure 12-68 Expanded results - flow data and model results for the RMA forecast beginning April 14th at SJR Brandt BR.....	205
Figure 12-69 Expanded results - flow data and model results for the RMA forecast beginning April 14th at SJR-Garwood.....	206
Figure 12-70 Expanded results - flow data and model results for the RMA forecast beginning April 14th at Threemile-SJR.....	207
Figure 12-71 Turbidity data and model results for the RMA forecast beginning Feb 25 th at Antioch.....	208
Figure 12-72 Turbidity data and model results for the RMA forecast beginning Feb 25 th at Cache-Ryer.....	209

Figure 12-73 Turbidity data and model results for the RMA forecast beginning Feb 25 th at Dutch SL.....	210
Figure 12-74 Turbidity data and model results for the RMA forecast beginning Feb 25 th at Georgiana-BLW.....	211
Figure 12-75 Turbidity data and model results for the RMA forecast beginning Feb 25 th at Georgiana-SAC.....	212
Figure 12-76 Turbidity data and model results for the RMA forecast beginning Feb 25 th at Grant Line.	213
Figure 12-77 Turbidity data and model results for the RMA forecast beginning Feb 25 th at Holland Cut.....	214
Figure 12-78 Turbidity data and model results for the RMA forecast beginning Feb 25 th at LIT-POT-SL-TERM.....	215
Figure 12-79 Turbidity data and model results for the RMA forecast beginning Feb 25 th at Middle R-Holt.....	216
Figure 12-80 Turbidity data and model results for the RMA forecast beginning Feb 25 th at Moke-at-SJR.	217
Figure 12-81 Turbidity data and model results for the RMA forecast beginning Feb 25 th at Mossdale.....	218
Figure 12-82 Turbidity data and model results for the RMA forecast beginning Feb 25 th at Old-R-Bacon.....	219
Figure 12-83 Turbidity data and model results for the RMA forecast beginning Feb 25 th at Old-R-Hwy 4.	220
Figure 12-84 Turbidity data and model results for the RMA forecast beginning Feb 25 th at Old-R-Quimby.	221
Figure 12-85 Turbidity data and model results for the RMA forecast beginning Feb 25 th at Rio Vista-U.	222
Figure 12-86 Turbidity data and model results for the RMA forecast beginning Feb 25 th at SAC at Decker.....	223
Figure 12-87 Turbidity data and model results for the RMA forecast beginning Feb 25 th at SJR-Garwood.....	224
Figure 12-88 Turbidity data and model results for the RMA forecast beginning Feb 25 th at SJR-JP.....	225
Figure 12-89 Turbidity data and model results for the RMA forecast beginning Feb 25 th at Threemile-SJR.	226
Figure 12-90 Turbidity data and model results for the RMA forecast beginning Feb 25 th at Turner Cut-Holt.....	227
Figure 12-91 Flow data and model results for the RMA forecast beginning Feb 25 th at Cache-Ryer.....	228

Figure 12-92 Flow data and model results for the RMA forecast beginning Feb 25 th at Georgiana-BLW.....	229
Figure 12-93 Flow data and model results for the RMA forecast beginning Feb 25 th at LIT-POT-SL-TERM.....	230
Figure 12-94 Flow data and model results for the RMA forecast beginning Feb 25 th at Middle R-Holt.....	231
Figure 12-95 Flow data and model results for the RMA forecast beginning Feb 25 th at Moke-at-SJR.....	232
Figure 12-96 Flow data and model results for the RMA forecast beginning Feb 25 th at Mossdale.....	233
Figure 12-97 Flow data and model results for the RMA forecast beginning Feb 25 th at Cache-Ryer.....	234
Figure 12-98 Flow data and model results for the RMA forecast beginning Feb 25 th at Old-R-Bacon.....	235
Figure 12-99 Flow data and model results for the RMA forecast beginning Feb 25 th at Old-R-Hwy 4.....	236
Figure 12-100 Flow data and model results for the RMA forecast beginning Feb 25 th at Rio Vista-U.....	237
Figure 12-101 Flow data and model results for the RMA forecast beginning Feb 25 th at SAC-ABV-DCC.....	238
Figure 12-102 Flow data and model results for the RMA forecast beginning Feb 25 th at SJR Brandt BR.....	239
Figure 12-103 Flow data and model results for the RMA forecast beginning Feb 25 th at SJR-Garwood.....	240
Figure 12-104 Flow data and model results for the RMA forecast beginning Feb 25 th at Threemile-SJR.....	241
Figure 13-1 Turbidity data (blue line) and Jan. 12 th model forecast (red dash) at Cache-Ryer.....	244
Figure 13-2 Turbidity data (blue line) and Jan. 12 th model forecast (red dash) at Dutch SL.....	244
Figure 13-3 Turbidity data (blue line) and Jan. 12 th model forecast (red dash) at Freeport.....	245
Figure 13-4 Turbidity data (blue line) and Jan. 12 th model forecast (red dash) at Grant Line.....	245
Figure 13-5 Turbidity data (blue line) and Jan. 12 th model forecast (red dash) at LIT-POT-SL-TERM.....	246
Figure 13-6 Turbidity data (blue line) and Jan. 12 th model forecast (red dash) at Martinez.....	246
Figure 13-7 Turbidity data (blue line) and Jan. 12 th model forecast (red dash) at Middel R-Holt.....	247
Figure 13-8 Turbidity data (blue line) and Jan. 12 th model forecast (red dash) at Old R-Bacon.....	247
Figure 13-9 Turbidity data (blue line) and Jan. 12 th model forecast (red dash) at Rio-Vista.....	248

Figure 13-10 Turbidity data (blue line) and Jan. 12 th model forecast (red dash) at SJR McCune.	248
Figure 13-11 Turbidity data (blue line) and Jan. 12 th model forecast (red dash) at SJR-JP.	249
Figure 13-12 Turbidity data at CCFB (blue line) and Jan. 12 th model forecast (red dash) at the SWP Intake.	249
Figure 13-13 Turbidity data (blue line) and Feb 11 th model forecast (red dash) at Cache-Ryer.	250
Figure 13-14 Turbidity data (blue line) and Feb 11 th model forecast (red dash) at Dutch Sl.	250
Figure 13-15 Turbidity data (blue line) and Feb 11 th model forecast (red dash) at Freeport.	251
Figure 13-16 Turbidity data (blue line) and Feb 11 th model forecast (red dash) at Grant Line. .	251
Figure 13-17 Turbidity data (blue line) and Feb 11 th model forecast (red dash) at LIT-POT-SL- TERM.	252
Figure 13-18 Turbidity data (blue line) and Feb 11 th model forecast (red dash) at Martinez.	252
Figure 13-19 Turbidity data (blue line) and Feb 11 th model forecast (red dash) at Middle R-Holt.	253
Figure 13-20 Turbidity data (blue line) and Feb 11 th model forecast (red dash) at Old R- Bacon.	253
Figure 13-21 Turbidity data (blue line) and Feb 11 th model forecast (red dash) at Rio Vista. ...	254
Figure 13-22 Turbidity data (blue line) and Feb 11 th model forecast (red dash) at SJR McCune.	254
Figure 13-23 Turbidity data (blue line) and Feb 11 th model forecast (red dash) at SJR-JP.	255
Figure 13-24 Turbidity data at CCFB (blue line) and Feb. 11 th model forecast (red dash) at the SWP Intake.	255
Figure 13-25 Turbidity data (blue line) and Feb 17 th model forecast (red dash) at Cache-Ryer.	256
Figure 13-26 Turbidity data (blue line) and Feb 17 th model forecast (red dash) at Dutch SL. ...	256
Figure 13-27 Turbidity data (blue line) and Feb 17 th model forecast (red dash) at Freeport.	257
Figure 13-28 Turbidity data (blue line) and Feb 17 th model forecast (red dash) at Grant Line. .	257
Figure 13-29 Turbidity data (blue line) and Feb 17 th model forecast (red dash) at LIT-POT-SL- TERM.	258
Figure 13-30 Turbidity data (blue line) and Feb 17 th model forecast (red dash) at Martinez.	258
Figure 13-31 Turbidity data (blue line) and Feb 17 th model forecast (red dash) at Middle R-Holt.	259
Figure 13-32 Turbidity data (blue line) and Feb 17 th model forecast (red dash) at Old R-Bacon.	259
Figure 13-33 Turbidity data (blue line) and Feb 17 th model forecast (red dash) at Rio-Vista. ...	260
Figure 13-34 Turbidity data (blue line) and Feb 17 th model forecast (red dash) at SJR McCune.	260
Figure 13-35 Turbidity data (blue line) and Feb 17 th model forecast (red dash) at SJR-JP.	261
Figure 13-36 Turbidity data at CCFB (blue line) and Feb. 17 th model forecast (red dash) at the SWP Intake.	261

Figure 13-37 Turbidity data (blue line) and April 7 th model forecast (red dash) at Cache-Ryer.	262
Figure 13-38 Turbidity data (blue line) and April 7 th model forecast (red dash) at Dutch SL....	262
Figure 13-39 Turbidity data (blue line) and April 7 th model forecast (red dash) at Freeport.	263
Figure 13-40 Turbidity data (blue line) and April 7 th model forecast (red dash) at Grant Line..	263
Figure 13-41 Turbidity data (blue line) and April 7 th model forecast (red dash) at LIT-POT-SL-TERM.....	264
Figure 13-42 Turbidity data (blue line) and April 7 th model forecast (red dash) at Martinez.....	264
Figure 13-43 Turbidity data (blue line) and April 7 th model forecast (red dash) at Middle R-Holt.	265
Figure 13-44 Turbidity data (blue line) and April 7 th model forecast (red dash) at Old R-Bacon.	265
Figure 13-45 Turbidity data (blue line) and April 7 th model forecast (red dash) at Rio Vista. ...	266
Figure 13-46 Turbidity data (blue line) and April 7 th model forecast (red dash) at SJR McCune.	266
Figure 13-47 Turbidity data (blue line) and April 7 th model forecast (red dash) at SJR-JP.	267
Figure 13-48 Turbidity data at CCFB (blue line) and Apr. 7 th model forecast (red dash) at the SWP Intake.....	267

Tables

Table 4-1 DWR modeled periods for near-real-time hindcasts.....	26
Table 4-2 RMA modeled periods, flow forecast period and flow sources used for near-real-time hindcasts	26
Table 4-3 Boundary conditions from DWR O&M.	27
Table 4-4 Data sources for historical and forecast boundary conditions implemented in RMA models.	28
Table 4-5 Boundary condition formulas for DWR forecast starting April 12, 2010.....	29
Table 4-6 Bin size (in NTU) for the Freeport flow category 30,000 cfs to < 35,000 cfs. 70 NTU, the average of the first two bins, was used for the 50 th percentile value.....	31
Table 4-7 Final values and categories for Freeport turbidity (SSC-based) boundary condition estimates.	32
Table 4-8 Final values and categories for Vernalis turbidity (SSC-based) boundary condition estimates.	32
Table 11-1 Inflows, outflows and turbidity data sources used to set model boundary conditions for 2007/8 calibration.	126
Table 11-2 Conversion from stage (ft.) to flow (cfs) at Sacramento R. at I street.	128
Table 11-3 Rating table to covert from stage (ft.) to flow (cfs) at Sacramento R. at I street for flows from 1 – 10 cfs.	129

This Page intentionally left blank.

1. Executive Summary

This document describes a methodology for forecasting turbidity, flow and EC using RMA2 and RMA11 models with a focus on the methodology for modeling turbidity. Once forecast in the RMA models, the hydrodynamic and water quality model outputs were used in RMA's adult delta smelt particle tracking model to predict the movement of delta smelt in the Delta, simulating their "habitat-seeking" behavior and their potential to become "salvage" in the SWP and CVP export locations.

In cooperation with DWR Operations and Maintenance (O&M) staff, RMA used DWR-supplied flow and salinity forecasts as a basis for developing a two-dimensional turbidity modeling protocol for short-term hydrodynamic, water quality and particle tracking forecasting. Starting in December 2009, new turbidity measurements have been gathered on a real-time basis at multiple locations in the Delta – these measurements supply a rich database on which turbidity forecast modeling is based. Starting with O&M's DSM2 flow forecast boundary conditions and HYDRO model output, flow boundary conditions for the Sacramento and San Joaquin Rivers and for the Yolo boundary were refined using forecast conditions obtained from the California-Nevada River Forecasting Center (CNRFC) website. A simple methodology using flow-based relationships was developed for forecasting approximate 50% and 90% exceedance values for turbidity boundary conditions at the Sacramento and San Joaquin River boundaries. Although adequate for a first cut, this methodology does not incorporate the longer-term episodic nature of upstream and in-Delta storage and release of sediments.

Using this newly expanded database of turbidity measurements, the previous RMA turbidity model using the decay coefficient approach was modified to improve the representation of Delta turbidity. The turbidity model developed for the current project settled on a three-region, three-parameter model. The previous model used a single decay coefficient throughout the entire model domain.

Forecast simulations were conducted roughly from December 2009 through May 2010 using weekly historical and forecast operations provided by DWR's Operations and Maintenance group as a basis for the hydrodynamics and salinity boundary conditions, and using new turbidity data and forecast boundary conditions developed by RMA. Although ten forecasts were prepared in total, some of the initial forecasts did not use the final three-region, three-parameter model for turbidity decay. At the request of Paul Hutton, a final set of six forecast models, including adult delta smelt particle distributions, were prepared using the final model parameterization – although these were essentially hindcasts, they were prepared as if they were forecasts using the methodology developed for this project.

For each forecast, the RMA modeled and forecast dates depended on the period in question. Although DWR forecast conditions extended three weeks into the future, the forecasts

themselves were generally delivered to RMA several days after the start of their forecast period so the RMA forecast period was offset from DWR's. Data was used to fill-in boundary conditions in the interim period (i.e., between the beginning of the DWR forecast and the date the RMA forecast was run) wherever possible. Each RMA flow, salinity and turbidity model run began at the beginning of a month, so the modeled period for a given forecast could cover two months. Each adult delta smelt model run, on the other hand, began on January 1, 2010 and proceeded through the end of a forecast period.

In order to improve model accuracy, RMA flow boundary conditions frequently differed from those supplied by DWR. For each forecast period, additional data was acquired and compared with DWR-supplied boundary conditions – if the additional data indicated the boundary values could be improved, DWR time series were not used. For example, the Yolo inflow boundary was prepared using additional data from the USGS and the CNRFC websites.

The turbidity model results for the 2009 – 2010 rainy period generally follow the magnitude and trend of turbidity measurements through most of the Delta with a few notable exceptions (*e.g.*, near Little Potato Slough at Terminous and near Stockton on the San Joaquin River). However, a turbidity model based on decay coefficients is not capable of capturing all processes in sediment transport, so some mismatch between the model and turbidity data is not unexpected as turbidity measurements are used as a proxy for suspended sediment concentration.

Although the turbidity model gives reasonable results throughout much of the Delta, several factors were identified that are needed for a more comprehensive and accurate conceptual model of the system: wind and rain events produce increases in turbidity that are not currently captured in the model; and, results at several locations suggest that inflow is not being adequately captured during high flow events. Lack of accurate inflow data may be producing problems with modeled turbidity particularly in the Eastern Delta. Also, areas where the decay-coefficient approach does not sufficiently capture decreases in measured turbidity are sometimes located in low-velocity channels or shallow water areas perhaps indicating the effects of accelerated sediment settling. Overall, the results indicate that measured turbidity will be better approximated by a model incorporating the effects of precipitation on turbidity changes due to runoff (although these may be difficult to quantify), of wind on re-suspension, and of sediment settling, and by additional and/or more accurate measurements of flow and turbidity at key locations during and shortly after storm events.

The adult delta smelt behavioral model results show only trivial losses at the export locations. This result is in general agreement with salvage data, as very few delta smelt were salvaged during this period. The timing of the salvaged delta smelt is in agreement with the modeled location of particles in central and south Delta regions. It is important to note that despite concurrent high flow and turbidity events on the Sacramento and San Joaquin Rivers that carried turbidity into the lower San Joaquin River and into the South Delta, respectively, a “turbidity

bridge” never formed in the central Delta to enhance the movement of modeled “delta smelt” particles into the south Delta.

The three-region, three-parameter turbidity model developed for the 2009 -2010 period might be improved by dividing the decay regions into subregions with selective changes to the decay coefficients. However, this sort of strategy generally reduces the predictive power of the model. The 2010-2011 wet season will provide an important test of the turbidity model.

One action that could be taken to improve model application without changing the basic turbidity model (*i.e.*, without incorporating meteorological effects and sediment settling) is to improve monitoring data. In particular, it is important to remove uncertainty about missing flow and runoff by obtaining better flow data at the locations discussed in this report and at other episodic inflow locations particularly during and shortly after rain events.

Comparison of forecast turbidity with measurements indicate that at least two turbidity forecasts should be run if increased flow is predicted to cover a range of possible turbidity outcomes, as the relationship between turbidity magnitude and flow magnitude is highly variable. CNRFC flow forecasts only use a five-day window, which limits the potential accuracy of the forecast results beyond that period.

There is room for improvement in the turbidity model process, in the acquisition of data at key locations and times, and in the protocol for forecasting turbidity at the inflow boundaries. Extending the forecast period using CNRFC forecast flows enhanced the quality of the turbidity forecast although it did require additional time and effort. At this time, the process of producing a forecast is quite demanding and it requires considerable modeling experience and professional judgment to set poorly constrained or questionable boundary conditions either from DWR or from the available data sources, particularly for turbidity data which is frequently noisy or missing. Acquiring DWR forecast results and model boundary conditions earlier would provide a major improvement in the ease of producing a good forecast. However, it was possible to produce RMA-model-based turbidity and adult delta smelt forecasts within a reasonable turn-around time (~ 1.5 days) using DWR flow and salinity forecasts as a basis.

2. Objectives

The objective of the work summarized in this document is to prepare and demonstrate a methodology for near-real-time hydrodynamic, water quality (EC and turbidity), and adult delta smelt behavioral forecasting using the RMA particle tracking simulations in conjunction with real-time data monitoring activities. Using previous work funded by Metropolitan Water District (MWD) as a starting point, the current work includes a new reconnaissance level recalibration of the existing RMA turbidity model using an expanded set of stations collecting turbidity data since Dec. 2009. In addition, a near-real-time forecasting methodology for flow, EC and turbidity was developed for use in the RMA models, and applied in near-real-time to RMA’s

adult delta smelt behavior model developed for the 2-Gate Fisheries Protection Plan. A preliminary methodology for forecasting turbidity loading is documented, along with the incorporation of recent model geometry enhancements for the north Delta that were initially developed for DWR's Through-Delta-Facility investigations.

Adult delta smelt particle distributions were predicted for six forecast periods, and estimates of particle ("delta smelt") entrainment and fate have been prepared. Forecasts of turbidity are particularly important during high flow events as the movement of adult delta smelt is hypothesized to be cued to increases in turbidity. If turbidity increases reach the Old+Middle River corridor, delta smelt following turbidity increases are at an increased risk from Delta export if their hypothesized habitat-seeking behavior leads them in that direction.

Forecast simulations were conducted roughly from December 2009 through May 2010 using historical and forecast operations provided by DWR's Operations and Maintenance group for the hydrodynamics and salinity boundary conditions, and using new turbidity data and forecast boundary conditions developed by RMA.

In a related report (in preparation), results produced by running the newly calibrated turbidity model for a selection of years prior to 2010 are being documented, along with results produced by running the adult delta smelt behavior model. A comparison is made in that document of computed salvage estimates with salvage data.

3. Background

To date, nearly all of the modeling for near-term Delta solutions has simulated historic conditions. While this was necessary for planning and environmental documentation, a forecast of future conditions is needed to successfully operate Delta infrastructure to improve water operations by reducing fish conflicts. In addition, particle tracking models have historically used passive, neutrally-buoyant particles to determine the potential movement and fate of delta smelt in the Delta. However, it has become increasingly evident that at least two distinct particle tracking techniques are needed: one to represent the adult life stage of delta smelt and another to represent the larval/juvenile life stages.

Larval and juvenile delta smelt are considered to be poor enough swimmers to be represented as passively transported particles. Adult delta smelt are not well represented using passive particle tracking techniques as they are sufficiently strong swimmers to resist tidal flows, for example, by moving out of the current and into shoals or near the bed where velocities are low. Some scientists have postulated that the adult smelt may be "surfing" the tides as a means of staying within their desirable habitat range.

Entrainment of adult delta smelt occurs during the period when the fish move upstream for spawning. Researchers have observed that the behaviors of delta smelt can be associated with

turbidity changes. Analyses done by Fullerton have shown patterns of salinity and turbidity habitat may correlate with smelt location. In the period from December through March when adult delta smelt are moving upstream to spawn, there appears to be strong correlation between salvage of adult delta smelt at the state and federal export facilities and turbidity near the export pumps. Periods of peak entrainment at the south Delta export locations are correlated with high turbidity resulting from storm flows reaching the neighborhood of the export pumps.

A particle tracking behavior model, developed by RMA with support from MWD, has been used to simulate the movement of adult delta smelt during periods of high Delta inflow based on simulated distributions of salinity (represented as electrical conductivity, EC) and turbidity (RMA 2008). Because turbidity is hypothesized as an important driver for the distribution of adult delta smelt, the ability to minimize adult entrainment is assumed to be dependent on monitoring and potentially controlling and reducing the progress of turbidity plumes from the Sacramento and San Joaquin Rivers into the central Delta through Old and Middle Rivers downstream of the export facilities.

Previous work funding RMA for the development of an adult delta smelt behavior model used (1) the electrical conductivity (EC) and turbidity gradient-based behavior model for delta smelt and (2) flow balancing relationships for modeling delta smelt behavior. In addition to historical simulations, several modified operations scenarios were simulated with the RMA Bay-Delta Model and RMA-PTRK model for revised export flows according to OCAP guidelines and 2-Gate Fish Protection Measures (RMA 2009a). Many simulations were performed for the 2000, 2002, 2003, 2004 and 2008 historic periods. Predicted delta smelt distribution, entrainment and fate were also developed in simulations by adding 2-Gate Project operations to the OCAP BO baseline operations.

During the CALFED Science Review of the 2-Gate Project proposal, questions were raised regarding the calibration of the RMA Delta model for the flow split between the Mokelumne River and Little Potato Slough. This flow split is important to the simulation of turbidity because it impacts the distribution of Sacramento River turbidity passing through the Cross Channel or Georgiana Slough into the Mokelumne River and its adjoining channels, which, in turn, impacts the distribution of turbidity across the Old and Middle River Corridors. An improved grid was developed as part of DWR's Through-Delta-Facility investigations that improved the representation of the flow split in the RMA models discussed in this report.

The turbidity model developed for the 2-Gate project used a decay coefficient regime based on limited turbidity data, and used a grid that did not adequately represent the flow split between the Mokelumne River and Little Potato Slough. With the inclusion of numerous new turbidity data collection sites and a refinement of the RMA grid, a recalibration of the turbidity model in the current project resulted in a different decay coefficient regime. In order to check the recent calibration and the inclusion of the improved grid in the vicinity of the Mokelumne River and

Little Potato Slough, a comparison of the turbidity model with the new decay regime and previous data will be made to assess the new turbidity model by running turbidity hindcasts – those results will be described in a separate report, currently in draft stages. Modeled turbidity results will be compared with the turbidity data available for Water Years 2007/8 and 2008/9, as well as a selection of earlier years which may include additional years though to be particularly interesting¹. The adult delta smelt behavior model will also be run with the new turbidity model for these years to compare computed salvage estimates with salvage data.

However, the main application of the new turbidity model summarized in this document is its use in a near-real-time context to forecast water quality parameters that are used in the prediction of delta smelt distributions using the RMA adult delta smelt behavioral model.

3.1. Relationship between turbidity and suspended-sediment measurements

The modeling in this project relies on a combination of suspended sediment concentration (SSC) and turbidity measurements and to some extent on understanding the relationship between the two. Suspended sediment concentration can be defined as the ratio of the mass of dry sediment in a water-sediment mixture to the mass of the mixture, and it is expressed in milligrams of dry sediment per liter of water-sediment mixture² (Gray *et al.* 2000). Turbidity is an expression of the optical properties of a liquid that cause light to be absorbed or scattered rather than transmitted through a sample³. Turbidity is caused by the presence of suspended and dissolved matter in the water column¹ (*e.g.*, clay, silt, organic matter).

Suspended-sediment concentration is typically reported in units of mg L⁻¹ while turbidity is typically reported in units of NTU, Nephelometric Turbidity Units. A third related measurement, total suspended solids (TSS), is not used in this project. The analytical methods for TSS and SSC differ, and the measurements are not comparable as sediment sizes vary, particularly when sand-size material composes a substantial fraction of the sediment sample (Gray *et al.* 2000). The SSC method produces reliable results, while the TSS method has been reported as unreliable for the analysis of natural-water samples (Gray *et al.* 2000).

Instruments have been developed that allow for nearly continuous monitoring and data logging of turbidity. Different instrument designs for turbidity measurement have different capabilities in

¹ Suggested by Pete Smith: 1988, 1993, 1997 and 1999.

² https://encrypted.google.com/search?hl=en&defl=en&q=define:suspended+sediment+concentration&sa=X&ei=sFiJTOMkHo_msQOk-eG7BA&ved=0CA8QkAE

³ http://water.usgs.gov/owq/FieldManual/Chapter6/6.7_contents.html, Chapter 6.7, Version 2.1 (dated 9/2005) , by Chauncey W. Anderson

terms of range of application and the ability to account for different properties of the turbid water, such as the color of the mixture. As a consequence, different instruments do not yield equivalent results in all situations. SSC measurements are made from samples collected in the field and brought back to the laboratory for analysis, so real-time monitoring is not practical. When using standard sample collection and processing methods, SSC measurements are reported to produce reliable results (Gray *et al.* 2000).

USGS researchers have documented the relationships between the SSC and NTU at several locations in San Francisco Bay using two types of turbidity sensors recording data at 15-minute intervals (Buchanan and Lionberger 2006). SSC samples included all insoluble particles not passing through 0.45-micrometer membrane filter. Turbidity sensor data was deemed invalid if voltage outputs were unusually high and of short duration or if voltage outputs increase rapidly. Sensors were calibrated before and after cleaning using water-sample data - cleaning sensors resulted in a decrease in sensor output. Detection of the point where instrument fouling rendered data unusable was somewhat subjective.

Due to various factors such as instrument fouling and interference by local organisms (e.g., fish), linear statistical relationships between SSC and NTU developed using non-parametric regression could vary by more than a factor of two between locations. Simplifying their analysis considerably, the authors found SSC in mg L^{-1} could range from $0.9 \cdot \text{NTU}$ to $2.3 \cdot \text{NTU}$ (plus or minus a constant), depending on parameters such as depth of instrument (surface, mid-depth or bottom) and sensor type (Buchanan and Lionberger 2006). However, output of side-by-side sensors with different instrument designs were “virtually identical” (Buchanan and Lionberger 2006). Other researchers (Ganju *et al.* 2006) have found that turbidity and SSC are proportional throughout San Francisco Bay. As this study used data collected at Rio Vista in arriving at this conclusion, it is reasonable to assume that turbidity and SSC are also proportional along the Sacramento River mainstem.

3.2. Previous turbidity/suspended sediment models

Models simulating the winters of 1999-2000 through 2003-2004 used suspended sediment data for setting turbidity boundary values with SSC values multiplied by two for rivers. In the earliest turbidity simulations used in the delta smelt behavior model, turbidity was simulated as a conservative constituent. In-Delta data for the models simulating the winters of 1999-2000 through 2003-2004 were not adequate to determine if this was a reasonable approximation.

Hydrodynamics and turbidity were simulated and turbidity was calibrated (a “reconnaissance” level calibration) using the RMA Bay-Delta Model for the period of December 1, 2007 through March 31, 2008 using turbidity data for boundary conditions. Boundary conditions for this model are shown in the Appendix, Table 11-1. This period was selected as turbidity measurements were more numerous for this period than for previous periods, and because large delta smelt salvage

spikes were seen at the south Delta export facilities. Increased turbidity resulting from the high flows in the Sacramento River and reverse flows in the south Delta are suspected to have contributed to the large delta smelt salvage numbers.

In the initial 2007-2008 simulation, turbidity was simulated as a conservative constituent. However, computed turbidity concentrations were found to be higher than observed at all monitoring stations. A complete sediment transport simulation was not feasible due to lack of data (e.g. particle size information on SSC in inflow) and limitations on time and budget. Therefore, the reconnaissance level calibration of turbidity was performed using an exponential decay rate to approximate sediment settling and other losses. An exponential decay rate was applied rather than a constant settling rate because it more closely approximated a sediment transport simulation by allowing more rapid decline in turbidity when concentrations are high. Through iterative calibration simulations, the decay rate found to result in the best fit with observed data was -0.05/day.

Measured turbidity data from CDEC and BDAT were used for the model calibration. There were eleven turbidity monitoring stations with available data for the December 2007 – March 2008 calibration period. Locations are shown in Figure 11-1.

3.3. RMA Delta model configuration

3.3.1. RMA numerical models

The RMA suite of finite element hydrodynamic and water quality models employed for this study have been used extensively since 1977 in engineering applications to examine flow and transport of constituents in surface water systems (RMA, 1997; 1998a; 1998b; 1999; 2001; 2003). One of the unique characteristics of this suite of models is their ability to represent a physical system using 1, 2, and/or 3 dimensional approximations within a single computational network. This allows construction of efficient computational networks where the level of spatial resolution varies according to the needs of the problem. Originally developed with the support of the U.S. Army Corps of Engineers Waterways Experiments Station (King, 1975), the models have undergone continued development and refinement by RMA (King, 1986). One of the most important additions has been the capability to accurately represent wetting and drying in shallow estuaries (RMA, 2009b).

The RMA finite element model of the San Francisco Bay and Sacramento – San Joaquin Delta has been calibrated and refined through many previous studies (for a detailed description of the most rigorous recent calibration effort, see <http://rmanet.com/zip/FloodedIslandsCalibrationFinalReport-2005-06-30.zip>).

Hydrodynamics have been simulated for this study using RMA-2, a two-dimensional depth-averaged finite element model that solves the shallow water equations to provide temporal and

spatial descriptions of velocities and water depths throughout the regions of interest. The model uses the Smagorinski formulation for modeling of turbulent momentum transfer (King *et al.*, 1975). Due to its capability for simulating the de-watering of tidal flats, RMA-2 is uniquely suited for modeling of inter-tidal hydrodynamics in the marshes and mudflats that characterize boundaries of the Bay-Delta.

RMA-11 has been successfully applied in numerous previous projects to simulate the fate and transport of sediments and other conservative and non-conservative water quality constituents in surface water systems. Velocities and water depths obtained from hydrodynamic model results are used to solve the advection-dispersion equation for each constituent simulated. RMA-11 has been designed for compatibility with model results obtained from one-, two-, or three-dimensional hydrodynamic simulations (King, 1995).

Hydrodynamic and water quality model output from RMA's Delta models, RMA2 and RMA11 respectively, provide temporal and spatial descriptions of velocities and water depths and water quality throughout the model domain. The results of the flow simulation are saved and used by the water quality model, assuming flow is independent of concentration. The computational time step used for modeling the depth-averaged flow and water quality transport in the Delta is 7.5 minutes, and output from each model is saved every 15 minutes.

Due to the variable grid capability of the finite element method, fine detail can be added to emphasize specific areas in the vicinity of the current project without increasing detail elsewhere in the model grid. During the Suisun Marsh Levee Breach modeling project (RMA, 2009b), considerable detail was added to the representation of Suisun Bay and the western Delta. Wetting and drying of the tidal mudflats was represented in sufficient detail to provide a good definition of change in the tidal prism with change in tidal stage.

3.3.2. Grid and bathymetry

The RMA finite element grid of the Delta, shown in Figure 3-1 extends from Martinez to the confluence of the American and Sacramento Rivers and to Vernalis on the San Joaquin River. A two-dimensional depth-averaged approximation is used to represent the Suisun Bay region, the Sacramento-San Joaquin confluence area, Sherman Lake, Liberty Island, the Sacramento River up to Rio Vista, Big Break, the San Joaquin River up to its confluence with Middle River, False River, Franks Tract and surrounding channels, Old River south of Franks Tract, and the Delta Cross Channel area. Delta channels and tributary streams are represented using a one-dimensional cross-sectionally averaged approximation.

The size and shape of elements are dictated by changes in bottom elevation and other hydraulic and salinity considerations, such as the wetting and drying of tidal mudflats. Bottom elevations and the extent of mudflats are based on bathymetry data collected by National Oceanic and Atmospheric Administration (NOAA), California Department of Water Resources (DWR), U.S.

Army Corps of Engineers (USACE) and U.S. Geological Survey (USGS). These data sets can be downloaded from DWR's Cross Section Development Program (CSDP) website at <http://baydeltaoffice.water.ca.gov/modeling/deltamodeling/models/csdp/index.html>. Additional data were collected around Franks Tract by DWR and USGS in 2004. USGS 10 m resolution Delta Bathymetry grids were obtained from the Access USGS website at <http://sfbay.wr.usgs.gov/access/Bathy/Delta/>.

3.3.3. Stage and flow boundaries

Boundary conditions for hydrodynamics include tidal elevations at the Martinez boundary and tributary inflows to the system and exports (see Figure 3-1). Details on setting the hydrodynamic boundary conditions for the real-time model are covered under the specific sections as different strategies were used depending on the application.

Delta exports applied in the model include State Water Project (SWP), Central Valley Project (CVP), Contra Costa Water District diversions and exports at Rock Slough and Old River intakes, respectively, and exports at the North Bay Aqueduct.

3.3.4. Gates and barriers

Permanent gates and temporary barriers represented in the model include the Delta Cross Channel (DCC), Old River near Tracy (DMC) barrier, Old River at Head barrier, Middle River barrier, Montezuma Slough salinity control gates, Grant Line Canal barrier, and Lawler buffer ditch culvert (see Figure 3-2). In addition, there is a tidal gate at Rock Slough. Historical or forecast gate and barrier operations were applied in the models as appropriate.

3.3.5. DICU (flow)

Delta Island Consumptive Use (DICU) values were applied on a monthly average basis and were derived from monthly DSM2 input values⁴.

3.3.6. Salinity and turbidity

Salinity and turbidity concentration time series are required at all inflow locations and at the stage boundary at Martinez. Electrical conductivity (EC) is used as a surrogate for salinity and modeled as a conservative constituent. Turbidity is conceptualized as a non-conservative constituent with decay. When SSC is used as a surrogate for turbidity measurements, a factor of two could be applied in some cases (RMA 2009a).

At DICU locations, the turbidity of the inflow is assumed to be the ambient concentration (i.e., the DICU inflow concentration is equal to the concentration in that cell during the computational step). EC concentration at DICU locations was derived from DSM2 input values.

⁴<http://baydeltaoffice.water.ca.gov/modeling/deltamodeling/models/dicu/dicu.cfm>

3.3.7. Grid changes for the current project

The RMA-Delta network used for the RMA forecast modeling incorporates several updates to the Delta network used in the 2-Gates study:

- 1) Liberty Island is represented with two-dimensional elements.
- 2) The eastside streams and sloughs were updated to more recent bathymetry and calibrated to flow monitoring data from a USGS 2005 field data collection program for the Mokelumne River system.
- 3) The channels of the north Delta were updated and calibrated with more recently available bathymetry and flow monitoring data.
- 4) The network detail and calibration for the Suisun Marsh region was improved, using the grid developed for a previous project modeling this region (RMA 2009b).

These update particularly improved the flow calibration for the Delta Cross Channel.

3.3.8. Turbidity – regional decay values for the current project

The previous model used a single decay coefficient for the entire Delta. Sequential runs varying a single decay coefficient illustrated that although the previous value was too low, a higher decay coefficient produced too much decay when applied over the entire Delta. Near the Martinez boundary, outside of high turbidity events, it was evident that little or no decay of turbidity was needed. A three-region model, shown in Figure 3-3, was developed to capture the main features of the 2009-2010 turbidity regime with three decay parameters.

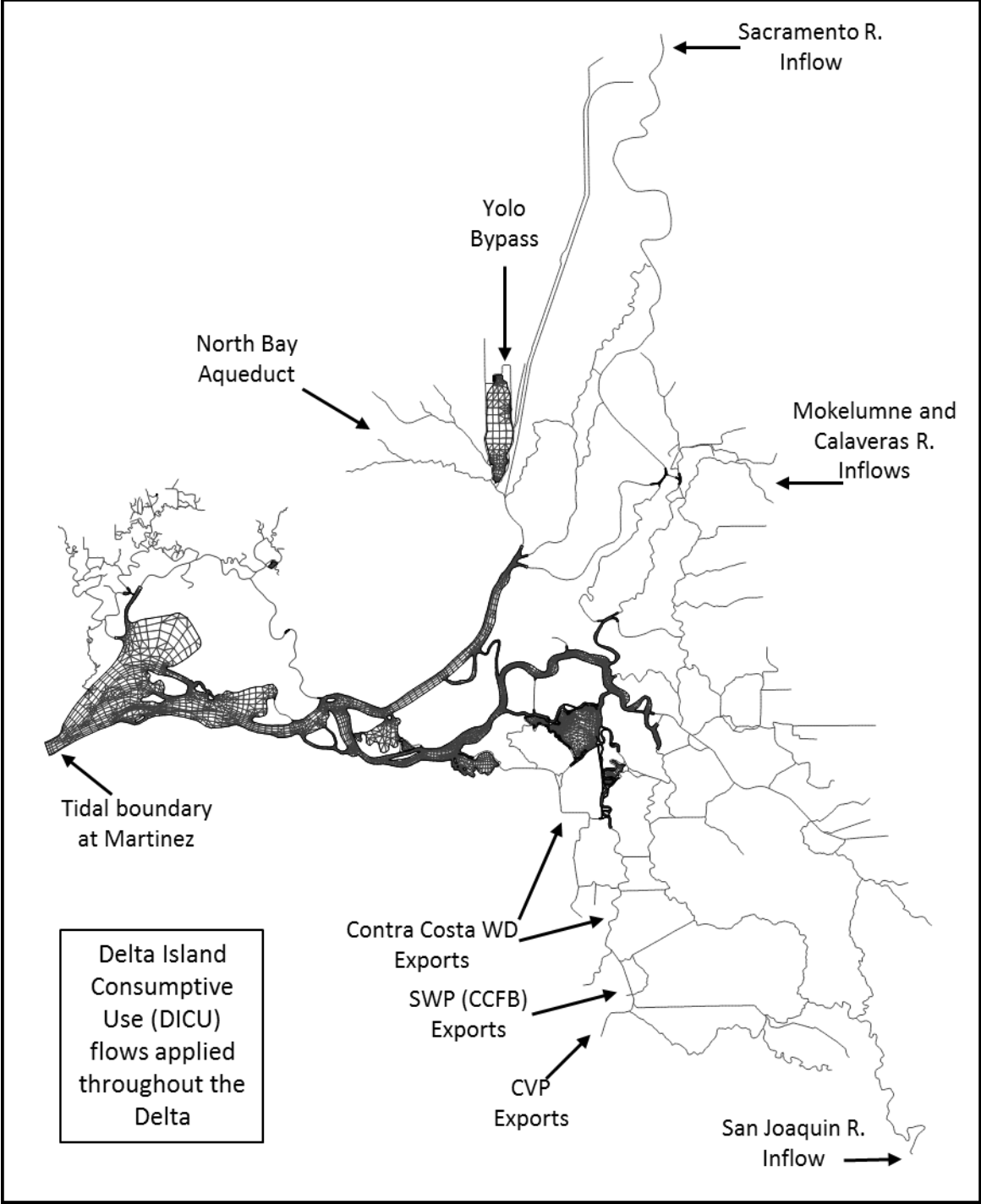


Figure 3-1 Finite element model configuration of the Sacramento – San Joaquin Delta.

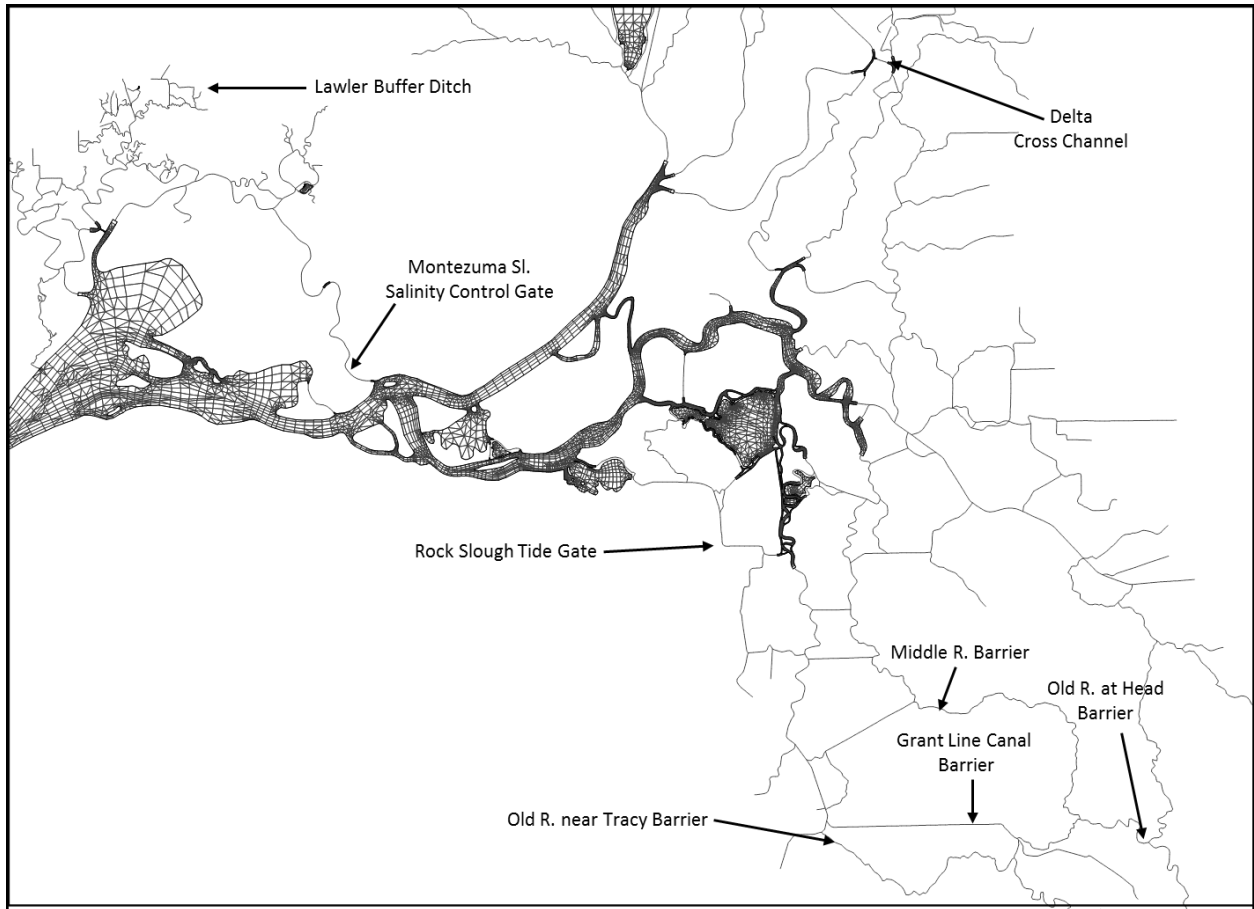


Figure 3-2 Approximate gate and barrier locations in the RMA grid.

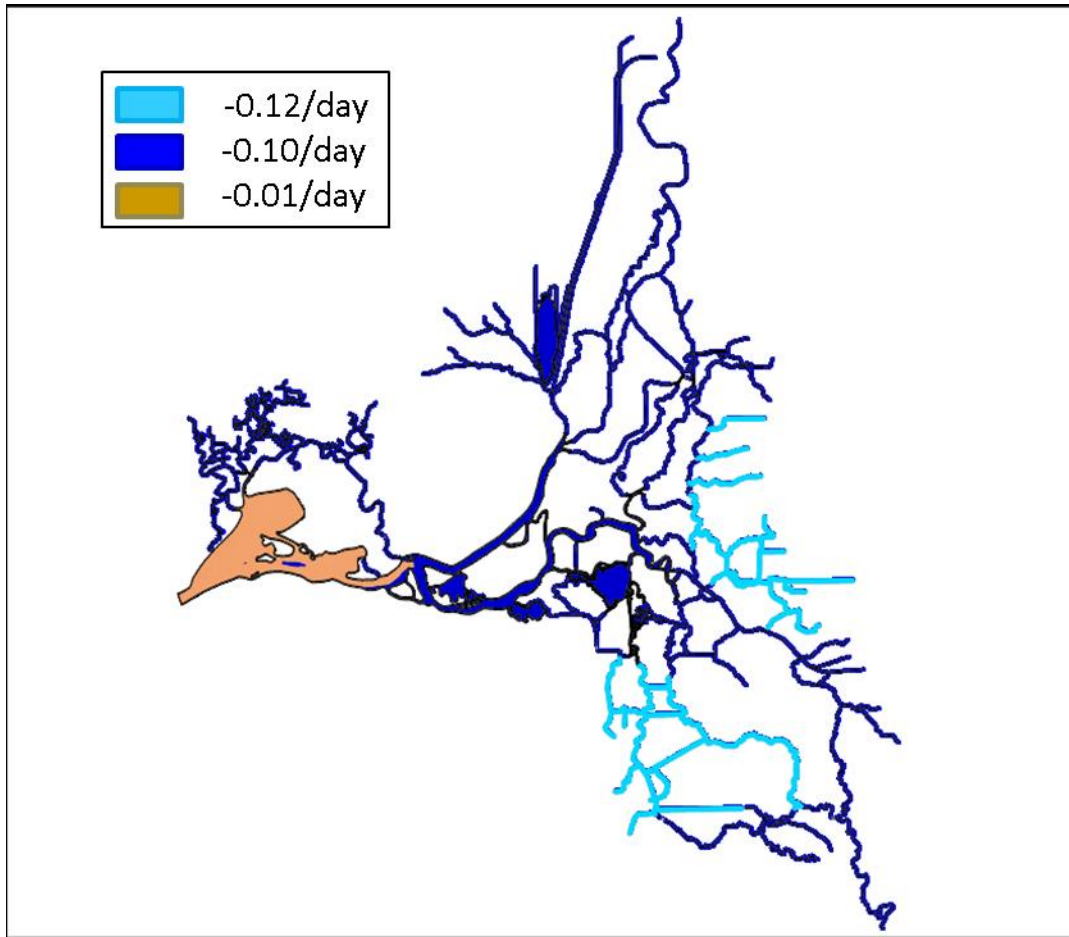


Figure 3-3 Final decay values and regions used in the current turbidity model.

4. Near-Real-time modeling

4.1. *Turbidity recalibration*

4.1.1. *Turbidity data*

Starting in December 2009, a large number of turbidity monitoring stations were added to the real-time network accessible through CDEC – these stations are shown in the Delta outline in Figure 4-1.

4.1.2. *Meteorological data (CIMIS)*

It is known that tidally-induced current velocities and wind waves in shallow waters are capable of resuspending bottom sediments (Powell et al, 1989; Schoellhamer, 1996). In comparing turbidity data with meteorological data, it was apparent that wind, rain and/or runoff had

influenced turbidity levels in various locations in the south and central Delta and along the San Joaquin River.

In order to better document these effects, automatic generation of current CIMIS data was requested on a weekly basis at several CIMIS locations – Hastings Tract, Lodi West, Tracy and Twitchell – the approximate locations are shown in Figure 4-2. Wind and rainfall data for the RMA forecast periods from these four locations are shown in Figure 11-2 through Figure 11-5 in the Appendix.

4.1.3. Flow data

We observed that there may be insufficient inflow in some regions of the model after storm events – *i.e.*, additional flow is seen in data that is not seen in the model in the eastern Delta (Mokelumne River area) and along the San Joaquin River near the Calaveras R. Hypotheses for this missing flow include local runoff during rain periods, additional flow entering the rivers or channels downstream of the flow gauges, and improperly calibrated flow gauges. These observations and associated hypotheses are discussed in greater detail in Section 5.2.

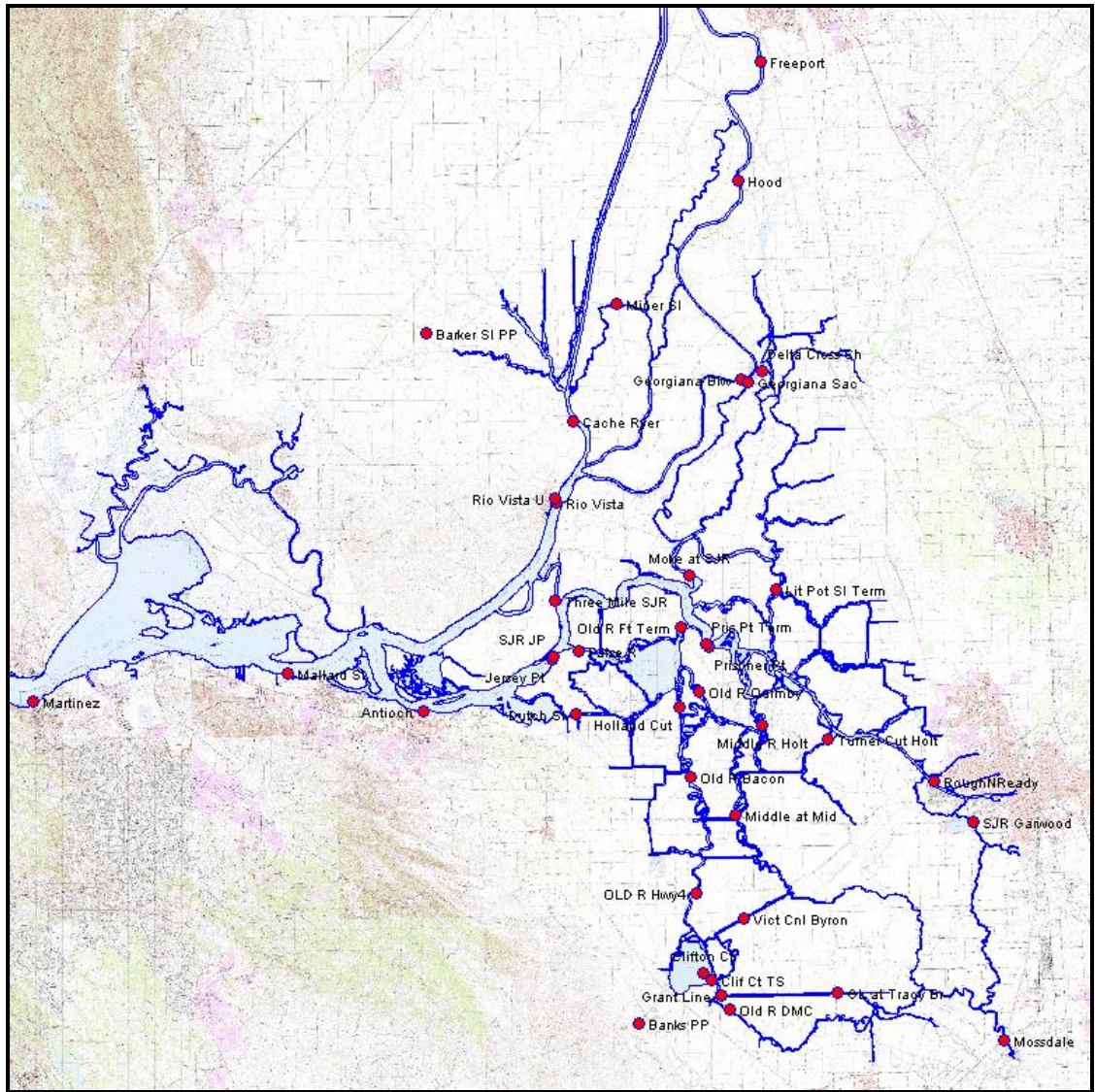


Figure 4-1 Locations of new turbidity monitoring stations.

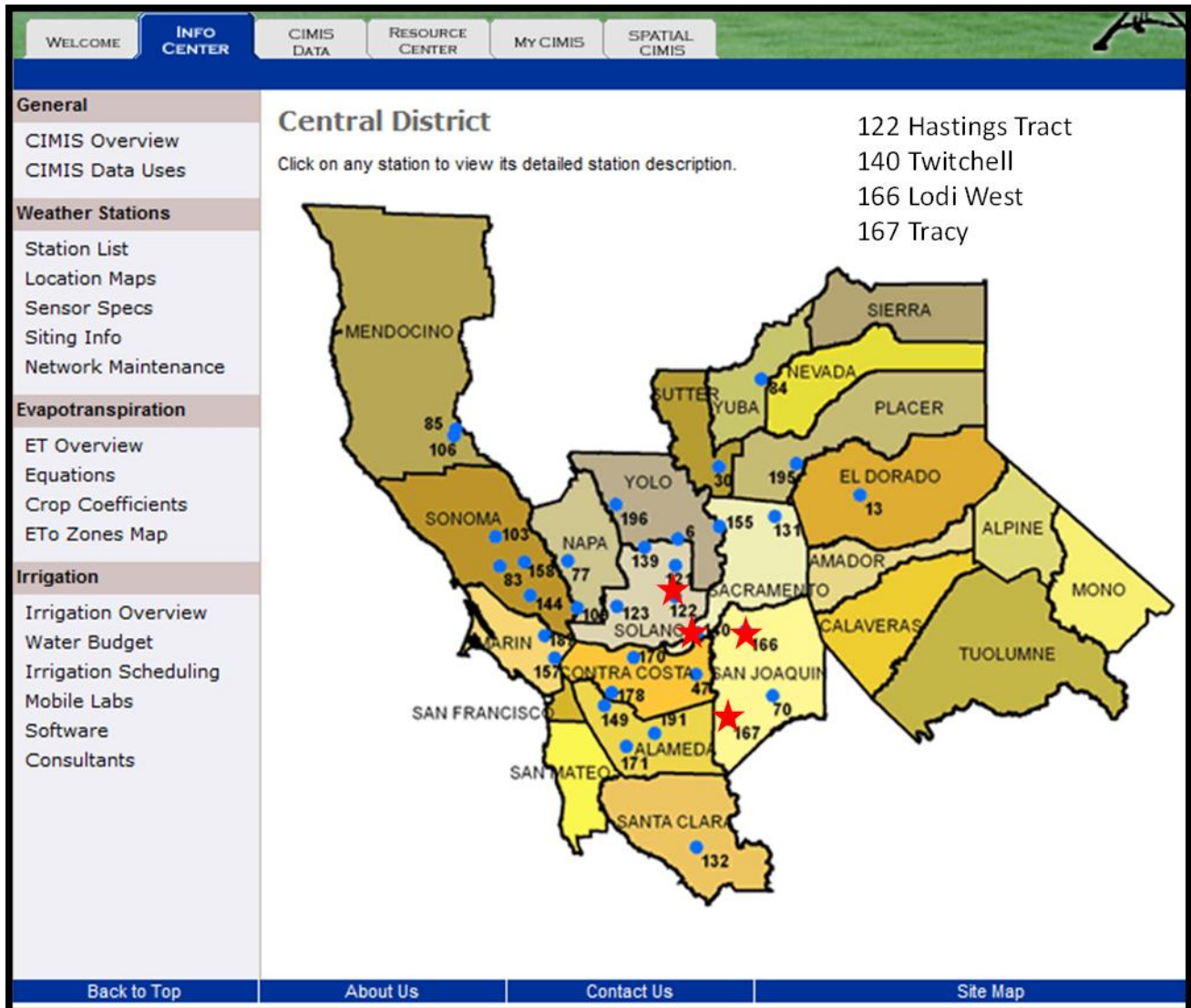


Figure 4-2 The CIMIS website map with the location of the four stations whose meteorological data was downloaded on a weekly basis (red stars).

4.2. Developing weekly forecasts using RMA2 and RMA11

4.2.1. Background

On a weekly basis, DWR's O&M section emailed RMA a set of DSS files containing flow and EC forecasts for a three-week period, information on in-Delta gate operations and DSM2 model output (Clifton-Court Node 72 in DSM2 terminology) that RMA used to specify Clifton Court export operations. The information flow for this process is shown in Figure 4-3.

Typically, the DWR forecast period began on the day before RMA received information, so the forecasts are (more appropriately) called "near-real-time". On occasion the DWR information arrived later, so the RMA forecast had two additional days of real data and forecast data to use in the development of the forecast.

As the project progressed, weekly near-real-time forecasts were developed and the calibration and the RMA forecast methodologies were refined. As turbidity at the Sacramento and San Joaquin boundaries did not necessarily peak during the later forecast periods which used the refined methodology, a set of near-real-time hindcasts were developed using the final forecast methodology during earlier periods when turbidity increased due to higher boundary inflows. As part of the development process, RMA refined some of the DWR-boundary conditions for flow, both for the historical period and for the RMA forecast period.

Six "near-real-time" hydrodynamic, water quality, and particle tracking modeling hindcasts were performed during the winter and spring period (Jan. - Apr., 2010). Model runs include actual and predicted field conditions that were developed at the time. Model forecast results include:

- Time series of instantaneous and averaged flow and turbidity at selected physical monitoring locations. Flow is tidally averaged while turbidity is smoothed as a three-day running average.
- Spatial contours of selected turbidity results.
- Particle tracking model estimates of potential salvage at the State and Federal export facilities using the adult delta smelt behavior model, and a comparison to measured salvage.

The periods selected for near-real-time model hindcasts are shown in Table 4-1.

4.2.2. DWR-supplied flow and EC boundary conditions

DWR Operations and Maintenance (O&M) provided RMA with boundary conditions used in the DSM2 HYDRO and QUAL/salinity models for each forecast period.

Table 4-3 lists the information supplied by O&M, while Table 4-4 lists the information that RMA used in the 2-dimensional forecasts. Some boundary inflow and EC values were supplied by O&M but not used in the modeling - these were instead developed by RMA from a variety of data sources (Table 4-4) that are considered in some cases to be more representative than the DWR-supplied values.

4.2.3. Turbidity forecast development

At the two inflow locations where SSC data was available historically, Freeport and Vernalis, a flow-based methodology was developed to forecast turbidity at times of high inflow (*i.e.*, at peak flows). Turbidity was estimated using SSC data and the relationship $NTU=SSC$ (*i.e.*, turbidity approximately equal to SSC). In the remainder of this document, references to turbidity estimated by SSC will use this relationship unless otherwise stated.

As shown in Figure 4-4 and Figure 4-11 for the Sacramento and San Joaquin River boundaries, respectively, turbidity was analyzed as a function of flow. SSC data was available for these rivers at Freeport and Vernalis from 1990 to 2006 or 2007, respectively. Three parameters need to be estimated for the turbidity forecast values – the maximum height of the turbidity peak, the width of the peak, and the timing of the turbidity peak in relation to the flow peak. An estimate of turbidity was also needed when a peak flow did not occur during the RMA forecast period, although non-peak flow estimates are somewhat less important in terms of the adult delta smelt forecast model assumptions.

For each water year at each location, flow, turbidity and EC on each river were separated into two periods – the rainy period between the first and final flow/turbidity maximum, generally December to April, and the rest of the year. The rainy periods were collated, and several analyses were performed on data sets for the two sites. In order to develop the flow/turbidity magnitude relationships (Figure 4-4 and Figure 4-11), the collated data were sorted by flow magnitude for each site, and then separated into flow categories. Figure 4-5 shows a scatter plot of the collated data at Freeport. Within each flow category, turbidity data was then binned to calculate approximate percent exceedance values for that flow category. The procedure was similar for the two locations, but the details vary.

At Freeport, turbidity bin sizes were reduced in regular step sizes until 50% and 90% exceedance values could be estimated. An example of this estimation procedure is given in Table 4-6 and the final values and flow categories are given in Table 4-7 - Figure 4-4 is the plot of this table. These values represent the final values intended for use in future forecasts developed following a refinement in the initial methodology – however, the forecasts documented herein used slightly different values for the flow-turbidity relationships.

The intended use of the 50% exceedance estimate is during the period preceding or following a peak flow pulse or during periods of constant flow. The intended use of the approximate 90%

exceedance estimate is during the peak flow period. The 75% exceedance estimate was not used in the current set of forecasts. However, they would be used in the future during periods of moderate increases in Sacramento R. inflow, so are included as additional information on the variability of the turbidity estimation procedure. Figure 4-6 illustrates the potential use of the 50% and 90% exceedance values for a large turbidity pulse in early February, 2010.

Figure 4-7, Figure 4-8 and Figure 4-9 compare the approximate 50%, 75% and 90% turbidity exceedance estimates, respectively, with turbidity data collected at Freeport starting in December 2009. The 50% estimate (Figure 4-7) corresponds with the turbidity data within about 5 NTU (overestimate) during periods of rapidly decreasing or relatively low or constant flow at Freeport. The magnitude of the 90% estimate (Figure 4-9) corresponds with the turbidity data maxima in mid-January and early February, 2010, although the timing of the estimated February peak is early by several days. The magnitude of the 75% estimate (Figure 4-8) corresponds with the smaller turbidity data maxima in late January and early March, 2010 that occur during a second pulse flow and a smaller pulse flow at Freeport, respectively.

Several other parameters were investigated using the collated rainy period data set at Freeport, including the timing of the turbidity peak in relation to the flow pulse peak. During the rainy period, the dates of the turbidity peak and the flow peak were compared on a daily basis, and the difference between them was calculated. Figure 4-10 shows the results of the analysis. Although the distribution is skewed toward turbidity peaking before the flow, the maximum of the distribution occurs at zero days, i.e., the turbidity peak occurs on the same day as the flow peak. In developing the turbidity forecast values, the turbidity peak was estimated to occur on the same day as the flow peak.

Attempts to develop a rationale for the width of the turbidity maximum during high flow periods, i.e. peak width to use with the 90% exceedance value, did not produce a satisfactory result. As the flow forecast from CNRFC was limited to five days, the decision on the values for the width of the turbidity peak was made on a case-by-case basis, typically 1 – 3 days.

A similar strategy to the one developed for Freeport was employed for the forecast of Vernalis turbidity. The rainy periods were collated, the collated data were sorted by flow magnitude into bins, and turbidity data was then binned to calculate approximate 50% and 95% percent exceedance values for each flow category. Table 4-8 lists the results of that analysis, and Figure 4-11 is a plot of the table. Figure 4-12 and Figure 4-13 compare the approximate 50% and 95% turbidity exceedance estimates, respectively, with turbidity data collected at Vernalis starting in December 2009. The intended use of the 50% exceedance estimate is during the period preceding or following a peak flow pulse or during periods of low or relatively constant flow. The intended use of the 95% exceedance estimate is during a peak flow period.

The estimate for the 50% exceedance corresponds reasonably well with the turbidity during periods of rapidly decreasing or relatively constant flow at Vernalis, but the 95% exceedance estimate is much too low for the peak flow and turbidity occurring in January 2010. In fact, it is much lower than the maximum SSC value used as an estimate for turbidity during the historical record 1990 – 2004.

At times when there were no peak flow periods on the Sacramento or San Joaquin Rivers (i.e., when there were no projected incoming flow pulses), the turbidity value for the RMA forecast period could be set either at a constant or at the 50% turbidity exceedance values for the predicted flows. For the forecasts documented herein, turbidity for the RMA forecast period was simply modeled as a constant extending from the last available data value for each inflow boundary outside of the 5-day CNRFC forecast period.

4.2.4. Turbidity boundary conditions

Turbidity data was available at the Sacramento and San Joaquin River boundaries and at Martinez for the historical portion of the modeled period. For the RMA forecast period, turbidity was developed using the flow-based methodology at Sacramento and San Joaquin River inflow boundaries (see Section 4.2.3). Turbidity was set as a constant at Martinez using the final real-time value available.

Turbidity boundary conditions were synthesized for both historical and forecast periods at boundaries where data was lacking. For the Yolo, Cosumnes, Mokelumne and Calaveras River boundaries, turbidity was modeled as a linear function of inflow as documented in Table 4-5 for the RMA forecast period starting Apr. 12th. The inflow magnitude was scaled to data values consistent with low and high flow periods - MWQI grab sample data was used to provide these linear relationships. Figure 4-14 illustrates the application of this method at the Yolo boundary.

4.2.5. Synthesized EC boundary conditions

Forecast salinity boundary conditions supplied by DWR O&M were accepted as given as several boundaries, but were synthesized as functions of flow for several other boundaries (see Table 4-4). EC boundary conditions were accepted at the Mokelumne, Cosumnes, Sacramento and San Joaquin Rivers and at Martinez. Forecast EC was calculated as an inverse function of flow at the Yolo and Calaveras River boundaries. The inflow magnitude was linearly scaled to data values consistent with low and high flow periods - MWQI grab sample data was used to provide these limits. Table 4-5 documents the functions used to scale the flow data to obtain both historical and forecast EC values at these locations. Figure 4-14 illustrates the application of this method at the Yolo boundary.

4.2.6. Development of initial conditions

Initial conditions were developed using RMA utility functions. For the initial forecast developed in January, EC and turbidity locations were selected from raw data on Dec. 04, 2009 at numerous locations in the Delta (at all available turbidity locations) and a diffusion solution (using RMA 11) was applied to obtain an initial condition (IC) for the full grid. The initial condition for the RMA2 flow model was developed using a 3-day-spin-up period starting Dec. 01, 2009. IC for other model periods were set similarly.

4.2.7. Gate and barrier operations

Historical gate and barrier operations were developed from raw text data at:

http://www.iep.water.ca.gov/dsm2pwt/Bay-Delta_barriers_activ.txt

4.2.8. Flow boundary conditions using CNRFC and USGS

The California-Nevada River Forecasting Center (CNRFC) develops forecasts of hourly flows and/or stage on many California Rivers using a five-day forecast window. To improve flow forecast accuracy, RMA used CNRFC-calculated forecast flows for the initial five-days of the RMA forecast period, and then reverted to DWR O&M forecast flows for the remainder of the RMA forecast period. Table 4-4 lists those inflow locations that were supplemented with CNRFC data (Sacramento R. at I St., San Joaquin R. at Vernalis and Yolo Bypass at Lisbon). A utility program implemented within HEC-DSSVue was developed to automate download of the available CNRFC data, which included both five days of observed hourly data and five days of forecast hourly data, directly into DSS format. The Sacramento R. at I St. CNRFC data only had stage forecasts – in this case, ratings curves supplied by DWR or CNRFC staff were used to calculate the RMA forecast flow. Details and discussion of the Sacramento R. at I St. rating table are found in Appendix I (Section 11.3.1).

DWR forecasts were often received by RMA 1 – 2 days after the beginning of their forecast period. For RMA forecasts, the most current CNRFC forecast data were used. This strategy extended the period of combined historical plus CNRFC forecast period. This difference in forecast period of DWR flow boundary conditions and RMA flow boundary conditions is documented in Table 4-2.

The Yolo boundary flow for pre-forecast values was developed from three sources of data – CDEC (Yolo Bypass at Lisbon, station LIS), CNRFC (Yolo Bypass – Lisbon) and USGS (site #11453000⁵, Yolo Bypass at Woodland). Discrepancies between the data sets complicated the process of deciding which values should be applied at this boundary in some periods. The final decision was based on “professional judgment”, which entailed combining the data sets to

⁵http://waterdata.usgs.gov/ca/nwis/uv?site_no=11453000

provide a consistent, logical time series for inflow. At the USGS site (Yolo at Woodland), the provisional real-time discharge data (presented in the real-time record at the USGS website) includes the flow at this station plus flow entering the Yolo bypass from the Sacramento Weir. The published discharge record for this station, including peak flows, does not include flow from the Sacramento Weir. Discharge below 1000 cfs is not published for this site.

4.3. Forecast methodology

4.3.1. General guidelines

The following are steps used in the RMA forecast methodology – the timing of the implementation of each step could vary depending on the date of receipt of the flow and salinity forecast from DWR O&M section. Note that Table 4-3 and Table 4-4 have the source of data used for each of the boundary conditions for flow, EC, turbidity and stage.

- 1) Evaluate information sent by DWR O&M – *forecast.dss* contains historical and forecast BC for inflow and EC, while the file *hydro.dss* has the historical and forecast stage and the file *quality.dss* has the combined historical and forecast Martinez EC BC.
- 2) Download and perform QA on data from CNRFC (current and forecast flow and stage), CDEC (turbidity, flow and EC) and USGS (flow at Yolo-Lisbon) using HECDSSVue and the supplied text files (for automated download). Data from CDEC and USGS was stored in DSS records as time series.
- 3) Develop inflow BC:
 - a. Evaluate the three data sources at the Yolo/Lisbon Toe Drain location to create a consistent historical time series.
 - b. Add the CNRFC forecast data to the end of the Sacramento and San Joaquin flow data (either use DWR's BC or use CDEC flow data that has been QA'd), and to the Yolo boundary flow data if indicated. Note that the Sacramento I-street CNRFC data forecast stage must be converted to flow using supplied rating tables (Table 11-2 and Table 11-3). Two options are possible for extending the RMA forecast time period to three weeks from the end of the CNRFC time period at Freeport and Vernalis: 1.) Set the inflow to a constant using the final value in the CNRFC time series, or, 2.) Set the inflow to the values supplied by DWR for the remainder of the RMA forecast period (Note: there may be problems with data inconsistency with this latter method).
 - c. Inflow BC from DWR O&M are used as-is for the Mokelumne and Cosumnes Rivers. For the Calaveras River, check the Mormon Sl. flow data to check that

enough flow is incorporated at the Calaveras inflow location and check Table 4-5 to implement a time shift if high flows have been identified on Mormon Sl.

- 4) Develop export BC by using the DWR-supplied values for DSM2 for all export locations, except Clifton Court. For Clifton Court, the file *RMAOUTPUT.dss* has a time series used for export levels (identified by DSS A-part “CLFCT-NODE72”).
- 5) Increase the Martinez stage BC by 0.3 feet to better approximate the standard stage level used in RMA2 models. Accept the EC boundary at Martinez supplied in the file *quality.dss*. (Note: ordinarily, the RMA MTZ BC for EC is composed of the average of top and bottom EC – for these model runs, we are accepting that EC will not be accurately simulated in the interest of reduced model preparation time. This compromise is justified because under the high flow conditions of interest to adult delta smelt movement, Martinez salinity has little influence on salinity in the Delta).
- 6) Use Table 4-4 and Table 4-5 to develop EC BC at all inflow boundaries.
- 7) Update the gate and barrier operations using information in http://www.iep.water.ca.gov/dsm2pwt/Bay-Delta_barriers_activ.txt
- 8) Developing forecast turbidity is different depending on the location, but in all cases relies on relationships developed between flow and turbidity.
 - a. At Cosumnes, Mokelumne and Calaveras R. inflow locations, apply the formulas in Table 4-5 to the combined historical and forecast flow time series.
 - b. At Freeport and Vernalis, develop turbidity BC using the values supplied in Table 4-7 and Table 4-8, respectively, to the inflow for the combined historical and forecast time periods. Note that this requires using “professional judgment”. Suggested guidelines are discussed below in Section 4.3.2.

The boundary conditions needed for running RMA2 and RMA11 forecasts are ready for application at this point. The synthesized BC should be evaluated visually to assure the calculated values are sensible.

4.3.2. Suggested guidelines for developing turbidity forecasts at Vernalis and Freeport

The major difficulty in developing the RMA forecast turbidity values at Freeport and is deciding the correct exceedance level to use if a peak flow is expected during the RMA forecast period. Generally, at both locations, the 50% exceedance forecast level was used during relatively constant flow periods (see Figure 4-7 and Figure 4-12) as these values match historical turbidity fairly well. For high flow periods (e.g., after rain storms), the 90% exceedance value was used

for Freeport for a one to three day period (see Figure 4-9) as it matches the high turbidity values fairly well. It is recommended that for intermediate flow pulses (see Figure 4-8), the 75% exceedance levels be used, although these were not implemented in the forecasts to date. At Vernalis, the 95% exceedance values should be used for higher flows (see Figure 4-13).

It is recommended that for each period in which higher than average flows are expected (e.g., after a rain storm), that two separate forecasts be run – one scenario with a 50 or 75% exceedance value at Freeport and a 50% exceedance value at Vernalis, and one scenario with a 90% exceedance value at Freeport and a 95% exceedance value at Vernalis.

Table 4-1 DWR modeled periods for near-real-time hindcasts.

MODEL PERIOD	DWR FORECAST PERIOD
12/04/09 – 02/04/10	01/12/10 – 02/04/10
12/04/09 – 03/02/10	02/09/10 – 03/02/10
12/04/09 – 03/11/10	02/16/10 – 03/11/10
12/04/09 – 03/16/10	02/23/10 – 03/16/10
01/01/10 – 04/26/10	04/06/10 – 04/26/10
01/01/10 – 05/05/10	04/12/10 – 05/05/10

Table 4-2 RMA modeled periods, flow forecast period and flow sources used for near-real-time hindcasts

MODEL PERIOD	RMA FORECAST PERIOD	FLOW SOURCE
12/04/09 – 02/04/10	01/12/10 – 02/04/10	DWR
12/04/09 – 03/02/10	02/11/10 – 03/02/10	CNRFC
12/04/09 – 03/11/10	02/17/10 – 03/11/10	CNRFC
12/04/09 – 03/16/10	02/25/10 – 03/16/10	CNRFC
01/01/10 – 04/26/10	04/08/10 – 04/26/10	CNRFC
01/01/10 – 05/05/10	04/14/10 – 05/05/10	CNRFC

Table 4-3 Boundary conditions from DWR O&M.

PARAMETER	DWR O&M	Used by RMA (Y/N)	DWR Filename
INFLOW	RSAC155	N	
	RSAN112	N	
	RCAL009	N	
	RMKL070	Y	Hydro.dss, Forecast.dss
	RCSM075	Y	Hydro.dss, Forecast.dss
	BYOLO040	N	
STAGE	RSAC054	Y	Hydro.dss
EXPORTS	CHSWP003	N	
	CHDMC004	Y	Hydro.dss, Forecast.dss
	CHCCC006	Y	Hydro.dss, Forecast.dss
	ROLD034	Y	Hydro.dss, Forecast.dss
	SLBAR002	Y	Hydro.dss, Forecast.dss
EC	RSAC054	Y	Quality.dss
	RSAN112	Y/N	Quality.dss, Forecast.dss
	RSAC142	N	
DCC Operation	RSAC128	N	
DSM2 MODEL OUTPUT	CLFCT-NODE 72 FLOW	Y (SWP EXPORT)	RMAOutput.dss

Table 4-4 Data sources for historical and forecast boundary conditions implemented in RMA models.

PARAMETER	LOCATION	DATA SOURCES
INFLOW	RSAC155	CDEC, CNRFC
	RSAN112	CDEC, CNRFC
	RCAL009	CDEC
	BYOLO040	CDEC, USGS, CNRFC
EC	RSAN112	CDEC/DWR
	RSAC142	CDEC/DWR
	RCAL009	SYNTHESIS/MWQI
	BYOLO040	SYNTHESIS/MWQI
	RMKL070	Constant (125 uS/cm)
	RCSM075	Constant (125 uS/cm)
	RSAC054	CDEC/DWR
TURBIDITY	RSAN112	CDEC
	RSAC142	CDEC
	RSAC054	CDEC
	RCAL009	SYNTHESIS/MWQI
	BYOLO040	SYNTHESIS/MWQI
	RMKL070	SYNTHESIS/MWQI
	RCSM075	SYNTHESIS/MWQI

Table 4-5 Boundary condition formulas for DWR forecast starting April 12, 2010.

Location	Parameter	Time Shift	Formula
Freeport	Turbidity	Back 9 hours	N/A
	EC	Back 11 hours	+ 20
Yolo	Turbidity	N/A	$(\text{flow magnitude})/50 + 10$
	EC	N/A	$(-1)*(\text{flow magnitude})/70 + 350$
Calaveras	Turbidity	Back 2 days	$(\text{flow magnitude})/15 + 20$
	EC		$(-0.3)*(\text{flow magnitude}) + 600$
Cosumnes	Turbidity	N/A	$(\text{flow magnitude})/10$
Mokelumne	Turbidity	N/A	$(\text{flow magnitude})/10 + 10$
Vernalis/SJR-McCune	Turbidity	N/A	N/A
	EC	N/A	N/A

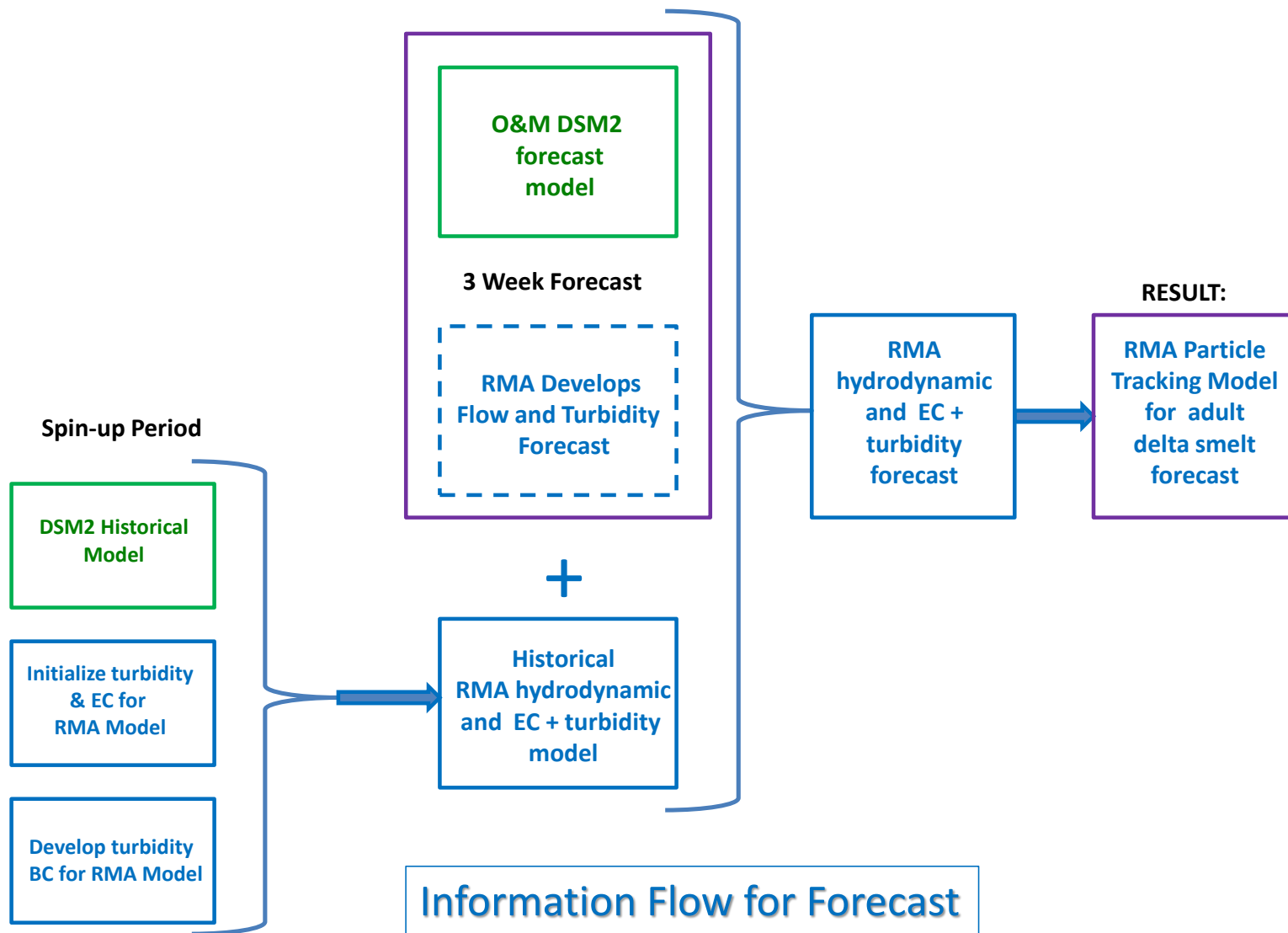


Figure 4-3 Information flow for developing turbidity and adult delta smelt forecasts.

Table 4-6 Bin size (in NTU) for the Freeport flow category 30,000 cfs to < 35,000 cfs. 70 NTU, the average of the first two bins, was used for the 50th percentile value.

Bins	Frequency	Percentage	Cumulative Percentage
40	24	0.2	0.19
60	25	0.2	0.39
80	27	0.2	0.61
100	5	0.0	0.65
120	9	0.1	0.72
140	4	0.0	0.75
160	4	0.0	0.78
180	2	0.0	0.80
200	3	0.0	0.82
220	3	0.0	0.85
240	2	0.0	0.86
260	1	0.0	0.87
280	2	0.0	0.89
300	4	0.0	0.92
320	3	0.0	0.94
340	2	0.0	0.96
360	1	0.0	0.97
380	0	0.0	0.97
400	2	0.0	0.98
420	0	0.0	0.98
440	1	0.0	0.99
More	1	0.0	1.00

Table 4-7 Final values and categories for Freeport turbidity (SSC-based) boundary condition estimates.

	Min	~ 50 %	~ 75 %	~ 90 %	Max
FLOW < 10K	4	10	15	20	31
FLOW 10K to < 15K	1	20	30	40	155
FLOW 15K to < 20K	4	30	40	70	161
FLOW 20K to < 25K	7	40	60	100	243
FLOW 25K to < 30K	11	60	100	160	464
FLOW 30K to < 35K	12	70	140	280	456
FLOW 35K to < 40K	20	90	160	280	493
FLOW 40K to < 50K	22	100	170	350	725
FLOW 50K to < 60K	13	100	175	300	805
FLOW 60K to < 70k	10	90	140	240	682
FLOW > 70 K	19	100	140	180	418

Table 4-8 Final values and categories for Vernalis turbidity (SSC-based) boundary condition estimates.

	Min	~ 50 %	~ 95%	Max
FLOW 0 to < 2K cfs	8	15	45	193
FLOW 2 to < 3.5K cfs	6	20	65	177
FLOW 3.5 to < 5 K cfs	15	25	75	97
FLOW 5K to < 10K cfs	8	25	60	90
FLOW 10K to < 20Kcfs	10	20	45	58
FLOW > 20K cfs	6	15	45	65

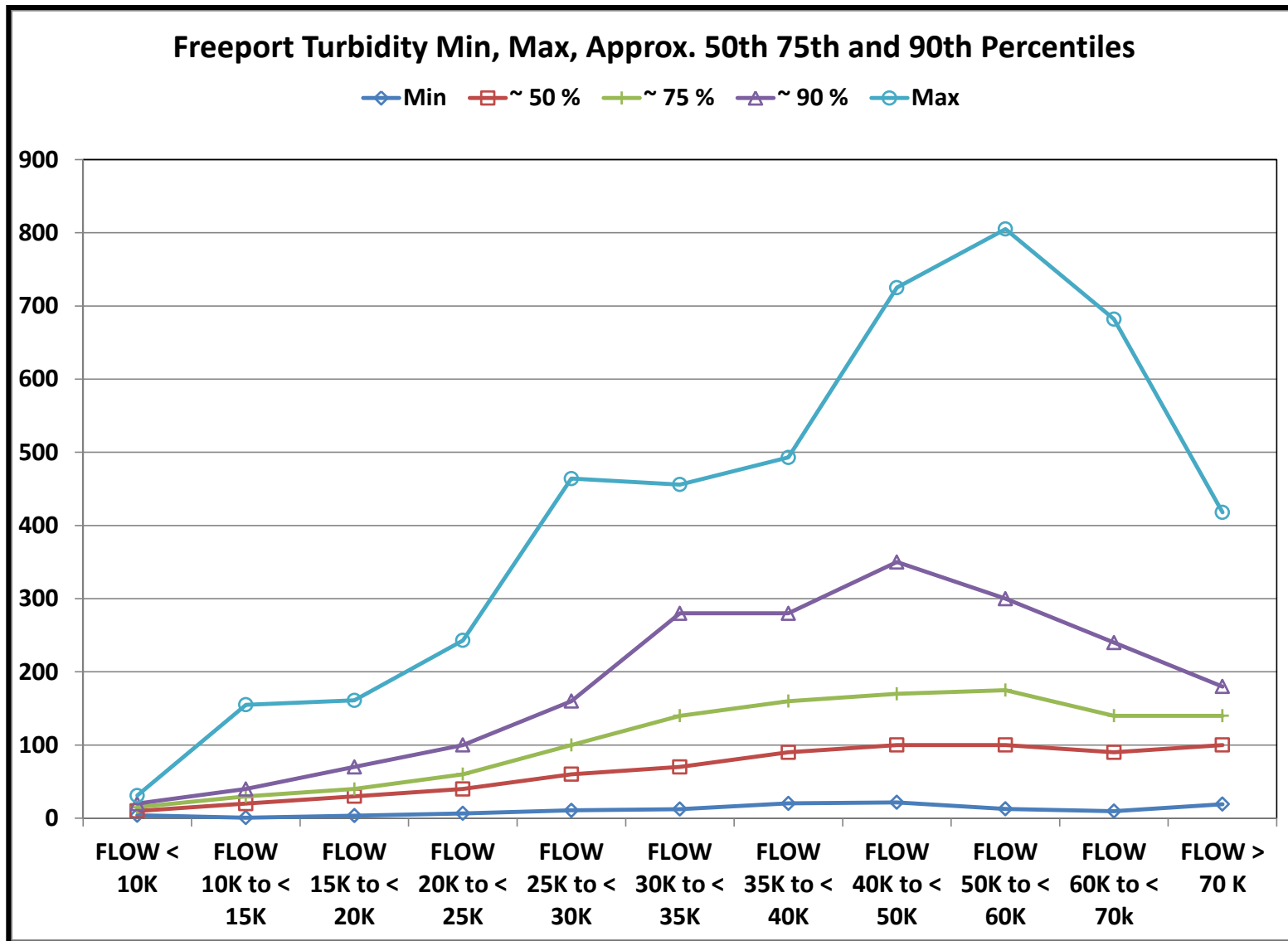


Figure 4-4 Plot of categorization of Freeport turbidity (SSC-based) during rainy seasons 1991 – 2007.

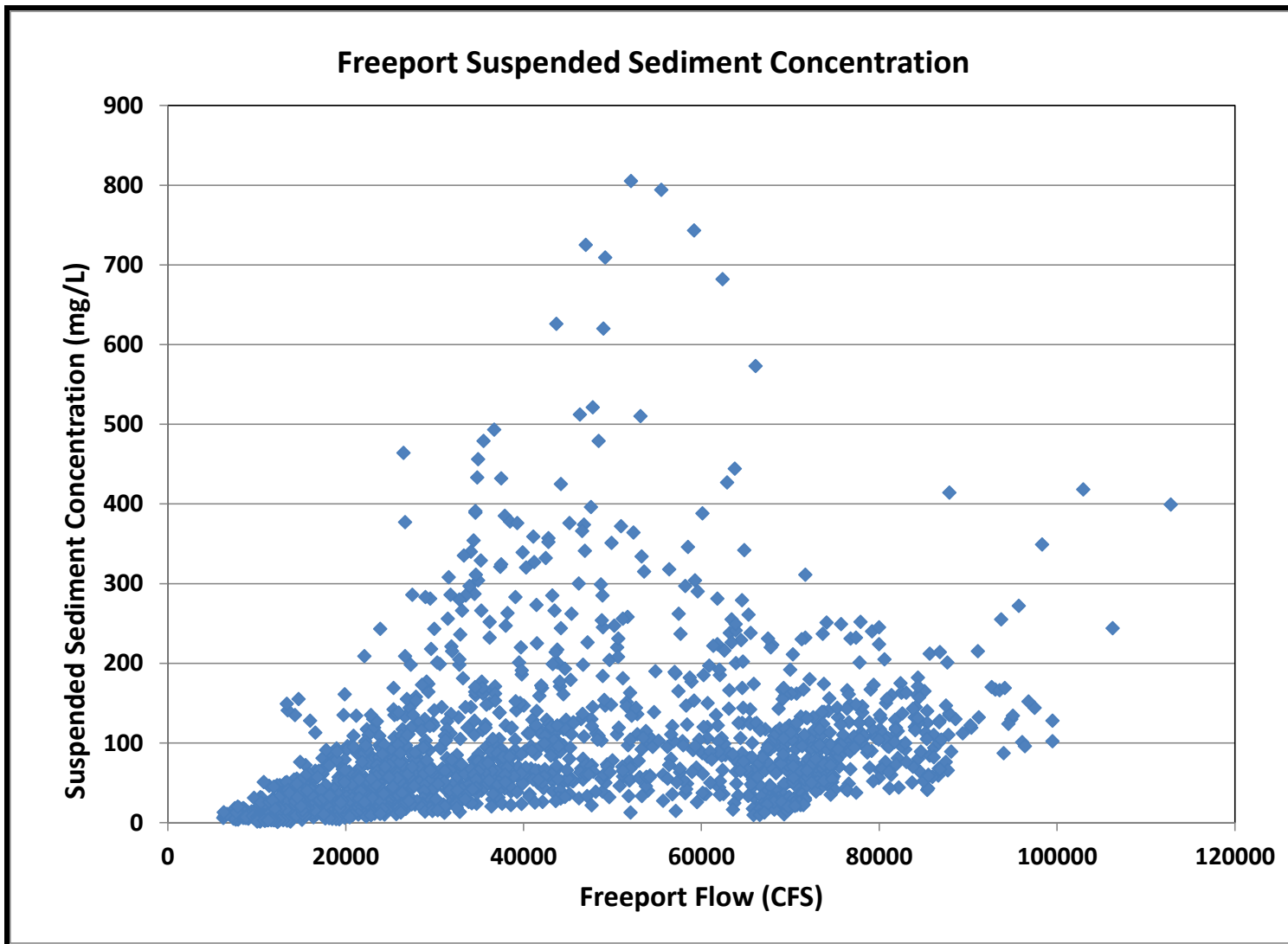


Figure 4-5 Scatter plot of the high flow/rainy period data set of flow vs. suspended sediment at Freeport used to create the turbidity/flow relationships.

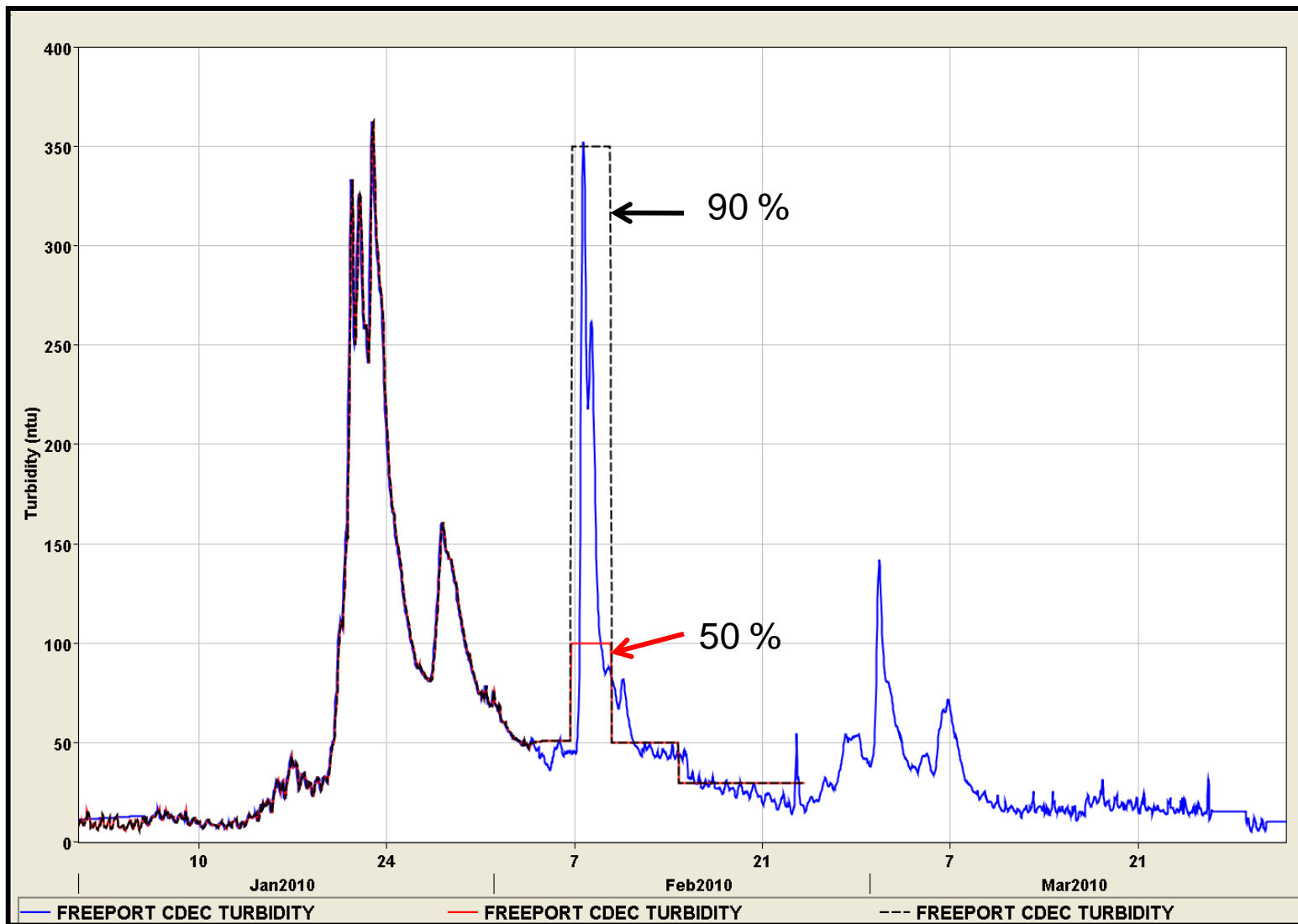


Figure 4-6 Possible values for a turbidity forecast during the highest flow event on the Sacramento in Feb. 2010.

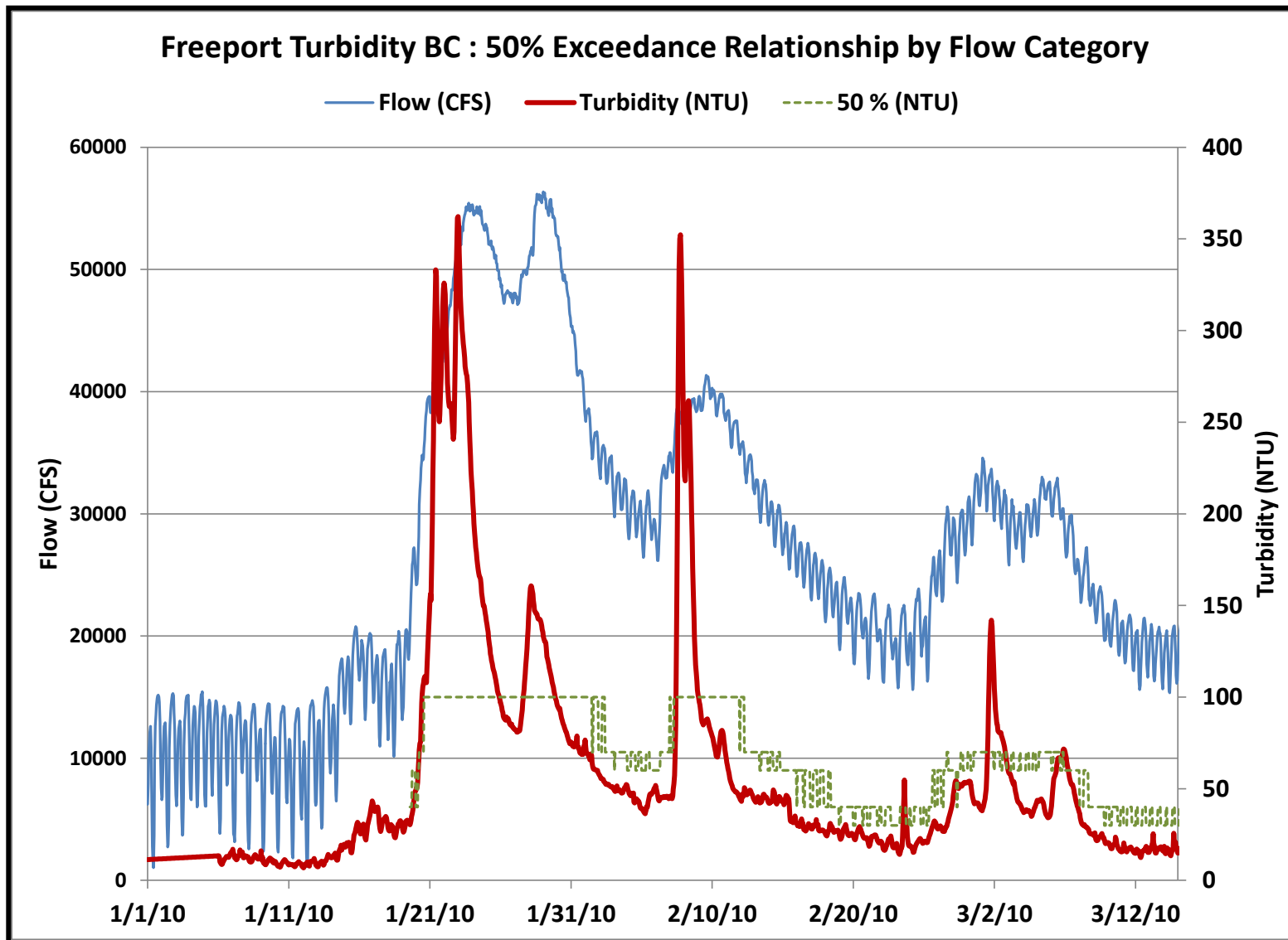


Figure 4-7 Comparison of data with 50% turbidity-flow relationship at Freeport.

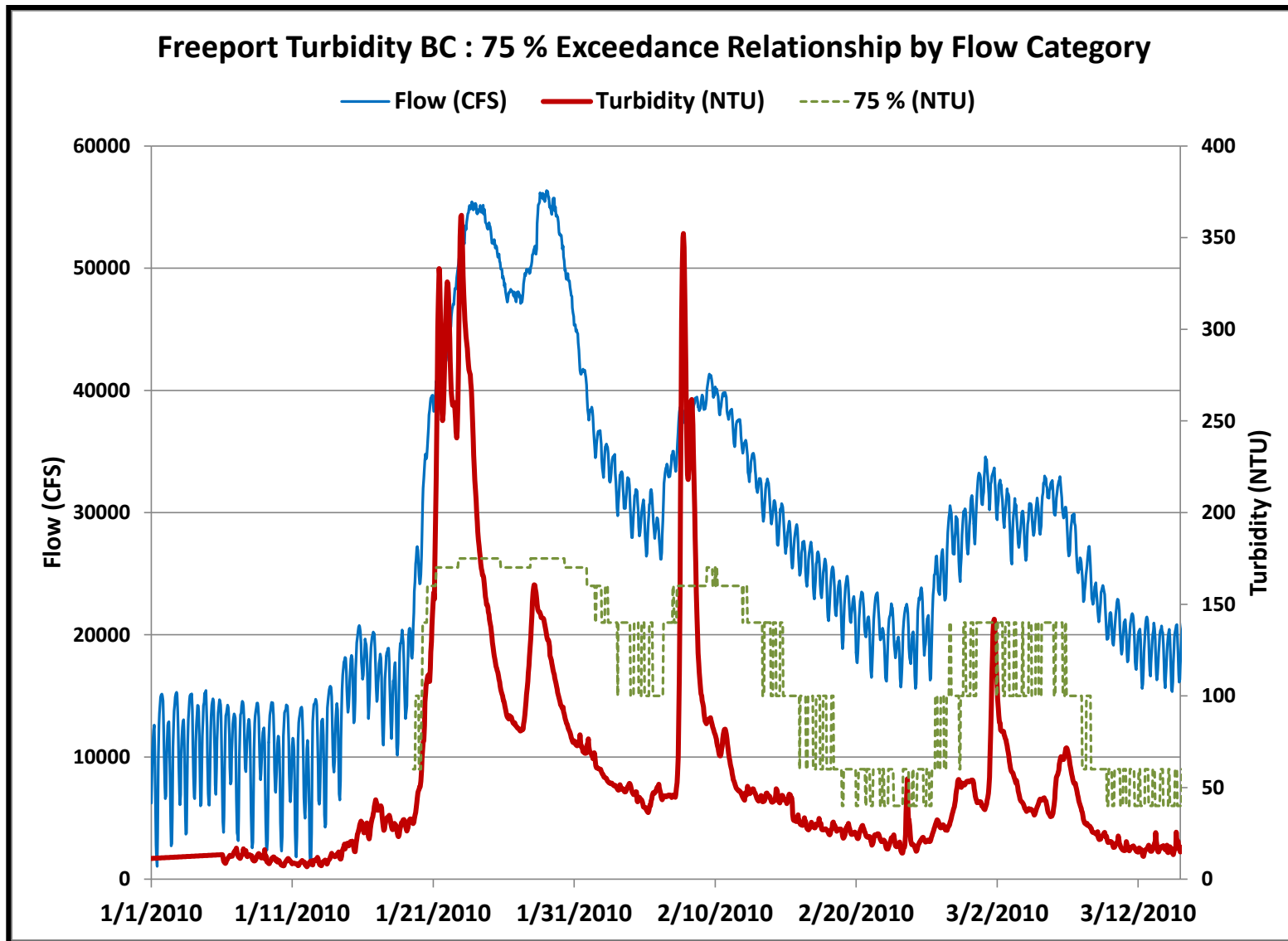


Figure 4-8 Comparison of data with 75% turbidity-flow relationship at Freeport.

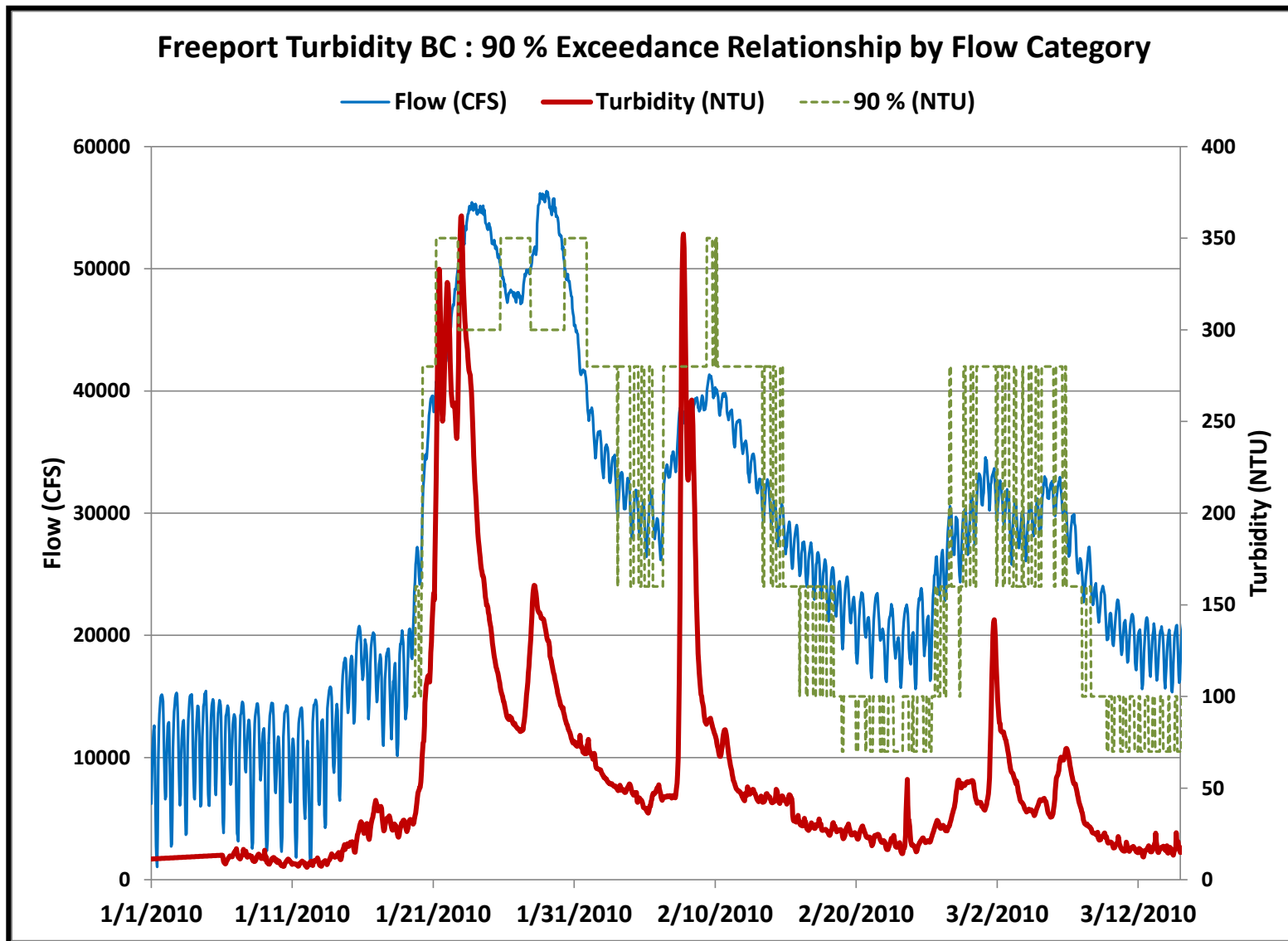


Figure 4-9 Comparison of data with 90% turbidity-flow relationship at Freeport.

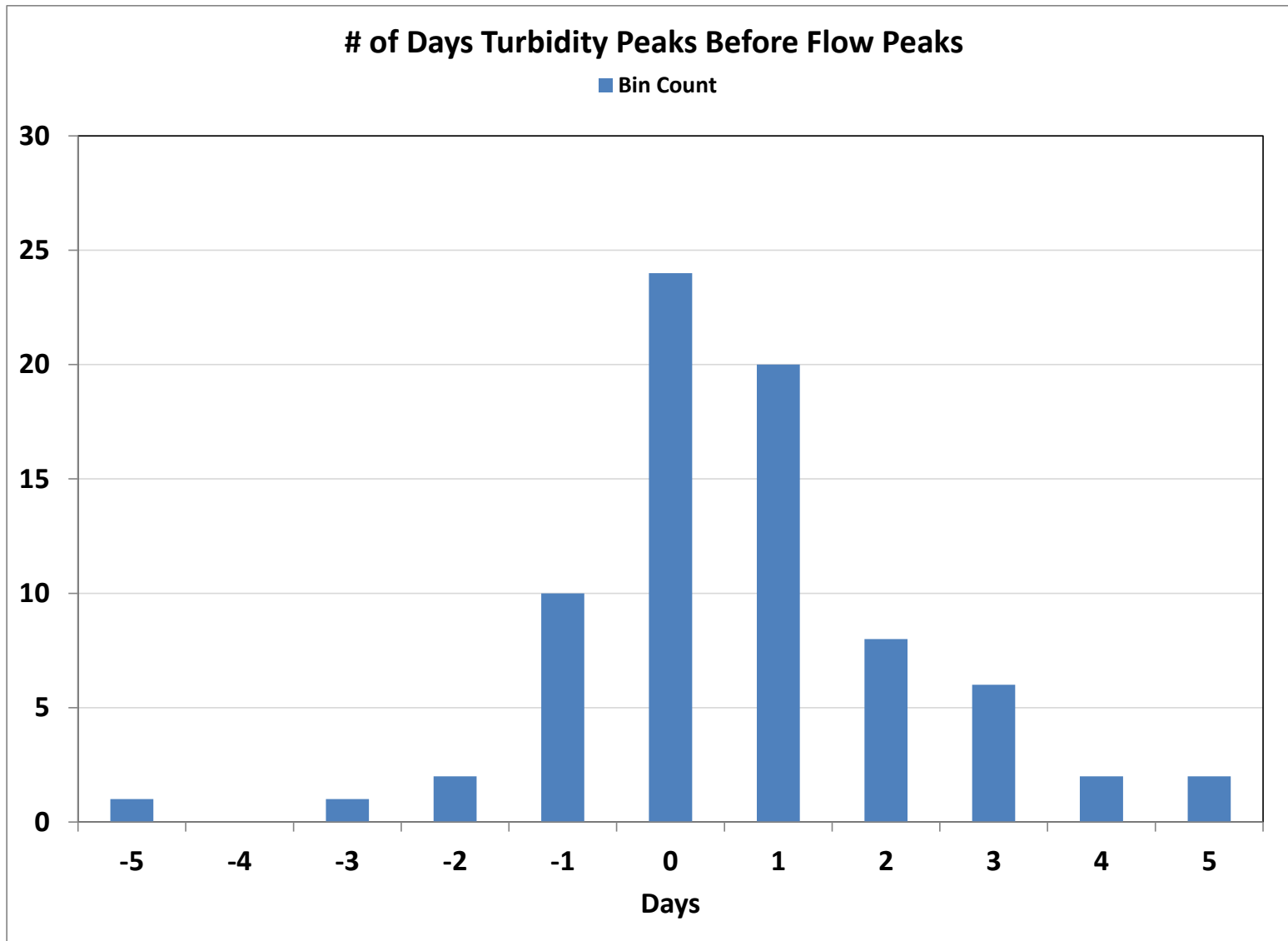


Figure 4-10 Turbidity peak timing vs. flow peak timing at Freeport is skewed – turbidity tends to peak before flow.

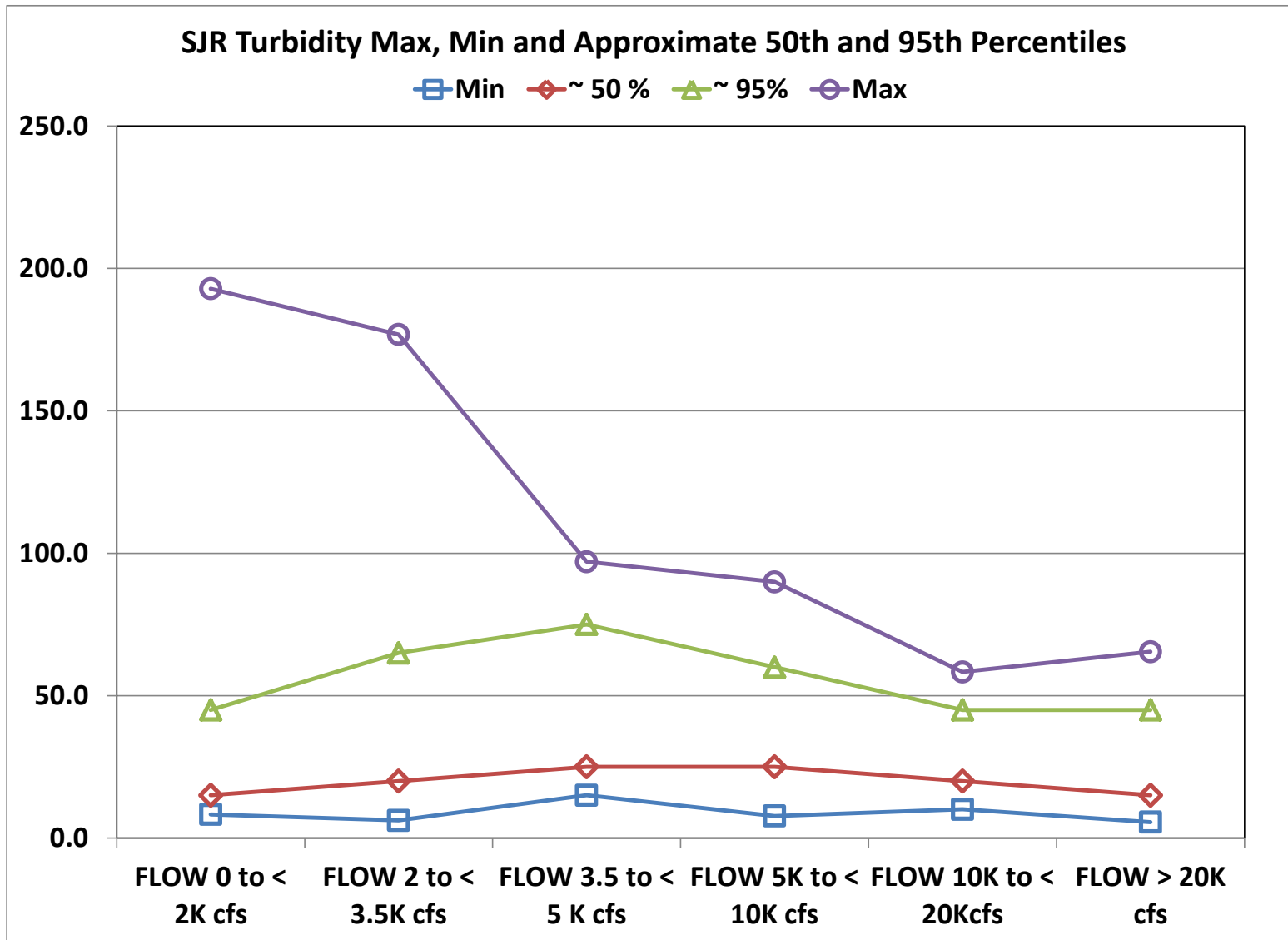


Figure 4-11 Categorization of Vernalis turbidity (SSC-based) during rainy seasons 1991 – 2007.

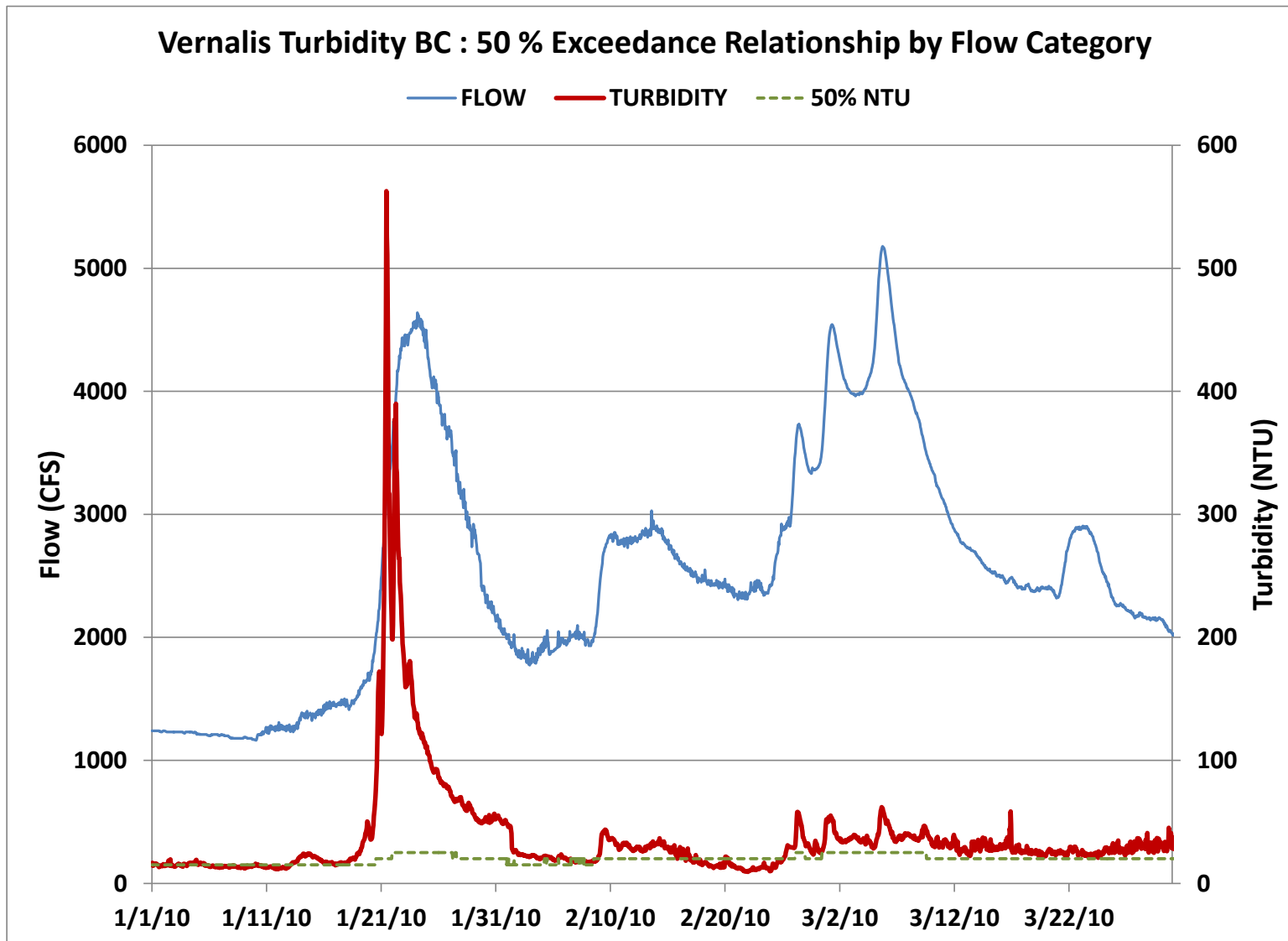


Figure 4-12 Comparison of data with 50% turbidity-flow relationship at Vernalis.

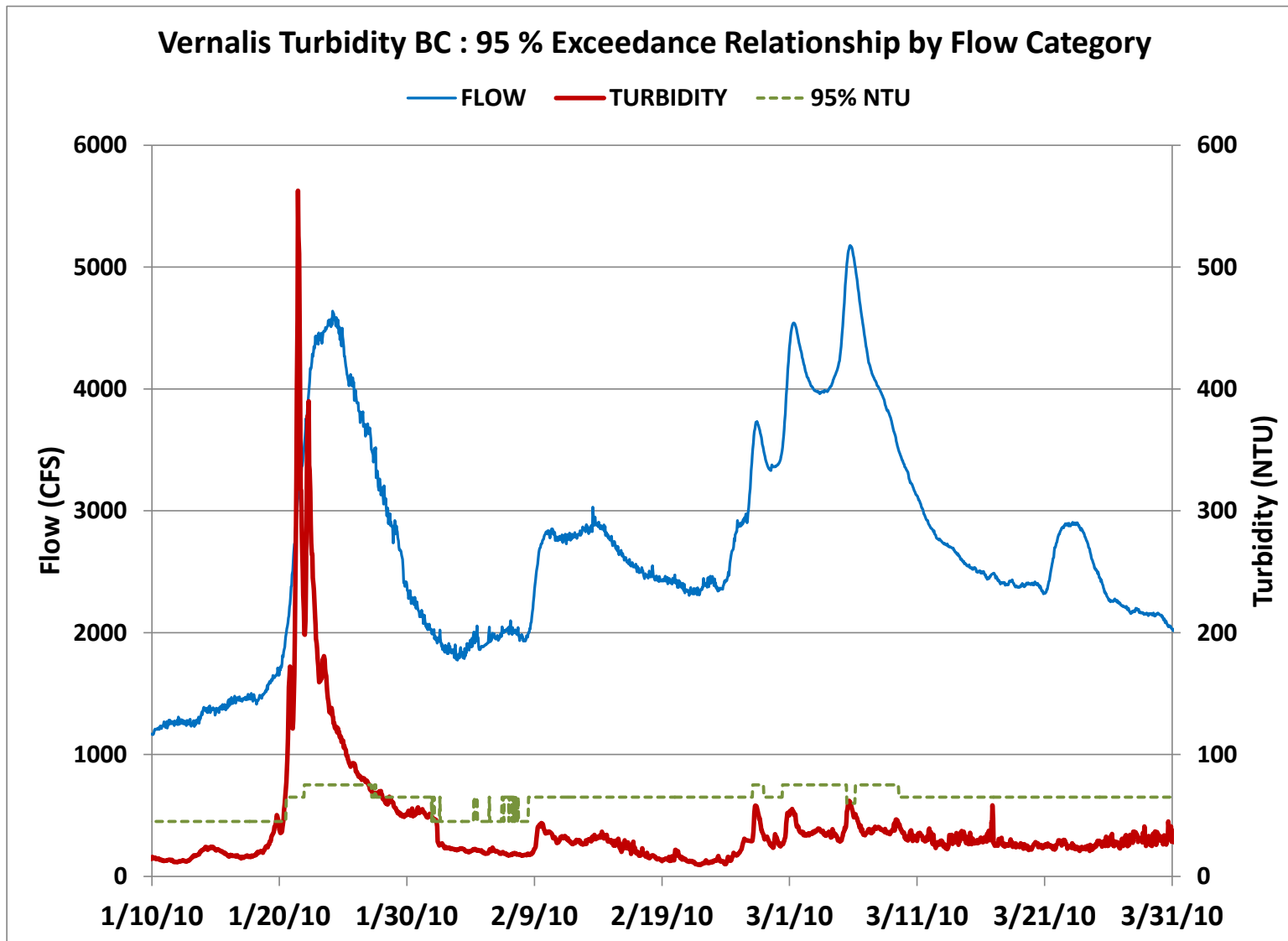


Figure 4-13 Comparison of data with 95% turbidity-flow relationship at Vernalis.

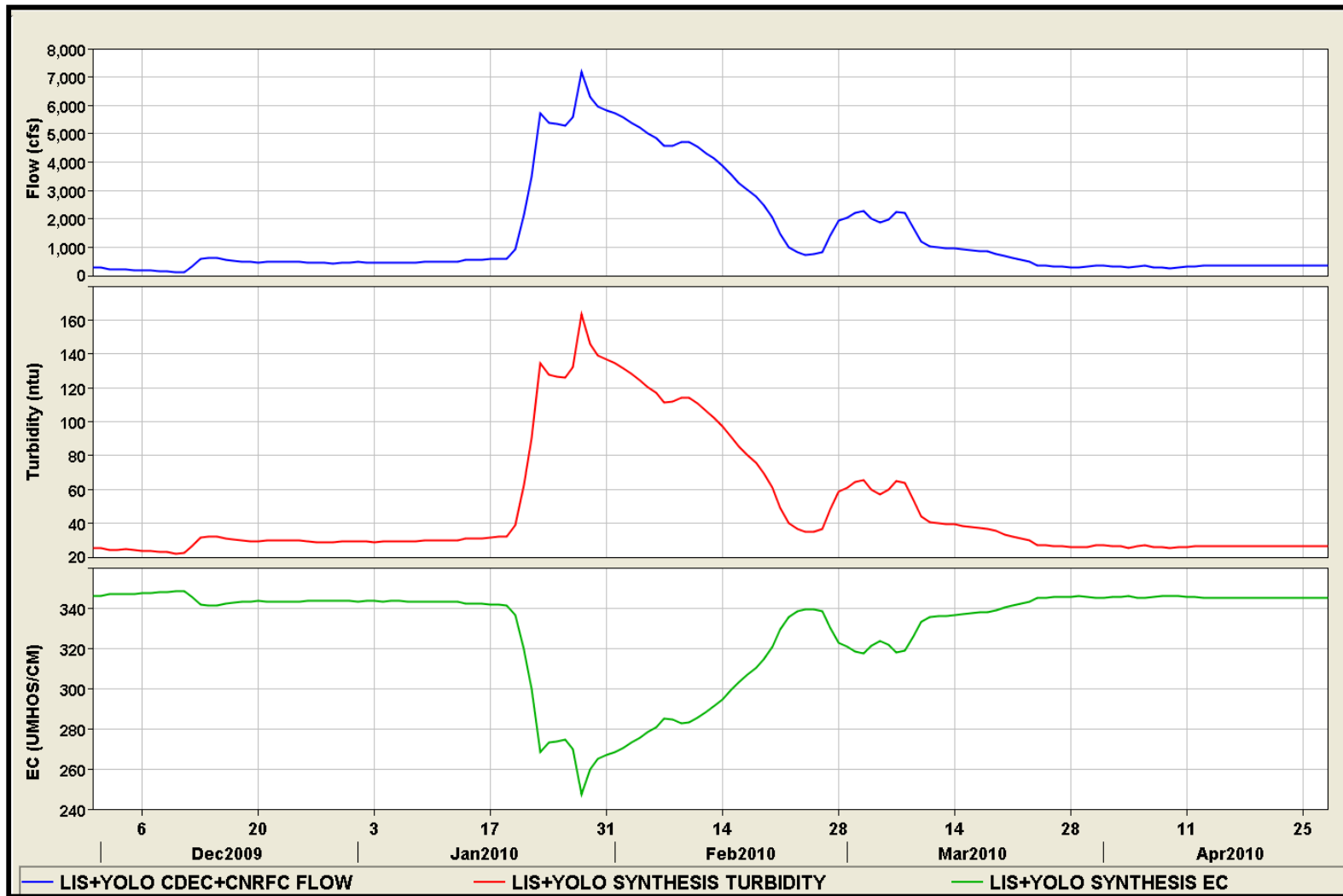


Figure 4-14 Time series of measured flow, and time series of turbidity (center) and salinity (bottom) synthesized as a function of flow at the RMA model Yolo-boundary.

5. Final Turbidity Model

The results of the DWR April 12th forecast, started by RMA on April 14th (the final forecast), are presented in this section to demonstrate the quality of the new decay coefficient parameterization of the turbidity model. The magnitude, timing and shape of modeled turbidity in the Delta are generally within reasonable agreement with the range of turbidity data. However, there are locations where the model discrepancies are more pronounced. In these cases, meteorological (wind, rain) or physical (dilution, settling) influences provide possible explanations for the mismatch between model and data.

5.1. *Single-parameter model examples*

The initial turbidity model used a single region for the decay parameter set at 0.05 day^{-1} . The initial attempts to improve the turbidity model started with single parameter region – the model was tested with a high decay coefficient and with a low decay coefficient, and the results were compared with data. At ROLD034 (Figure 5-1), Old River at Hwy 4, the low decay coefficient model result is too high in comparison with data, and the high decay coefficient model is generally too low except at the peak turbidity. At Little Potato Sl. at Terminous (Figure 5-2), even the high decay coefficient model does not reduce modeled turbidity enough to match data. Finally, at Jersey Point (Figure 5-3), the high decay coefficient model produces a fair match with data (apart from the effects of wind, lower plot), although the decay of turbidity arriving from the Sacramento boundary needed to be reduced somewhat. These results (and others) indicated the model would best be represented by a regional model with more than one decay coefficient. The final three regions and decay coefficient values are shown in Figure 3-3.

5.2. *Results*

This section reviews the quality of the new turbidity model showing locations where data and model match well and where there are mismatches, presents information that can potentially explain the differences.

5.2.1. *Effects of wind and rain; missing runoff flow*

Comparison of data and model results indicated that either sediment re-suspension and/or external sources of turbidity in ungauged inflow were causing discrepancies between the model output and turbidity data at several locations in the Delta. Figure 5-4 and Figure 5-6 illustrate this point at Jersey Point and at Dutch Slough, respectively. Other locations in the Delta showed evidence of influence due to meteorological conditions, for example at Old River near Bacon (Figure 5-7 and Figure 5-8). Although many of these locations are in the south and central Delta, there was also evidence of meteorological influences at Cache-Ryer (not shown).

Rain events may also be accompanied by local inflow from runoff, although measurements to verify this possibility are lacking. In the area along the San Joaquin River downstream of Mossdale, the potential for significant dilution is evidenced in both salinity and turbidity data.

Salinity data shows evidence of dilution downstream of Mossdale (Figure 5-9, upper plot) after rain events (Figure 5-10) that are corroborated by data-model mismatches (Figure 5-9, lower plots). A similar story is indicated by turbidity data (Figure 5-11, upper plot) downstream of Mossdale, and by data-model mismatches in these locations (Figure 5-11, lower plots). Figure 5-12 illustrates this point in the turbidity model at Garwood on the San Joaquin River, where modeled turbidity during and after the rain event is significantly higher than the measured turbidity.

5.2.2. Effects of velocity and potential for sediment settling

Although dilution and runoff are two possible causes for data-model mismatches, it is also possible that settling of larger size fractions may explain the discrepancies. There is possible evidence for this effect at Grant Line Canal (Figure 5-13) and at Little Potato Sl. at Terminous (Figure 5-14), where modeled turbidity is much higher than measured turbidity during the high flow event(s).

Low channel velocity may contribute to rapidity of sediment settling, as some data model discrepancies appear to be accentuated in low velocity locations. In these locations, little Potato Sl. at Terminous (Figure 5-15), Garwood and Grant Line (both shown in Figure 5-16), data shows a rapid decrease in turbidity that is not seen in the model. Rapid decrease in turbidity data is generally not seen at higher velocity locations such as Georgiana-Sac (Figure 5-15).

5.2.3. Potential for missing flow during high flow events

There are other possible explanations for modeled turbidity being higher than measured. It is clear that there is inflow to the Delta that isn't captured by gauges, as is demonstrated at three locations in the model domain (Figure 5-17). In Figure 5-18, gauged flow at Freeport is up to 5,000 cfs less during the peak flow event than measured at downstream locations (the sum of the flows at Steamboat Sl. between Sac and Sutter, Sutter Sl. at Courtland, and Sacramento R. above the DCC).

Similarly, Figure 5-19 (upper plot) shows that flow out of the Mokelumne system (measured at the locations Little Potato Sl. at Terminous and at Mokelumne at SJR locations) is frequently higher than the flow into the system (measured at Georgiana Sl. and the Mokelumne and Cosumnes Rivers) when the DCC is closed. When comparing flow or tidally-averaged flow between data and model, the biggest problems of the mismatch occur at times when peak flow due to rainfall events is missing at the Mokelumne at SJR location. DWR staff (J. Christen, personal communication) indicated that 3000 – 5000 cfs ungauged flow was likely reaching the

eastern Delta out of the foothills during and after rain events. Finally, along the San Joaquin River (Figure 5-20), flow at Garwood and at Brandt Bridge should be close as there are no intervening sources but there is instead a considerable mismatch. This may be due to measurement error, to changes in bathymetry along the flow path, or perhaps due to ungauged sources.

5.2.4. Turbidity model results at additional locations

A comparison of final turbidity model output with measurement is presented at several other locations: Rio Vista (Figure 5-21), Cache Slough at Ryer (Figure 5-22), Middle River near Holt (Figure 5-23) and at Antioch (Figure 5-24). At the two northern Delta locations, the model result shows a close comparison with data, with little effect from meteorological forcing, sediment settling or dilution. The model result at Cache-Ryer (Figure 5-22) greatly benefitted from estimating the magnitude of the turbidity in Yolo inflow, as illustrated in Figure 4-14.

5.2.5. Turbidity contour plots – data and model

The series of figures Figure 5-27 through Figure 5-30 illustrate a two-dimensional comparison of spatially interpolated time series data in the RMA grid (RMA 2010) and model output. The spatial interpolation methodology leads to an approximately linear variation on turbidity between observation stations (see Figure 4-1) – areas of the Delta within the RMA grid without data have been removed from the contour plots as indicated in Figure 5-26.

Figure 5-27 through Figure 5-30 show the progression of the turbidity plumes originating at Freeport and Vernalis in mid-January, 2010 shortly after a major storm event. The contour plots show the correspondence between the interpolated data and modeled turbidity at 21:00 on January 21, 23, 25 and 30, 2010. As indicated in the time series plots discussed earlier in this section, turbidity in the north Delta is very well represented by the model. The lack of data, in addition to potential problems with gauged flow, in the east Delta hampers the ability of the model to accurately represent this region. As the turbidity from Vernalis advances into the south Delta, by Jan. 23rd the model overestimation along Grant Line canal and in the San Joaquin River near Stockton is clear (Figure 5-28). By Jan. 25th (Figure 5-29), the spatial progression of the plume into the lower San Joaquin and the central Delta is similar, with most of the turbidity along the lower San Joaquin originating from Freeport and travelling through Georgiana and the North Fork of the Mokelumne. The final contour plot (Figure 5-30) with an expanded color scale shows that a “turbidity bridge” never *formed* in the central Delta, with Victoria Canal and the southern sections of Middle and Old Rivers remaining relatively low in turbidity.

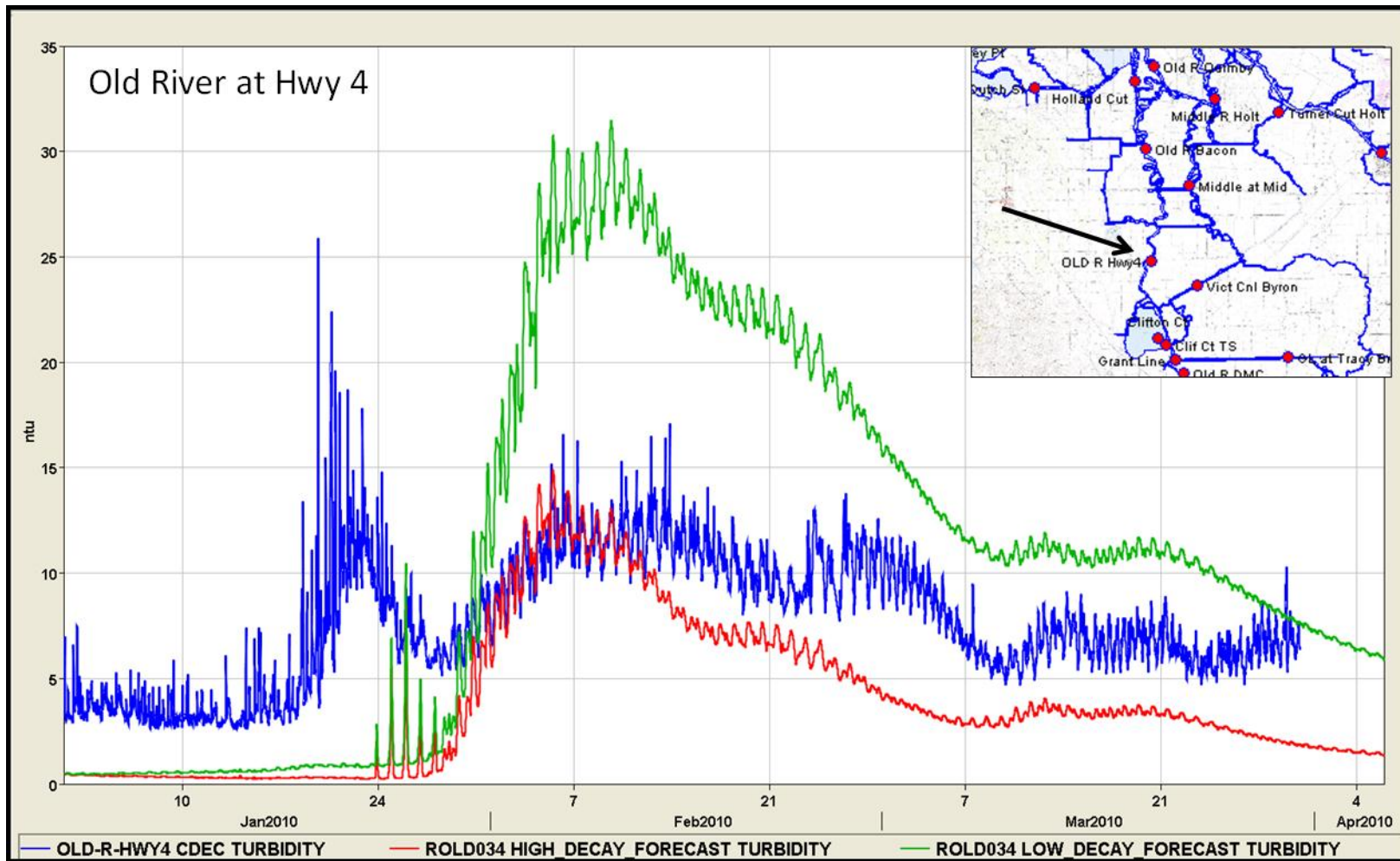


Figure 5-1 Low decay (green) and high decay (red) coefficient models in comparison with data (blue) at Old River at Hwy 4.

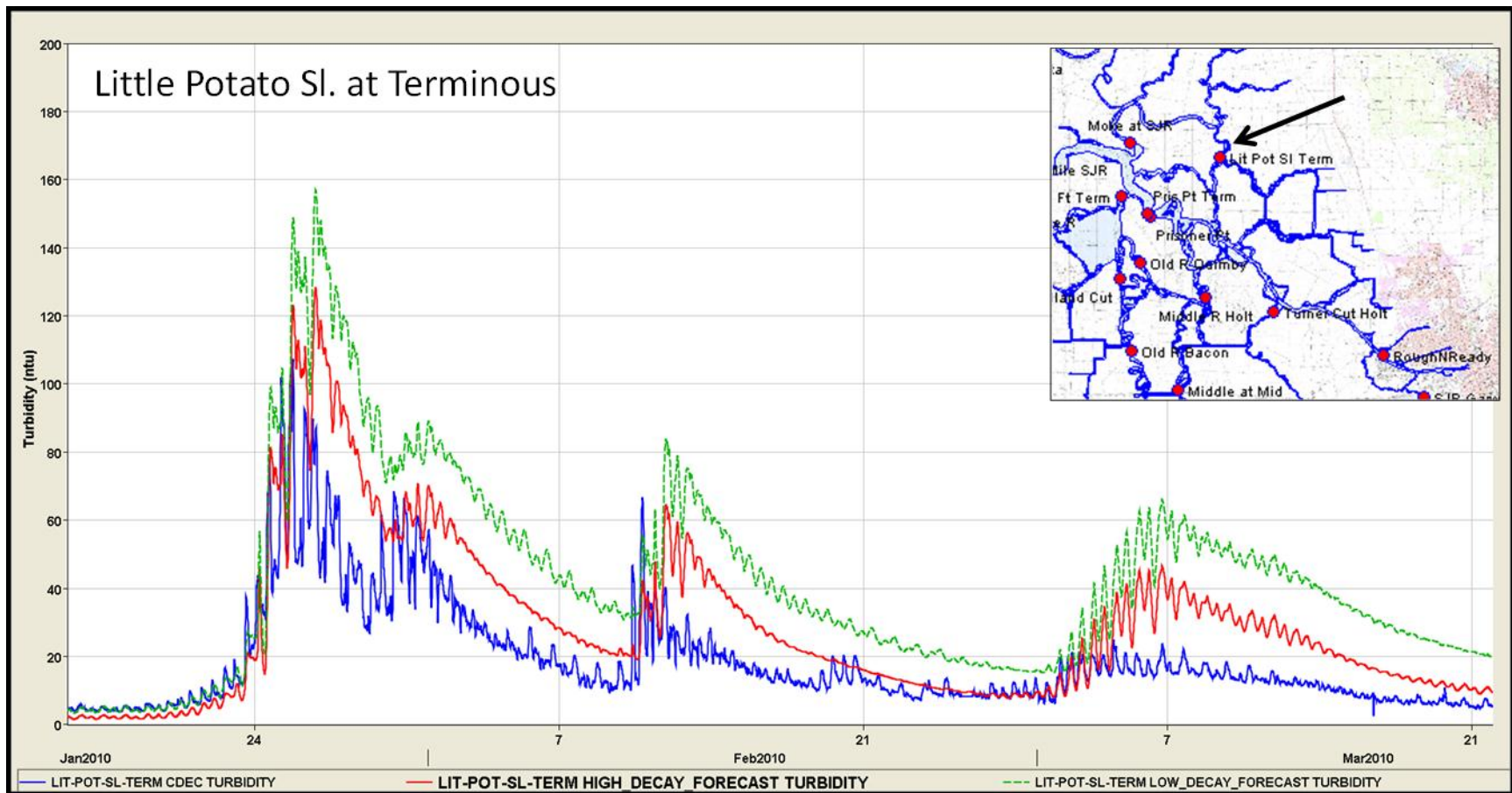


Figure 5-2 Low decay (green) and high decay (red) coefficient models in comparison with data (blue) at Little Potato Slough at Terminous.

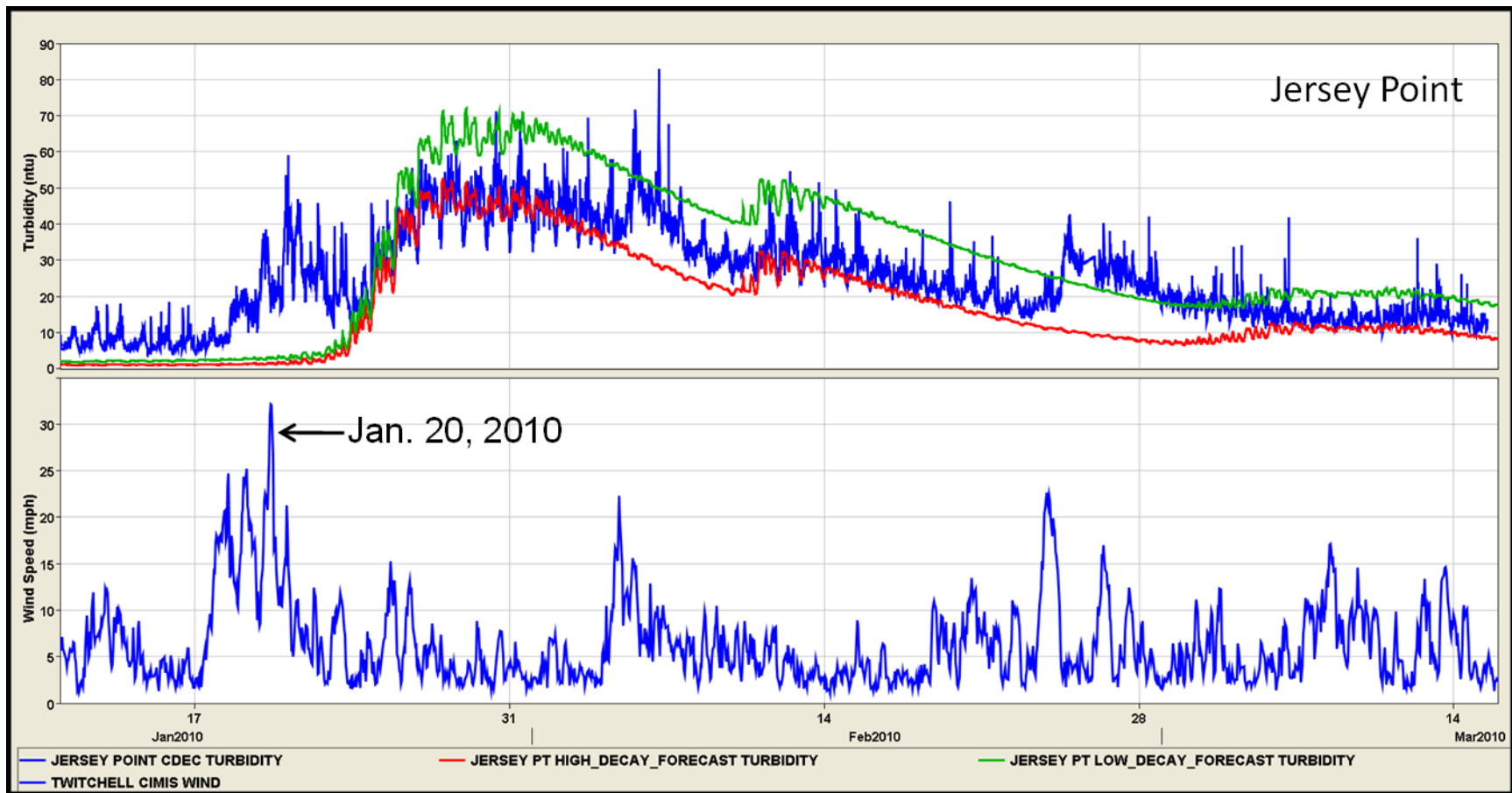


Figure 5-3 Low decay (green) and high decay (red) coefficient models in comparison with data (blue) at Jersey Point, with CIMIS (Twitchell) wind data (lower plot).

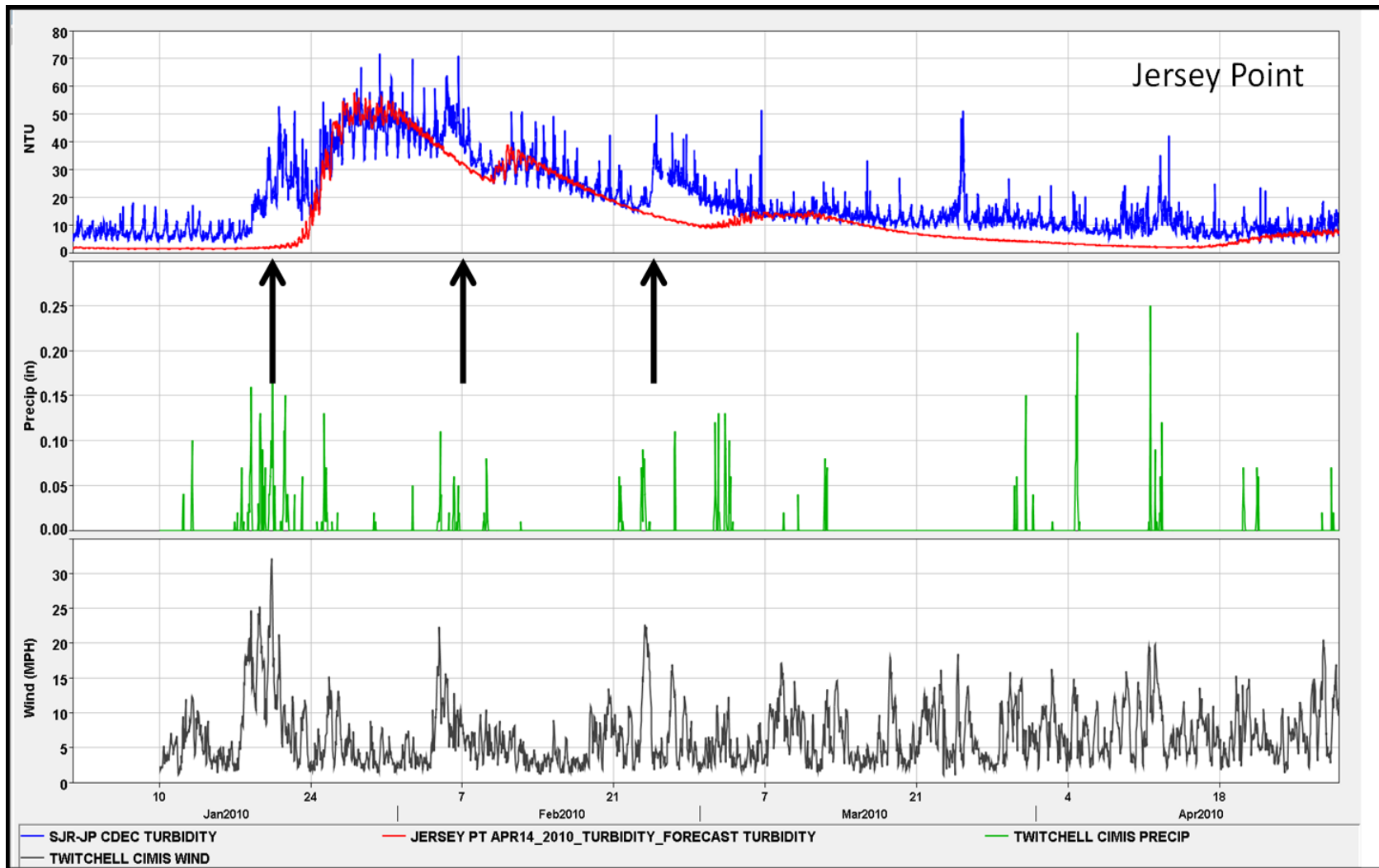


Figure 5-4 Turbidity data/model comparison with wind and precipitation data from CIMIS (Twitchell) indicates that the effects of meteorological conditions may be significant – turbidity increases near Jersey Point during wind and rain events.

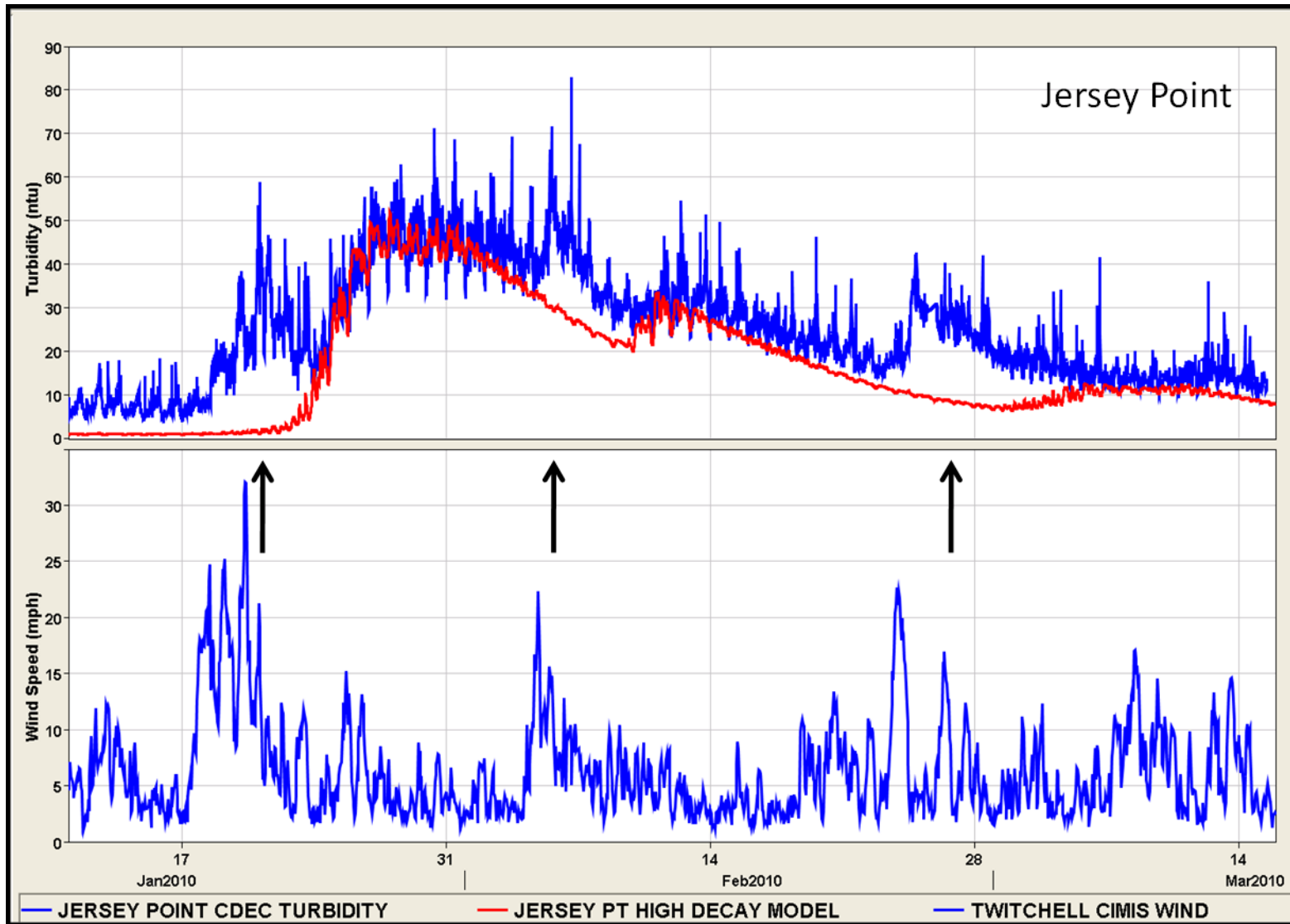


Figure 5-5 Expanded scale of data/model comparison at Jersey Point in comparison with CIMIS (Twitchell) wind data.

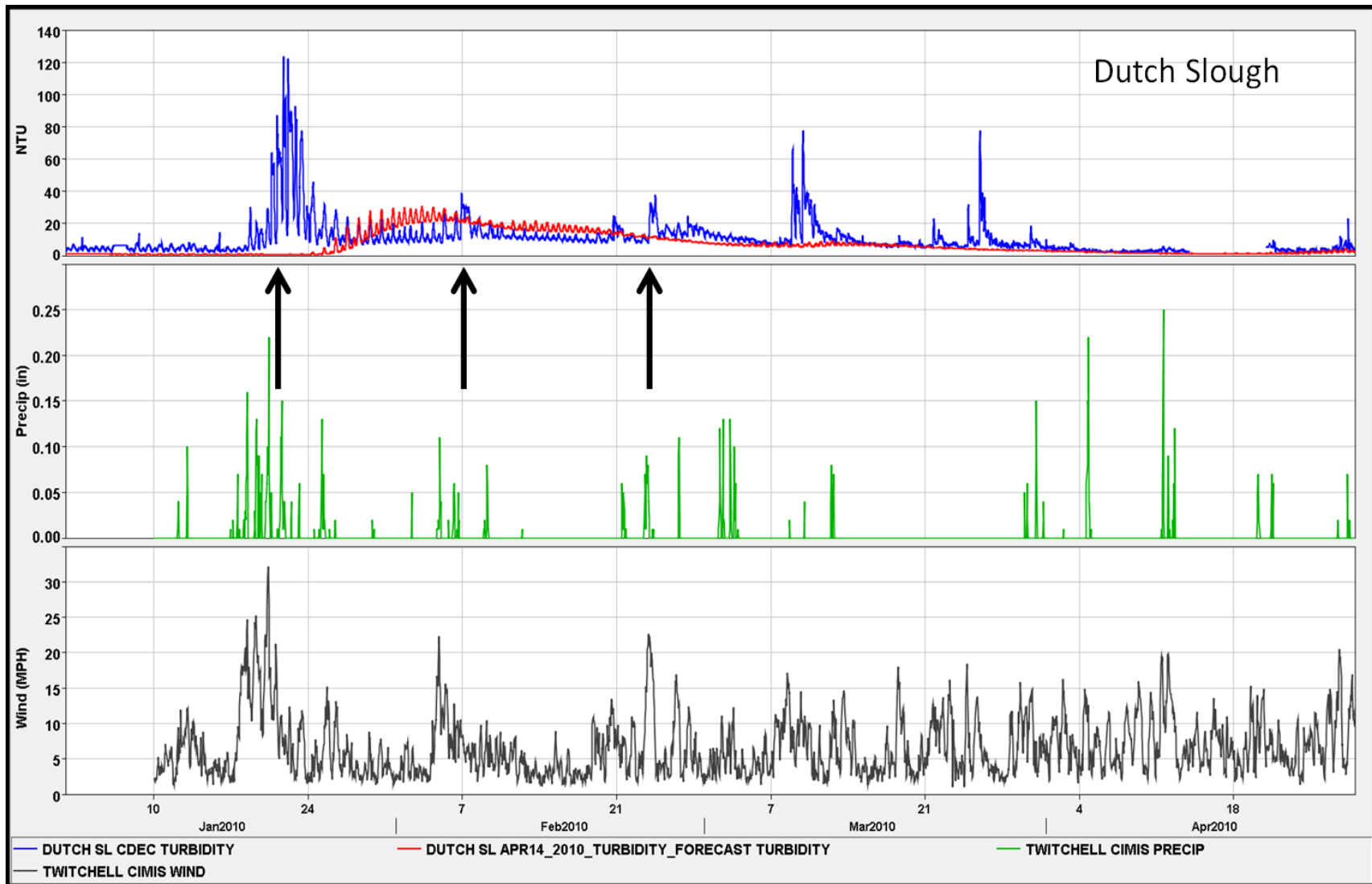


Figure 5-6 Turbidity data/model comparison with wind and precipitation data from CIMIS (Twitchell) indicates that the effects of meteorological conditions may be significant – turbidity increases near Dutch Slough during wind and rain events.

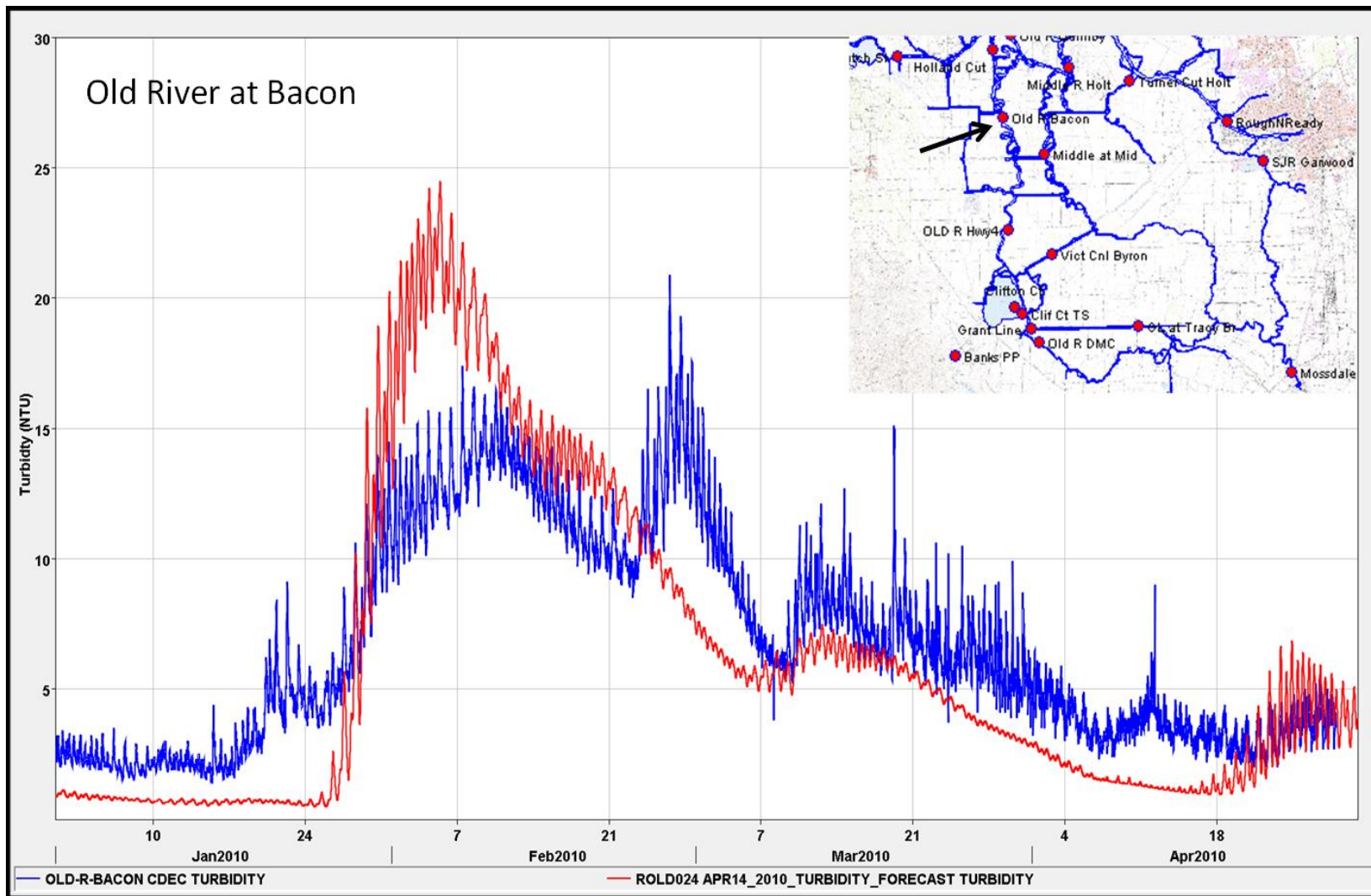


Figure 5-7 Turbidity data/model comparison at Old River at Bacon (ROLD024).

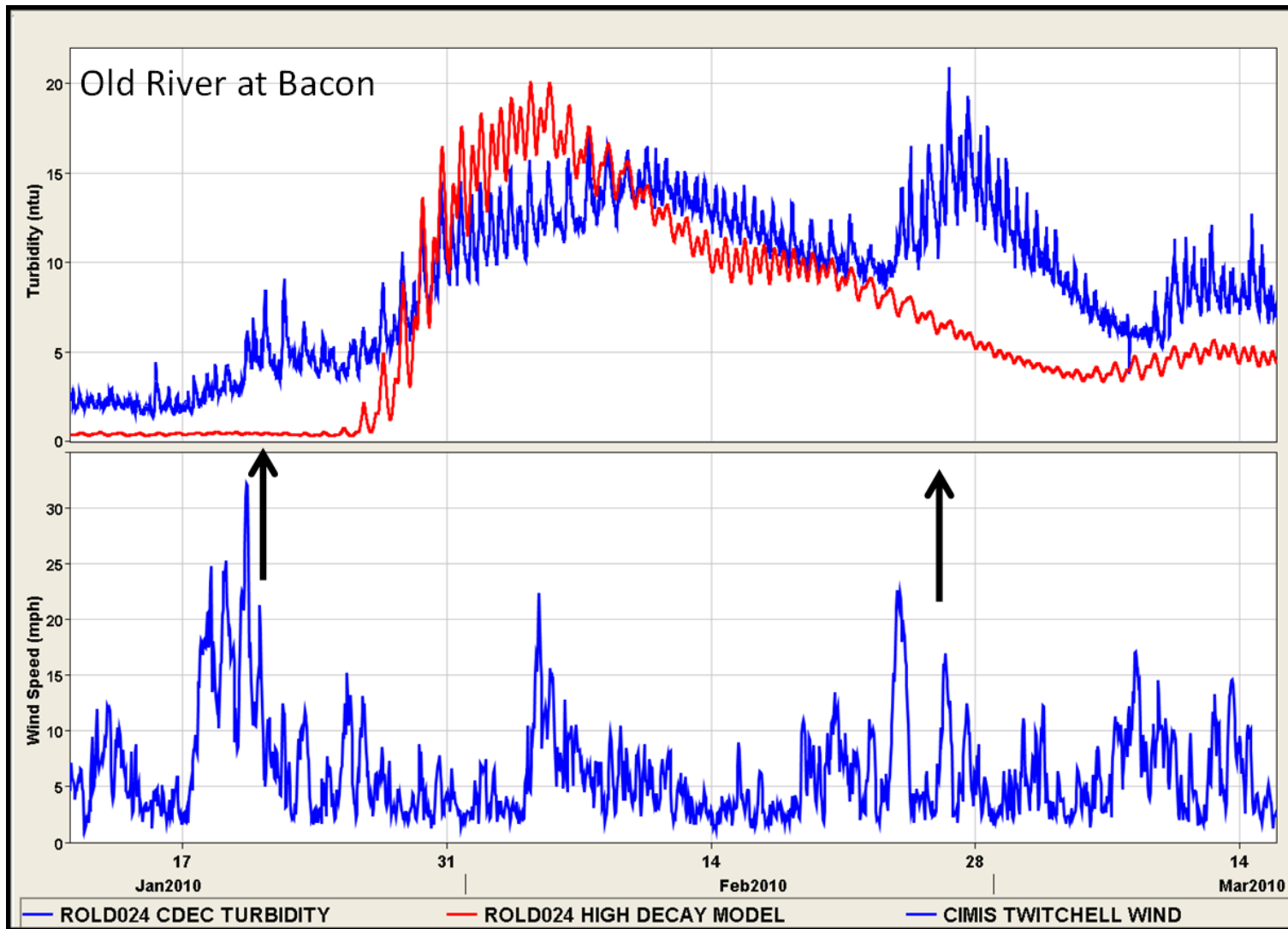
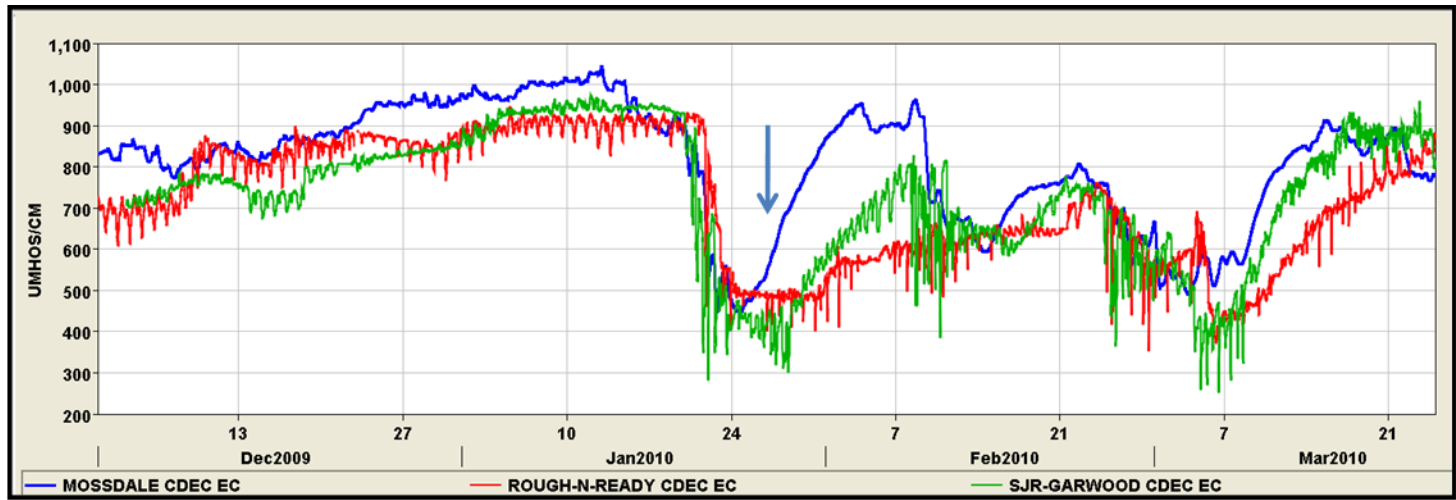


Figure 5-8 Turbidity data/model comparison at Old River at Bacon in comparison with CIMIS wind data.



Significant dilution indicated in data downstream of Mossdale during and after storms: Modeled EC (below) is too high during periods where data (above) shows dilution

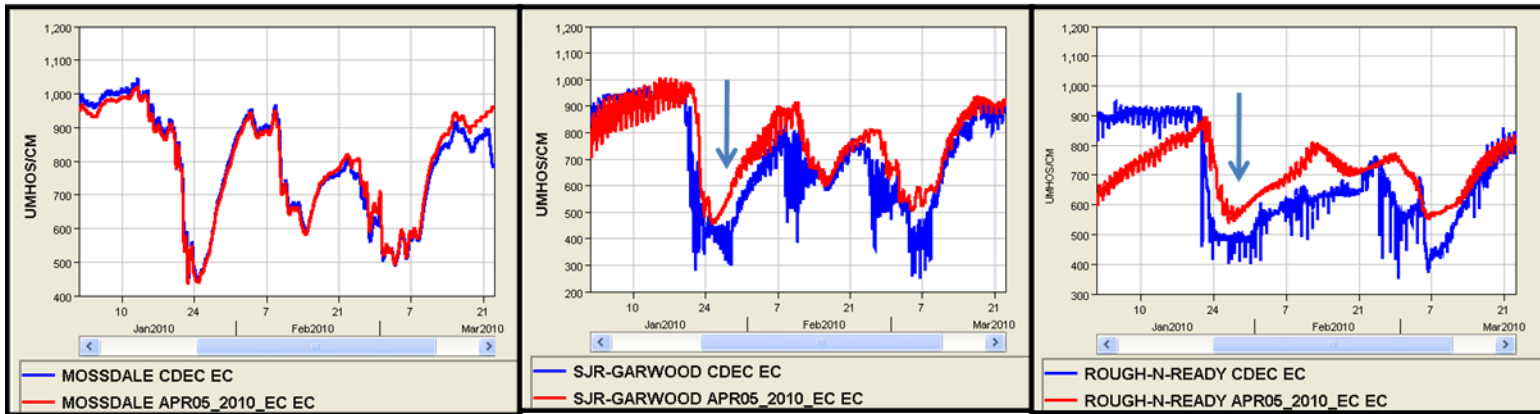


Figure 5-9 Data (Upper plots) show EC dilution downstream of Mossdale after late January rain event (arrow) - modeled EC (lower plots) is good at Mossdale but too high downstream, also indicating possible dilution from local inflow sources.

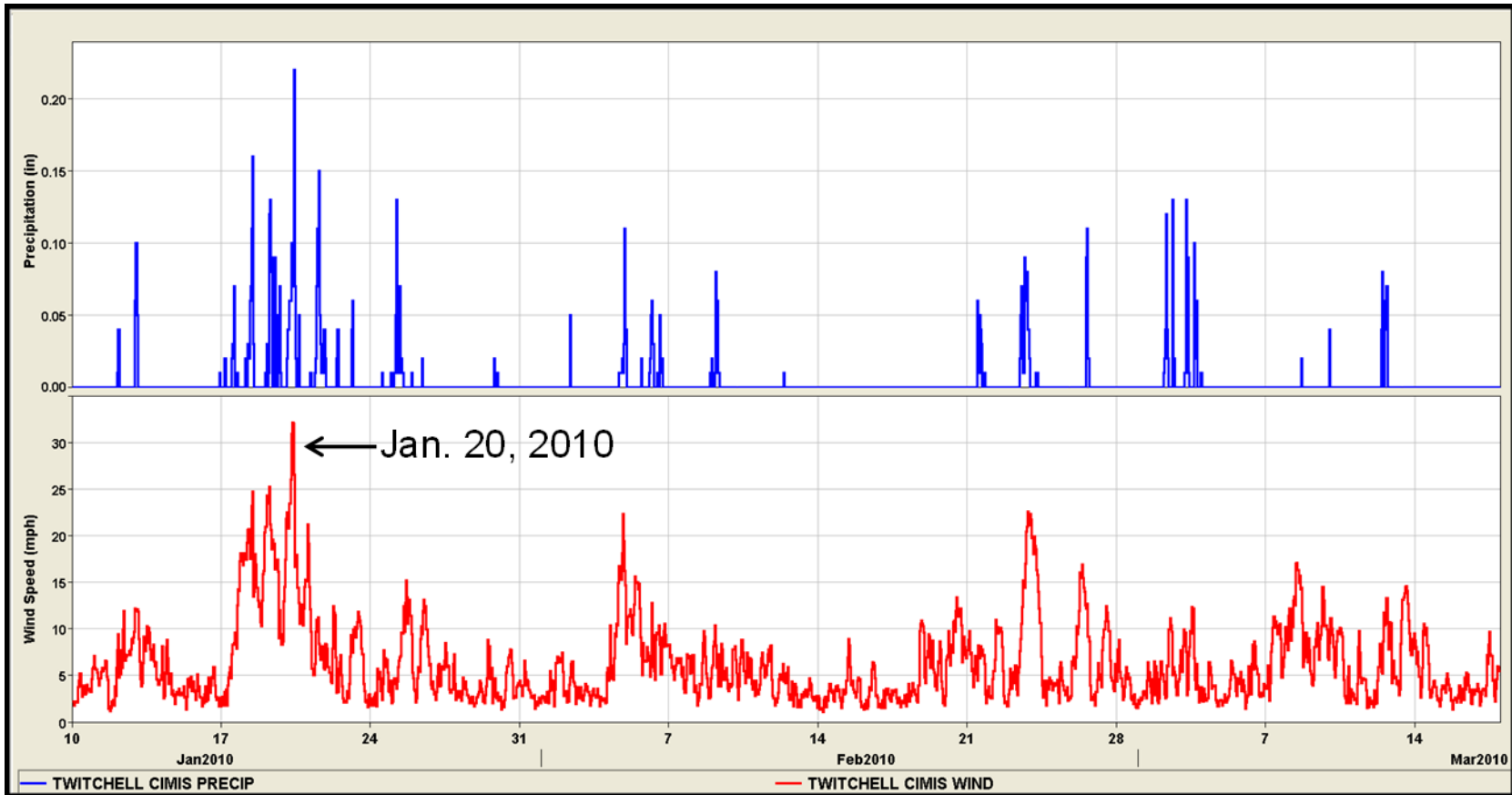
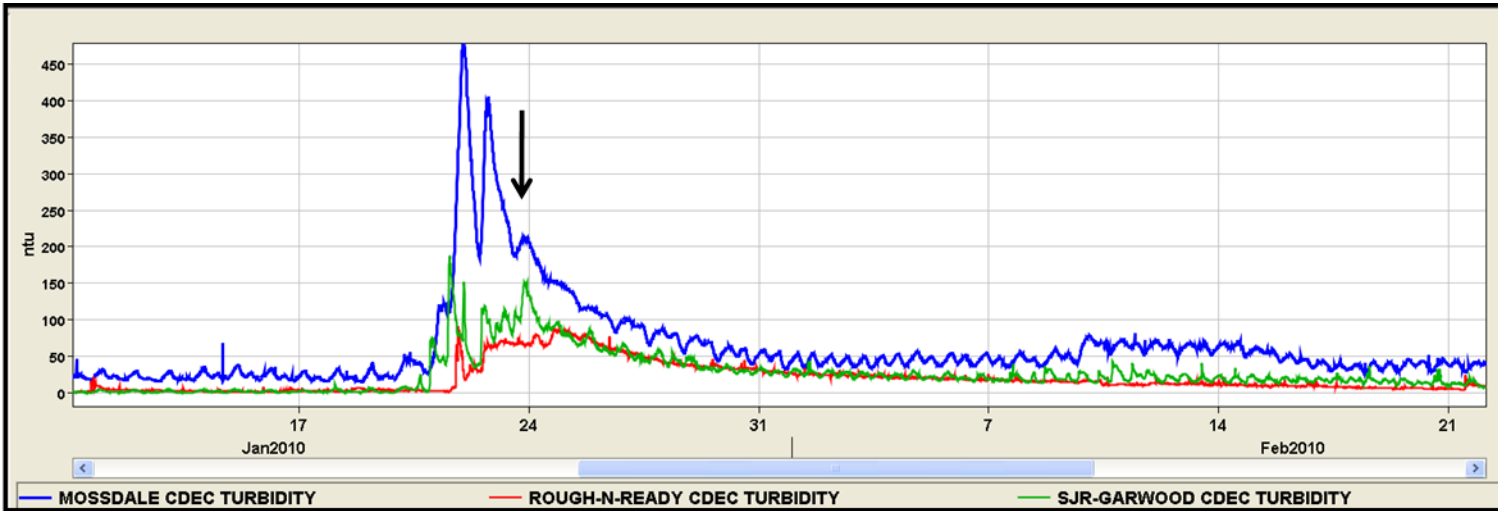


Figure 5-10 CIMIS data at the Twitchell station shows the timing of the wind and rain events January to mid-March, 2010.



Significant dilution also indicated in turbidity data downstream of Mossdale after storms: Modeled turbidity is too high during periods where data shows dilution.

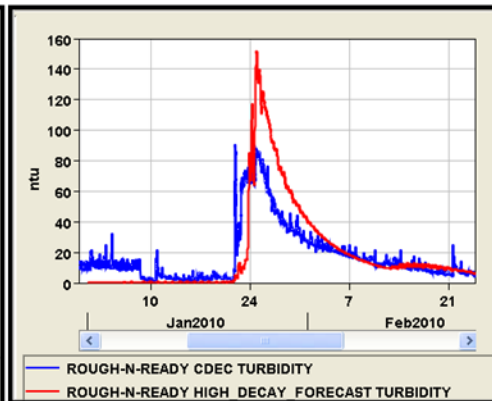
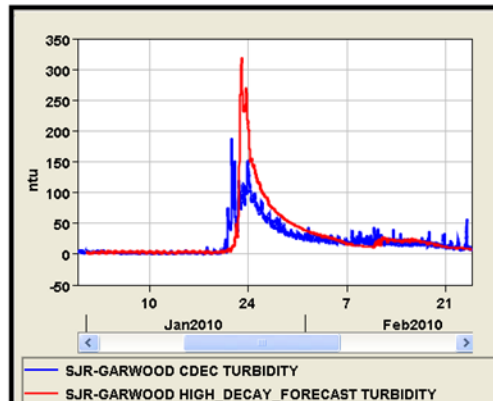
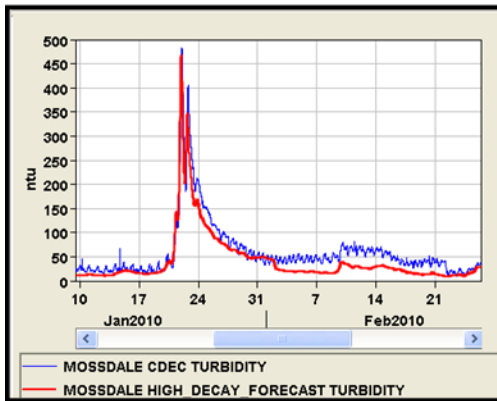


Figure 5-11 Data (upper plot) show turbidity dilution downstream of Mossdale after late January rain event (arrow) - modeled turbidity (lower plots) is good at Mossdale but too high downstream, also indicating possible dilution from local inflow sources.

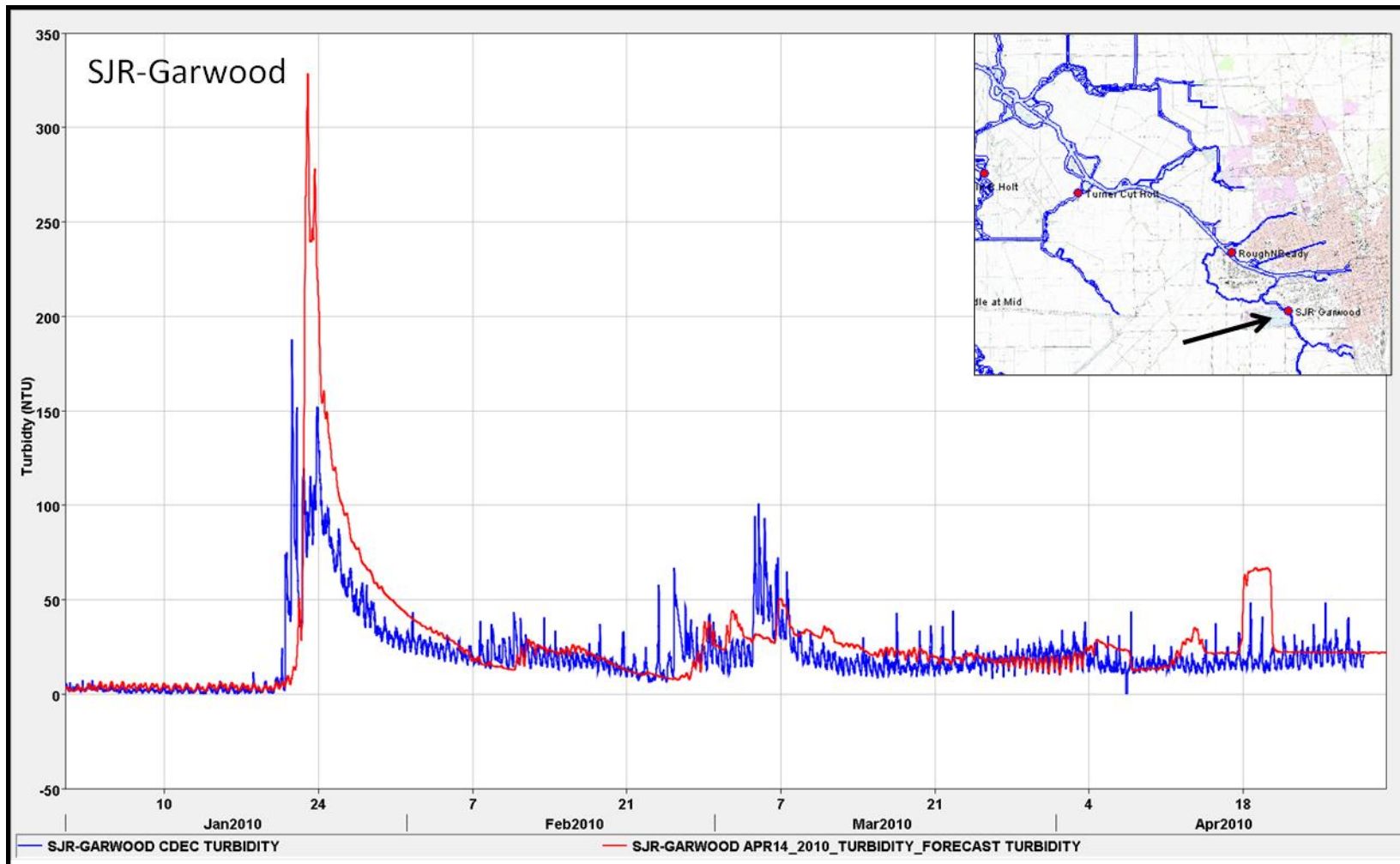


Figure 5-12 Turbidity data/model comparison at Garwood on the San Joaquin R. indicates possible evidence of missing effects of dilution.

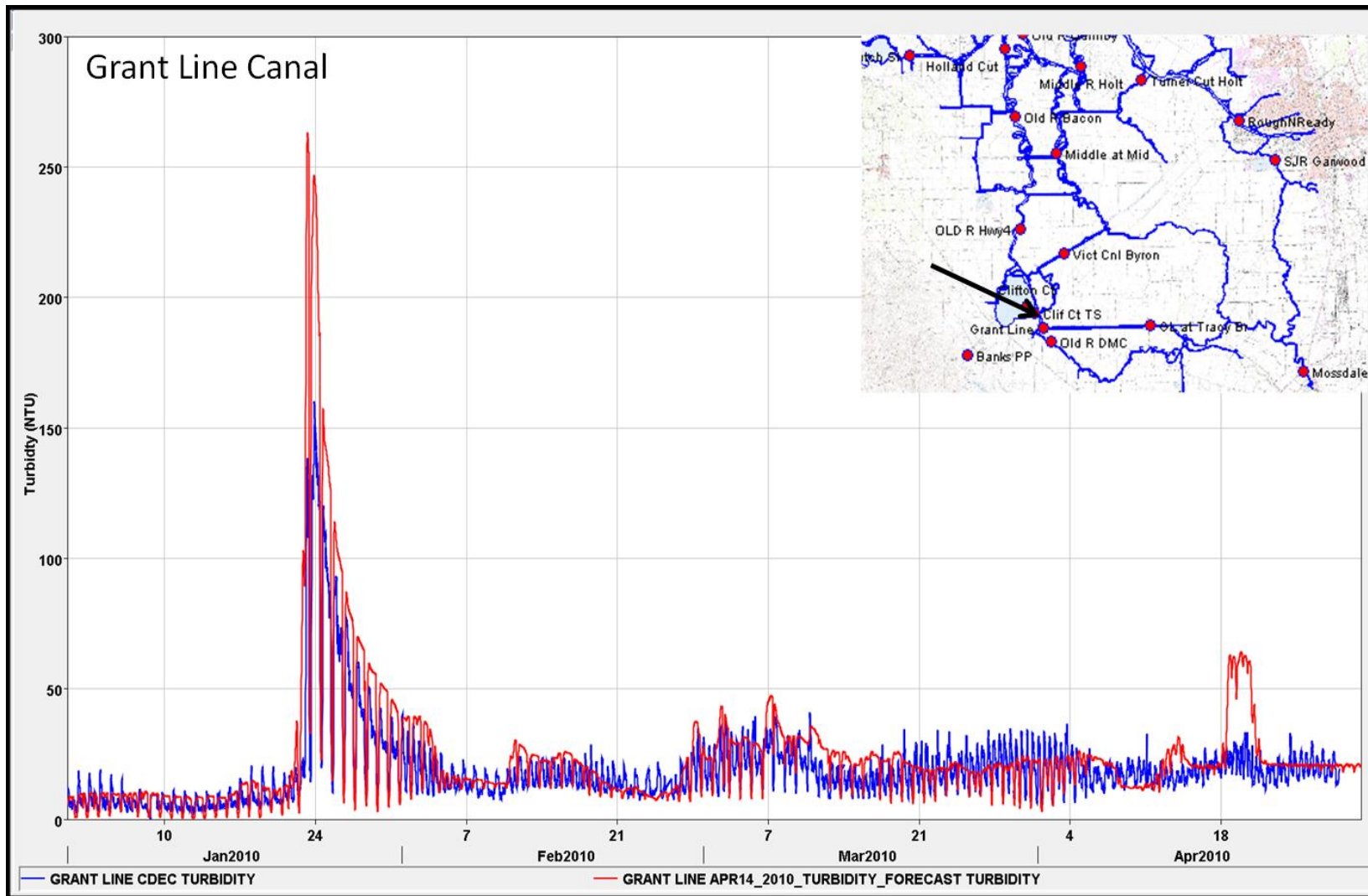


Figure 5-13 Turbidity data/model comparison at Grant Line Canal indicates possible evidence of missing effects of sediment settling.

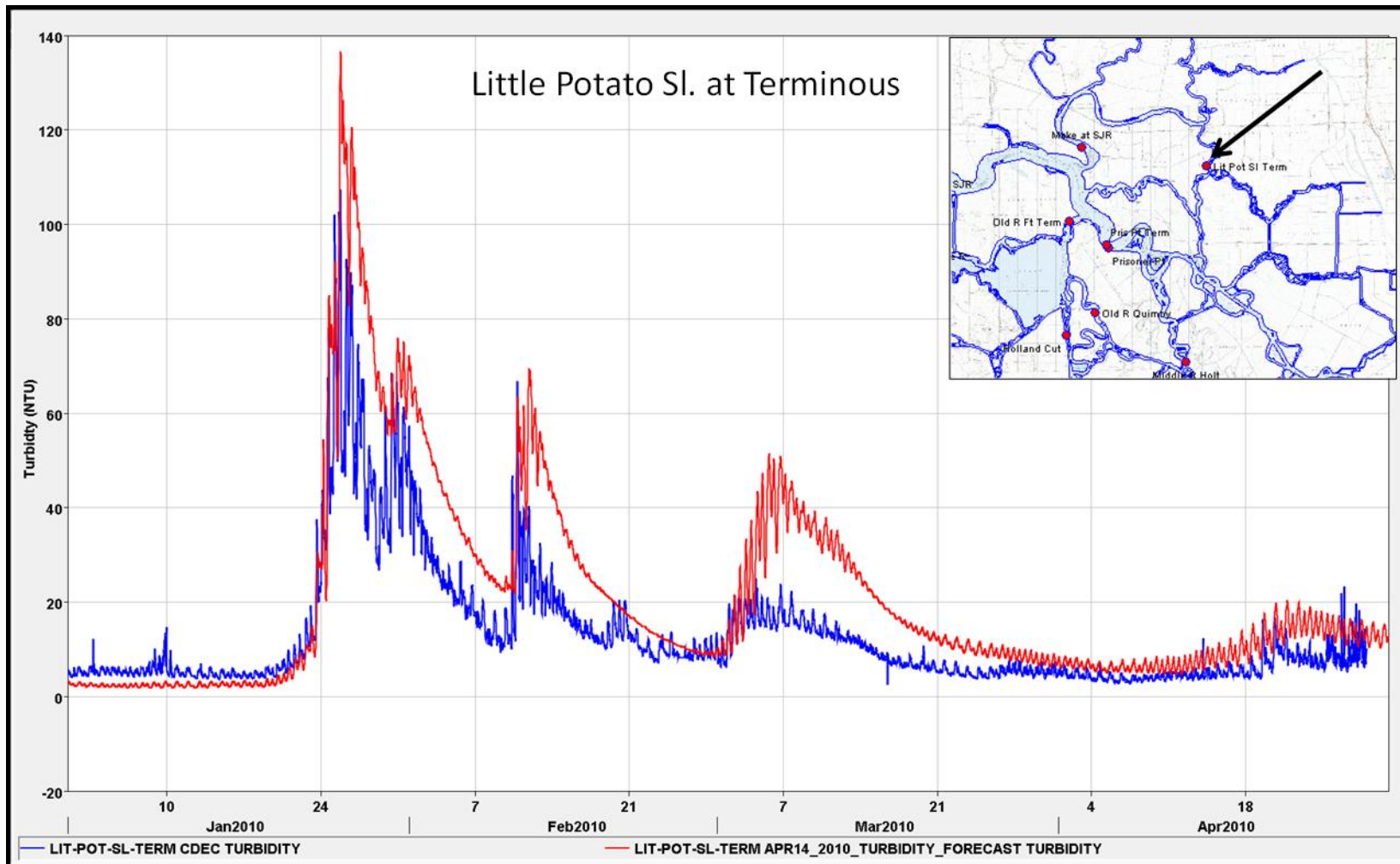


Figure 5-14 Turbidity data/model comparison at Little Potato Sl. at Terminous indicates possible evidence of missing effects of sediment settling.

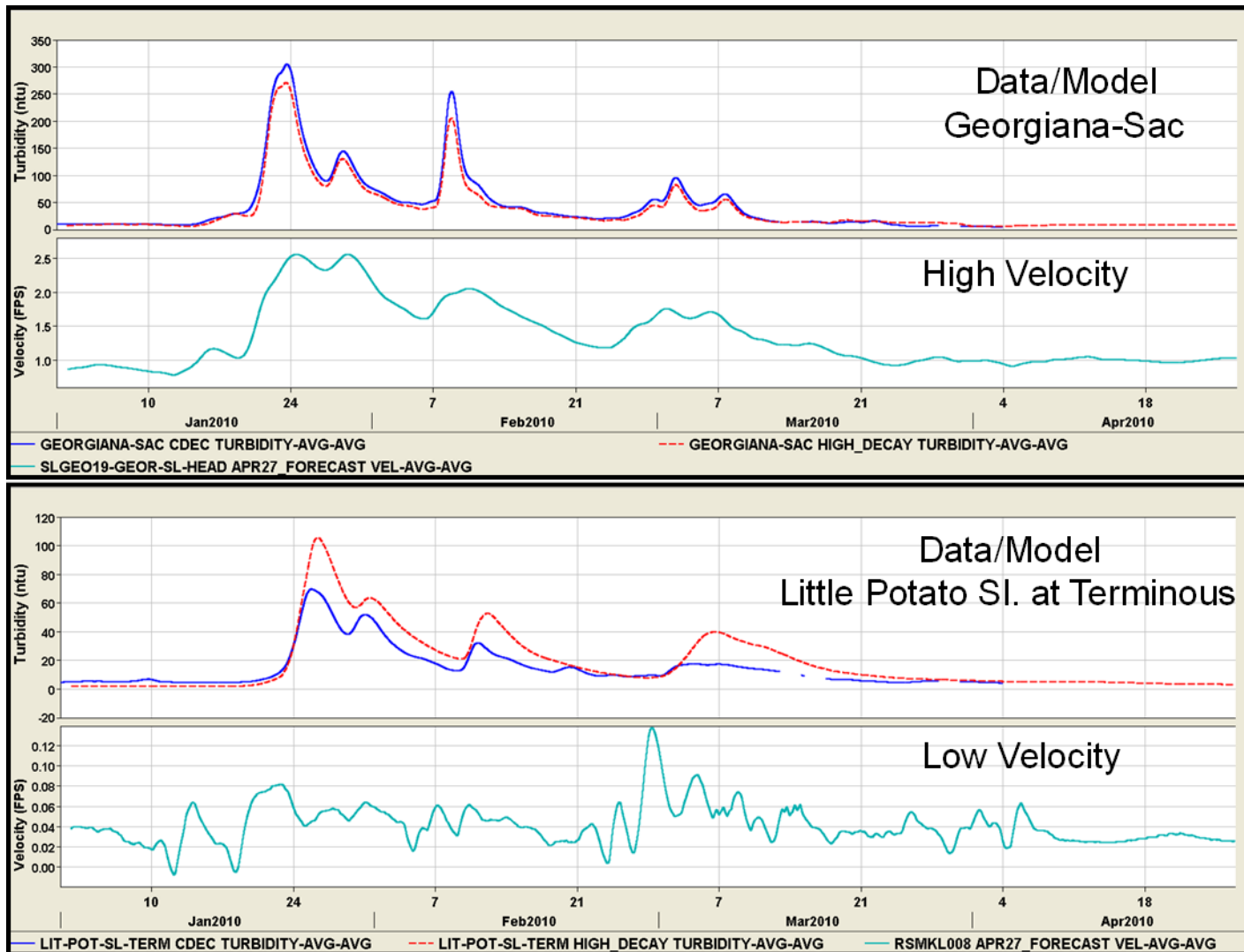


Figure 5-15 Local low velocity is associated with model over-prediction of turbidity during high turbidity events at Little Potato Sl. at Terminous – this is not evidence of this at high velocity locations such as Georgiana-Sac.

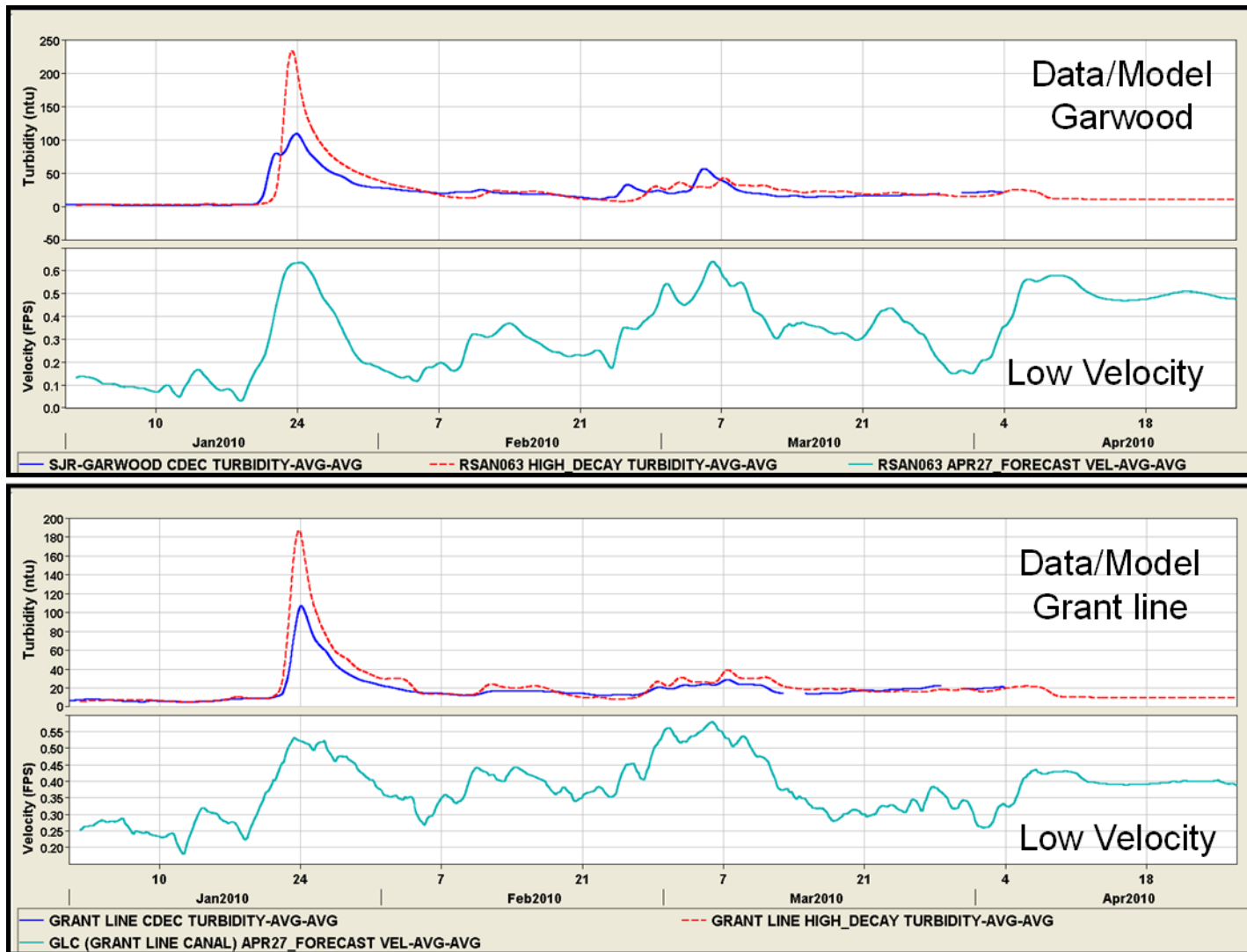


Figure 5-16 Local low velocity is associated with model over-prediction of turbidity during high turbidity events at Garwood on the San Joaquin R. and in Grant Line canal.

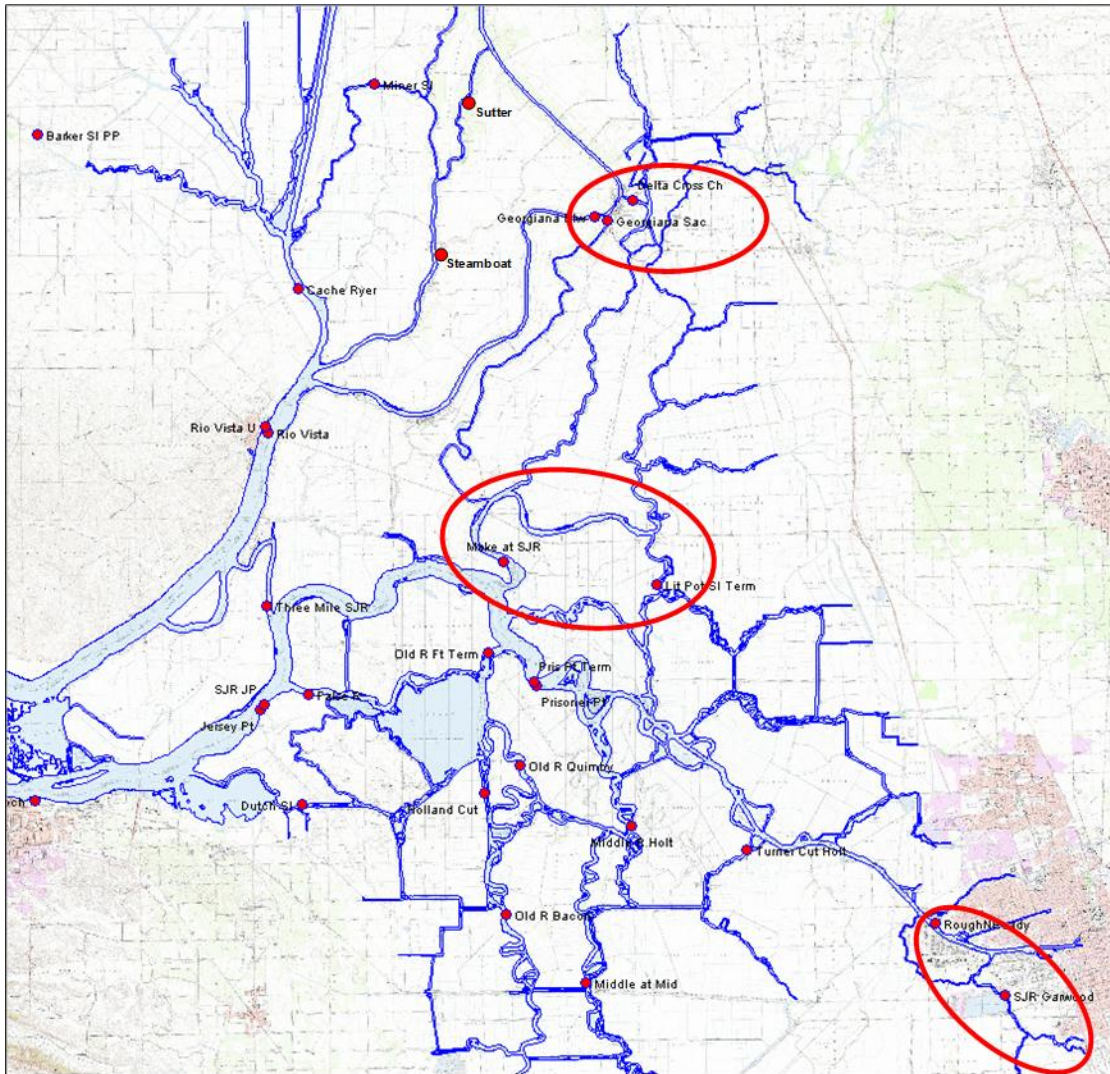


Figure 5-17 Three areas were identified as having problems with missing flow – i.e., where gauged data upstream and downstream didn't match.

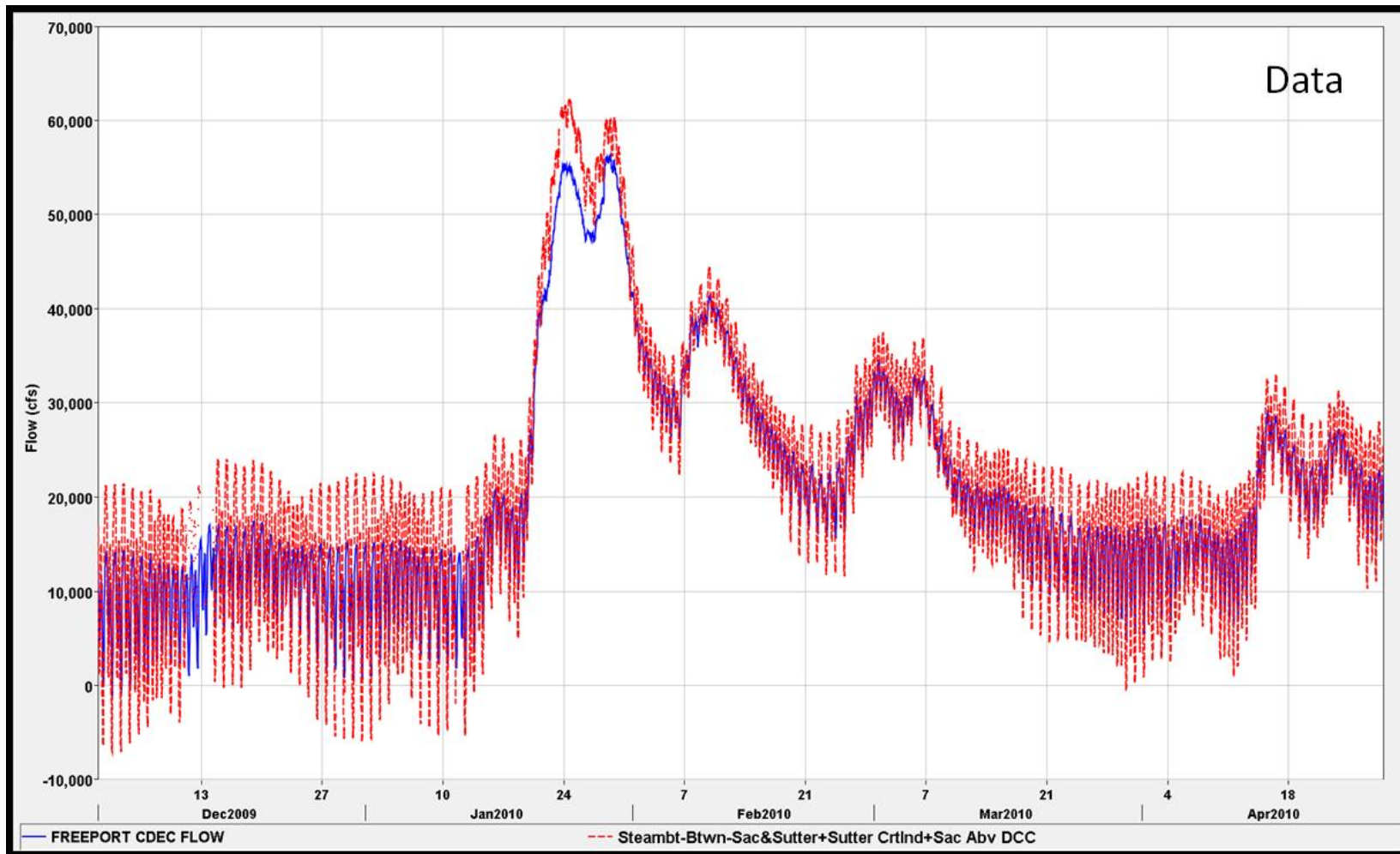


Figure 5-18 Flow at Freeport (blue) is up to 5,000 cfs less than gauged downstream flow around the time of the late January storm – this flow difference is not accounted for in the model.

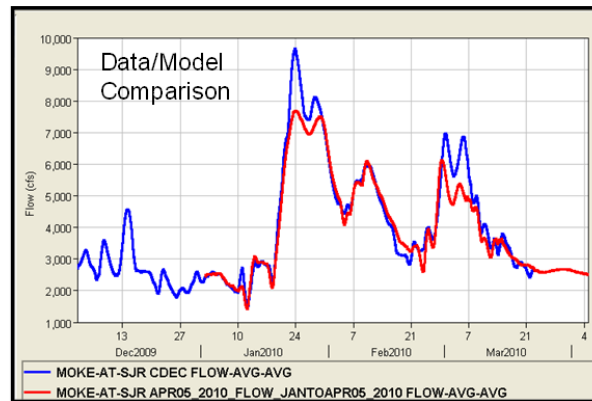
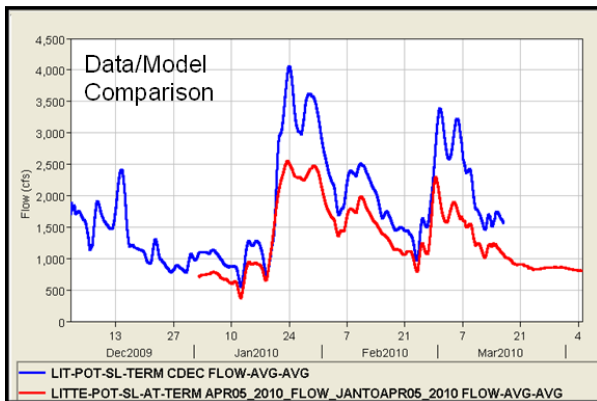
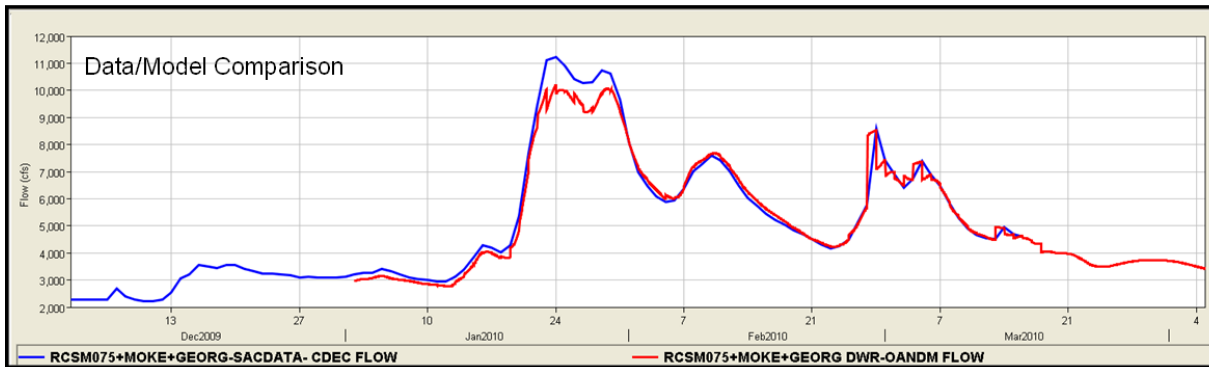
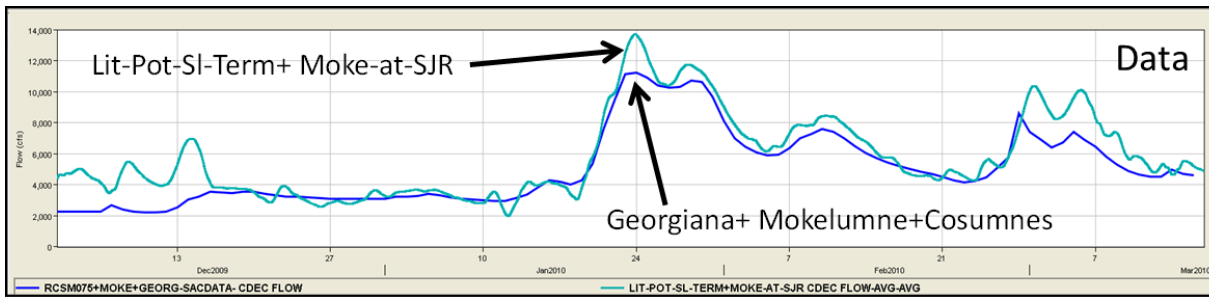


Figure 5-19 Flow into the Mokelumne system does not match flow out of the Mokelumne system.

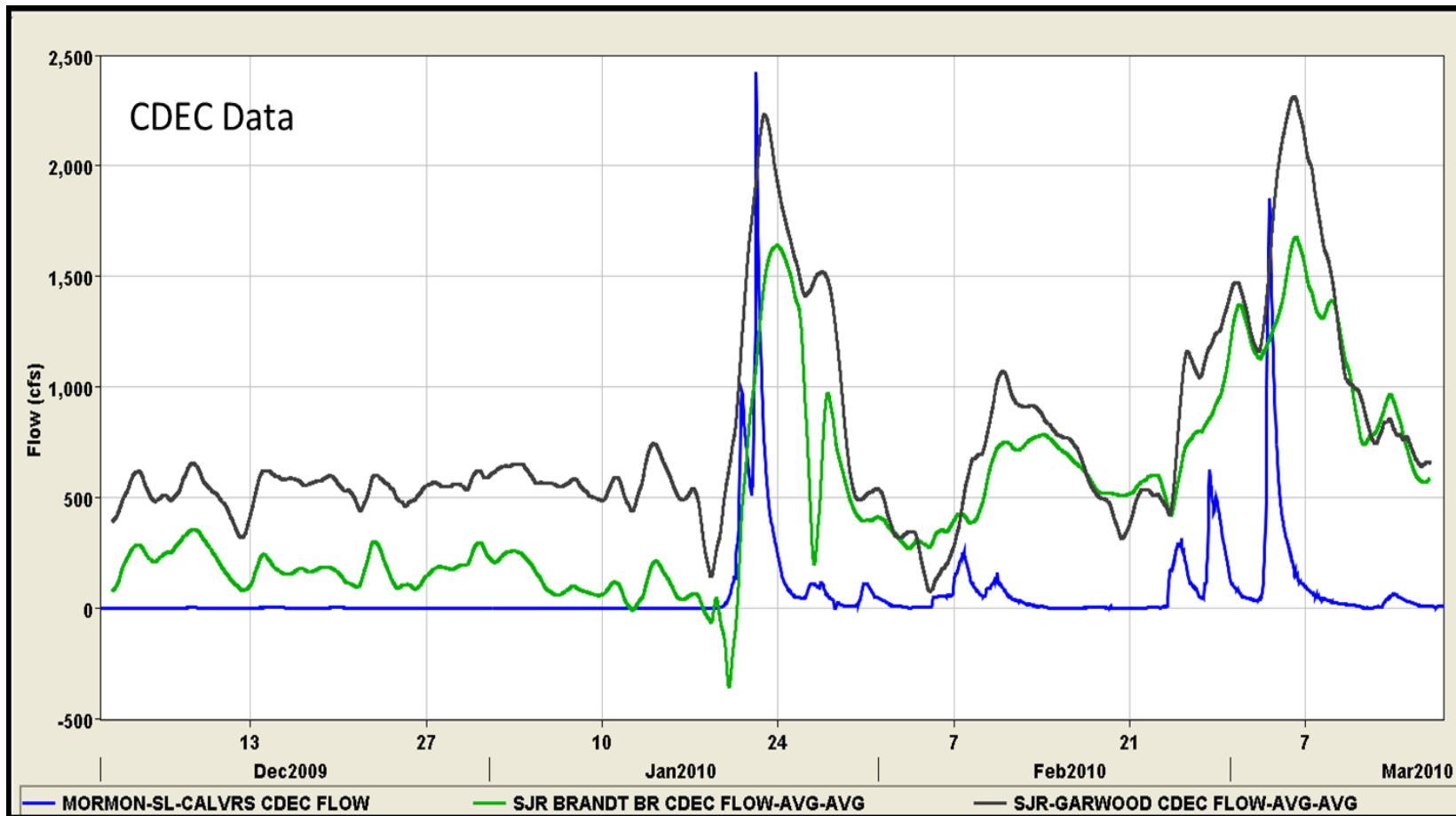


Figure 5-20 Gauged flow (shown here as tidally-averaged flow) at Brandt Br. (green) and at Garwood (black) does not add up on the San Joaquin R., upstream and downstream of the Calaveras R. Note that peak flows on the Calaveras include flow from Mormon Sl. (blue line).

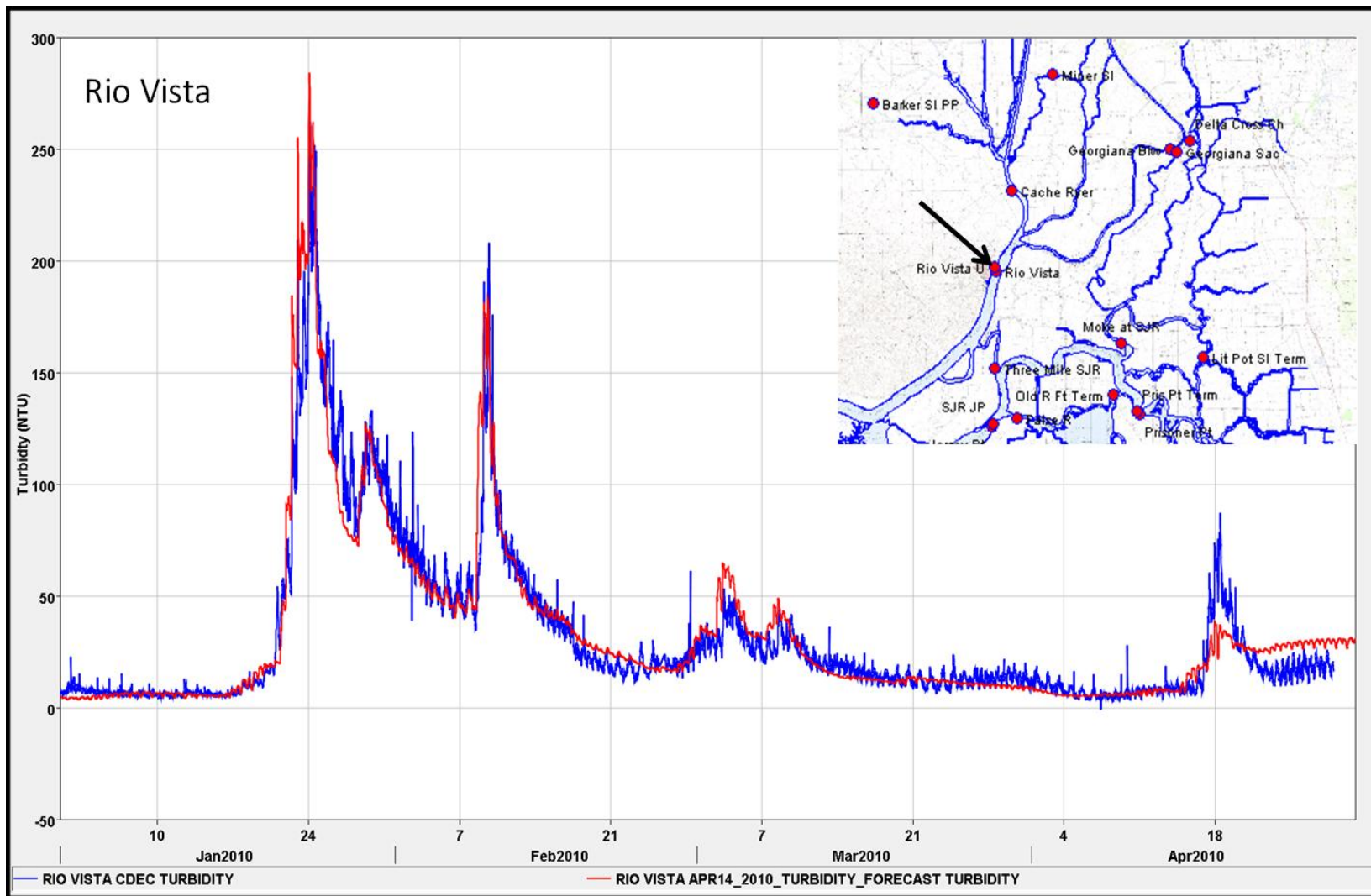


Figure 5-21 Turbidity data (blue) and model results (red) at Rio Vista.

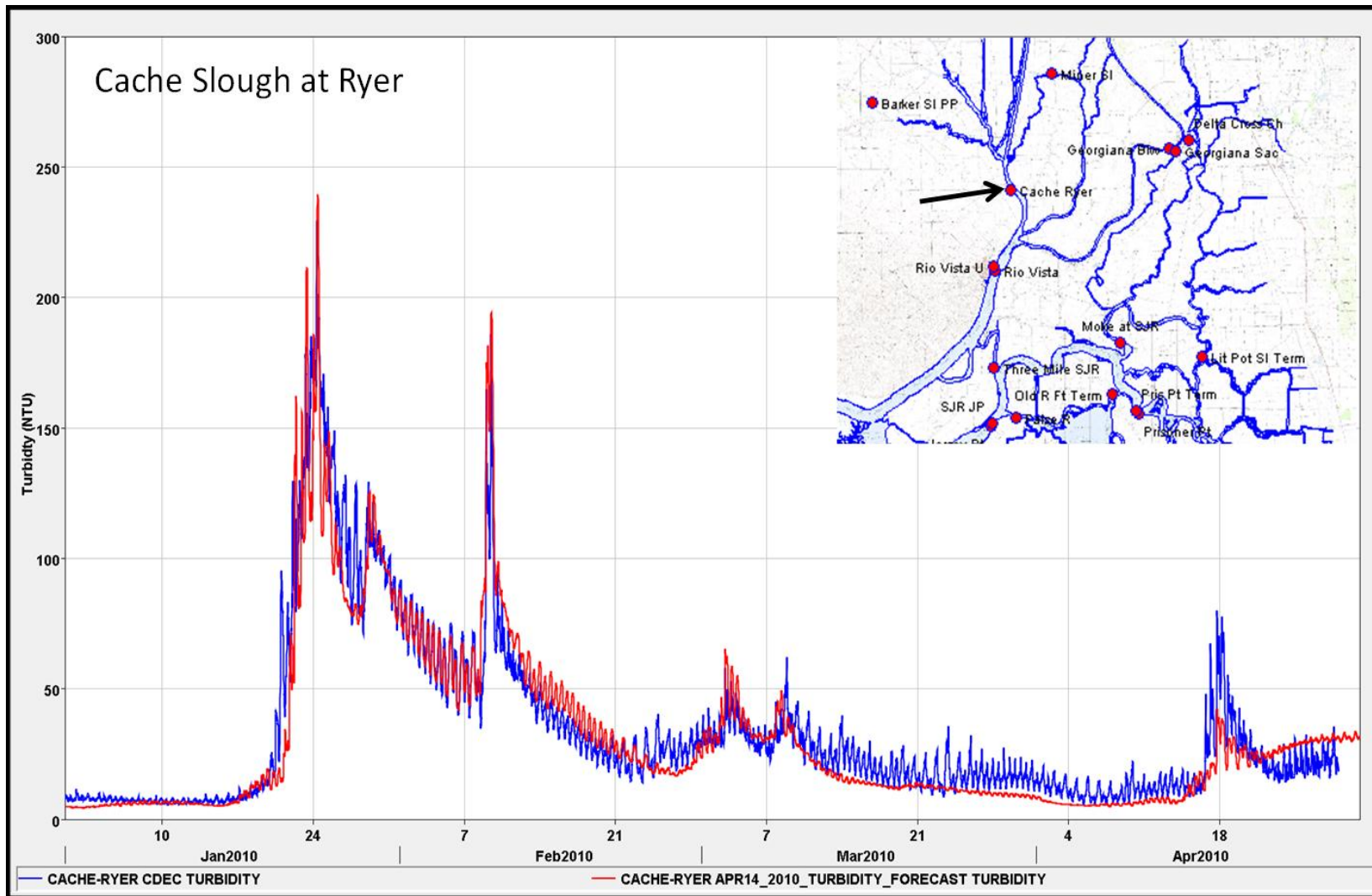


Figure 5-22 Turbidity data (blue) and model results (red) at Cache-Ryer.

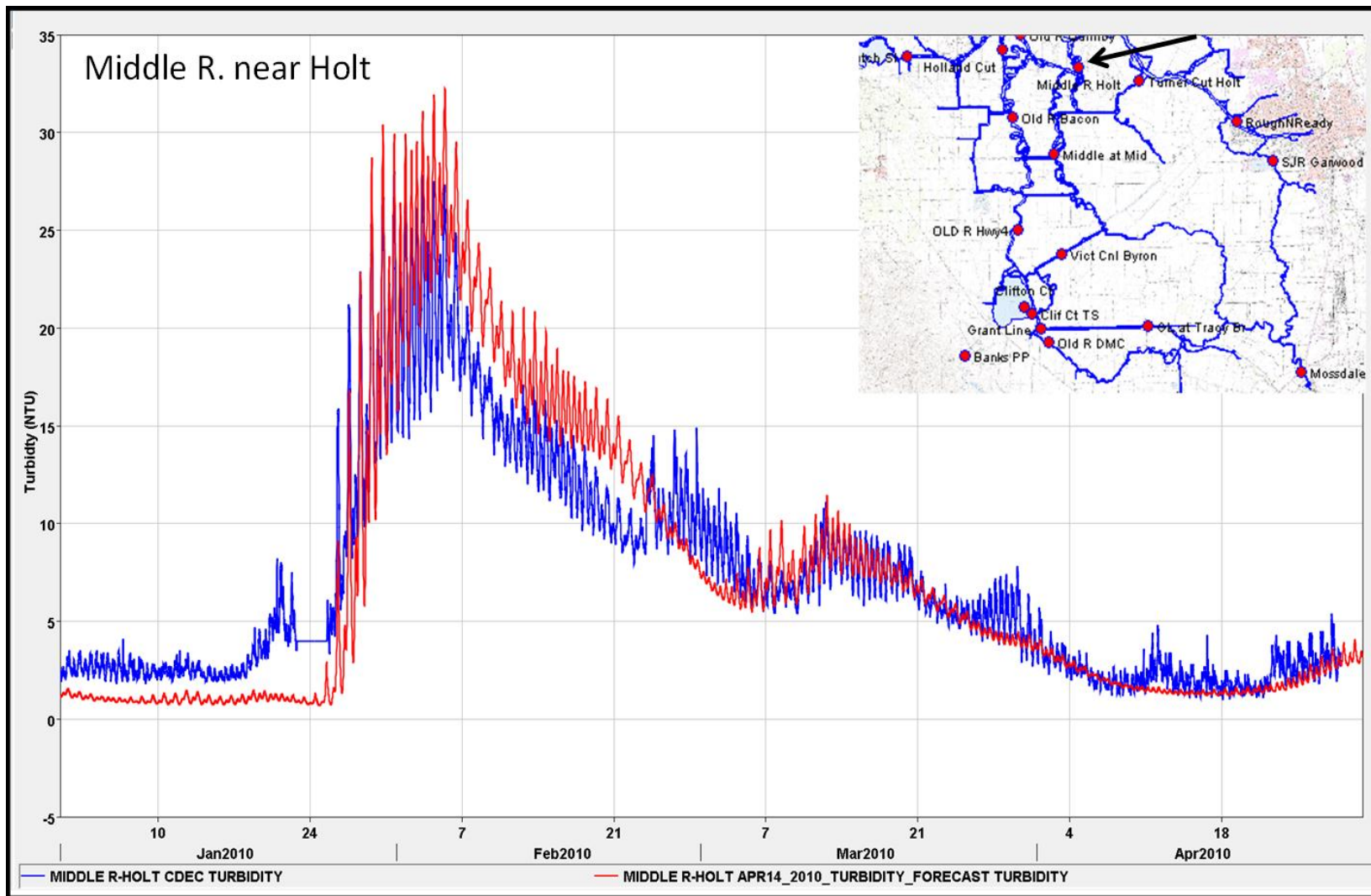


Figure 5-23 Turbidity data (blue) and model results (red) at Middle River near Holt.

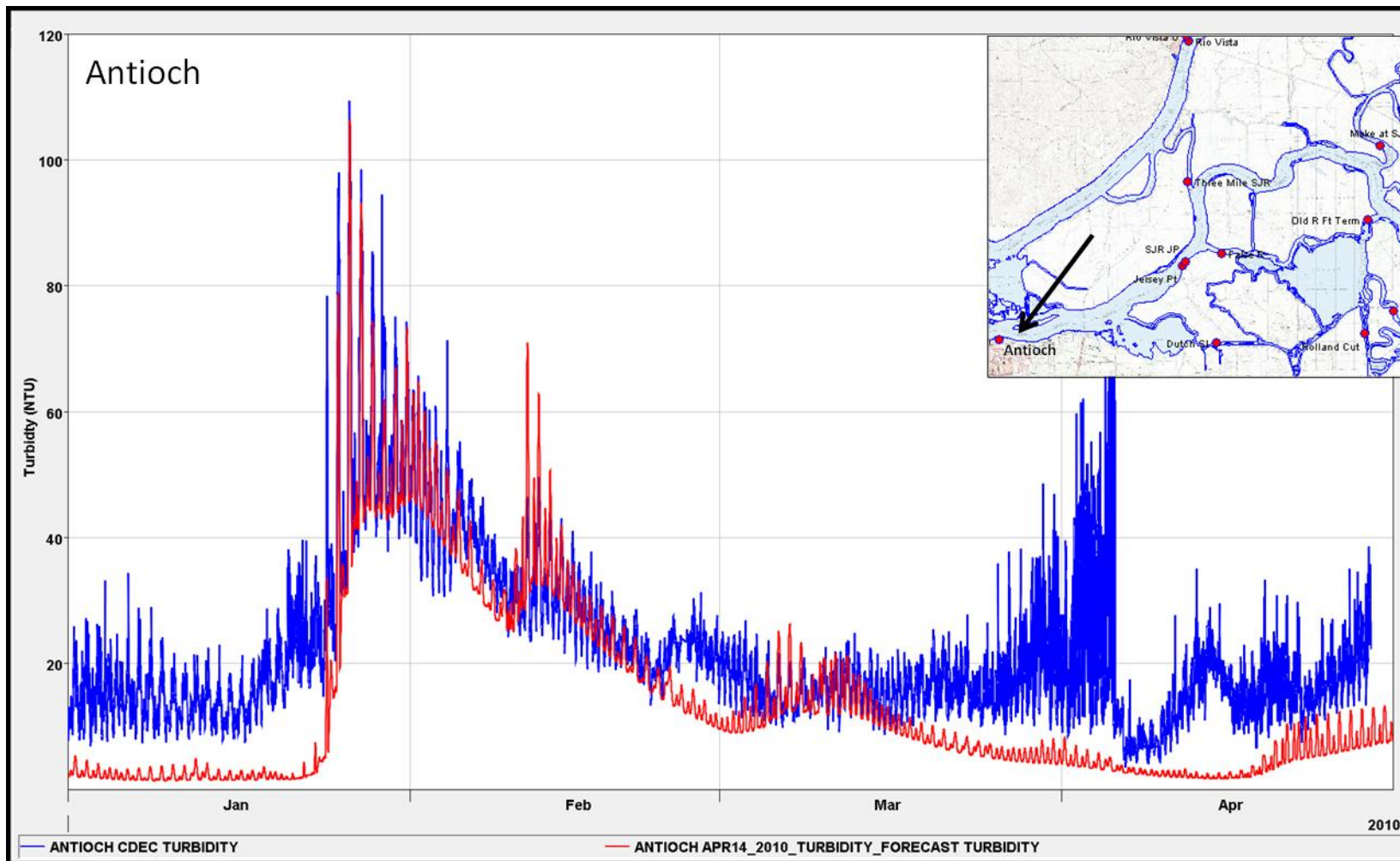


Figure 5-24 Turbidity data (blue) and model results (red) at Antioch.

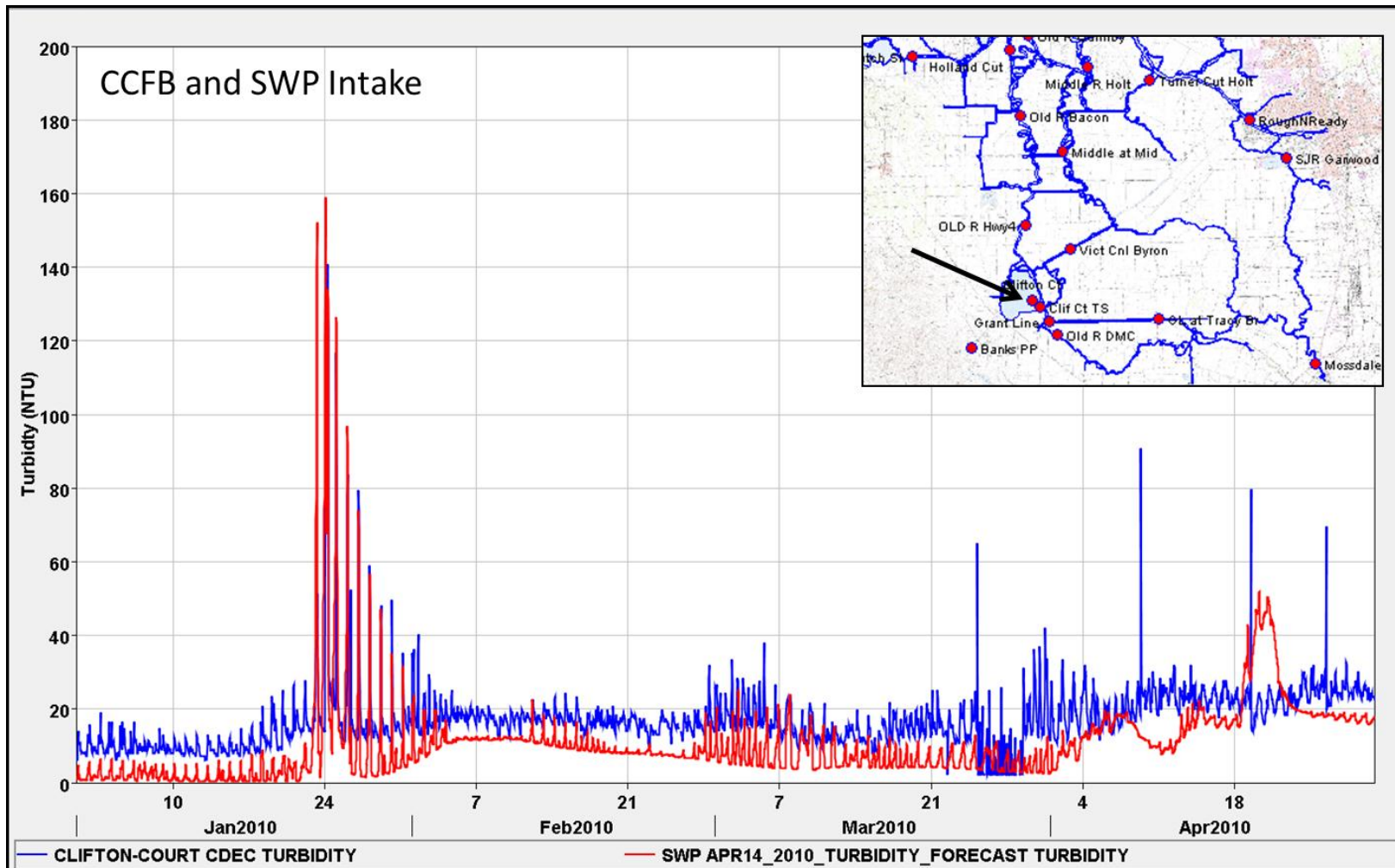


Figure 5-25 Turbidity data (blue) in Clifton Court Forebay (CCFB) and model results (red) at the intake to CCFB (SWP intake).

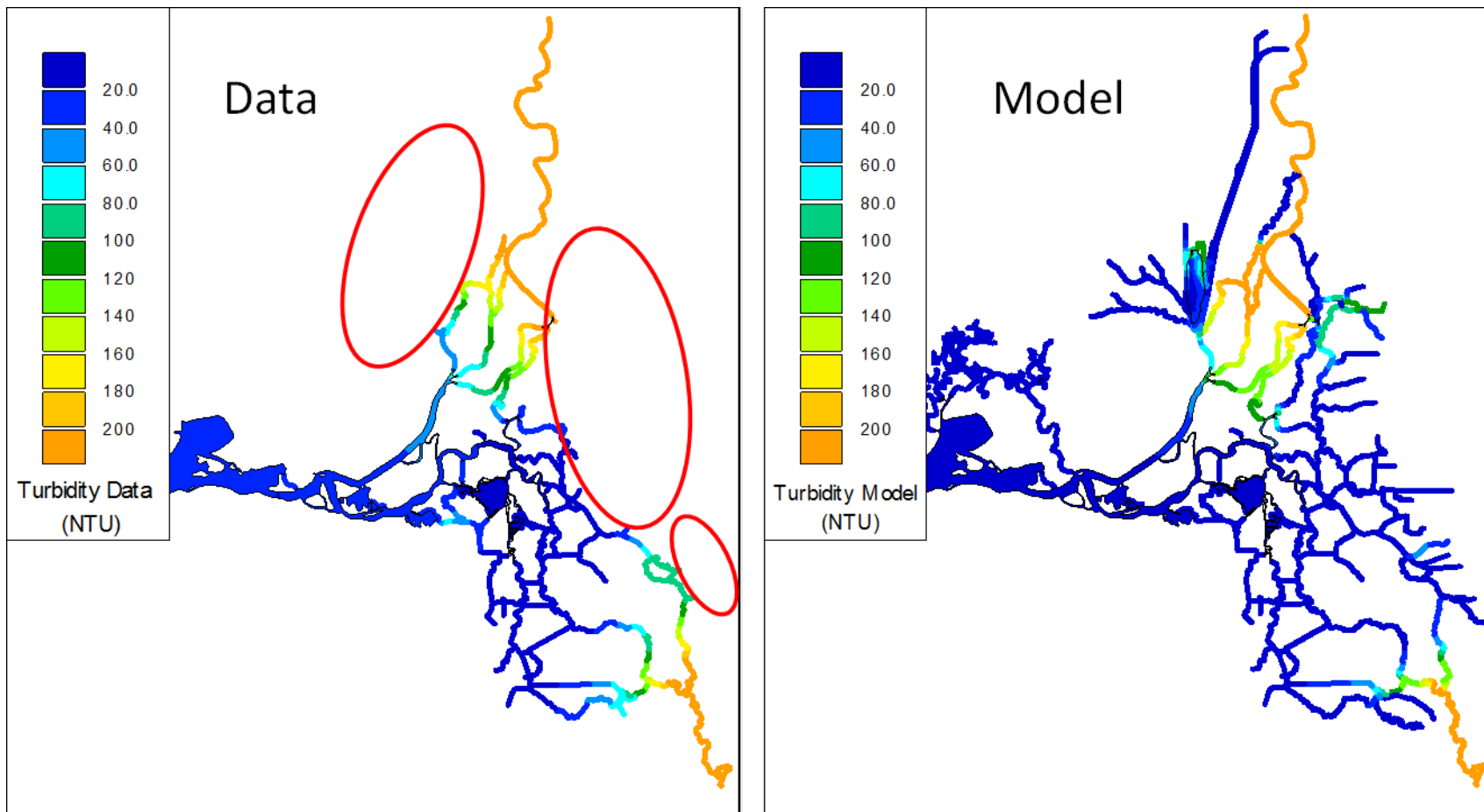


Figure 5-26 Contour plot of spatially interpolated data (left) is missing some regions (red circles) within the RMA 2-D model grid (right) due to a lack of data.

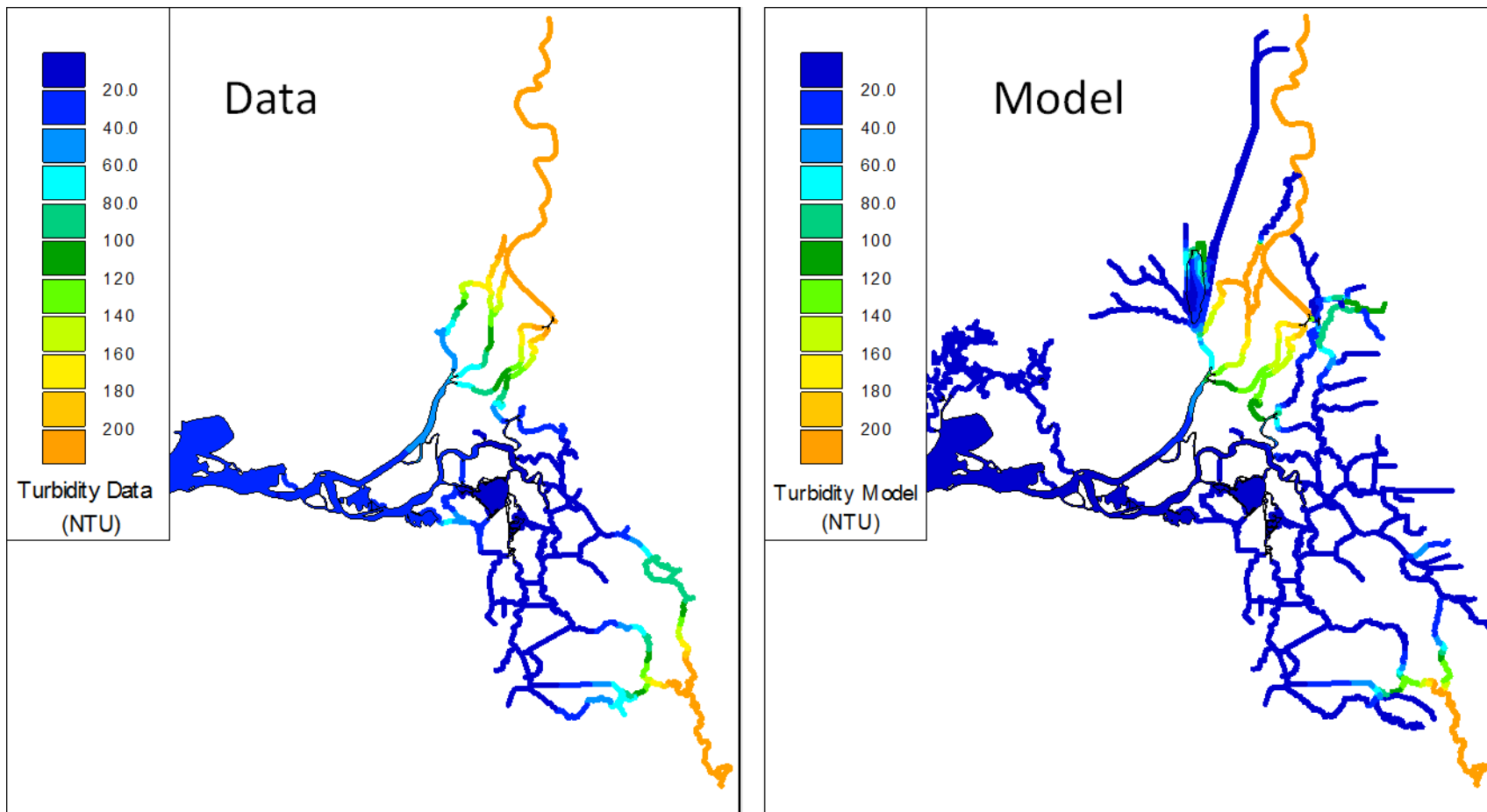


Figure 5-27 Contour plots of spatially interpolated data (left) and model output (right) at 21:00 on January 21, 2010.

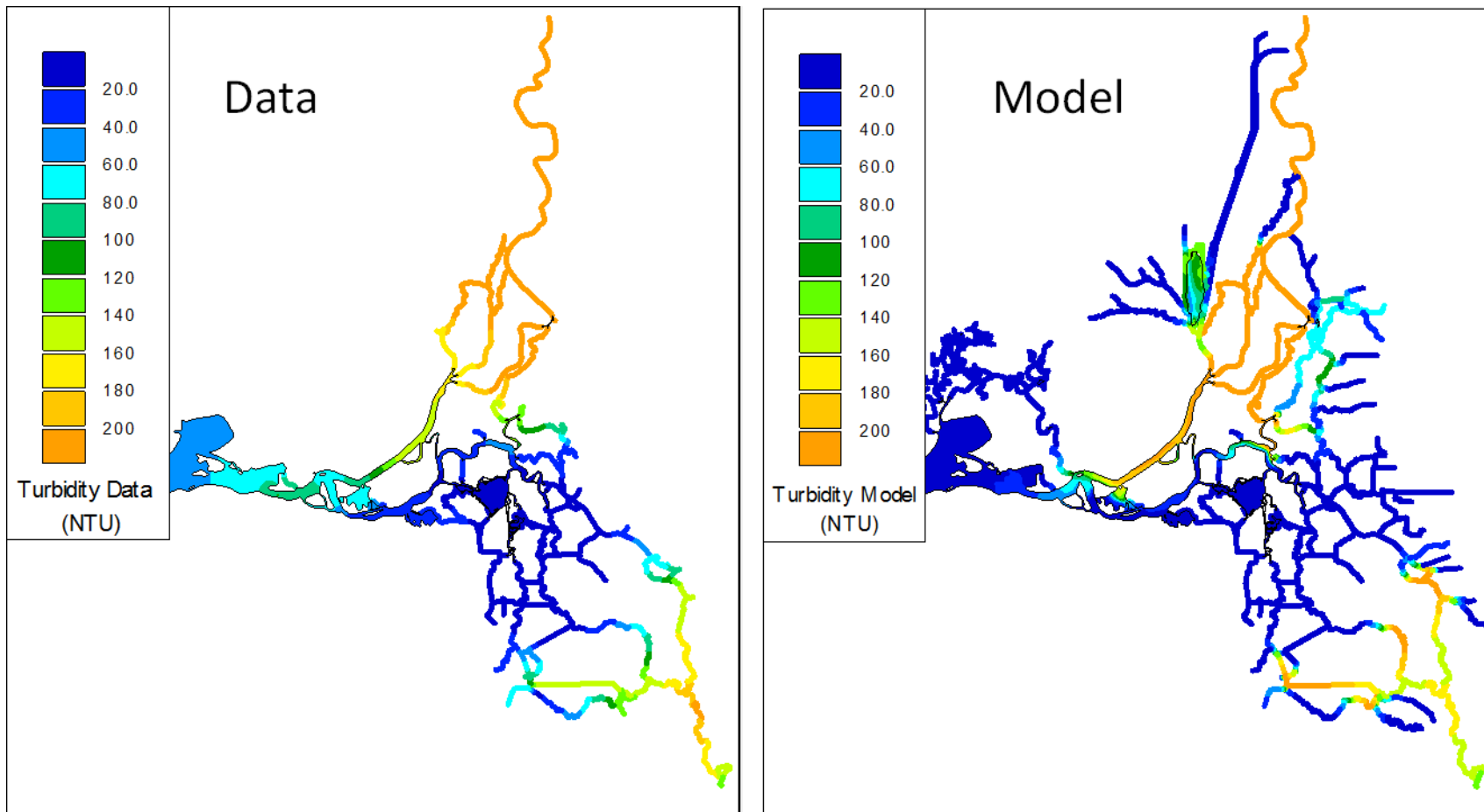


Figure 5-28 Contour plots of spatially interpolated data (left) and model output (right) at 21:00 on January 23, 2010.

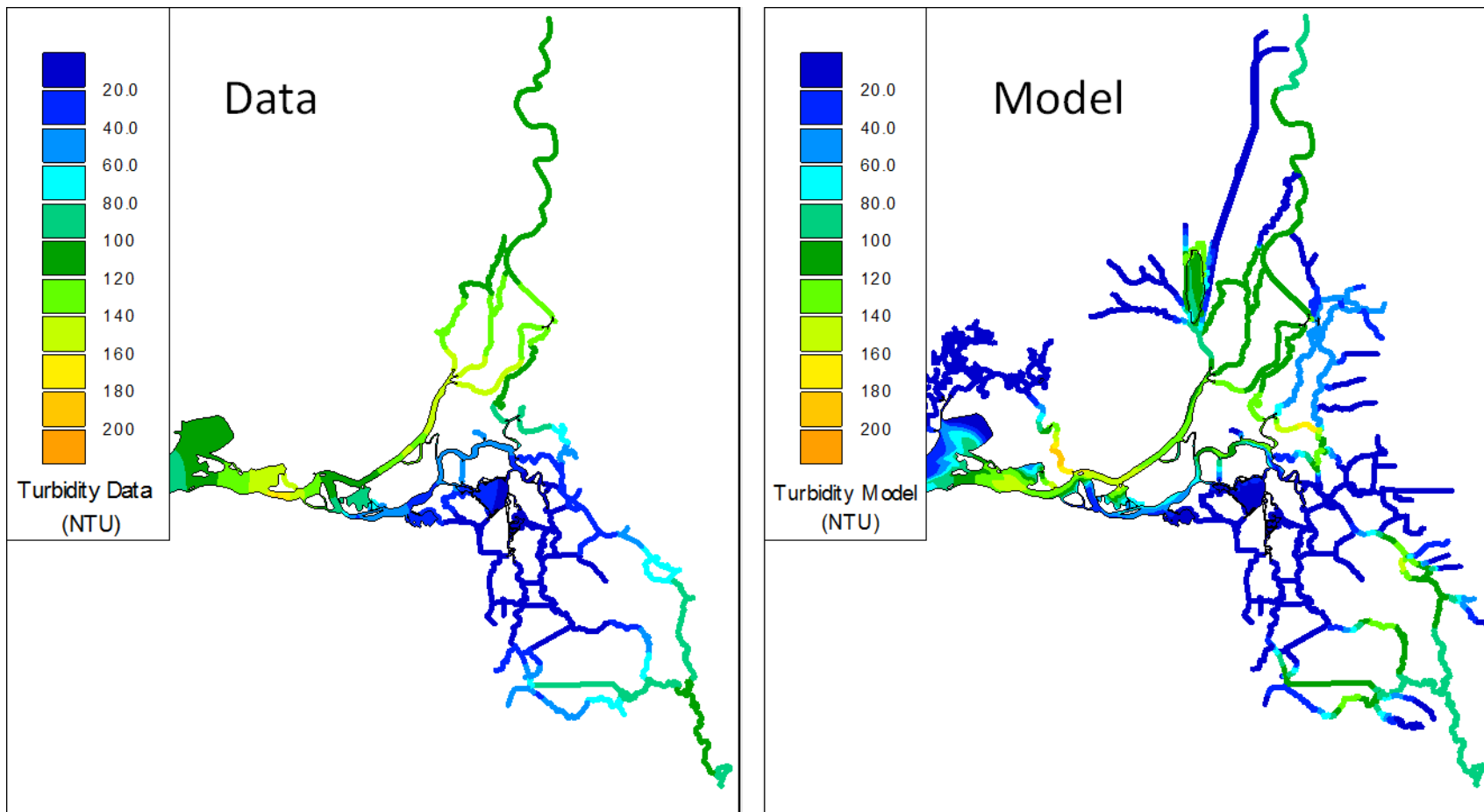


Figure 5-29 Contour plots of spatially interpolated data (left) and model output (right) at 21:00 on January 25, 2010.

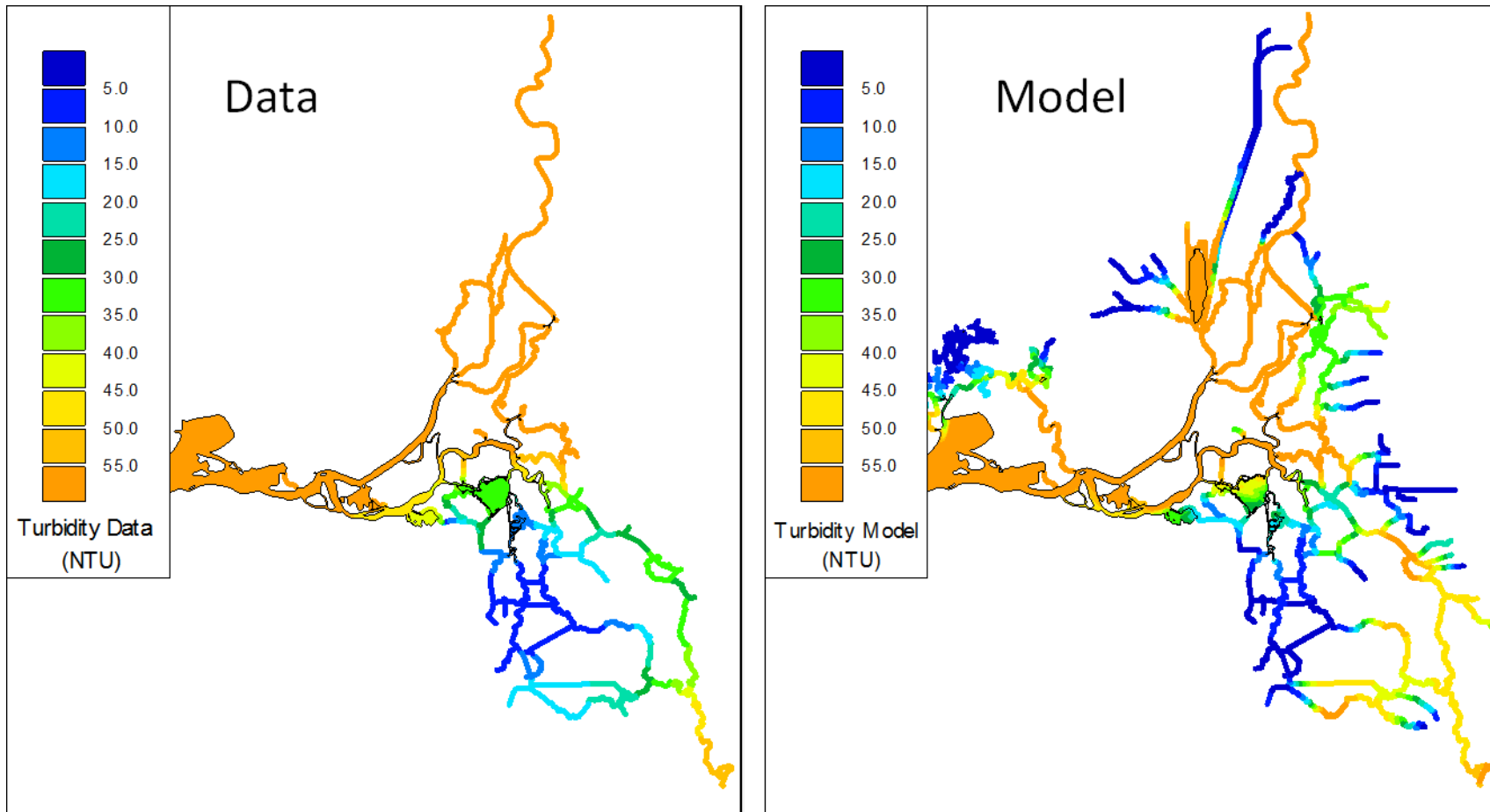


Figure 5-30 Contour plots of spatially interpolated data (left) and model output (right) at 21:00 on January 30, 2010. Note change in color contour scale from previous plots.

6. Adult delta smelt particle tracking models

6.1. *Hypotheses behind the behavior model (ref:RMA 2009)*

The basic hypothesis of the behavior model is as follows. Adult delta smelt desire to move upstream from the Suisun Bay region during the late fall or early winter to spawn. The fish wait until the first storm events of the season increase the turbidity in the interior of the Delta. The fish prefer to avoid water with very low turbidity because of higher risk of predation and/or lack of food supply. The fish determine the desired direction of travel by sensing local gradients of salinity and turbidity. Initially, when they are in the Suisun Bay Region, the upstream direction is determined by a decreasing gradient for salinity. Once into the interior of the Delta where the salinity gradient is very small, the fish randomly explore the Delta channels to find suitable spawning habitat. If the turbidity is too low, the fish will move in the direction of increasing turbidity. If the turbidity gradient is too small however and it cannot be determined which direction leads to higher turbidity, the fish will hide.

Delta smelt are relatively small fish and not strong swimmers, so it is hypothesized that they will use a “surfing” mechanism with tidal flows to move through the Delta channels without expending a large amount of energy. In open channel flow, peak velocities are near the surface toward the middle of the channel, while near the bed or along shallow banks the velocity is very low. If a fish chooses to move with the tidal flow, it can easily move toward the surface where the velocity is highest. Conversely, if the fish chooses not to move with the tidal flow, then it can move toward the bottom where the velocity is very low. This allows the fish to ride the tidal flow in a preferred direction. For example, if the turbidity at the current location is too low and the fish desires to move toward more turbid water, it would tend to hold its position (move to the bottom) if the turbidity gradient along the direction of flow was such that the tidal flow was bringing higher turbidity water toward it. When the tide turned and flow directions reversed, the fish would move toward the surface to go with the tidal flow. Because tidal excursions in the Delta channels are quite large, often on the order of several kilometers, fish can move very quickly using this surfing mechanism.

Recent evidence suggests that delta smelt may use lateral movement across a channel in order to maintain their position or move upstream against the net current. The fish would move into the shallows where velocities are low during ebb tide, and move into the deeper main channel where velocity is higher on flood tide. While the current formulation of the adult delta smelt behavior model does not utilize lateral movement to perform tidal surfing, it would be possible to include this mechanism. This would enable the model to test the sensitivity of results to incorporation of the lateral movement hypothesis.

6.2. *Adult delta smelt behavior model*

The behavior model is implemented on top of the RMATRK particle tracking model. At each tracking step, the transport velocity is computed for a neutrally buoyant passive particle moving with the streamline velocity computed by the RMA Bay-Delta Model and subject to a random velocity component representing turbulent dispersion. The behavior model is then used to determine an adjustment to the transport velocity. The behavior algorithm utilizes the local concentration and gradient of electrical conductivity (EC, simulated as a surrogate for salinity) and turbidity computed by the RMA Bay-Delta Model to determine the adjustment to the transport velocity.

The behavior algorithm is implemented as follows:

- If the local EC is greater than the required maximum limit
 - Surf toward lower EC.
- Else if the local turbidity is lower than the required minimum limit
 - If the local turbidity gradient is greater than the minimum detectible gradient
 - Surf toward higher turbidity
 - Else if the local turbidity gradient is lower than the minimum detectible gradient
 - Hide
- Else if the local EC is lower than the desired minimum limit
 - Surf toward higher EC.
- If the local EC and local turbidity are within required limits
 - Randomly move (explore desirable habitat).

The surfing behavior is implemented by applying a scalar velocity factor to the transport velocity vector computed for neutrally buoyant particles. The velocity factors for moving with the tidal flow and resisting tidal flow are user defined constants. Reasonable limits for these factors are zero as a minimum and 1.2 as a maximum factor. Assuming a logarithmic vertical velocity profile the peak velocity is approximately 1.2 times the depth averaged velocity. Hiding is also implemented with a user defined scalar velocity factor, which causes the particles to move slowly or stop.

Random movement to explore desirable habitat is currently implemented as addition random mixing. When a particle is at a location where the EC is below the required maximum limit and the turbidity is above the required minimum limit a random velocity component is computed based on user defined dispersion coefficients in the longitudinal (streamline) and transverse directions. The velocity component is computed as:

$$v = \sqrt{\frac{2K * g}{dt}}$$

where:

v is the velocity component in the longitudinal or transverse direction (m/s),

K is the user defined dispersion coefficient in the longitudinal or transverse direction (m²/s),

dt is the tracking time step(s), and

g is a randomly selected value from a standard normal Gaussian distribution (i.e., with a mean 0.0 and a standard deviation of 1.0).

6.3. Particle tracking model parameters

In addition to the “standard” settings that need to be implemented in any RMA particle-tracking model (see Figure 6-1, Figure 6-2), such as the location, timing and distribution of particles, the adult delta smelt behavior model requires the settings of behavioral parameters (Figure 6-3). For the current project, the behavioral parameters were set as in previous applications.

The user defined calibration parameters for the current implementation of the adult delta smelt behavior model are:

- Required maximum EC limit (umhos/cm)
- Required minimum turbidity limit (NTU)
- Minimum detectable horizontal turbidity gradient (NTU/m)
- Desired minimum EC limit (umhos/cm)
- Velocity factor for moving with tide flow
- Velocity factor for resisting tidal flow
- Velocity factor used when hiding
- Longitudinal dispersion coefficient (m²/s) for random exploration
- Transverse dispersion coefficient (m²/s) for random exploration

6.4. *Adult delta smelt modeled period and particle count.*

For the near-real-time simulations, near the start of the simulation and before turbidity starts to increase due to a high flow event, 40,000 particles are randomly distributed in the Suisun Bay Region. This insertion occurred at the beginning of January 2010 (Figure 6-2) for all of the forecasts. Through the course of the simulation period, the particle movement through the Delta is based on the behavior algorithm described above. Particles are removed from the system only at the CVP and SWP exports. It is assumed that losses of adult delta smelt are negligible for the Contra Costa Water District intakes on Old River and Rock Slough and for Delta island diversions.

6.5. *Particle observation locations*

Particle numbers can be recorded periodically during the simulation at individual locations, such as at the state (SWP) and federal (CVP) export locations, or in pre-defined regions of the model grid (Figure 6-4).

6.6. *Delta smelt salvage data*

Delta smelt salvage data was obtained from the Bureau of Reclamations Mid-Pacific region website. The Central Valley Operations office (CVO) maintains a repository of data on fish species of interest such as delta smelt that are lost or salvaged at the state and federal export facilities, SWP and CVP exports respectively. Although the official numbers are posted on the California Department of Fish and Game website, the numbers that appear in the CVO reports are verified with DFG reports. The web location that hosts the previous monthly reports is:

<http://www.usbr.gov/mp/cvo/fishrpt.html>

Links to current fish data, as well as other CVO operational data, can be found at:

<http://www.usbr.gov/mp/cvo/>

Figure 6-5 shows the observed salvage count for delta smelt at the state (SWP) and federal (CVP) fish facilities from January through mid-April 2010.

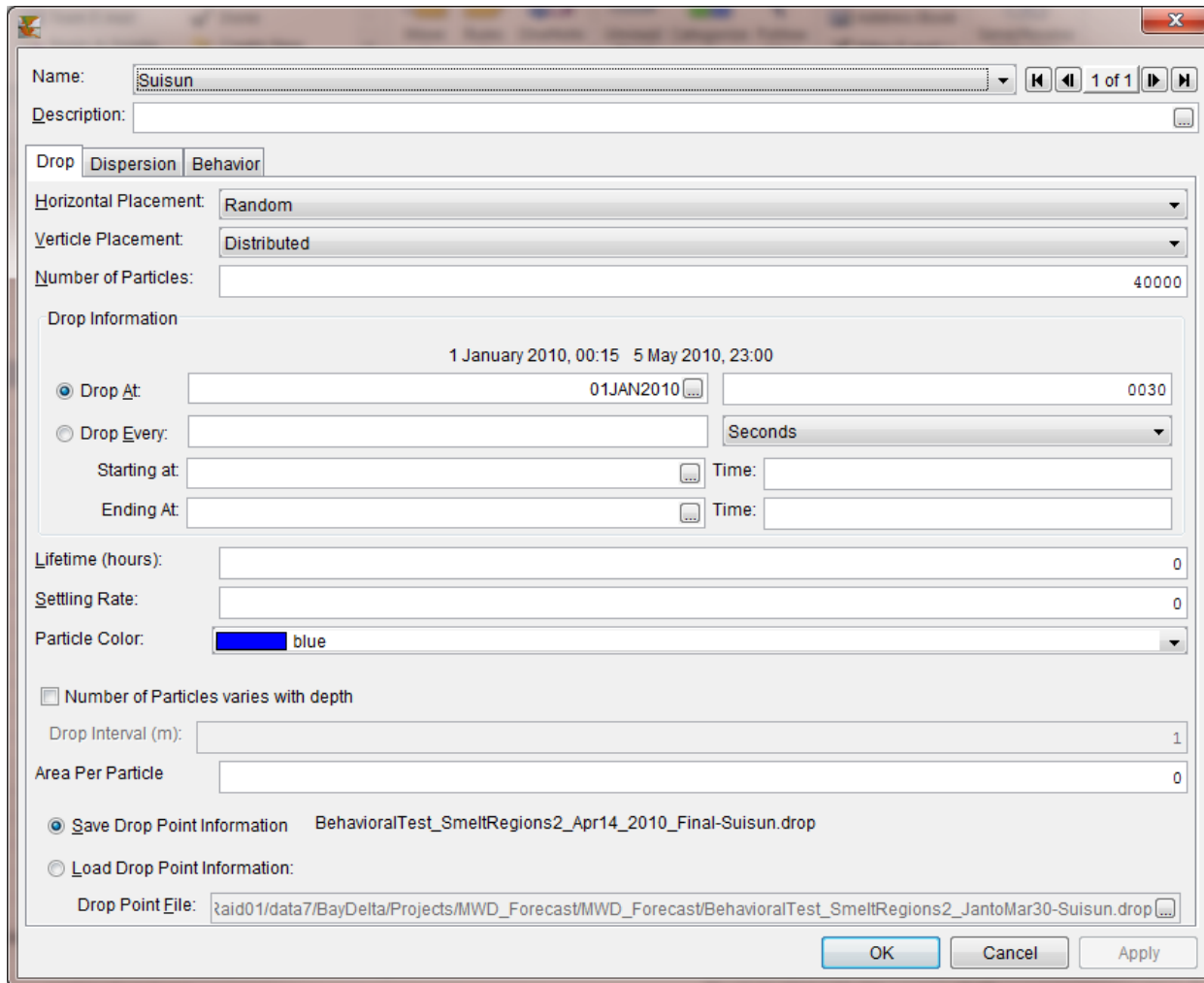


Figure 6-1 User interface for setting the initial location (Suisun region), timing (00:30, Jan. 01, 2010) and distribution (random distributed instantaneous vertical placement) of 40,000 particles.

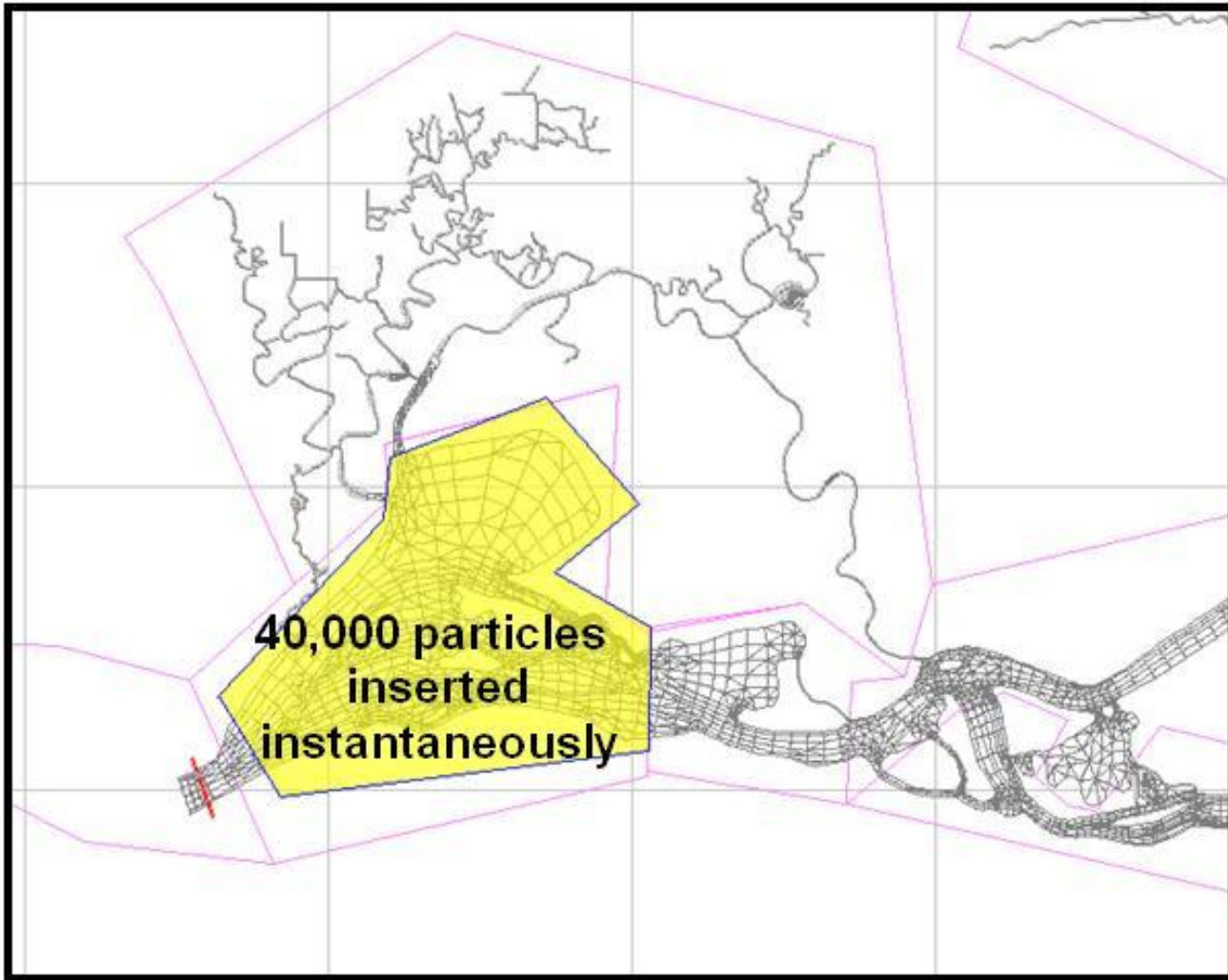


Figure 6-2 Insertion region for the delta smelt PTM model.

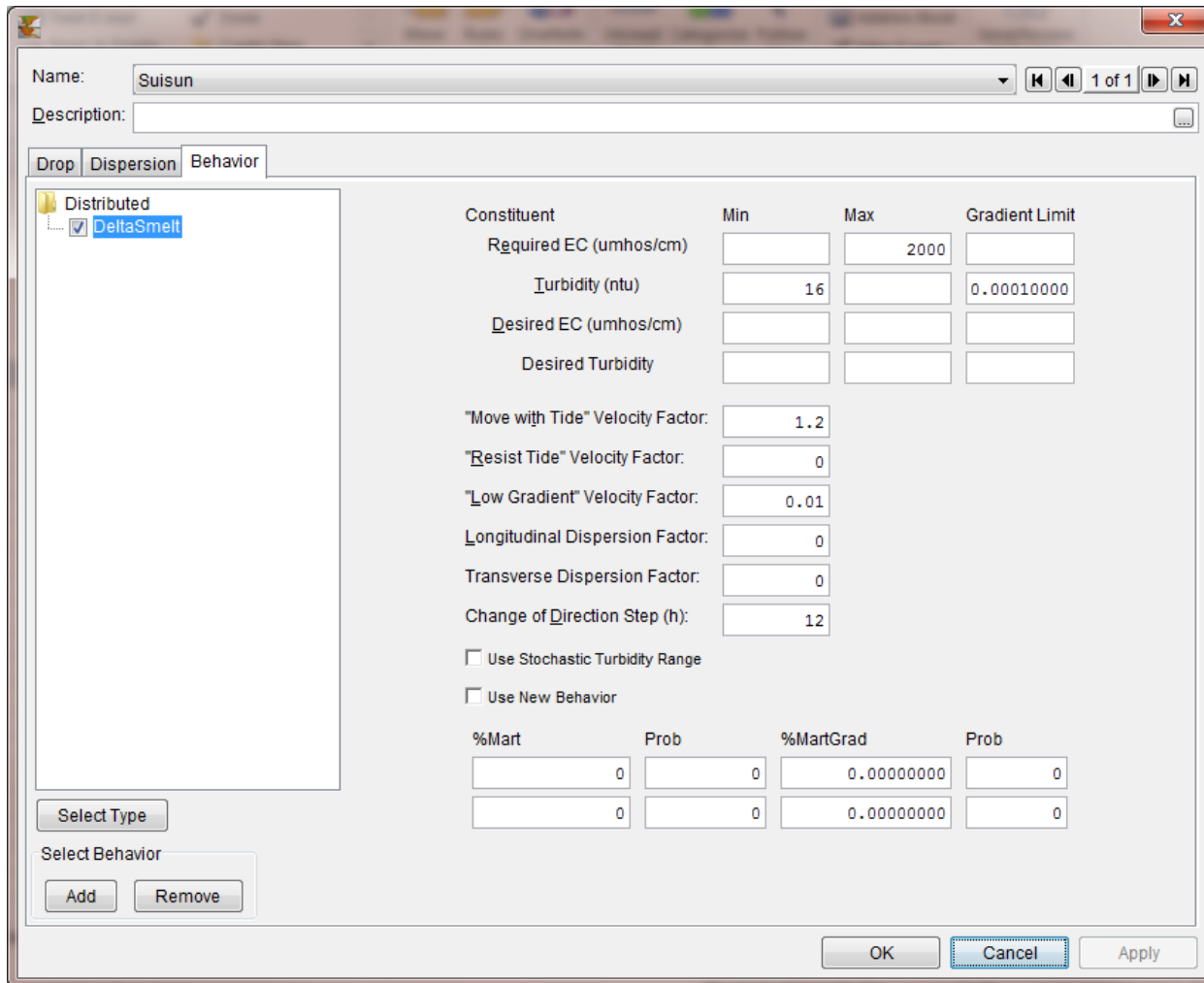


Figure 6-3 Behavioral parameters used in the delta smelt PTM Model.

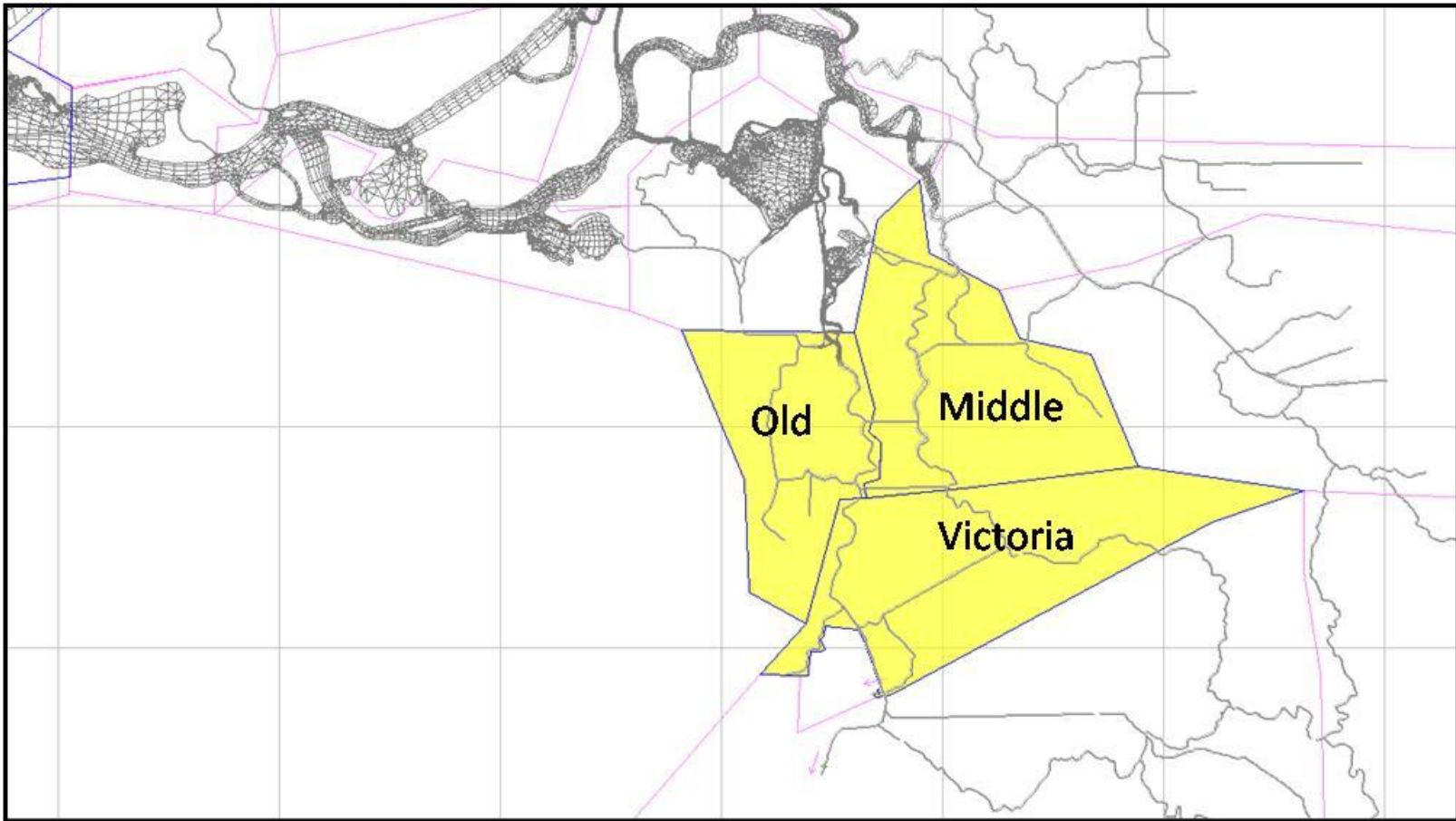


Figure 6-4 The fate of particles in the delta smelt PTM model is recorded in many regions including the three regions shown above. Particle fate is also recorded at the SWP and CVP export facilities.

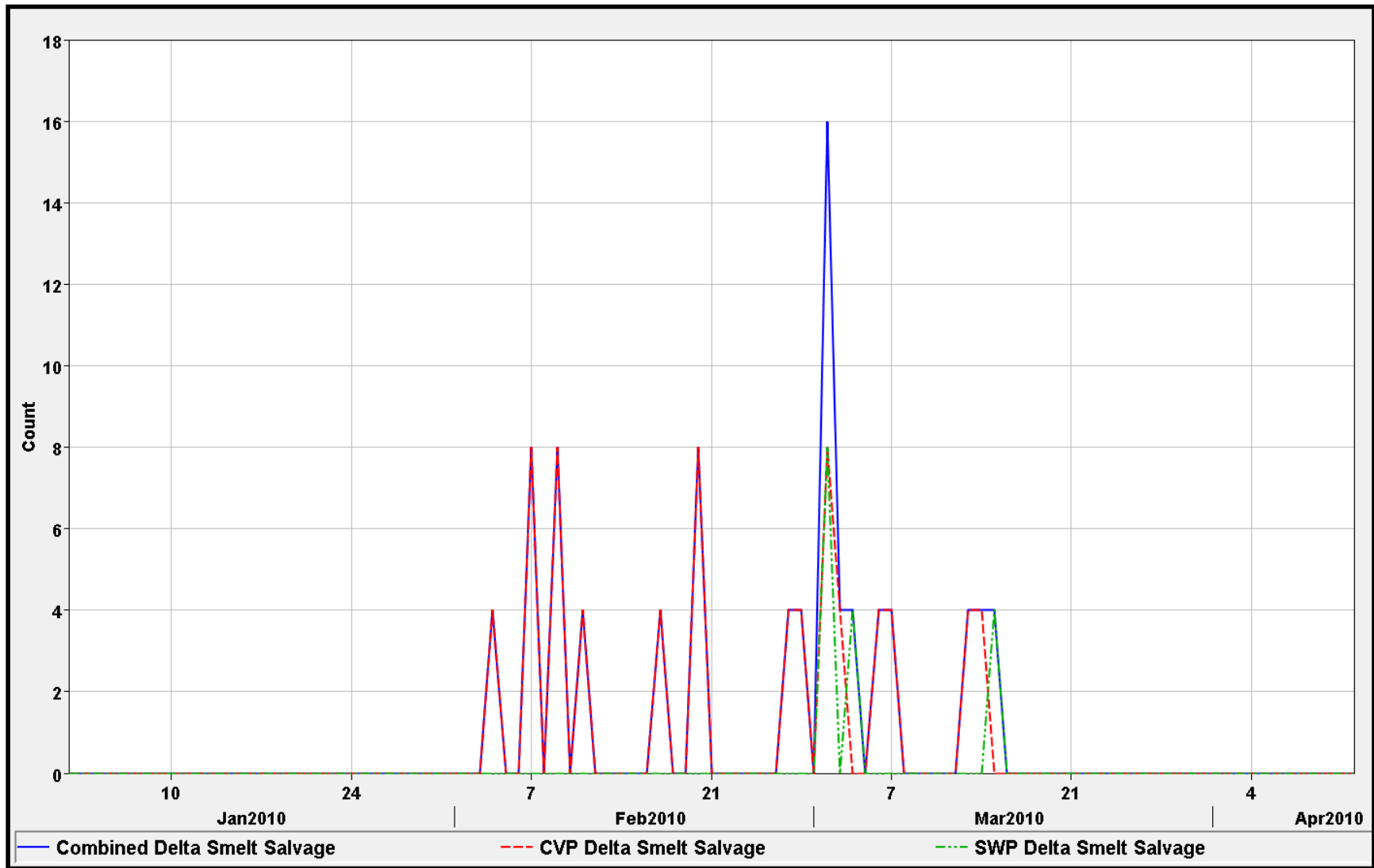


Figure 6-5 Observed delta smelt salvage combined (blue) from the state (SWP, green dash-dot) and federal (CVP red dash) fish salvage facilities January to mid-April, 2010.

7. Forecast results

The turbidity values used in forecasts documented herein used slightly different values for the flow-turbidity relationships shown in Table 4-7 for Freeport and in Table 4-8 for Vernalis, which were refined subsequent to the model simulations. The input files and model output for the six forecast periods are submitted separately in electronic format. The figures shown below illustrate methodology and results for three of the final six forecasts for flow and adult delta smelt particle tracking, respectively, and for the latter two of these forecasts for turbidity results. Selected results for the remaining three forecast are documented in Appendix III, Section 13.

7.1. Examples of flow and turbidity forecast boundary condition methodology

Figure 7-1, Figure 7-2, and Figure 7-3 illustrate the results of the methodology used to set Freeport flow forecast boundary values. The CNRFC data is downloaded, stage values are converted into forecast flow five days into the future, and then the flow is set as a constant for the remainder of the DWR forecast period.

Figure 7-4 shows a comparison of RMA-generated (red lines) and DWR-estimated (green lines) Freeport forecast inflows in comparison with data (blue lines) for these three forecast periods on 2010 – Feb 4th, Feb. 25th and April 12th. The DWR forecast is generally received a couple of days after the start of their forecast period, so the start of RMA boundary conditions based on CNRFC forecasts generally extend further into the future as additional historical data is available for the intervening period. The CNRFC forecast data reproduces the tidal variability at Freeport, so the first five days of the RMA forecast are generally superior to the DWR forecast, however for the remainder of the RMA forecast period the superior method (DWR or RMA-constant) is not clear. DWR may have forecast information from reservoir operators, so possibly have additional advance knowledge for a longer period than CNRFC.

Figure 7-5 illustrates the turbidity forecast methodology used at Freeport during these same periods. For the two February forecasts, using the 50% exceedance values proved most appropriate, while for the April 12th forecast, the 90% exceedance values were better despite lower flows at Freeport.

For the flow boundary at Vernalis on the San Joaquin River, the CNRFC forecast includes five days of observed hourly flow data and five days of forecast hourly flow data. The RMA forecast flow data from CNRFC was used directly in the forecast, and the final value was used to set a constant flow for the remainder of the RMA forecast period. Figure 7-6, Figure 7-7, and Figure 7-8 illustrate the results of the methodology used to set Vernalis flow forecast boundary values. Figure 7-9 shows a comparison of RMA-generated (red lines) and DWR-estimated (green lines) Freeport forecast inflows in comparison with data (blue lines) for these three forecast periods.

Figure 7-10 illustrates the turbidity forecast methodology used at Vernalis during these same periods. For the two February forecasts, the 50% exceedance values were used, while for the April 12th forecast, the 95% exceedance value was used for comparison. Note that flow at Vernalis was slightly higher during the April forecast period.

7.1.1. Forecast results

Results for two example forecast periods, DWR forecasts beginning on Feb. 25th and on Apr. 12th are shown in this section – the RMA forecast for the latter period beings April 14th. A more complete set of results for most of the available turbidity output locations during these periods are documented in Appendix II, Section 12. Selected results for the four remaining forecasts are also shown in Appendix III, Section 13.

Figure 7-13 shows the location of turbidity monitoring stations in the Delta – this figure should be used to reference the locations illustrated in the plots comparing model results and turbidity or flow data in this section and in the Appendices.

7.1.2. February 25th forecast

In this period, Vernalis experienced a relatively high flow but low turbidity regime, while Freeport experienced an intermediate flow and intermediate turbidity regime. Turbidity forecast boundary conditions for Freeport and Vernalis were each set at 50% exceedance levels (Figure 7-5 and Figure 7-10, respectively).

Figure 7-12 shows computed three-day average turbidity at three Delta locations, Prisoner Point, Holland Cut and Victoria Canal. According to the Biological Opinion for delta smelt, there is a turbidity trigger limiting Old+Middle River flows (OMR flows), known as FWS RPA Component 1 or simply RPA 1, based on turbidity conditions at these three locations in the Delta. When the three-day-average turbidity is ≥ 12 NTU at each of the three stations, RPA 1 is triggered and OMR flow must be moderated. During this period, as Victoria Canal turbidity never reaches 12 NTU, so RPA 1 was never triggered.

Figure 7-14 through Figure 7-20 illustrate selected model results during the period January 01 – March 15, 2010, with the upper plot comparing 15-min data (turquoise) and model (red) output and the lower plot comparing three-day forward moving averages of data and model. In Appendix II, Section 12 shows a full set of flow and turbidity results for this model period. During the forecast period, the high modeled turbidity at Rio Vista (Figure 7-14) is due to the high, constant values set for the Freeport BC inflow and turbidity. However, as shown in 15-min and the moving average turbidity plots, outside of the forecast period, the model and data were extremely close in timing and magnitude.

At Jersey Point, Figure 7-15 shows the effects of meteorological forcing, such as sediment resuspension due to wind events, are evident as specific events that cause a mismatch between

data and model. However, outside of these events, the model/data match is still quite good. Similar features are seen at Antioch (Figure 7-16), although here the effects of the low turbidity initial condition are seen in the low modeled turbidity at the beginning of the modeled period. Once the turbidity event moves down the Sacramento R. to Antioch, the data/model turbidity match improves. Figure 7-17 and Figure 7-18 illustrate results on Middle R. (Holt) and on Old R. (Bacon), respectively, in the Central Delta. The effects of meteorological forcing are still evident, although subdued. Modeled turbidity is high outside of these periods. At Grant Line Canal (Figure 7-19), the timing of the turbidity pulse from the Vernalis BC traveling down Old River is excellent, including stage effects, but significant sediment settling has taken place during the initial turbidity pulse that is not captured in the model. Data in Clifton Court (Figure 7-20) is compared with model output at SWP since the RMA model domain does not include Clifton Court.

7.1.3. April 14th forecast

In this modeled period, Vernalis experienced a relatively high flow, low turbidity regime similar to the Feb. 25th period, while Freeport again experienced an intermediate flow, but lower flow higher turbidity regime in comparison with Feb. 25th. Turbidity forecast boundary conditions for Freeport and Vernalis were set at 90% and 95% exceedance levels, respectively (Figure 7-5 and Figure 7-10).

Figure 7-21 through Figure 7-27 illustrate selected results during the period January 01 – May 03, 2010, with the upper plot comparing 15-min data (turquoise) and model (red) output and the lower plot comparing three-day forward moving averages of data and model. In Appendix II, Section 12 shows a full set of flow and turbidity results for this model period. At Rio Vista (Figure 7-21), we can see that the forecast period estimate of turbidity at Freeport was too low. At Grant Line (Figure 7-26), we can see that the forecast pulse of turbidity at Vernalis was too high. Model results are mixed at Antioch (Figure 7-23), Middle R. (Figure 7-24), Old River (Figure 7-25) and Jersey Point (Figure 7-22). Data in Clifton Court (Figure 7-27) is compared with model output at SWP since the RMA model domain does not include Clifton Court.

The moderate levels of turbidity at Freeport and at Vernalis do not produce any significant turbidity influence in the central Delta for this forecast.

7.2. Adult delta smelt model results

During the model forecast periods, delta smelt were salvaged at both the state and federal facilities, as shown in Figure 6-5, but the numbers were very small. It is important to note that despite concurrent sizable flow and turbidity events on the Sacramento and San Joaquin Rivers that traveled into the lower San Joaquin River and into the south Delta, respectively, a “turbidity bridge” never formed in the central Delta to entice delta smelt into the south Delta. Similarly, modeled turbidity never reached the Central and south Delta in concentrations high enough to

form a “turbidity bridge” to the export locations. As a consequence, in the adult delta smelt particle tracking model very few particles reached the export locations.

Figure 7-28 shows a comparison of adult delta smelt particle tracking model results for the Feb. 11th forecast. No particles reached the SWP or CVP export locations, but a small number of the 40,000 inserted particles make it into the south and central Delta in the Old, Middle and Victoria regions. Only a few delta smelt were salvaged at the export pumps during this period, as shown in the lower plot in Figure 7-28. Particle tracking results using the adult delta smelt behavior model in the south and central Delta regions are shown in the upper plot of Figure 7-28 - the timing of particles reaching these regions is very similar to salvage data.

Figure 7-29 shows a comparison of adult delta smelt particle tracking model results for the Feb. 25th forecast, which are very similar to the Feb. 11th forecast. No particles reached the SWP or CVP export locations, but a small number of the 40,000 inserted particles make it into the south and central Delta in the Old, Middle and Victoria regions.

Figure 7-30 and Figure 7-31 illustrate the adult delta smelt particle tracking model results for the Apr. 14th forecast. In this forecast period, (Figure 7-31), a few particles reach the export locations. The percentage of inserted particles reaching the pumps is low, and the timing of those particles that reach the pumps is somewhat delayed in comparison with the salvage data.

Figure 7-32 shows particle tracking results in the RMA Delta grid at two times, February 10th and March 10th. By February 10th, particles had moved into the central Delta following the adult delta smelt model turbidity cues, but only a few reach the south Delta. By March 10th, those few particles that had earlier moved into the south Delta and were “waiting” there, saw the increased turbidity to the south at this time, moved toward the pumps and were entrained as shown in Figure 7-31 model results (upper plot).

Additional adult delta smelt particle tracking model results are given in Appendix I, Section 11.3.3.

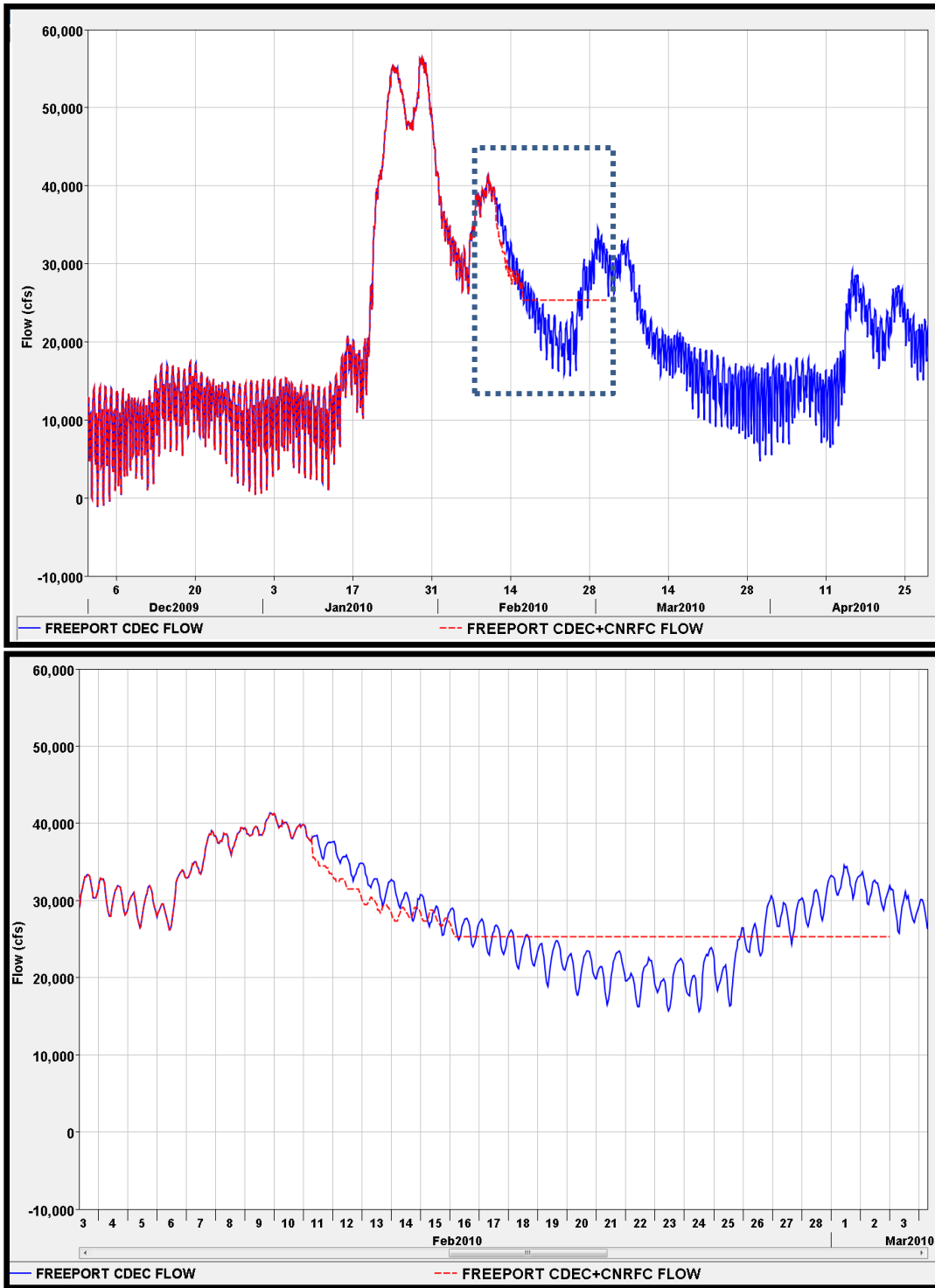


Figure 7-1 Three-week flow forecast period at Freeport February 11 – March 01, 2010.

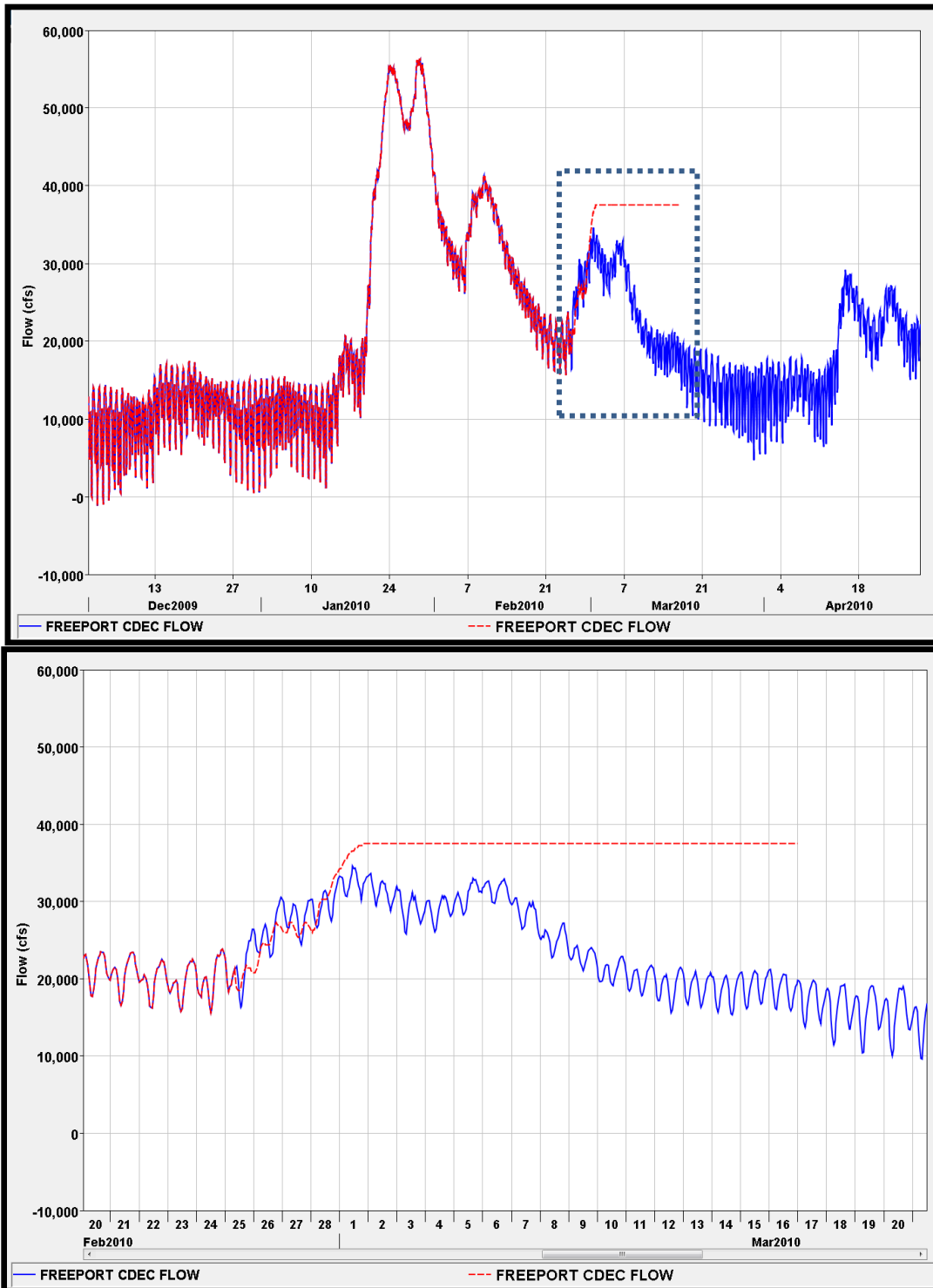


Figure 7-2 Three-week flow forecast period at Freeport February 25 – March 15, 2010.

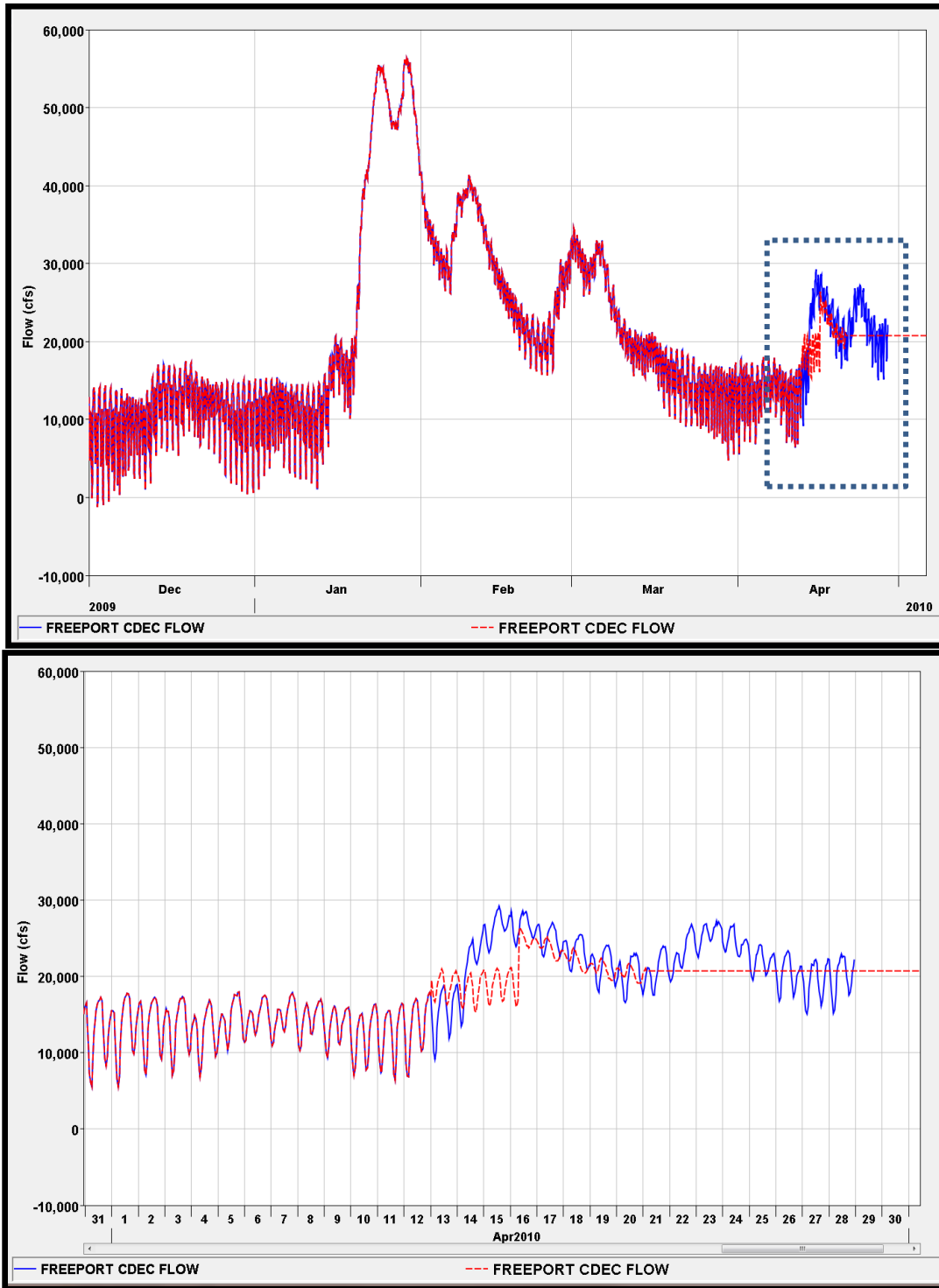


Figure 7-3 Three-week flow forecast period at Freeport April 12 – May 03, 2010.

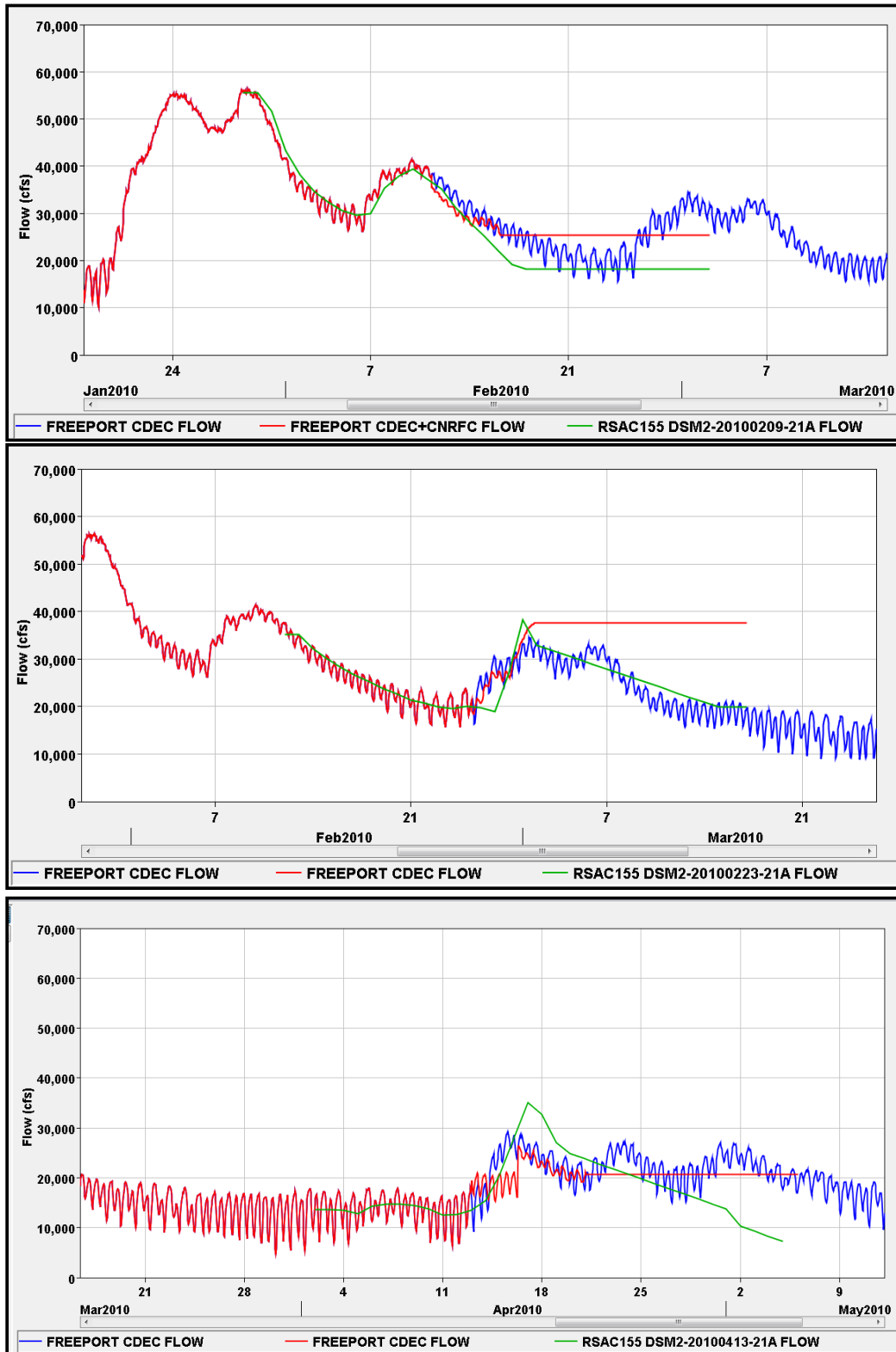


Figure 7-4 Comparison of Freeport flow data (blue) vs. forecast, RMA (red) and DWR (green), for forecast periods starting Feb. 11th, Feb. 25th, and April 14th (top to bottom).

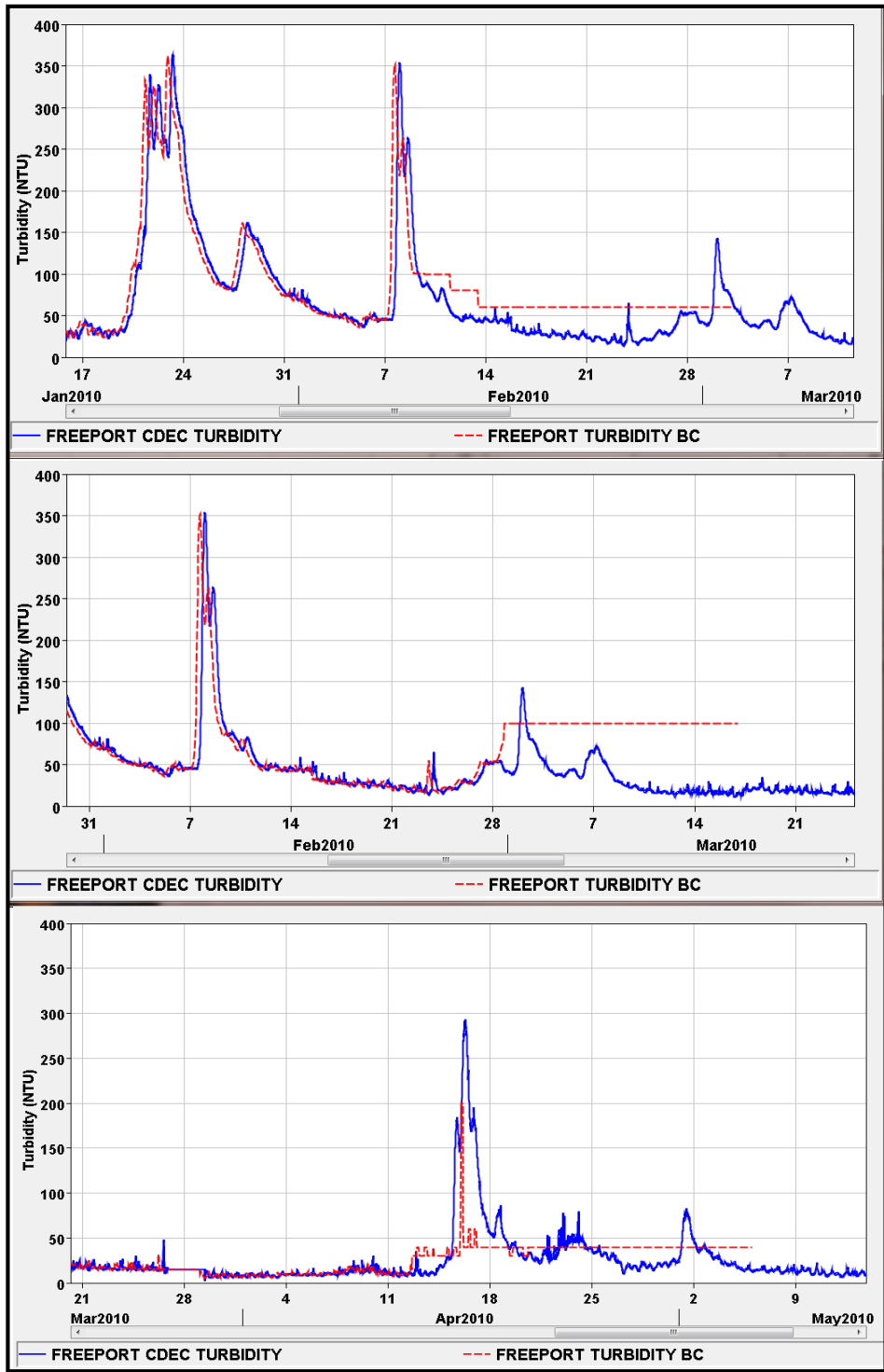


Figure 7-5 Freeport turbidity 50% exceedance forecast – Feb. 11th, 25th (top and center plots) and 90% exceedance forecast April 14th (bottom plot).

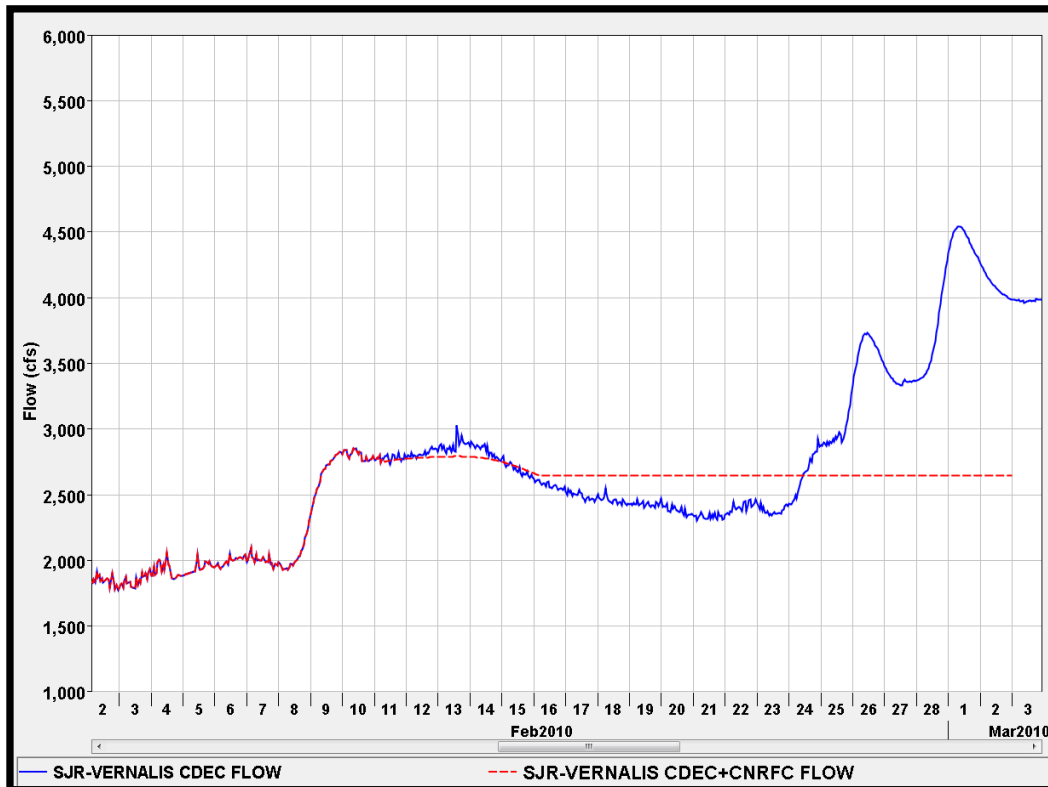
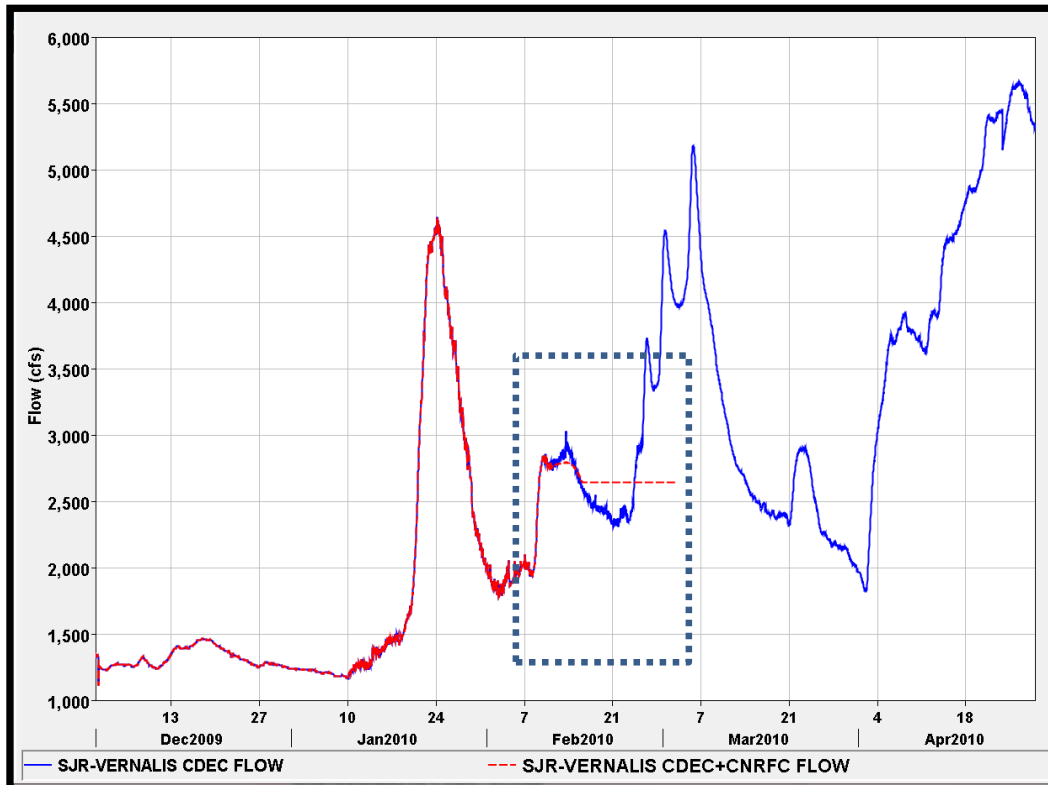


Figure 7-6 Three-week flow forecast period at Vernalis was February 11 – March 01, 2010.

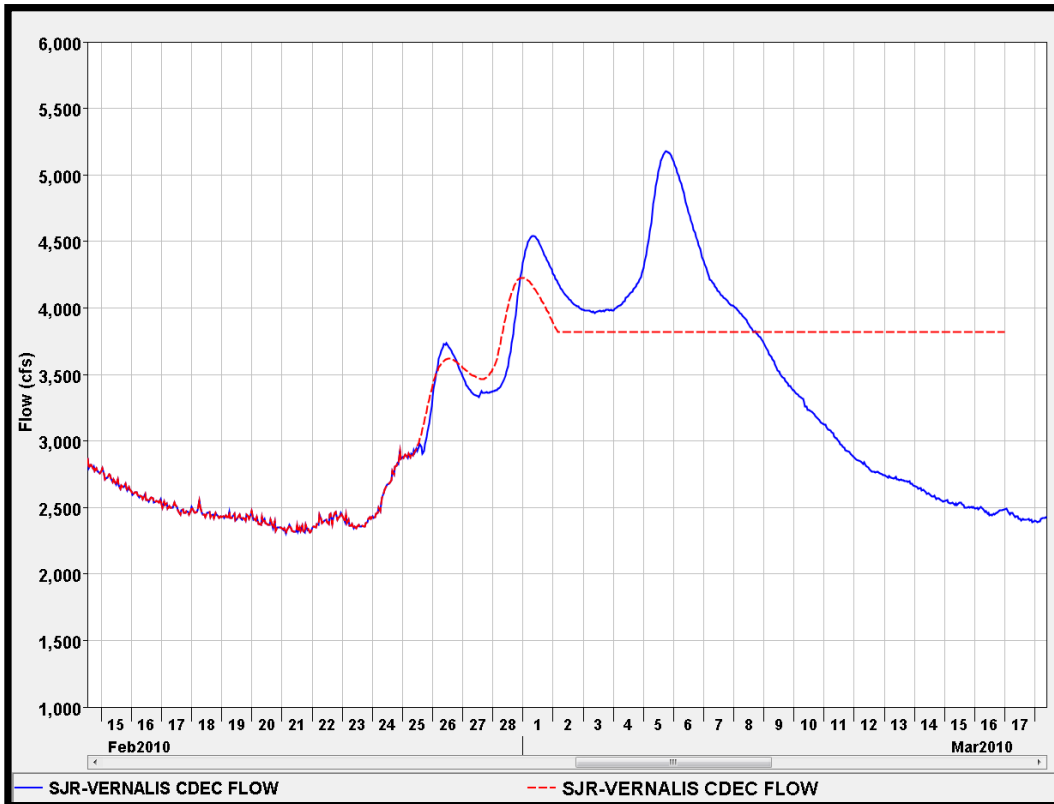
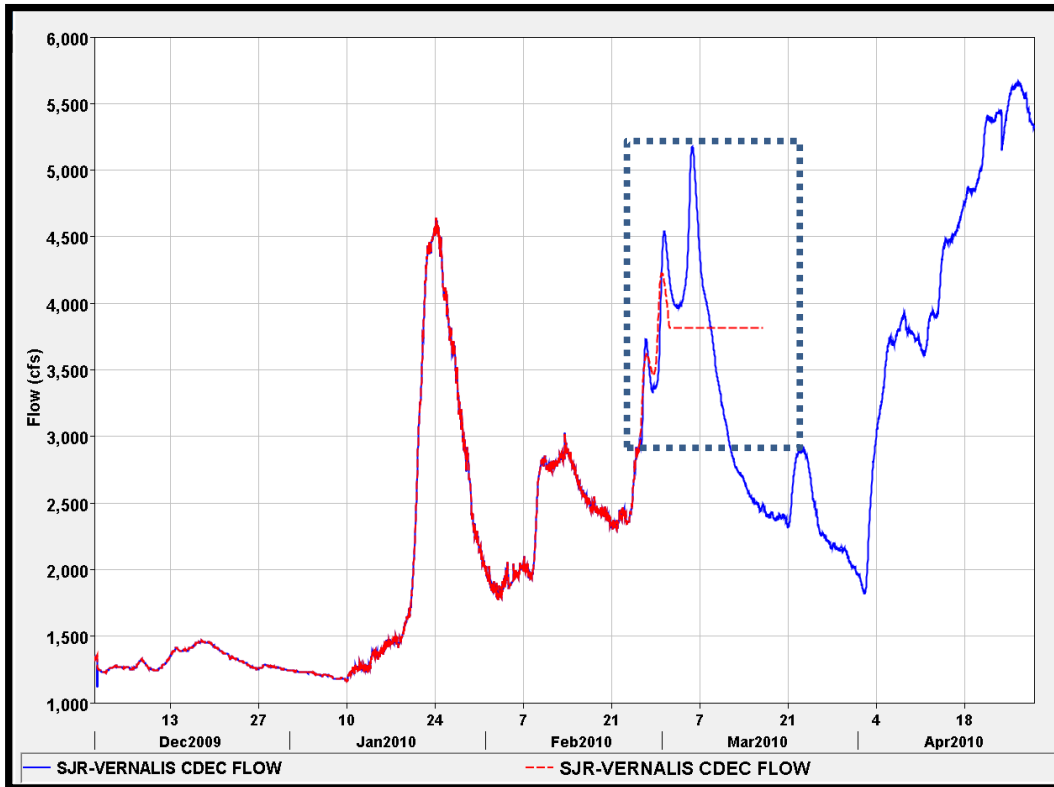


Figure 7-7 Three-week flow forecast period at Vernalis February 25 – March 15, 2010.

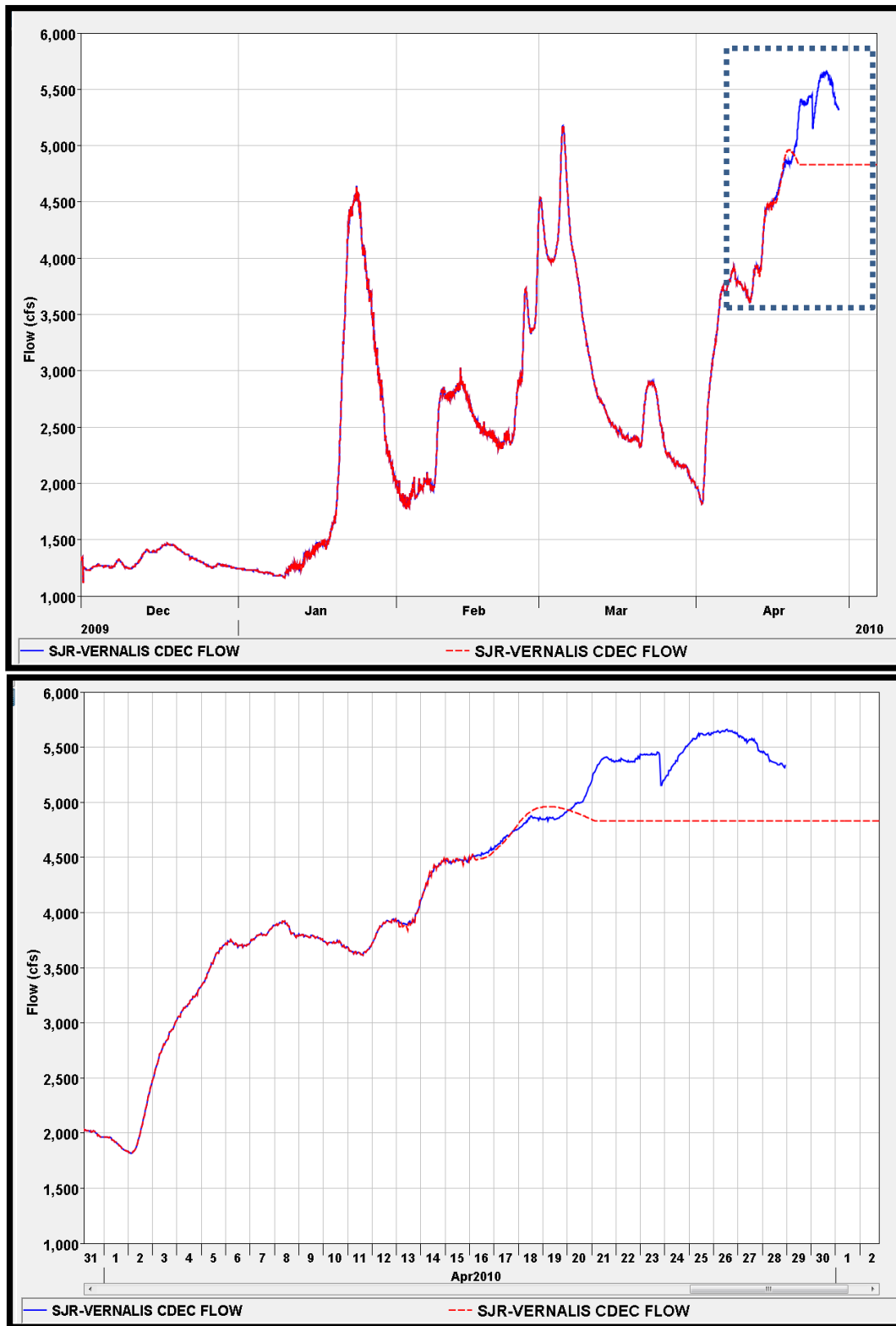


Figure 7-8 Three-week flow forecast period at Vernalis April 12 – May 03, 2010.

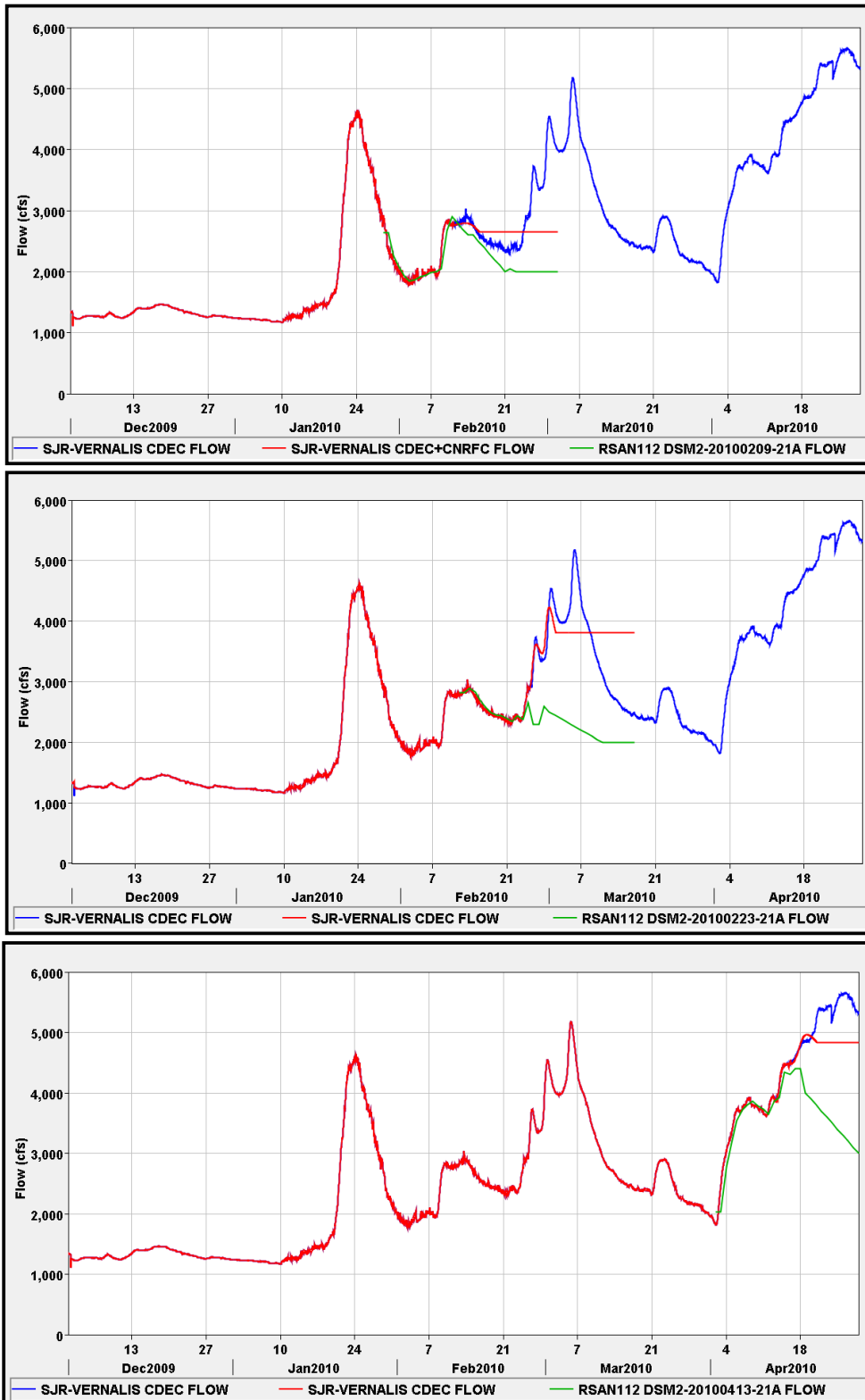


Figure 7-9 Comparison of RMA (red) and DWR (green) Vernalis flow for forecast periods starting Feb. 11th, Feb. 25th, and April 14th (top to bottom).

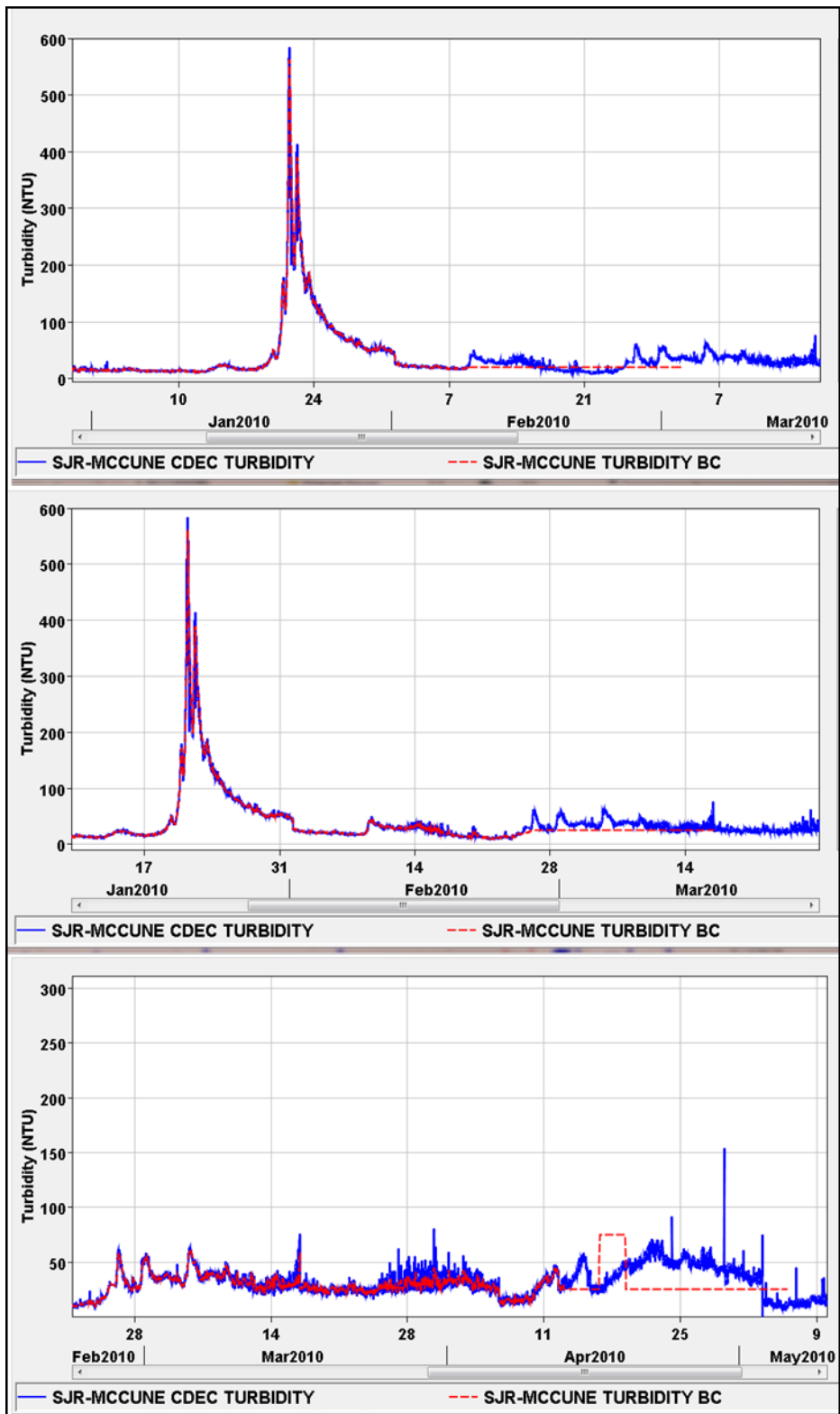


Figure 7-10 Vernalis turbidity 50% exceedance forecast Feb 11th, 25th and 95% exceedance estimate April 14th (top to bottom).

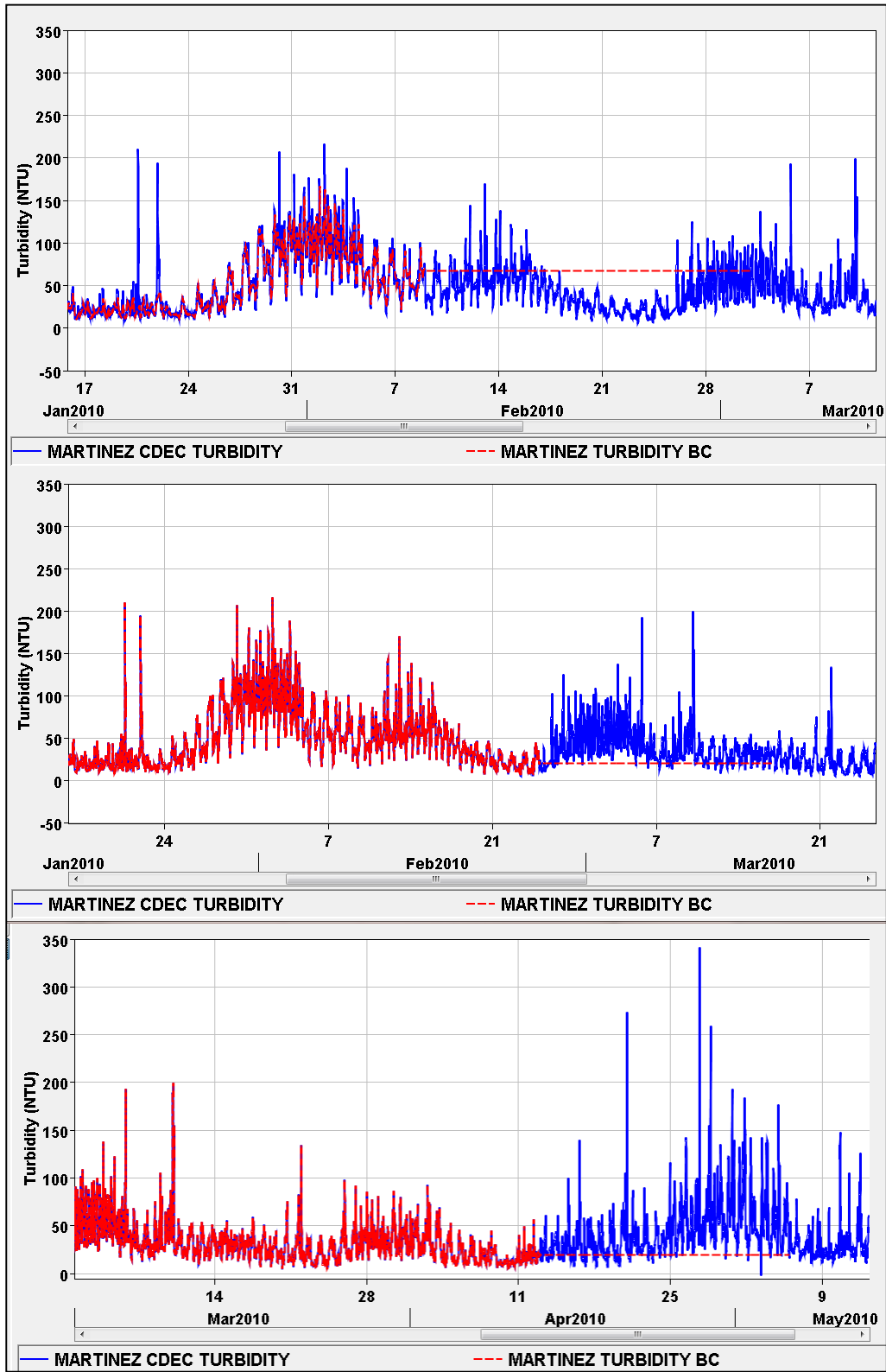


Figure 7-11 Martinez turbidity forecast – Feb 11th, 25th and April 14th (top to bottom).

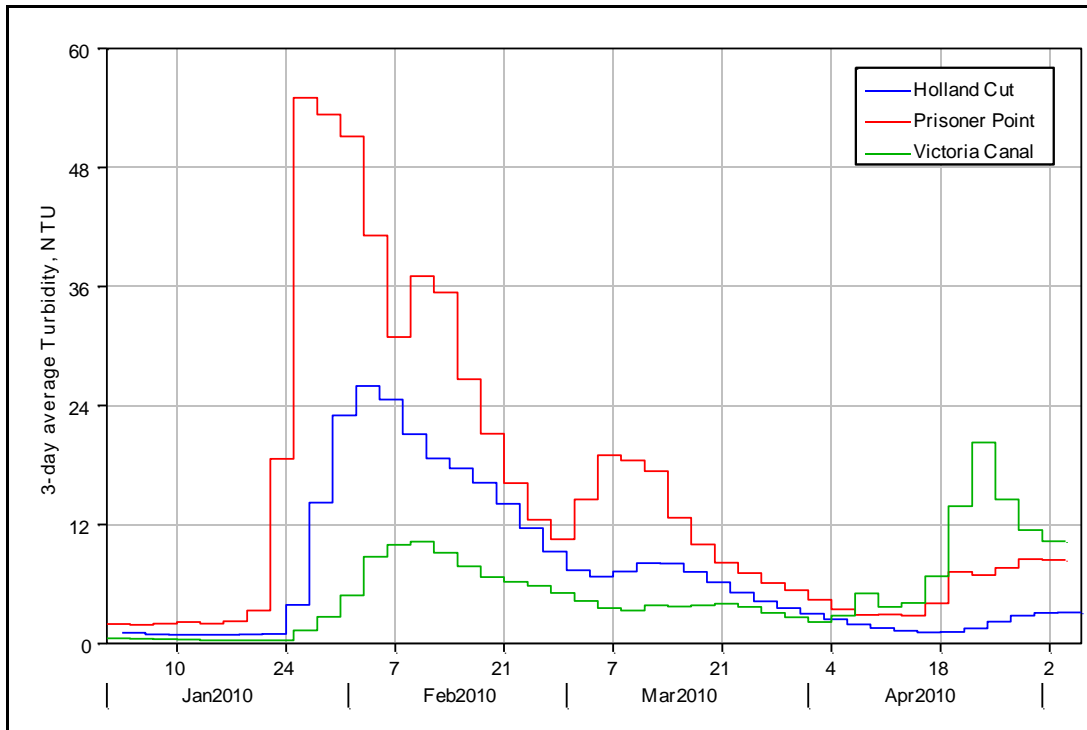


Figure 7-12 Computed 3-day average turbidity at Holland Cut, Prisoner Point and Victoria Canal.

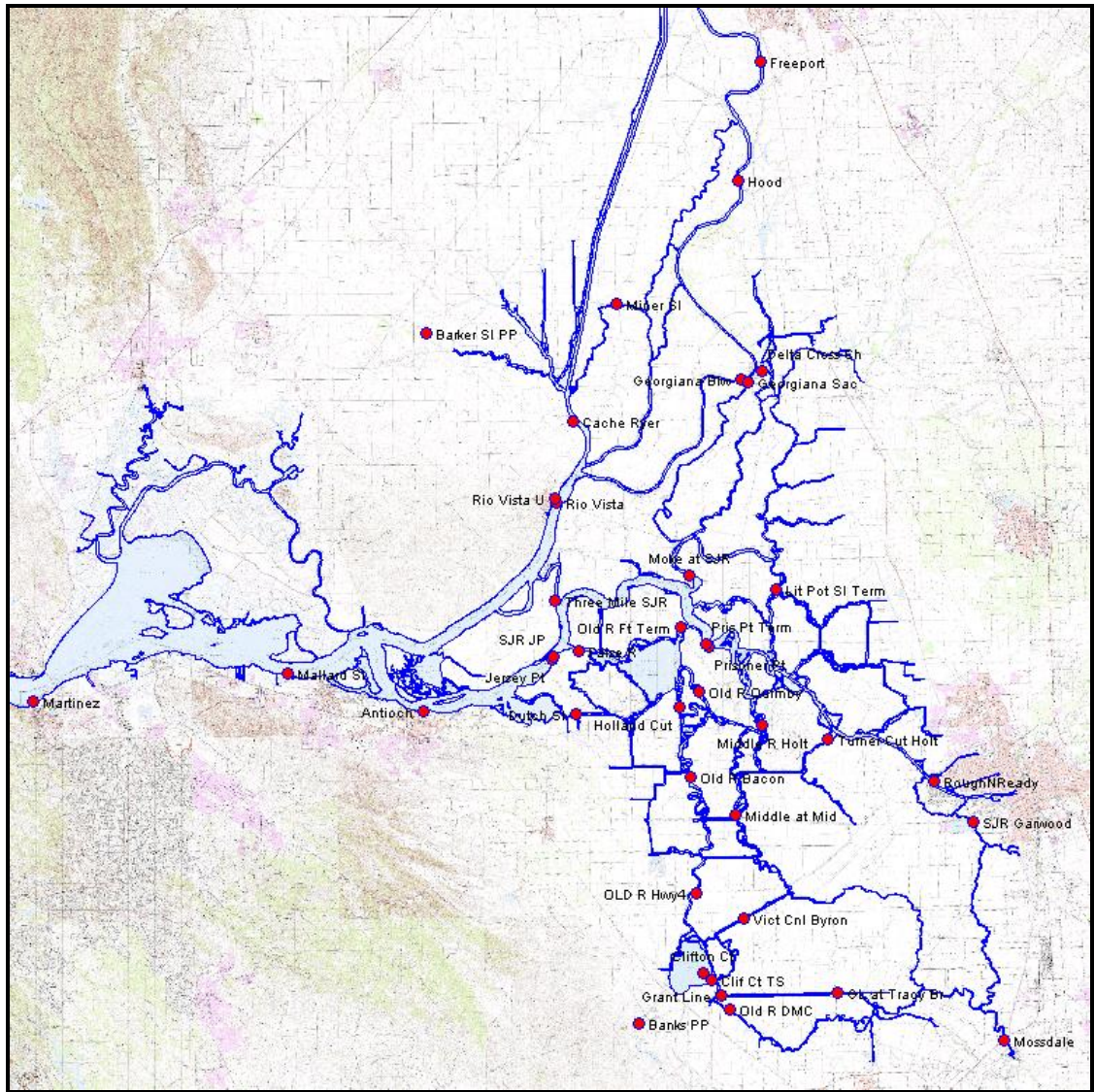


Figure 7-13 Location of turbidity monitoring stations in the Delta.

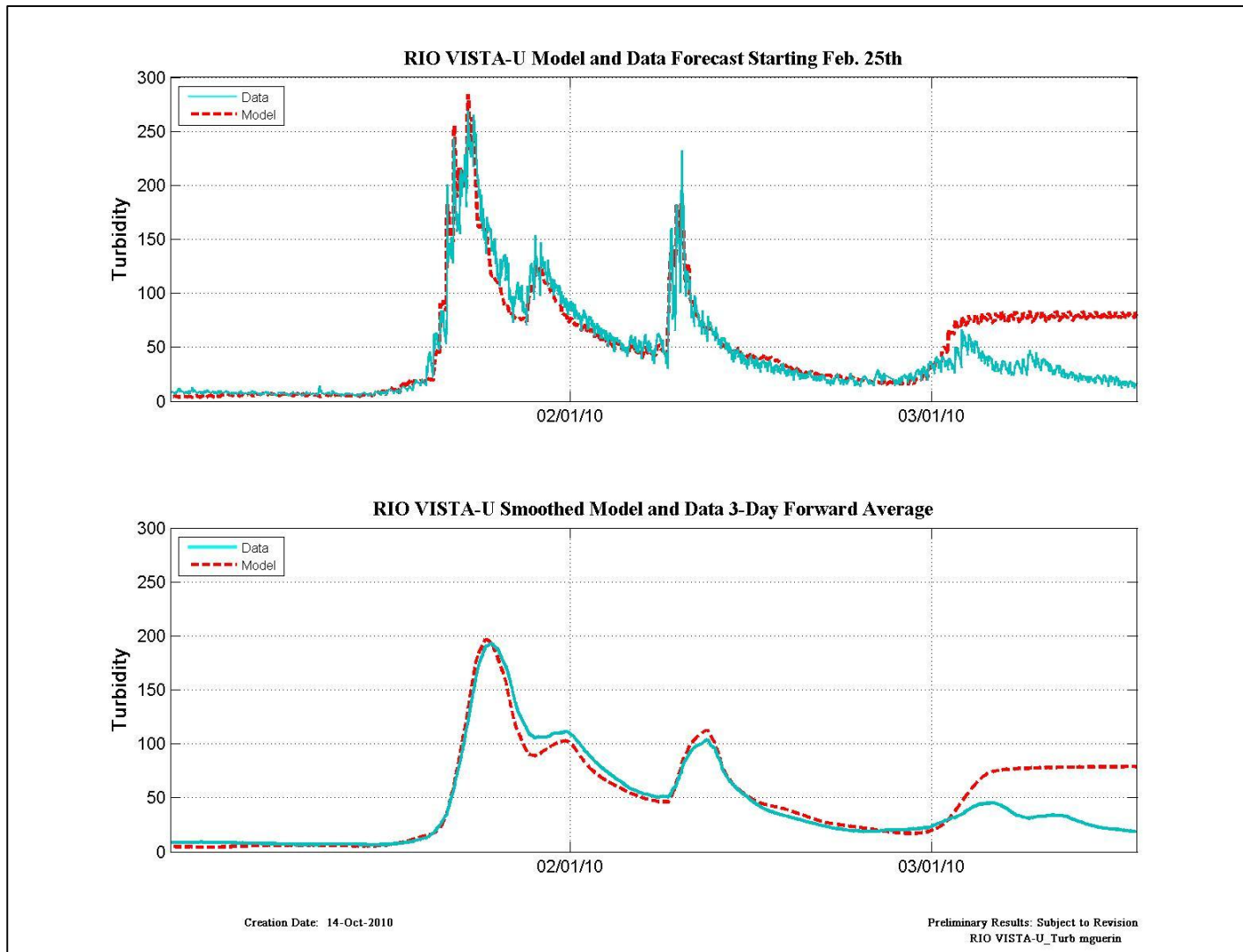


Figure 7-14 Turbidity data and model results for the forecast beginning Feb 25th at Rio Vista.

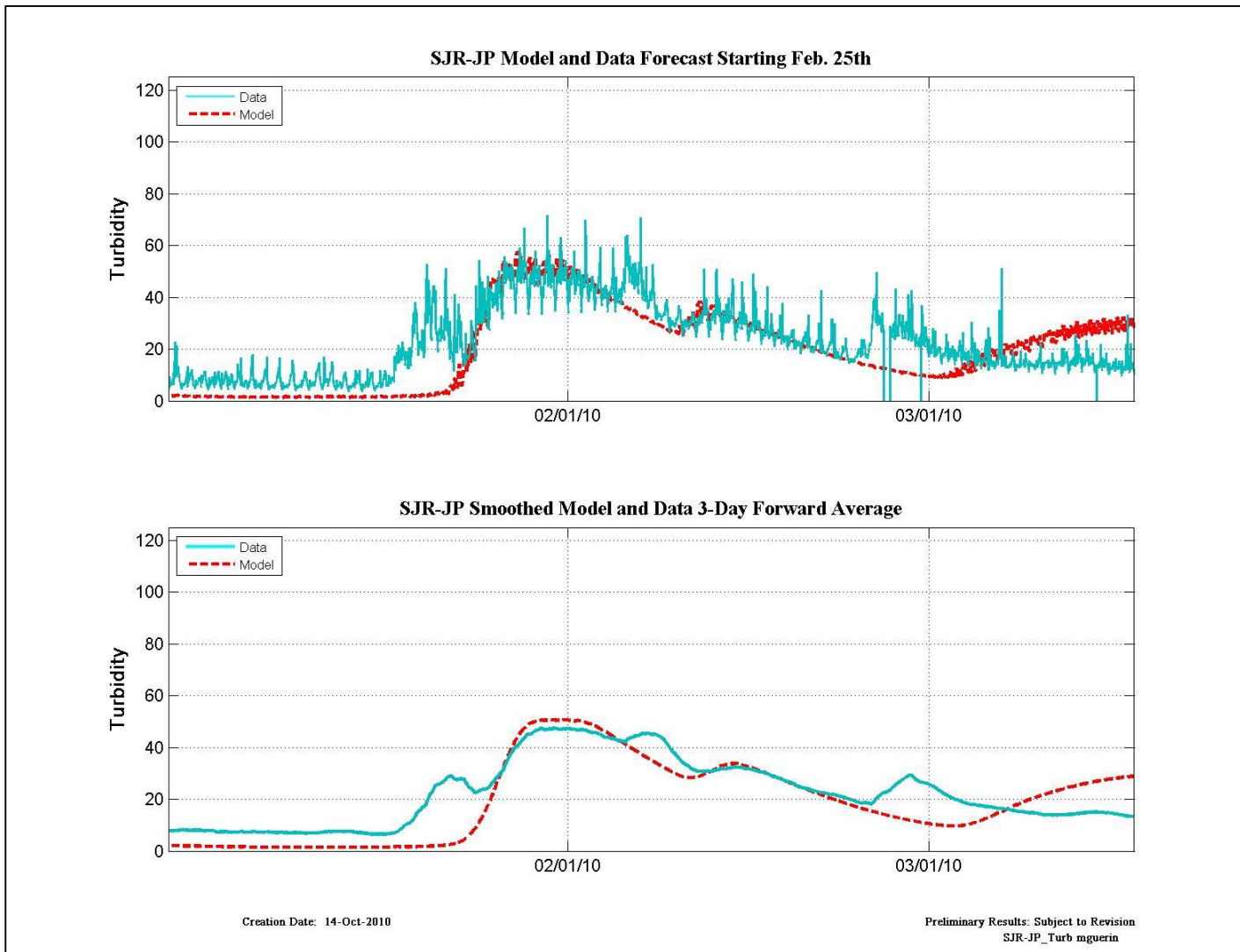


Figure 7-15 Turbidity data and model results for the forecast beginning Feb 25th at SJR-JP.

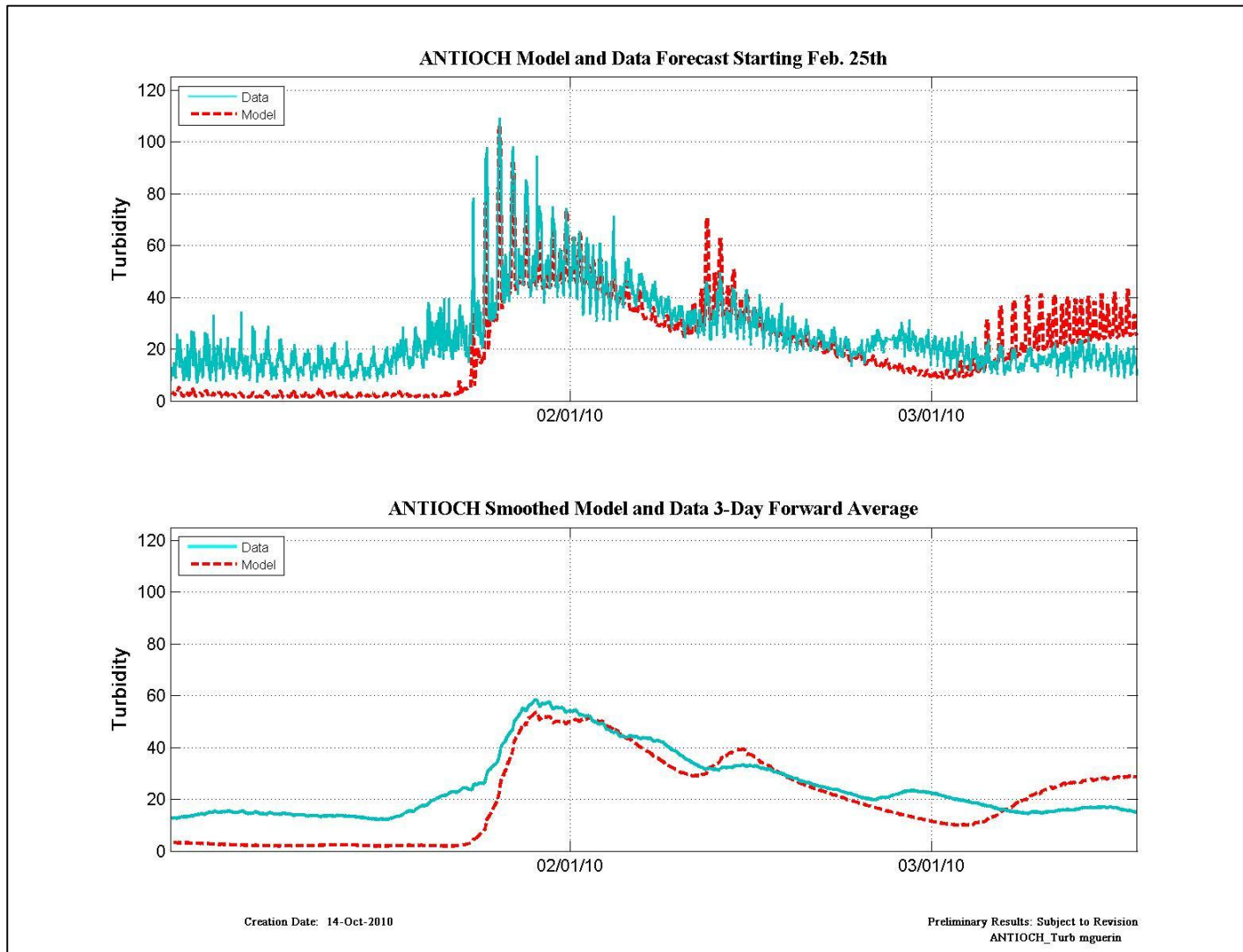


Figure 7-16 Turbidity data and model results for the forecast beginning Feb 25th at Antioch.

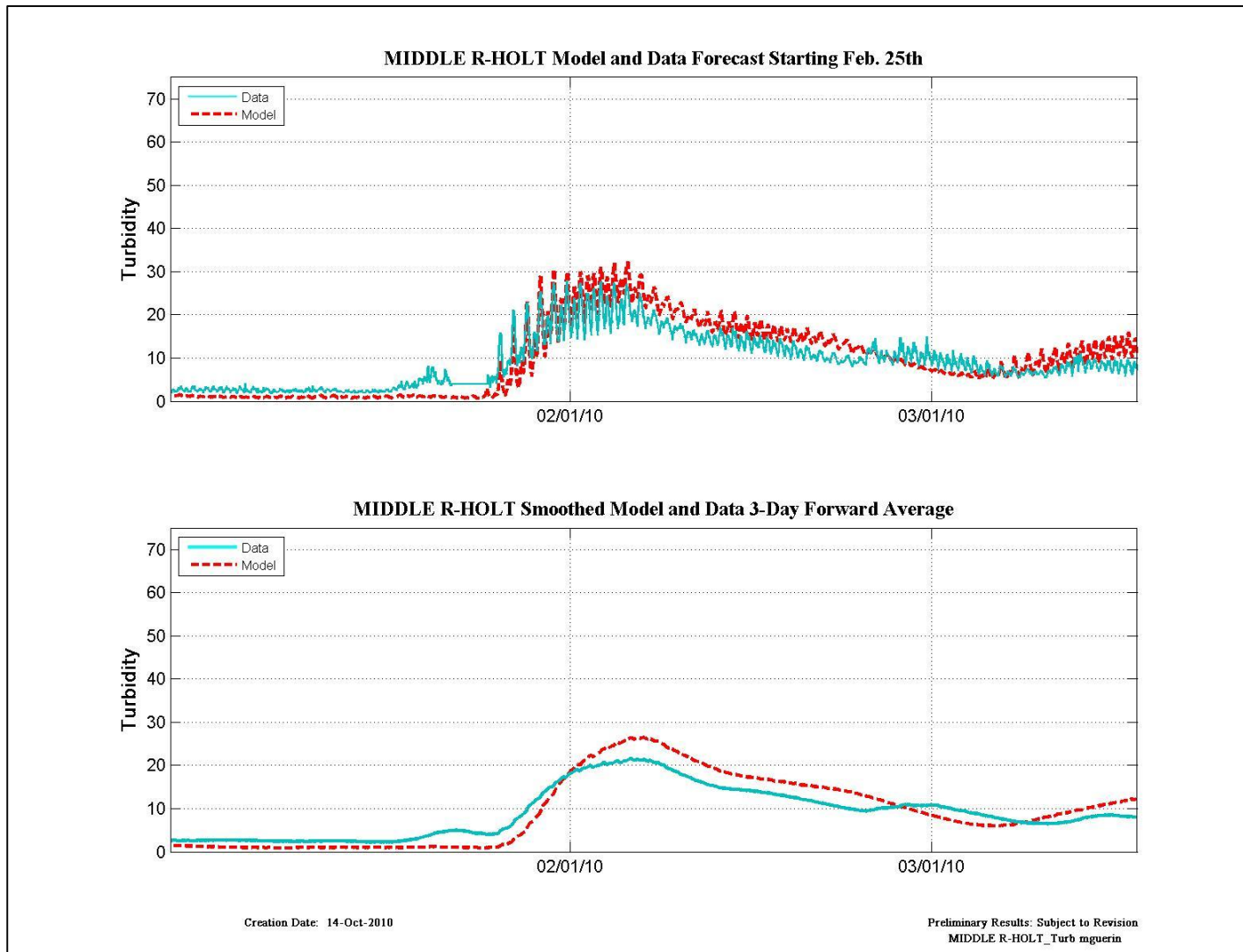


Figure 7-17 Turbidity data and model results for the forecast beginning Feb 25th at Middle R-Holt.

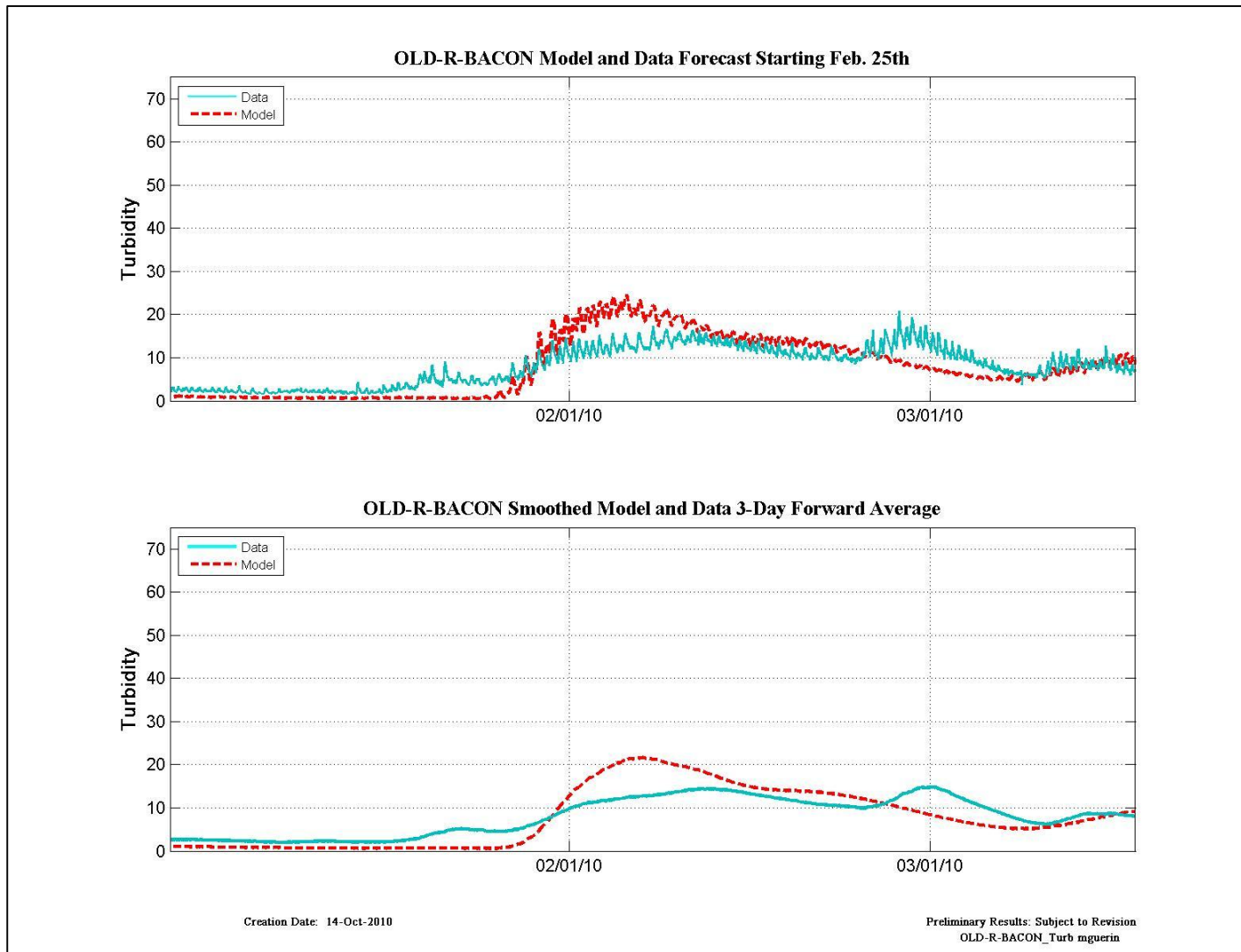


Figure 7-18 Turbidity data and model results for the forecast beginning Feb 25th at Old-R-Bacon.

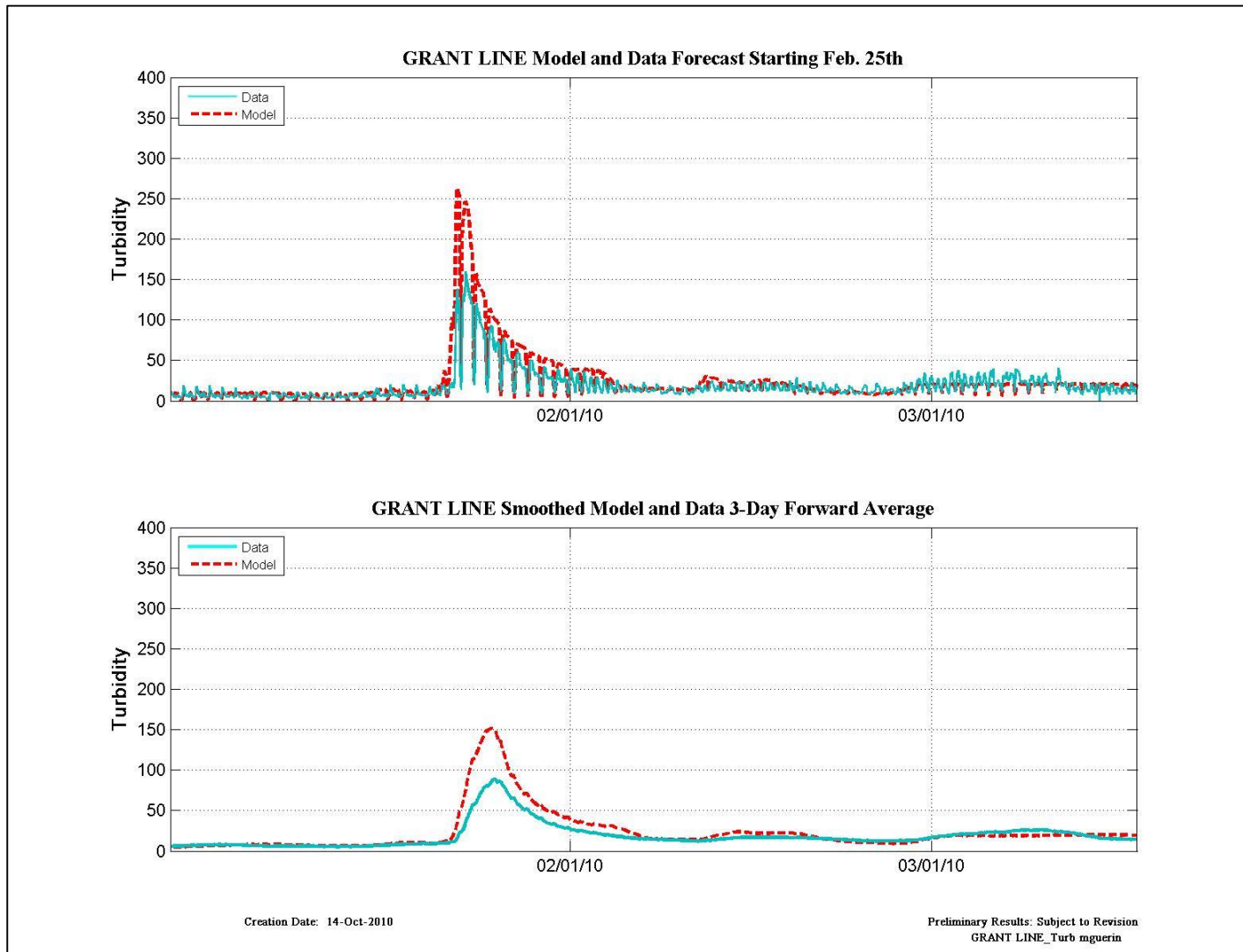


Figure 7-19 Turbidity data and model results for the forecast beginning Feb 25th at Grant Line.

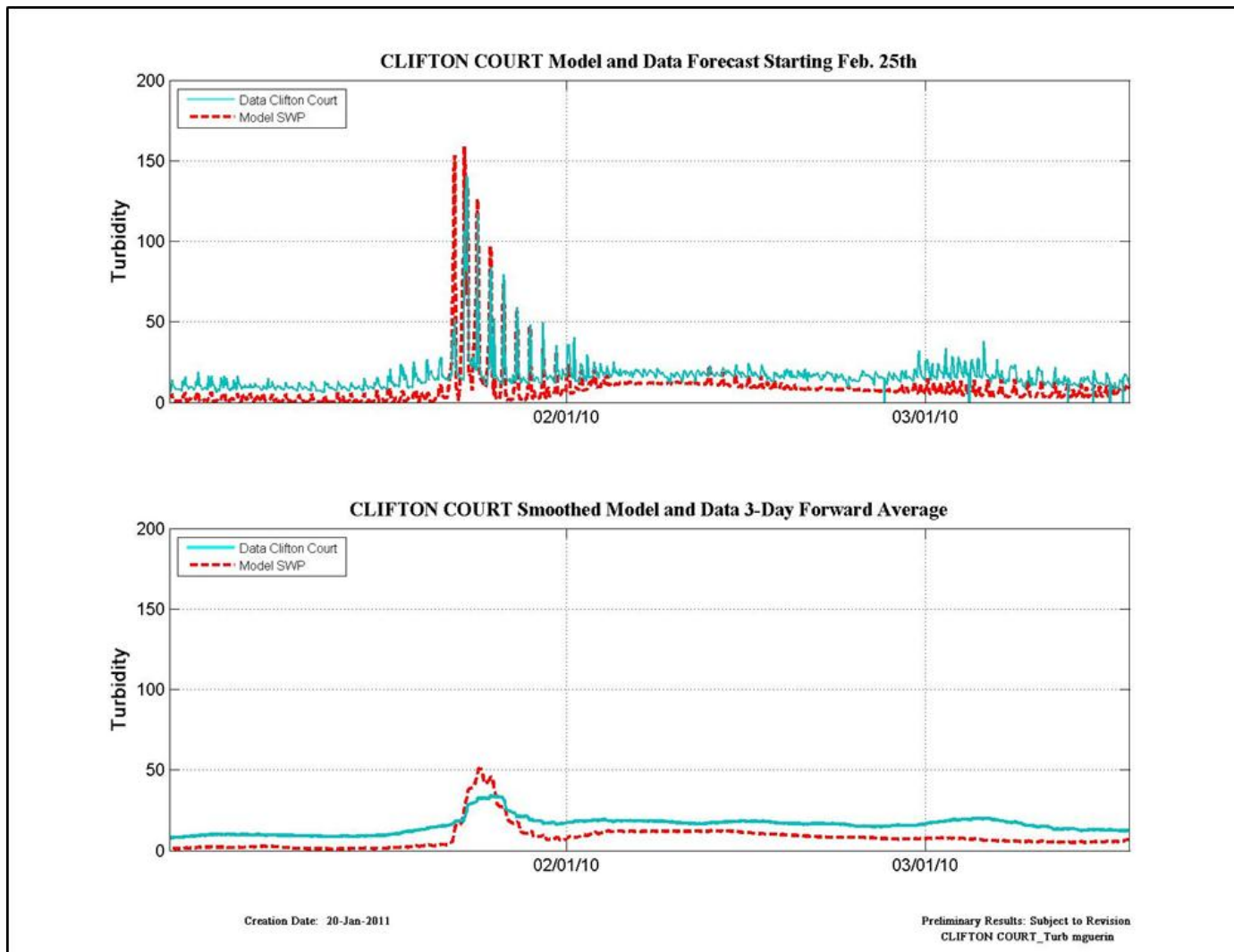


Figure 7-20 Turbidity data and model results for the forecast beginning Feb 25th at Clifton Court (data) and SWP (model).

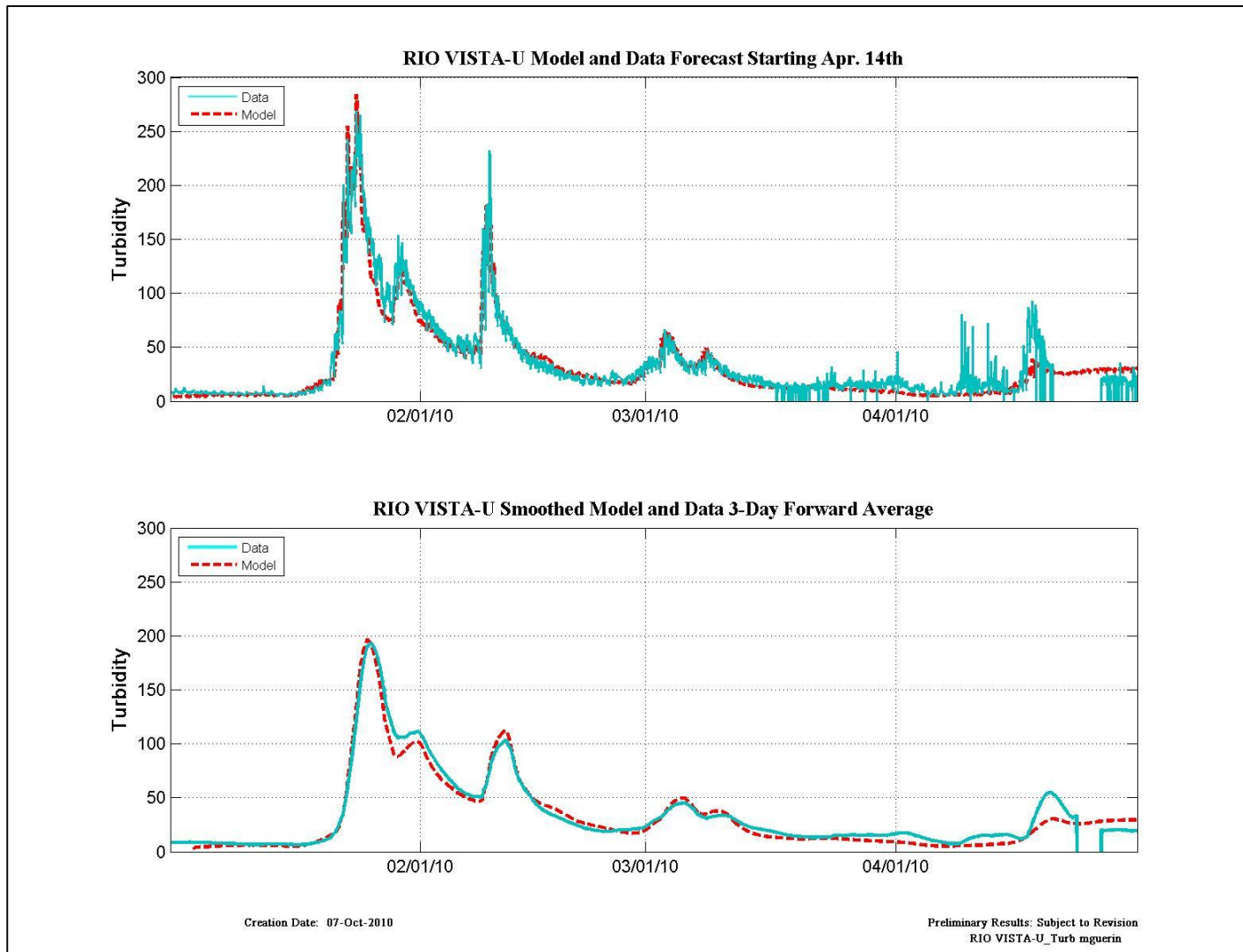


Figure 7-21 Turbidity data and model results for the forecast beginning April 14th at Rio Vista-U.

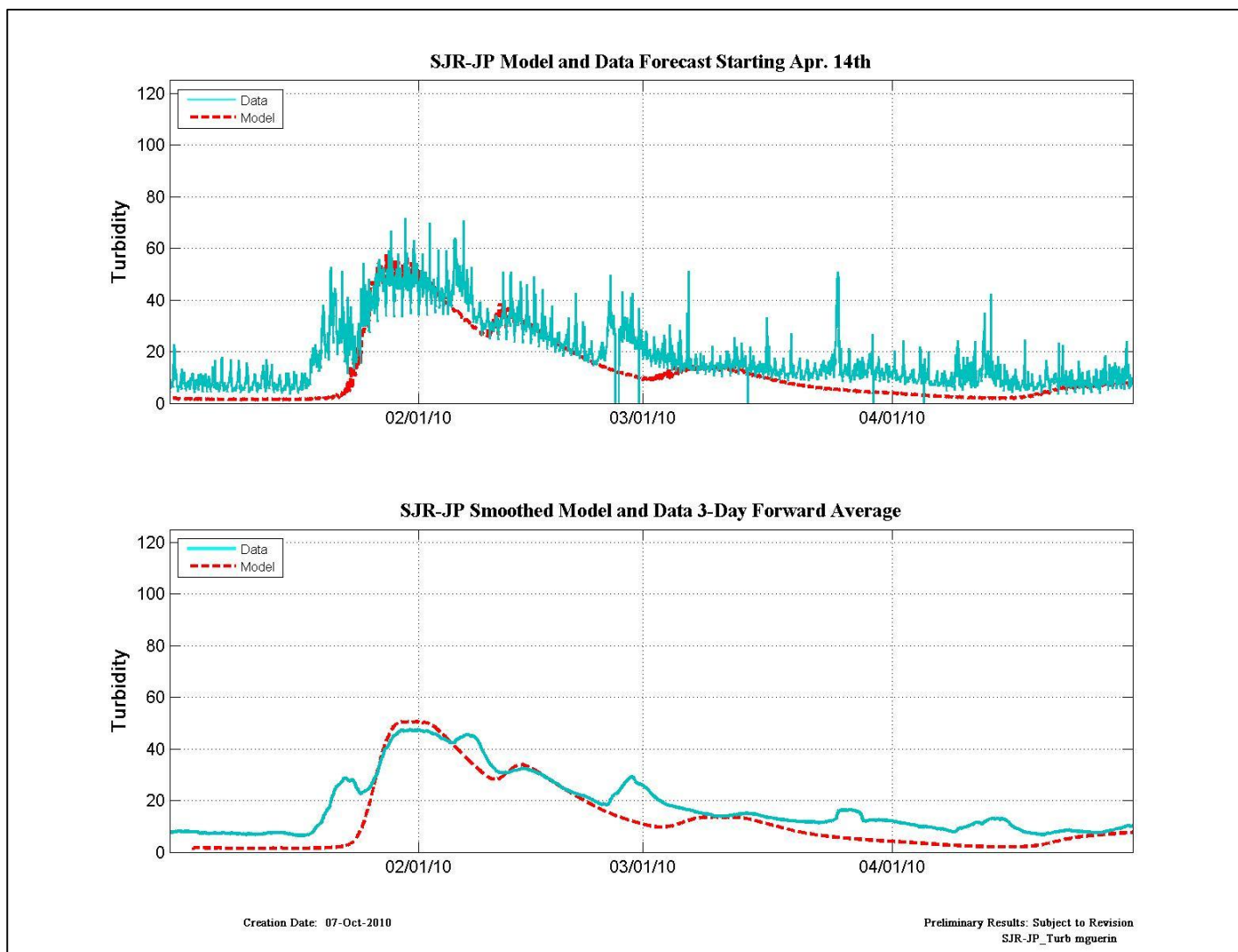


Figure 7-22 Turbidity data and model results for the forecast beginning April 14th at SJR-JP.

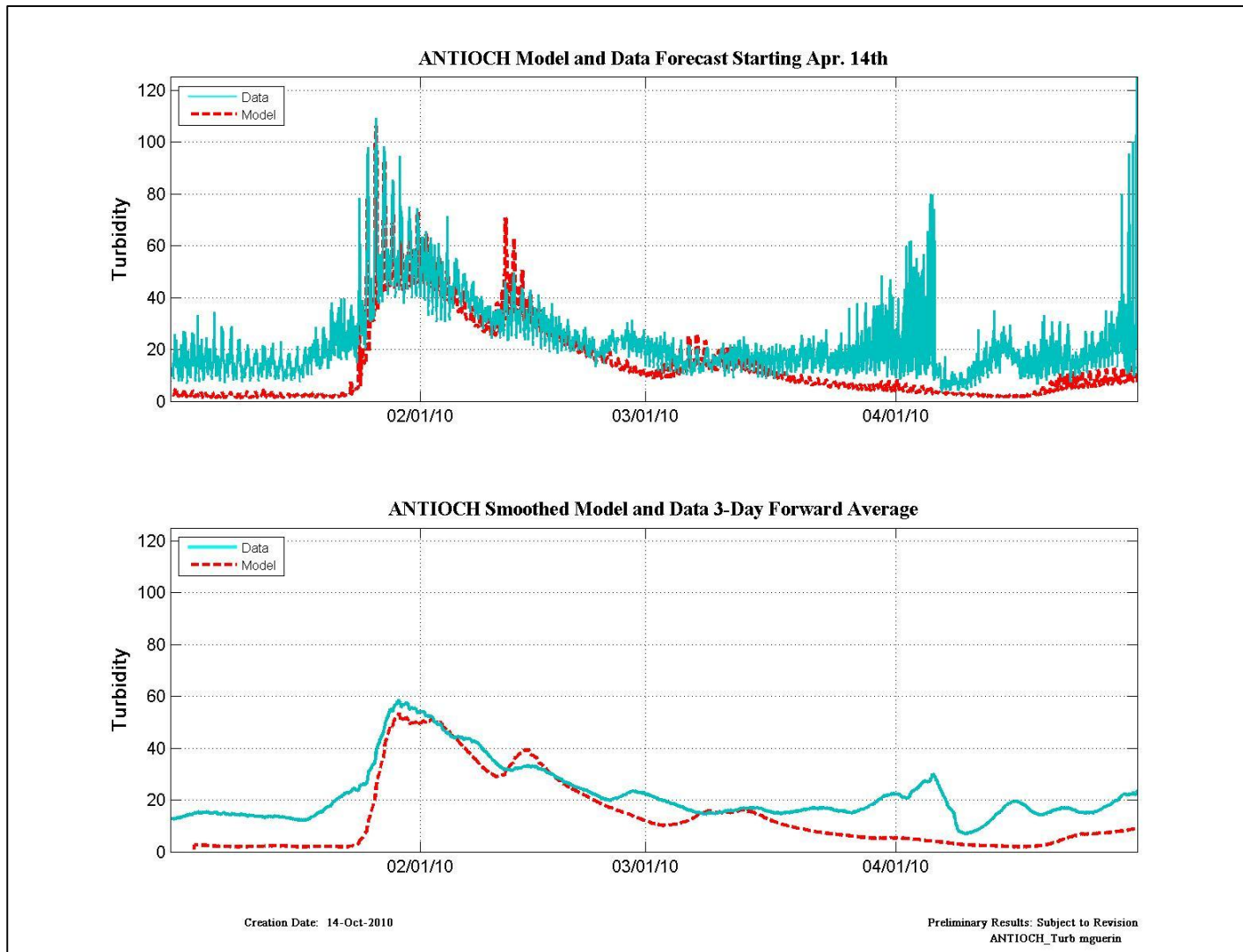


Figure 7-23 Turbidity data and model results for the forecast beginning April 14th at Antioch.

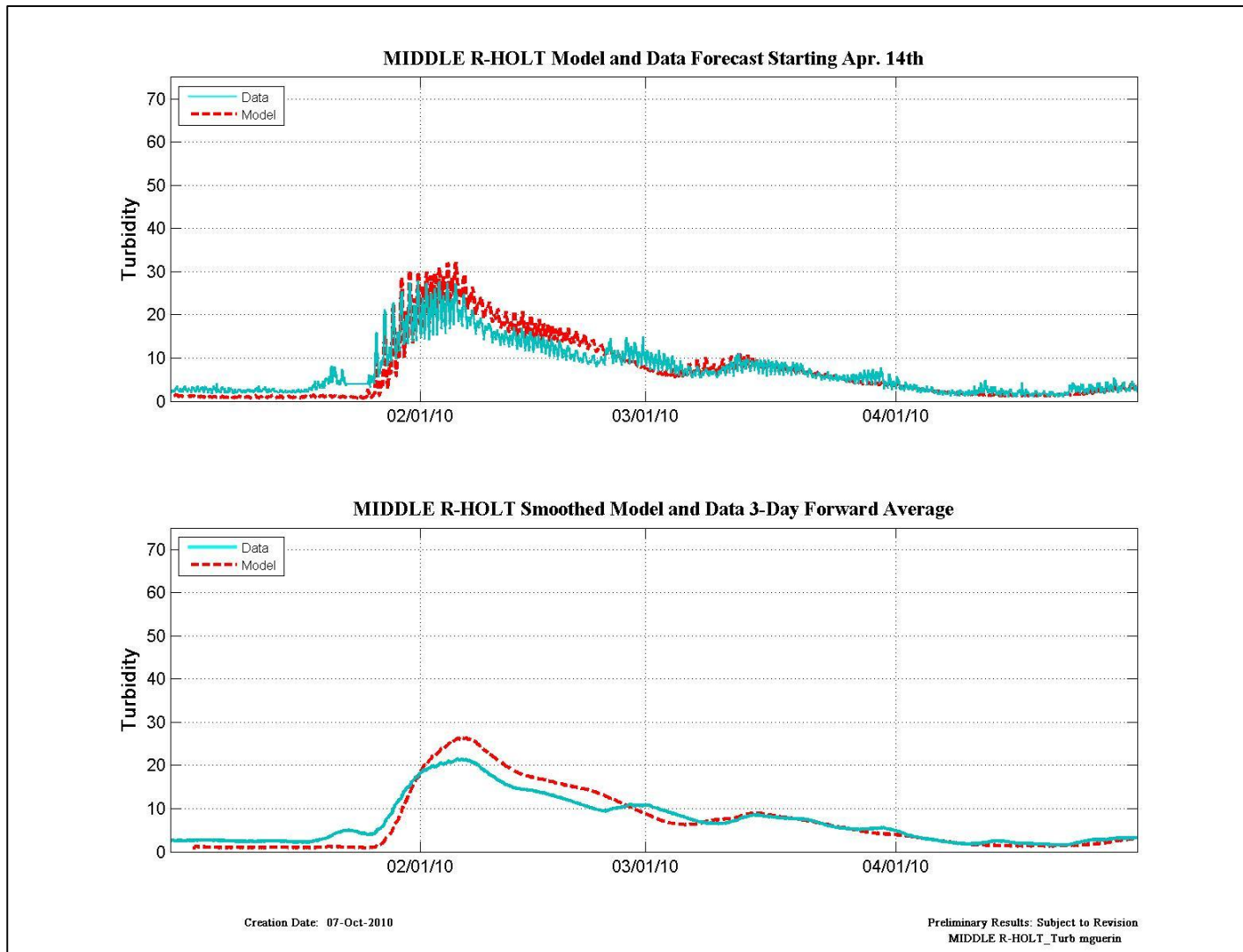


Figure 7-24 Turbidity data and model results for the forecast beginning April 14th at Middle R-Holt.

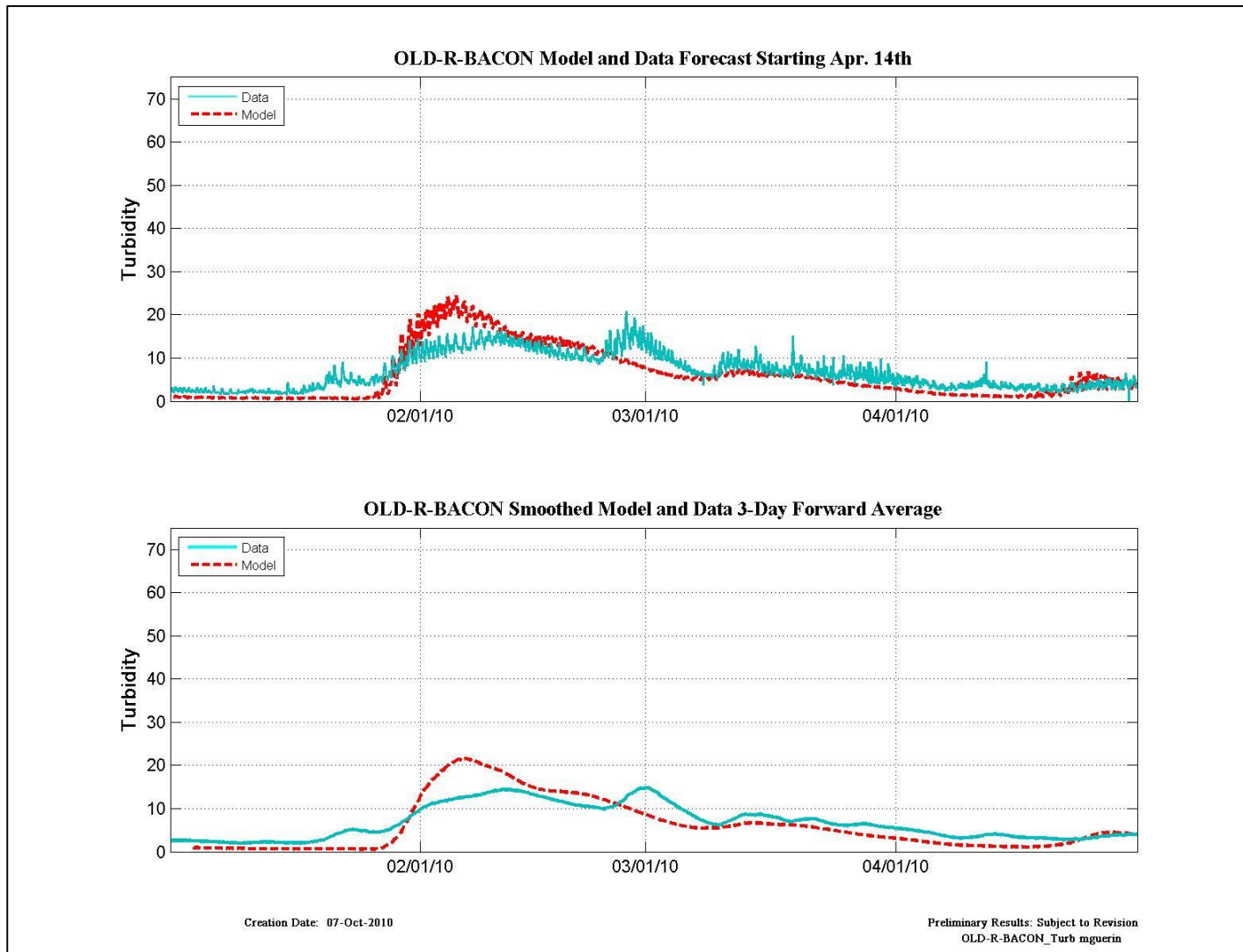


Figure 7-25 Turbidity data and model results for the forecast beginning April 14th at Old-R-Bacon.

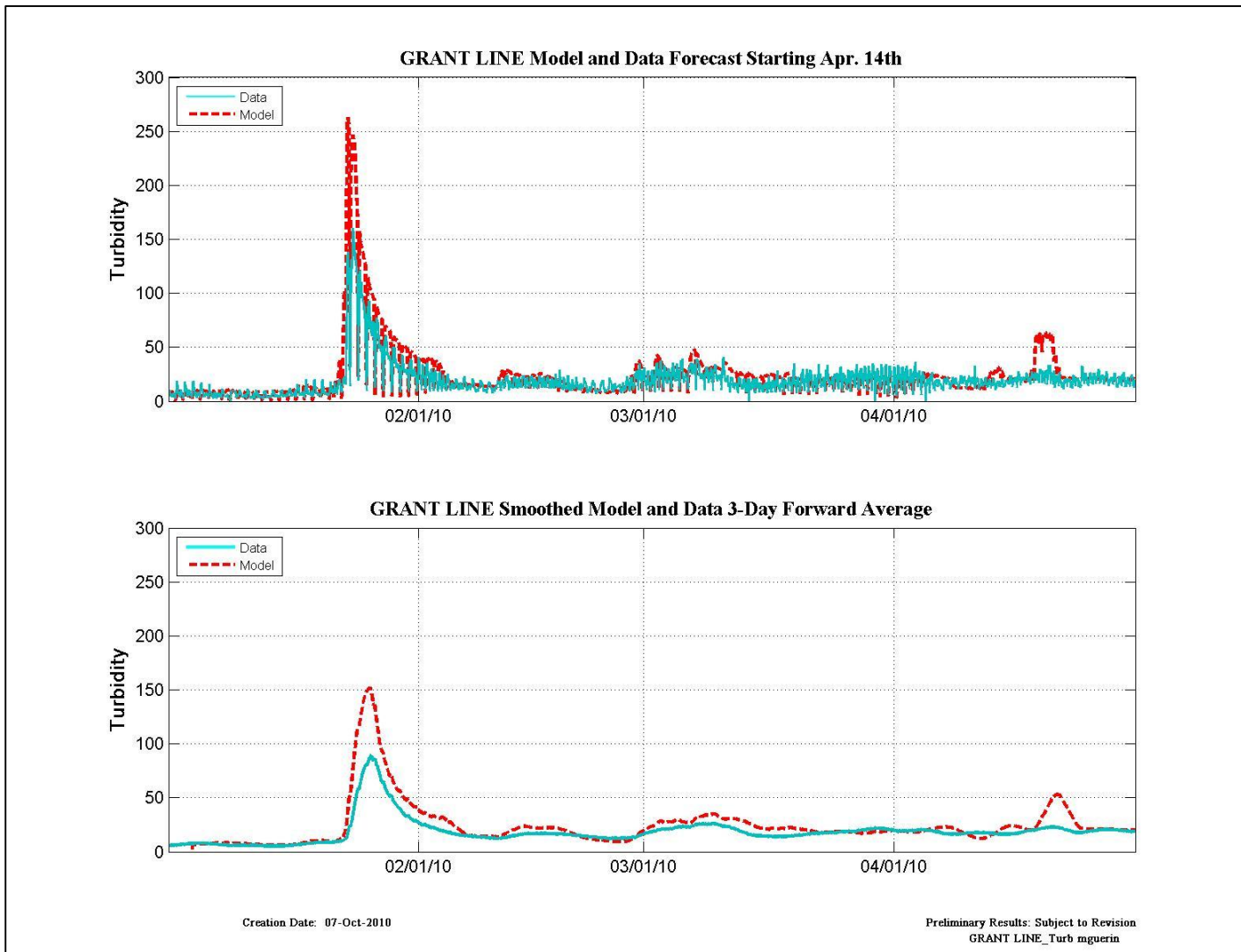


Figure 7-26 Turbidity data and model results for the forecast beginning April 14th at Grant Line.

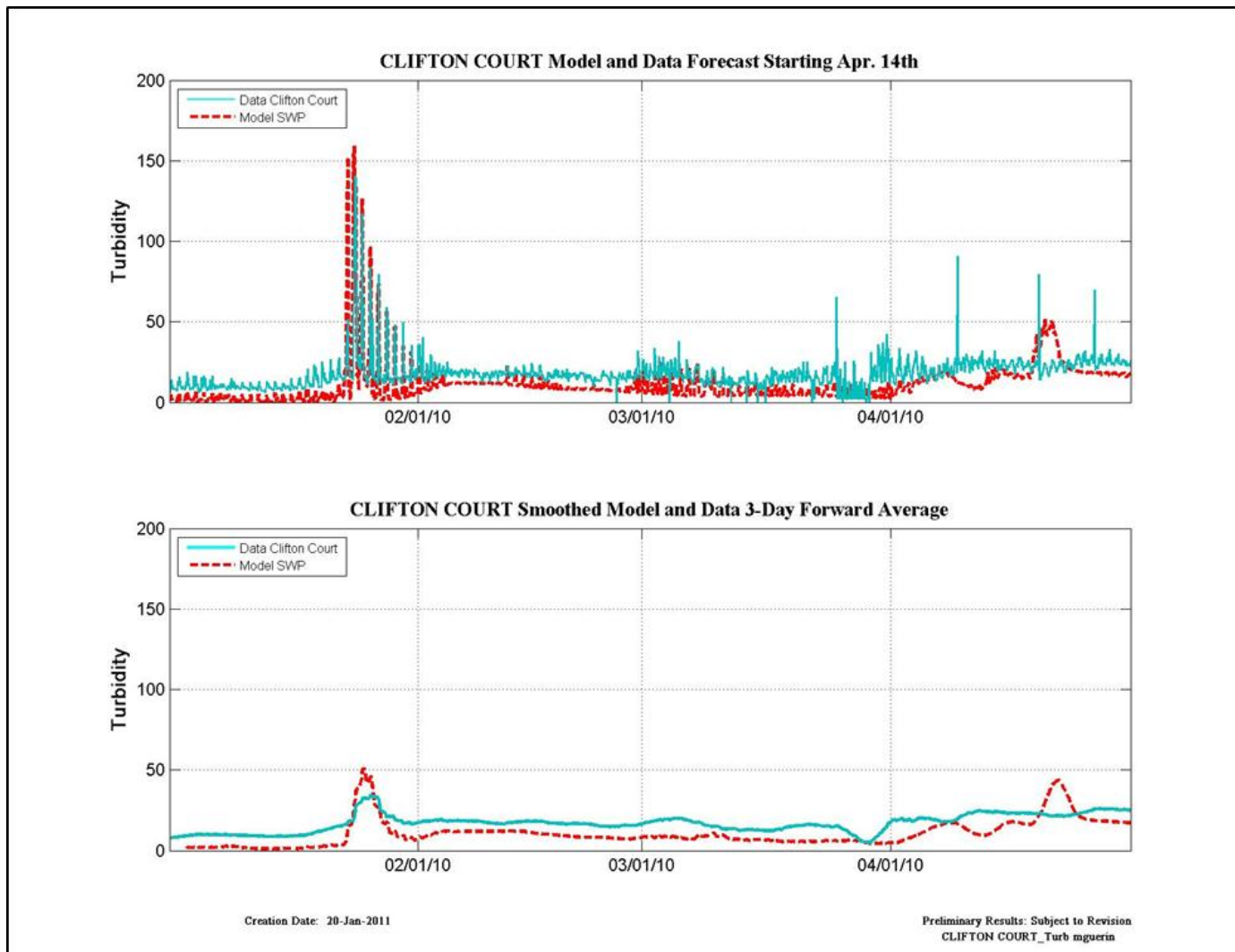


Figure 7-27 Turbidity data and model results for the forecast beginning April 14th at Clifton Court (data) and SWP (Model).

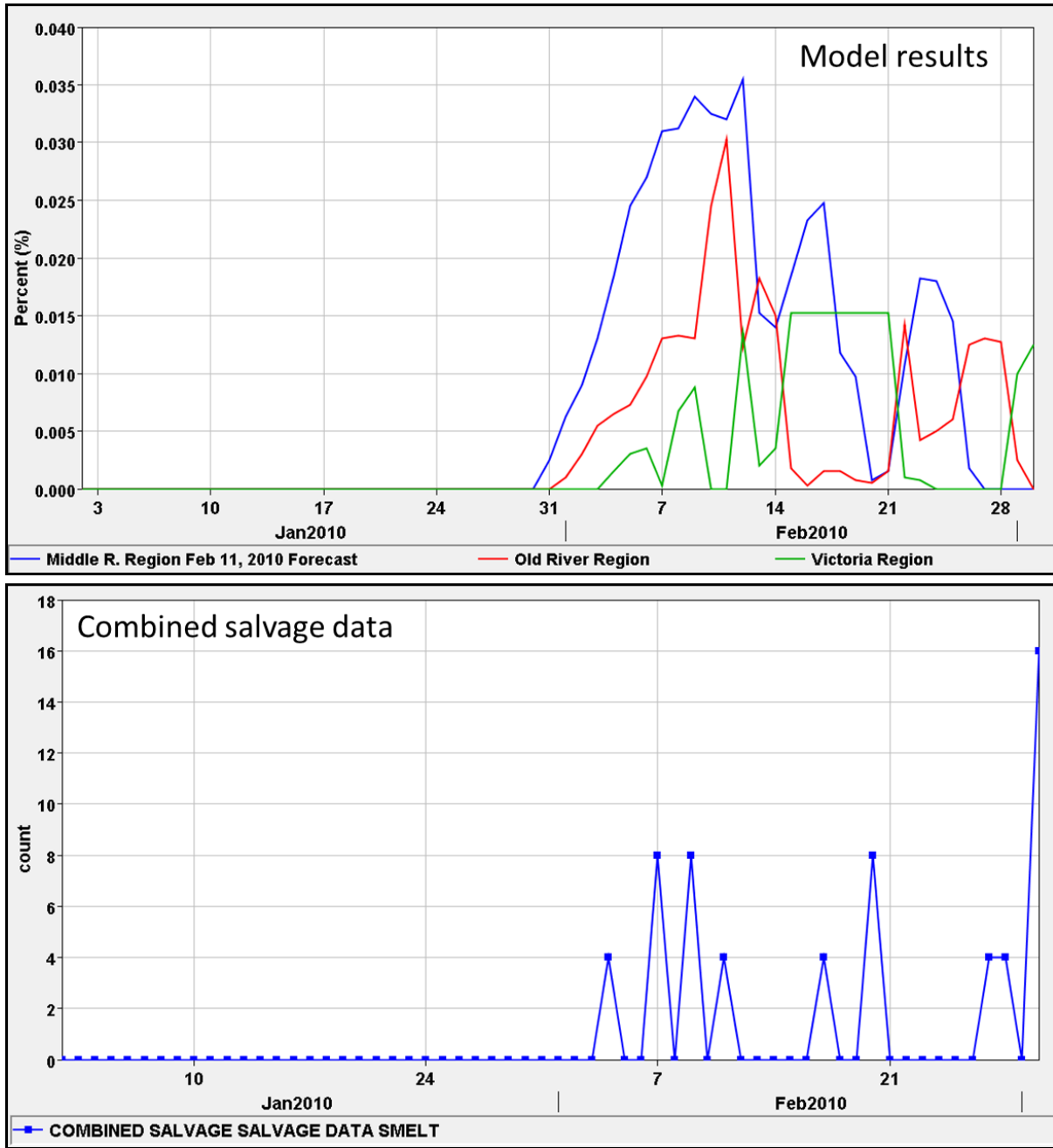


Figure 7-28 Adult delta smelt model results (top) for the RMA Feb. 11th forecast show a small percentage of particles (of 40,000 inserted) reached the Old, Middle and Victoria regions. The lower plot shows combined delta smelt salvage count at the SWP+CVP facilities.

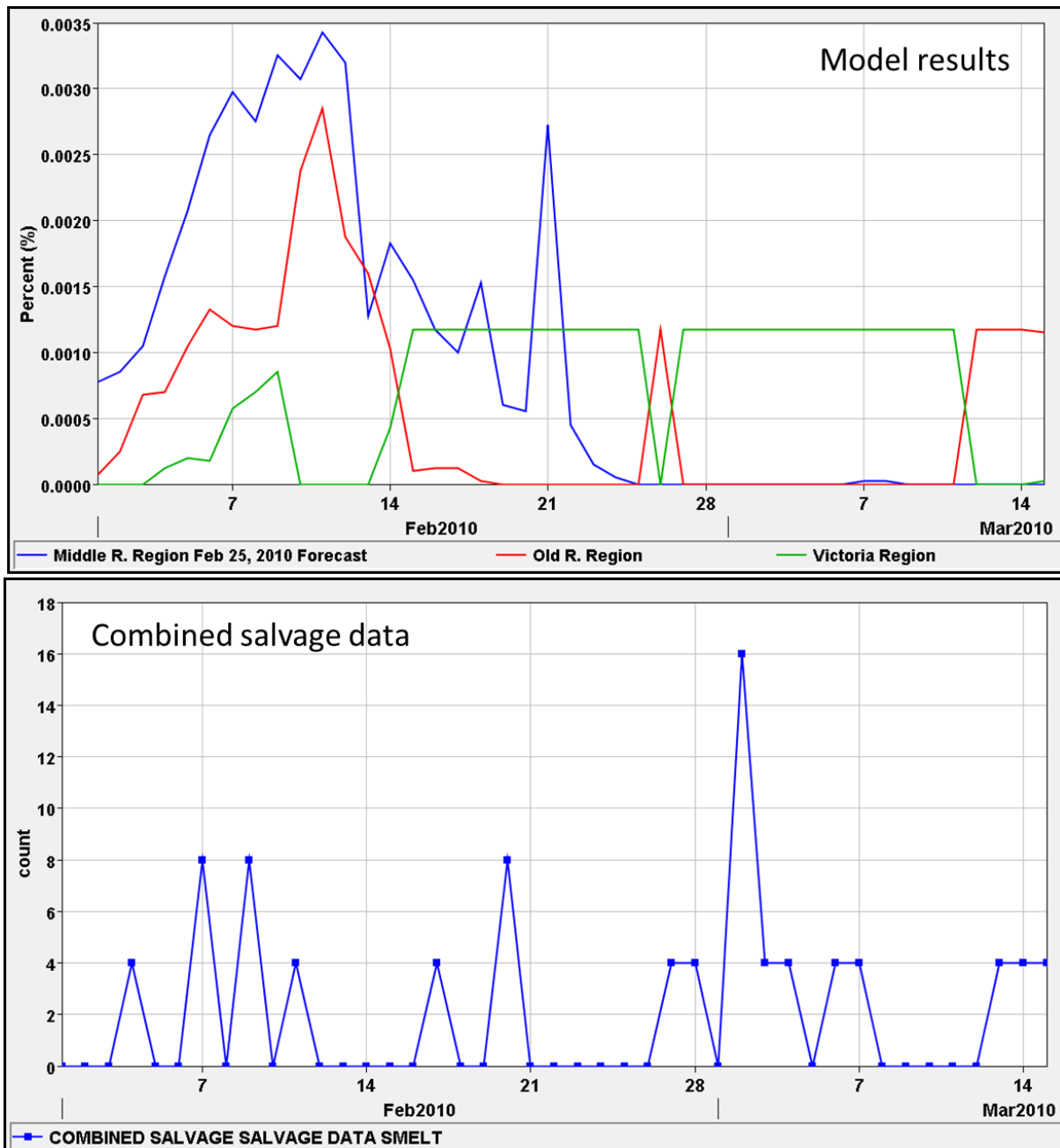


Figure 7-29 Adult delta smelt model results (top) for the RMA Feb. 25th forecast show a small percentage of particles (of 40,000 inserted) reached the Old, Middle and Victoria regions. The lower plot shows combined delta smelt salvage count at the SWP+CVP facilities.

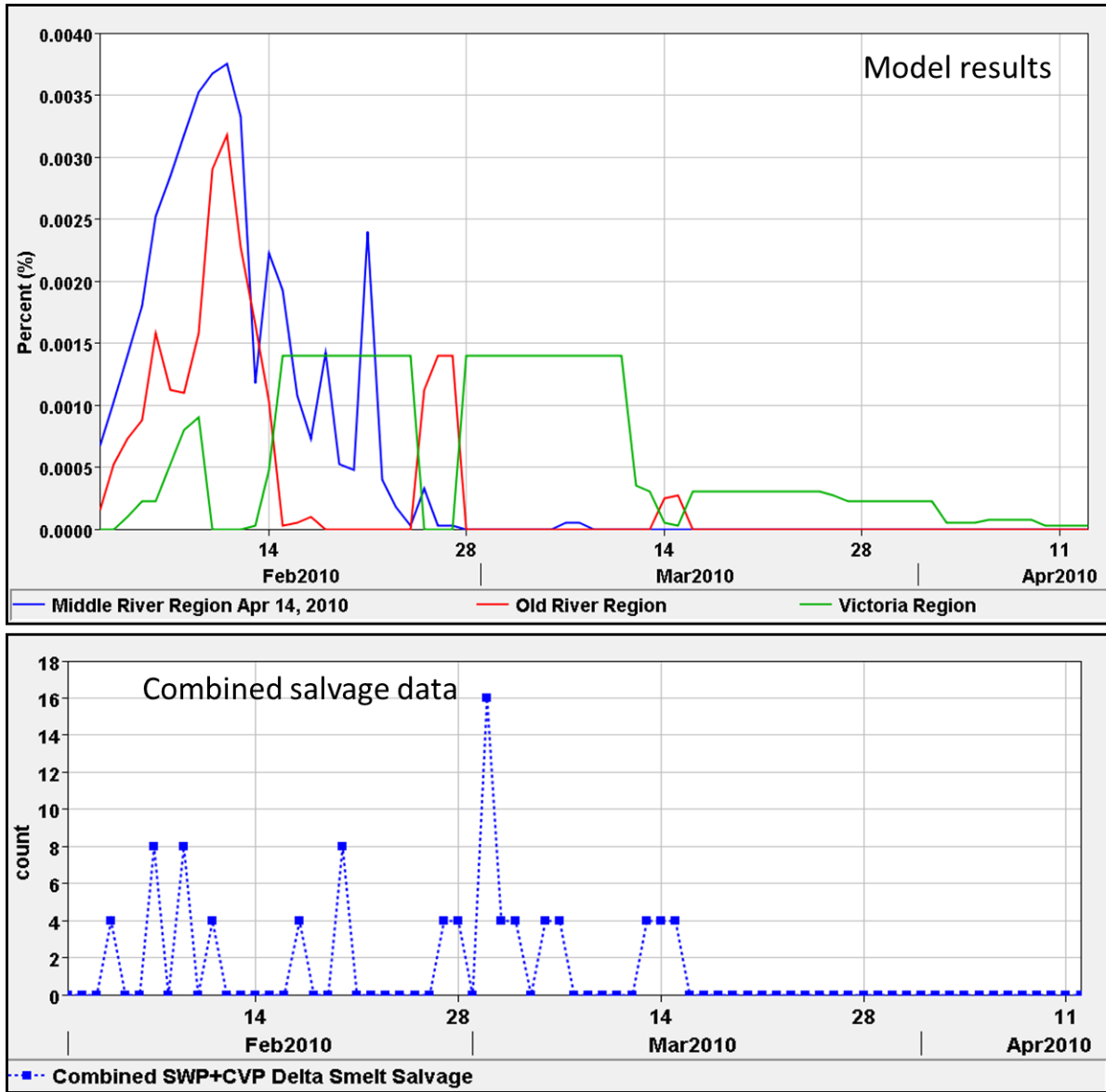


Figure 7-30 Adult delta smelt model results (top) for the RMA Apr. 14th forecast show a small percentage of particles (of 40,000 inserted) reached the Old, Middle and Victoria regions. The lower plot shows combined delta smelt salvage count at the SWP+CVP facilities.

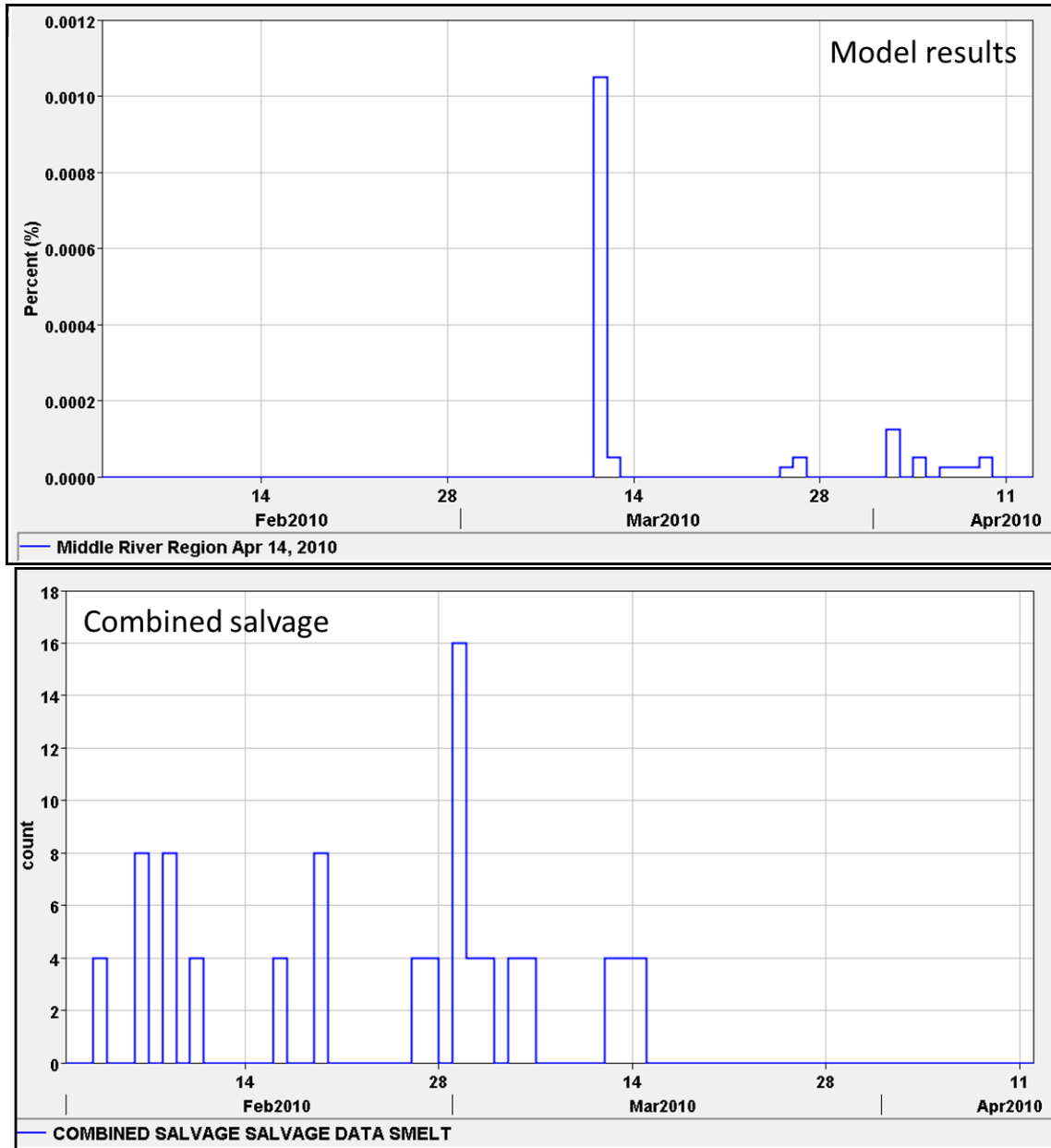


Figure 7-31 Adult delta smelt model results (top) for the RMA Apr. 14th forecast show a small percentage of particles (of 40,000 inserted) reached the SWP+CVP exports. The lower plot shows combined delta smelt salvage count at the SWP+CVP facilities.

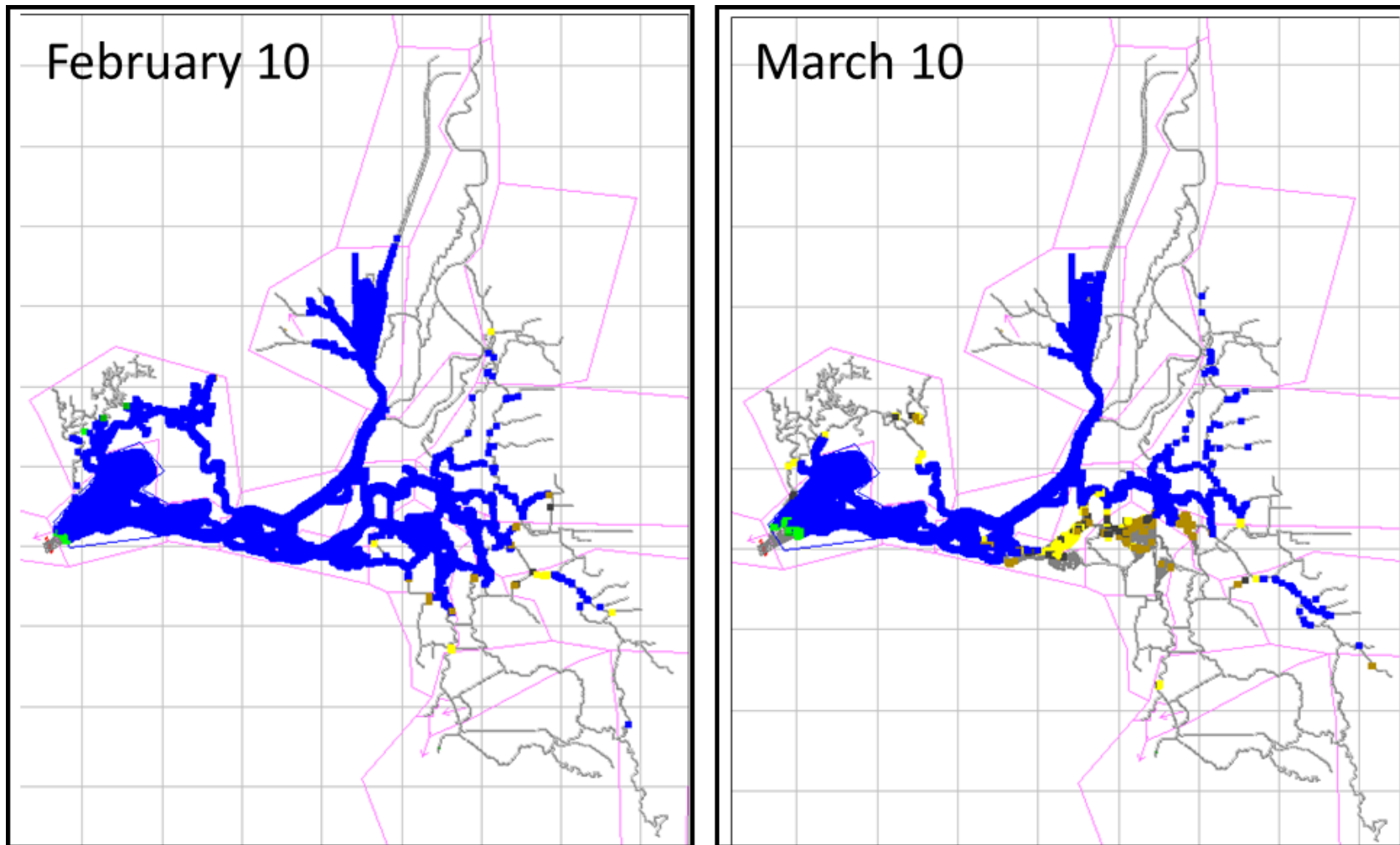


Figure 7-32 Particle tracking results using the adult delta smelt behavior model.

8. Discussion

A turbidity model based on decay coefficients is not capable of capturing all processes in sediment transport, so some mismatch between the model and turbidity data is not unexpected. However, the turbidity model results for the 2009 – 2010 rainy period generally follow the magnitude and trend of turbidity measurements through most of the Delta with a few notable exceptions (Little Potato Slough at Terminous and near Stockton on the San Joaquin River). Delta smelt salvage during this period was very low, and the adult delta smelt model results are consistent with this data as only a trivial percentage of particles reach the export locations.

The three-region, three-parameter turbidity model might be improved for the 2009-2010 period by refining the decay regions with selective changes to the decay coefficients. However, this sort of strategy generally reduces predictive power of the model. The 2010-2011 wet season will provide an important test of the current turbidity model formulation.

Adult delta smelt behavior model results for this time period suggest that higher export levels during the high turbidity events on the San Joaquin and Sacramento Rivers may have brought more delta smelt into the south Delta and into salvage. Scenarios with higher export levels and changes in the timing of exports could investigate the manipulation of turbidity levels in the south and central Delta to see if higher pumping levels would result in additional modeled salvage, and to see if a turbidity bridge would have formed under different export regimes.

The methodology developed to forecast turbidity is fairly rudimentary, and as such, needs to be applied using professional judgment. For example, CNRFC 5-day flow forecasts are viewed as more reliable than DWR forecasts, but then matching flow forecast with the beginning of the DWR flow forecast can be problematic, for example, at the Yolo inflow boundary. Similarly, deciding which exceedance value to use for an increasing Sacramento R, inflow requires some judgment – later in the rainy season there may be less upstream sediment available for suspension than earlier in the year. Developing at least two scenarios thus seems warranted to cover a range of magnitudes for forecasting turbidity pulses.

9. Conclusion

There is room for improvement in the turbidity forecast process, in the acquisition of data at key locations and times, and in the protocol for forecasting turbidity at the inflow boundaries. Extending the forecast period using CNRFC forecast flows enhanced the quality of the turbidity forecast although it did require additional time and effort. At this time, the process of producing a forecast is quite demanding, and it requires considerable modeling experience and professional judgment to set poorly constrained or questionable boundary conditions either from DWR or from the available data sources, particularly for turbidity data which is frequently noisy or missing. Acquiring DWR forecast and model output earlier would provide a major improvement in the ease of producing a good forecast. However, it was possible to produce RMA-model-based

turbidity and adult delta smelt forecasts within a reasonable turn-around time (~ 1.5 days) using DWR flow and salinity forecasts as a basis.

It was clear from the project this year that producing a successful forecast to provide information to the Delta Smelt Working Group or exporters considering changes to export operations would benefit from better event-driven data collection. The important flows and turbidity concentrations influencing turbidity in the central and south Delta were driven by a few days of high flows and turbidity at the Delta's boundaries. One action that could be taken to improve model application without changing the basic turbidity model (*i.e.*, without incorporating meteorological effects and sediment settling) is to improve monitoring data. In particular, it is important to remove uncertainty about missing flow and runoff by obtaining better flow and turbidity data at the locations discussed in this report particularly during and shortly after rain events. In addition, the Eastside inflows (Mokelumne, Calaveras, and Cosumnes Rivers) have the potential to significantly influence turbidity in Middle River and contribute to the development of a turbidity bridge in the central Delta if both flow and turbidity are high at one or more of these locations.

The modeling process itself could easily be streamlined by developing utility programs to combine the various data sets needed to develop the flow and water quality boundary conditions. During the forecast development process this year, programs to automate the weaving of the various data sources together were clearly needed – such utility programs could be developed within the HEC-DSSVue platform which supports the DSS data format used by DSM2 and by RMA models. This would not only decrease the time and effort involved in a weekly forecast, but increased automation would also reduce the likelihood of operator error. Another area where automation might streamline the forecasting process and our ability to visualize the turbidity data in the Delta falls under the category of “data cleaning”, or the detection and removal of outliers in the time series of turbidity data. In general, cleaning data requires some “human” intervention, but there are tools and methods available for time series data that could be utilized. However, automation alone would not reduce the requirement of familiarity with the basic data needed to run a successful forecast – flow, stage, salinity and turbidity – and with interpreting model output to assure the results are sensible.

The use of the RMA two-dimensional models provides a major improvement in the ability to understand the turbidity field in the Delta by using turbidity contour plots, for both technically sophisticated and general audiences. Similarly, visualizing the development of the turbidity fields through time as a “movie” could help inform decision-makers about the potential for impending conditions that may require a costly change in Delta operations.

10. References

- Buchanan, P.A., Lionberger, M.A., 2006. Summary of Suspended-Sediment Concentration Data, San Francisco Bay, California, Water Year 2004. p. 49. US Geological Survey Data Series 26.
- Ganju, N.K., Schoellhamer, D.H., Murrell, M.C., Gartner, J.W., and Wright, S.A., 2006, Constancy of the relation between floc size and density in San Francisco Bay. In: Maa, J.P., Sanford, L.H., and Schoellhamer, D.H., Eds., *Estuarine and Coastal Fine Sediment Dynamics - INTERCOH 2003*, Elsevier, Amsterdam, Netherlands, p. 75-91.
- Gray, J.R., G. D. Glysson, L. M. Turcios, and G. E. Schwarz. 2000, Comparability of Suspended-Sediment Concentration and Total Suspended Solids Data, Water-Resources Investigations Report 00-4191.
- Hills, "New Flow Equations for Clifton Court Gates", Technical Memorandum. California Department of Water Resources, State Water Project Division of Operations and Maintenance, Sacramento California, 1988.
- King, I. P., W. R. Norton and K. R. Iceman, 1975, A finite element solution for two-dimensional stratified flow problems', in R. H. Gallagher, J. T. Oden, C. Taylor and O. C. Zienkiewicz, *Finite Elements in Fluids*, J. Wiley, Chapter 7.
- King, I.P., Finite element modeling for two-dimensional depth averaged flow, RMA2V Version 3.3, Resource Management Associates, 1986.
- King, I.P., RMA11 – A two-dimensional finite element quality model, Resource Management Associates, 1995.
- McKee, L., Ganju, N.K., and Schoellhamer, D.H., 2006, Estimates of suspended sediment entering San Francisco Bay from the Sacramento and San Joaquin Delta, San Francisco Bay, California. *Journal of Hydrology*, 323, 335-352.
- Powell, T.M., Cloern, J.E., and Huzzey, L.M., 1989, Spatial and temporal variability in South San Francisco Bay (U.S.A.). I. Horizontal distributions of salinity, suspended sediments, and phytoplankton biomass and productivity: *Estuarine, Coastal and Shelf Science*, v. 28, p. 583–597.
- Resource Management Associates, Inc. (RMA), 1997 "Upper Newport Bay Final Model and GUI Development and Implementation Report", prepared for U.S. Army Corps of Engineers Los Angeles District, October 1997.
- Resource Management Associates, Inc. (RMA), 1998a "Upper Newport Bay Feasibility Report: Upper Newport Bay Salinity Study", prepared for U.S. Army Corps of Engineers Los Angeles District, October 1998.
- Resource Management Associates, Inc. (RMA), 1998b "Upper Newport Bay Feasibility Report: Upper Newport Bay Numerical Model Development Baseline Conditions Analysis", prepared for U.S. Army Corps of Engineers Los Angeles District, July 1998.

- Resource Management Associates, Inc. (RMA), 1999 “Upper Newport Bay Feasibility Report: Upper Newport Bay Alternative Analysis”, prepared for U.S. Army Corps of Engineers Los Angeles District, November 1999.
- Resource Management Associates, Inc. (RMA), 2001 “Newport Bay Water Quality Model Development” 3-D Stratified Flow Analysis, prepared for California Regional Water Quality Control Board, Santa Ana Region, February 2001.
- Resource Management Associates, Inc. (RMA), 2003 “Newport Bay Water Quality Model Update”, prepared for California Regional Water Quality Control Board, Santa Ana Region, November 2003.
- Resource Management Associates, Inc. (RMA), 2008 “San Francisco Bay-Delta Turbidity Modeling”, prepared for Metropolitan Water District of Southern California, October 2008.
- Resource Management Associates, Inc. (RMA), 2009a “Particle Tracking and Analysis of Adult and Larval/Juvenile Delta Smelt for 2-Gates Demonstration Project”, prepared for Metropolitan Water District of Southern California, July 2009.
- Resource Management Associates, Inc. (RMA), 2009b “Numerical Modeling in Support of Suisun Marsh PEIR/EIS: Technical Appendix”, prepared Jones and Stokes Associates, September 2009.
- Resource Management Associates, Inc. (RMA), 2010, Spatial animation of Observed Turbidity Time Series for the Sacramento-San Joaquin Delta.
- Schoellhamer, D.H., 1996, Factors affecting suspended-sediment concentrations in South San Francisco Bay, California: *Journal of Geophysical Research*, v. 101, no. C5, p. 12087–12095.
- Suits, B., 2002, Calibrating DSM2-QUAL Dispersion Factors to Practical Salinity, 23rd Annual Progress Report (Chapter 6), “Methodology for Flow and Salinity Estimates in the Sacramento-San Joaquin Delta and Suisun Marsh”.

11. Appendix I

11.1. Background

Table 11-1 Inflows, outflows and turbidity data sources used to set model boundary conditions for 2007/8 calibration.

Model Input Locations	BC type	Data Source	Monitoring Location	BC type	Data Source	Monitoring Location
Martinez	Tidal elevation	NOAA	Martinez	Turbidity	CDEC	Martinez
Sacramento River	Inflow	USGS	Sacramento River at Freeport	Turbidity	CDEC	Sacramento River at Hood
San Joaquin River	Inflow	USGS	San Joaquin River at Vernalis	Turbidity	CDEC	San Joaquin River at Mossdale
Yolo Bypass	Inflow	CDEC	Yolo Bypass at Lisbon	Turbidity	CDEC	Sacramento River at Hood
Cosumnes River	Inflow	CDEC	Cosumnes River at Michigan Bar	Turbidity	CDEC	Sacramento River at Hood
Mokelumne River	Inflow	CDEC	Comanche Reservoir Outflow	Turbidity	CDEC	Sacramento River at Hood
Calaveras	Inflow	CDEC	Mormon Slough at Bellota	Turbidity	CDEC	No boundary condition applied - set at ambient
SWP	Outflow	BDAT	Clifton Court	--	--	--
CVP	Outflow	CDEC	Tracy Pumping Plant	--	--	--
CCWD Rock Slough Intake	Outflow	CCWD	near Brentwood	--	--	--
CCWD Old River Intake	Outflow	CCWD	near Discovery Bay Flow diversion	--	--	--
North Bay Aqueduct	Outflow	CDEC	Barker Slough Pumping Plant	--	--	--

11.2. Historical turbidity locations (pre-12/2009)

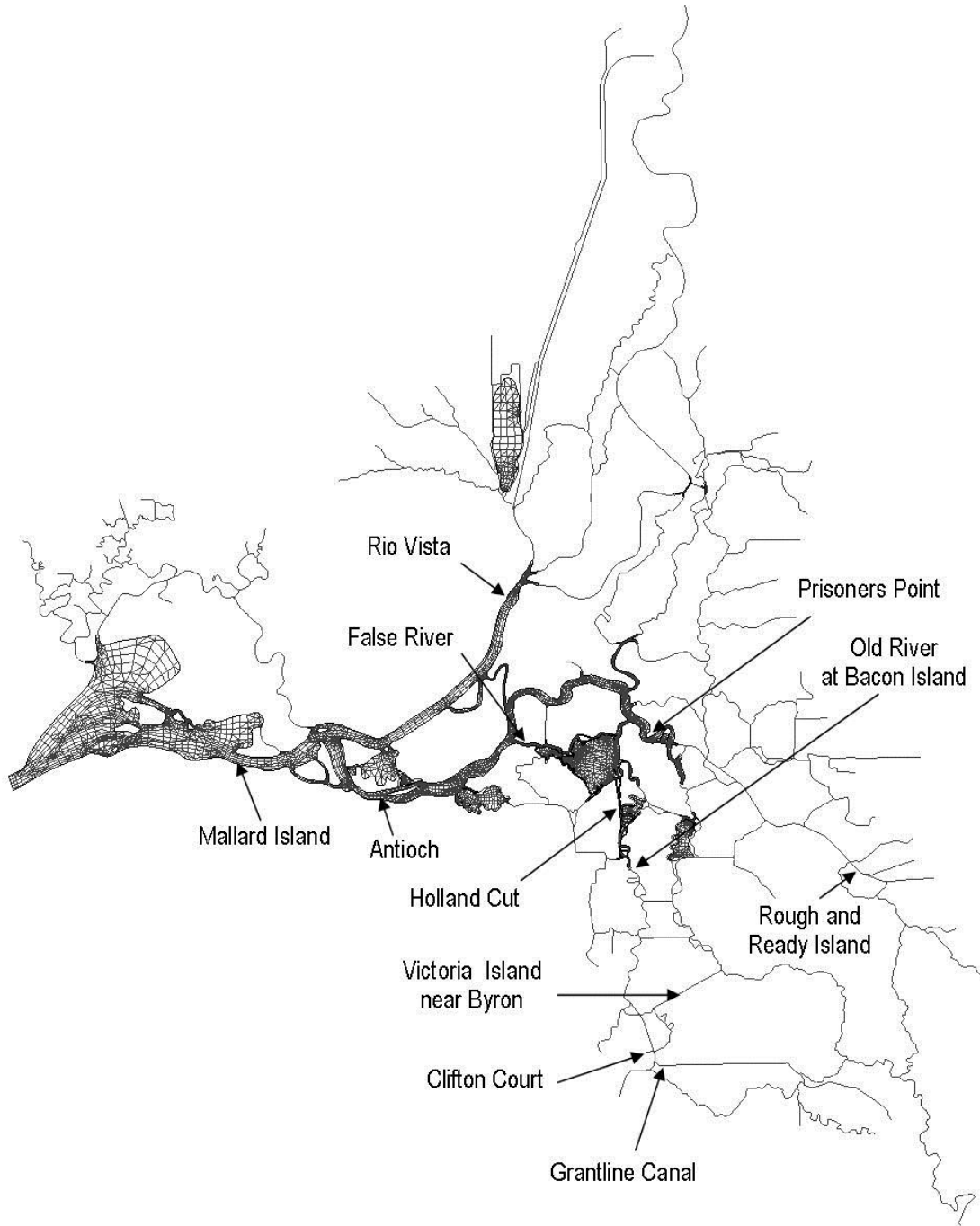


Figure 11-1 Locations of original turbidity monitoring stations in a previous grid.

11.3. *Setting flow boundaries*

11.3.1. *Sacramento River at I Street – CNRFC forecast – stage to flow conversion*

According to NOAA/CNRFC staff⁶, the I-Street rating is difficult since I-Street is "in tides" for most of the year. When the stage is below 7-10 feet, the flows at these levels are not officially rated. The rating available on the CDEC website (<http://cdec.water.ca.gov/rtables/IST.html>) (DWR rating curve) only goes from 10 to 31 feet, as shown in Table 11-2. NOAA/CNRFC staff have extended the DWR I-Street rating below 10 feet to allow modeling of the river flows throughout the year, and also made some adjustments to the DWR rating at higher flows (above 22 feet) based on their calibration efforts. The higher flow values in the NOAA/CNRFC synthetic rating have a better correlation to the flows that the USGS measured at Freeport; for stages above 22 feet, although there are two different ratings, the variation between them is minor.

The rating table available on the CDEC website is reproduced in the following Table:

Table 11-2 Conversion from stage (ft.) to flow (cfs) at Sacramento R. at I street.

From (Ft.)	To(Ft.)	Add (cfs) for each 0.01 Ft	Add (cfs) For Each 0.1 Ft	Add (cfs) For Each 1.0 Ft	To (cfs)
10	12.99	34	340	3400	31800
13	16.99	35	350	3500	42000
17	18.99	36	360	3600	56000
19	20.99	37	370	3700	63200
21	22.99	38	380	3800	70600
23	24.99	39	390	3900	78200
25	31	40	400	4000	86000

NOAA/CNRFC staff recommends that for a proof-of-concept model, such as the current turbidity model, for stages 10-22 feet the rating curves work sufficiently well. For stages below 10 feet, tides have an influence and the CNRFC synthetic rating does not really model true flow

⁶ Pete Fickenscher, Senior Hydrologist, NOAA/NWS/CNRFC

in the tidal range (e.g., a high tide would actually have a lower flow as the tide impedes flow downstream). The rating table is shown in Table 11-3. Since in this project we are interested in peak flows, this should not present any difficulty.

Table 11-3 Rating table to covert from stage (ft.) to flow (cfs) at Sacramento R. at I street for flows from 1 – 10 cfs.

Stage	Flow (cfs)	Stage	Flow (cfs)	Stage	Flow (cfs)
1	4100	11	35200	21	70600
2	6600	12	38600	22	74400
3	9300	13	42000	23	78500
4	12200	14	45500	24	83000
5	15300	15	49000	25	87800
6	18500	16	52500	26	92700
7	21700	17	56000	27	97700
8	25000	18	59600	28	102800
9	28400	19	63200	29	108000
10	31800	20	66900	30	113200
				31	118400

11.3.2. CIMIS wind and precipitation data

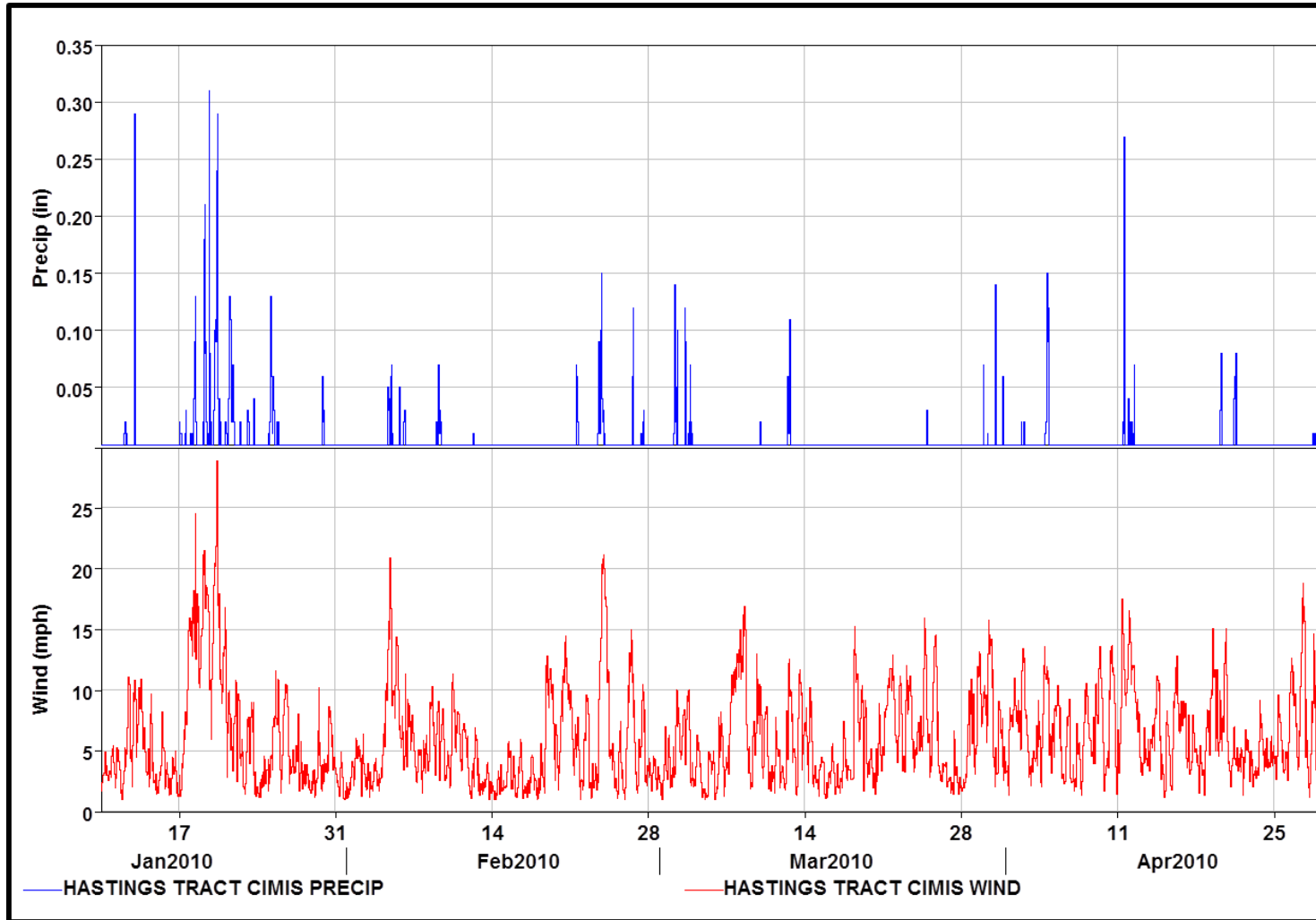


Figure 11-2 CIMIS wind and precipitation data at Hastings Tract.

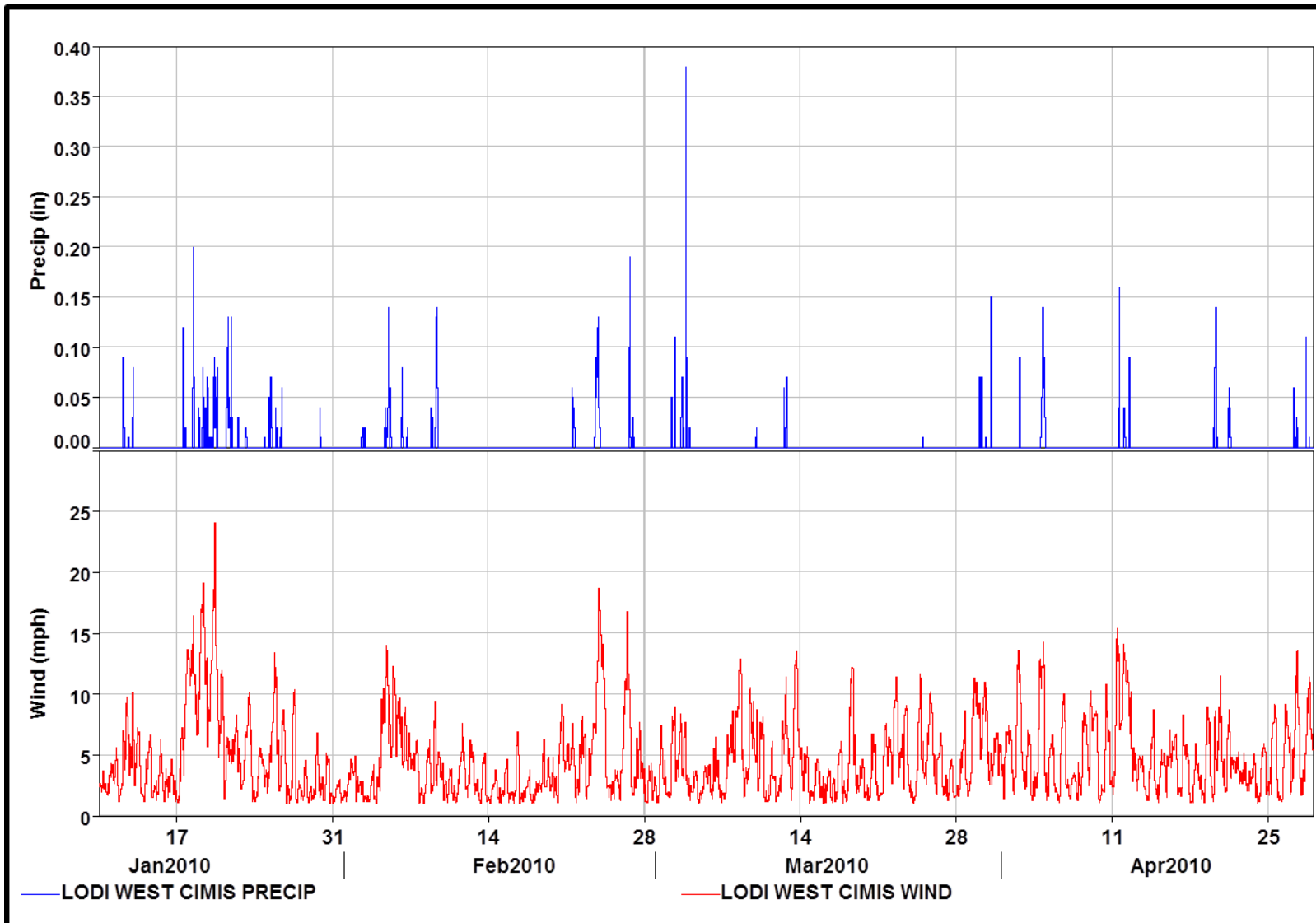


Figure 11-3 CIMIS wind and precipitation data at Lodi West.

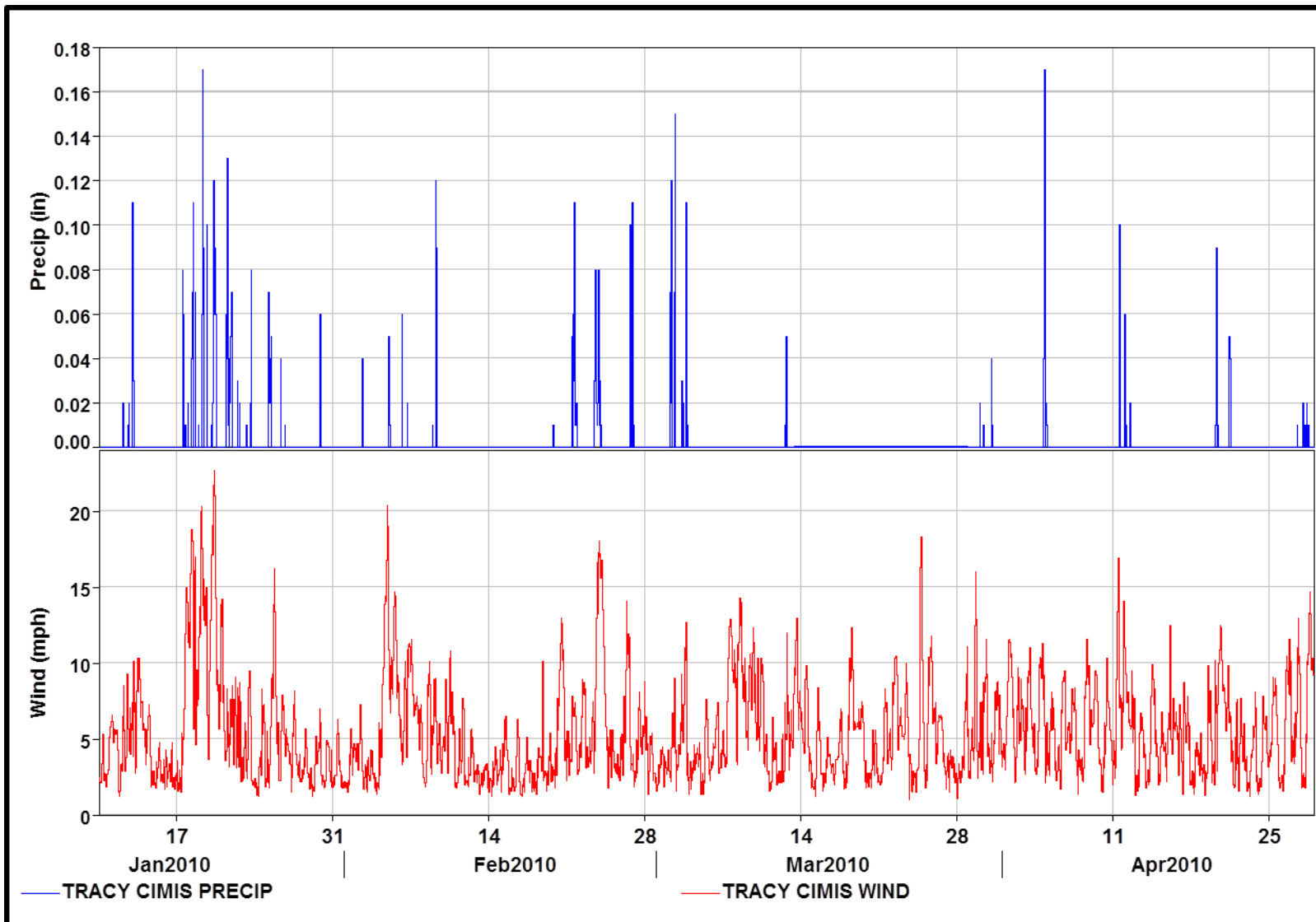


Figure 11-4 CIMIS wind and precipitation data at Tracy.

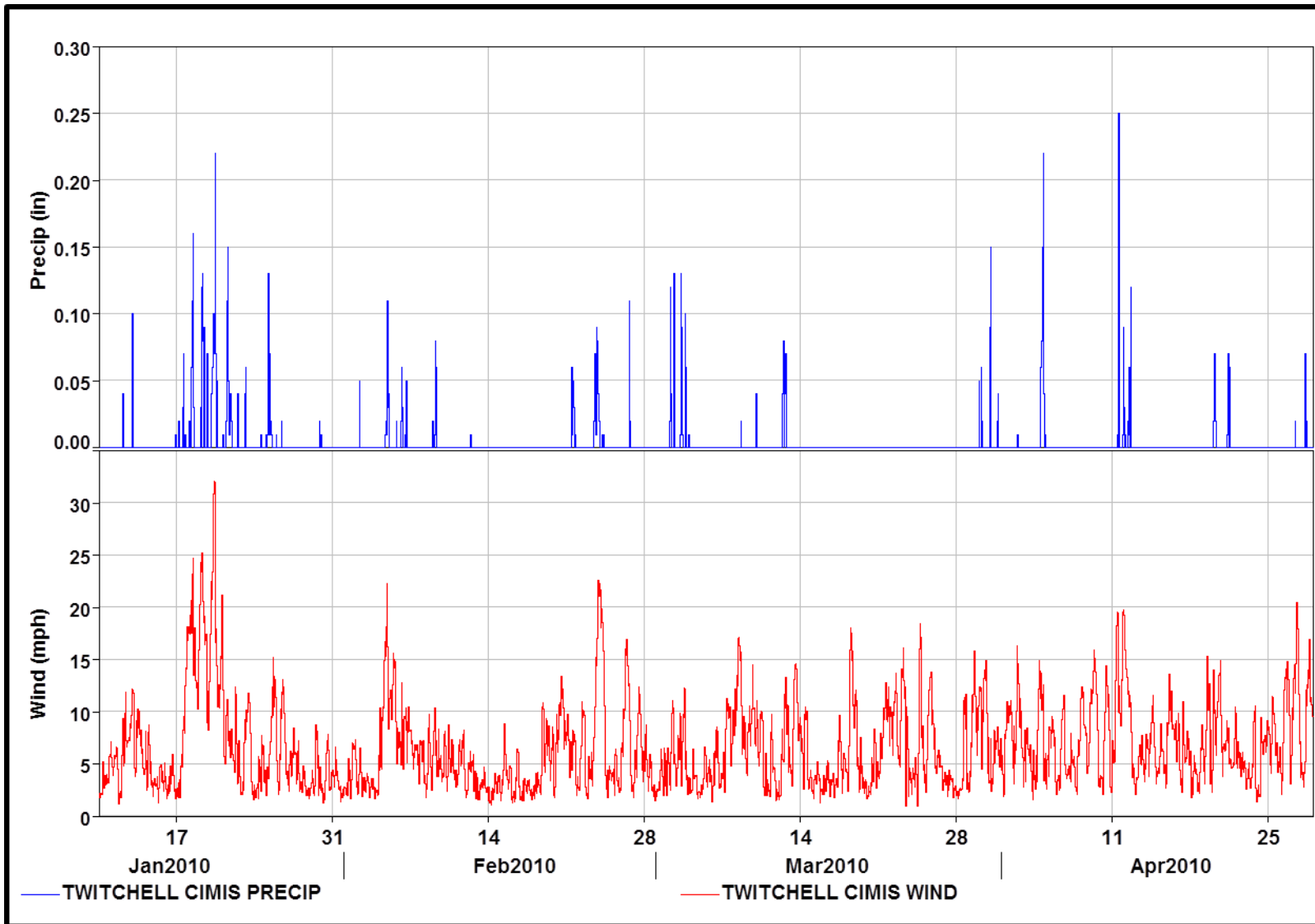


Figure 11-5 CIMIS wind and precipitation data at Twitchell.

11.3.3. Additional adult delta smelt model results

The Jan. 11th adult delta smelt model forecast showed that no particles reached the Old, Middle, or Victoria regions, or the export location within the three week forecast period – therefore no plots are shown for this period. For the other forecast periods covered in this section, note that these plots show particle count, not percentage of particles inserted as in previous plots.

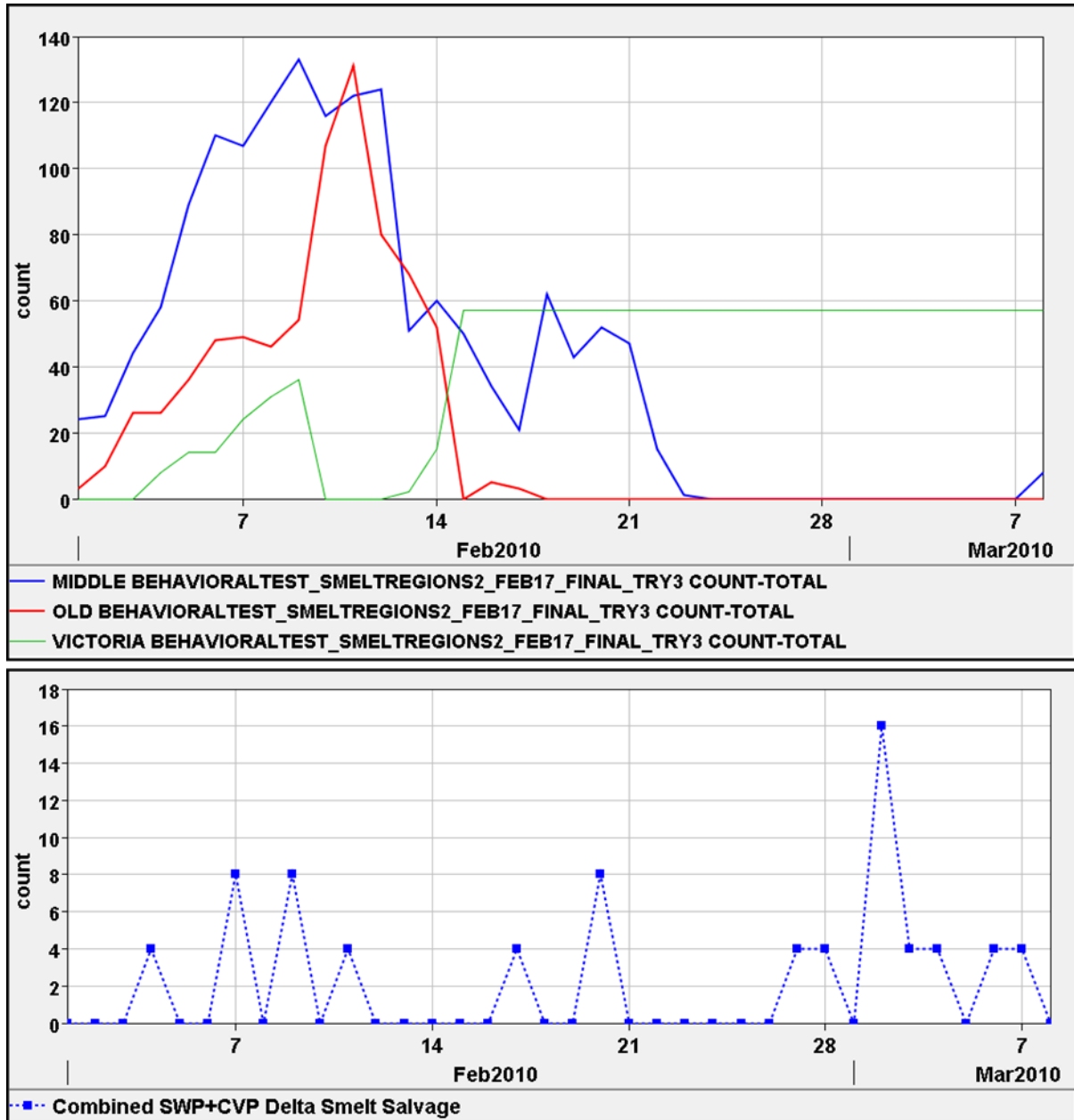


Figure 11-6 Adult delta smelt model results (top) for the Feb. 17th forecast show a small number of particles (40,000 inserted) reached the Old, Middle and Victoria regions. The lower plot shows combined delta smelt salvage count at the SWP+CVP facilities.

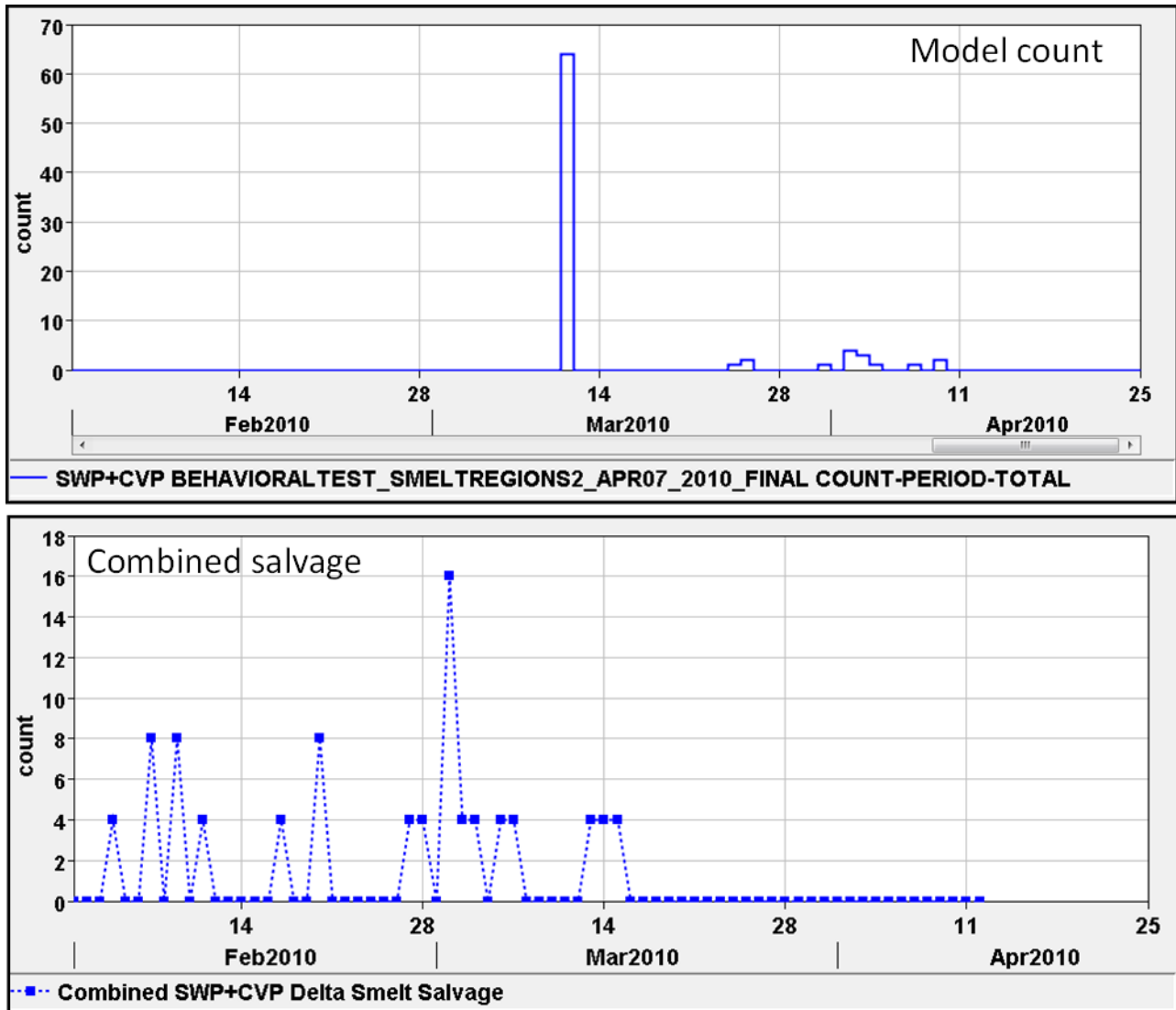


Figure 11-7 Adult delta smelt model results (top) for the Apr. 7th forecast show a small number of particles (40,000 inserted) reached the SWP+CVP exports. The lower plot shows combined delta smelt salvage count at the SWP+CVP facilities.

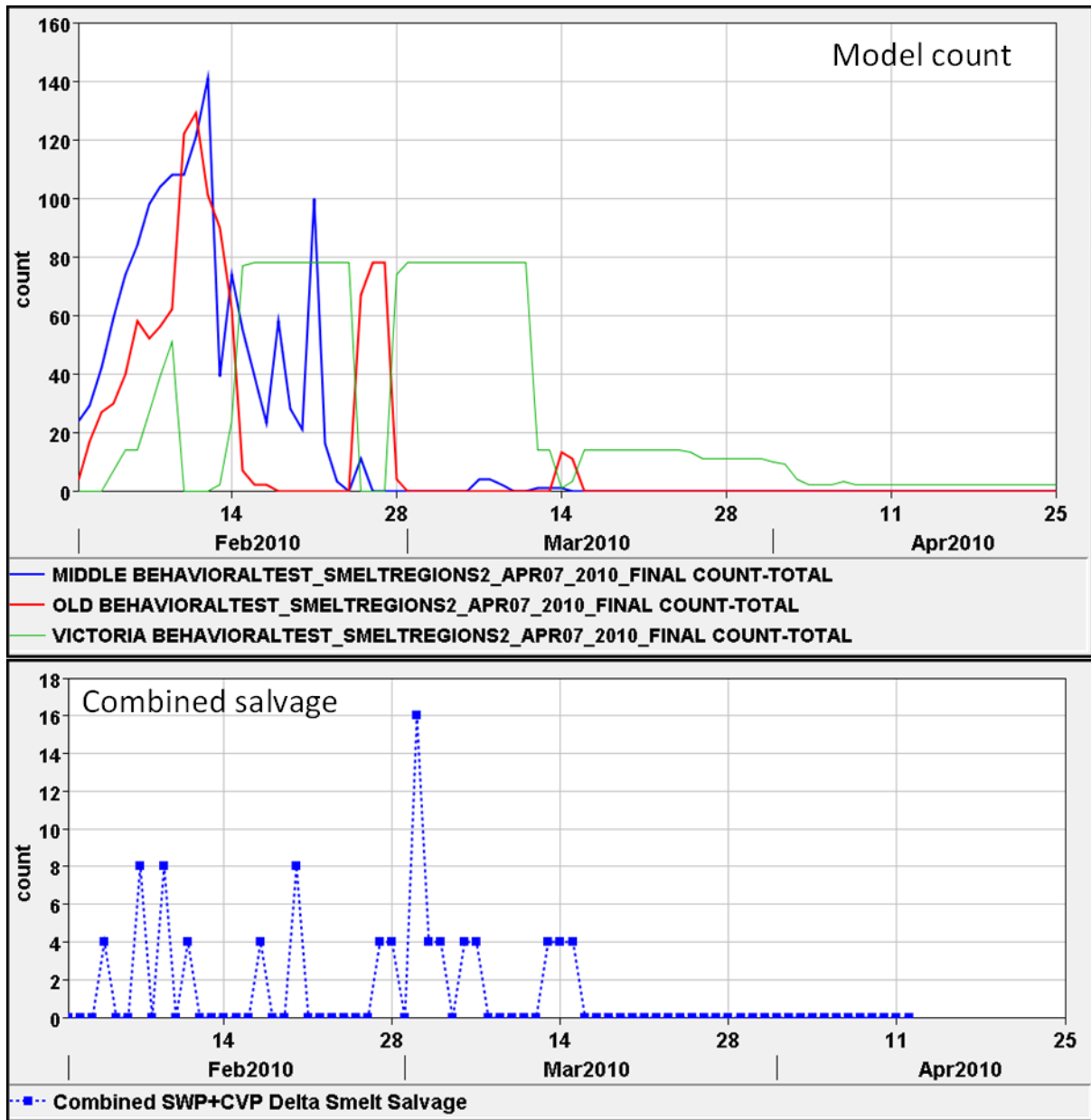


Figure 11-8 Adult delta smelt model results (top) for the Apr. 7th forecast show a small number of particles (40,000 inserted) reached the Old, Middle and Victoria regions. The lower plot shows combined delta smelt salvage count at the SWP+CVP facilities.

12. Appendix II - Detailed forecast model results for Apr. 14th and Feb. 25th

Model results and data for the RMA April 14th forecast are shown in Figure 12-1 through Figure 12-70, while model results for the RMA February 25th forecast are shown in Figure 12-71 through Figure 12-104. Results are shown for turbidity and flow, with plots of 15-minute and three-day running average (turbidity) or tidally averaged (flow). Results are also shown expanding the time scale to focus on the forecast period.

Raw turbidity data was assessed and sometimes (rarely) altered for the plots below to remove data points that were clearly wrong (e.g., negative values or extremely high values). Thus, much of the data was used as downloaded which influences the running average calculations – this is also the case with missing data. Where data was missing, the plot shows a step function down to zero (see Figure 12-25 and Figure 12-37, for example).

Model results show the effect of step function increases in turbidity boundary conditions used as approximations – these effects are particularly noticeable near the inflow boundaries (for example, see Figure 12-5 for effects from the Freeport BC and Figure 12-7 and Figure 12-33 for effects from the Vernalis BC).

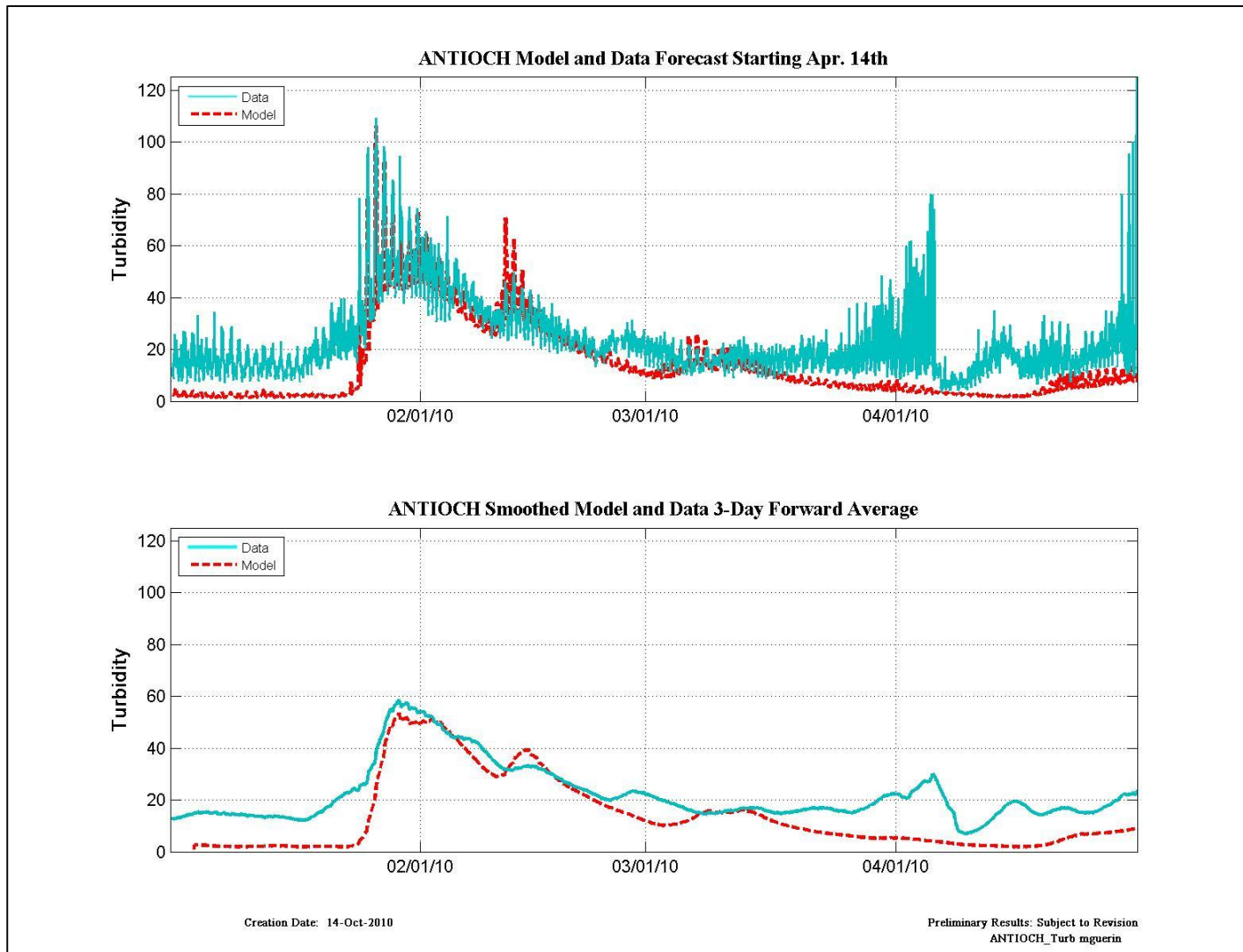


Figure 12-1 Turbidity data and model results for the RMA forecast beginning April 14th at Antioch.

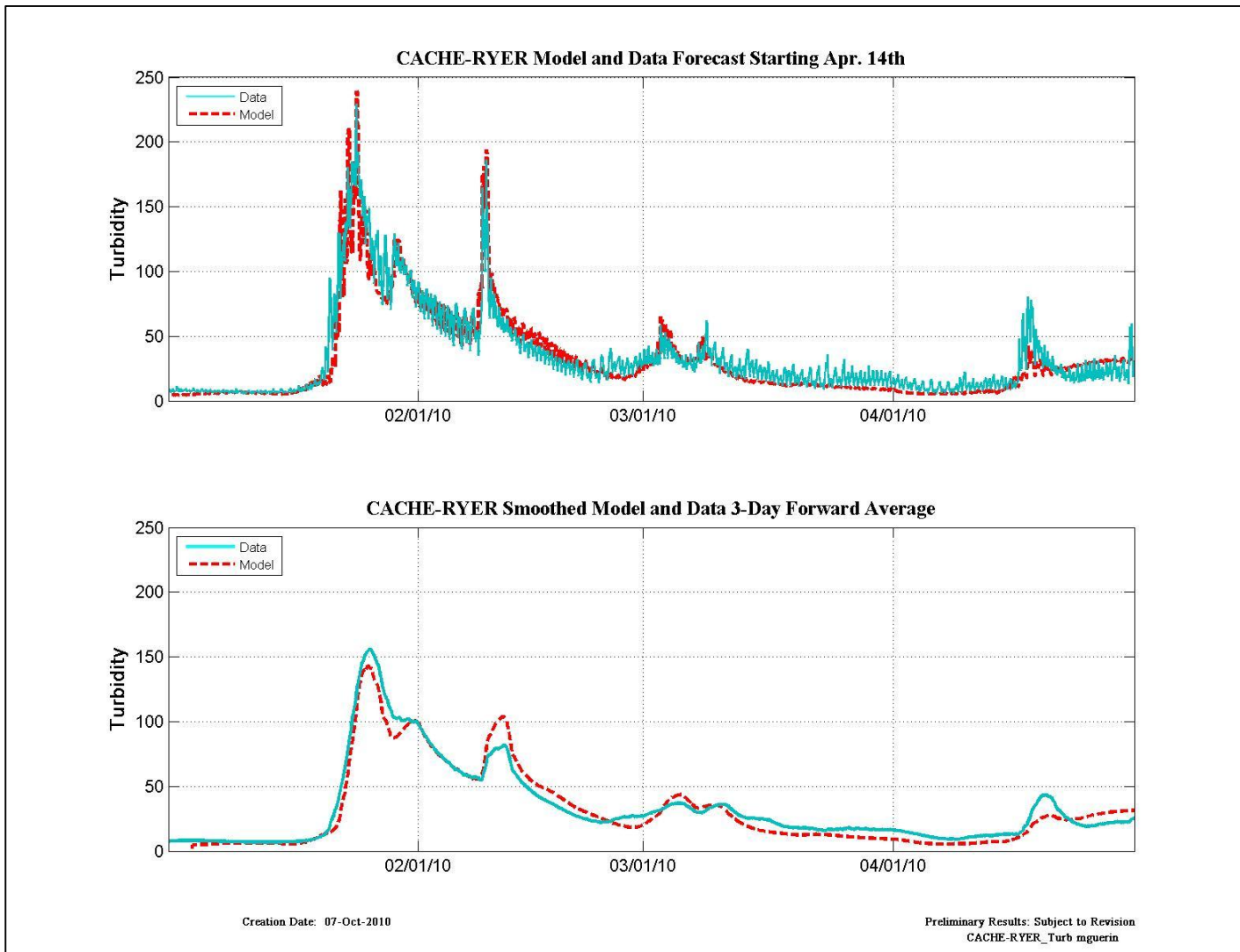


Figure 12-2 Turbidity data and model results for the RMA forecast beginning April 14th at Cache-Ryer.

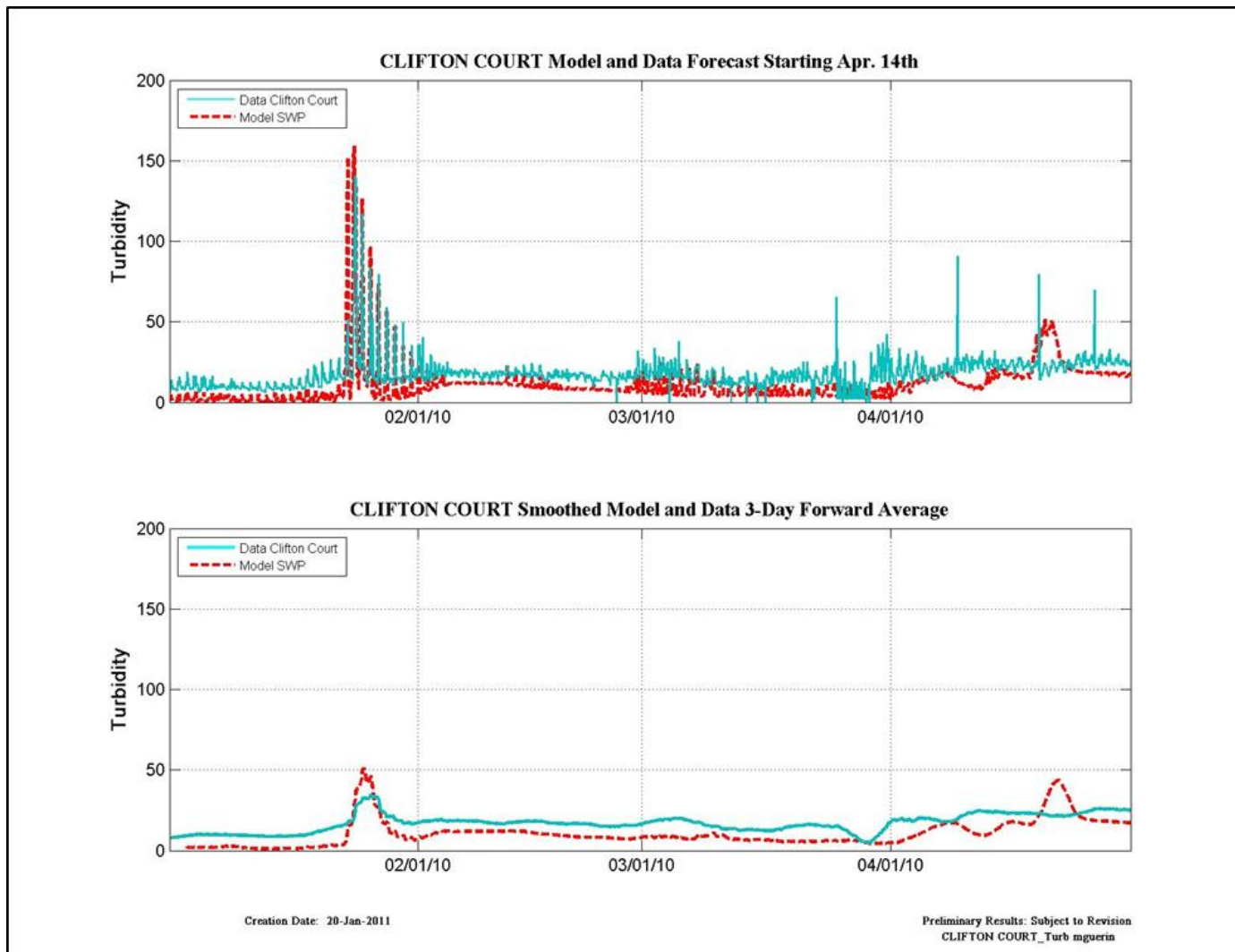


Figure 12-3 Turbidity data and model results for the RMA forecast beginning April 14th at Clifton Court (data) and SWP (model).

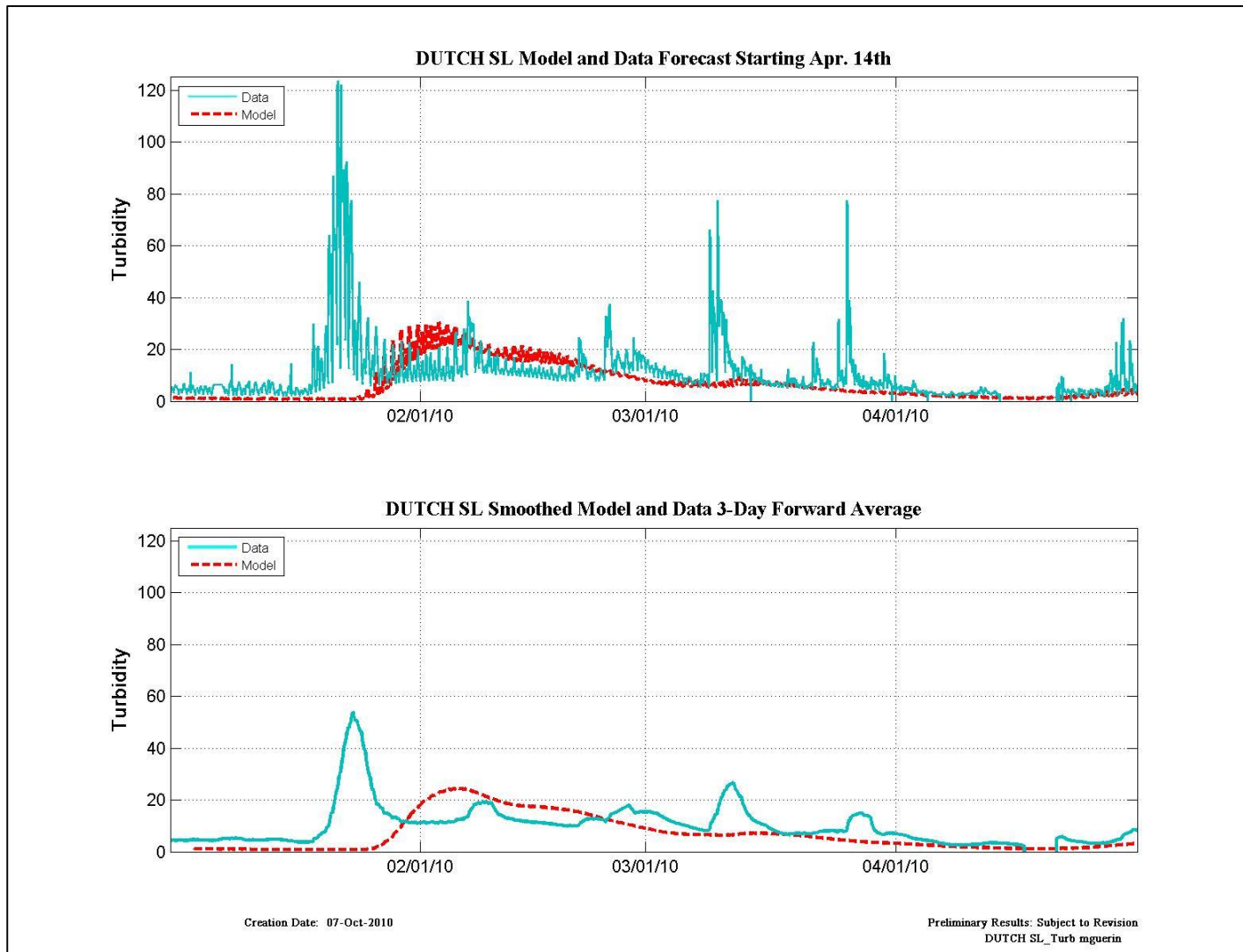


Figure 12-4 Turbidity data and model results for the RMA forecast beginning April 14th at Dutch SL.

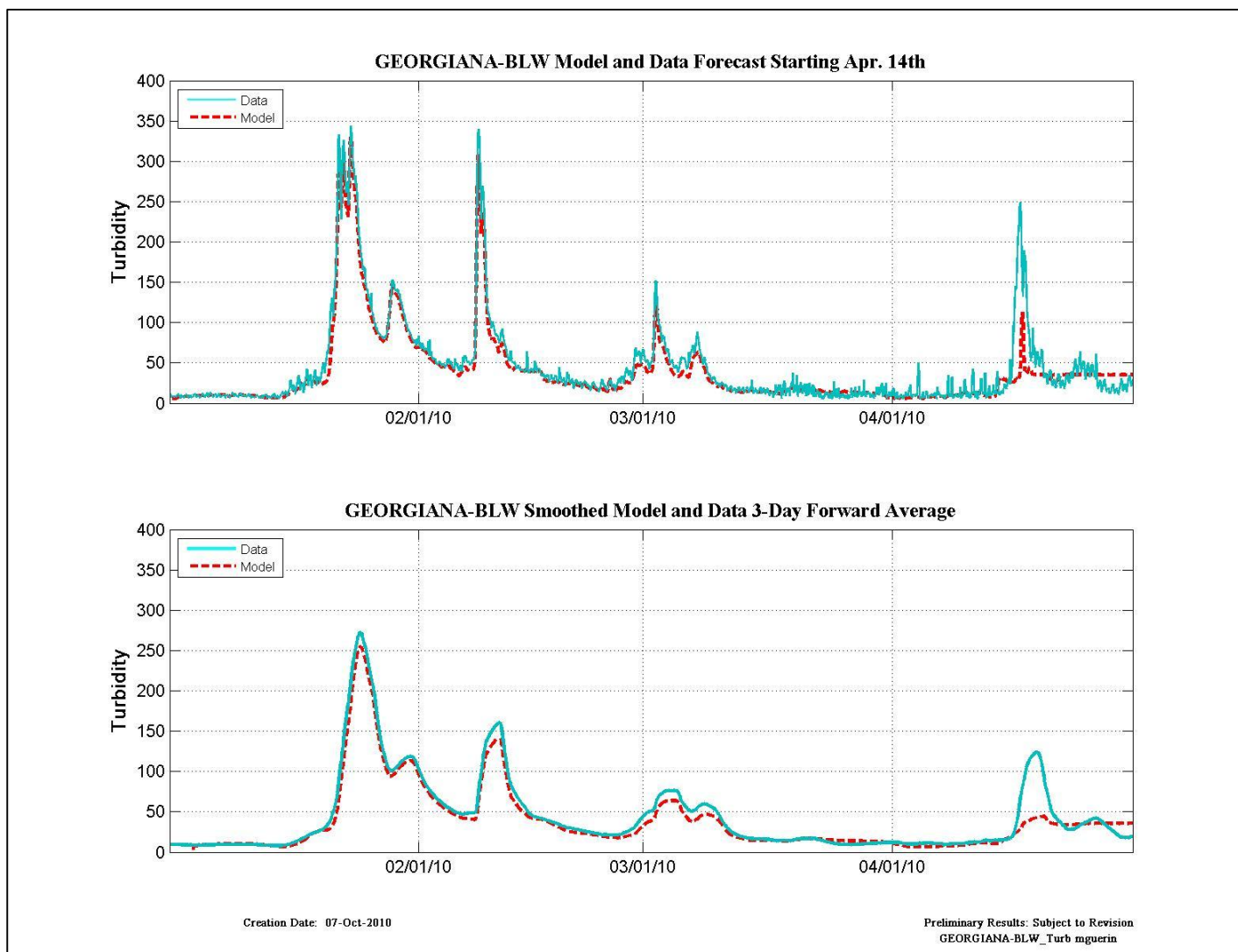


Figure 12-5 Turbidity data and model results for the RMA forecast beginning April 14th at Georgiana-BLW.

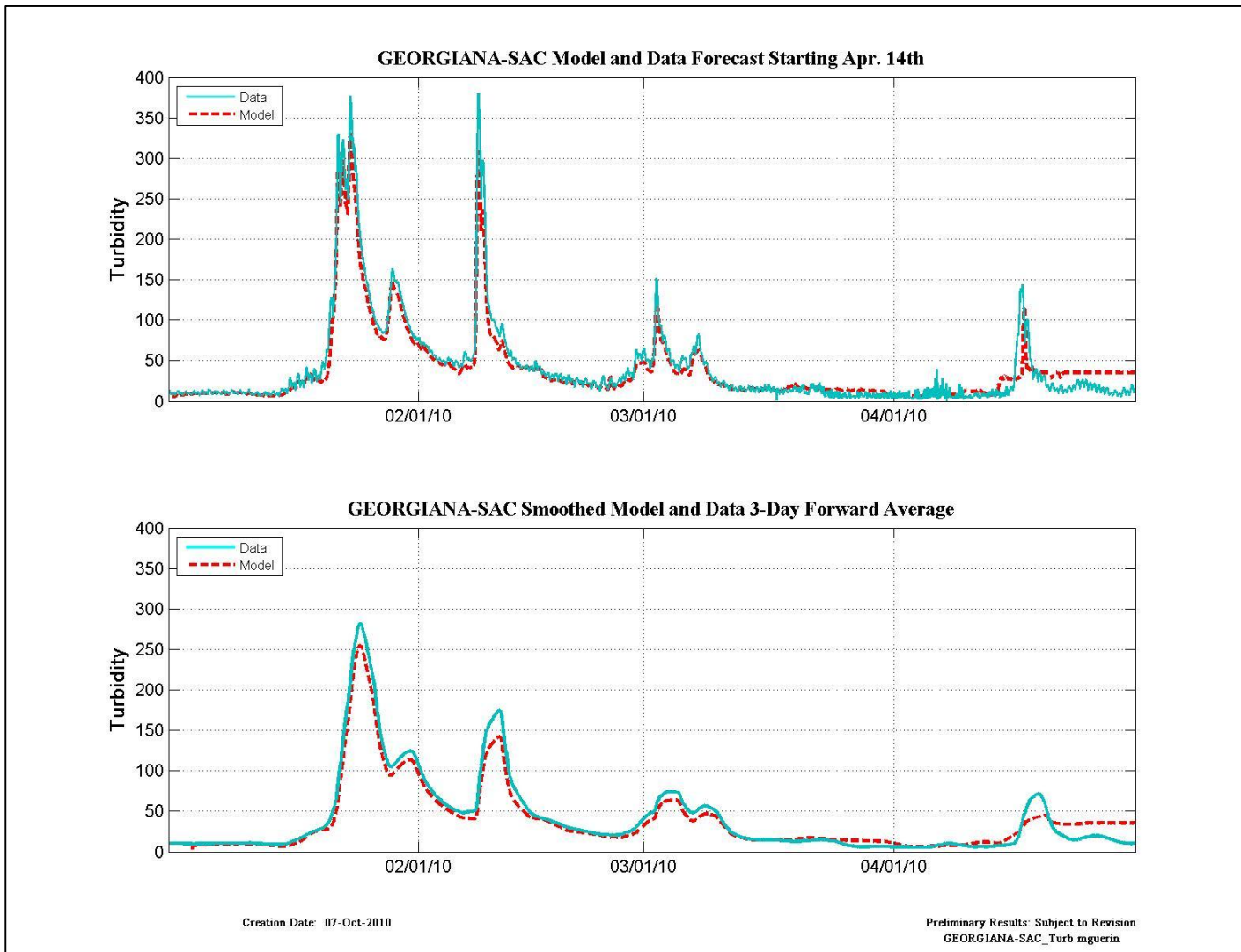


Figure 12-6 Turbidity data and model results for the RMA forecast beginning April 14th at Georgiana-SAC.

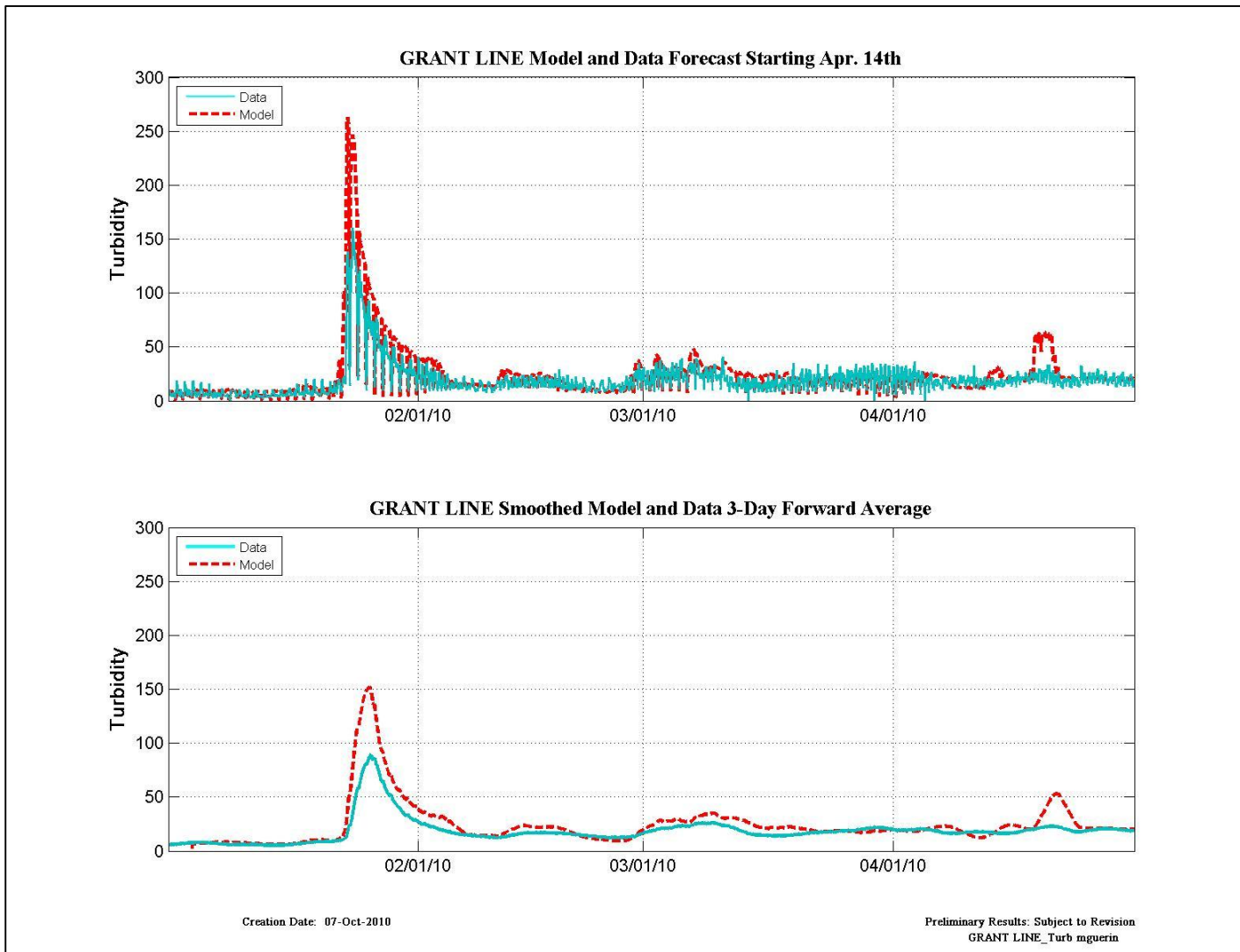


Figure 12-7 Turbidity data and model results for the RMA forecast beginning April 14th at Grant Line.

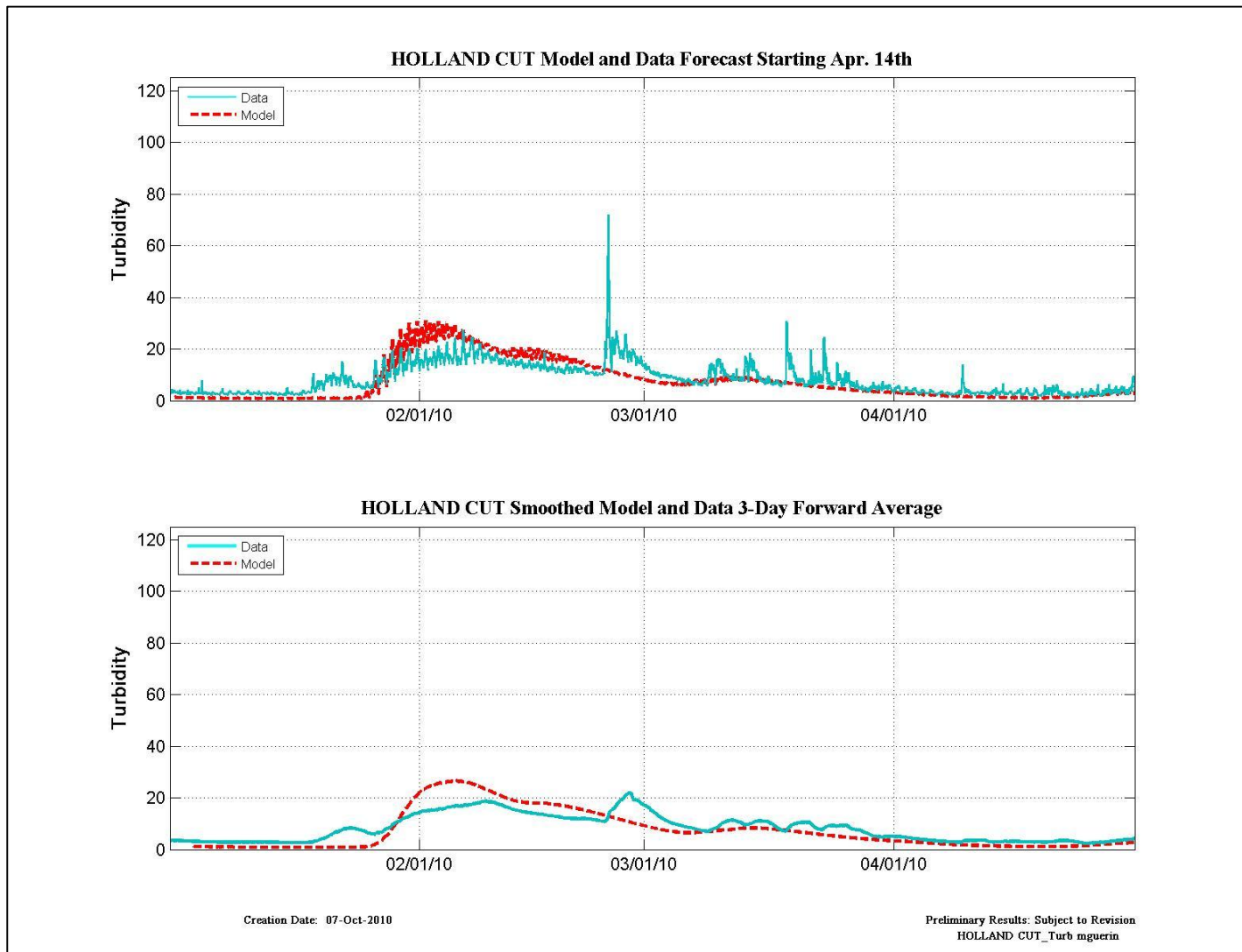


Figure 12-8 Turbidity data and model results for the RMA forecast beginning April 14th at Holland Cut.

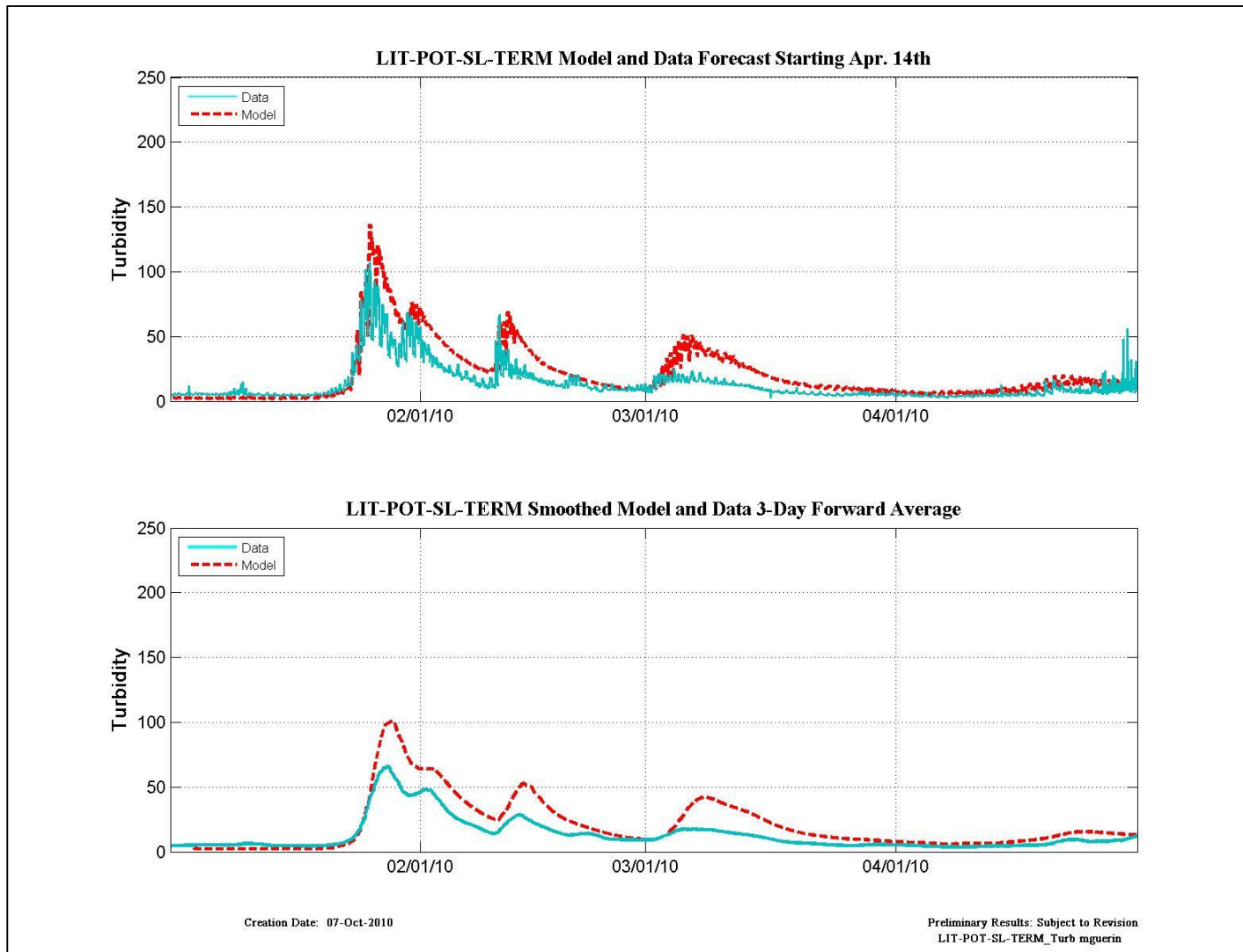


Figure 12-9 Turbidity data and model results for the RMA forecast beginning April 14th at LIT-POT-SL-TERM.

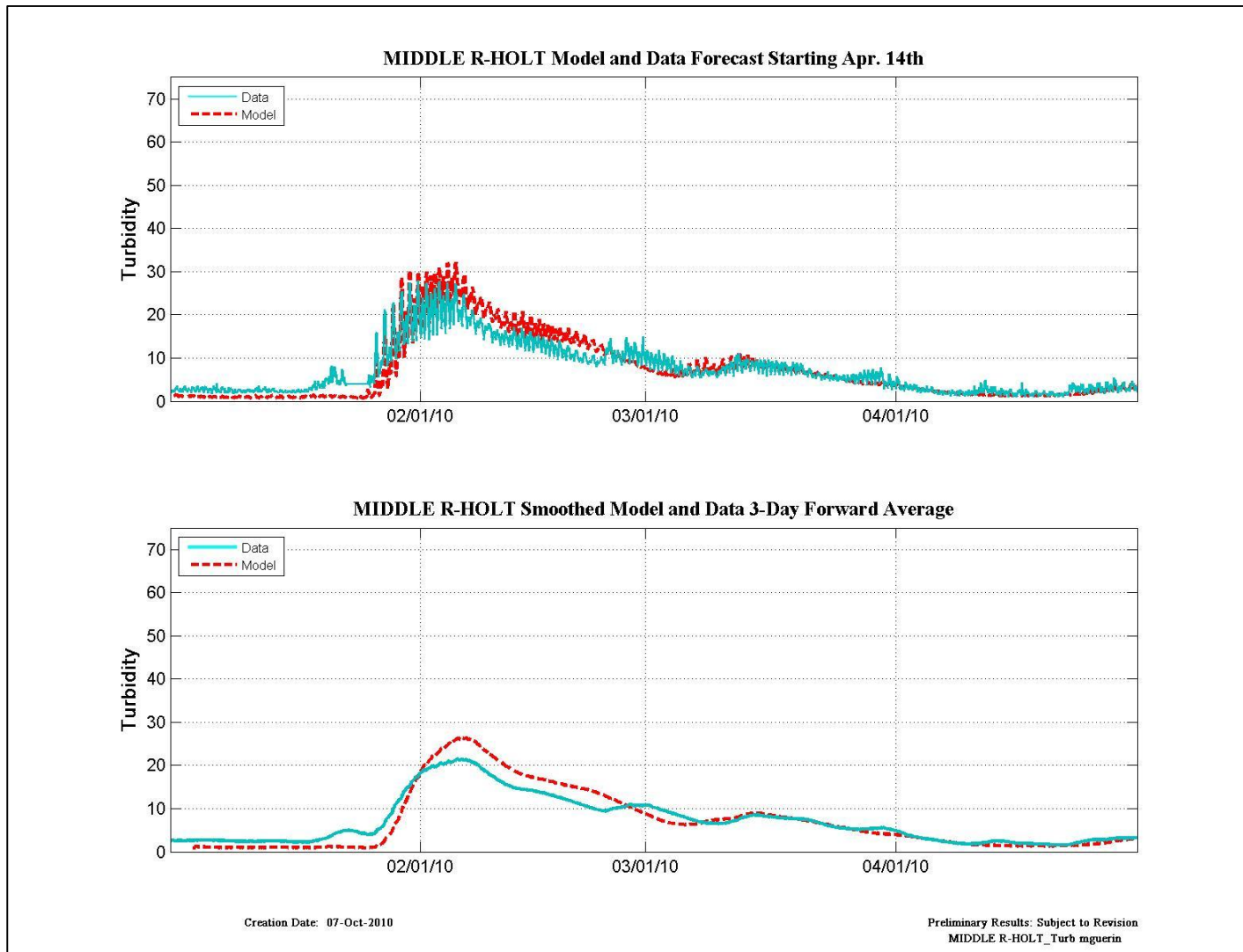


Figure 12-10 Turbidity data and model results for the RMA forecast beginning April 14th at Middle R-Holt.

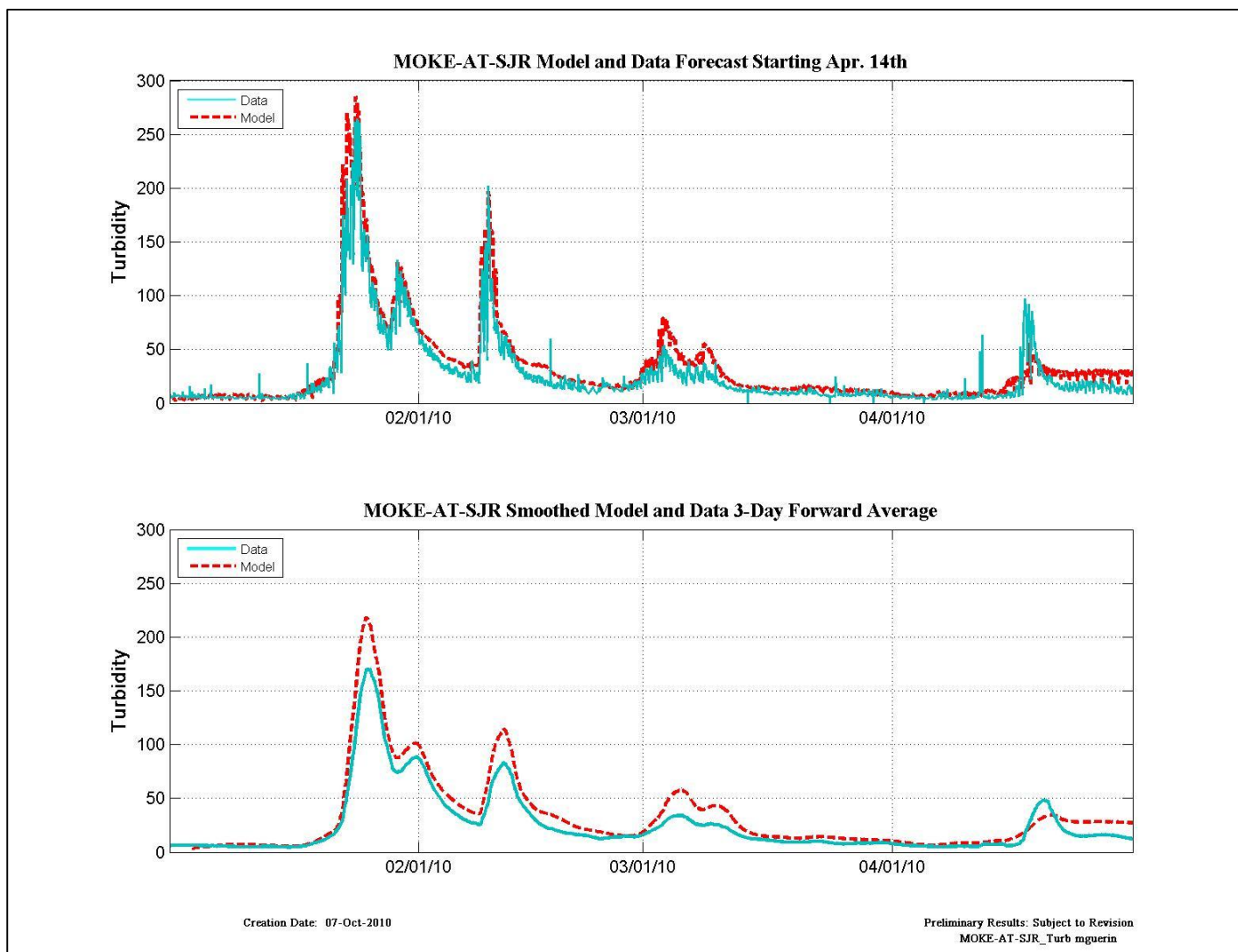


Figure 12-11 Turbidity data and model results for the RMA forecast beginning April 14th at Moke-at-SJR.

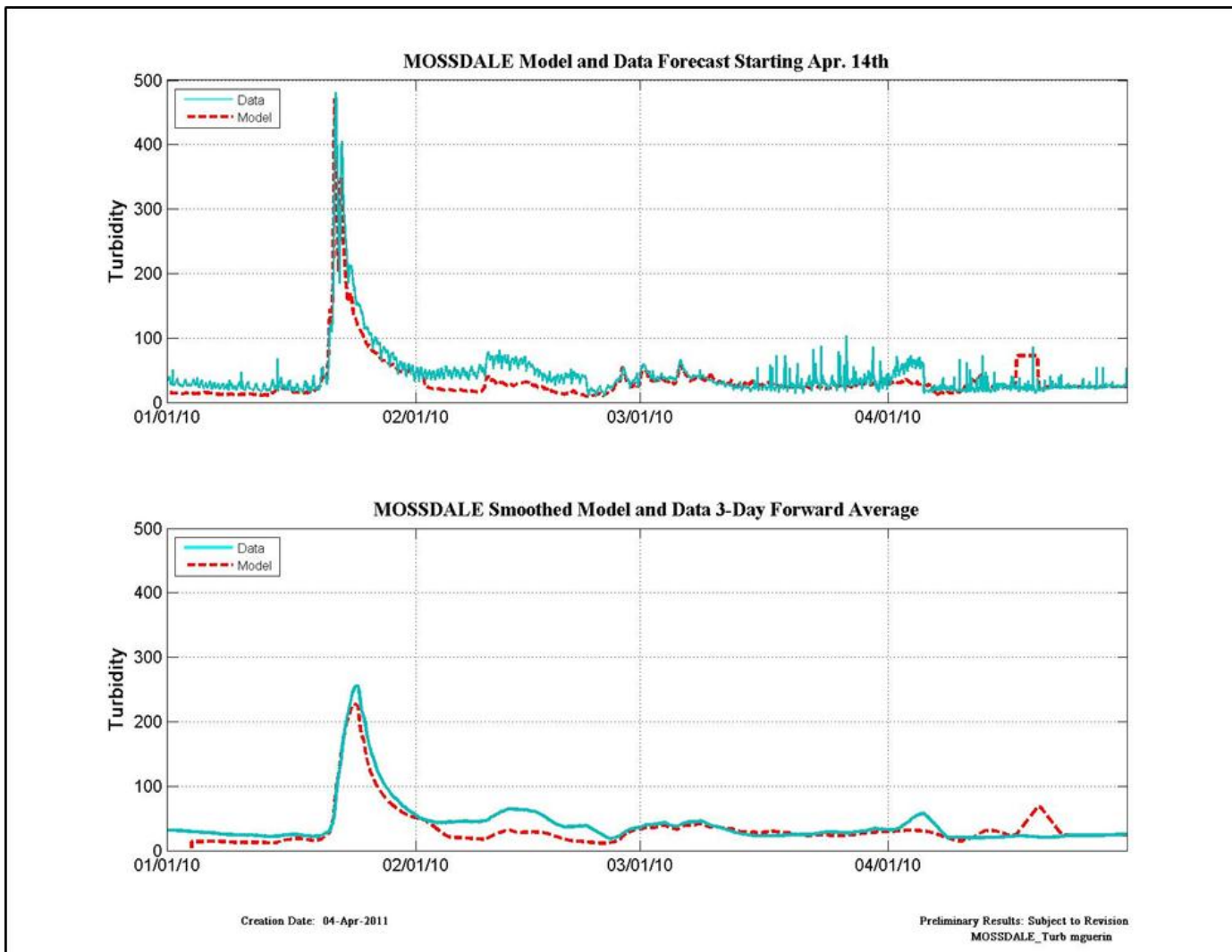


Figure 12-12 Turbidity data and model results for the RMA forecast beginning April 14th at Mossdale.

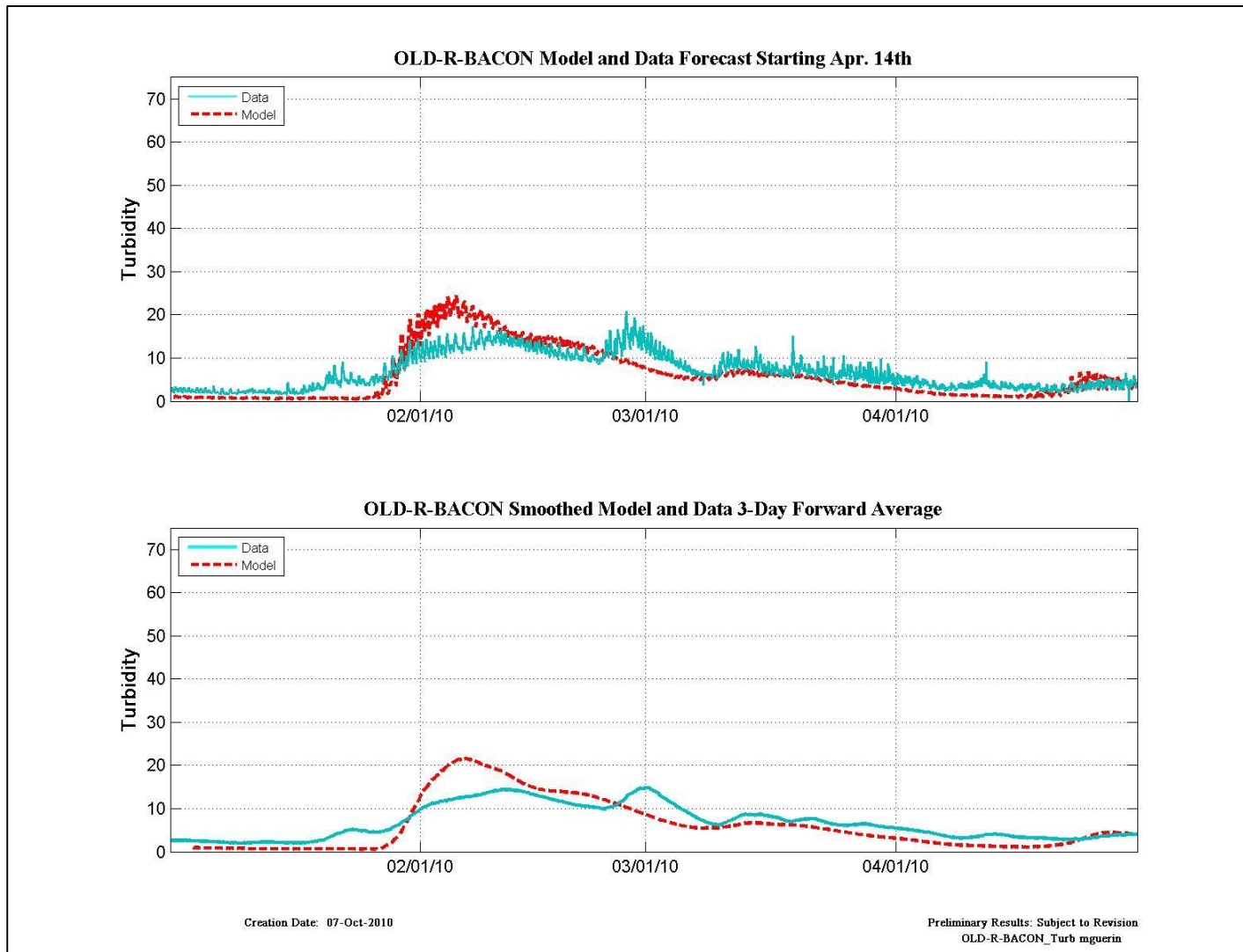


Figure 12-13 Turbidity data and model results for the RMA forecast beginning April 14th at Old-R-Bacon.

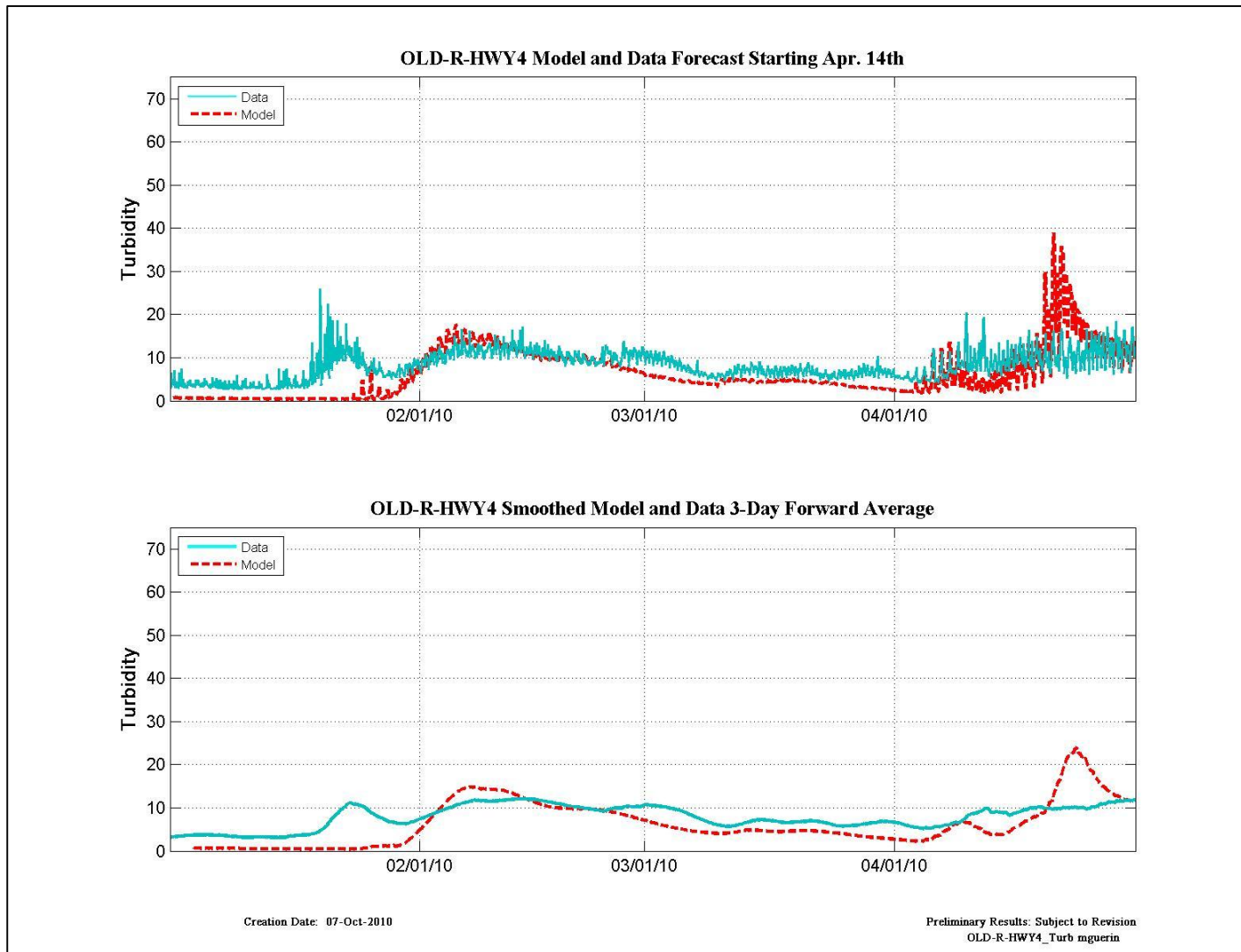


Figure 12-14 Turbidity data and model results for the RMA forecast beginning April 14th at Old-R-Hwy 4.

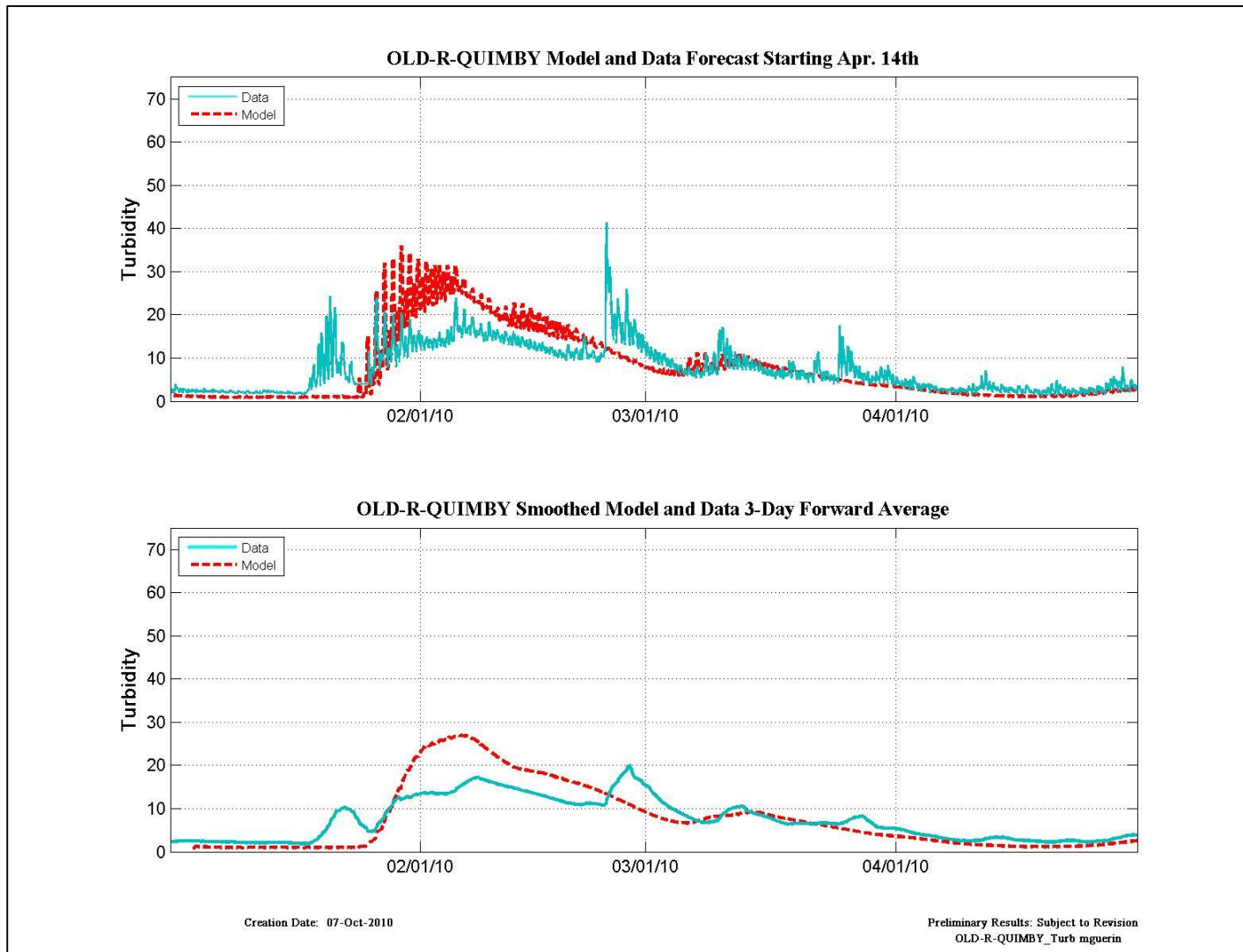


Figure 12-15 Turbidity data and model results for the RMA forecast beginning April 14th at Old-R-Quimby.

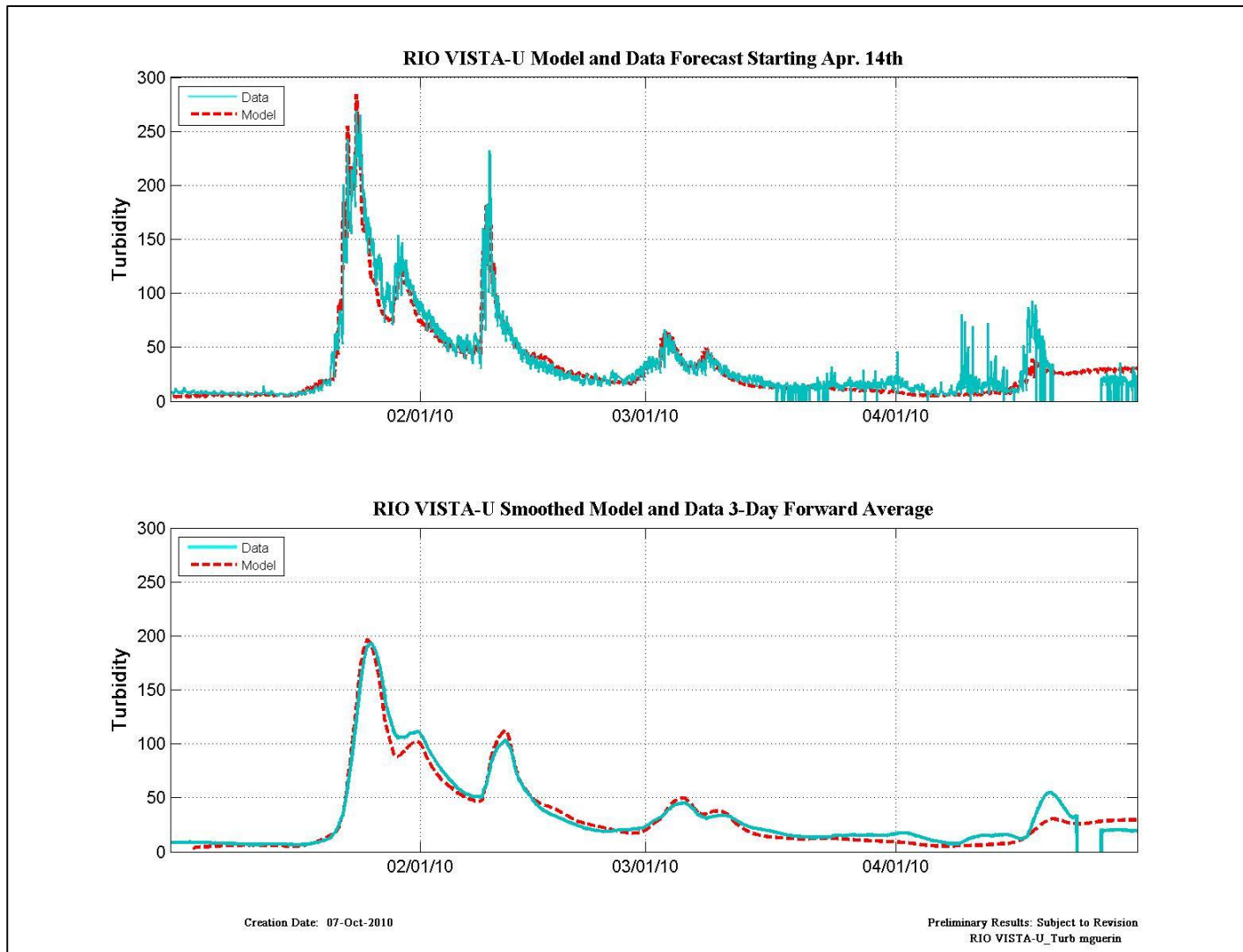


Figure 12-16 Turbidity data and model results for the RMA forecast beginning April 14th at Rio Vista-U.

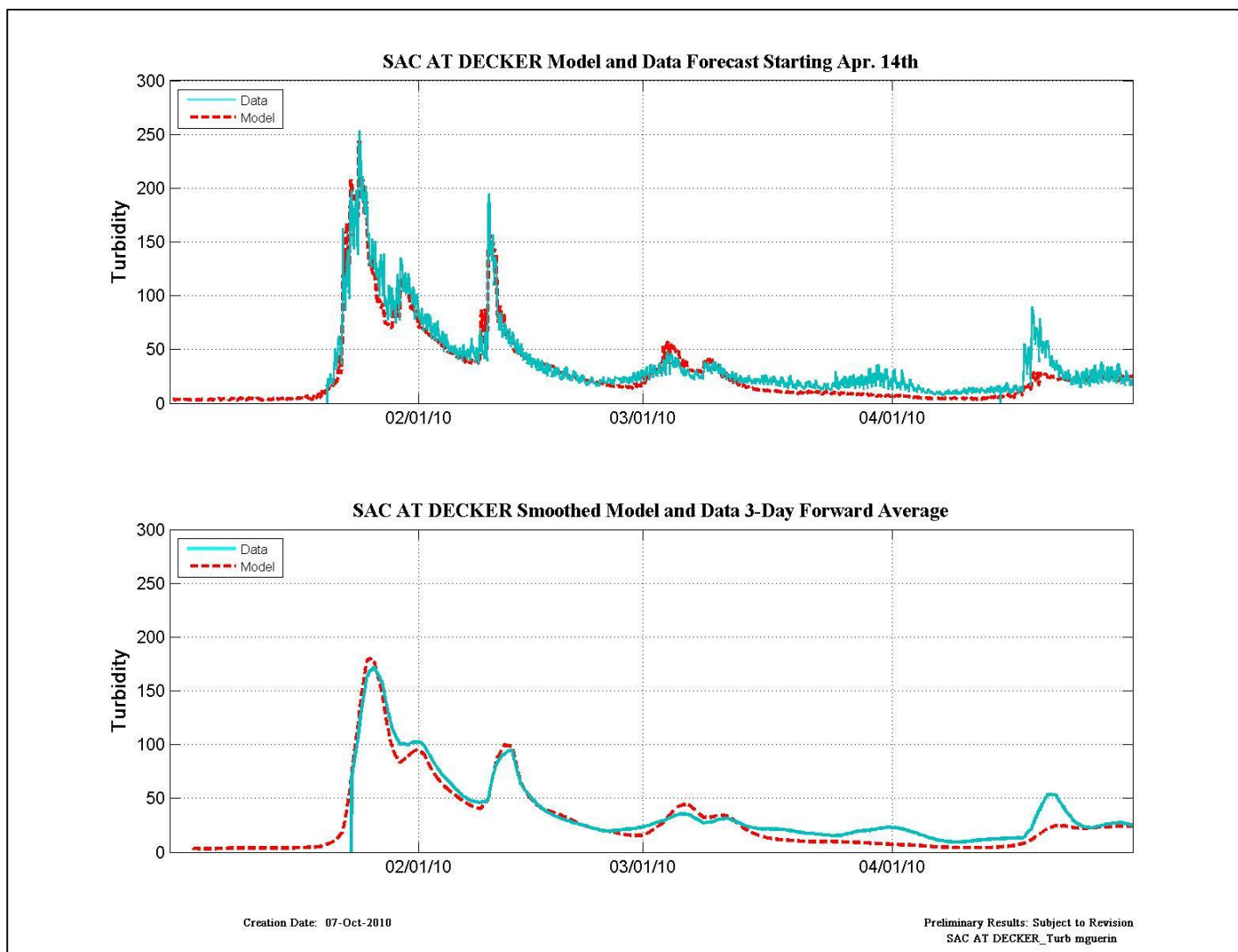


Figure 12-17 Turbidity data and model results for the RMA forecast beginning April 14th at SAC AT Decker.

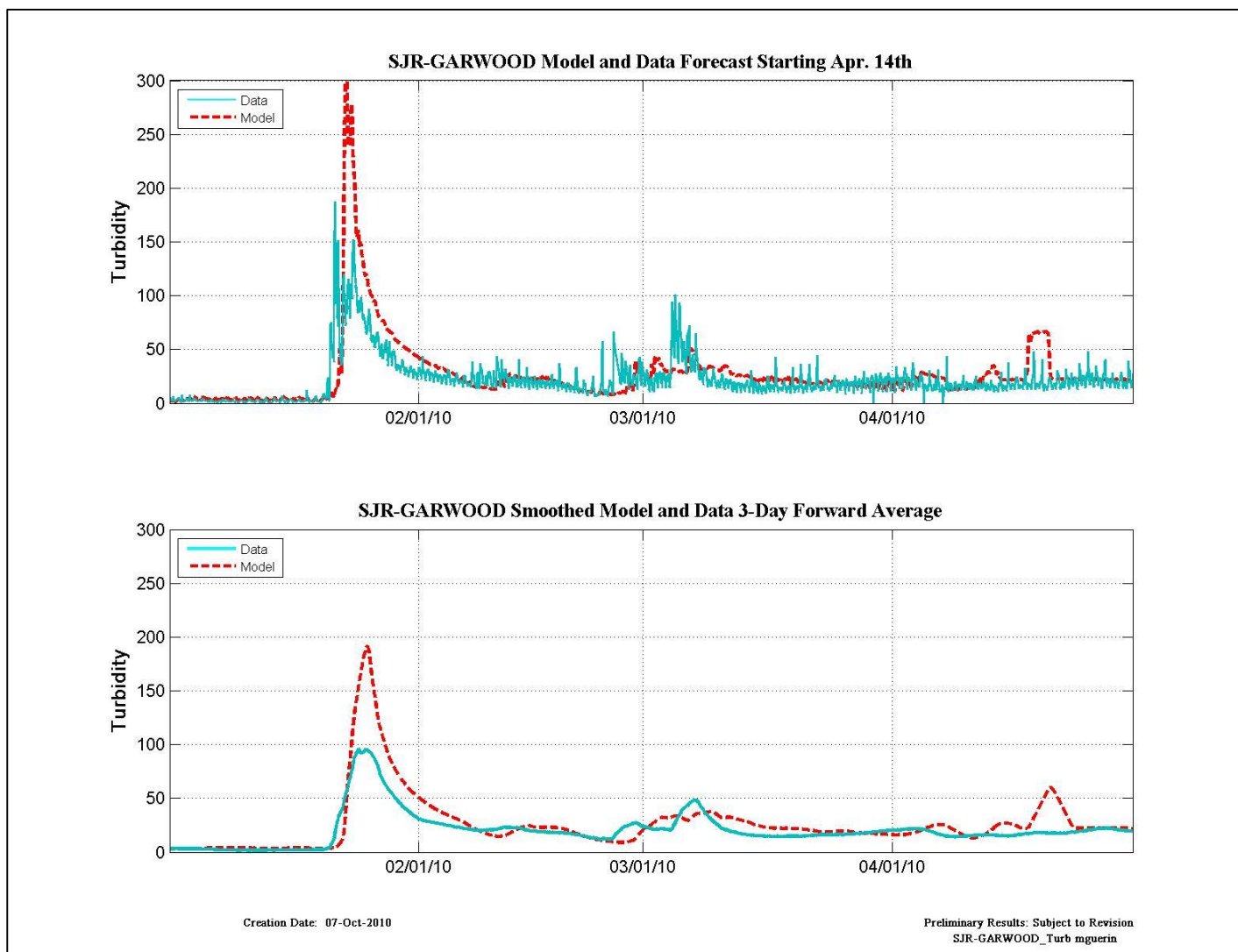


Figure 12-18 Turbidity data and model results for the RMA forecast beginning April 14th at SJR-Garwood.

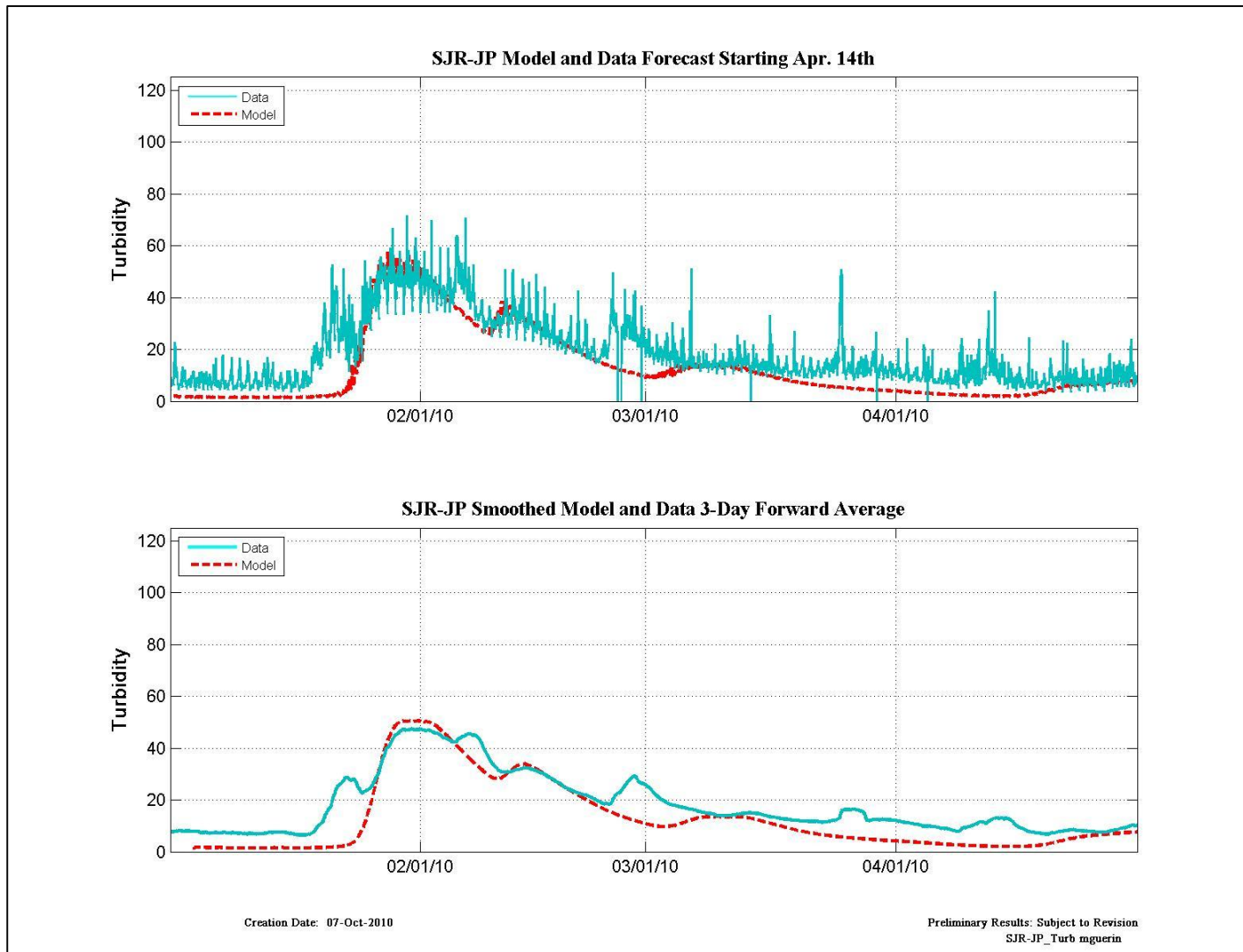


Figure 12-19 Turbidity data and model results for the RMA forecast beginning April 14th at SJR-JP.

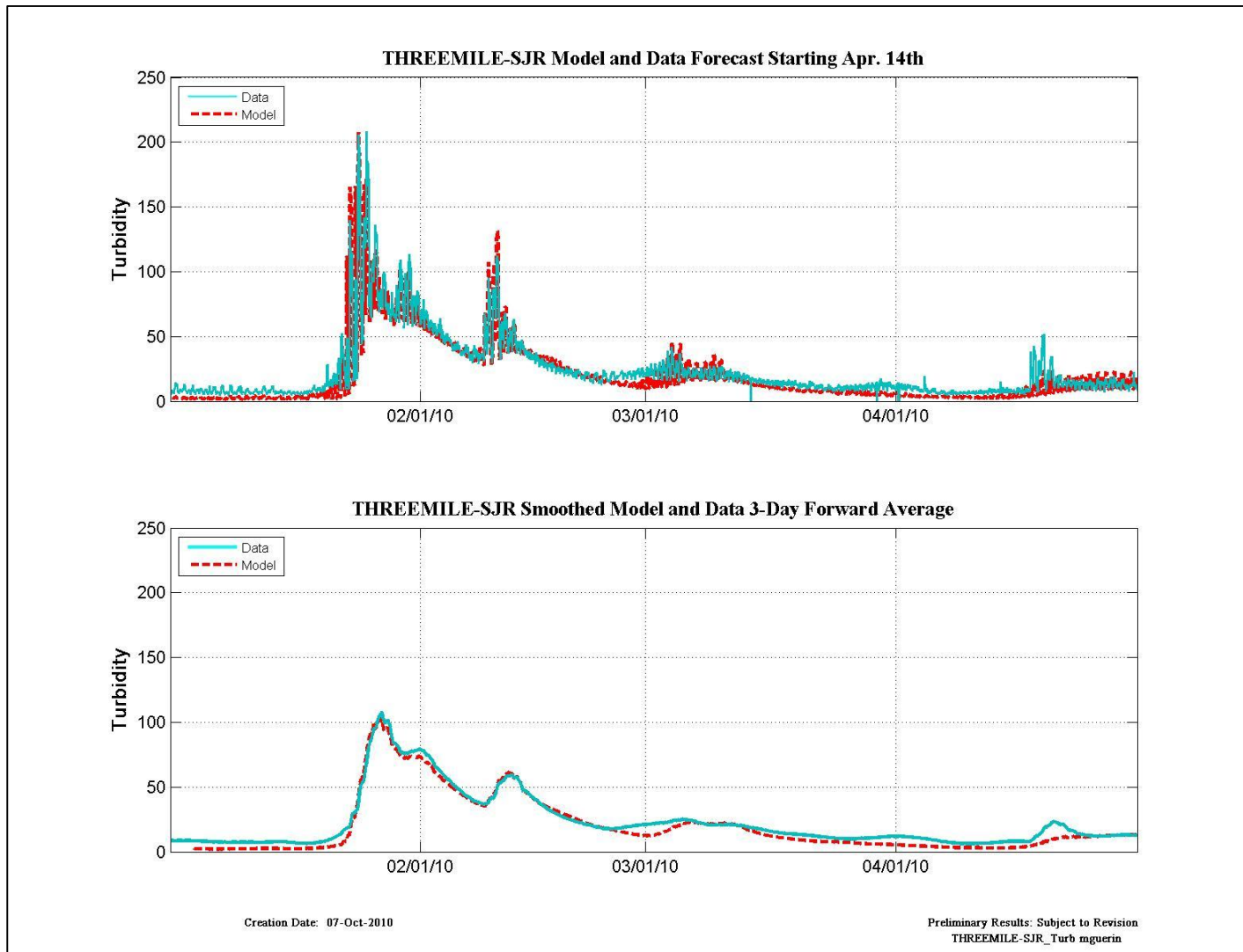


Figure 12-20 Turbidity data and model results for the RMA forecast beginning April 14th at Threemile-SJR.

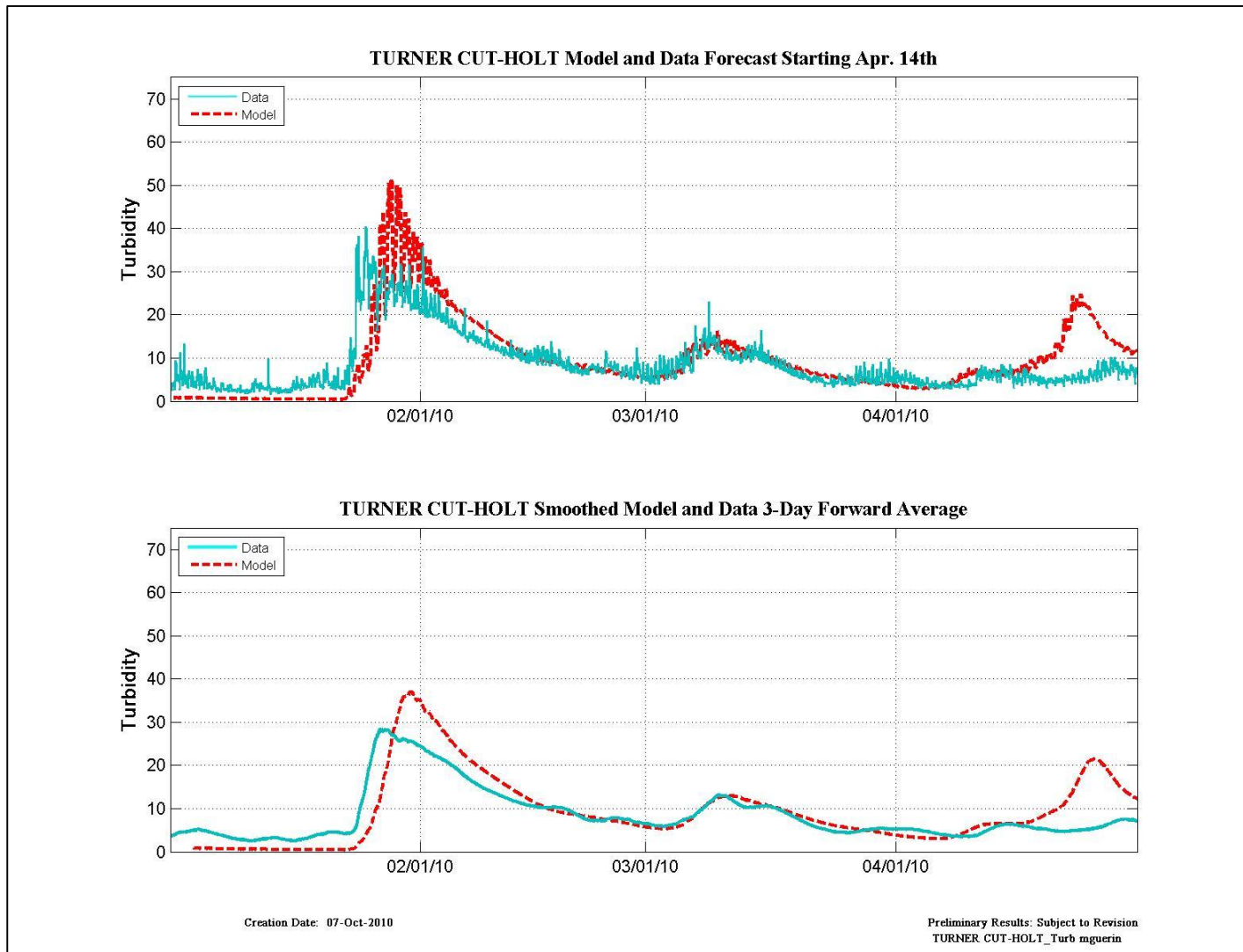


Figure 12-21 Turbidity data and model results for the RMA forecast beginning April 14th at Turner Cut-Holt.

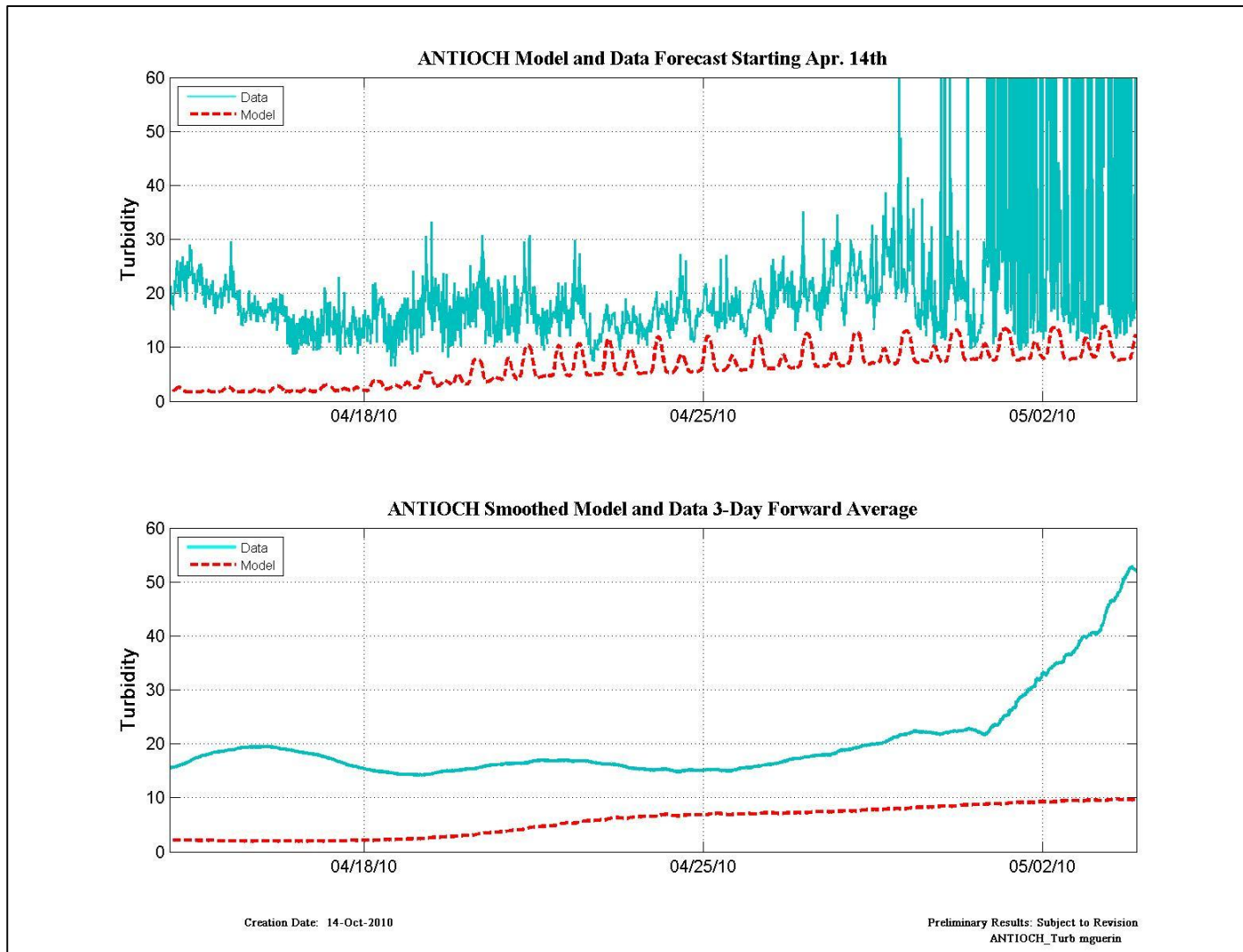


Figure 12-22 Expanded results - turbidity data and model results for the RMA forecast beginning April 14th at Antioch.

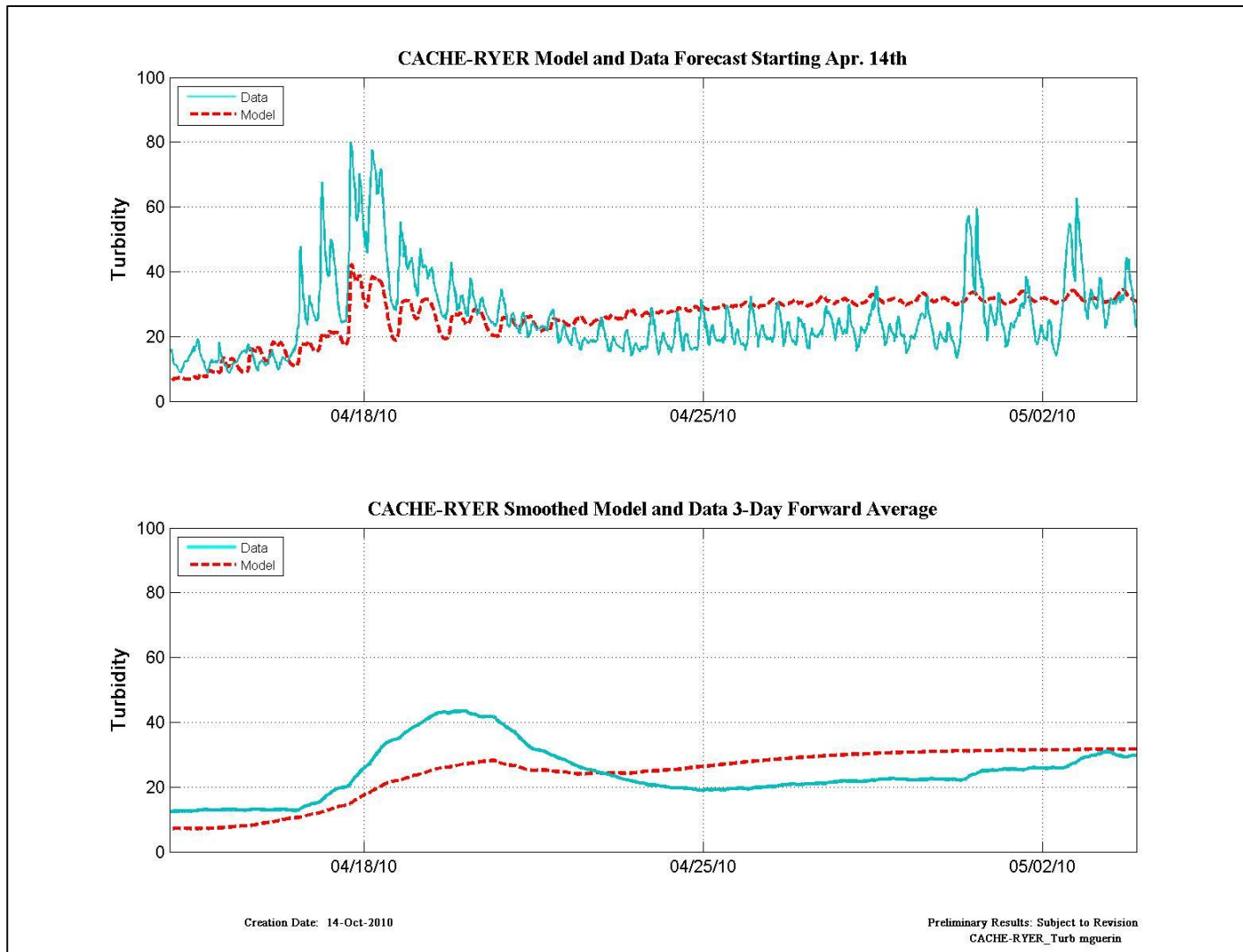


Figure 12-23 Expanded results - turbidity data and model results for the RMA forecast beginning April 14th at Cache-Ryer.

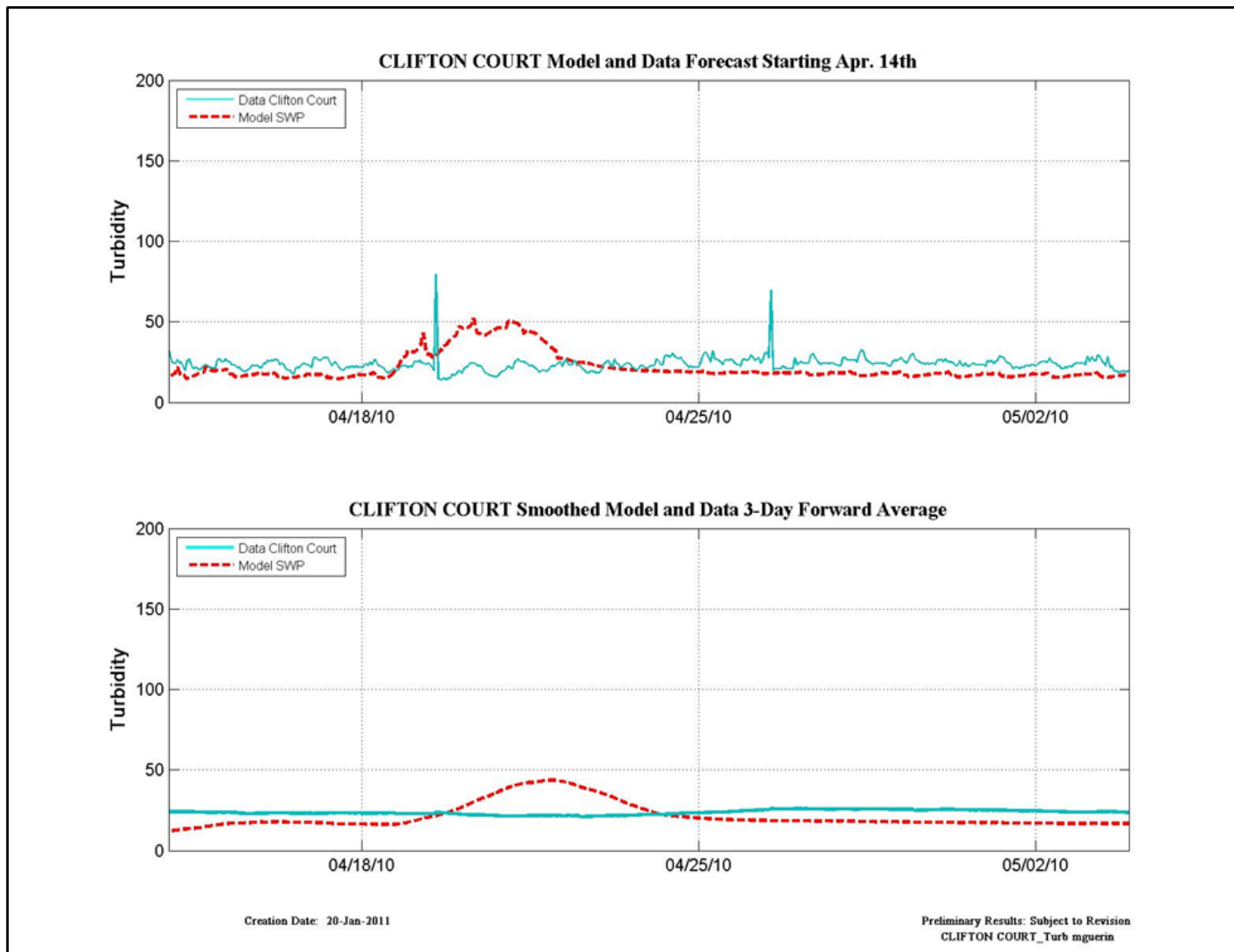


Figure 12-24 Expanded results - turbidity data and model results for the RMA forecast beginning April 14th at Clifton Court (data) and SWP (model).

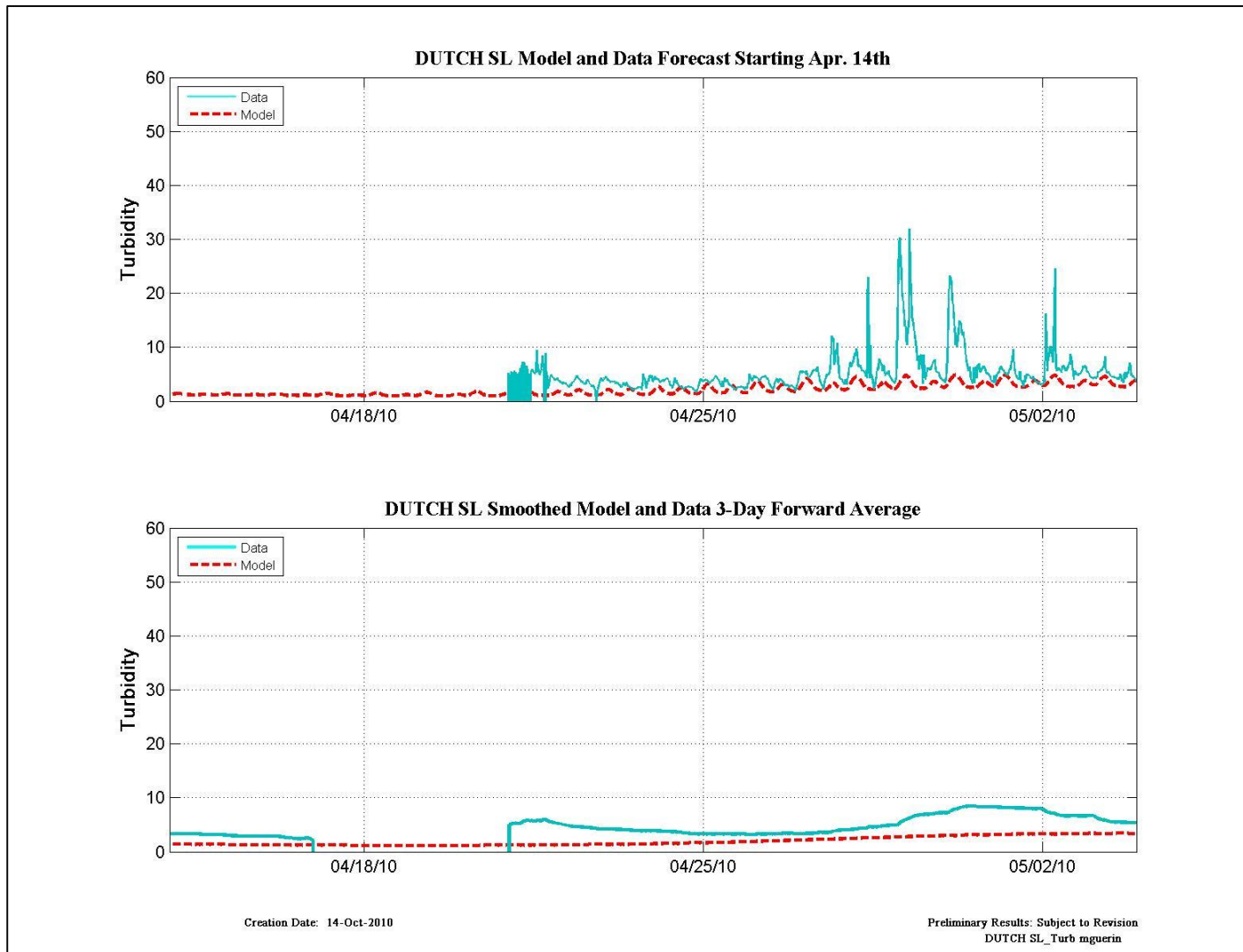


Figure 12-25 Expanded results - turbidity data and model results for the RMA forecast beginning April 14th at Dutch SL.

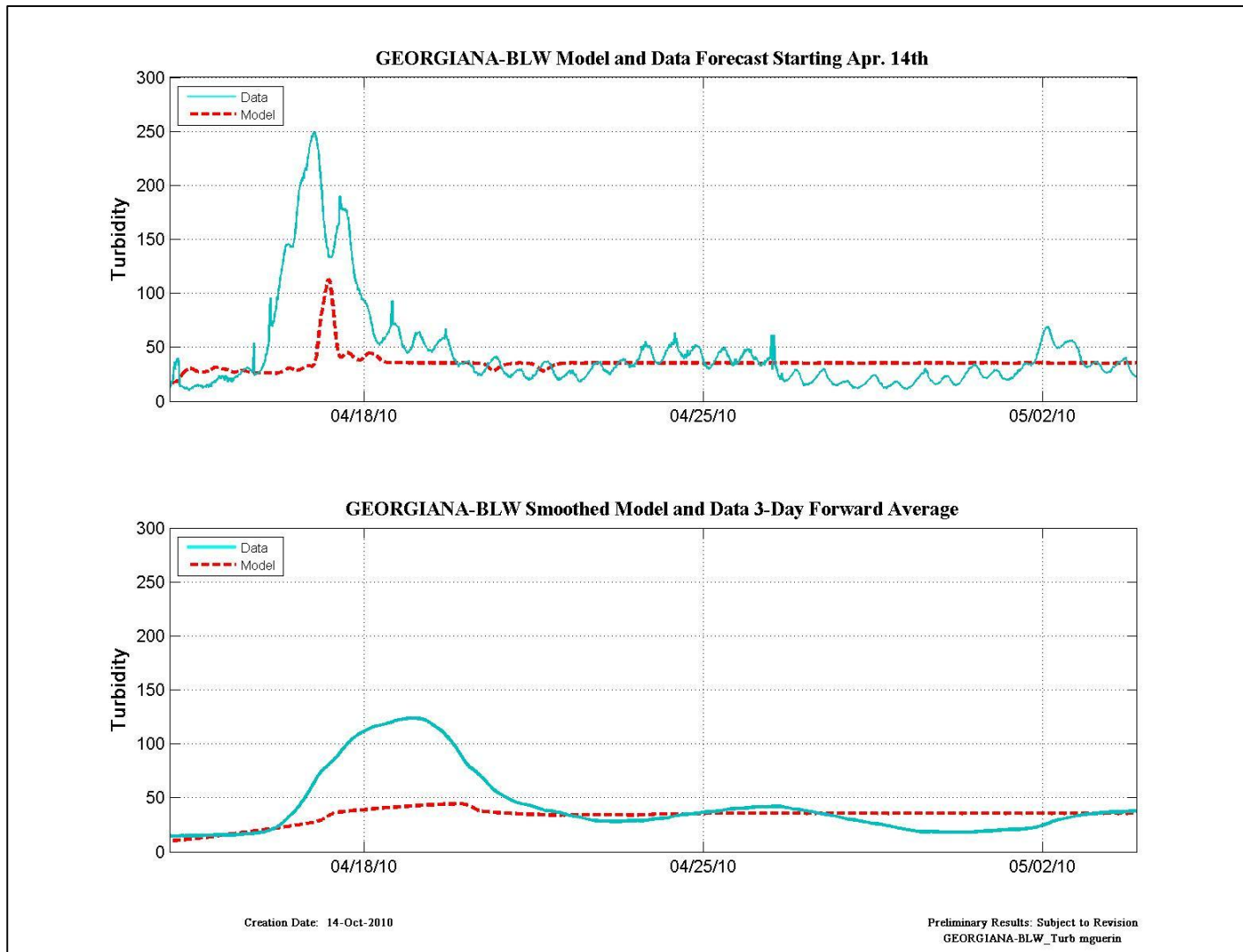


Figure 12-26 Expanded results - turbidity data and model results for the RMA forecast beginning April 14th at Georgiana-BLW.

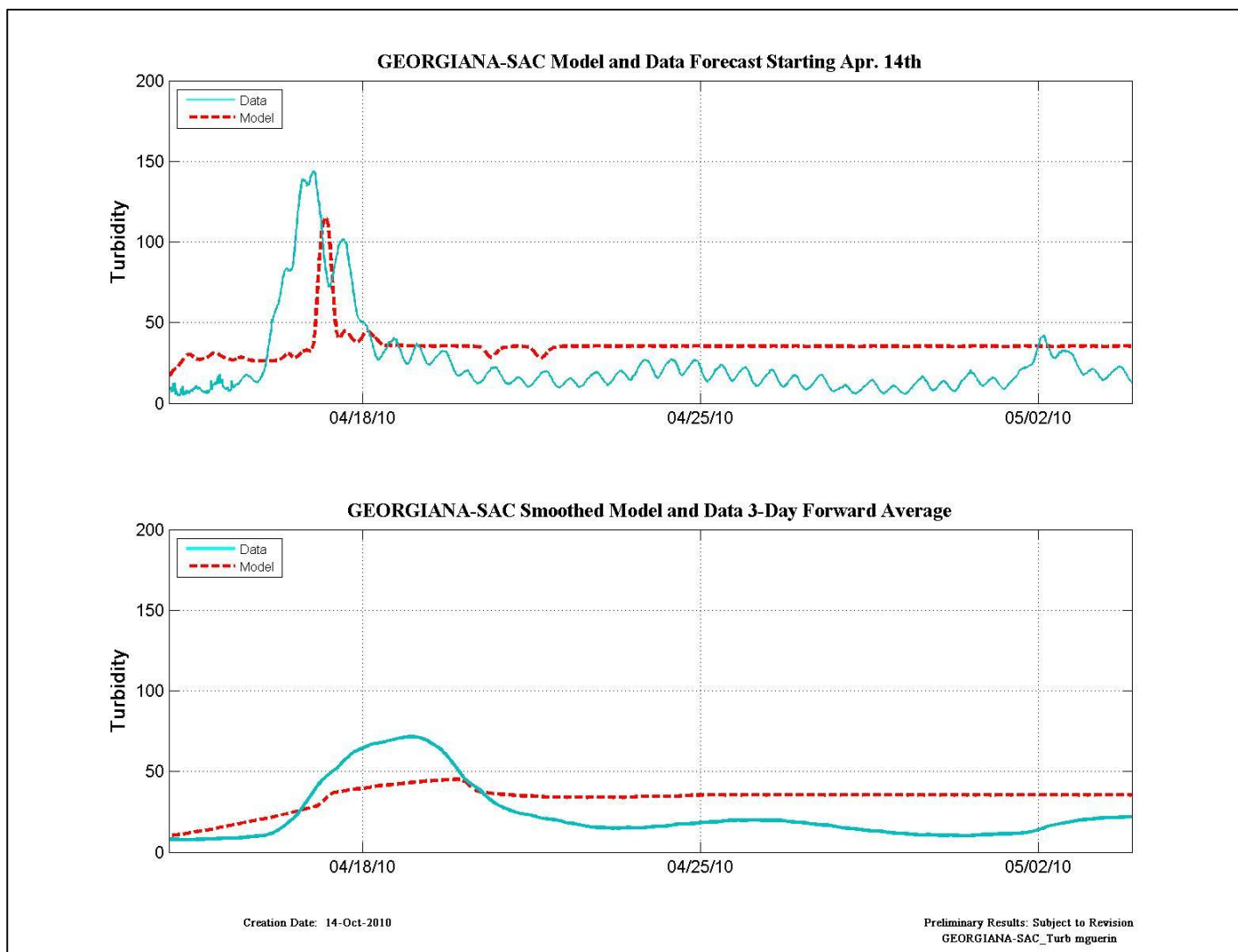


Figure 12-27 Expanded results - turbidity data and model results for the RMA forecast beginning April 14th at Georgiana-SAC.

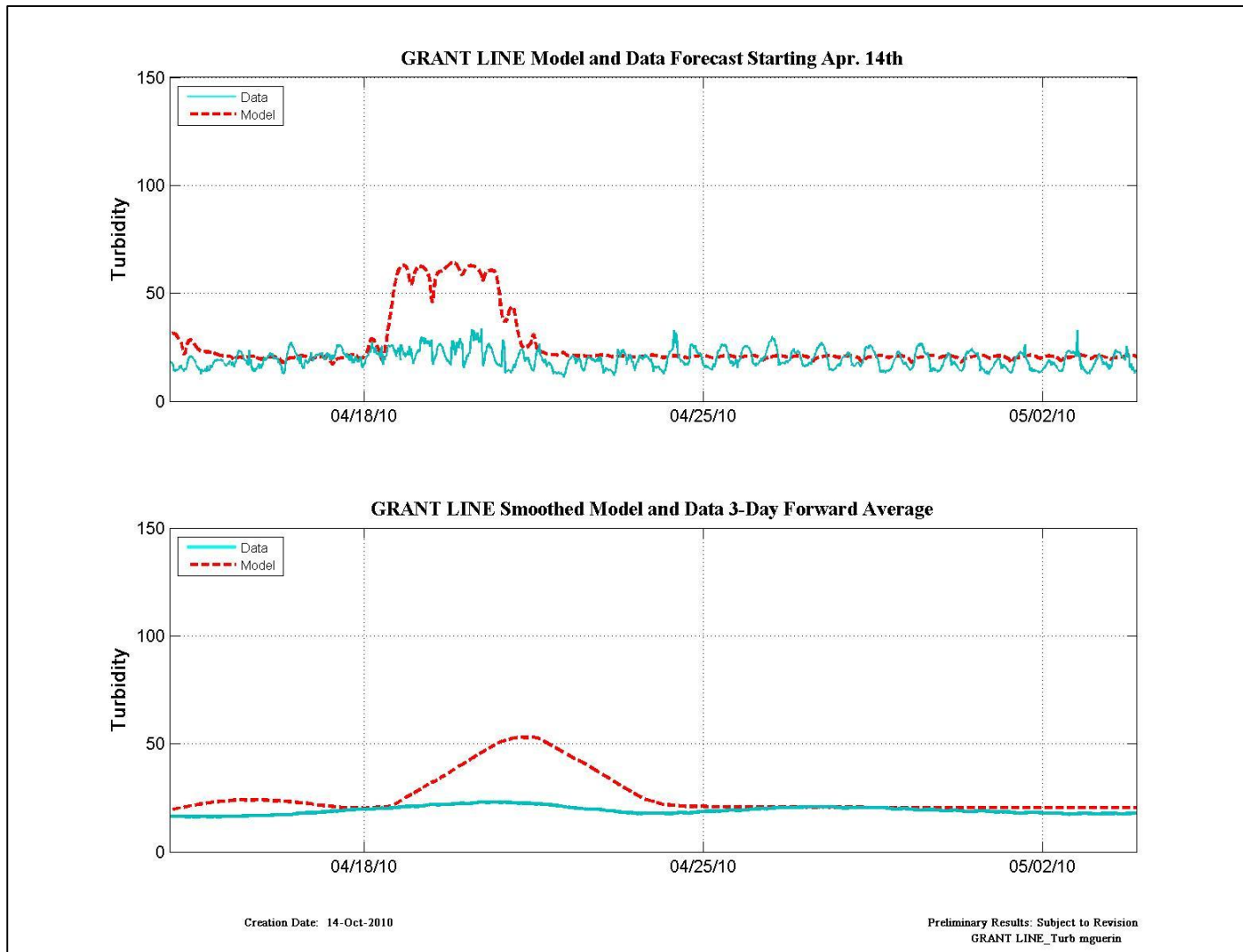


Figure 12-28 Expanded results - turbidity data and model results for the RMA forecast beginning April 14th at Grant Line.

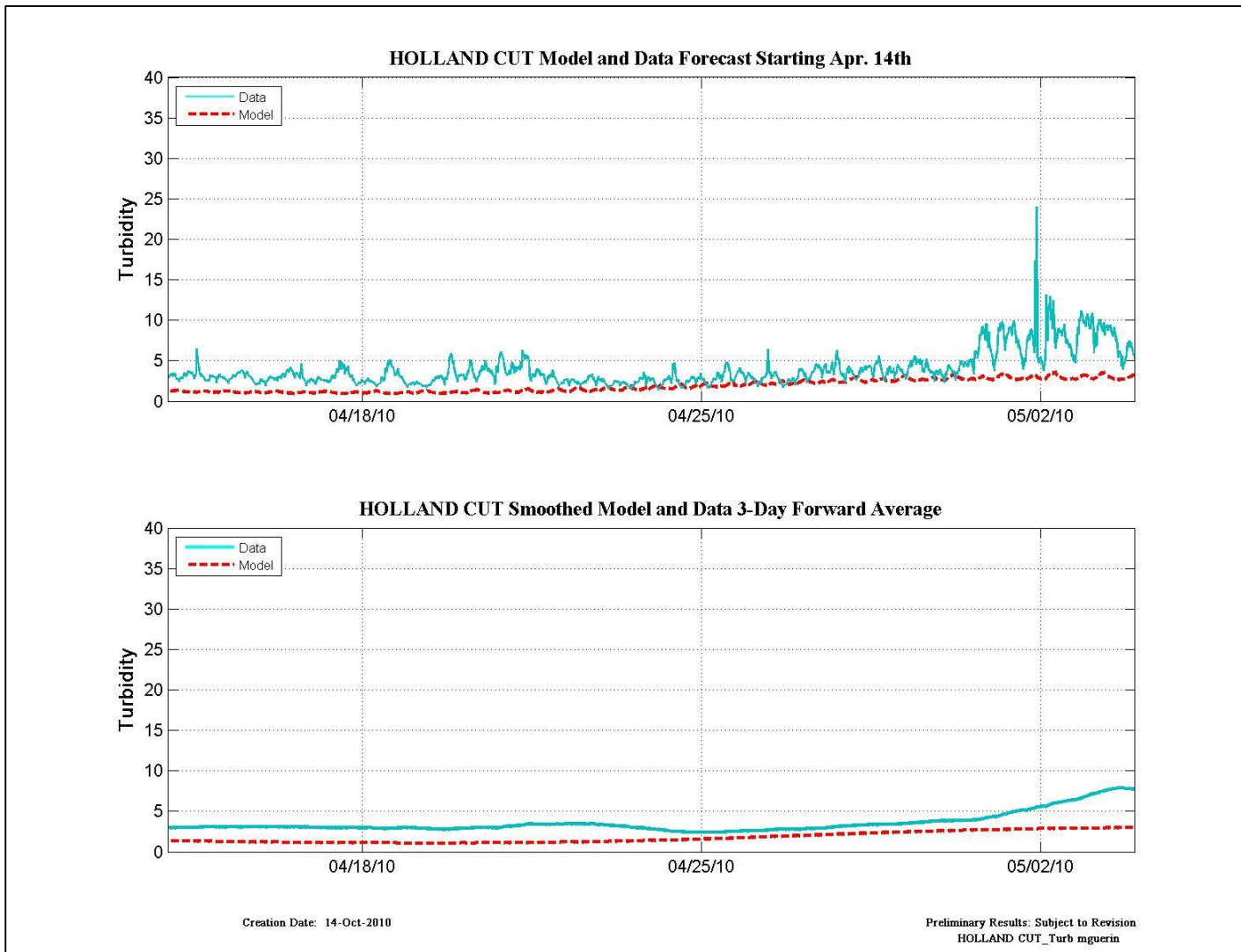


Figure 12-29 Expanded results - turbidity data and model results for the RMA forecast beginning April 14th at Holland Cut.

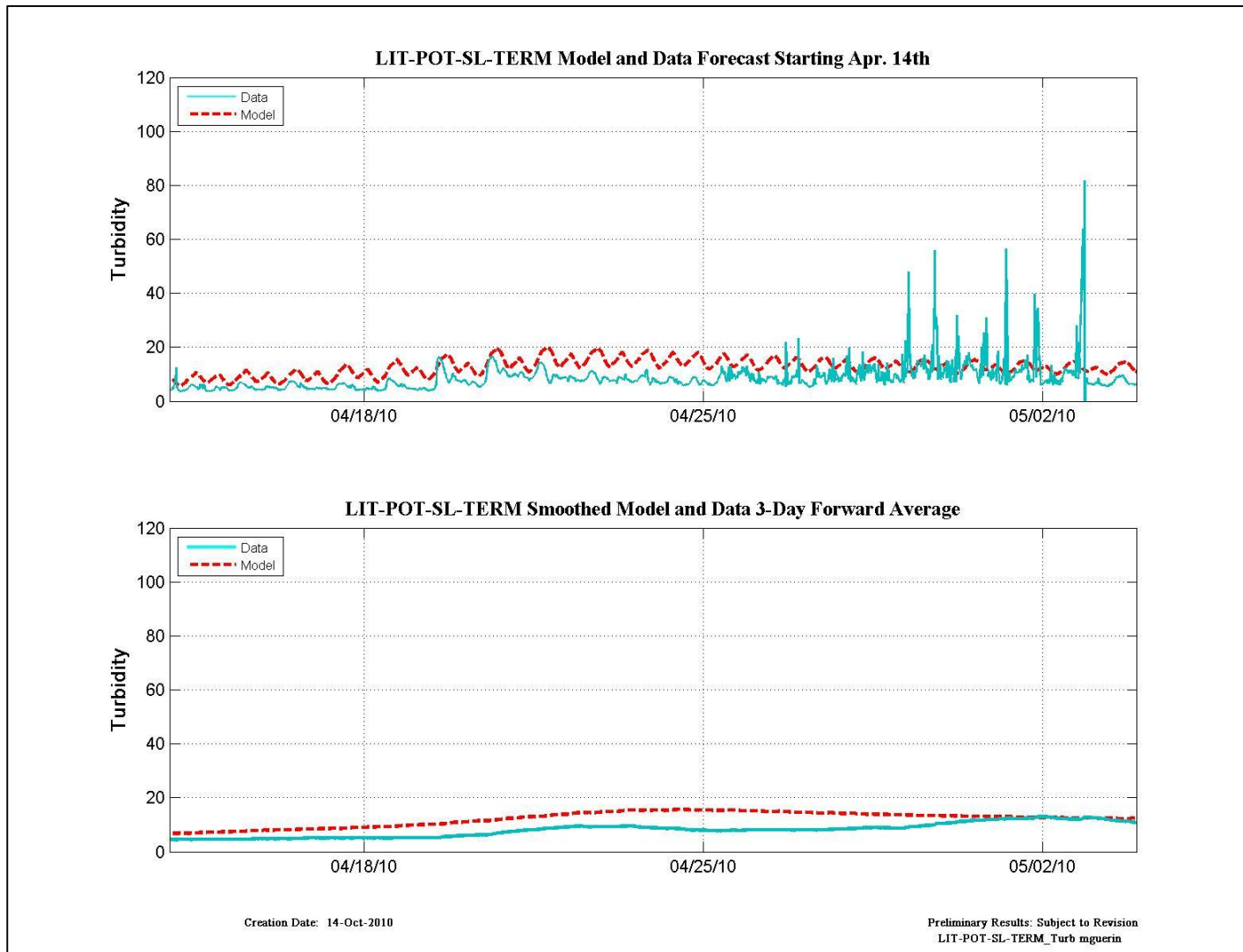


Figure 12-30 Expanded results - turbidity data and model results for the RMA forecast beginning April 14th at LIT-POT-SL.

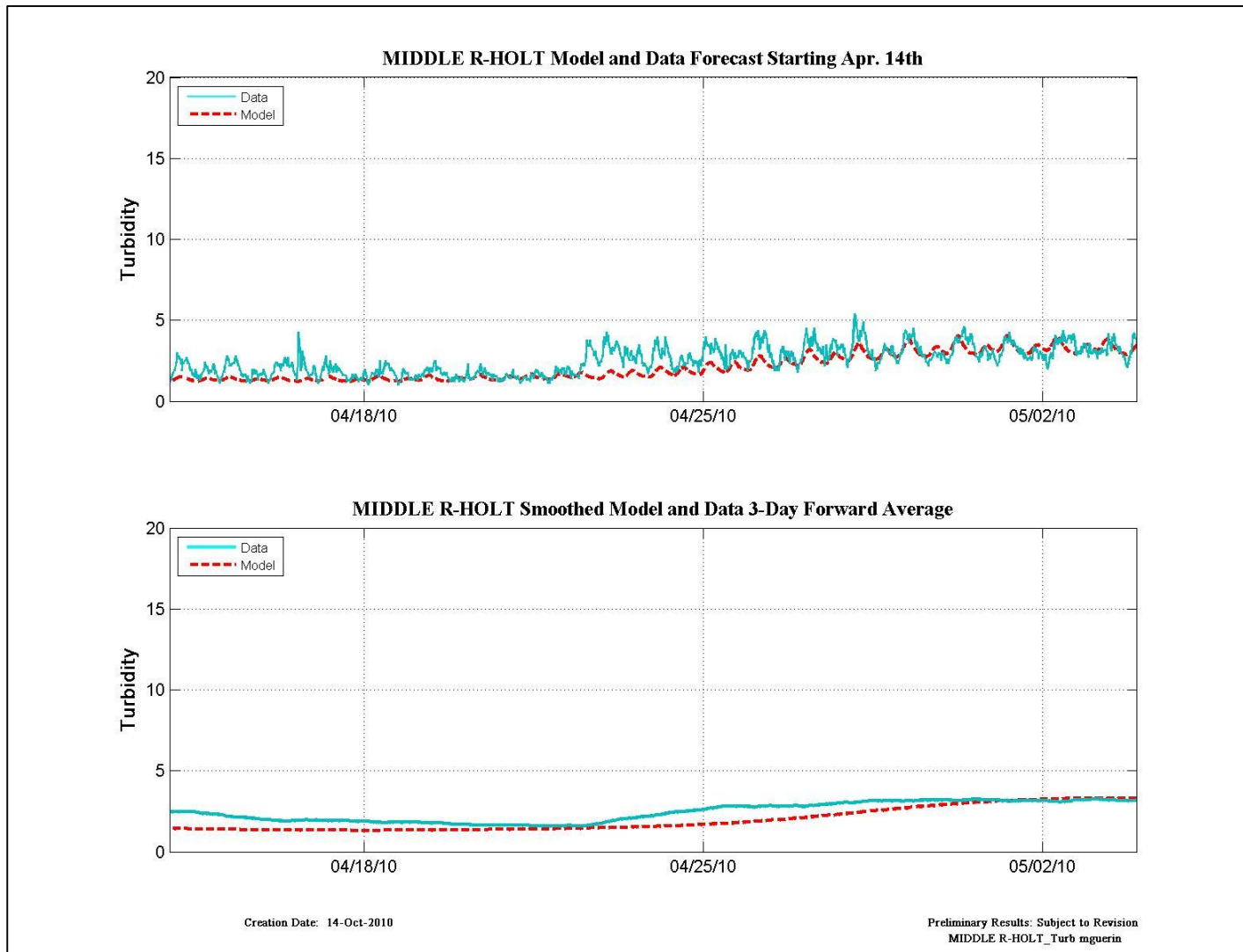


Figure 12-31 Expanded results - turbidity data and model results for the RMA forecast beginning April 14th at Middle R-Holt.

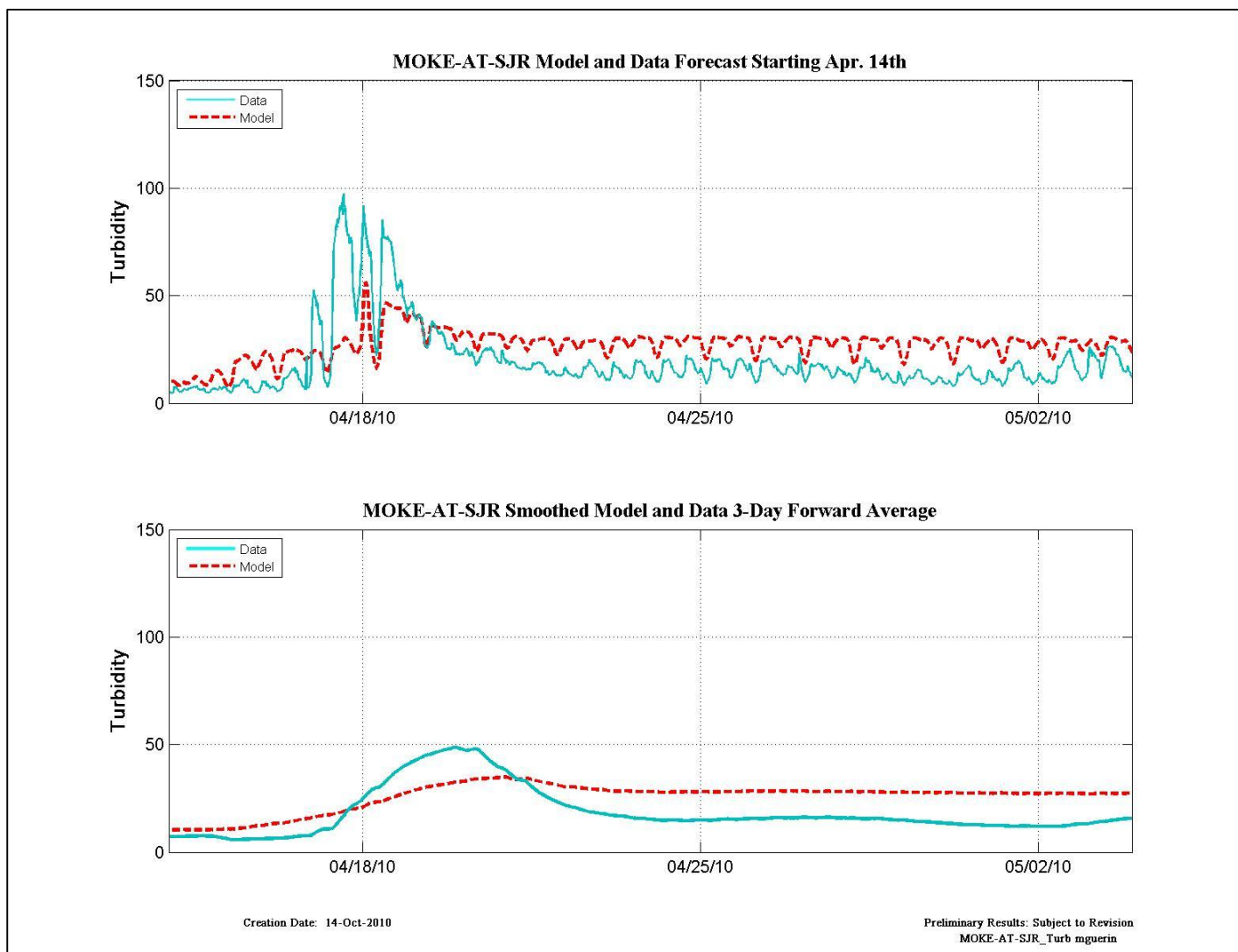


Figure 12-32 Expanded results - turbidity data and model results for the RMA forecast beginning April 14th at Moke-at-SJR.

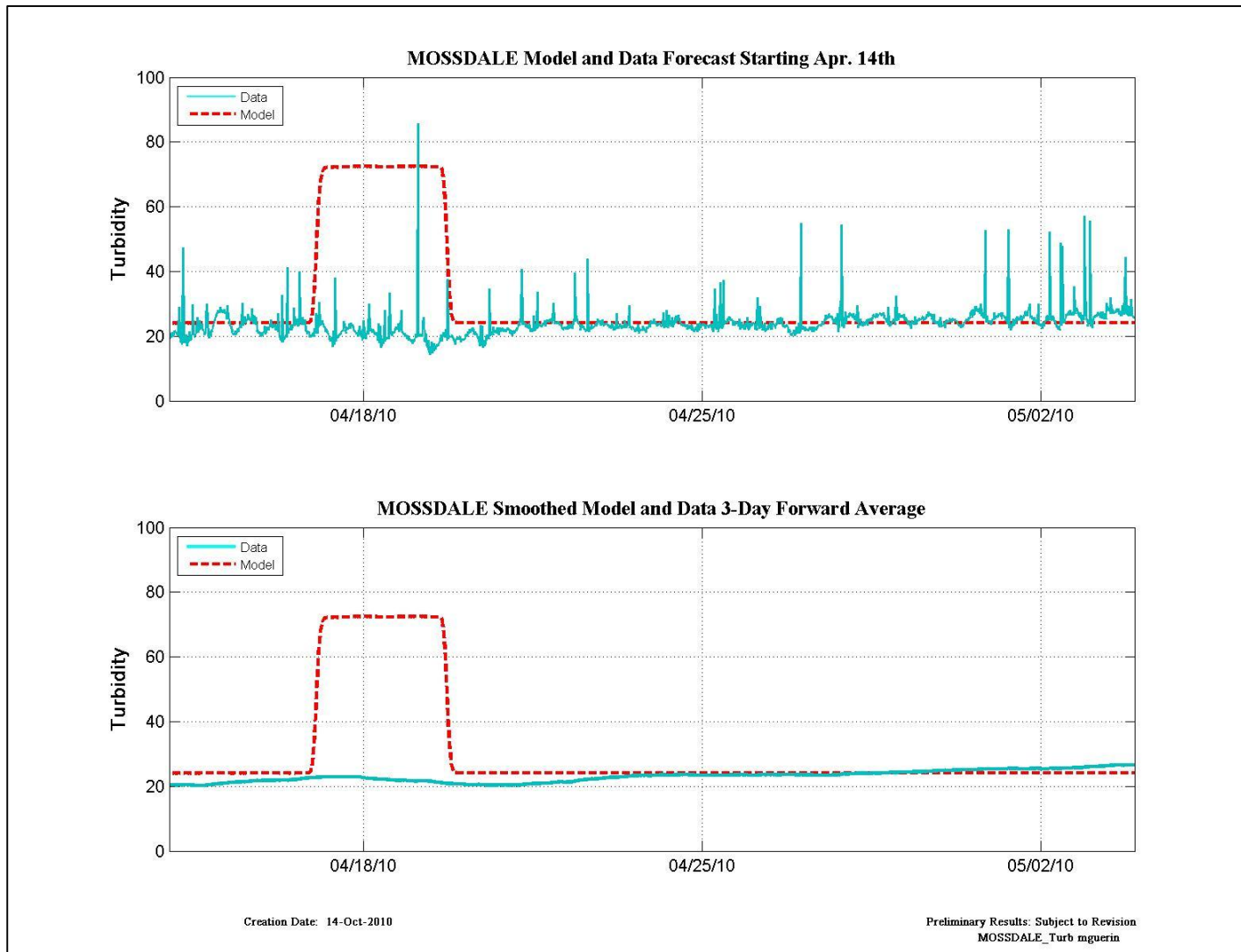


Figure 12-33 Expanded results - turbidity data and model results for the RMA forecast beginning April 14th at Mossdale.

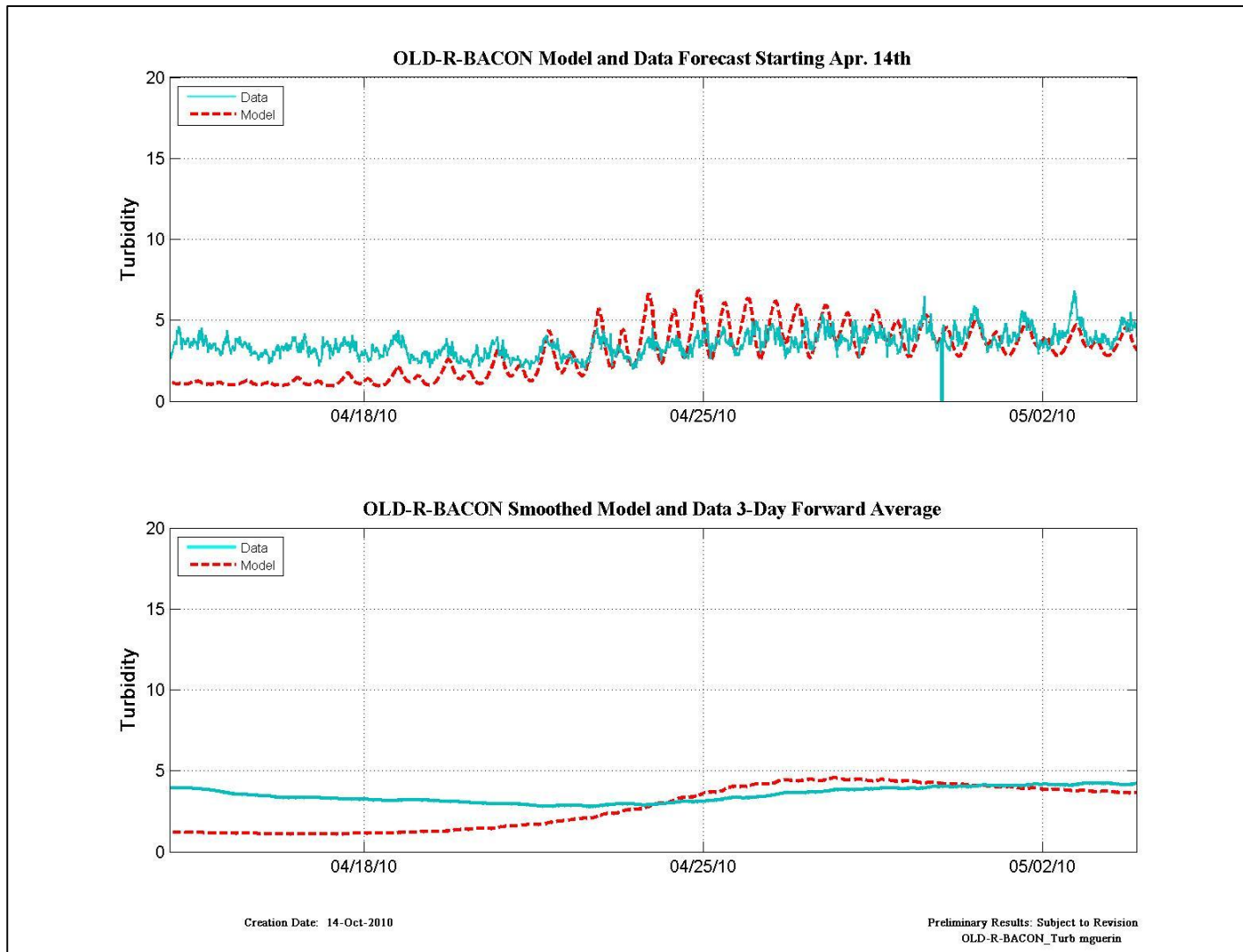


Figure 12-34 Expanded results - turbidity data and model results for the RMA forecast beginning April 14th at Old-R-Bacon.

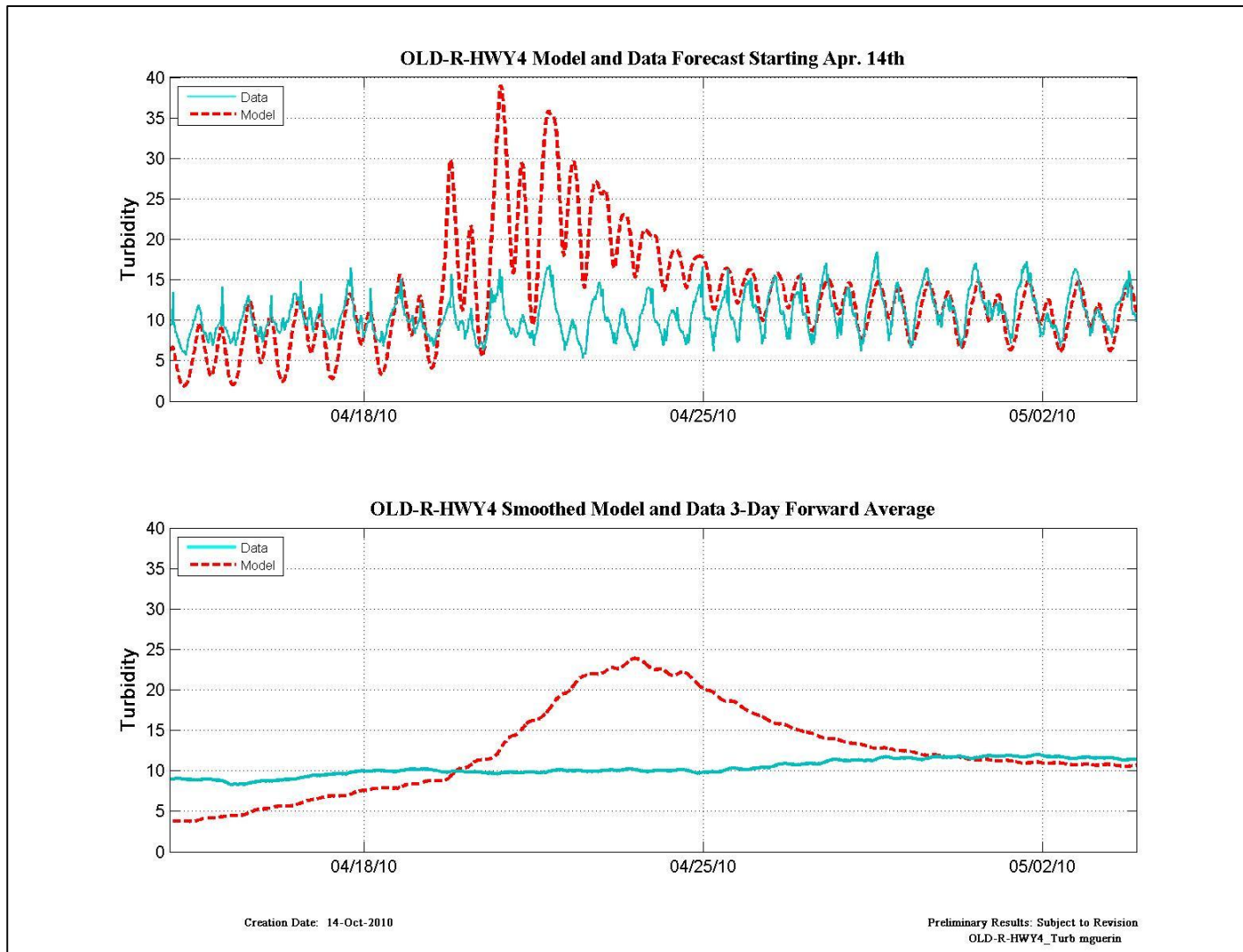


Figure 12-35 Expanded results - turbidity data and model results for the RMA forecast beginning April 14th at Old-R-Hwy 4.

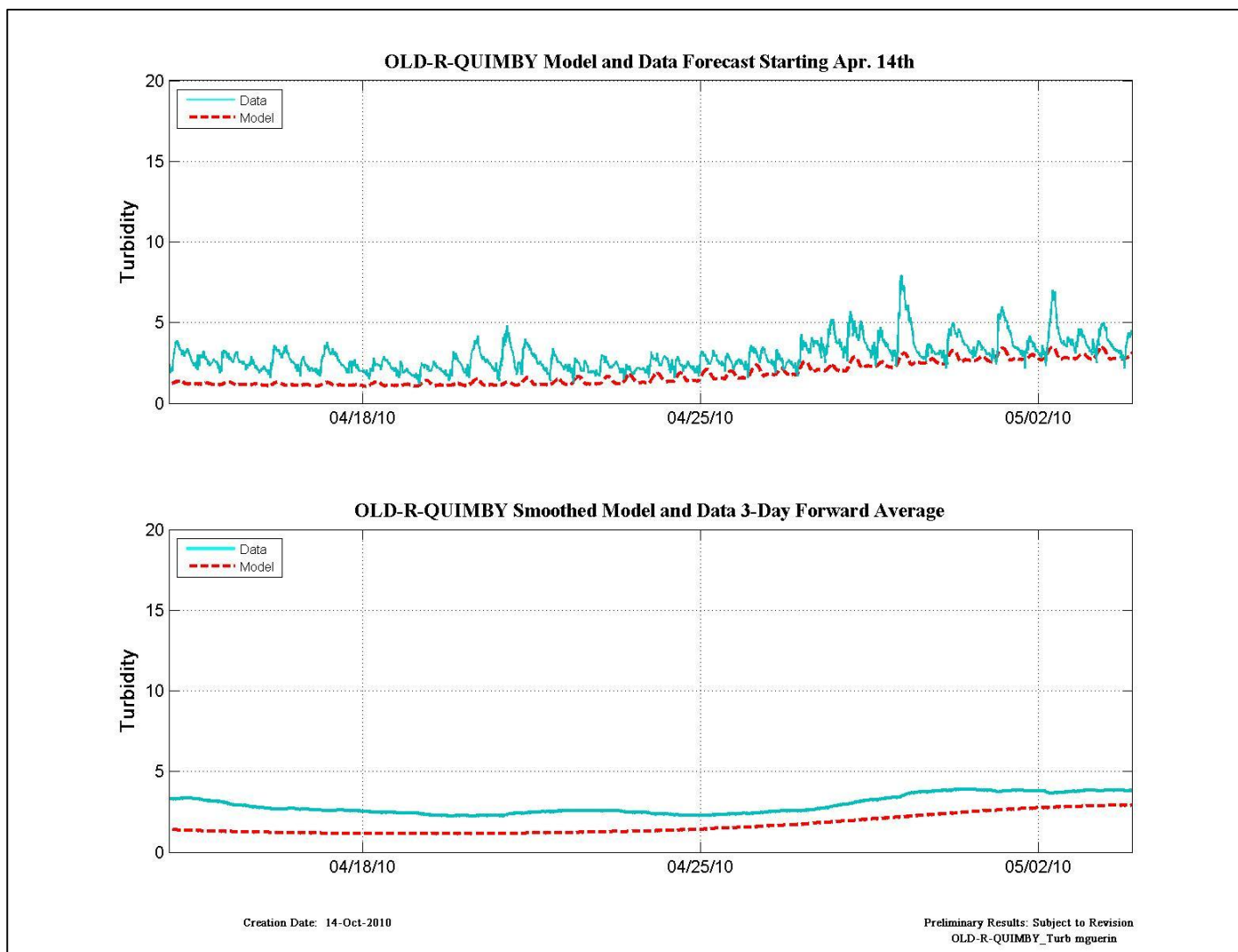


Figure 12-36 Expanded results - turbidity data and model results for the RMA forecast beginning April 14th at Old-R-Quimby.

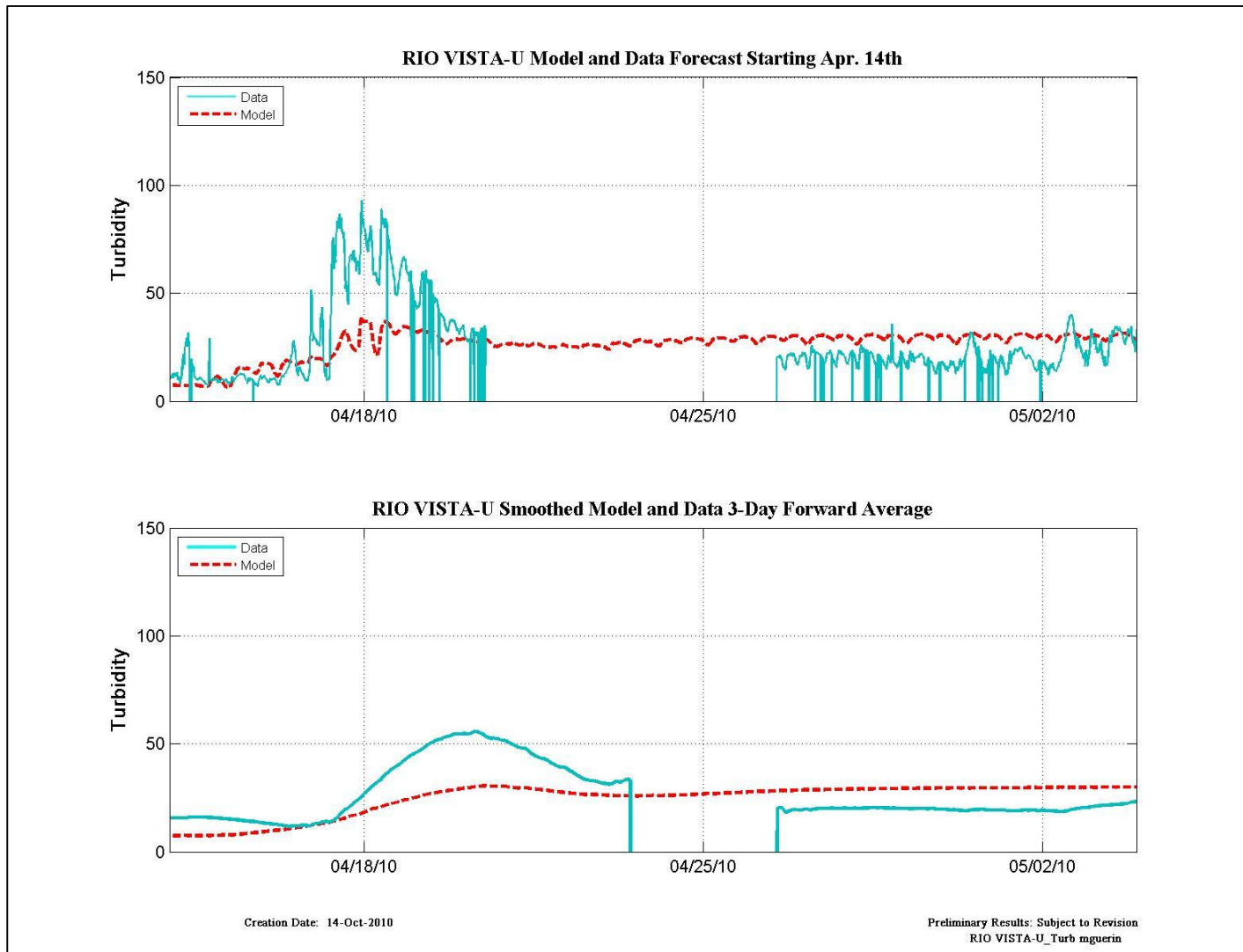


Figure 12-37 Expanded results - turbidity data and model results for the RMA forecast beginning April 14th at Rio Vista-U.

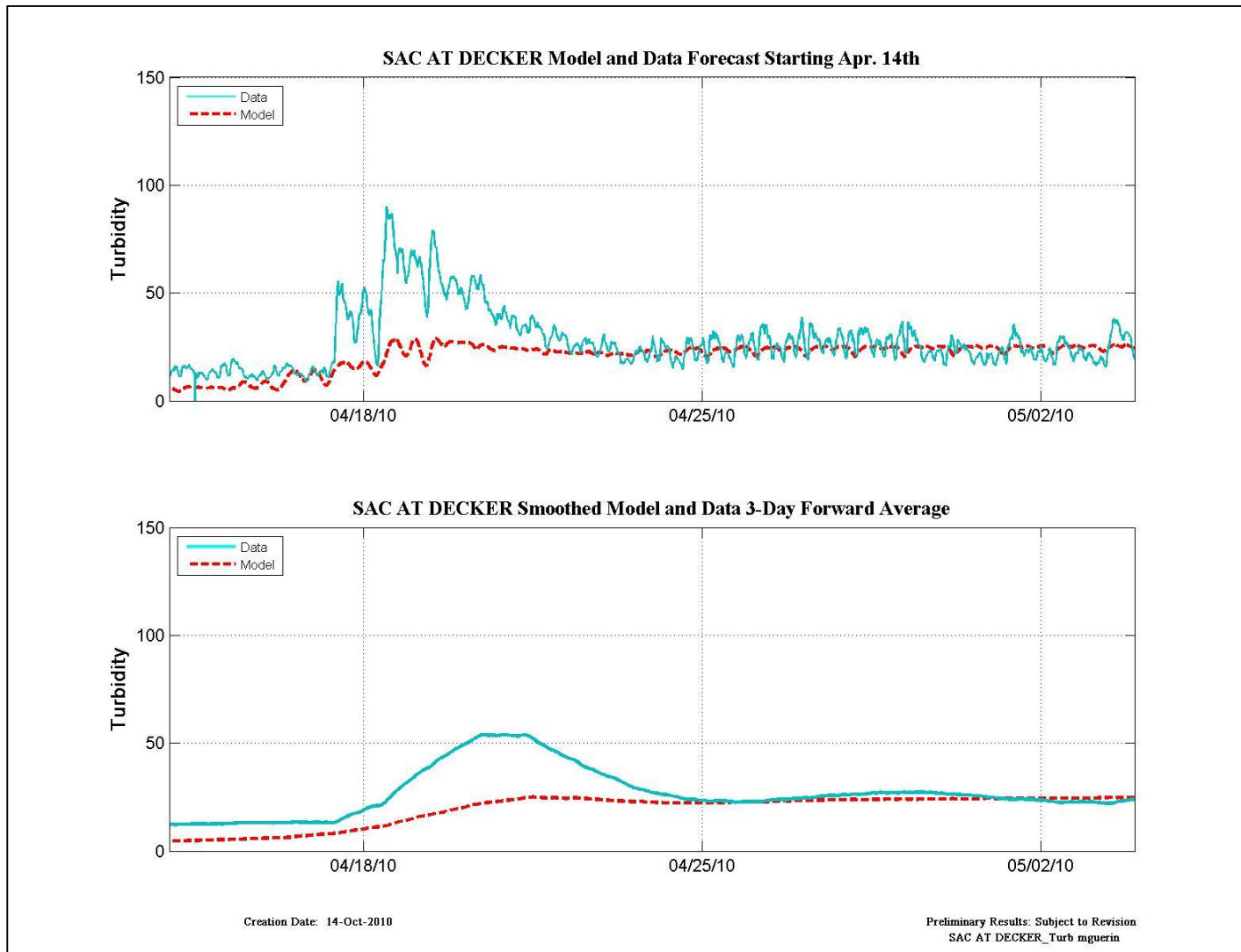


Figure 12-38 Expanded results - turbidity data and model results for the RMA forecast beginning April 14th at SAC at Decker.

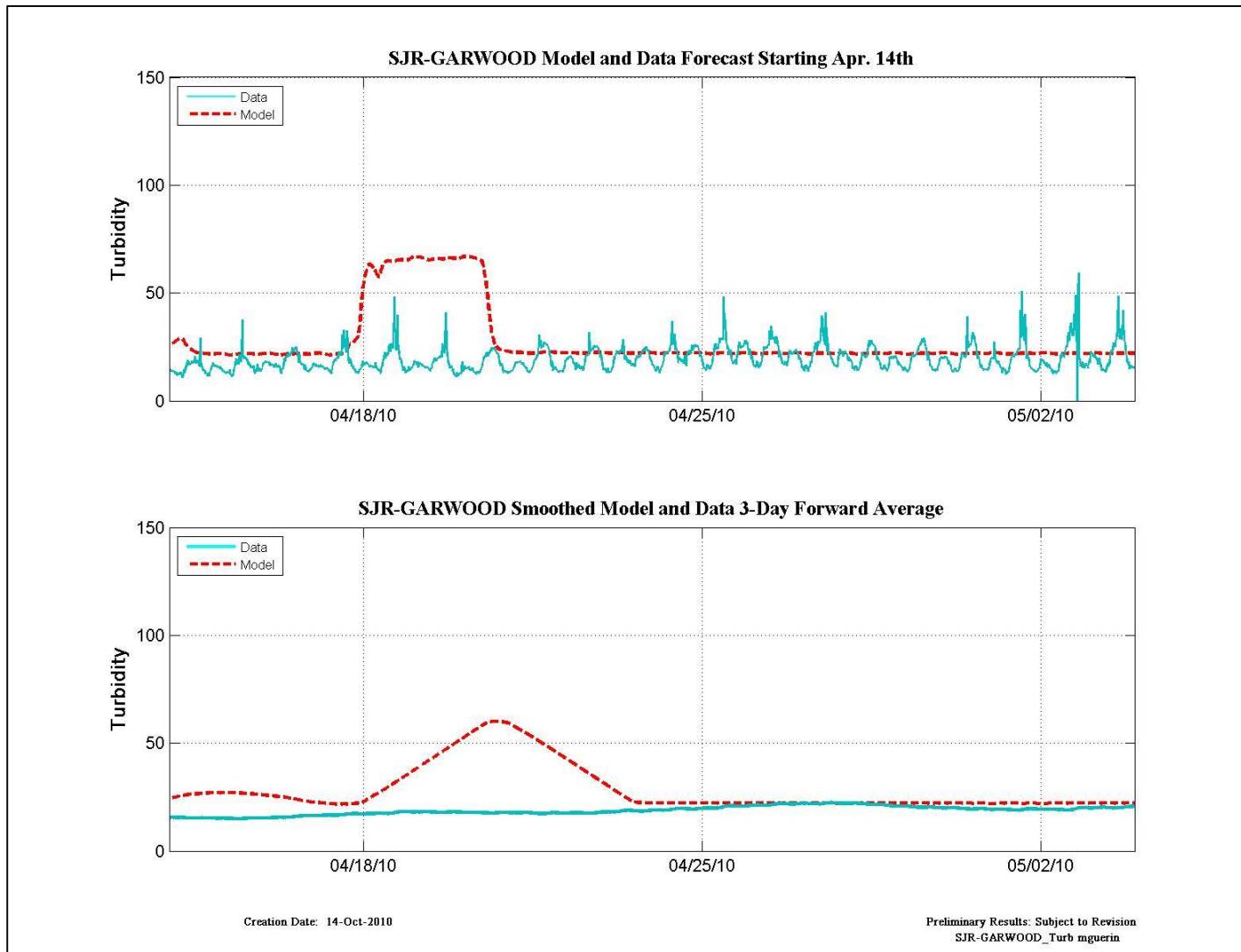


Figure 12-39 Expanded results - turbidity data and model results for the RMA forecast beginning April 14th at SJR-Garwood.

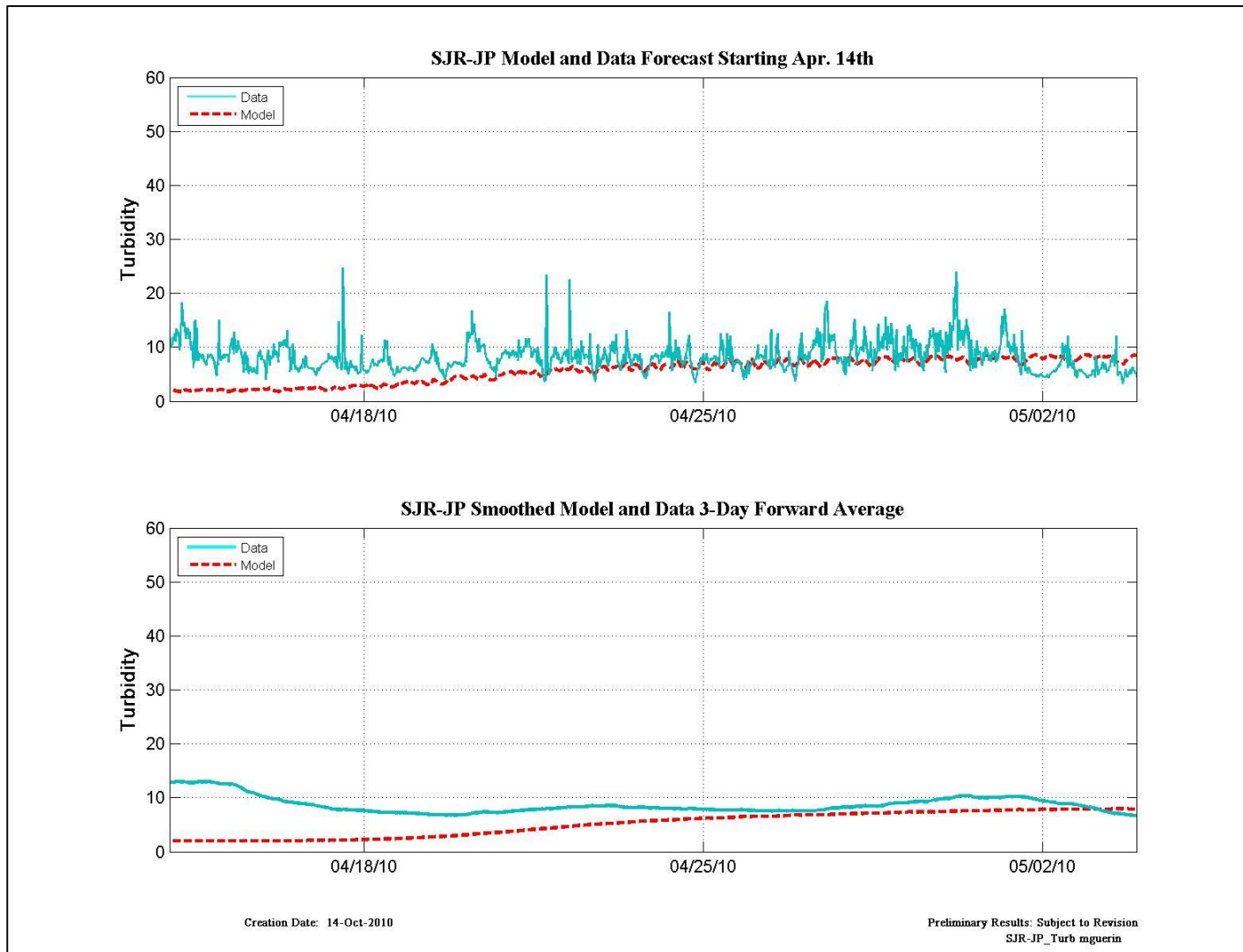


Figure 12-40 Expanded results - turbidity data and model results for the RMA forecast beginning April 14th at SJR-JP.

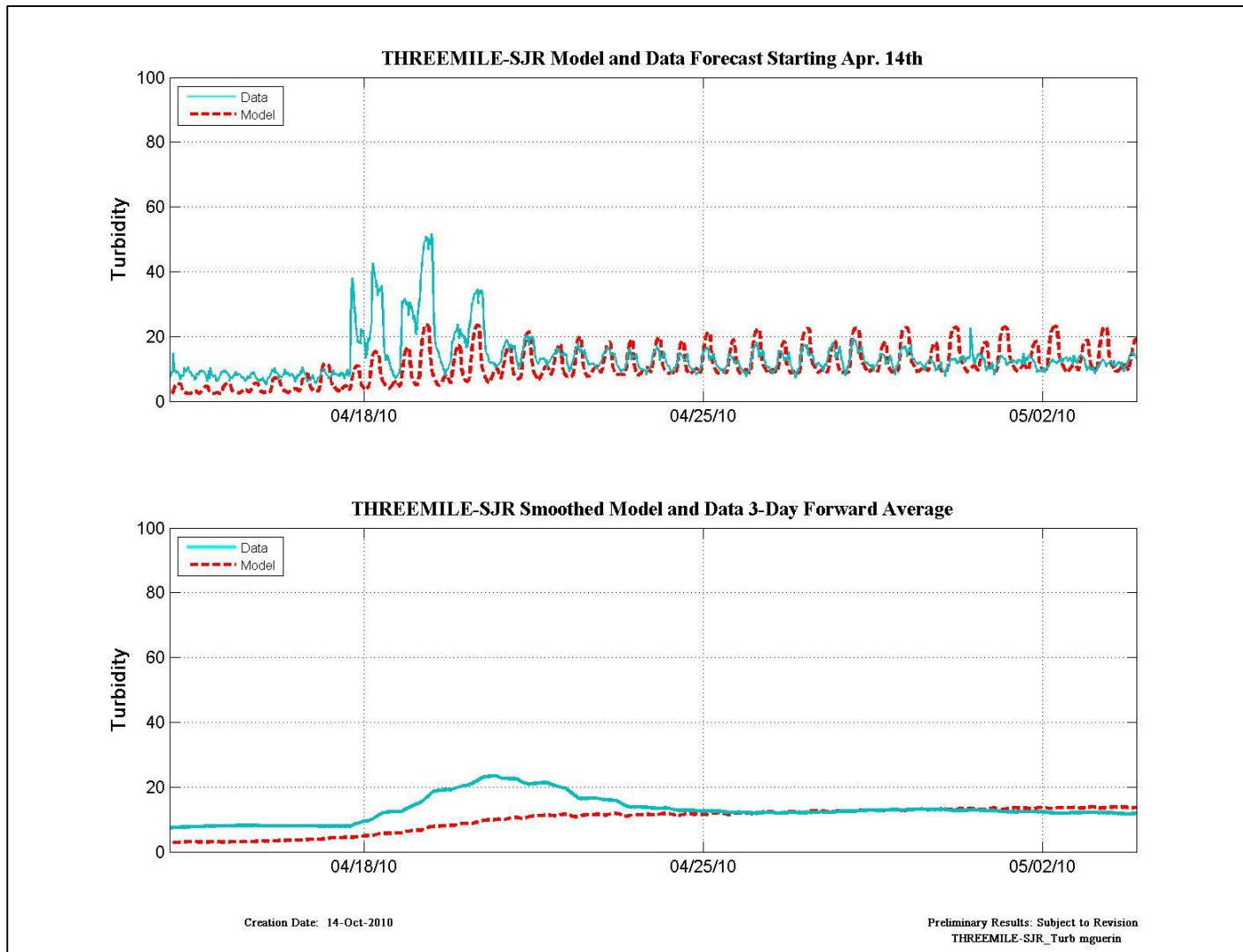


Figure 12-41 Expanded results - turbidity data and model results for the RMA forecast beginning April 14th at Threemile-SJR.

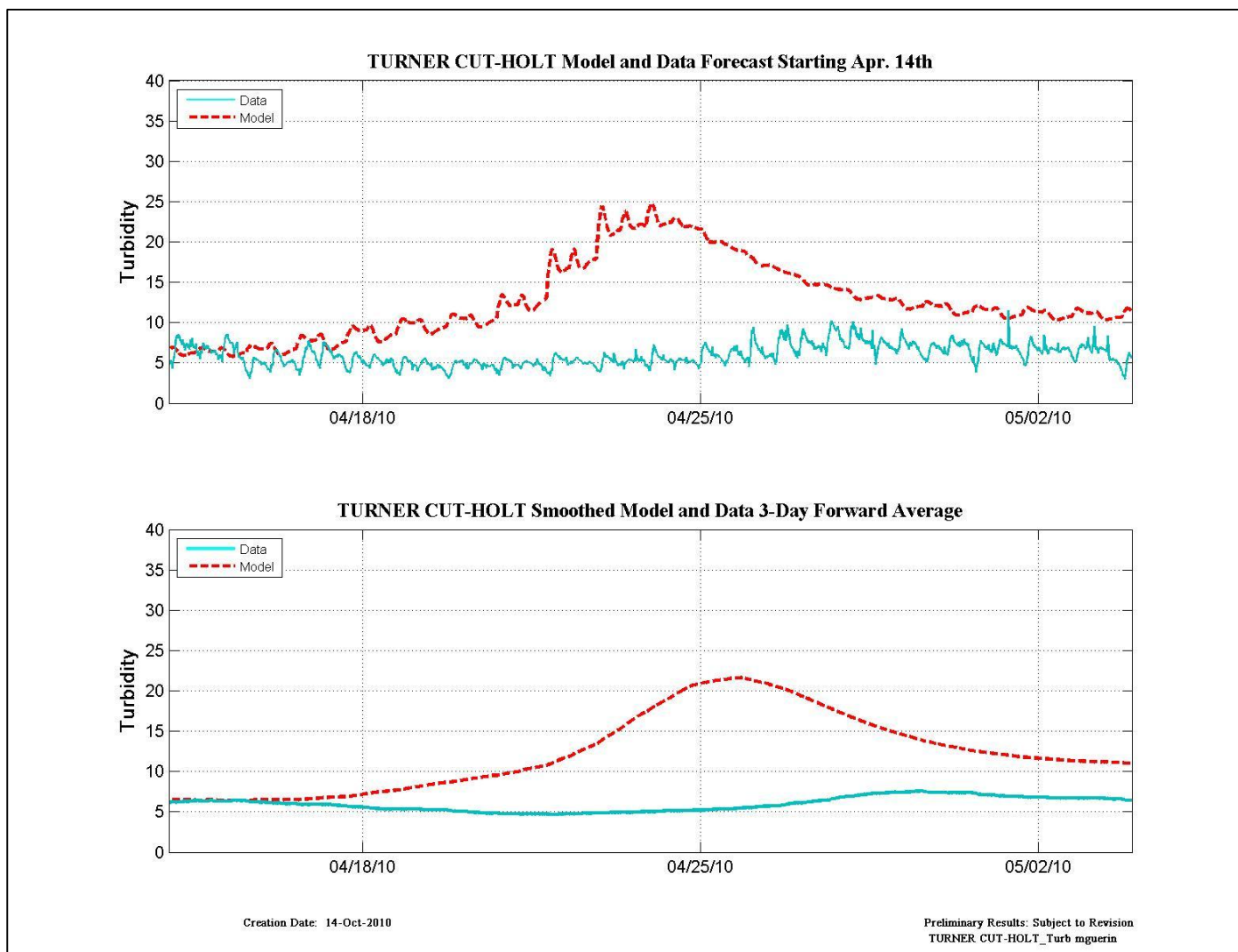


Figure 12-42 Expanded results - turbidity data and model results for the RMA forecast beginning April 14th at Turner Cut-Holt.

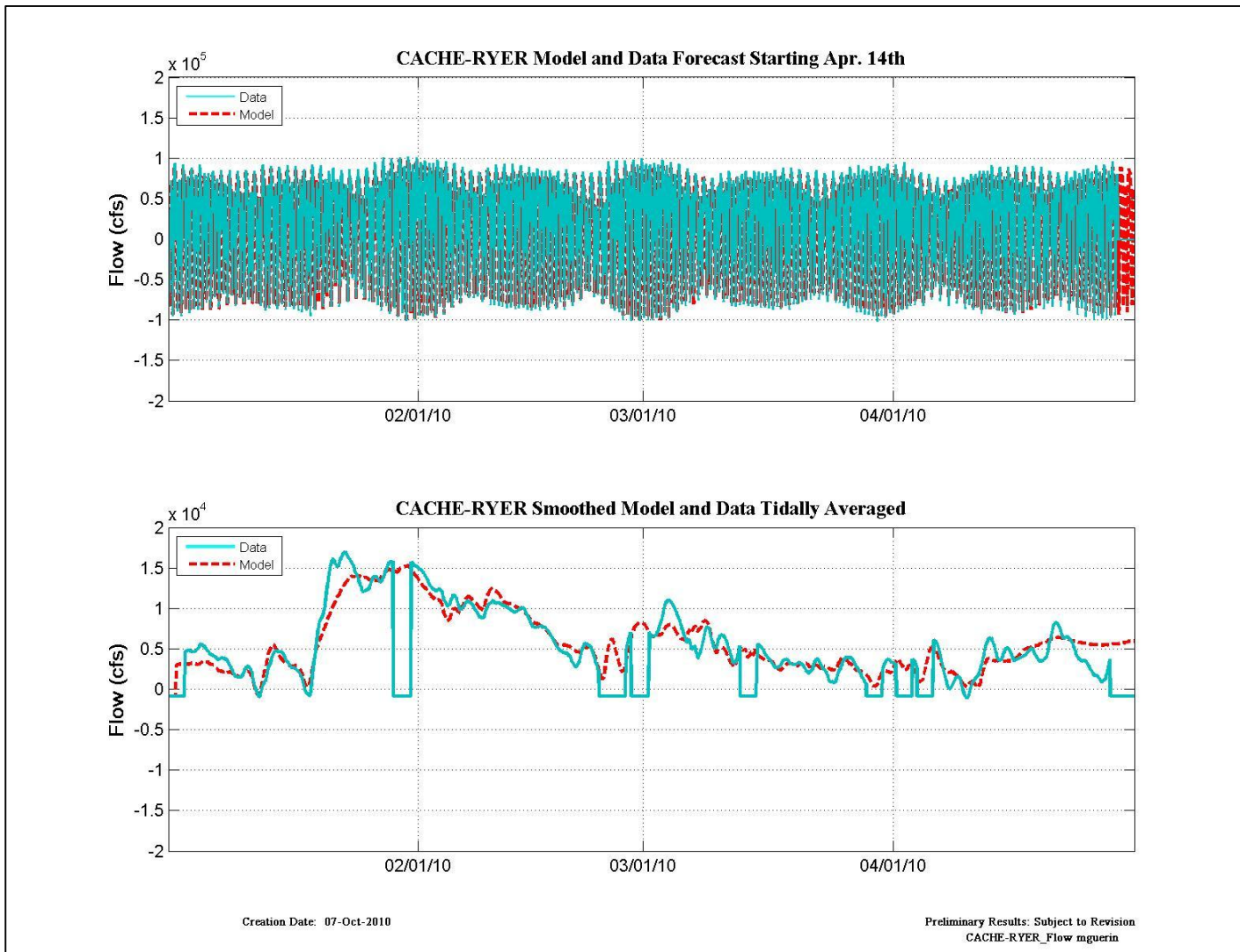


Figure 12-43 Flow data and model results for the RMA forecast beginning April 14th at Cache-Ryer.

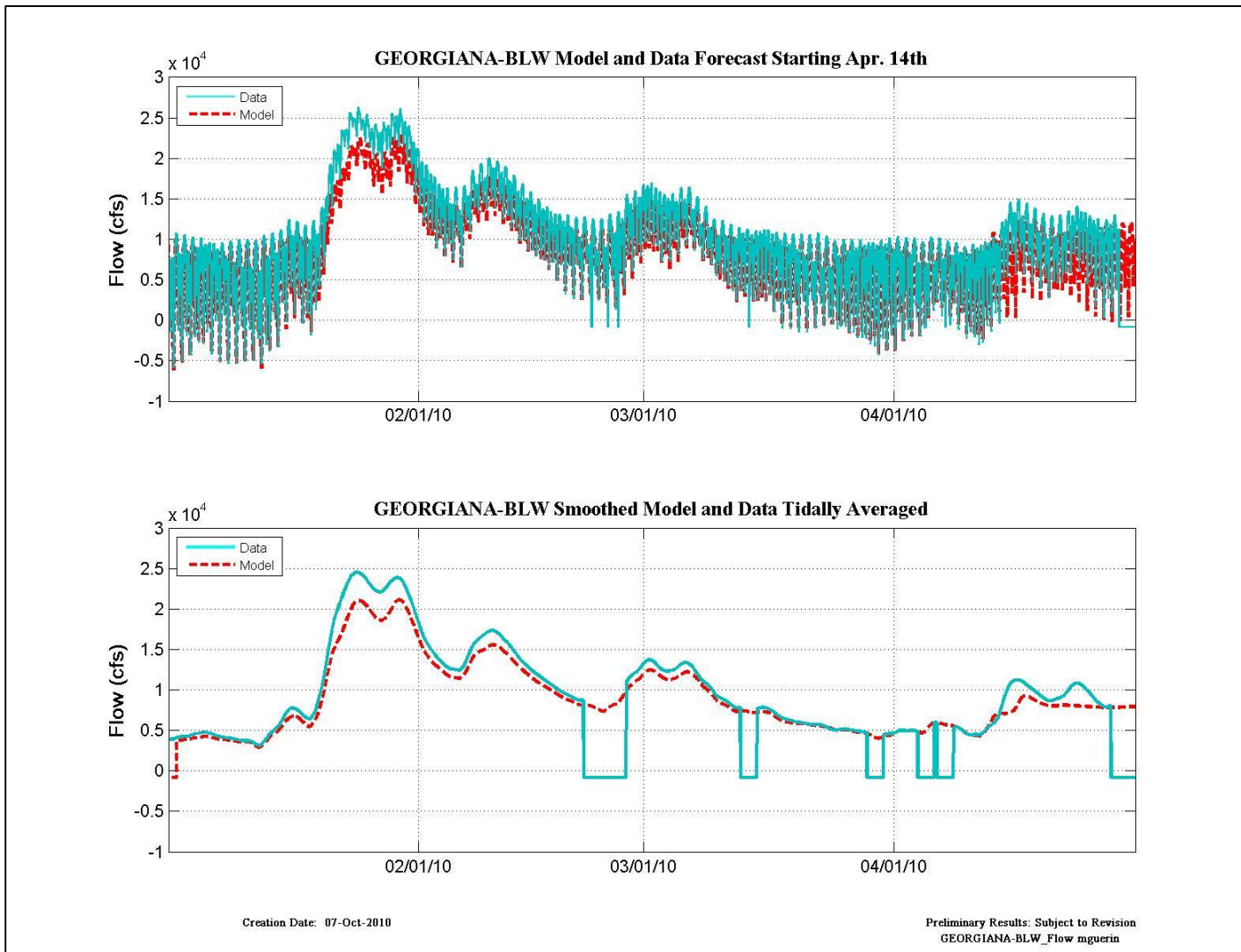


Figure 12-44 Flow data and model results for the RMA forecast beginning April 14th at Georgiana-BLW.

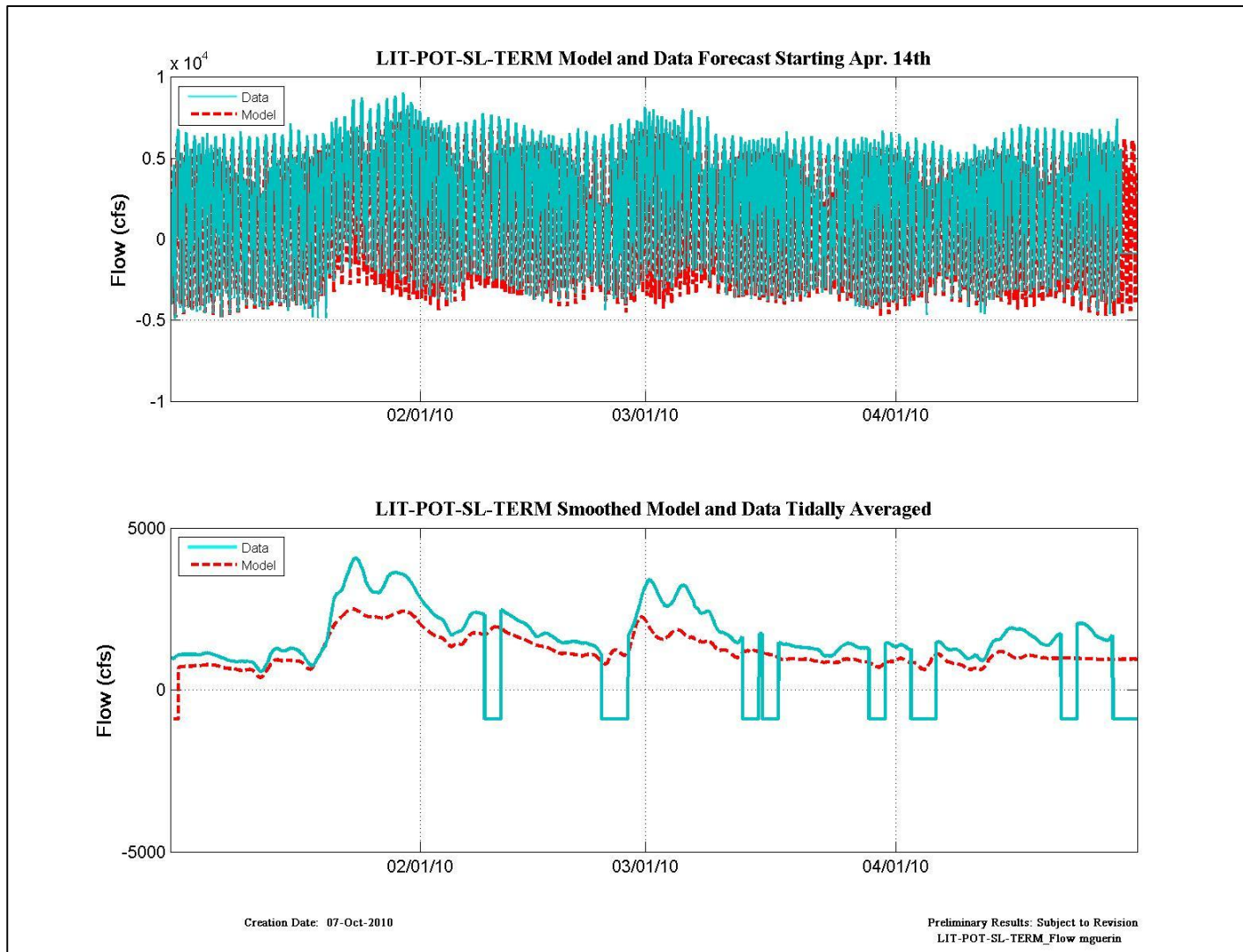


Figure 12-45 Flow data and model results for the RMA forecast beginning April 14th at LIT-POT-SL.

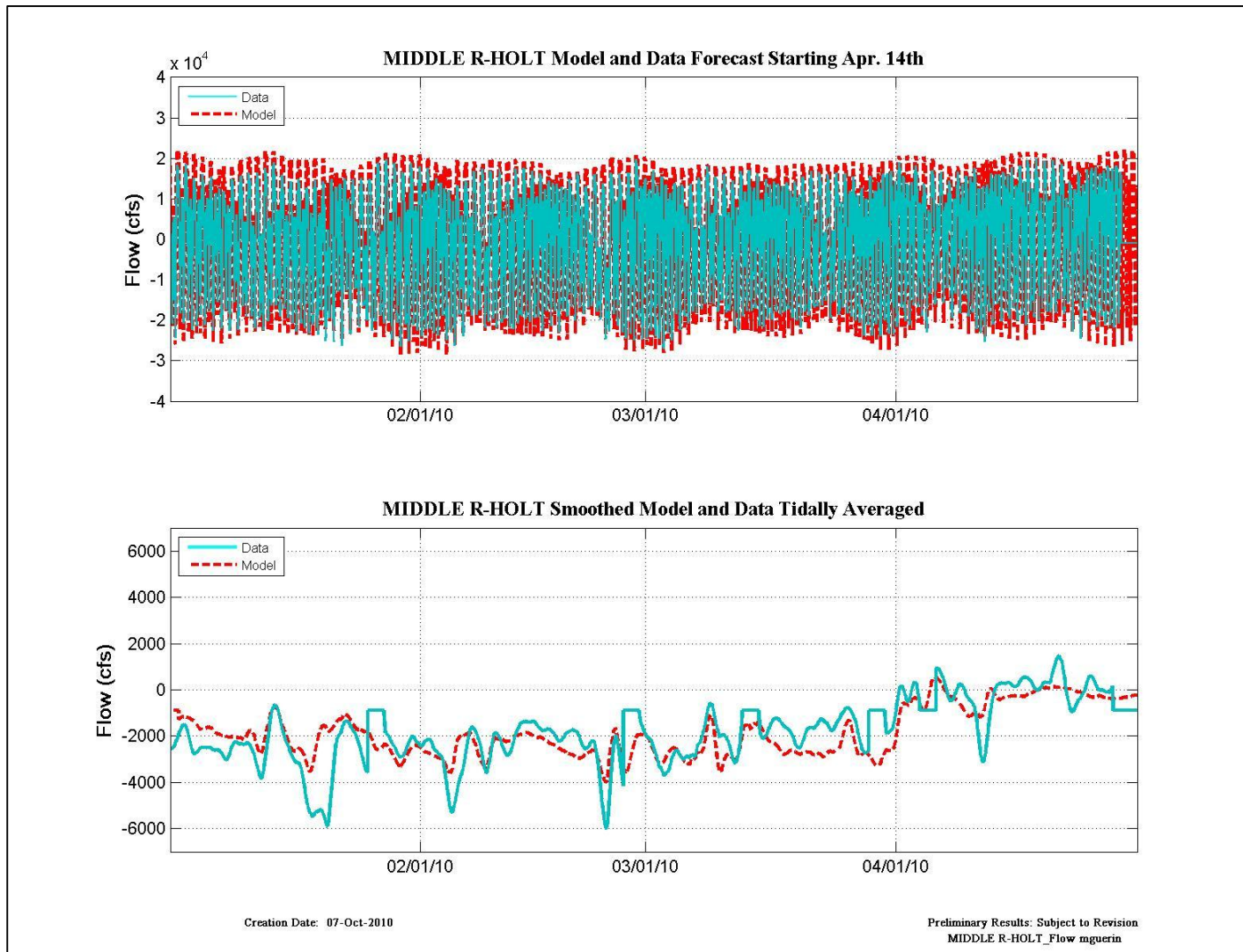


Figure 12-46 Flow data and model results for the RMA forecast beginning April 14th at Middle R-Holt.

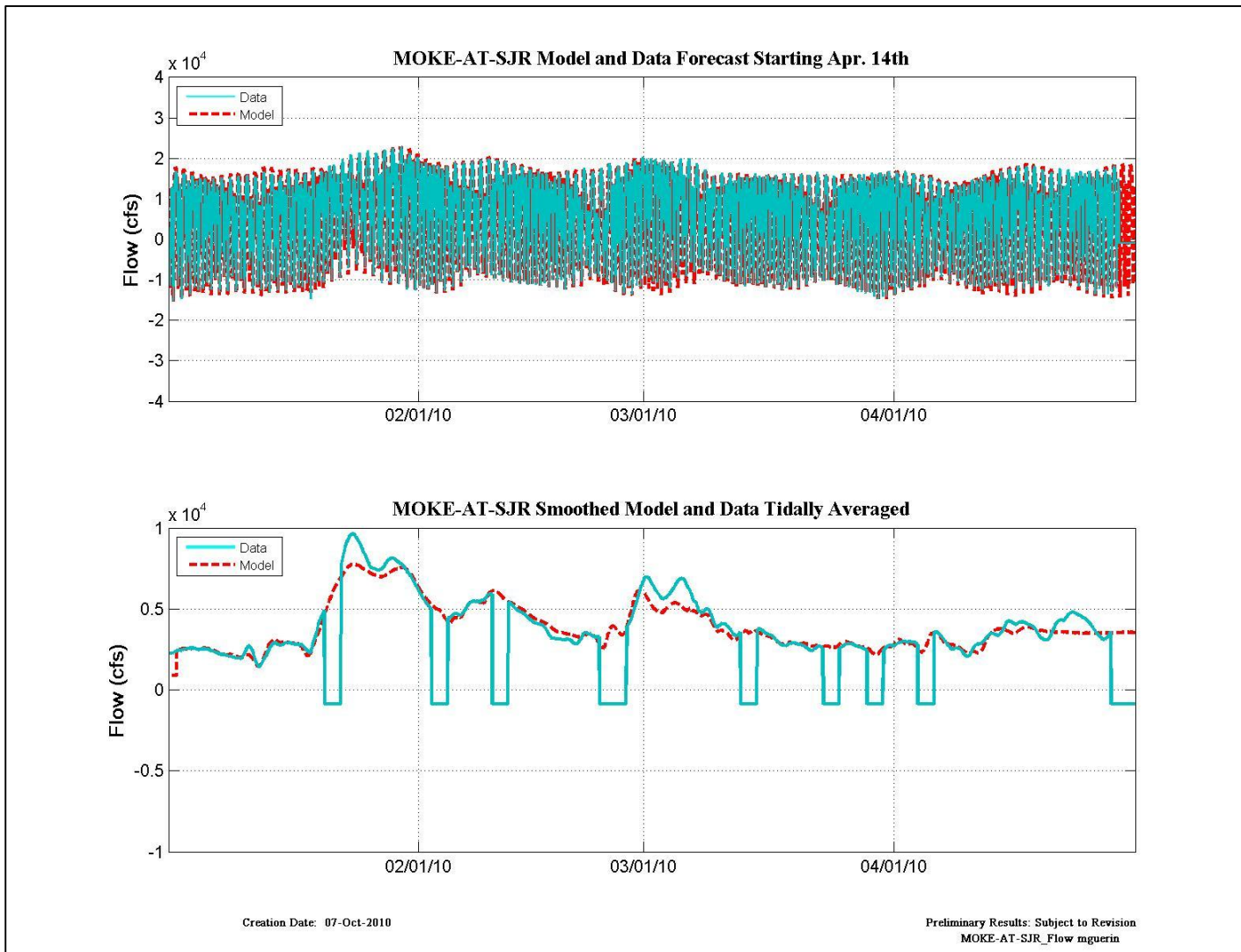


Figure 12-47 Flow data and model results for the RMA forecast beginning April 14th at Moke-at-SJR.

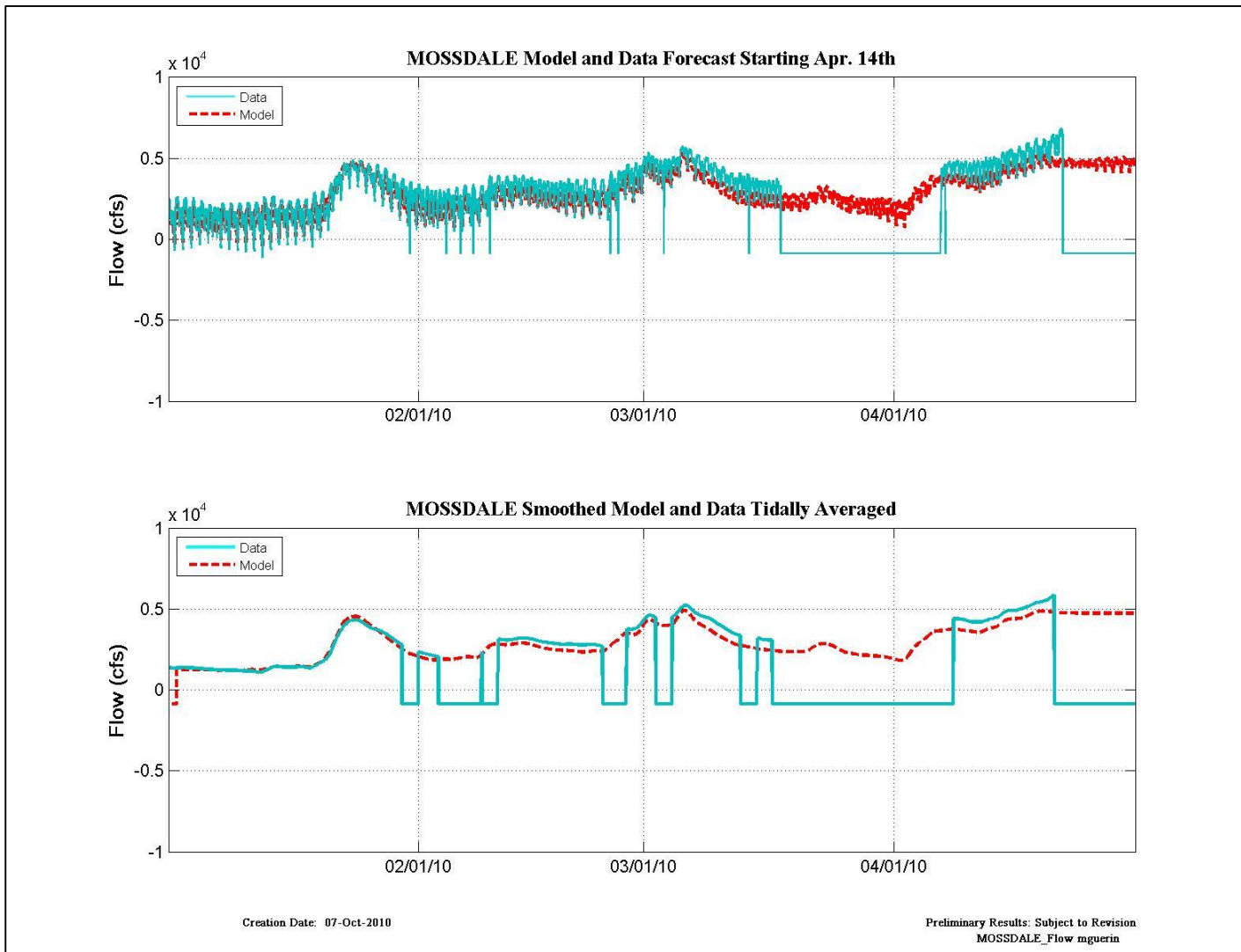


Figure 12-48 Flow data and model results for the RMA forecast beginning April 14th at Mossdale.

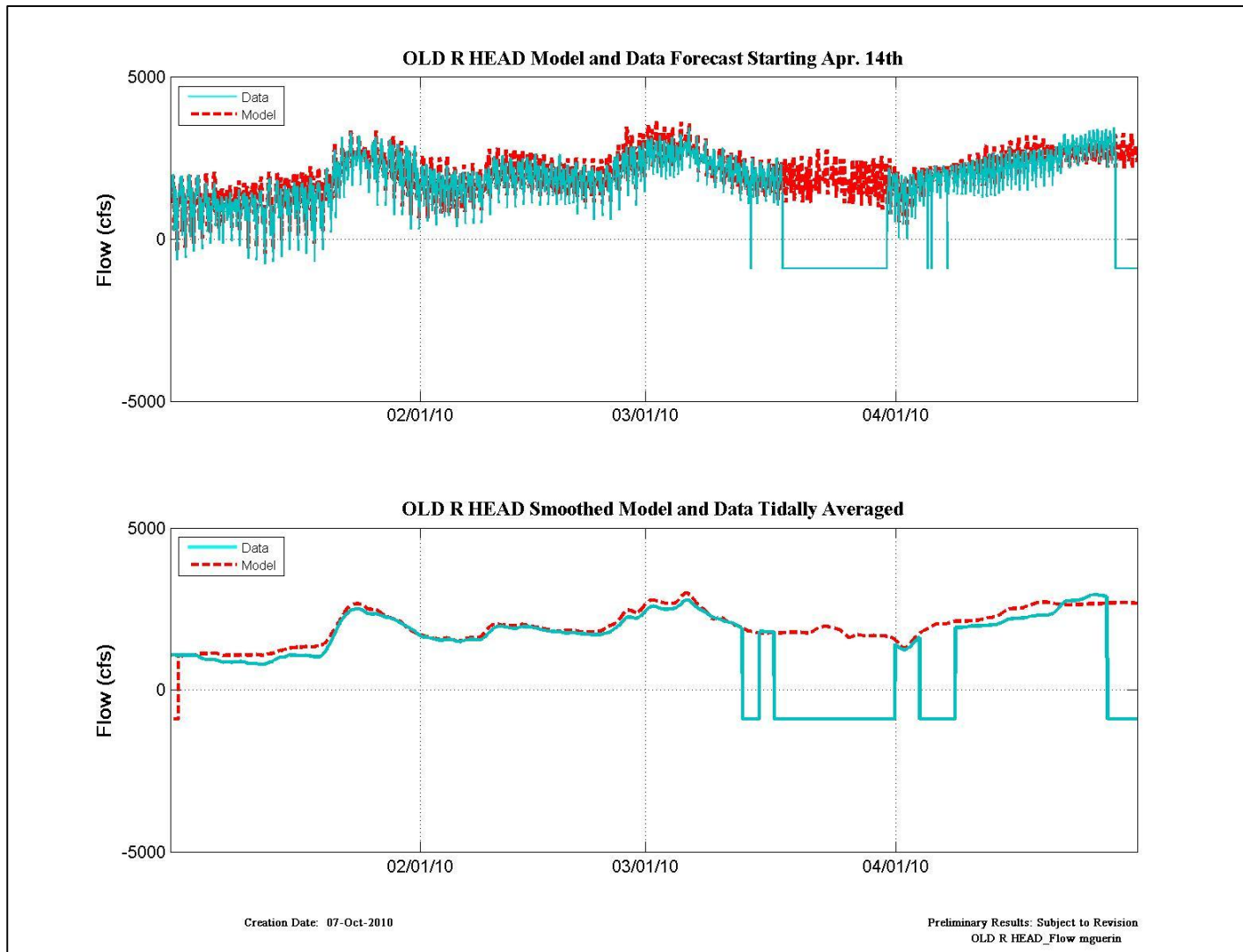


Figure 12-49 Flow data and model results for the RMA forecast beginning April 14th at Old R Head.

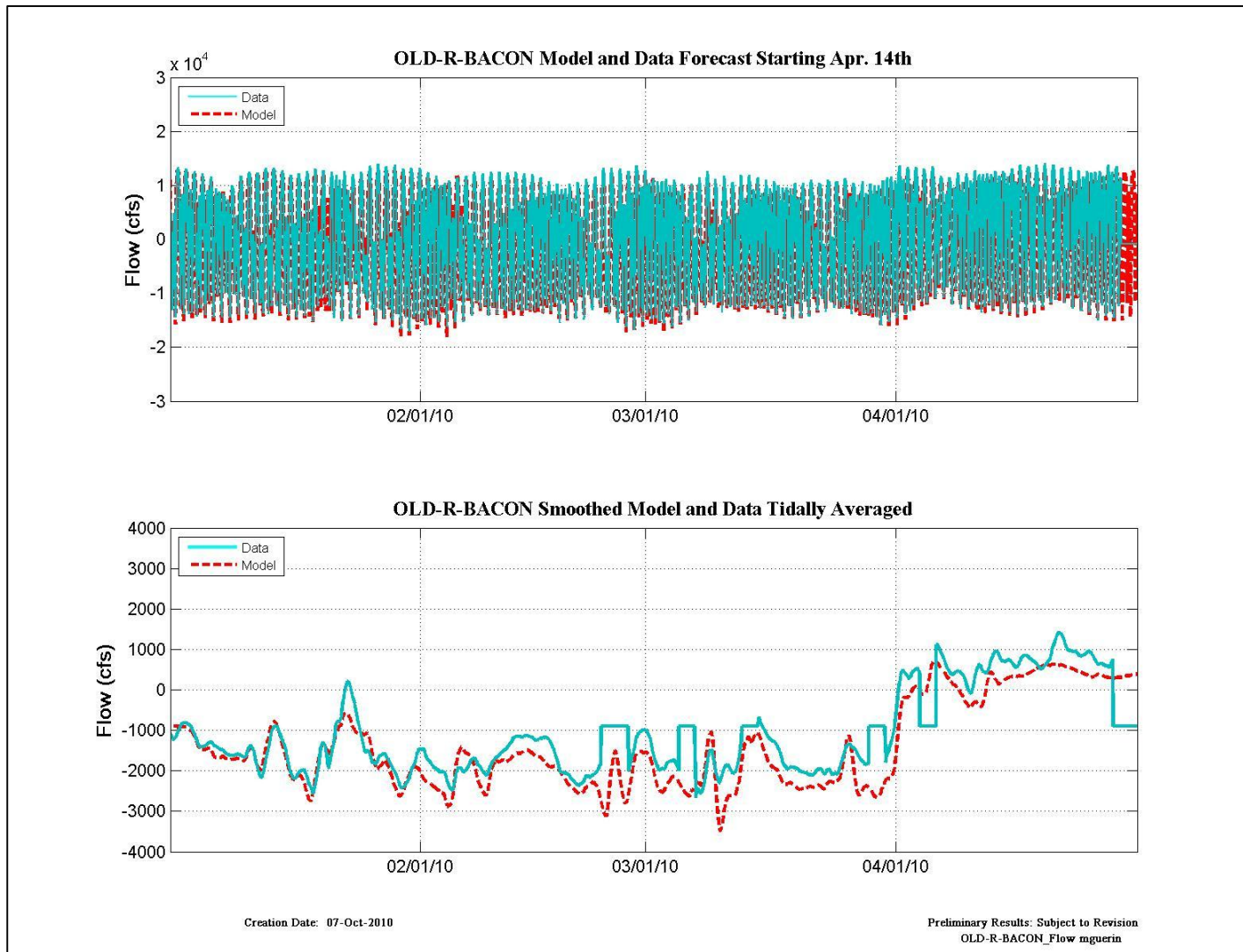


Figure 12-50 Flow data and model results for the RMA forecast beginning April 14th at Old-R-Bacon.

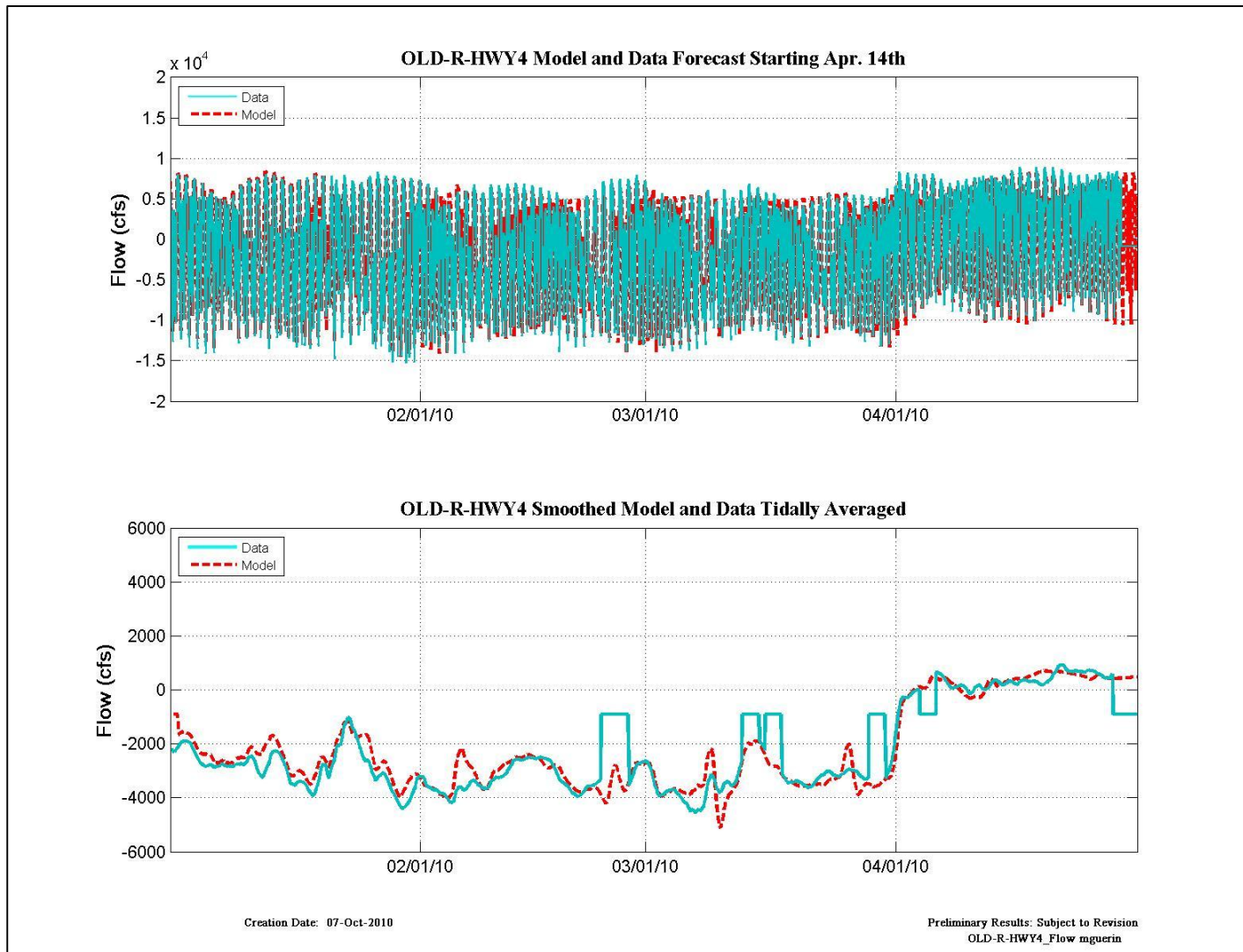


Figure 12-51 Flow data and model results for the RMA forecast beginning April 14th at Old-R-Hwy 4.

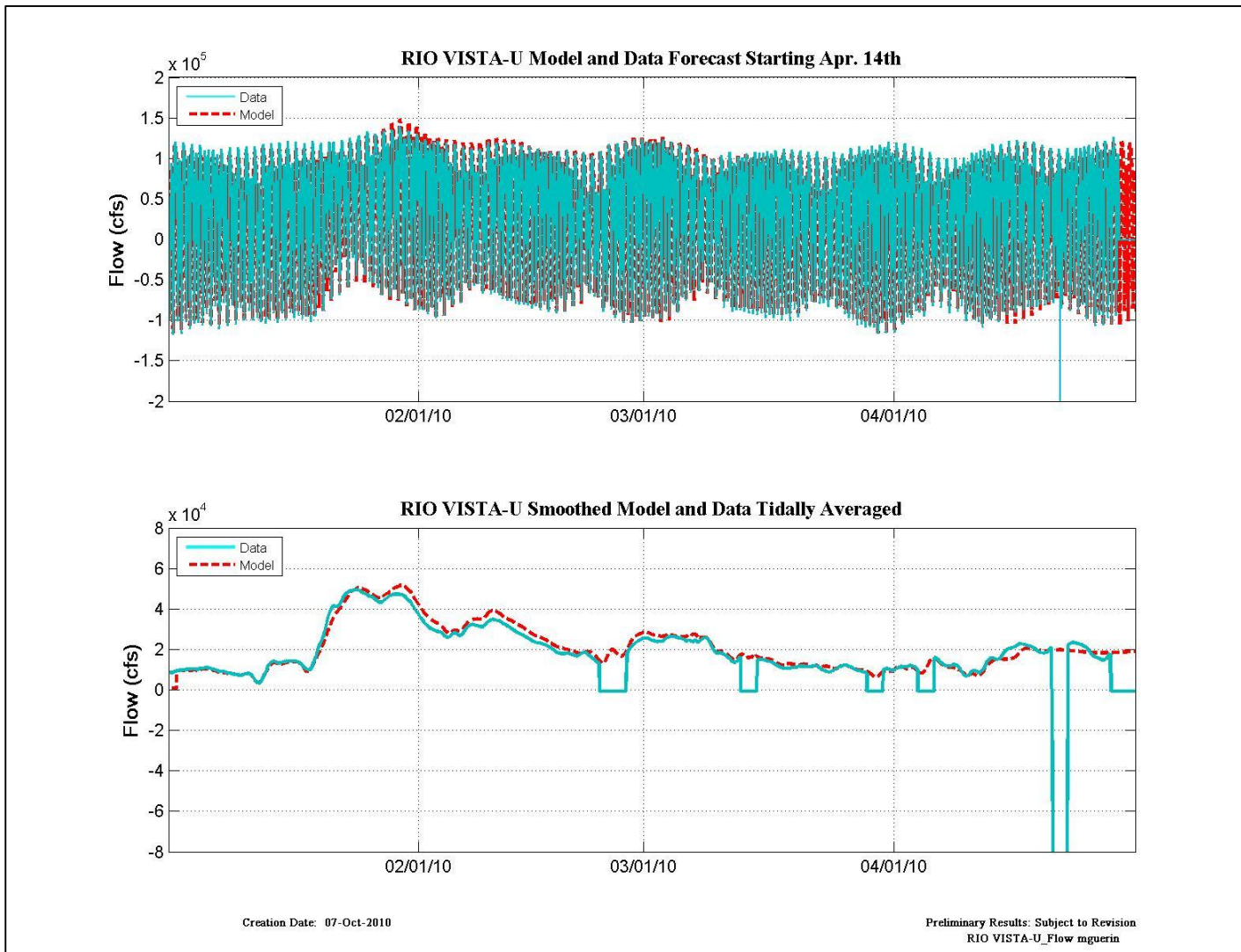


Figure 12-52 Flow data and model results for the RMA forecast beginning April 14th at Rio Vista-U.

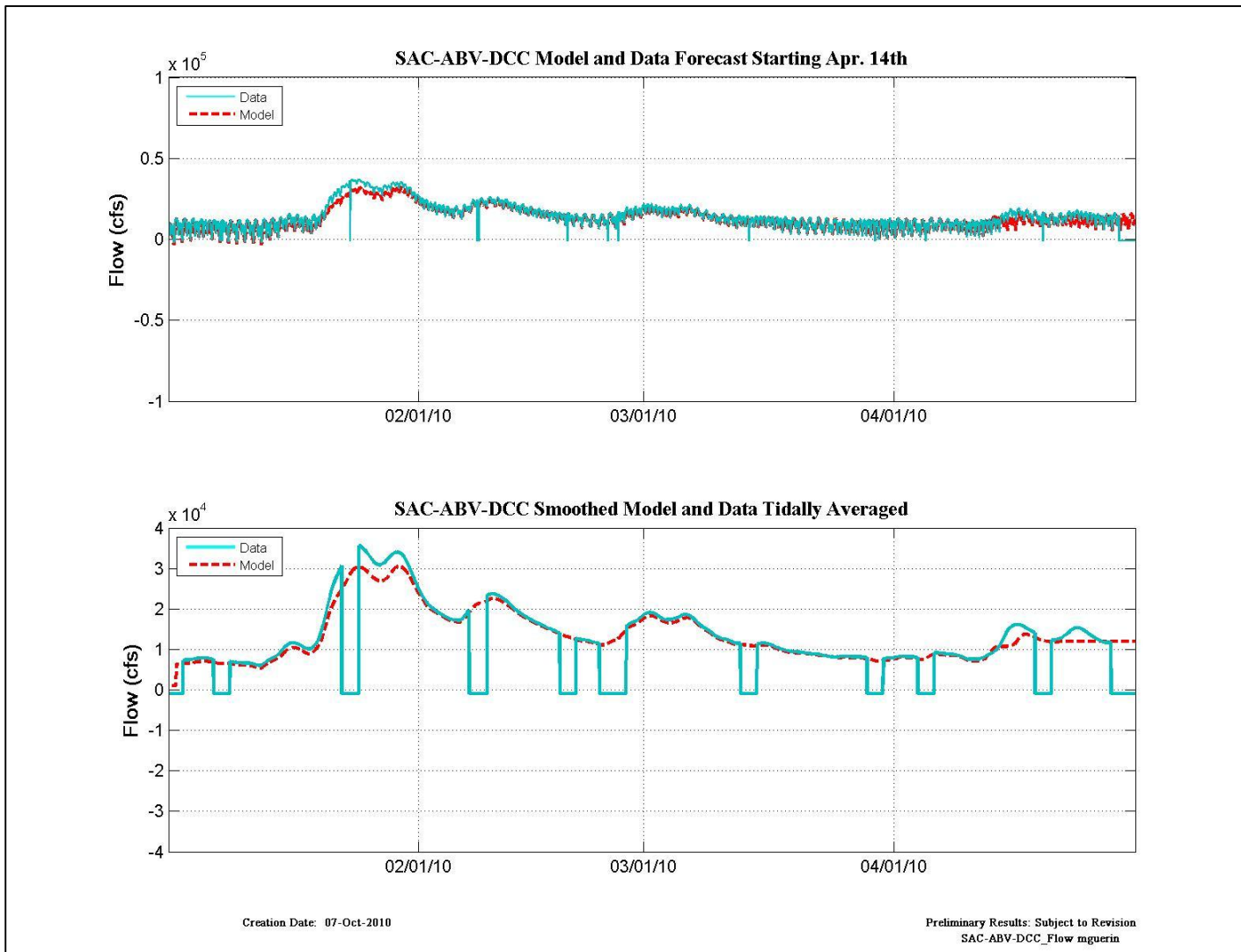


Figure 12-53 Flow data and model results for the RMA forecast beginning April 14th at SAC-ABV-DCC.

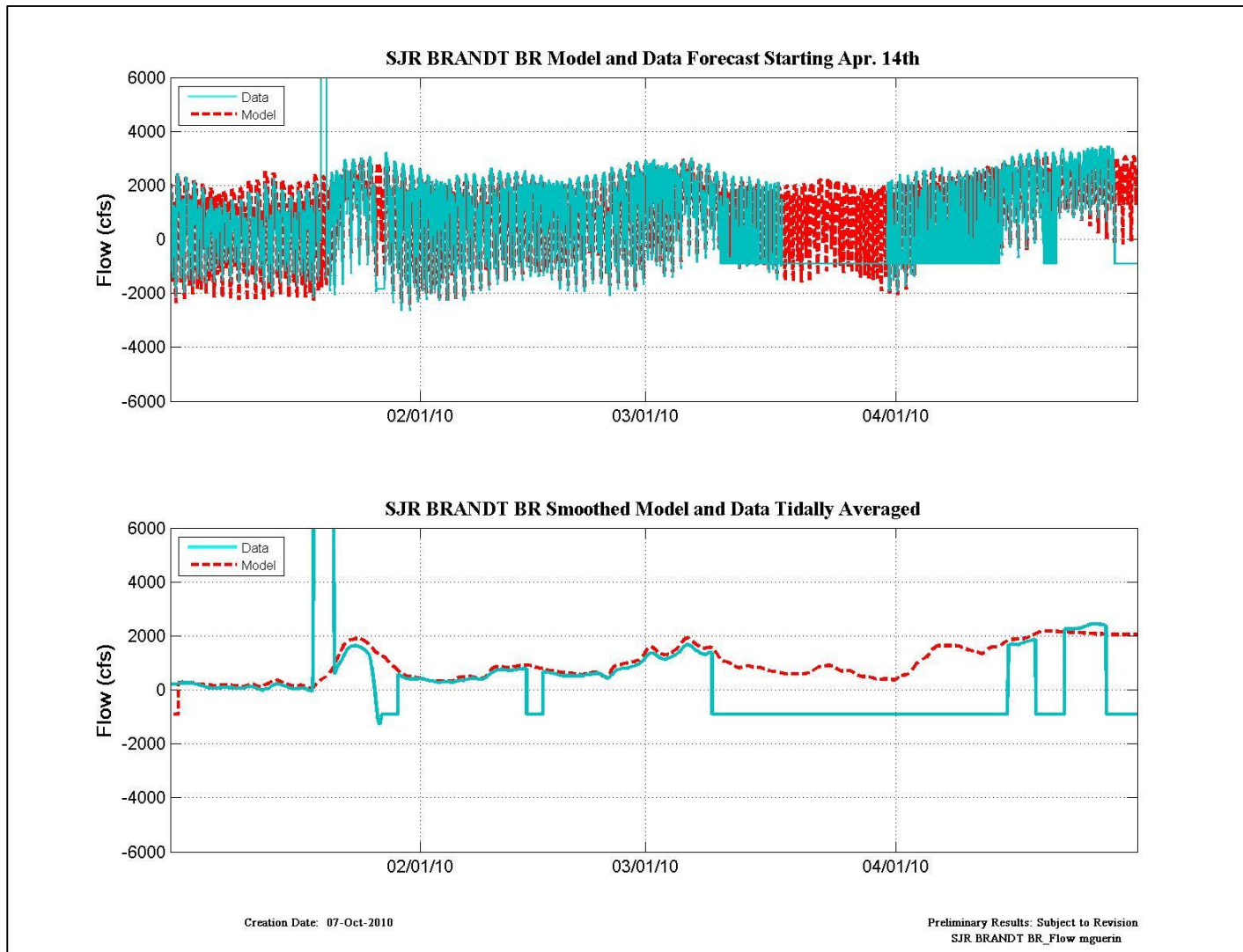


Figure 12-54 Flow data and model results for the RMA forecast beginning April 14th at SJR Brandt BR.

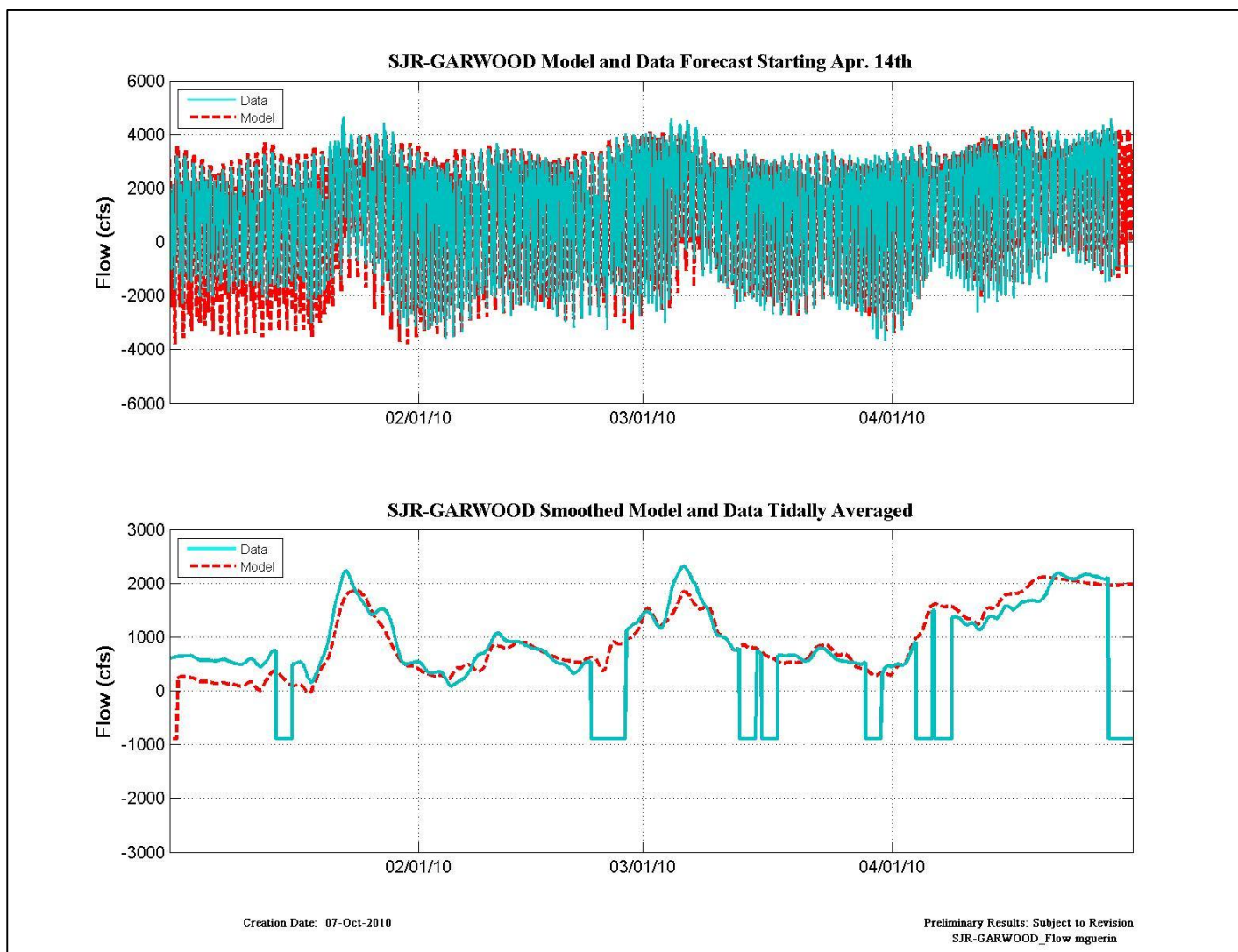


Figure 12-55 Flow data and model results for the RMA forecast beginning April 14th at SJR-Garwood.

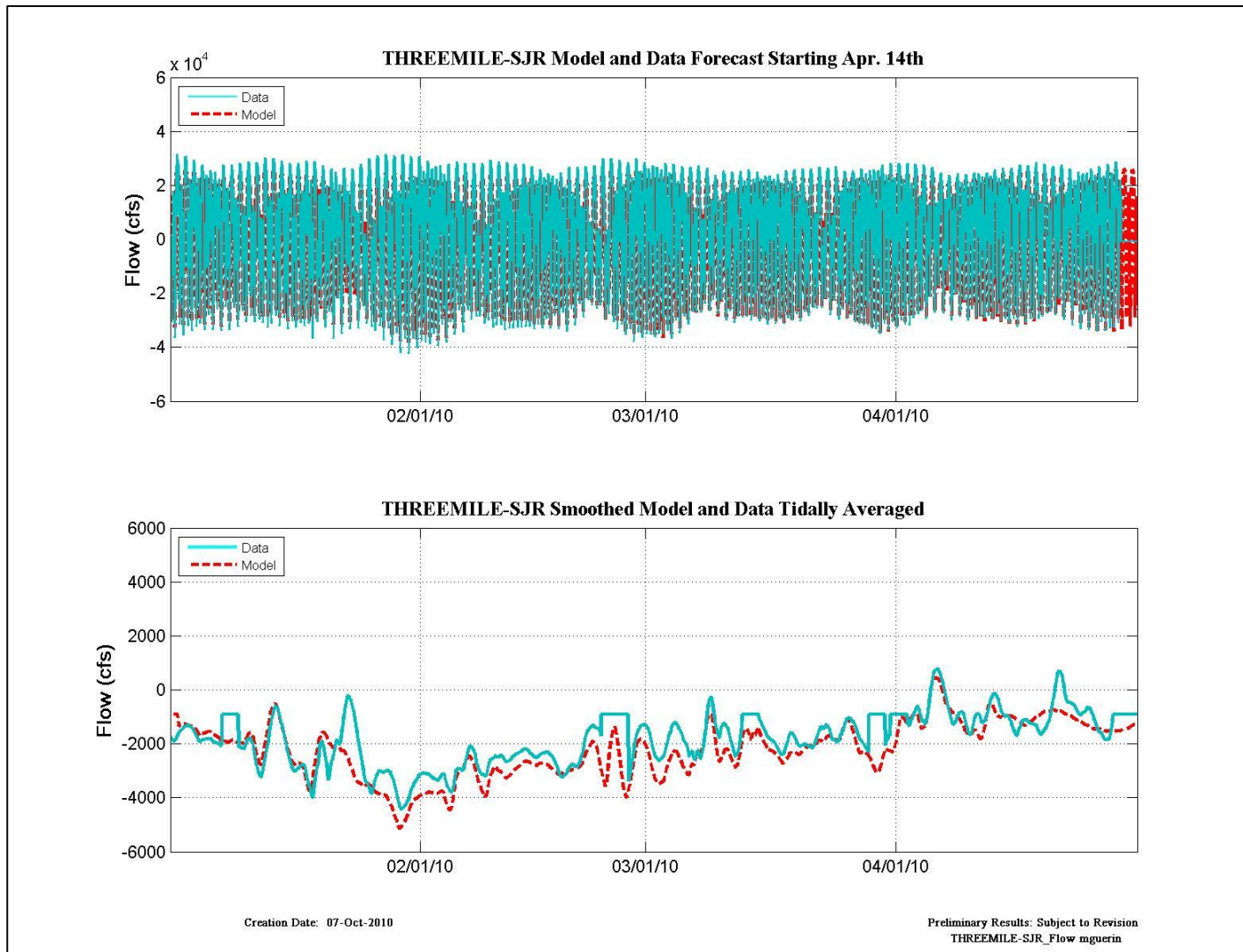


Figure 12-56 Flow data and model results for the RMA forecast beginning April 14th at Threemile-SJR.

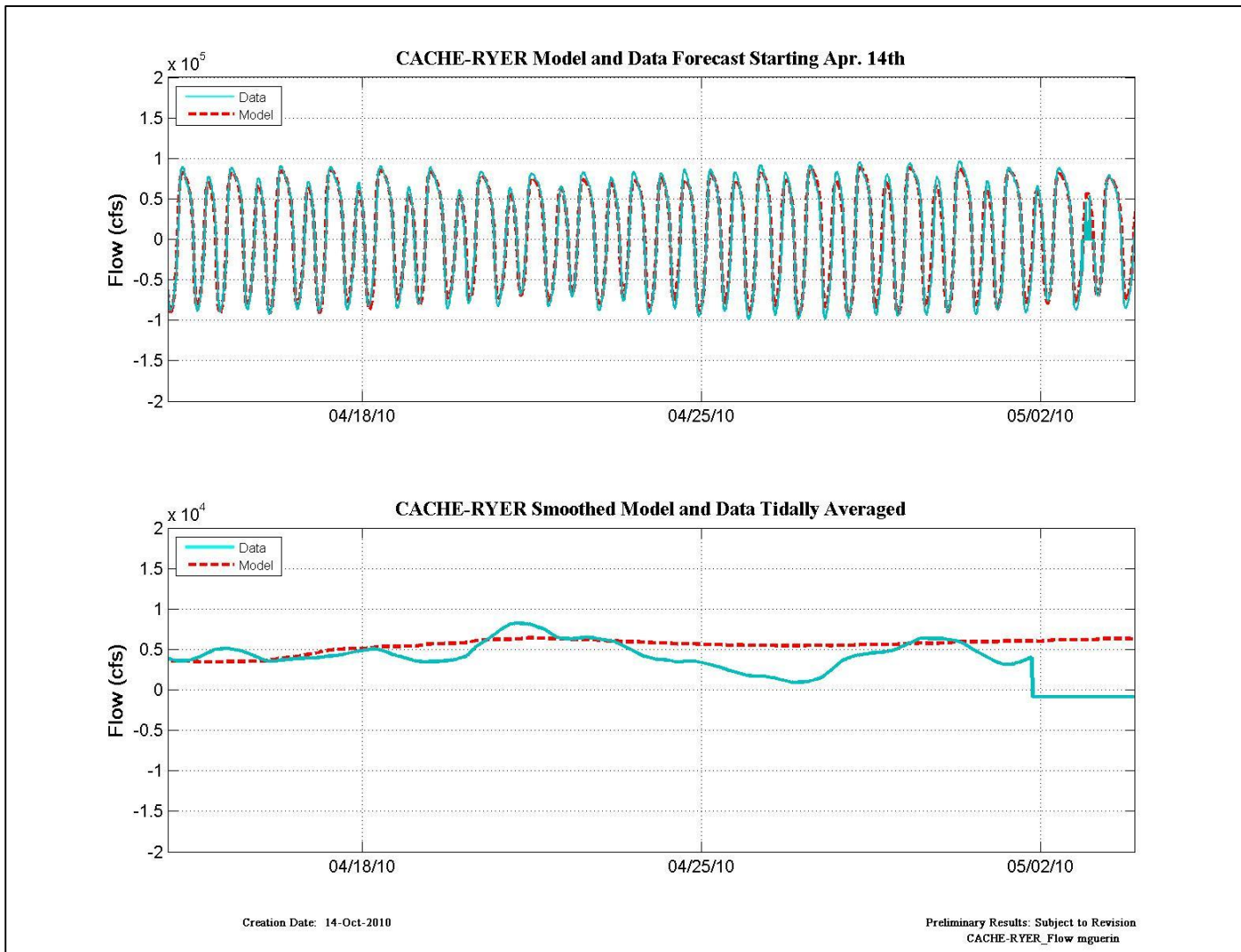


Figure 12-57 Expanded results - flow data and model results for the RMA forecast beginning April 14th at Cache-Ryer.

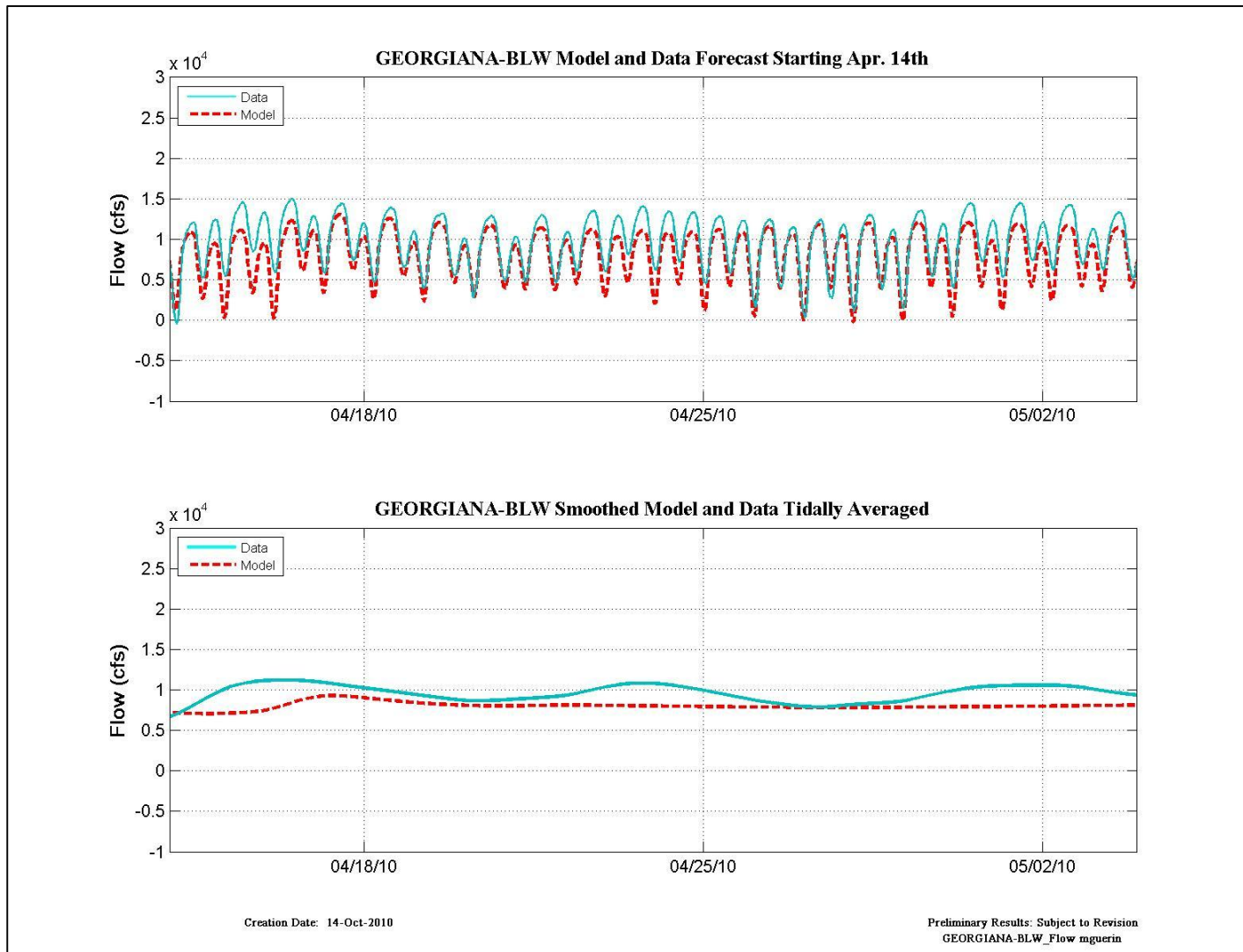


Figure 12-58 Expanded results - flow data and model results for the RMA forecast beginning April 14th at Georgiana-BLW.

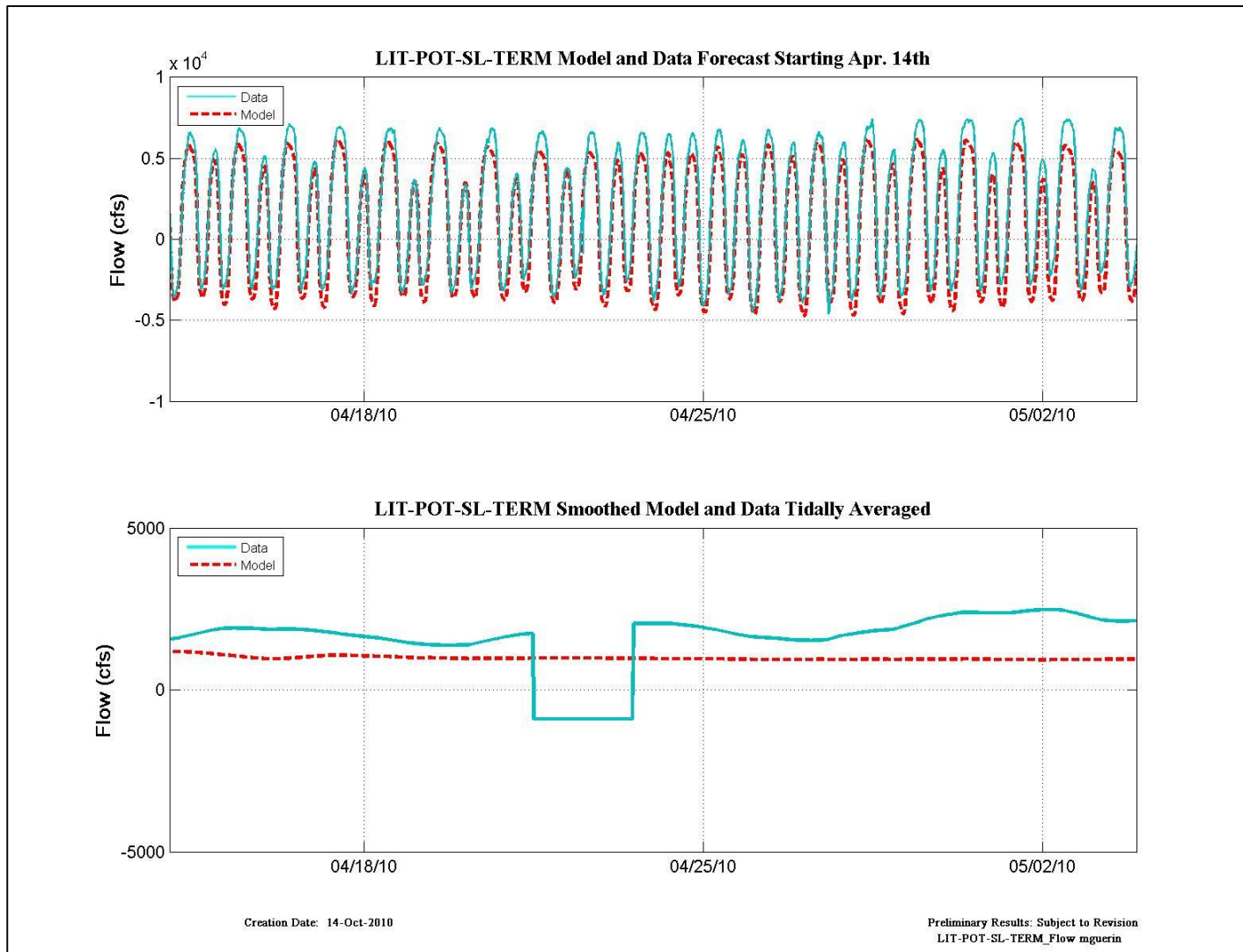


Figure 12-59 Expanded results - flow data and model results for the RMA forecast beginning April 14th at LIT-POT-SL-TERM.

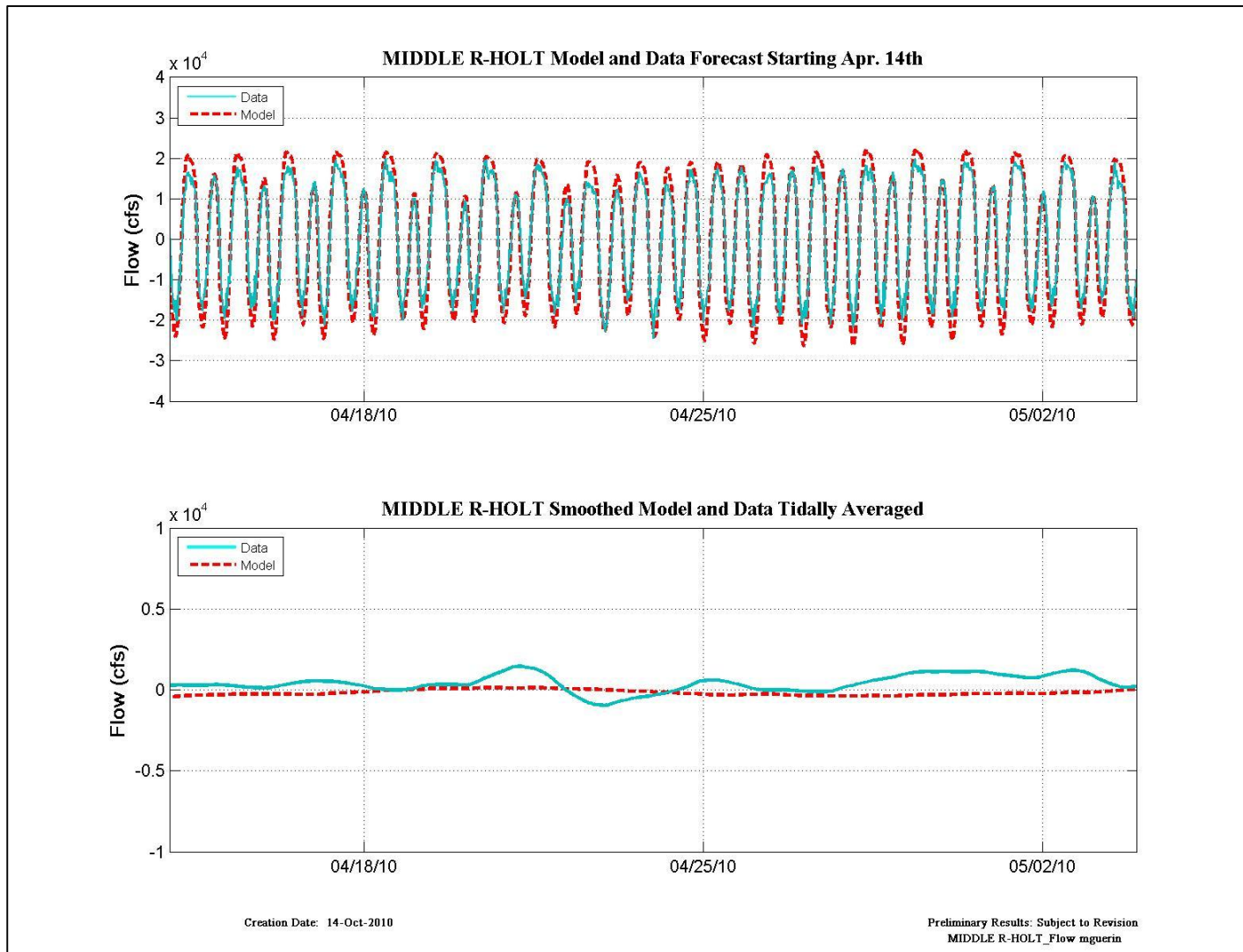


Figure 12-60 Expanded results - flow data and model results for the RMA forecast beginning April 14th at Middle R-Holt.

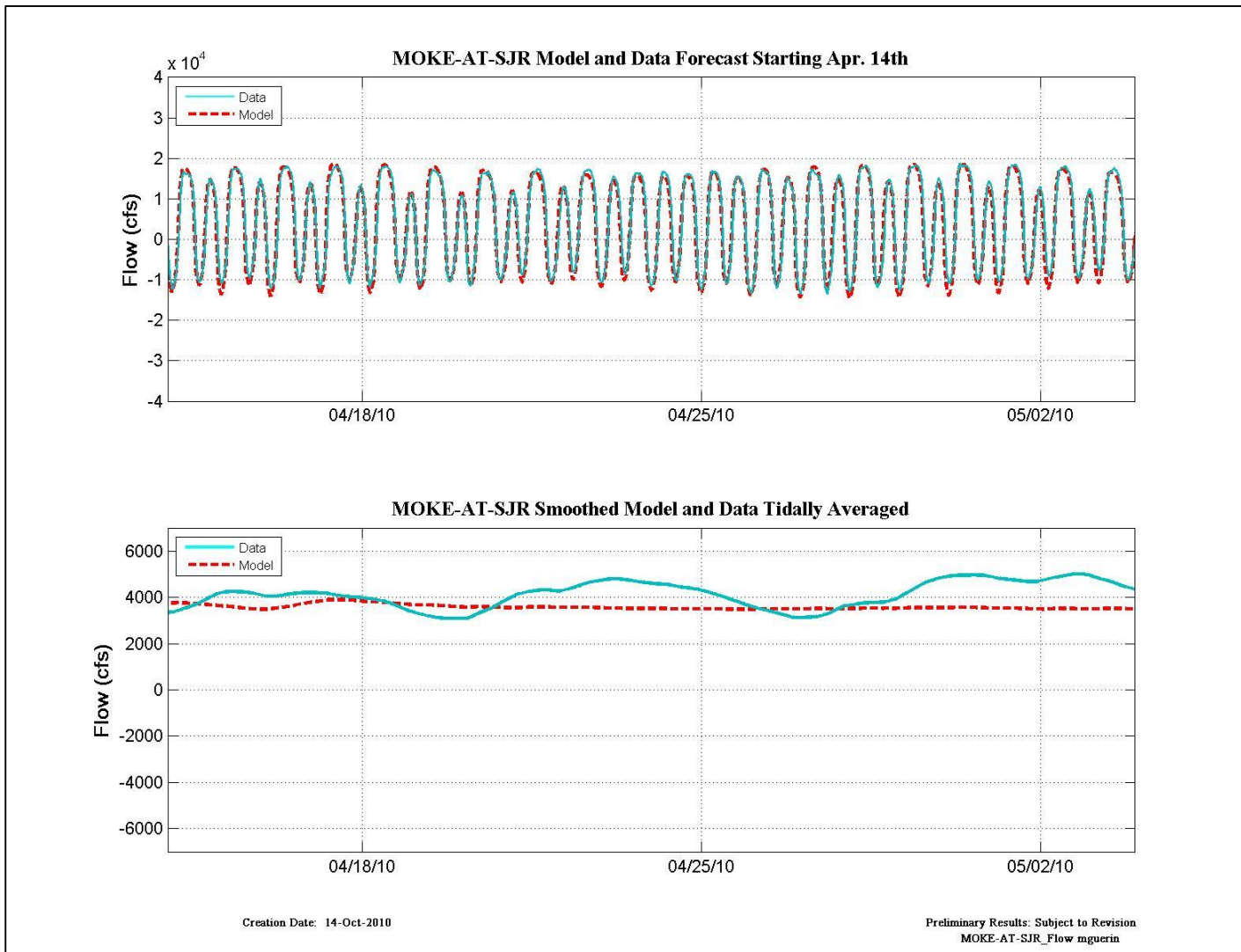


Figure 12-61 Expanded results - flow data and model results for the RMA forecast beginning April 14th at Moke-at-SJR.

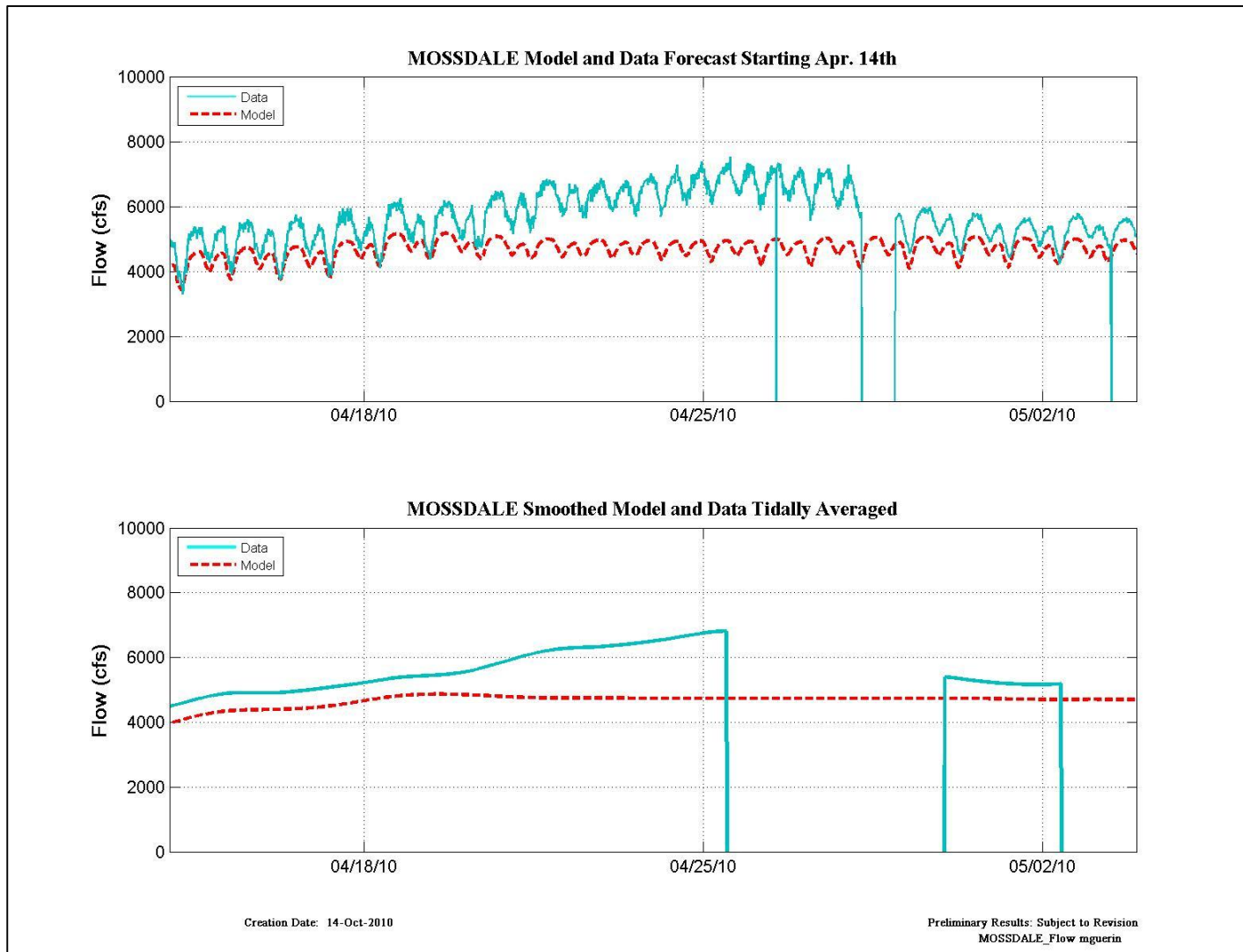


Figure 12-62 Expanded results - flow data and model results for the RMA forecast beginning April 14th at Mosedale.

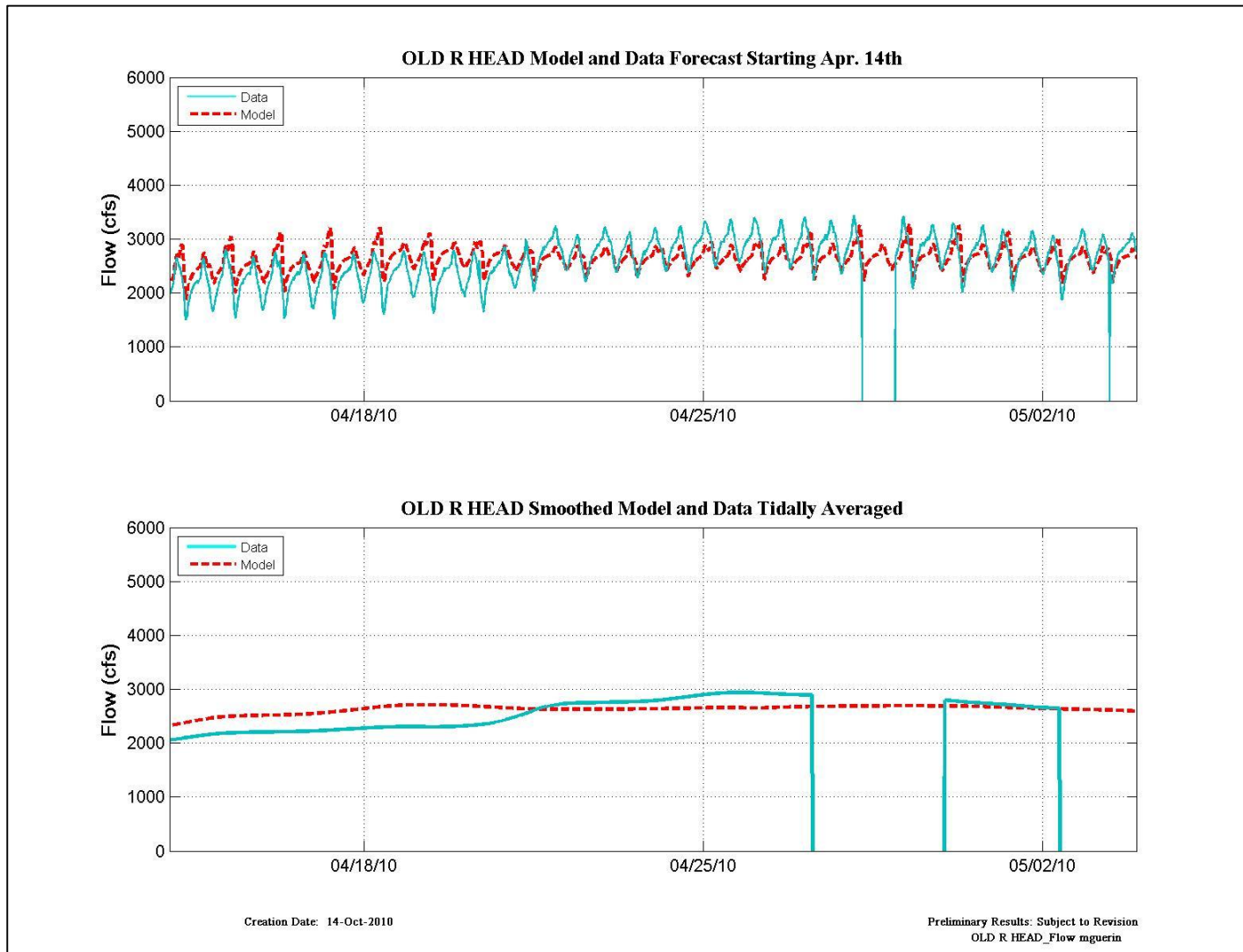


Figure 12-63 Expanded results - flow data and model results for the RMA forecast beginning April 14th at Old R Head.

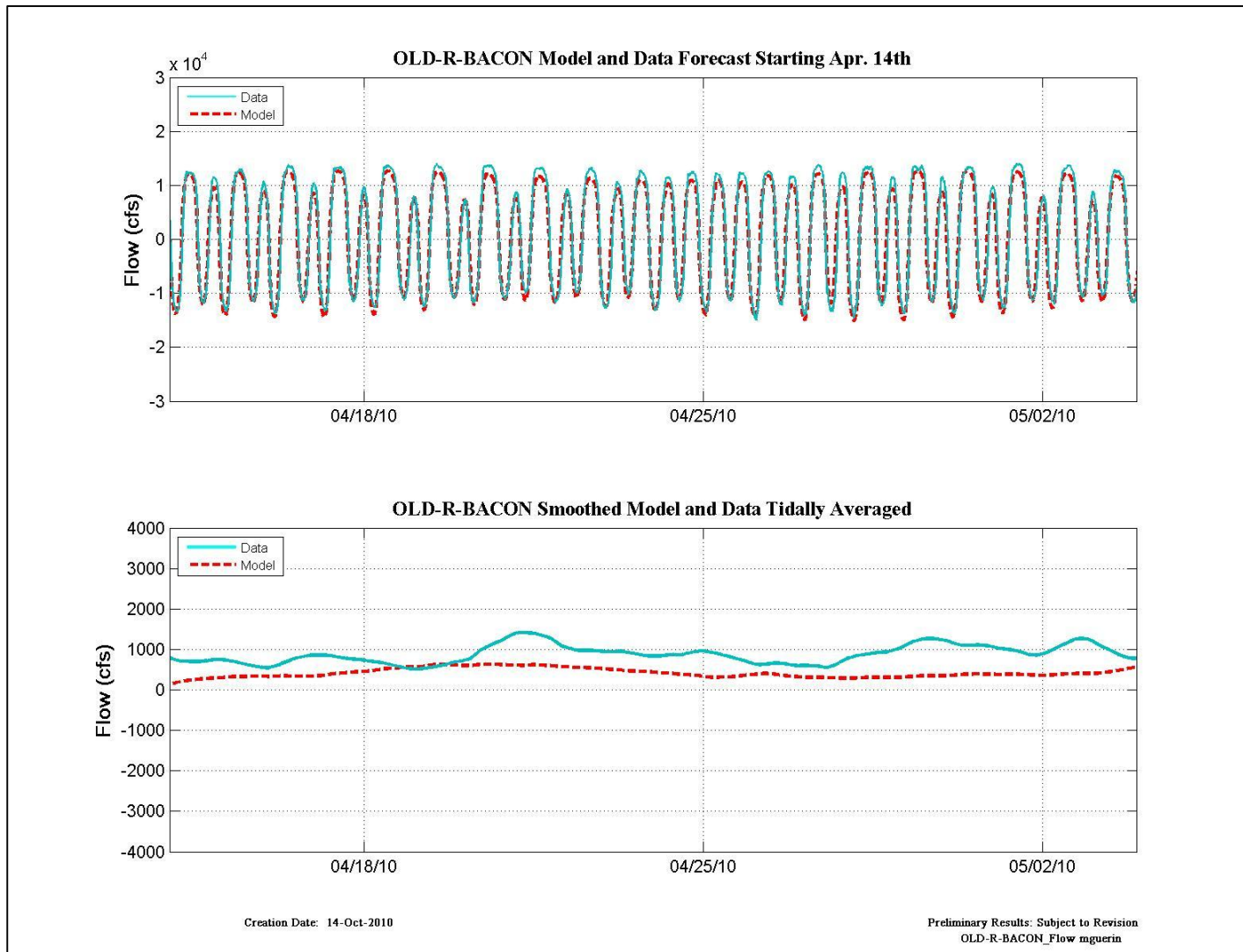


Figure 12-64 Expanded results - flow data and model results for the RMA forecast beginning April 14th at Old-R-Bacon.

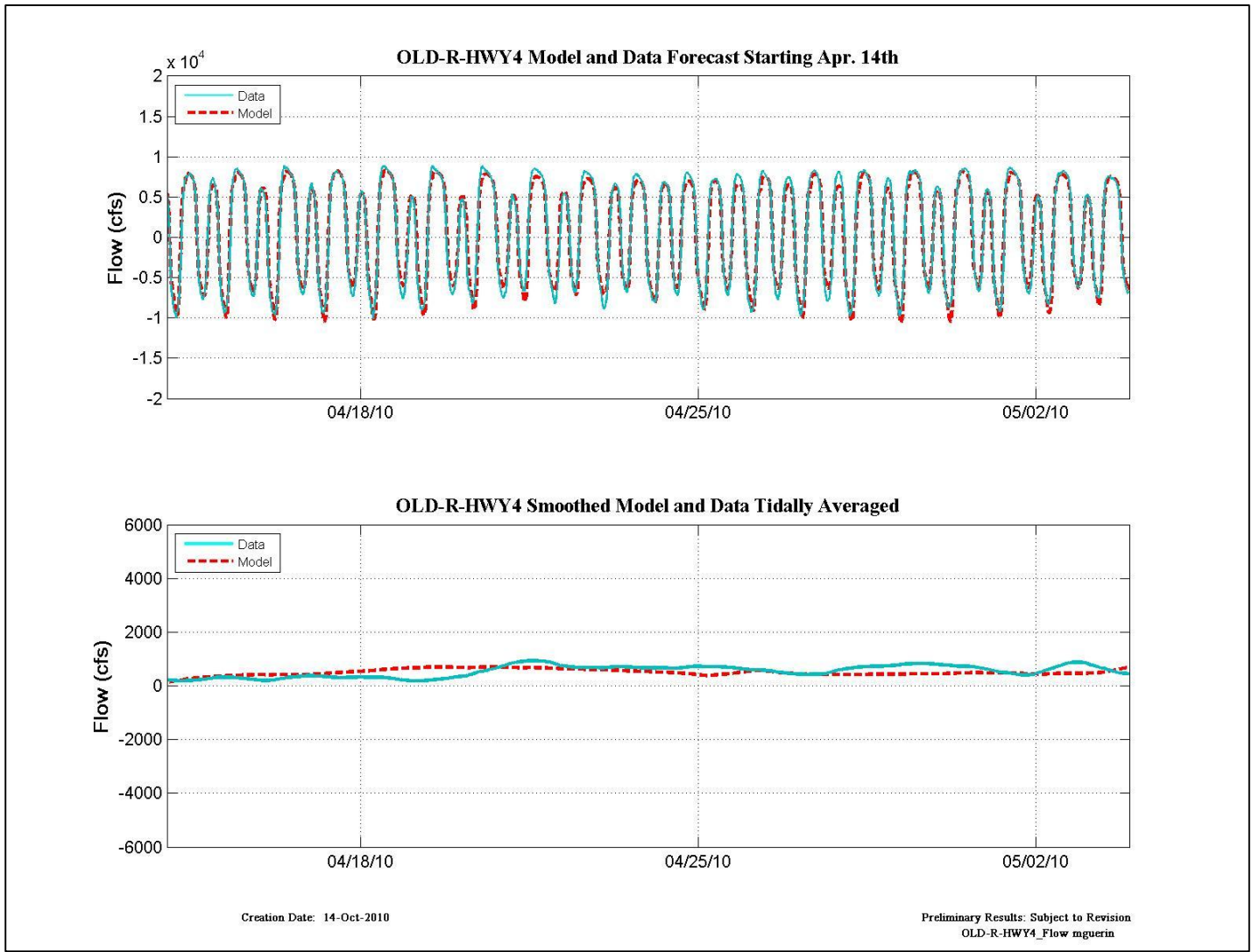


Figure 12-65 Expanded results - flow data and model results for the RMA forecast beginning April 14th at Old-R-Hwy 4.

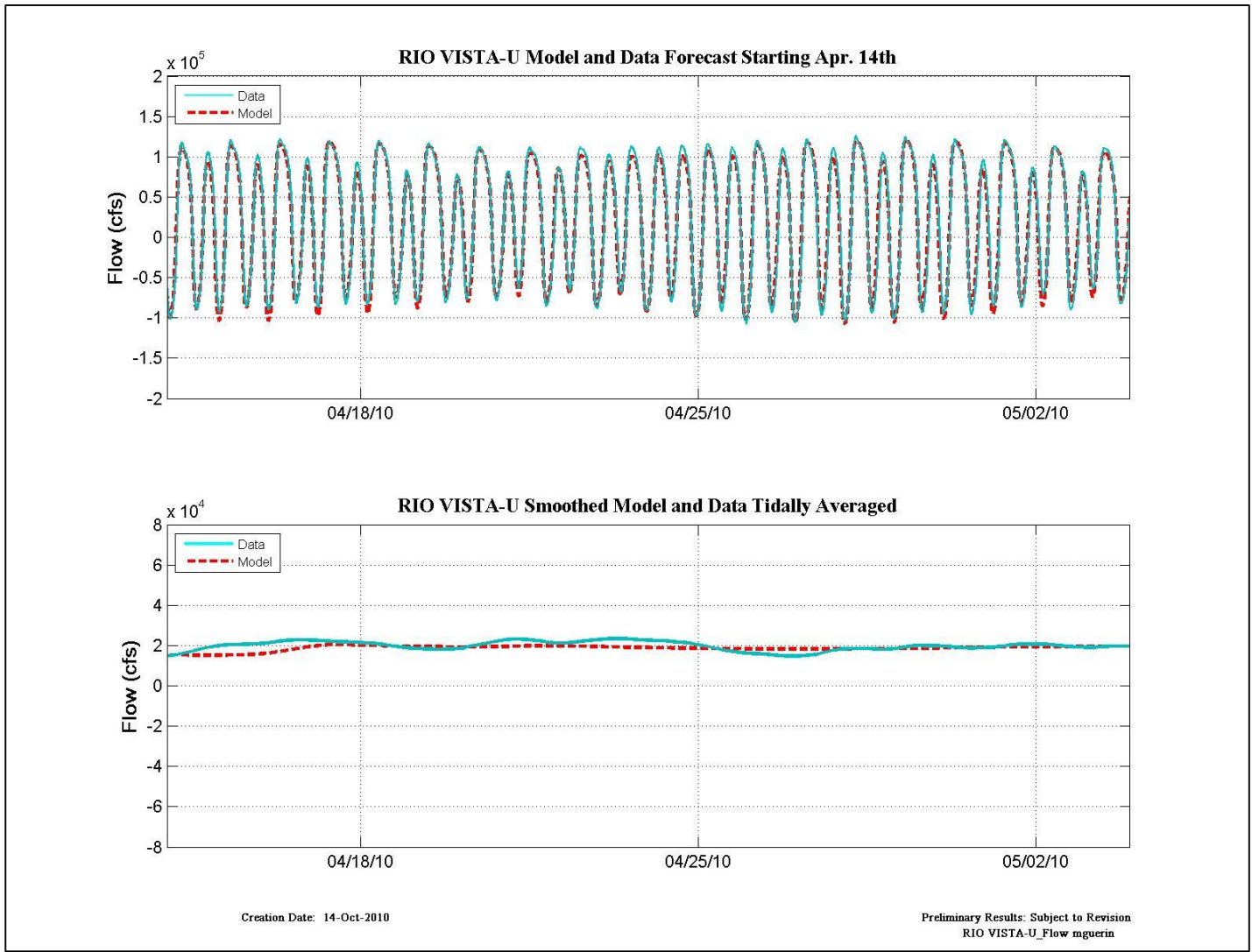


Figure 12-66 Expanded results - flow data and model results for the RMA forecast beginning April 14th at Rio Vista-U.

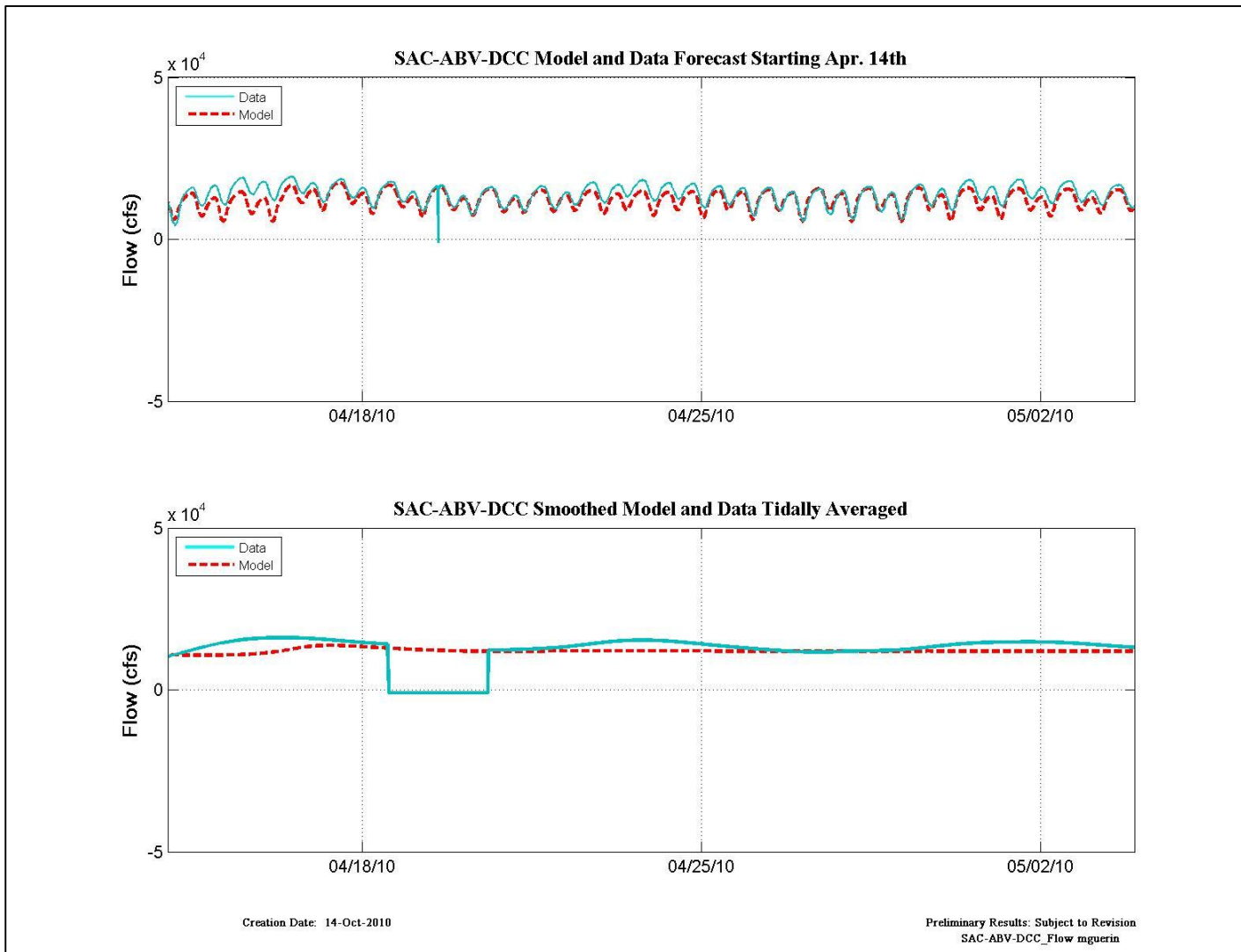


Figure 12-67 Expanded results - flow data and model results for the RMA forecast beginning April 14th at SAC-ABV-DCC.

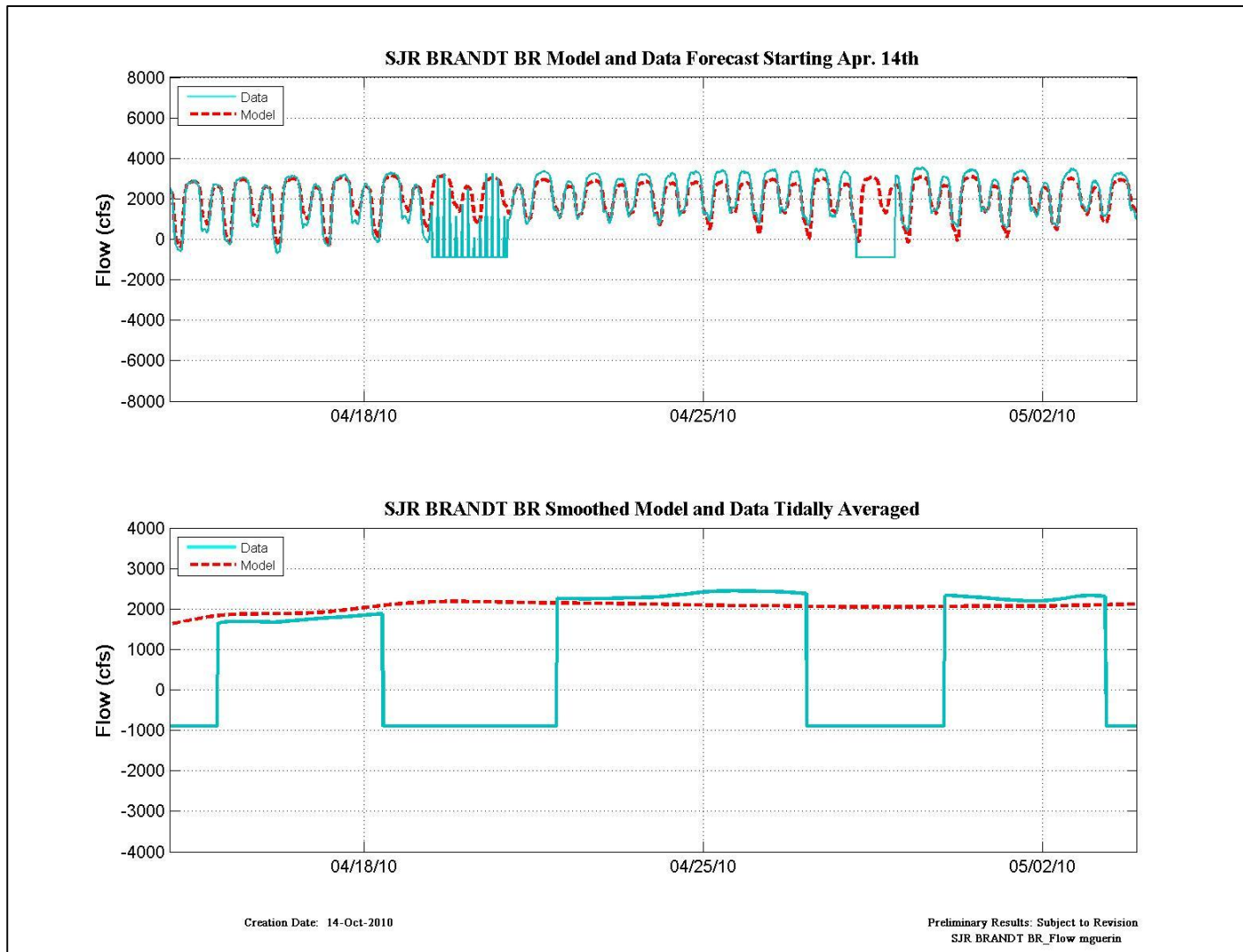


Figure 12-68 Expanded results - flow data and model results for the RMA forecast beginning April 14th at SJR Brandt BR.

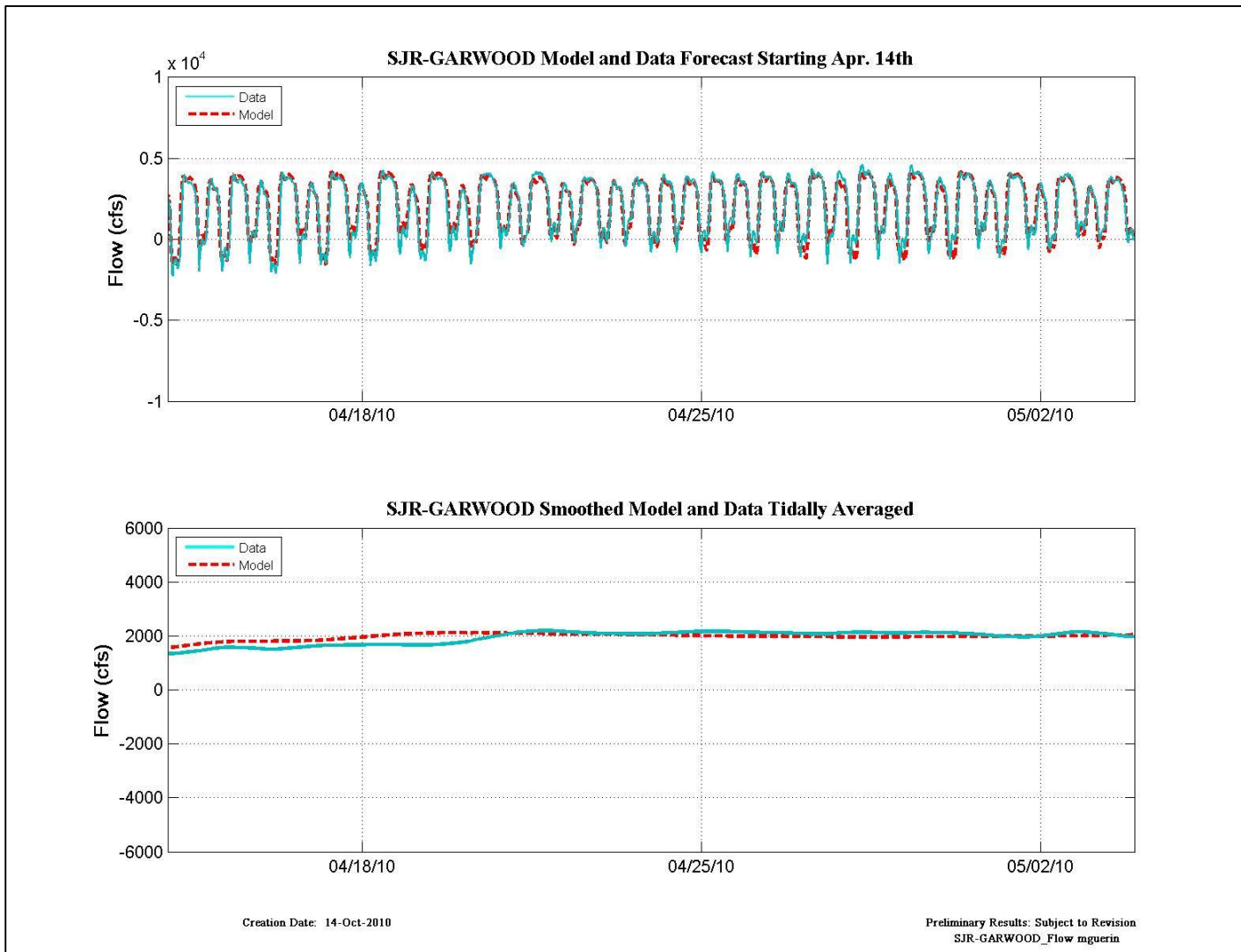


Figure 12-69 Expanded results - flow data and model results for the RMA forecast beginning April 14th at SJR-Garwood.

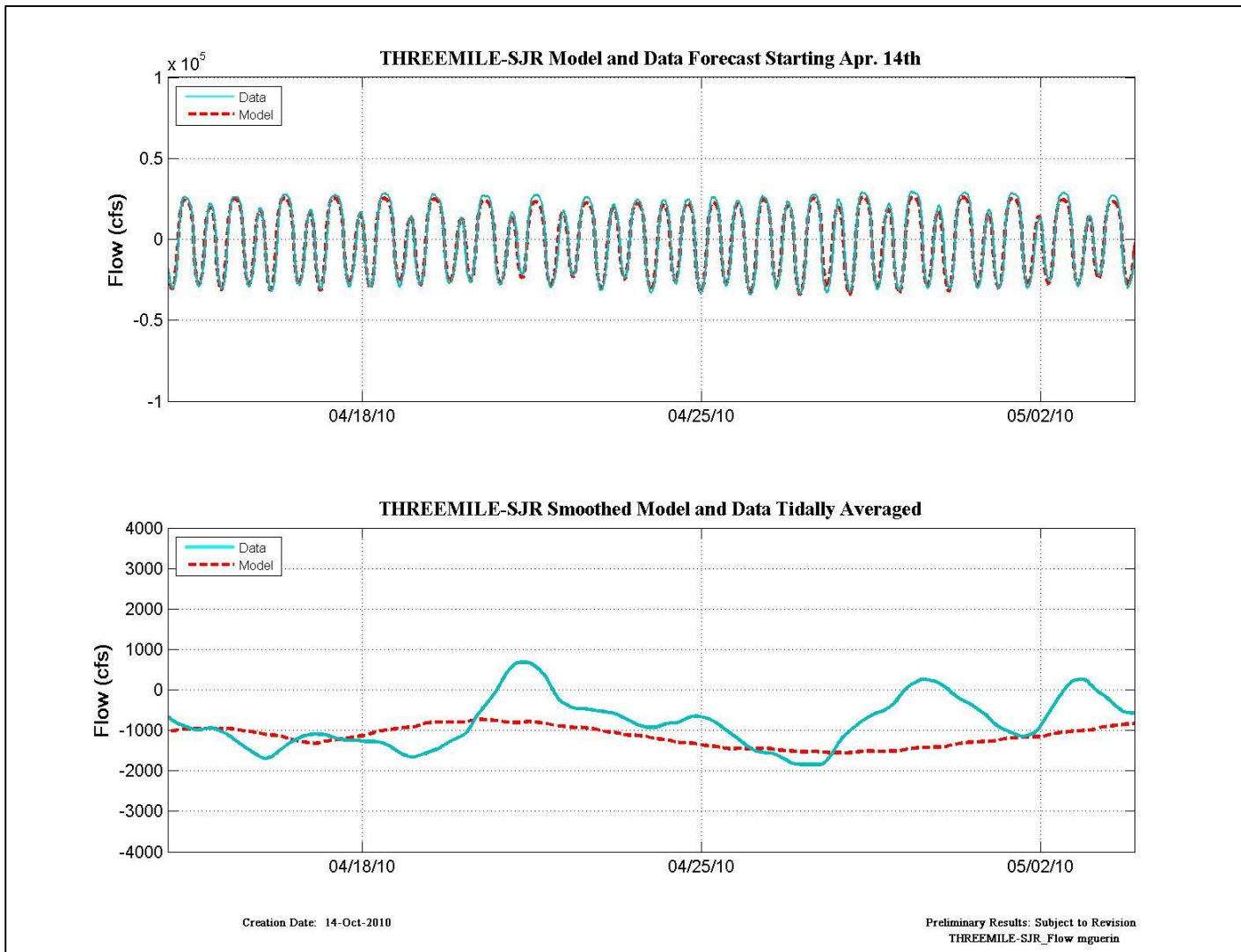


Figure 12-70 Expanded results - flow data and model results for the RMA forecast beginning April 14th at Threemile-SJR.

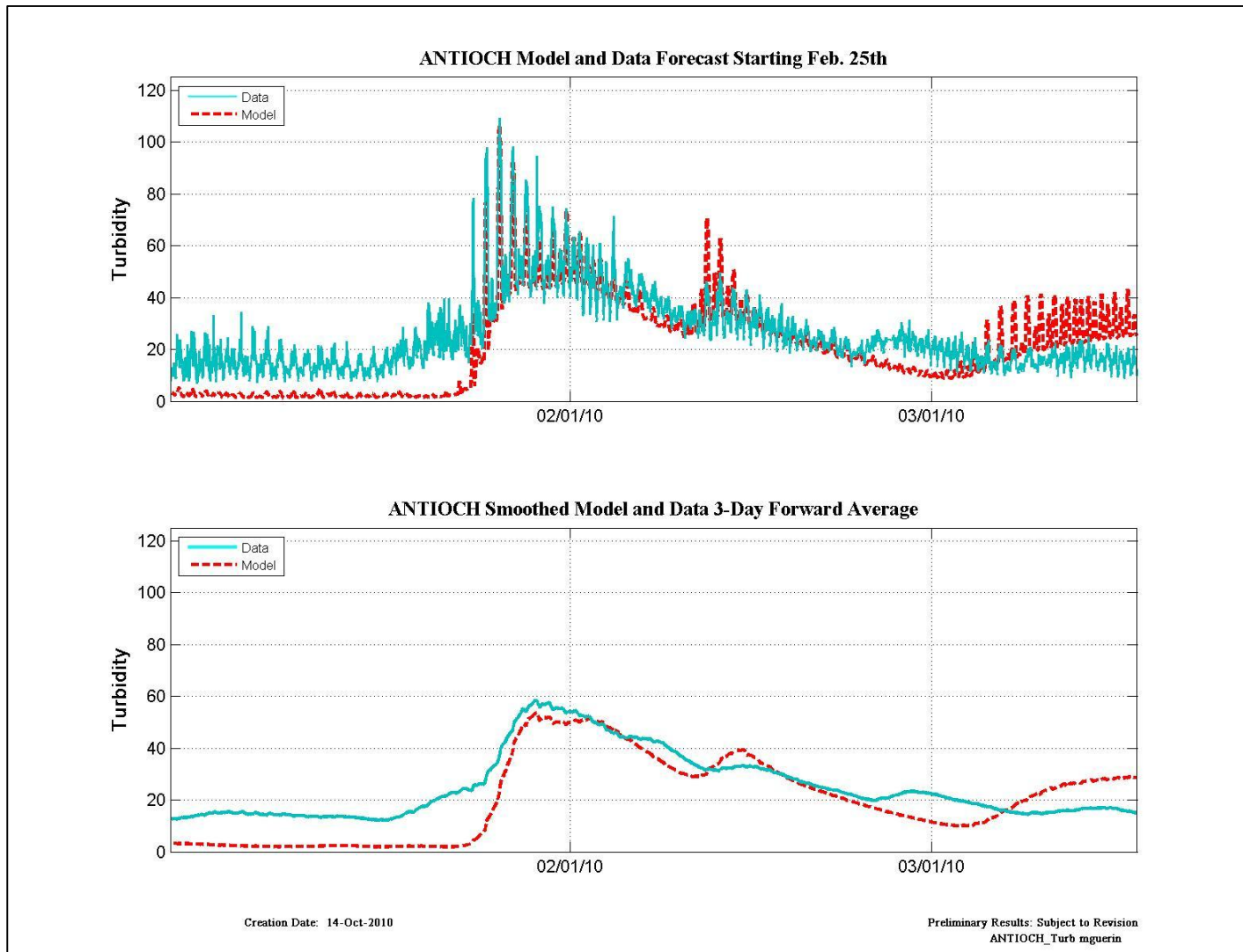


Figure 12-71 Turbidity data and model results for the RMA forecast beginning Feb 25th at Antioch.

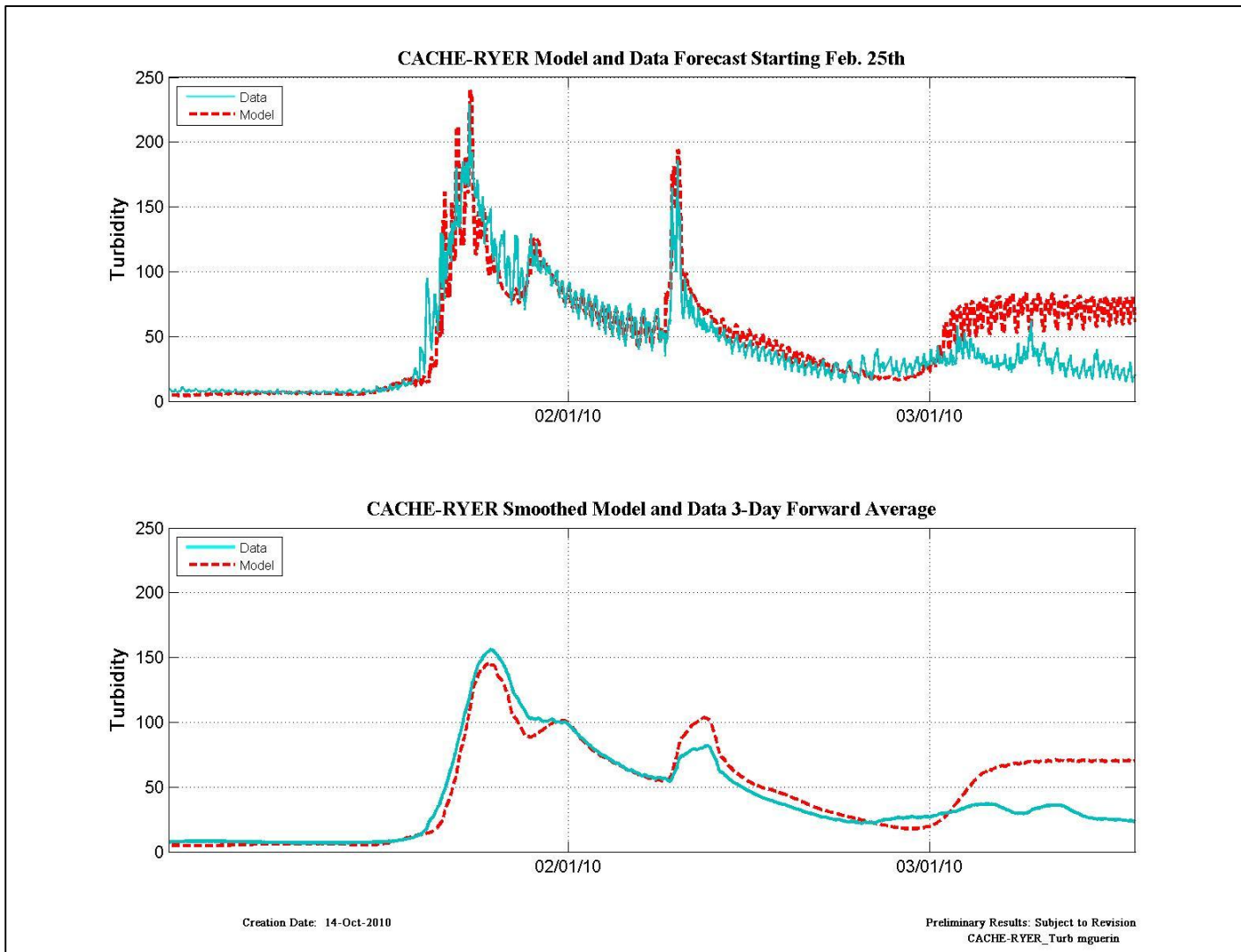


Figure 12-72 Turbidity data and model results for the RMA forecast beginning Feb 25th at Cache-Ryer.

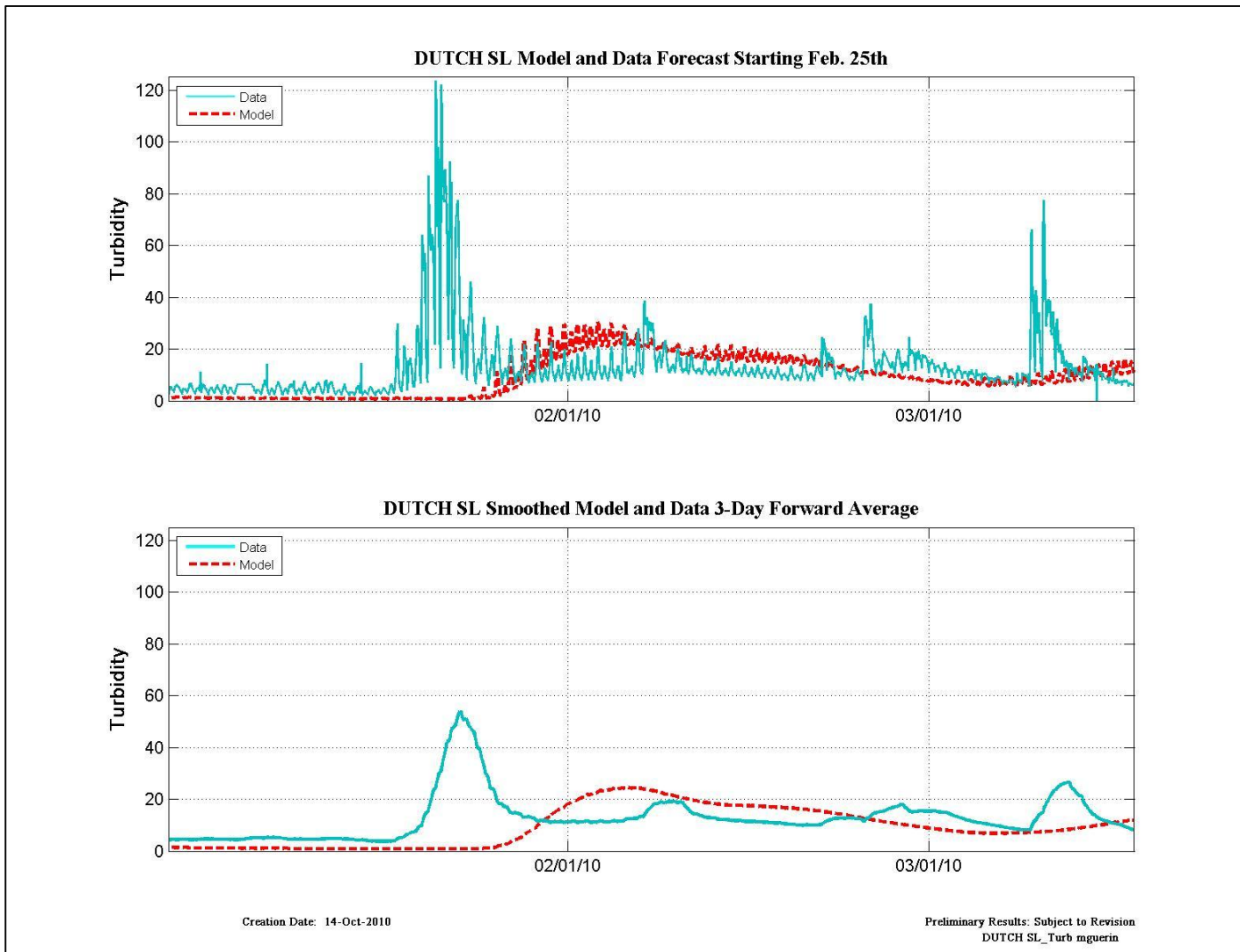


Figure 12-73 Turbidity data and model results for the RMA forecast beginning Feb 25th at Dutch SL.

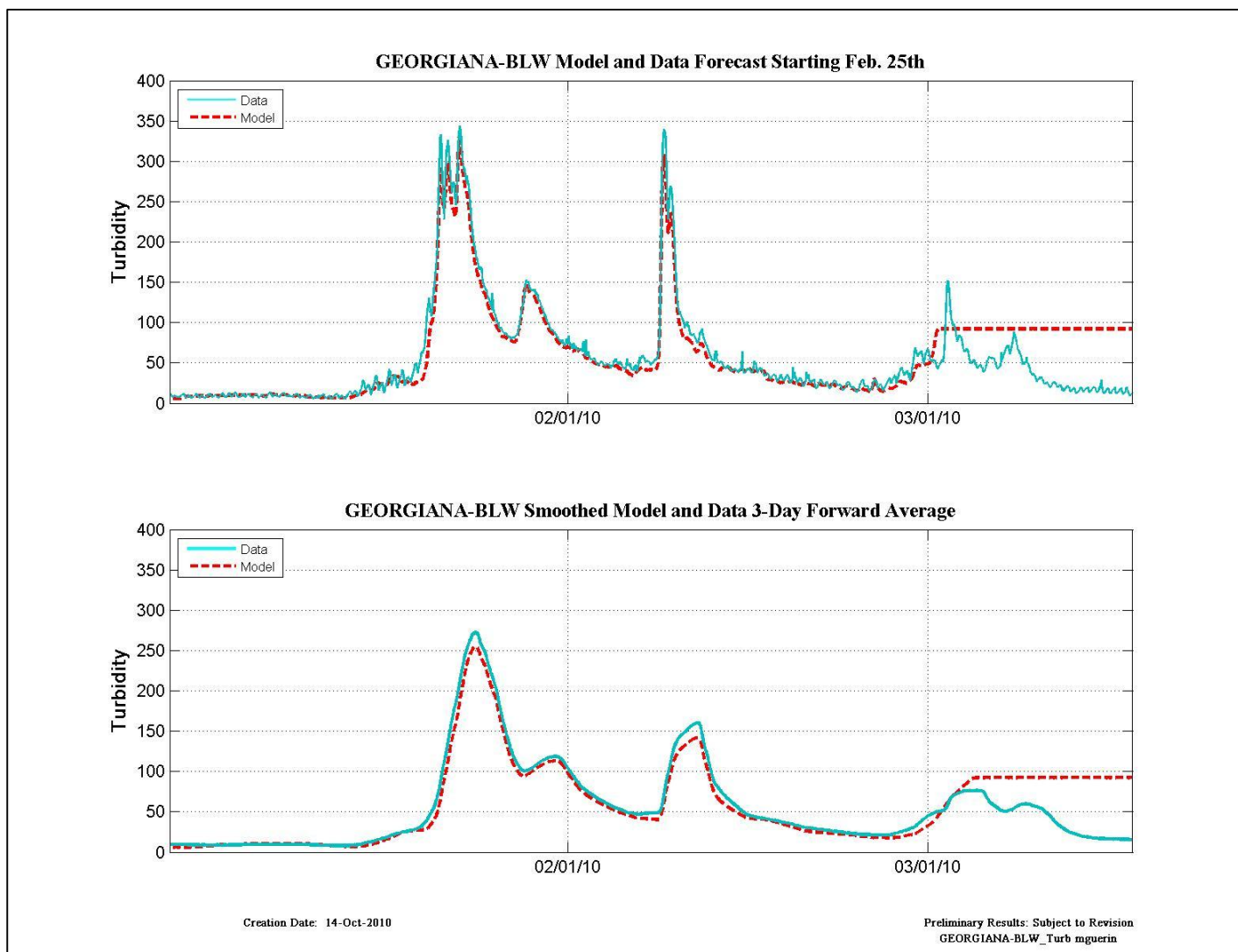


Figure 12-74 Turbidity data and model results for the RMA forecast beginning Feb 25th at Georgiana-BLW.

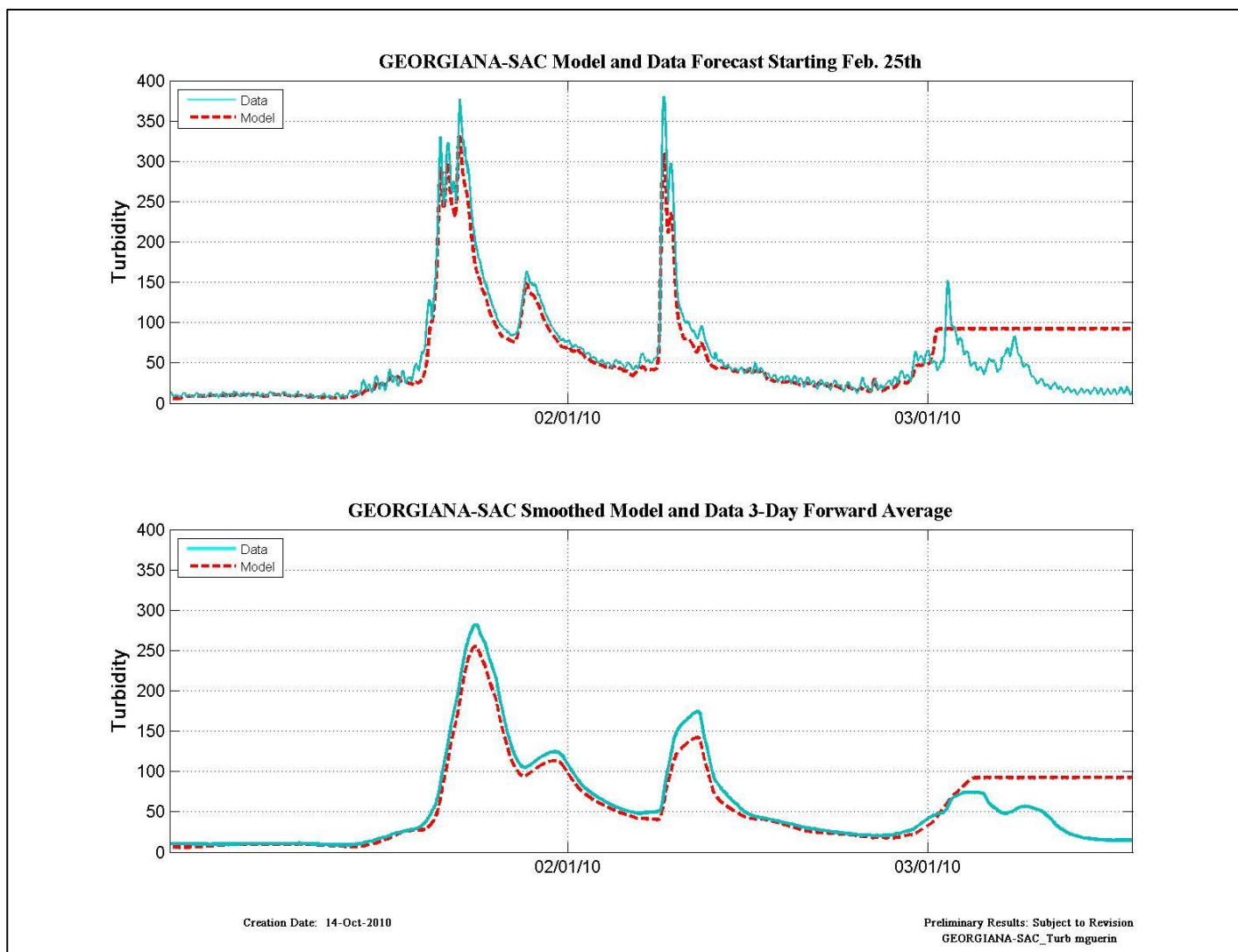


Figure 12-75 Turbidity data and model results for the RMA forecast beginning Feb 25th at Georgiana-SAC.

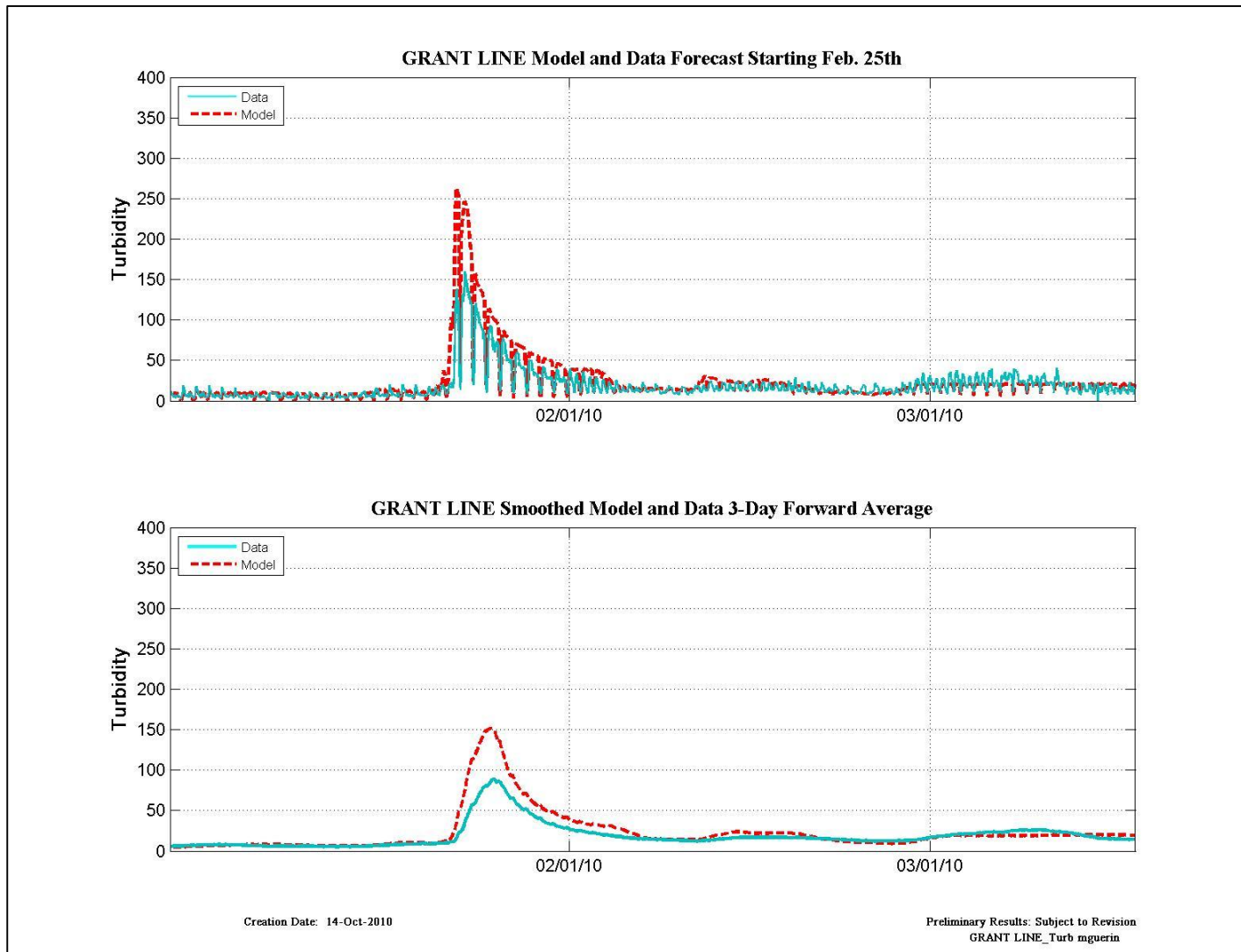


Figure 12-76 Turbidity data and model results for the RMA forecast beginning Feb 25th at Grant Line.

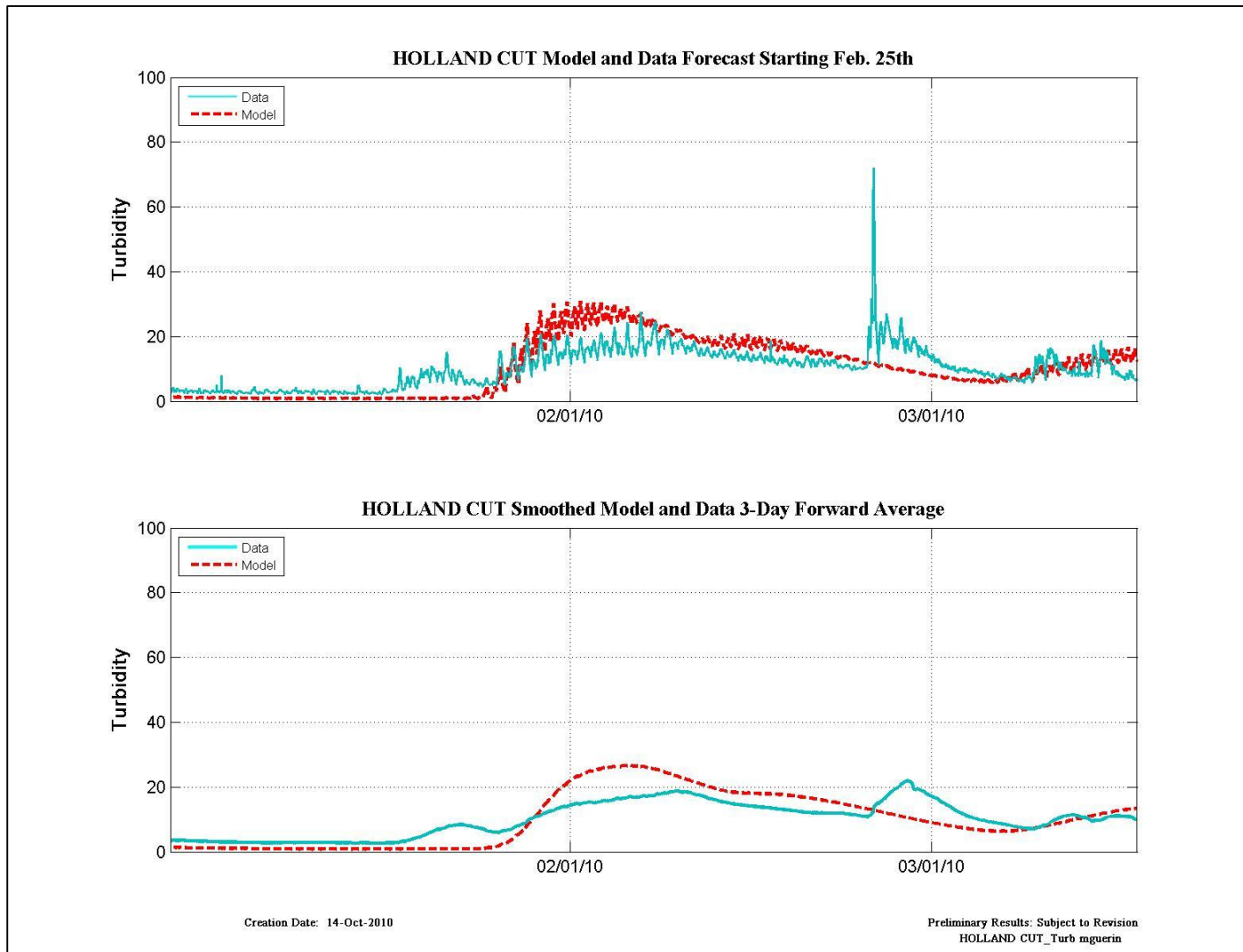


Figure 12-77 Turbidity data and model results for the RMA forecast beginning Feb 25th at Holland Cut.

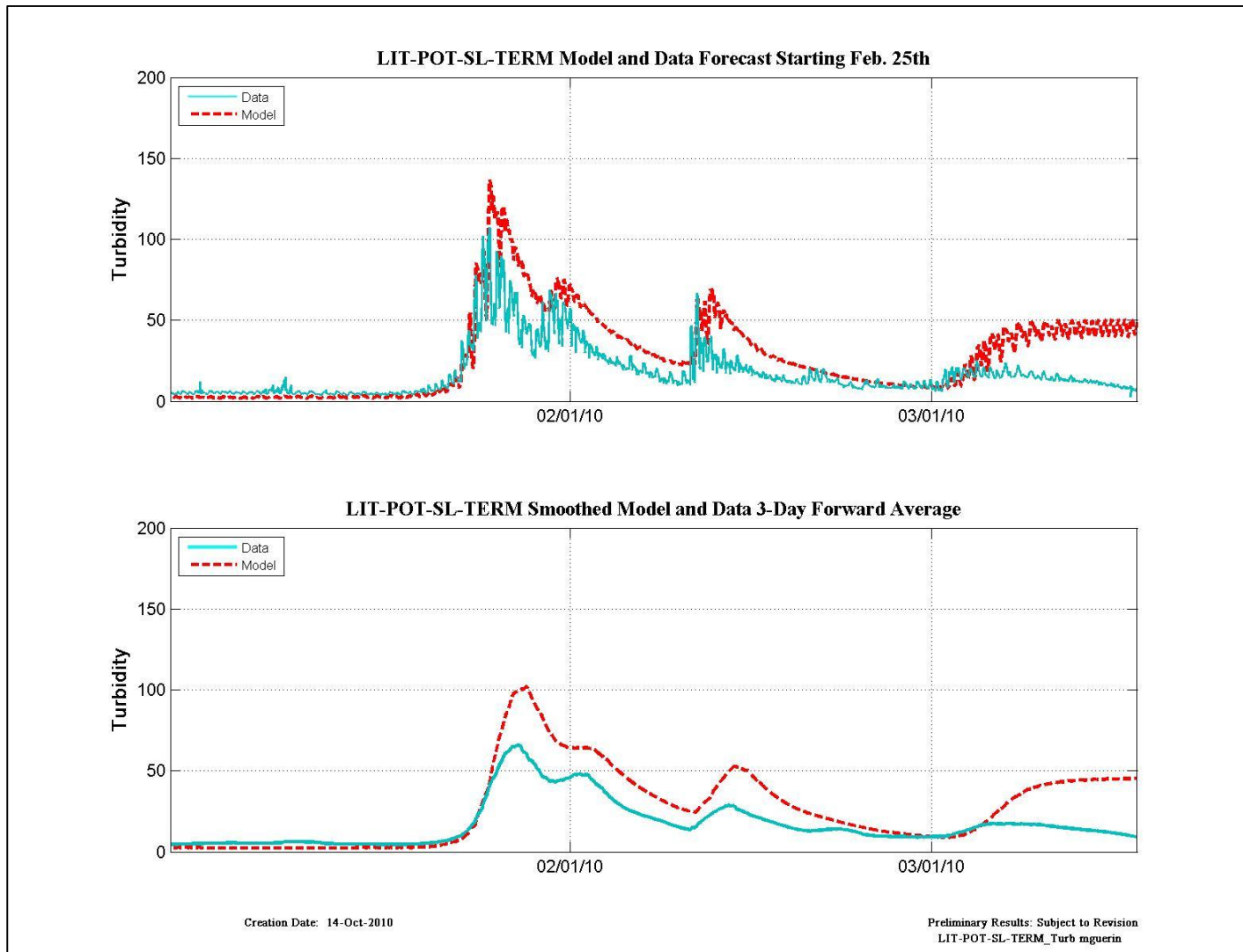


Figure 12-78 Turbidity data and model results for the RMA forecast beginning Feb 25th at LIT-POT-SL-TERM.

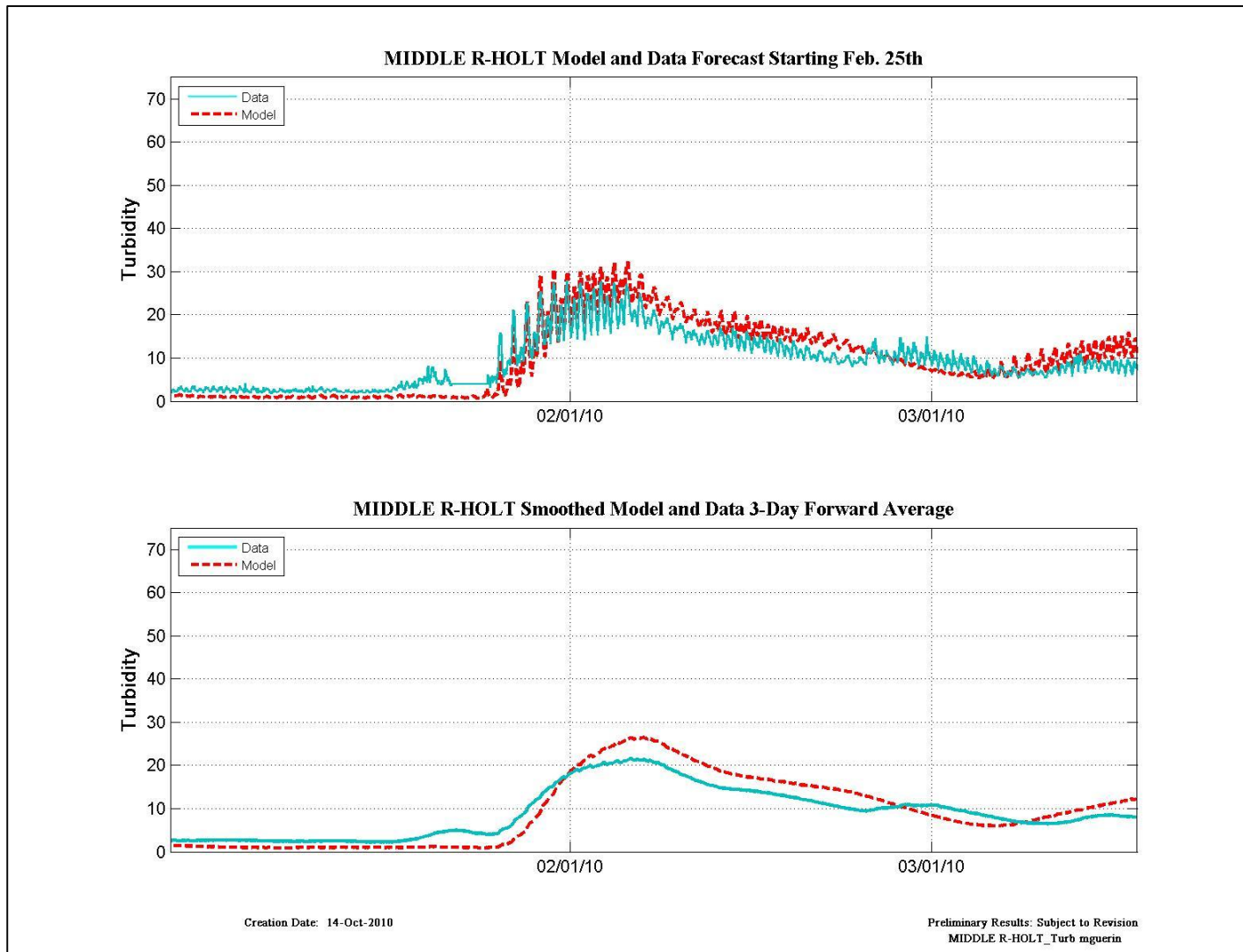


Figure 12-79 Turbidity data and model results for the RMA forecast beginning Feb 25th at Middle R-Holt.

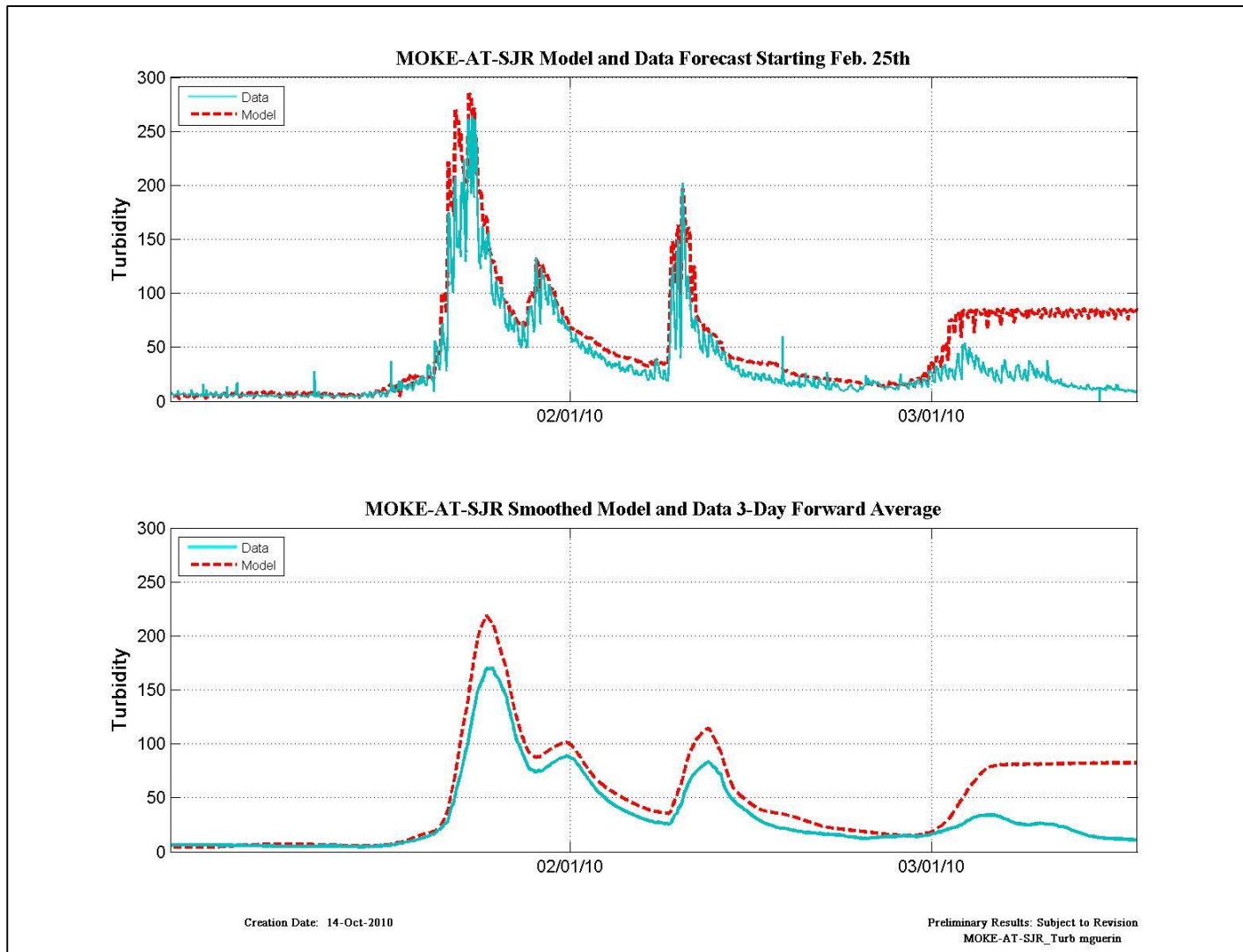


Figure 12-80 Turbidity data and model results for the RMA forecast beginning Feb 25th at Moke-at-SJR.

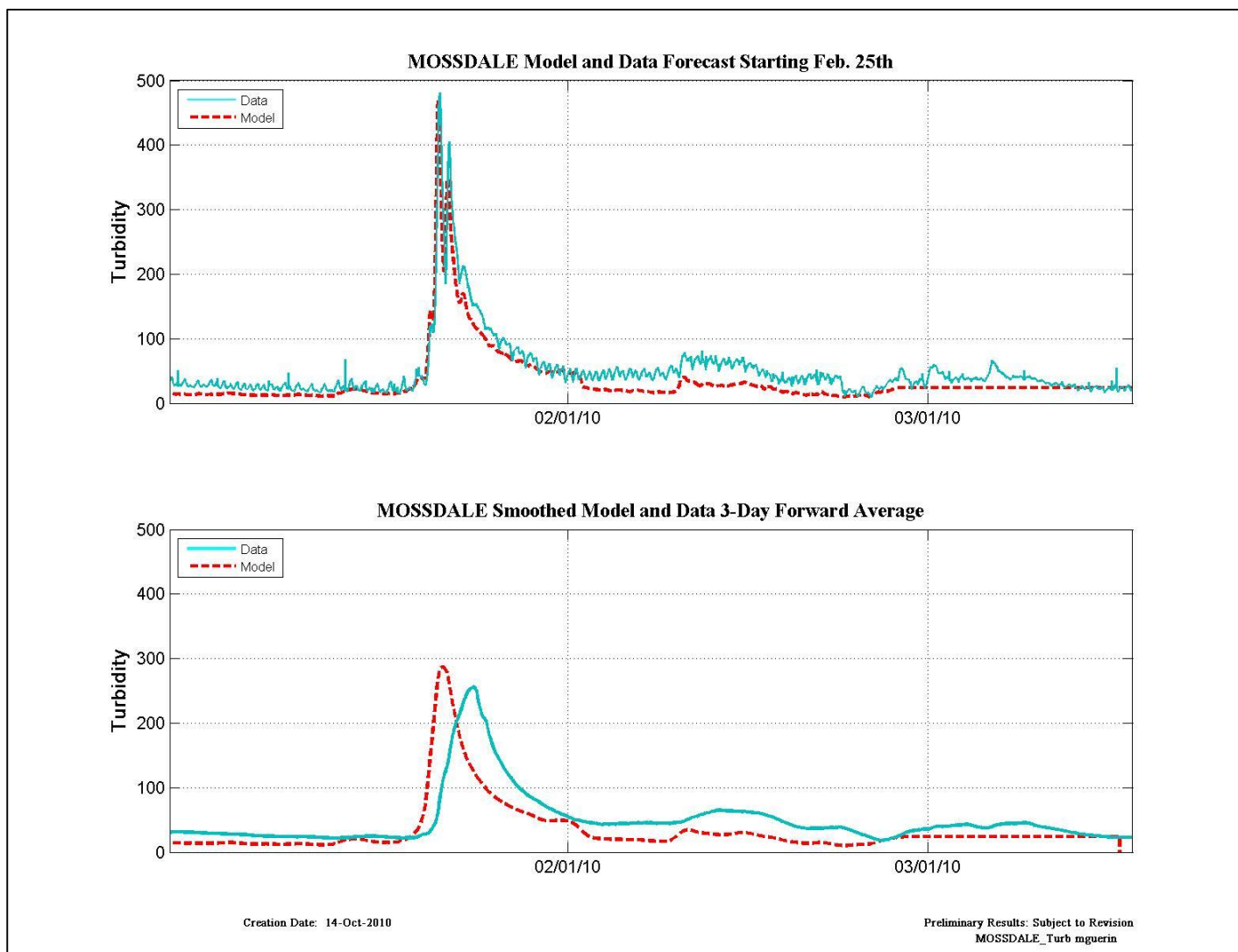


Figure 12-81 Turbidity data and model results for the RMA forecast beginning Feb 25th at Mossdale.

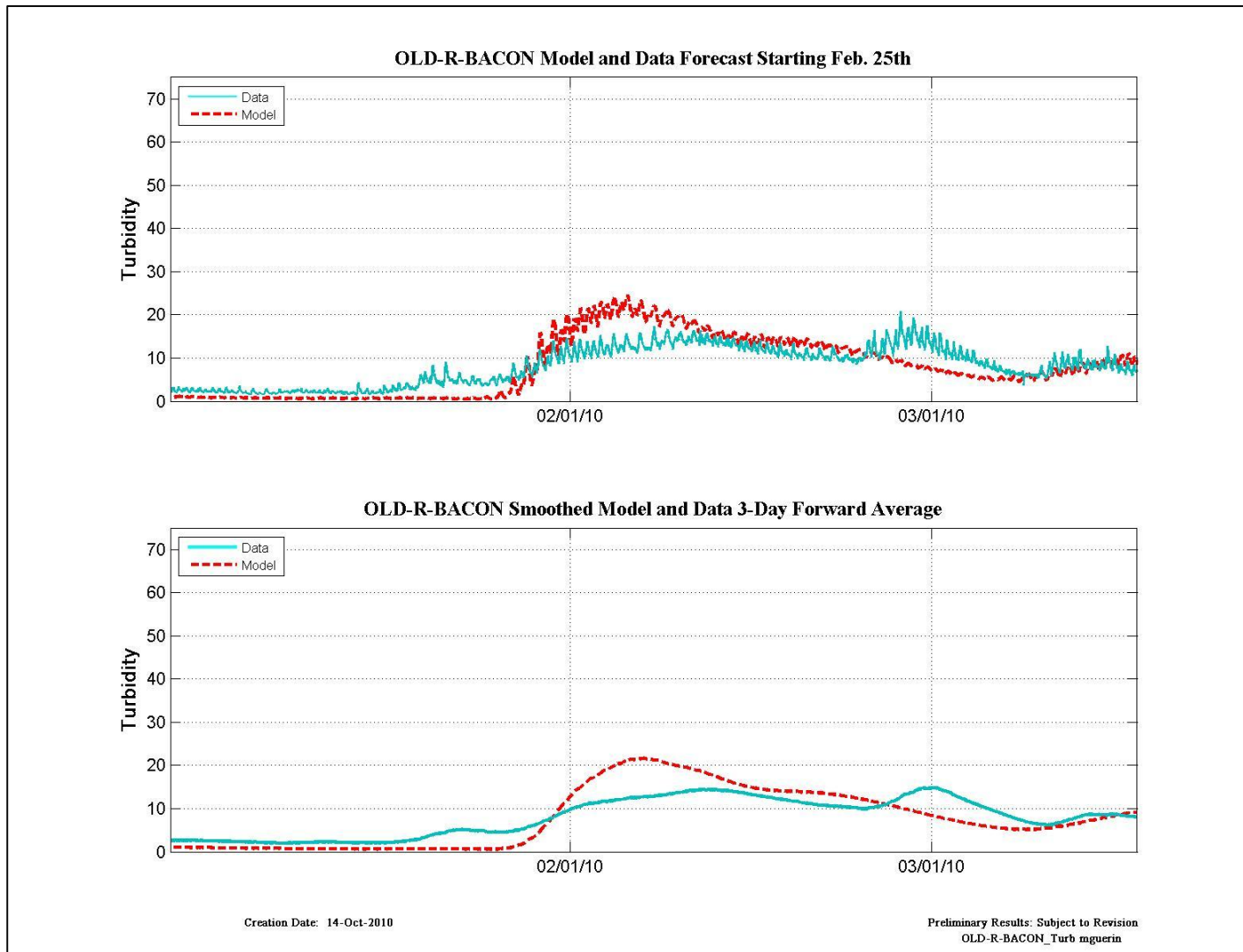


Figure 12-82 Turbidity data and model results for the RMA forecast beginning Feb 25th at Old-R-Bacon.

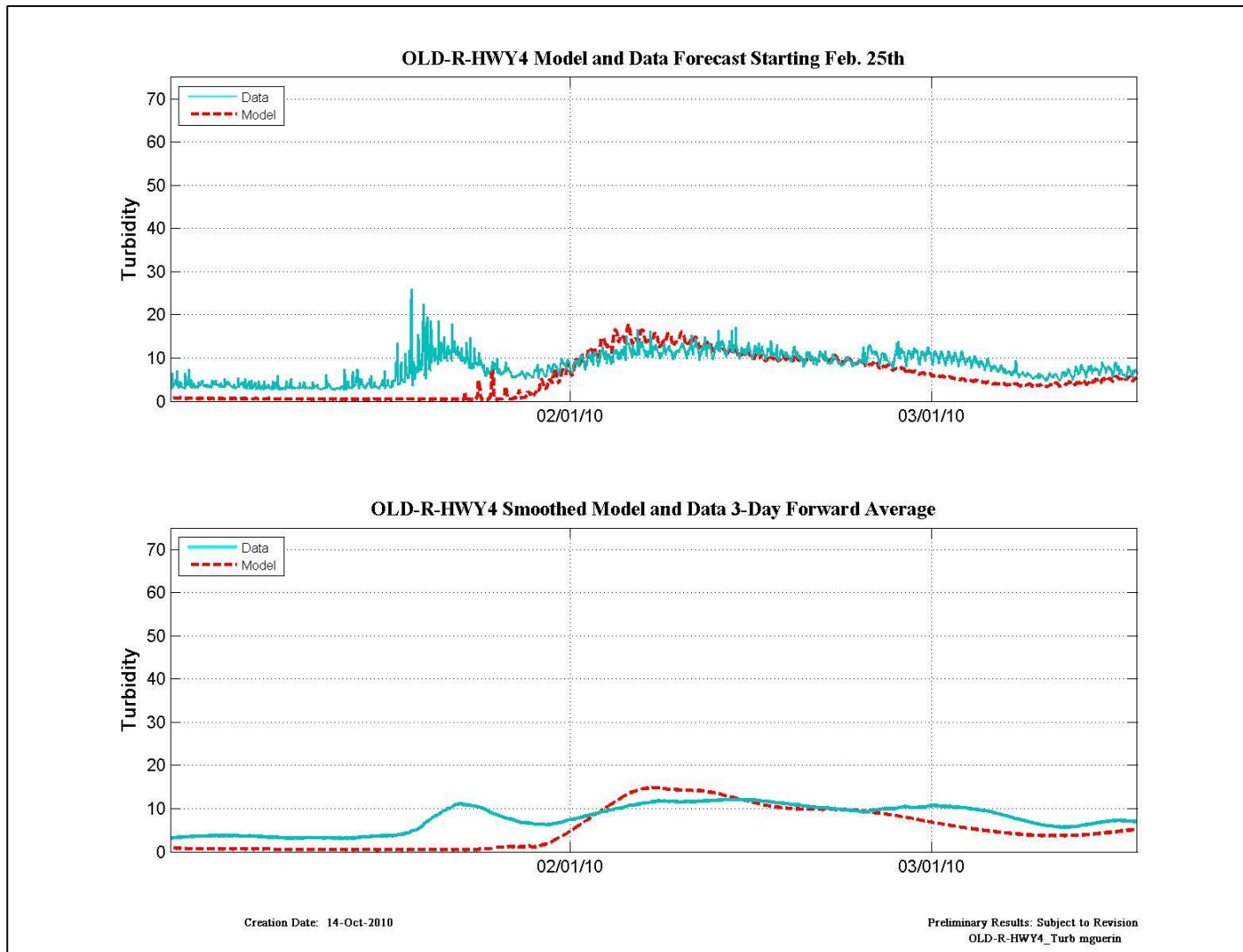


Figure 12-83 Turbidity data and model results for the RMA forecast beginning Feb 25th at Old-R-Hwy 4.

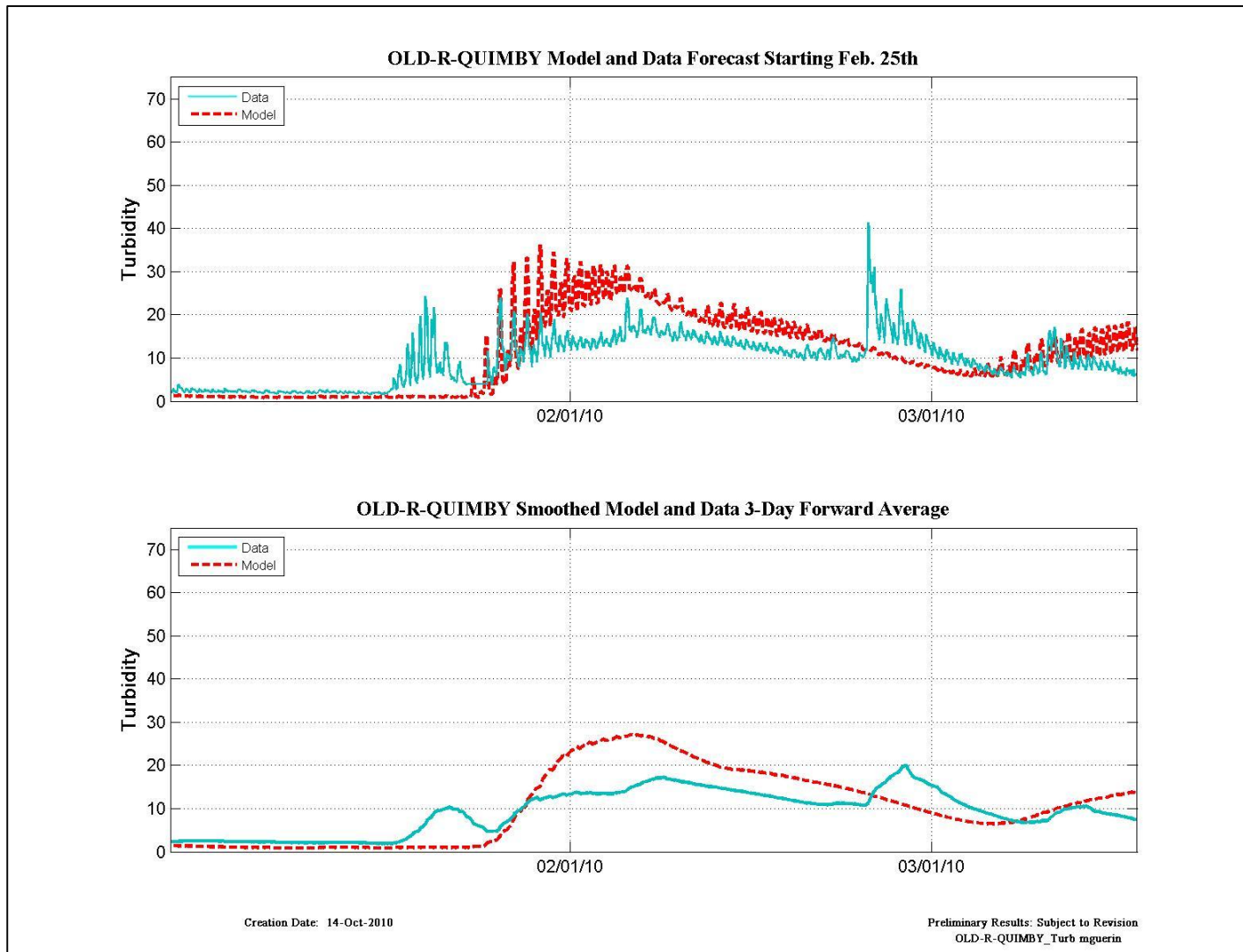


Figure 12-84 Turbidity data and model results for the RMA forecast beginning Feb 25th at Old-R-Quimby.

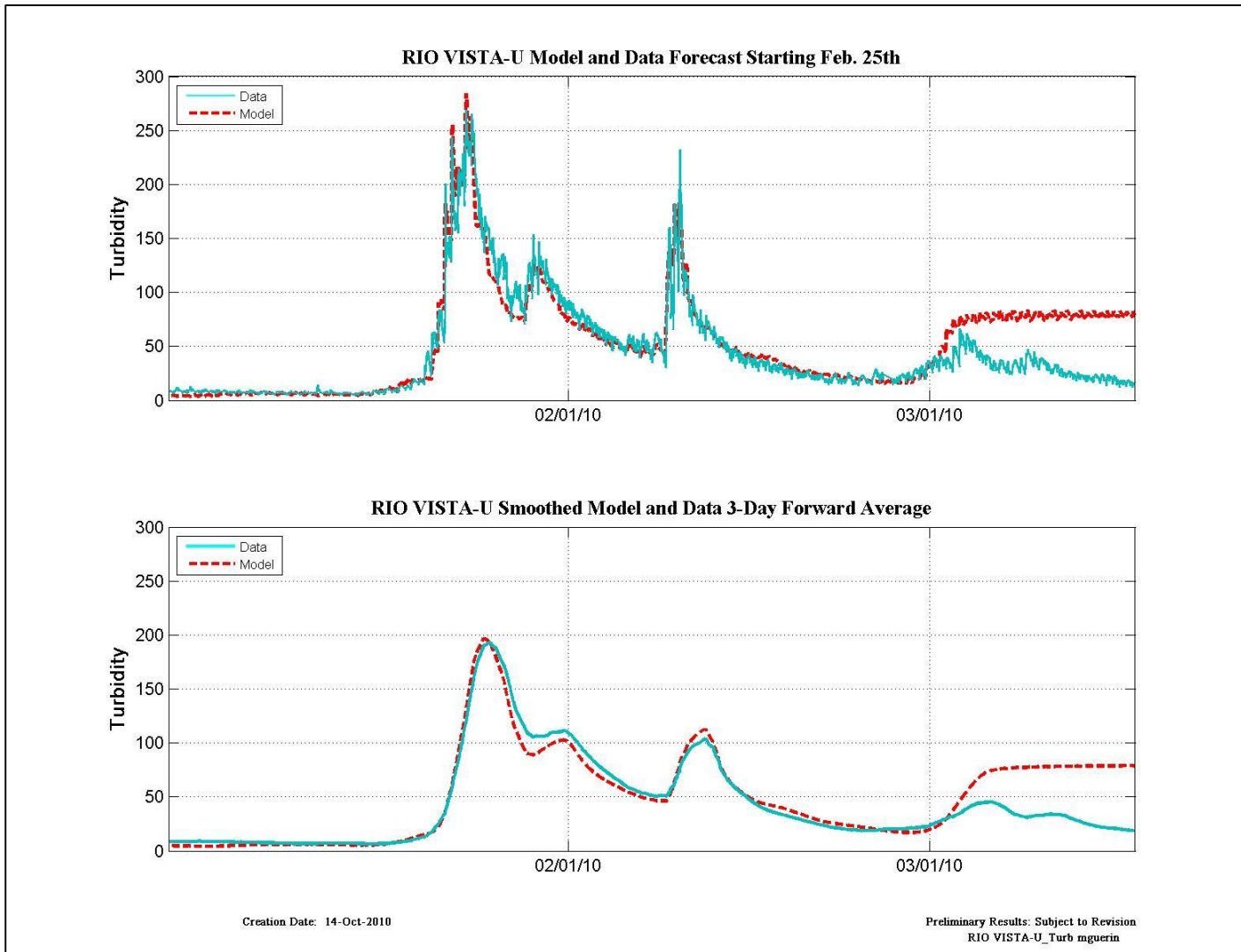


Figure 12-85 Turbidity data and model results for the RMA forecast beginning Feb 25th at Rio Vista-U.

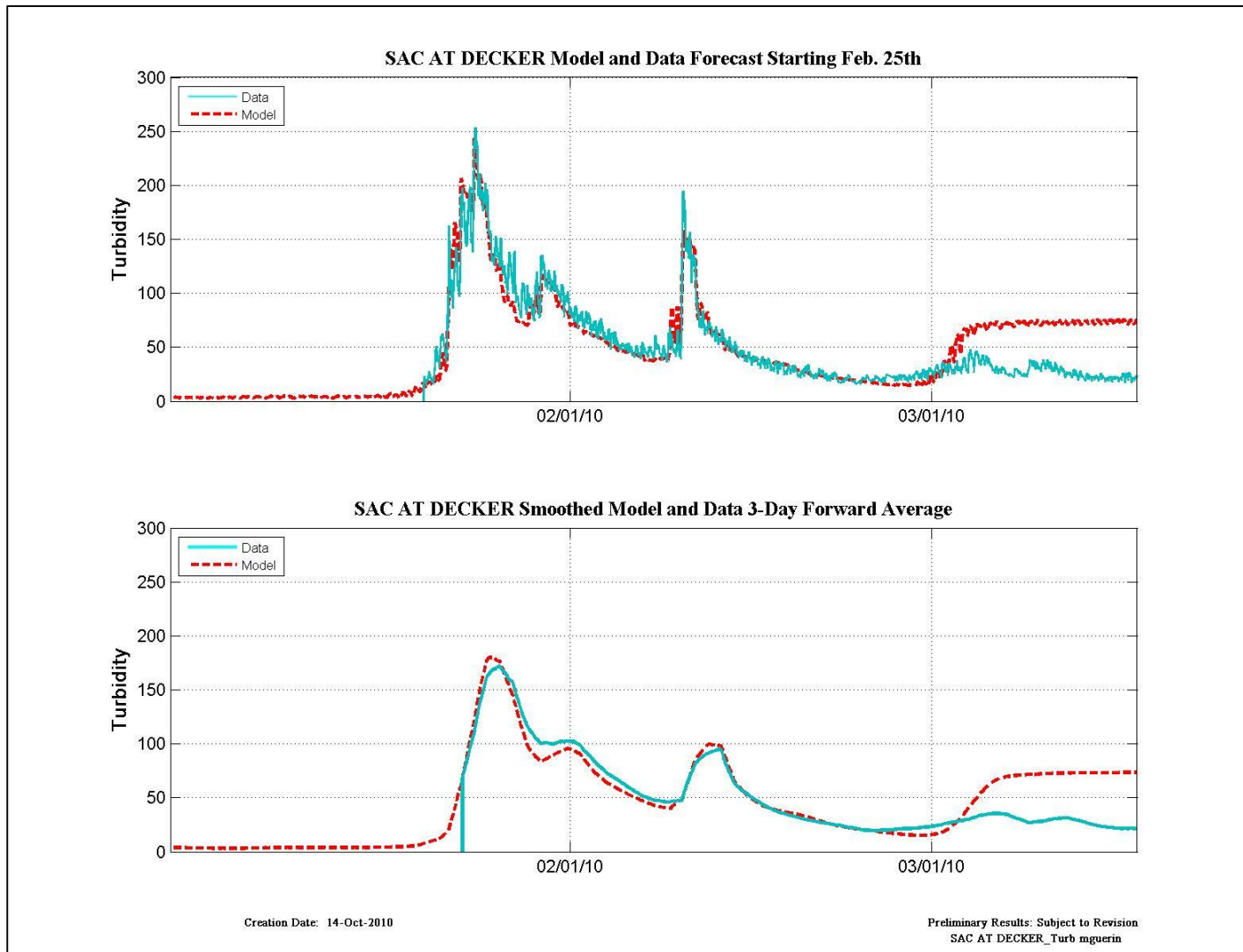


Figure 12-86 Turbidity data and model results for the RMA forecast beginning Feb 25th at SAC at Decker.

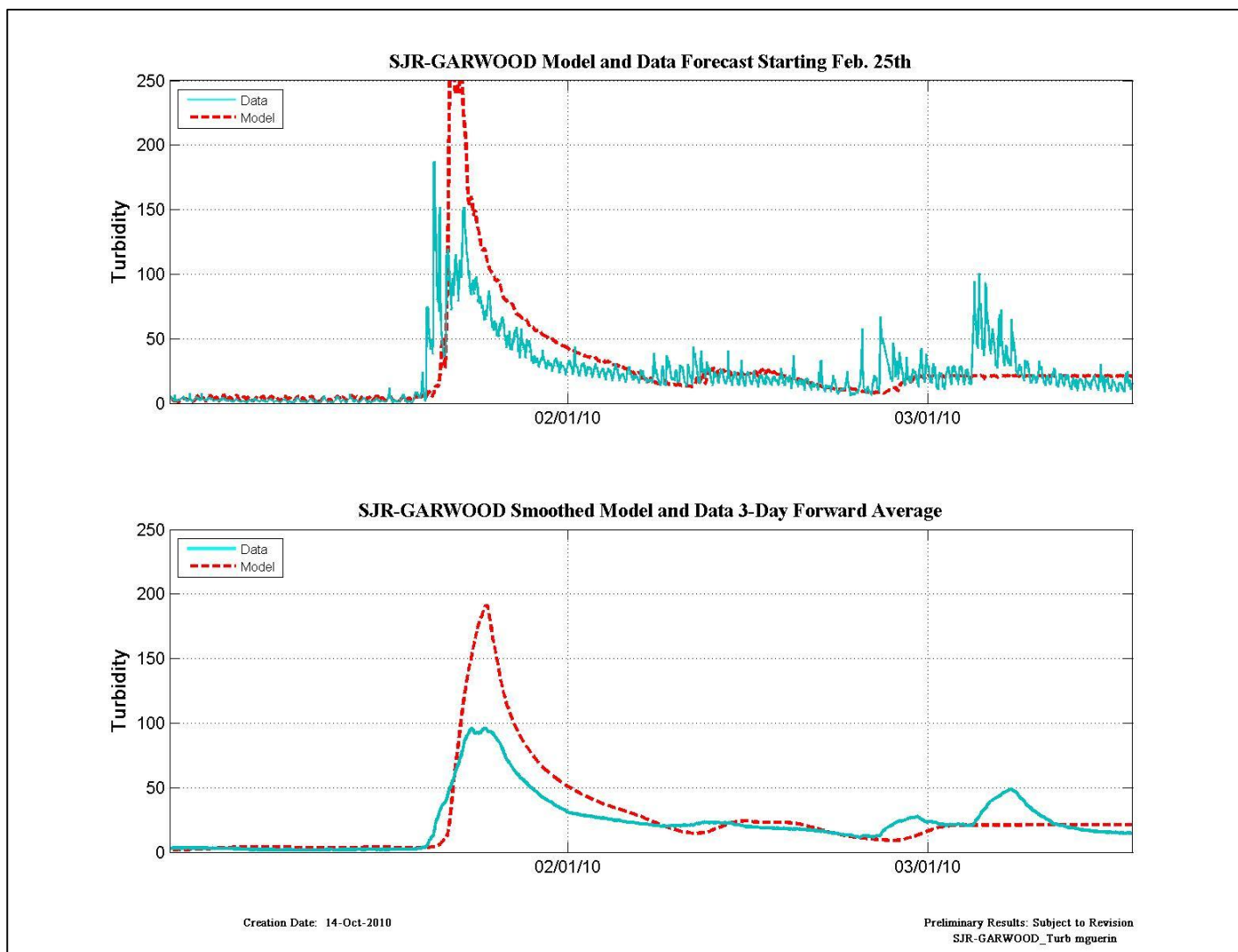


Figure 12-87 Turbidity data and model results for the RMA forecast beginning Feb 25th at SJR-Garwood.

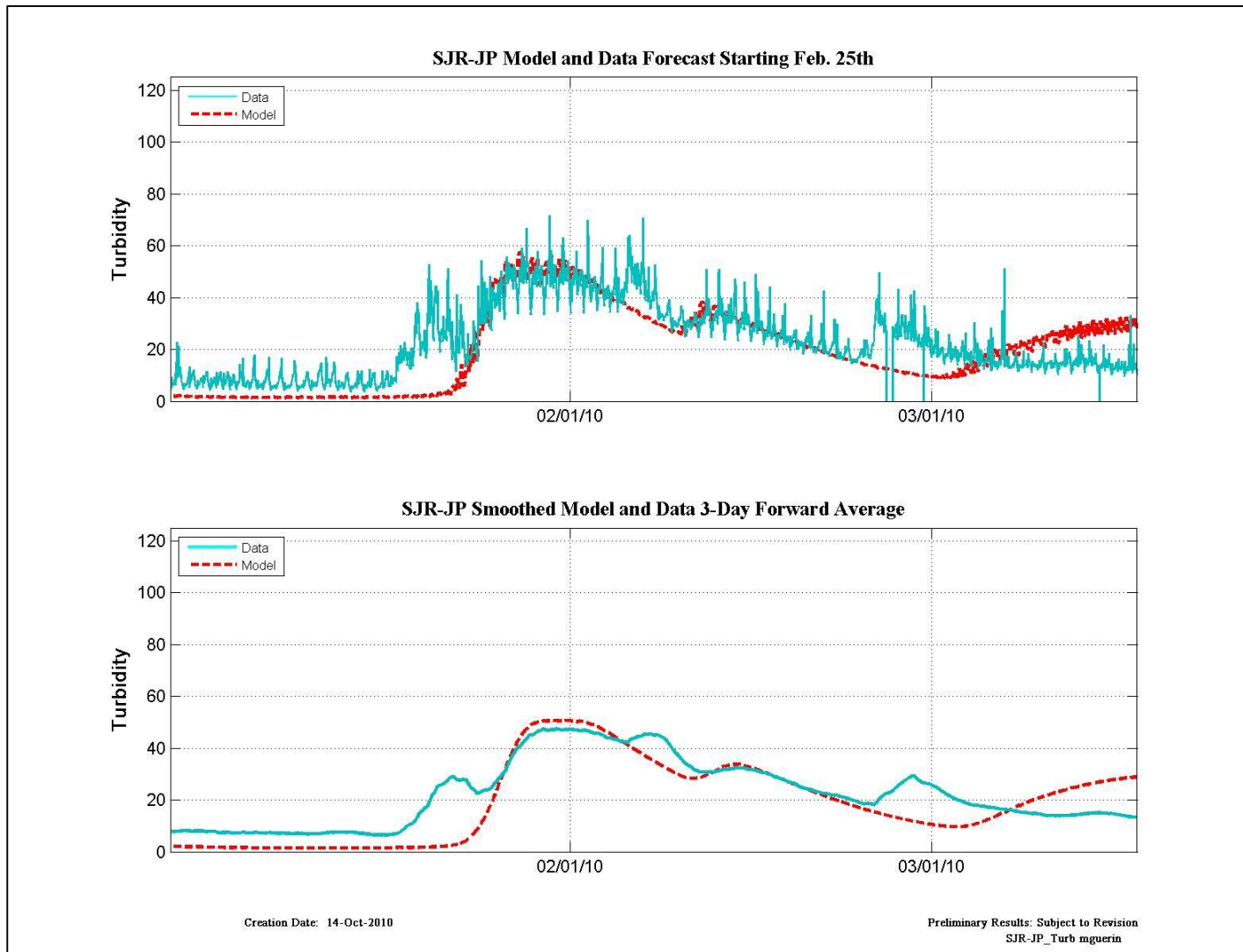


Figure 12-88 Turbidity data and model results for the RMA forecast beginning Feb 25th at SJR-JP.

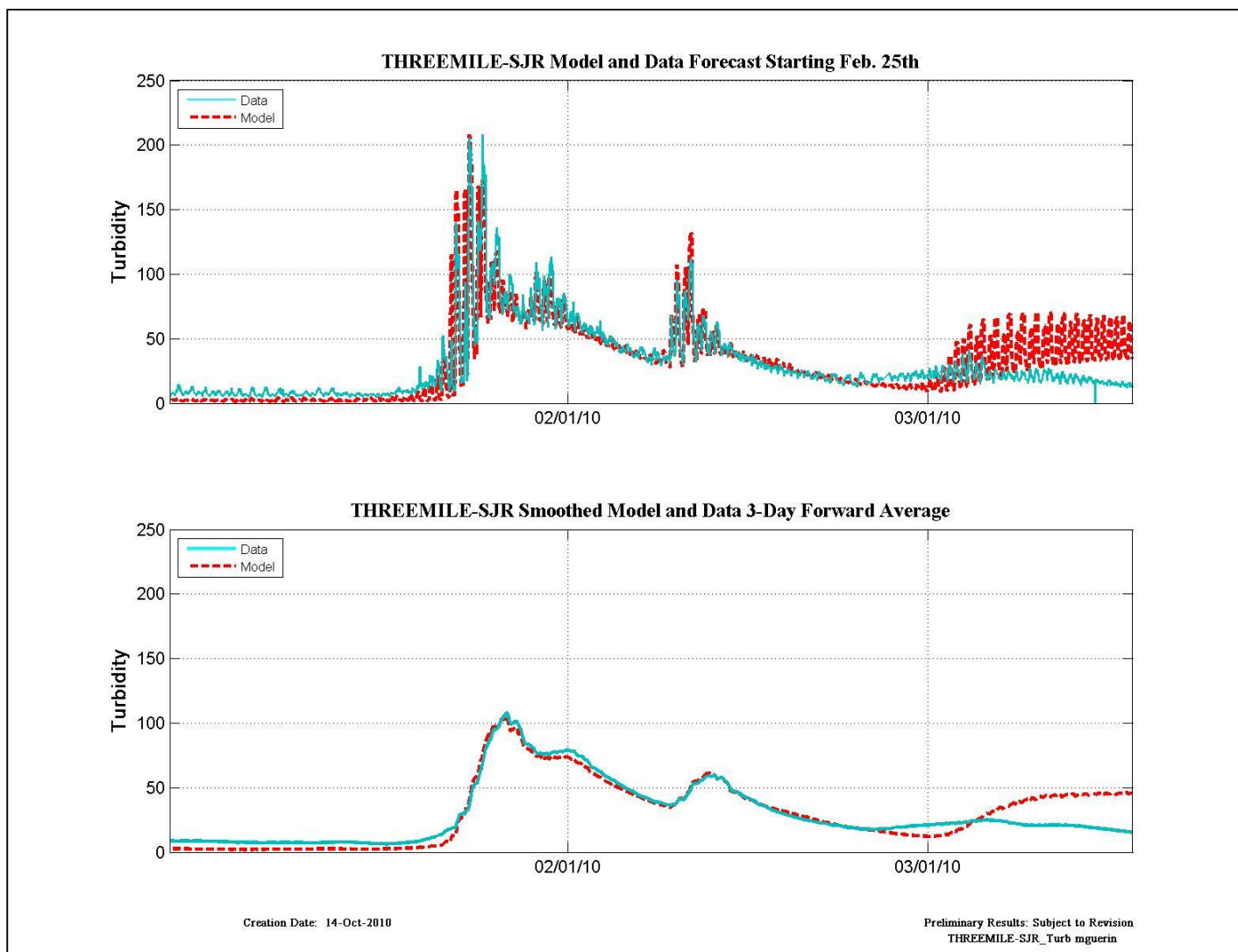


Figure 12-89 Turbidity data and model results for the RMA forecast beginning Feb 25th at Threemile-SJR.

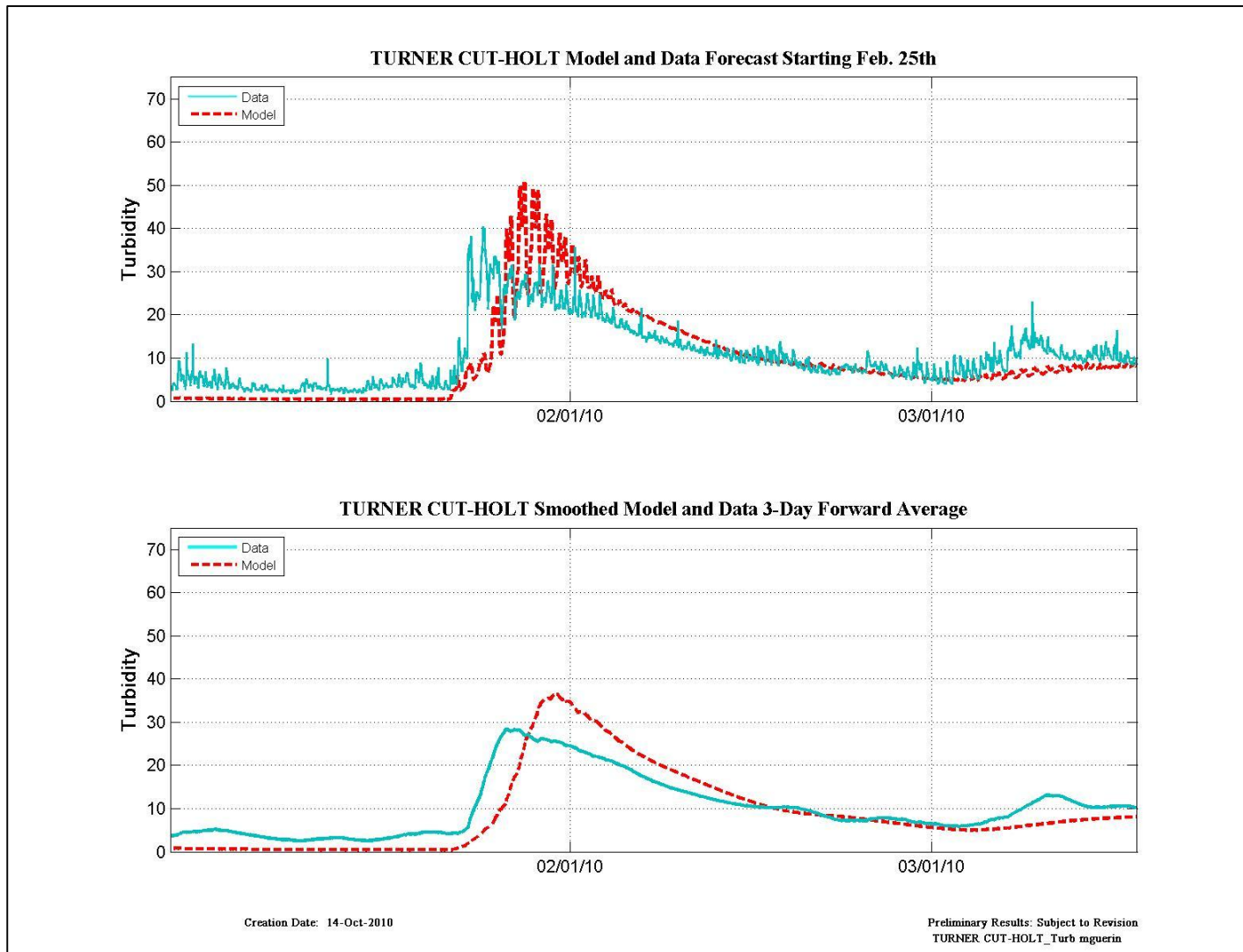


Figure 12-90 Turbidity data and model results for the RMA forecast beginning Feb 25th at Turner Cut-Holt.

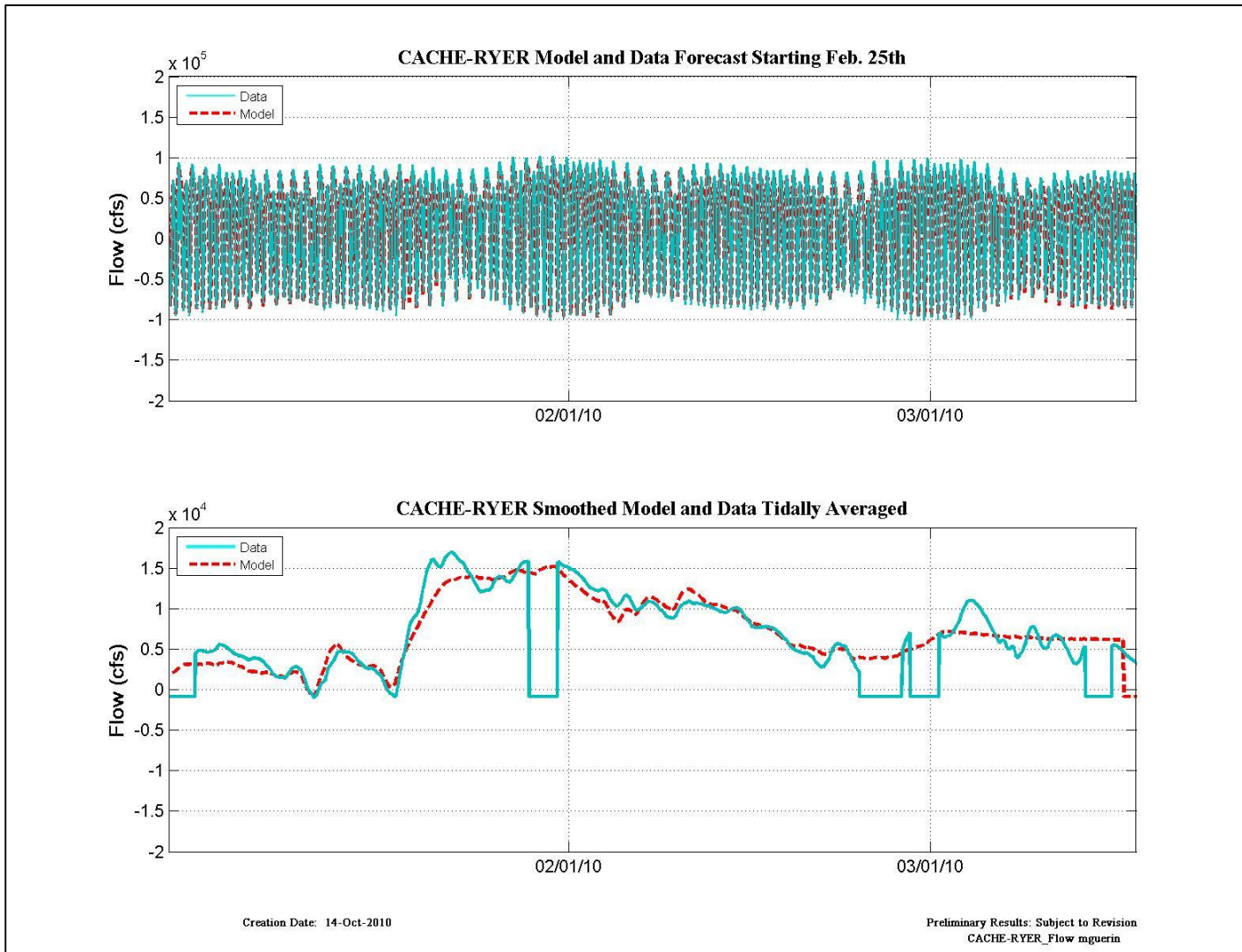
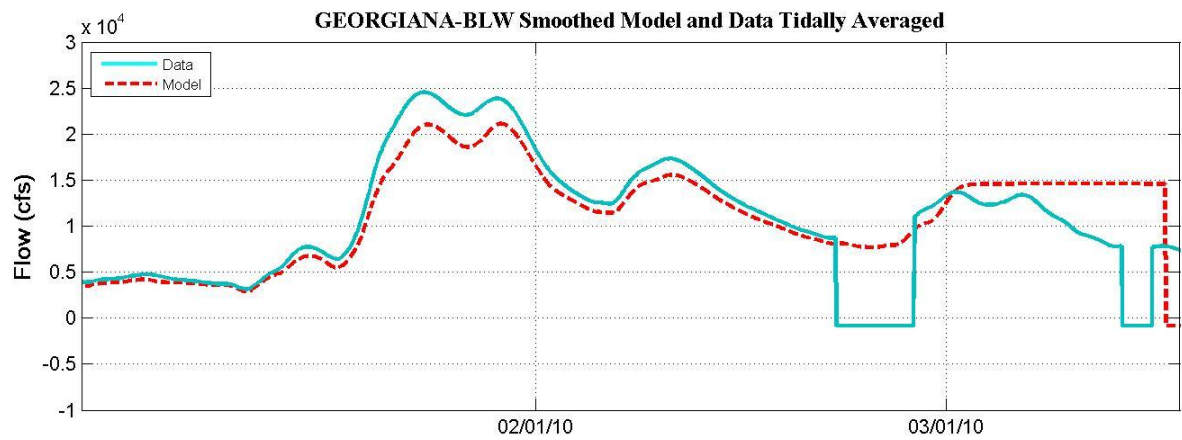
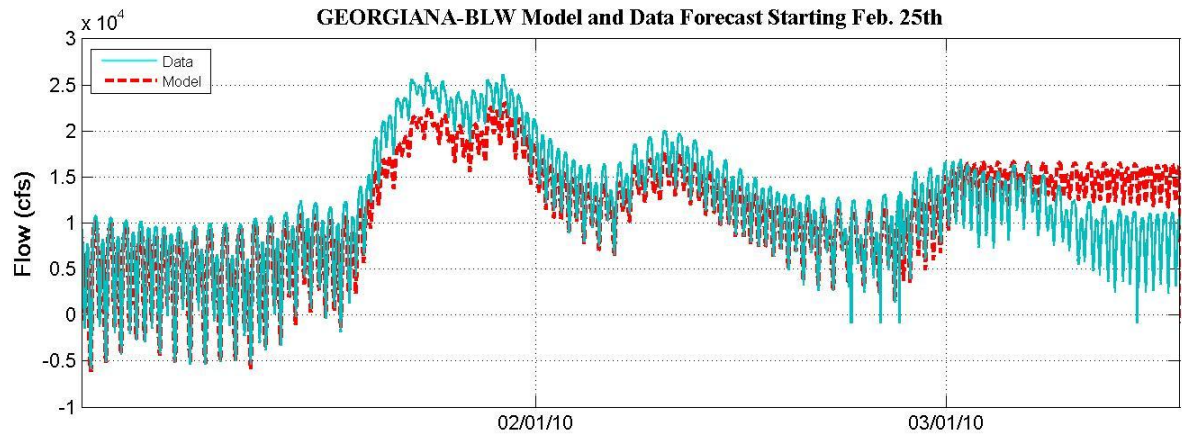


Figure 12-91 Flow data and model results for the RMA forecast beginning Feb 25th at Cache-Ryer.



Creation Date: 14-Oct-2010

Preliminary Results: Subject to Revision
 GEORGIANA-BLW_Flow mguerin

Figure 12-92 Flow data and model results for the RMA forecast beginning Feb 25th at Georgiana-BLW.

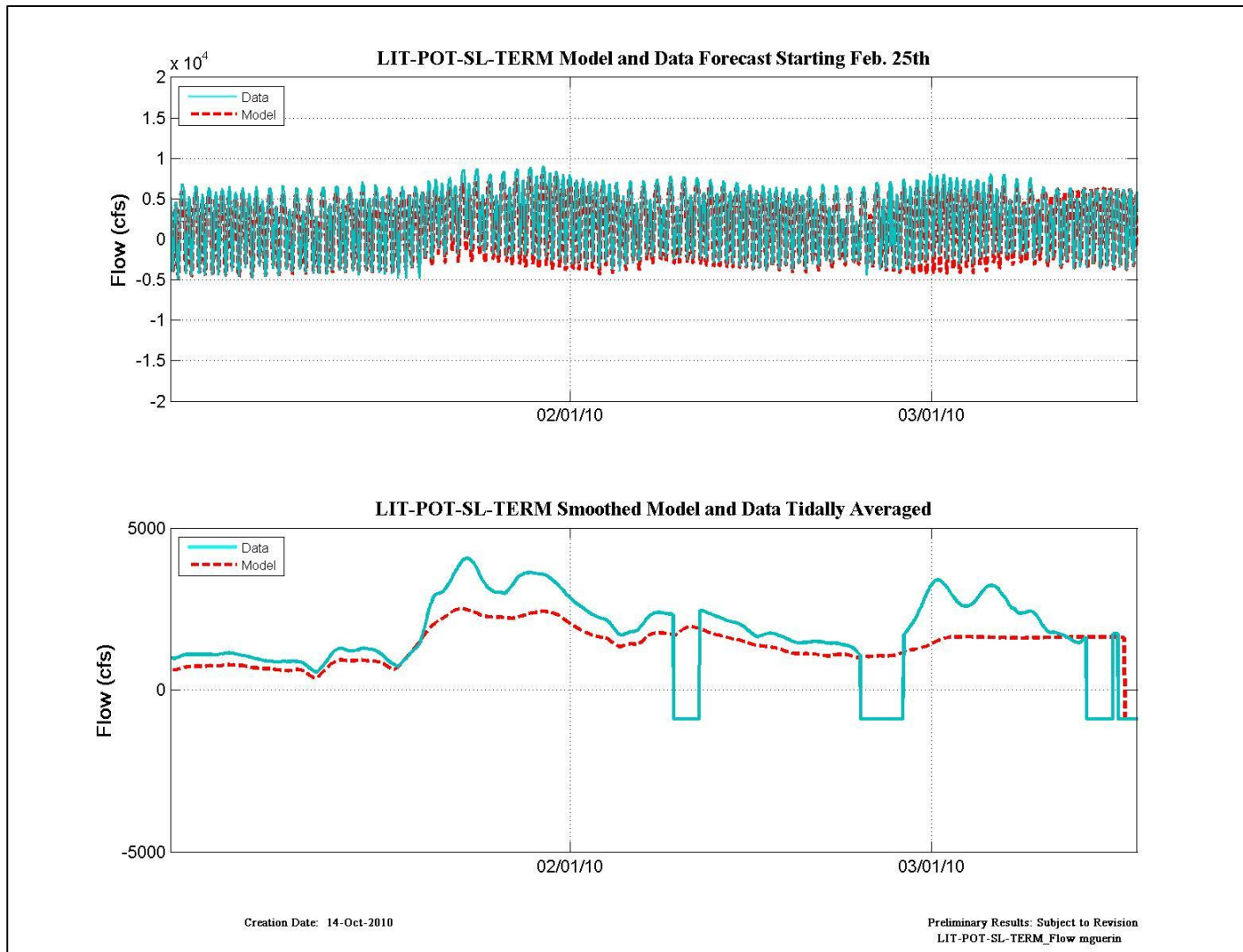


Figure 12-93 Flow data and model results for the RMA forecast beginning Feb 25th at LIT-POT-SL-TERM.

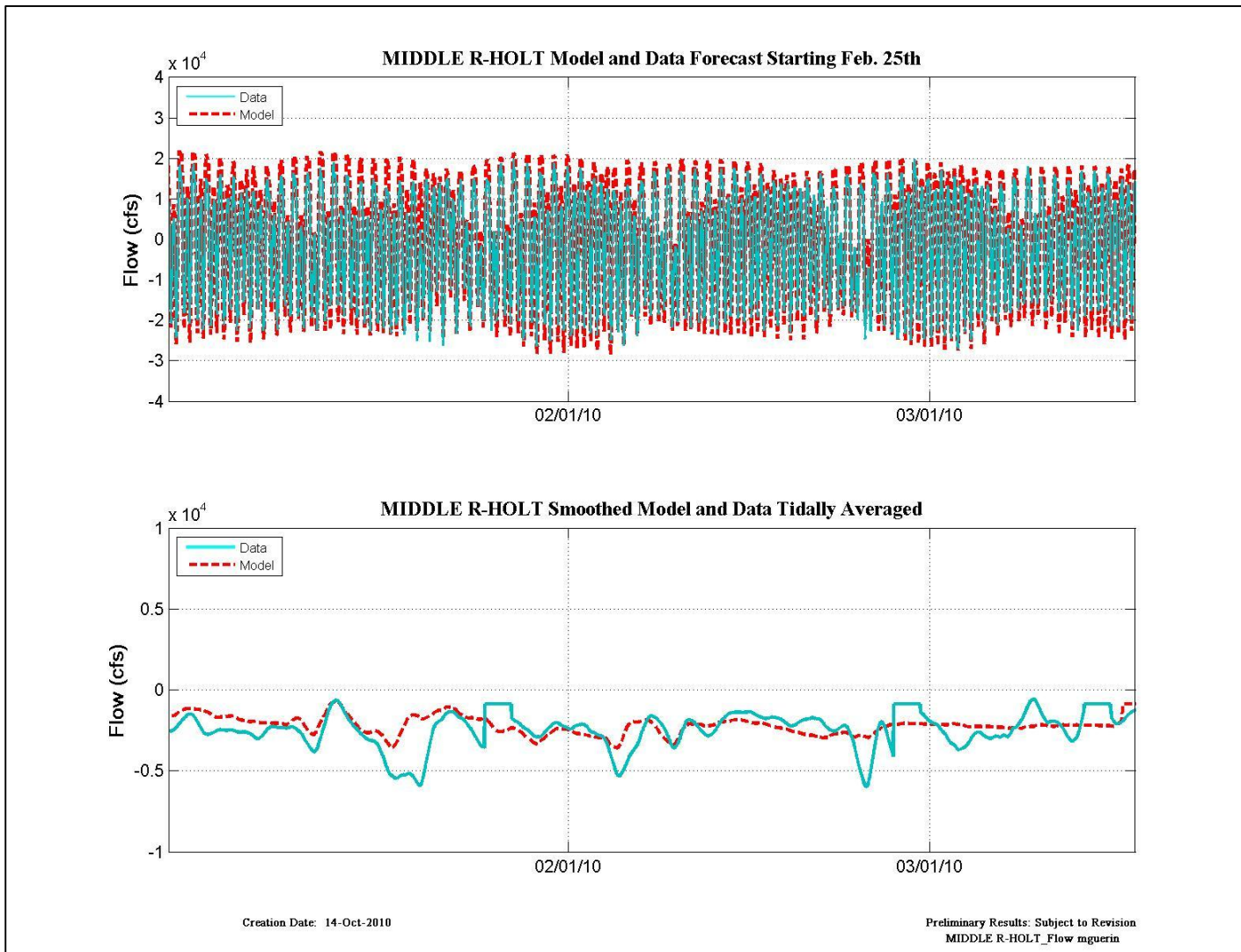


Figure 12-94 Flow data and model results for the RMA forecast beginning Feb 25th at Middle R-Holt.

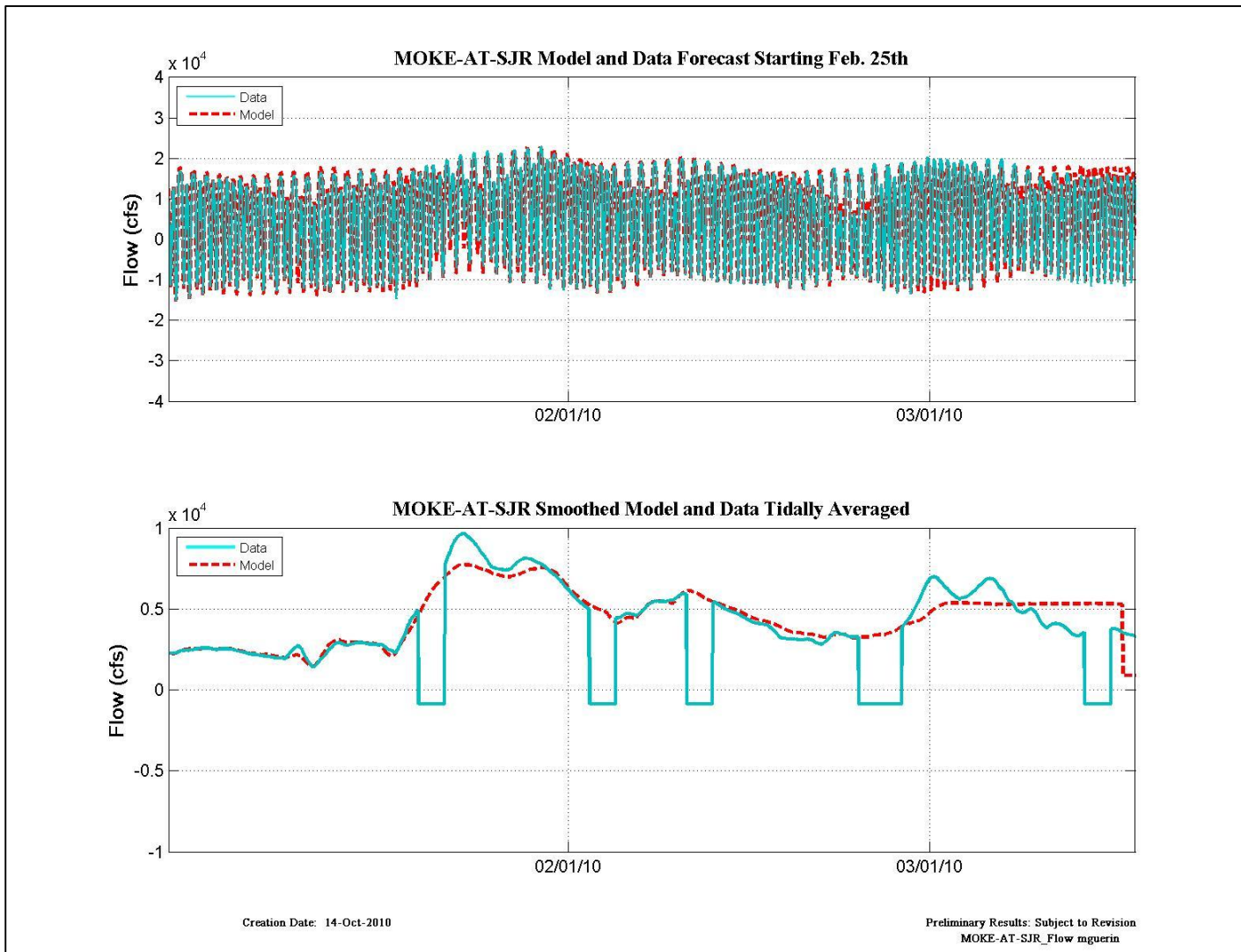


Figure 12-95 Flow data and model results for the RMA forecast beginning Feb 25th at Moke-at-SJR.

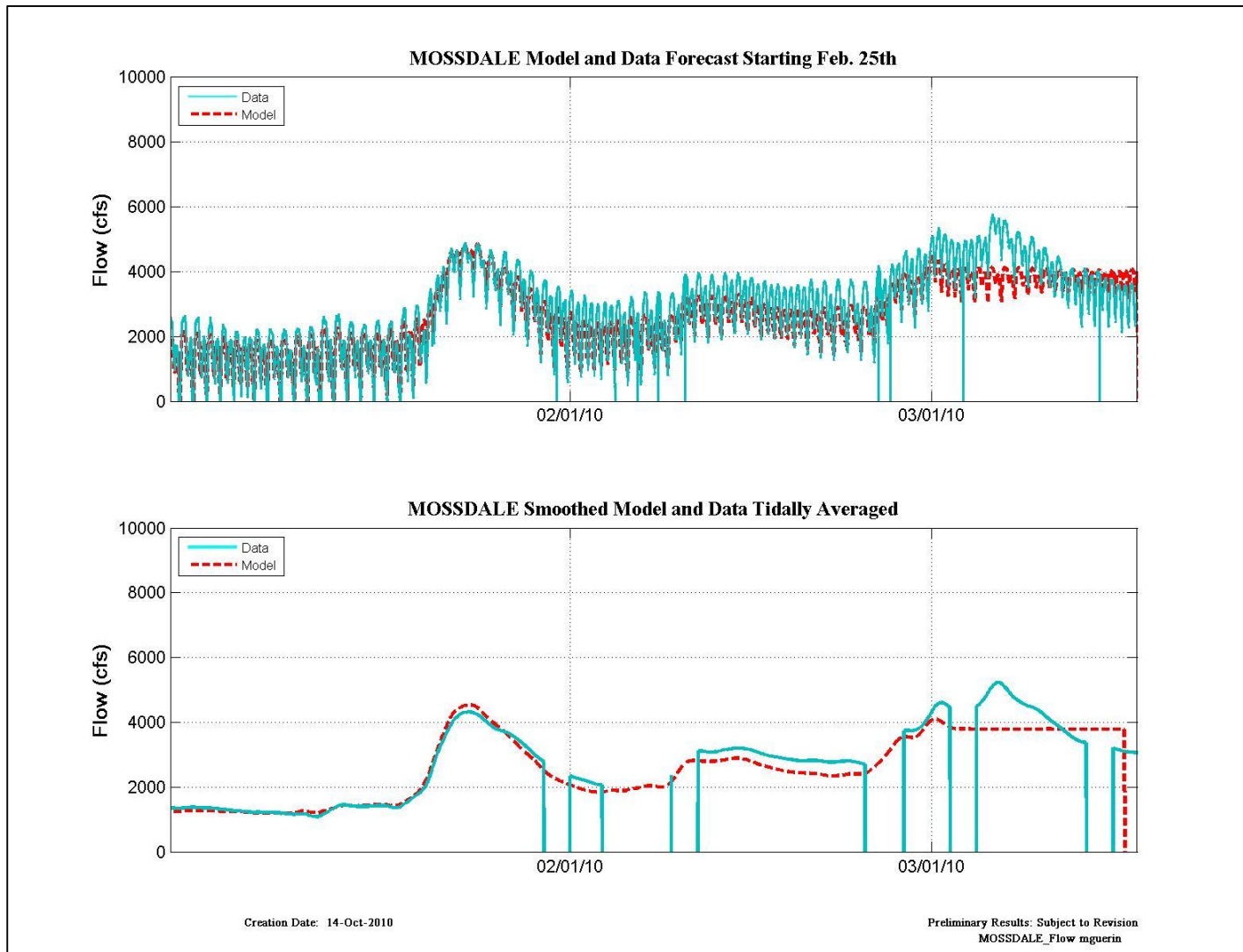


Figure 12-96 Flow data and model results for the RMA forecast beginning Feb 25th at Mossdale.

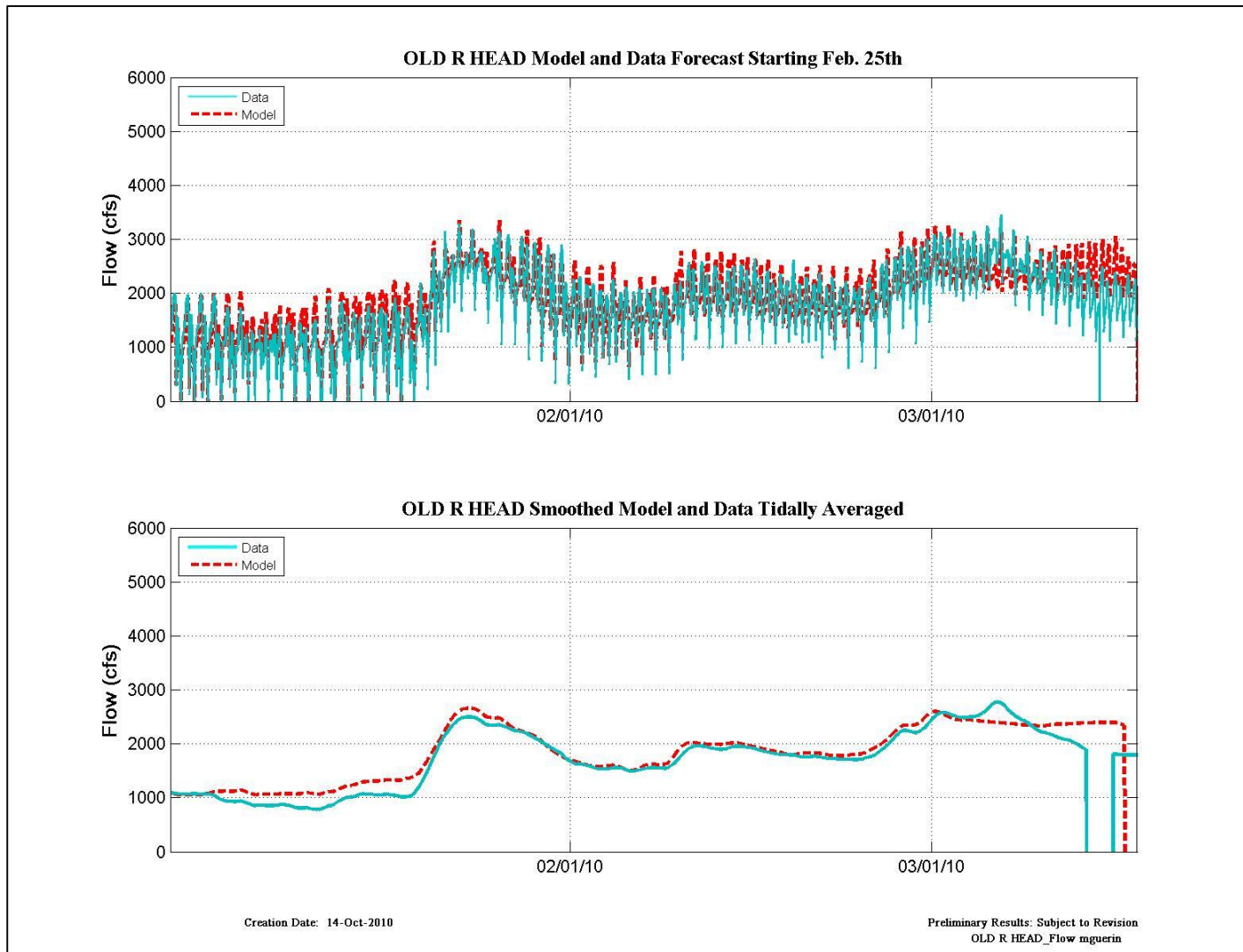


Figure 12-97 Flow data and model results for the RMA forecast beginning Feb 25th at Cache-Ryer.

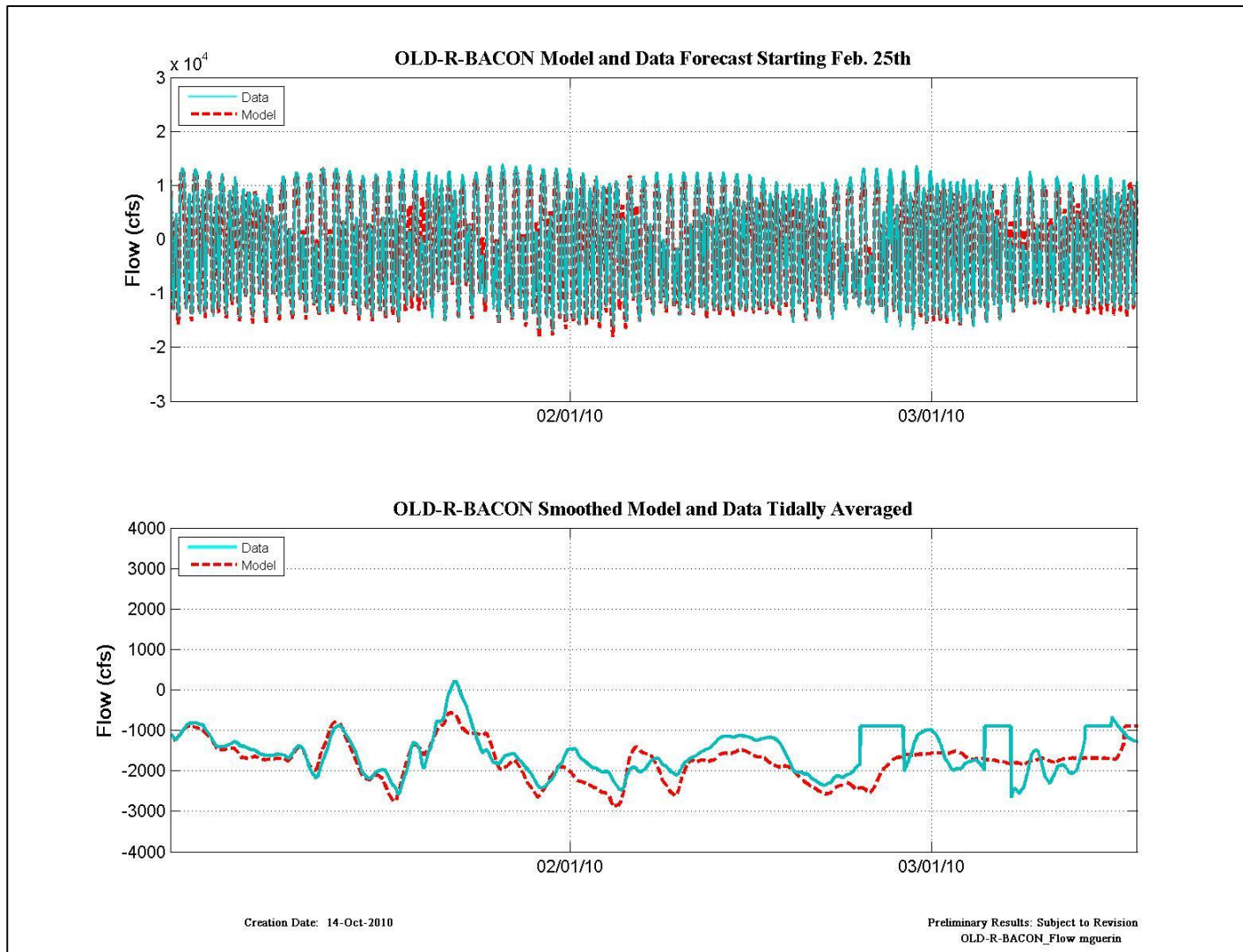


Figure 12-98 Flow data and model results for the RMA forecast beginning Feb 25th at Old-R-Bacon.

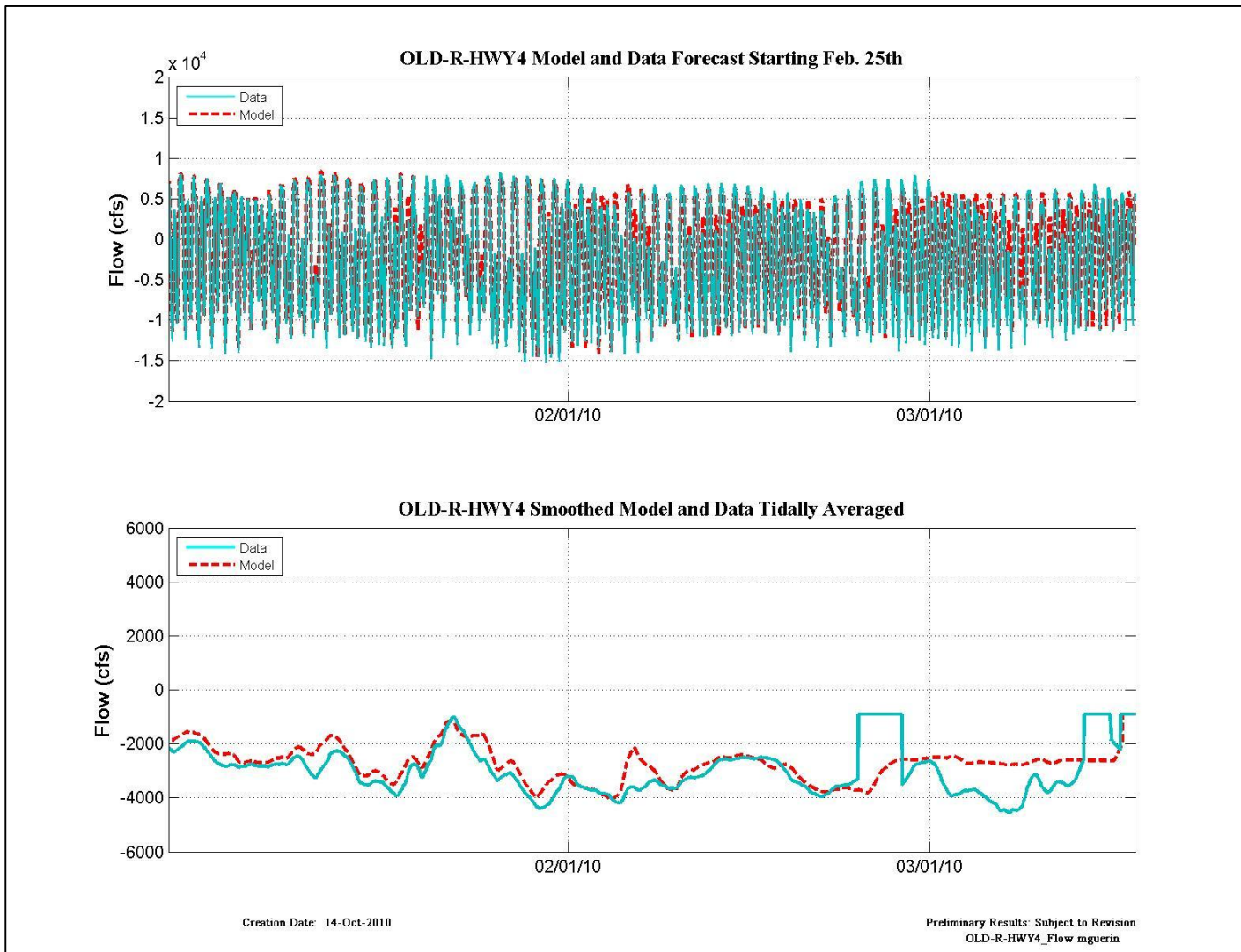


Figure 12-99 Flow data and model results for the RMA forecast beginning Feb 25th at Old-R-Hwy 4.

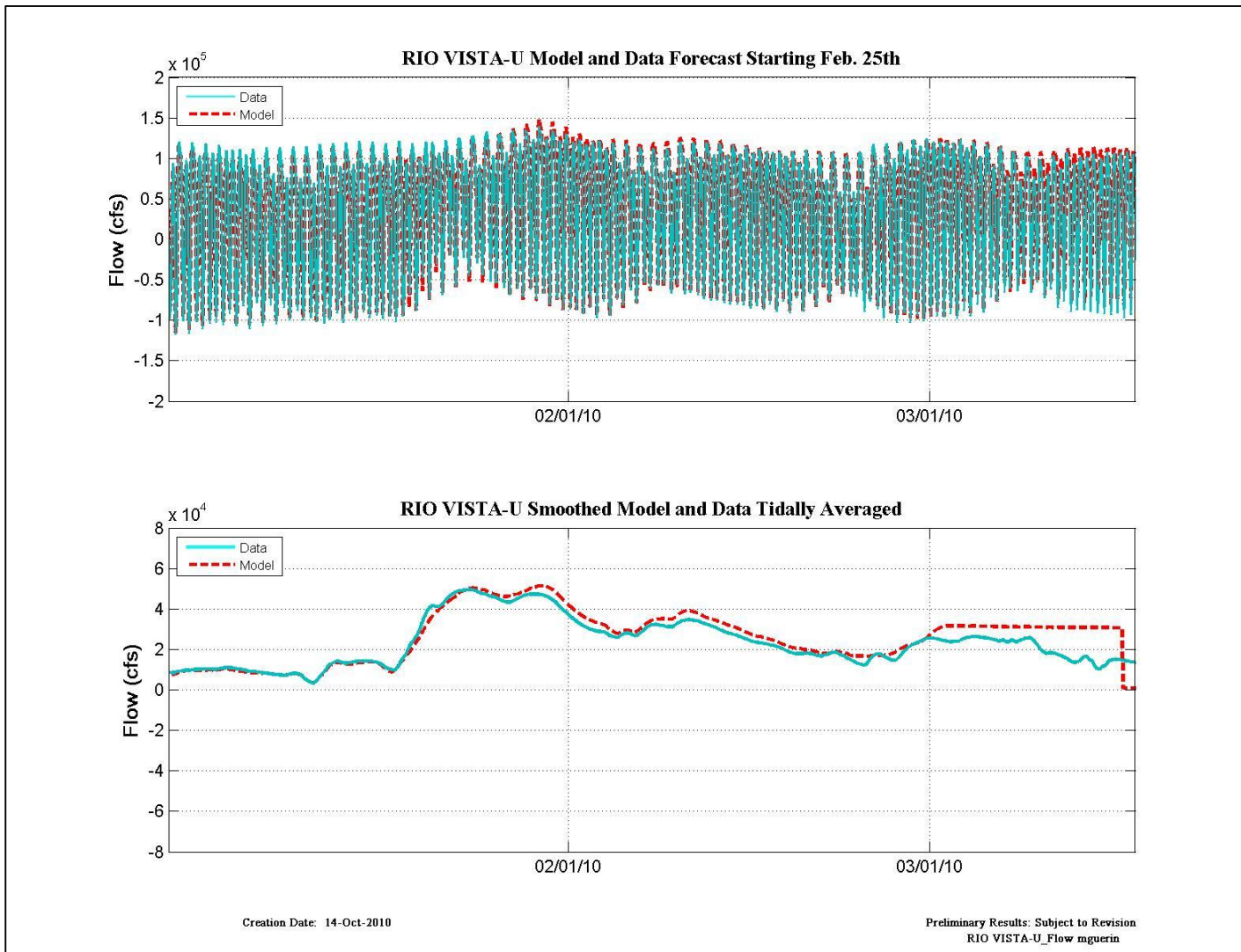


Figure 12-100 Flow data and model results for the RMA forecast beginning Feb 25th at Rio Vista-U.

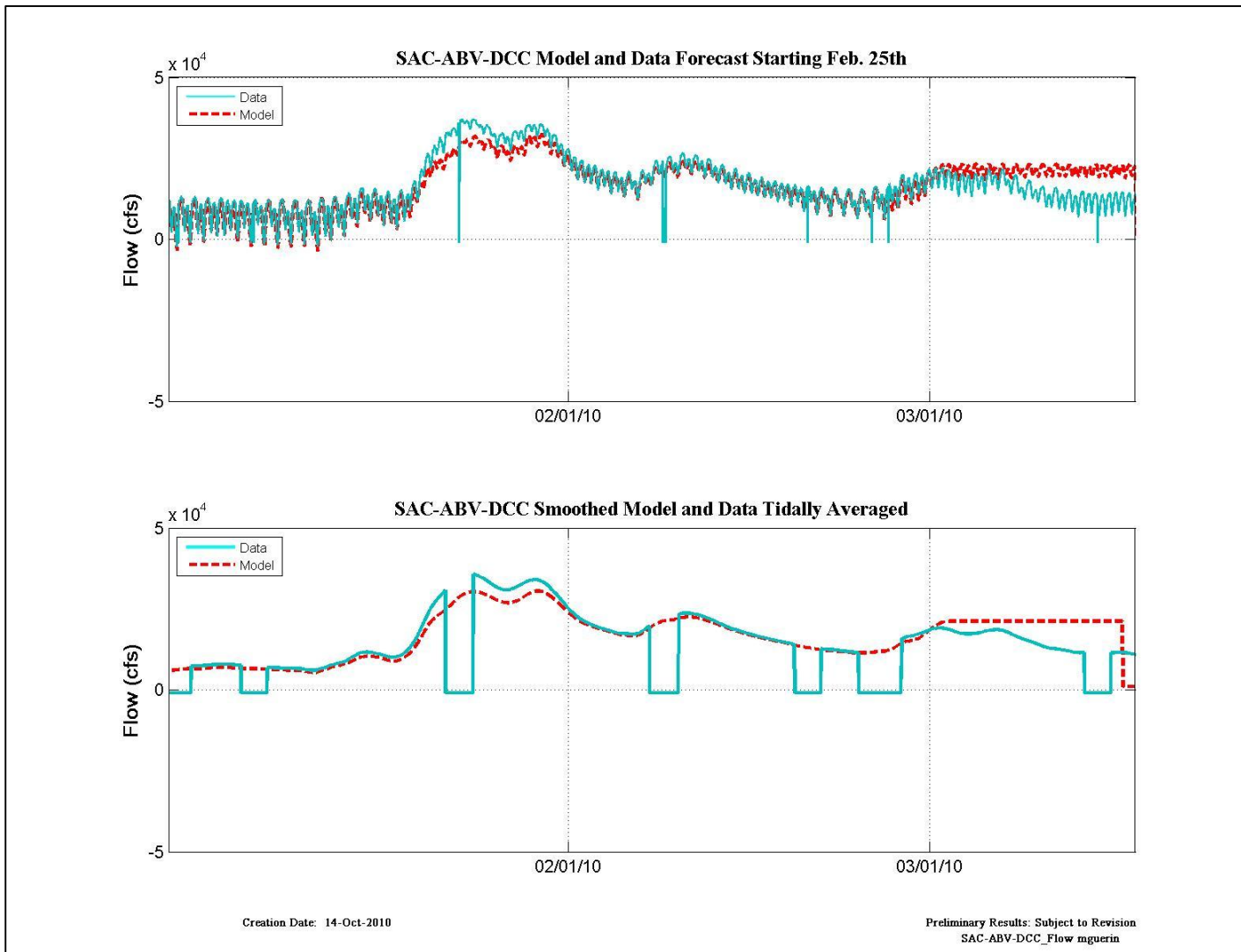


Figure 12-101 Flow data and model results for the RMA forecast beginning Feb 25th at SAC-ABV-DCC.

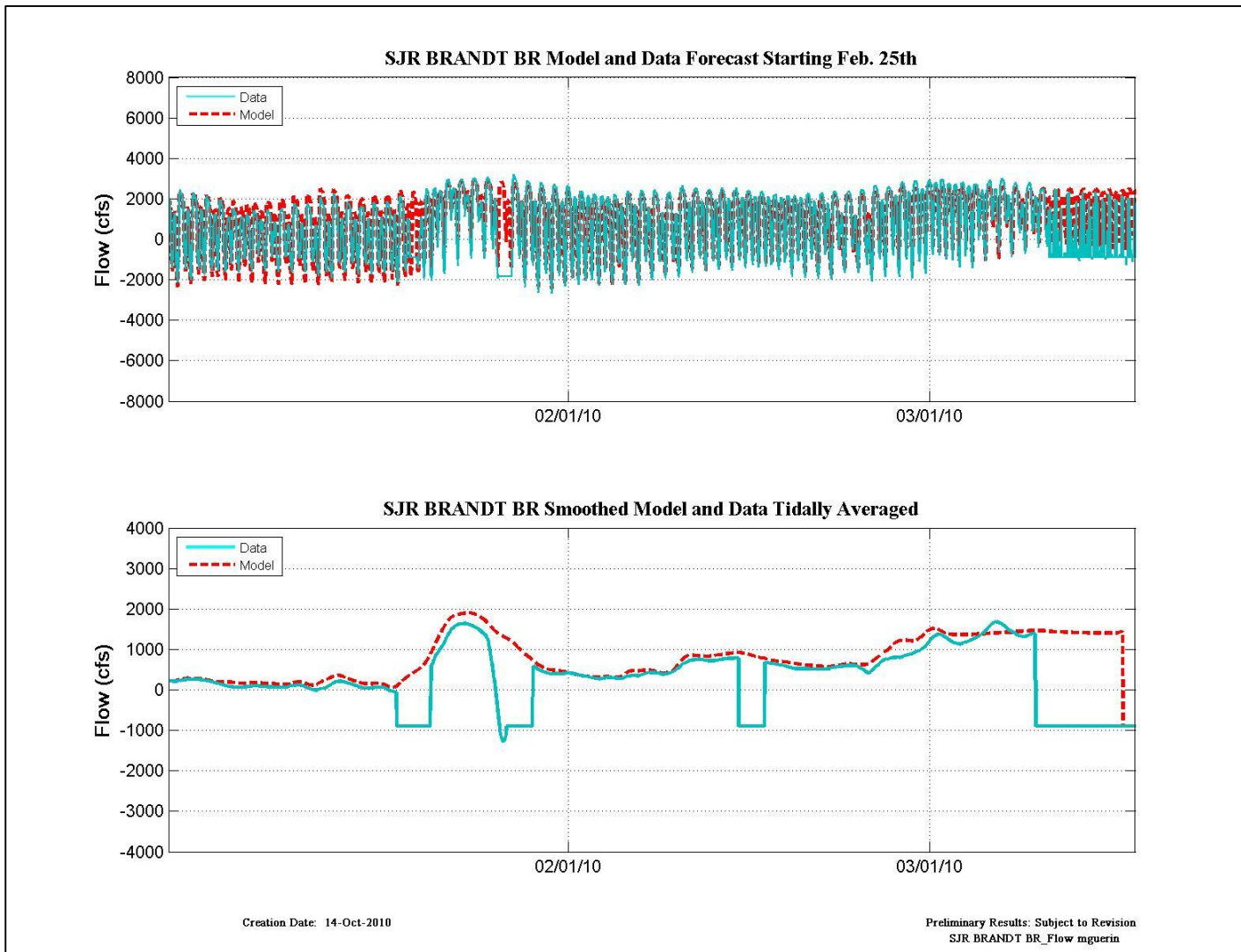


Figure 12-102 Flow data and model results for the RMA forecast beginning Feb 25th at SJR Brandt BR.

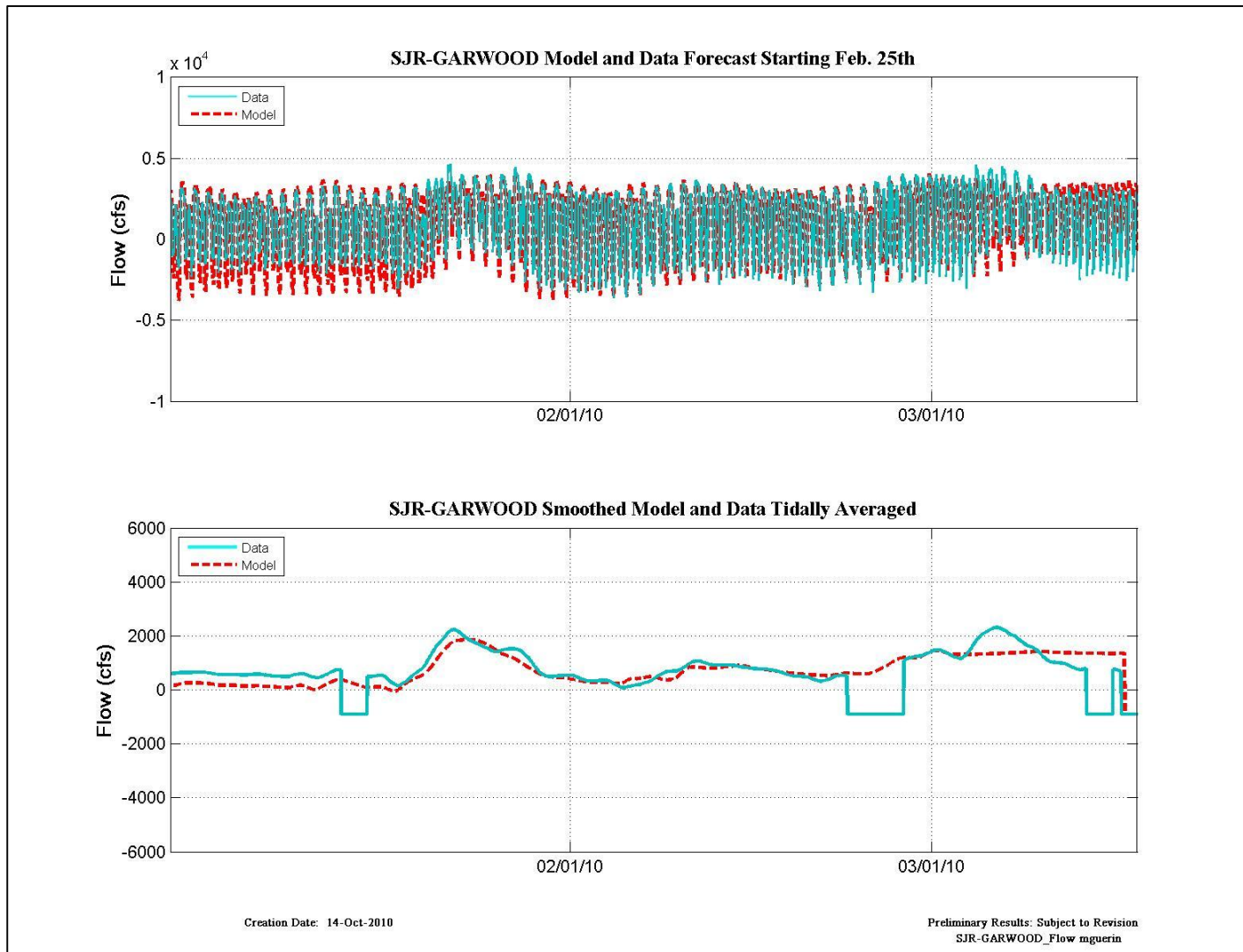


Figure 12-103 Flow data and model results for the RMA forecast beginning Feb 25th at SJR-Garwood.

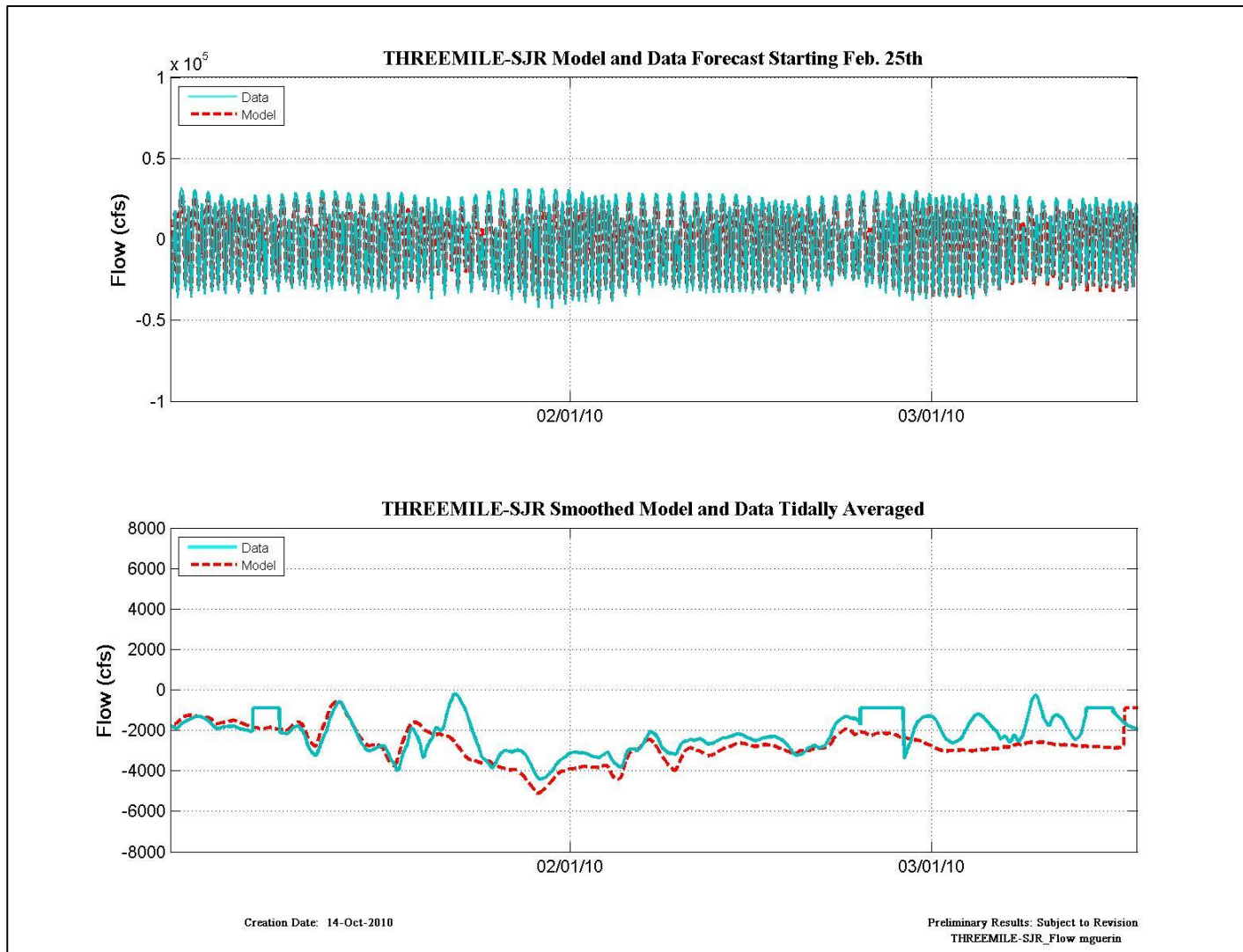


Figure 12-104 Flow data and model results for the RMA forecast beginning Feb 25th at Threemile-SJR.

**13. Appendix III - Model results for forecasts Jan. 12th, Feb. 11th,
Feb. 17th, Apr. 07th**

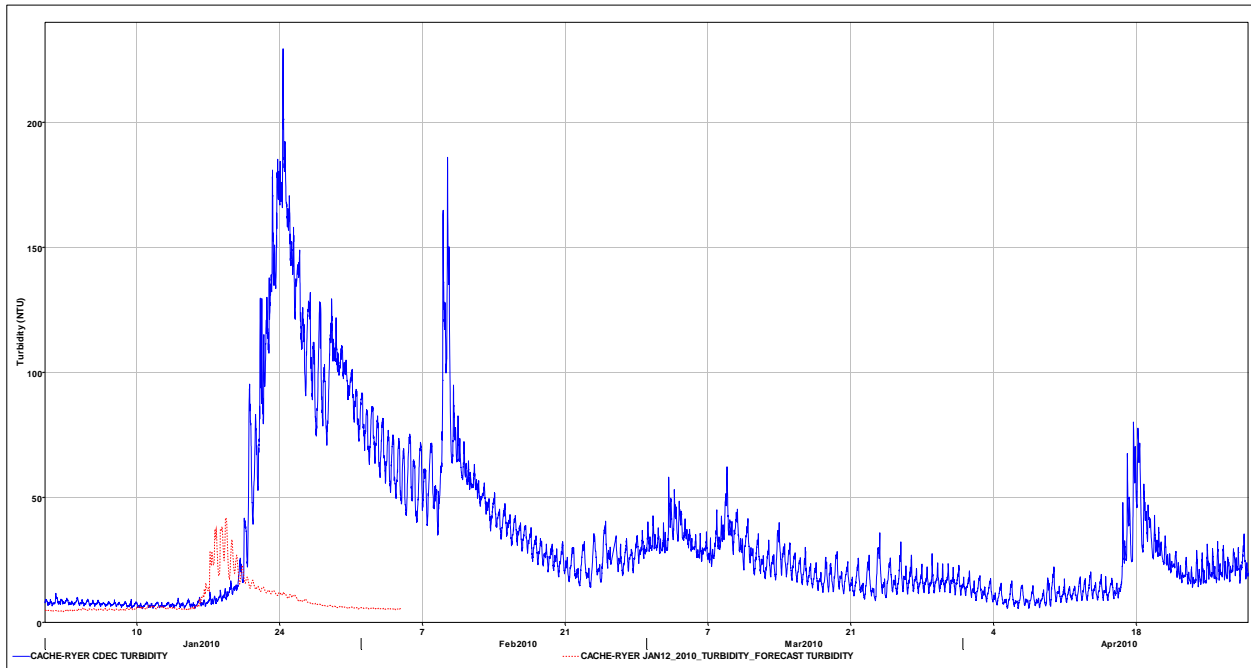


Figure 13-1 Turbidity data (blue line) and Jan. 12th model forecast (red dash) at Cache-Ryer.

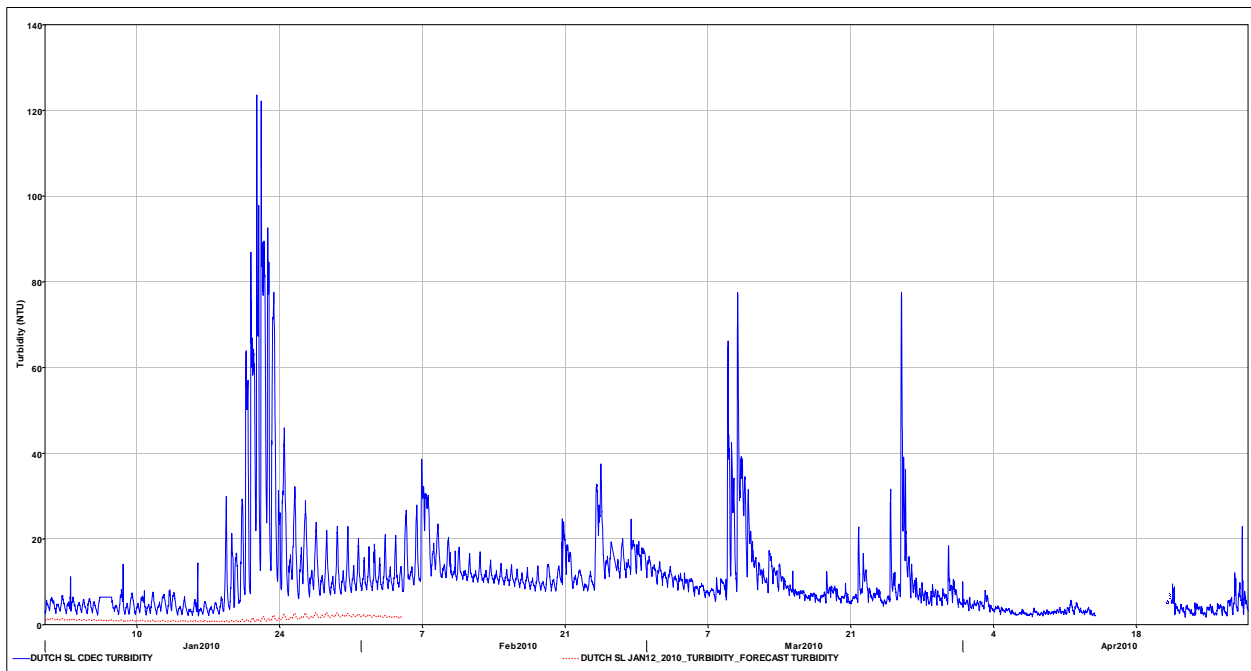


Figure 13-2 Turbidity data (blue line) and Jan. 12th model forecast (red dash) at Dutch SL.

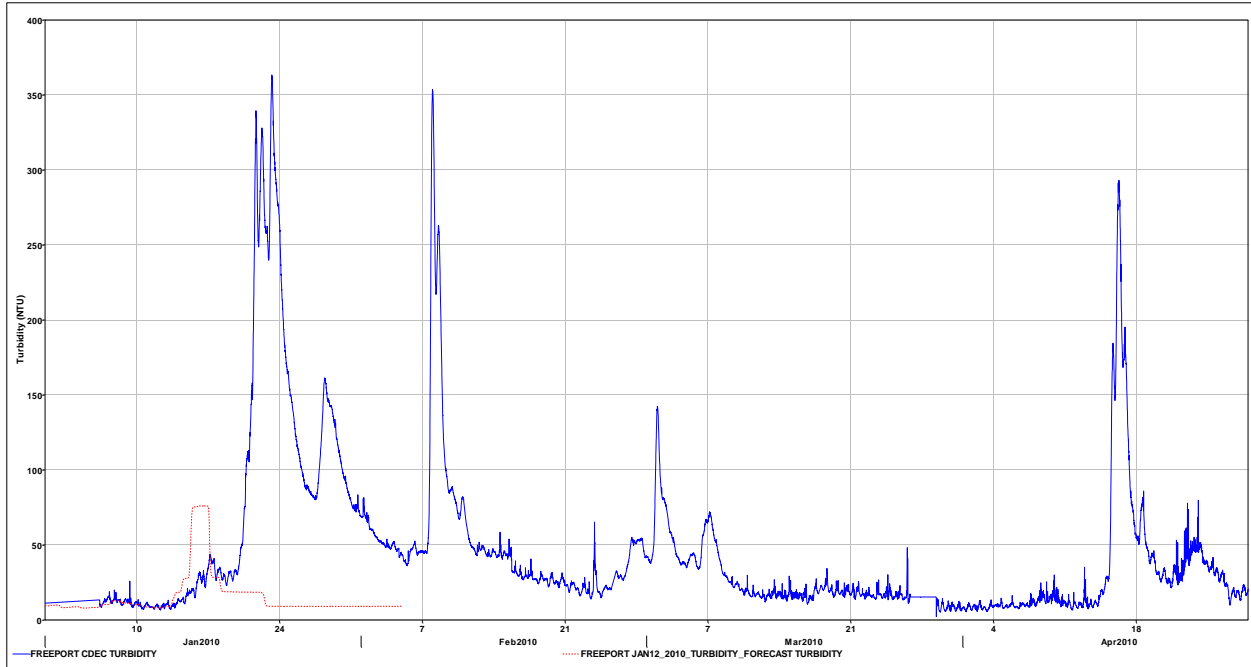


Figure 13-3 Turbidity data (blue line) and Jan. 12th model forecast (red dash) at Freeport.

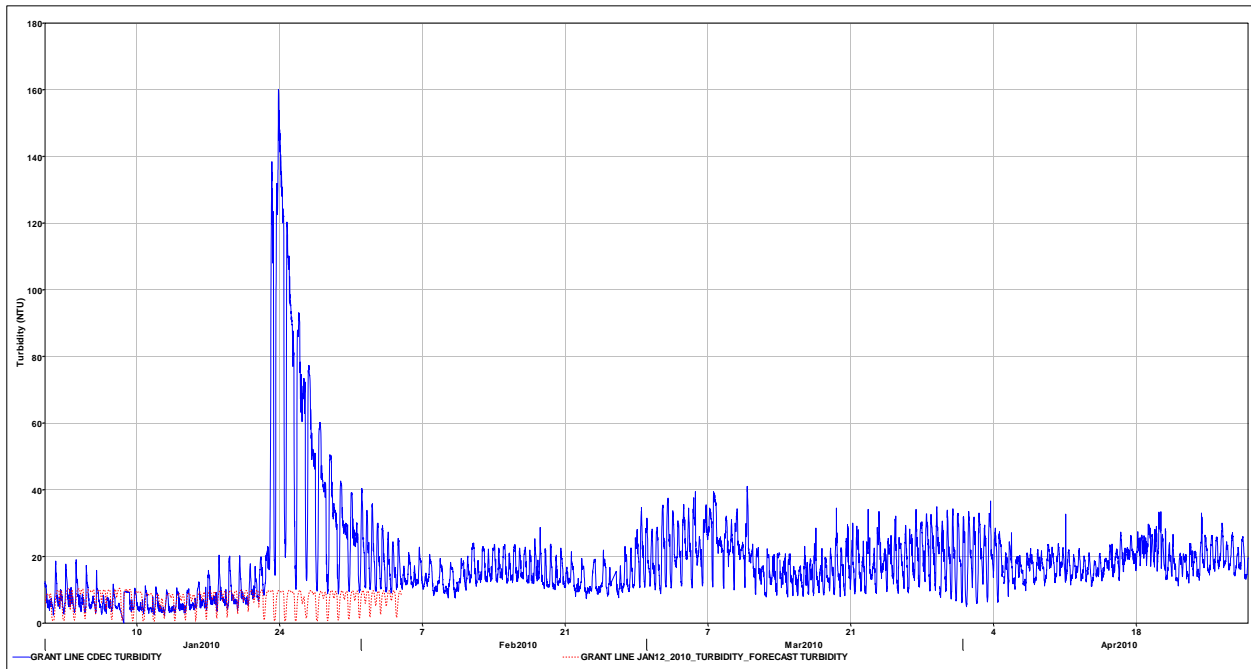


Figure 13-4 Turbidity data (blue line) and Jan. 12th model forecast (red dash) at Grant Line.

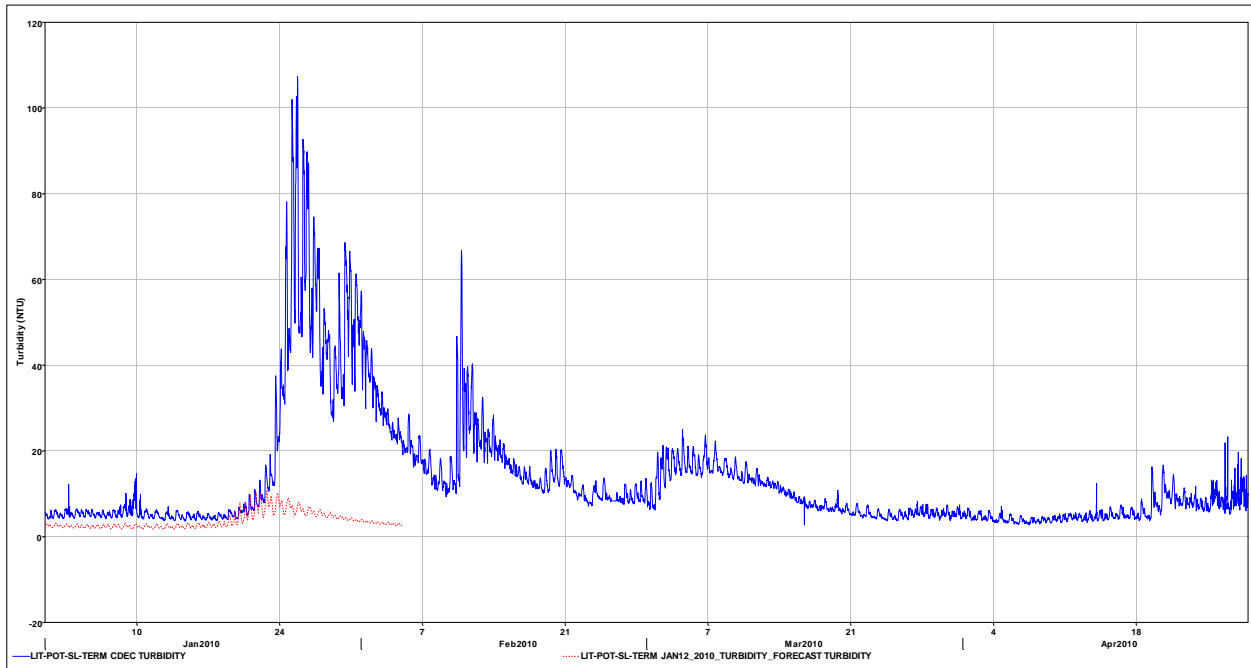


Figure 13-5 Turbidity data (blue line) and Jan. 12th model forecast (red dash) at LIT-POT-SL-TERM.

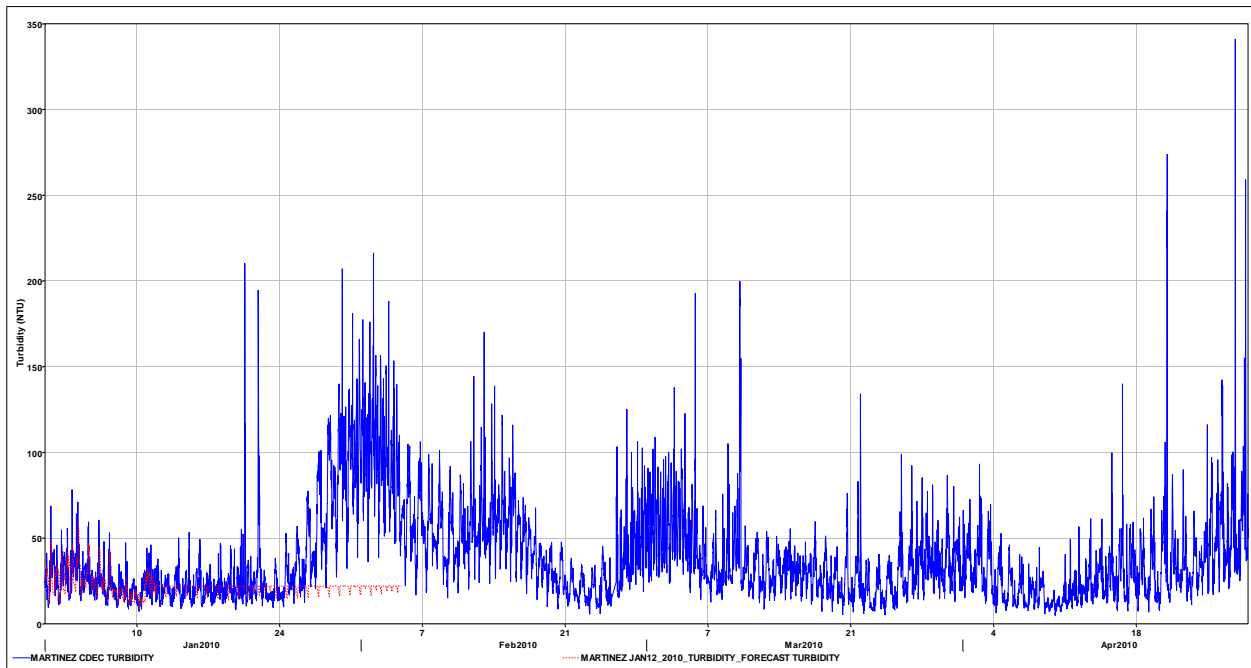


Figure 13-6 Turbidity data (blue line) and Jan. 12th model forecast (red dash) at Martinez.

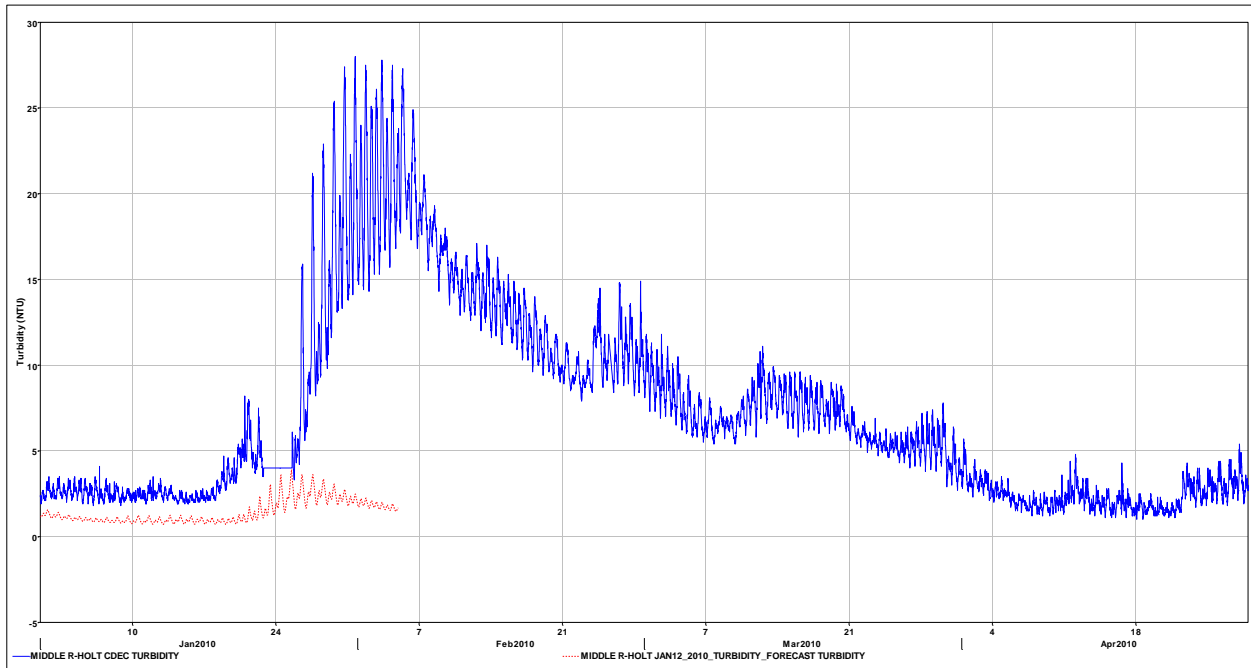


Figure 13-7 Turbidity data (blue line) and Jan. 12th model forecast (red dash) at Middel R-Holt.

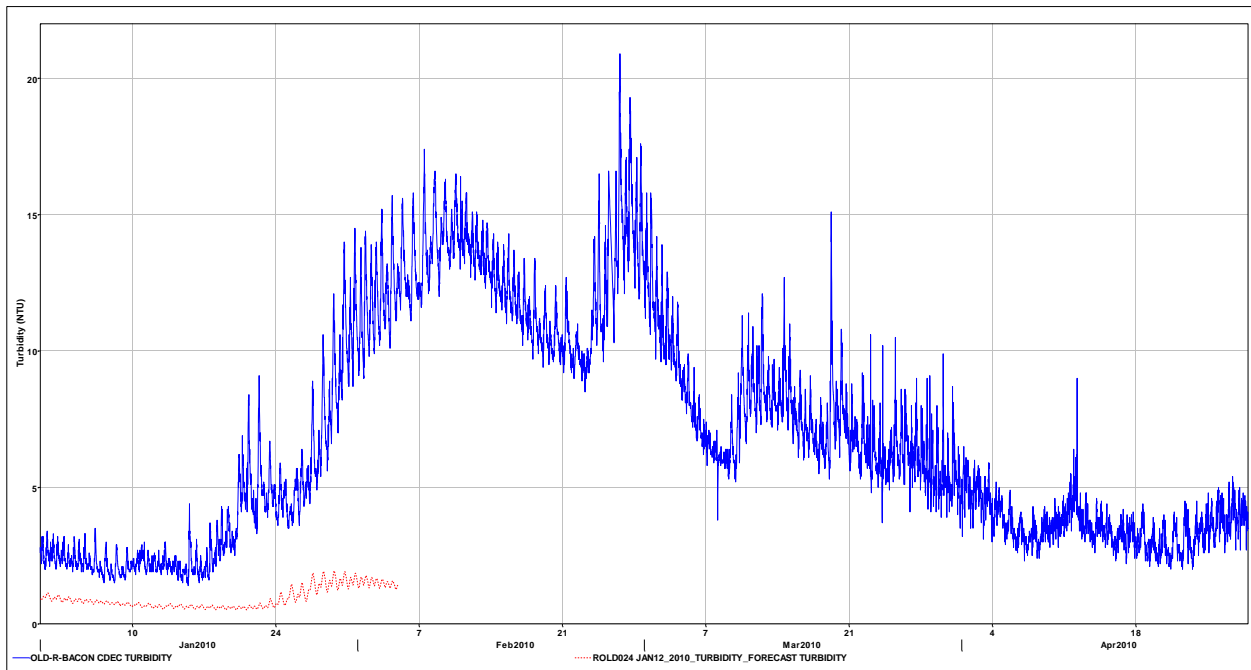


Figure 13-8 Turbidity data (blue line) and Jan. 12th model forecast (red dash) at Old R-Bacon.

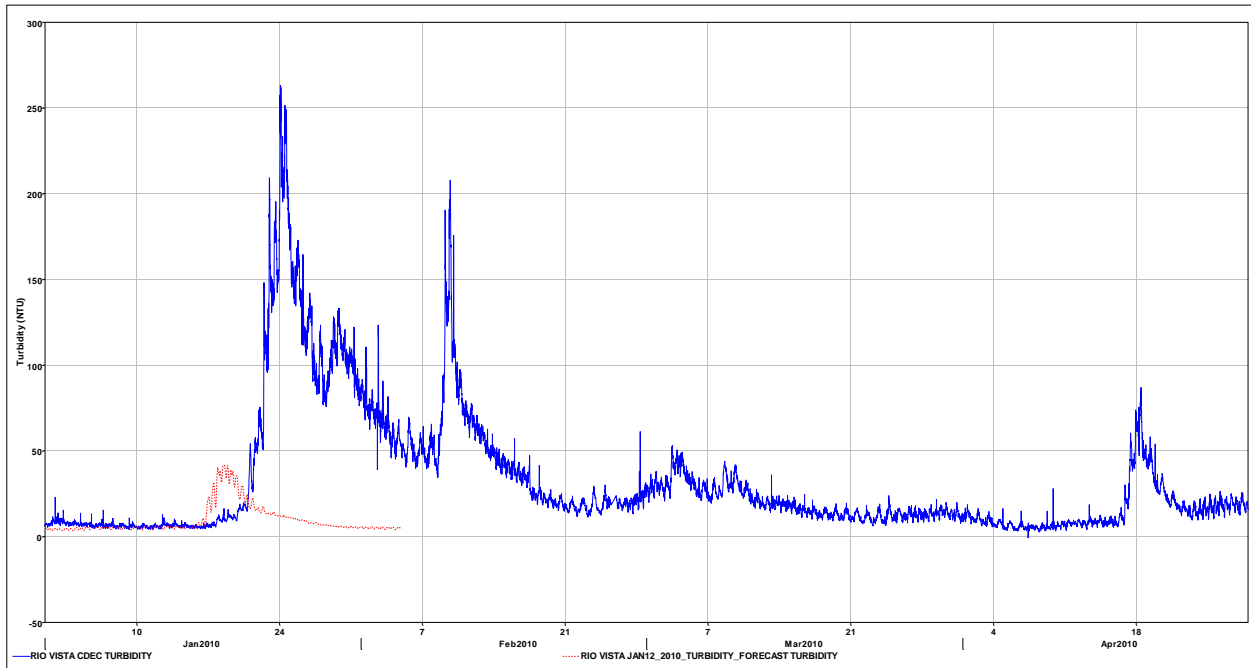


Figure 13-9 Turbidity data (blue line) and Jan. 12th model forecast (red dash) at Rio-Vista.

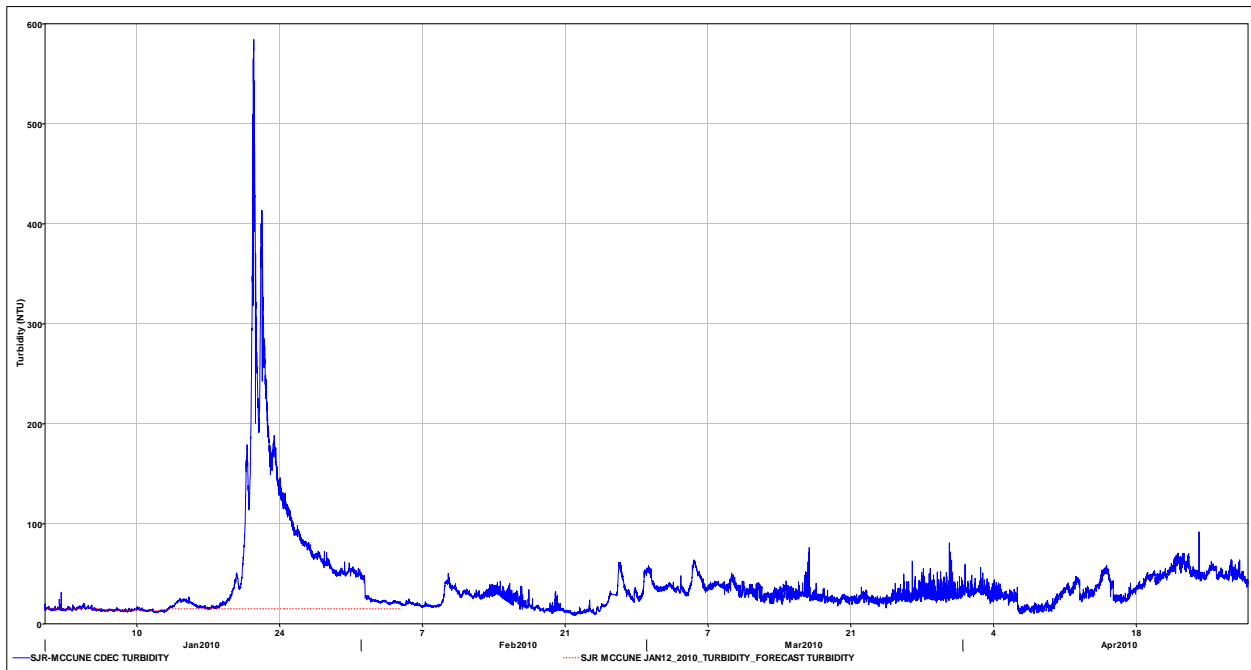


Figure 13-10 Turbidity data (blue line) and Jan. 12th model forecast (red dash) at SJR McCune.

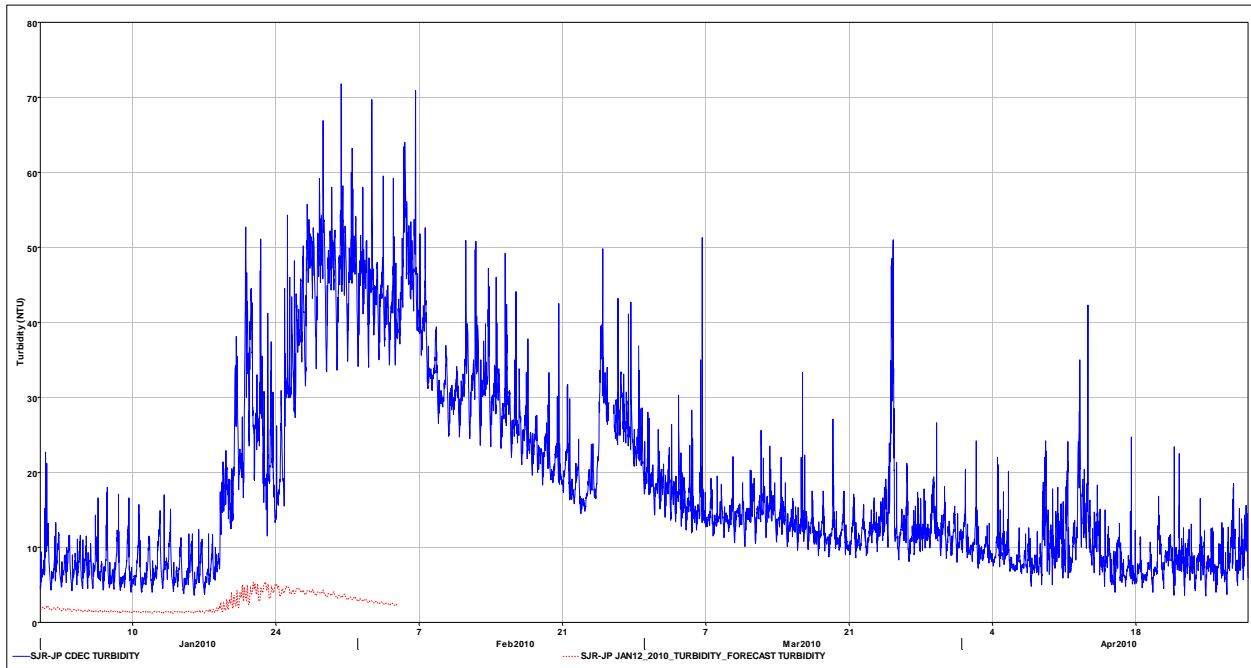


Figure 13-11 Turbidity data (blue line) and Jan. 12th model forecast (red dash) at SJR-JP.

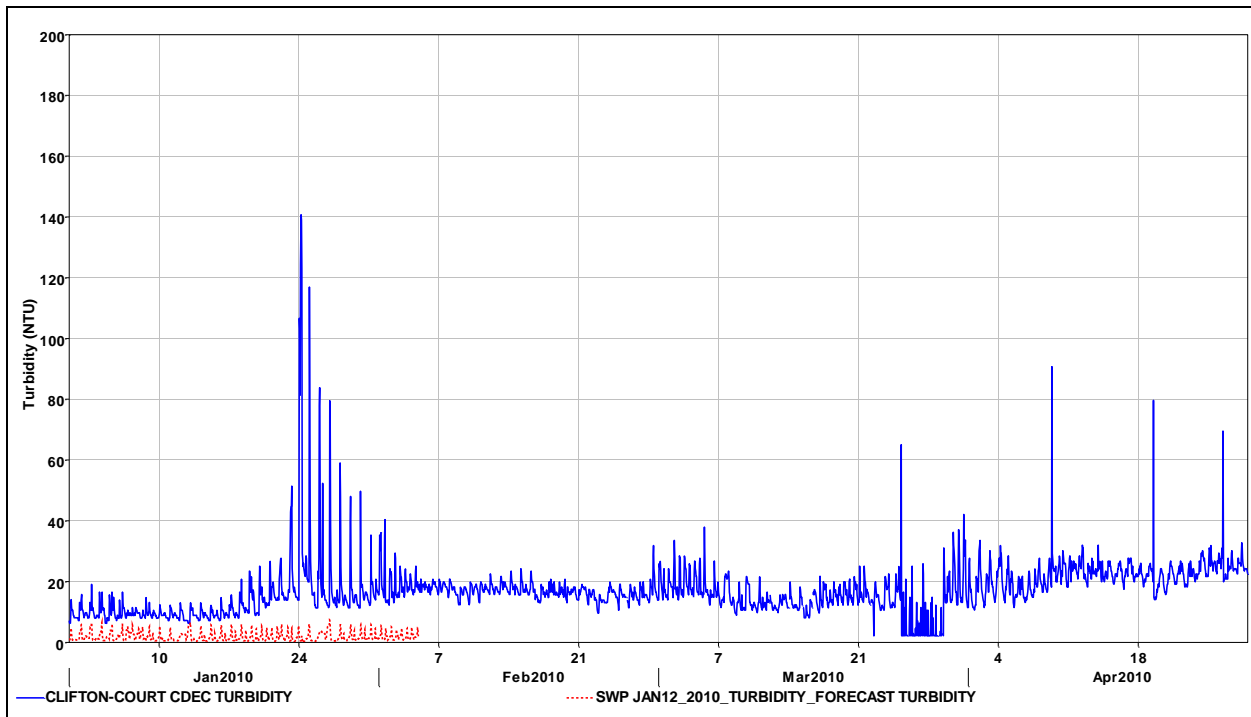


Figure 13-12 Turbidity data at CCFB (blue line) and Jan. 12th model forecast (red dash) at the SWP Intake.

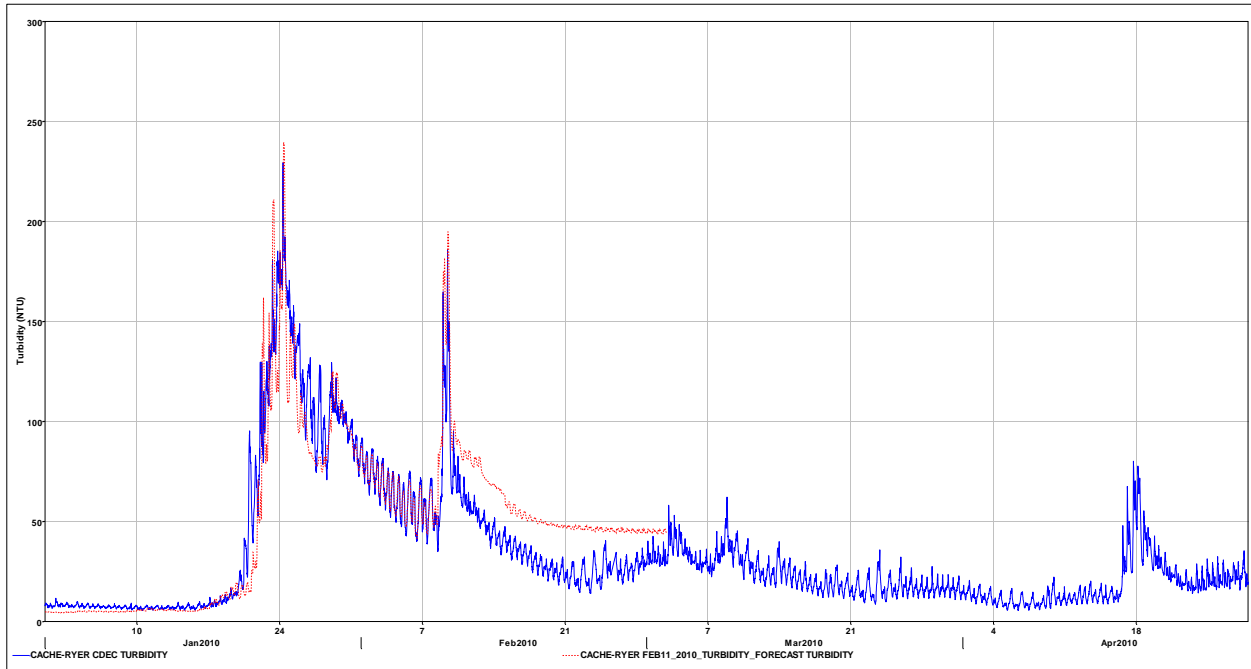


Figure 13-13 Turbidity data (blue line) and Feb 11th model forecast (red dash) at Cache-Ryer.

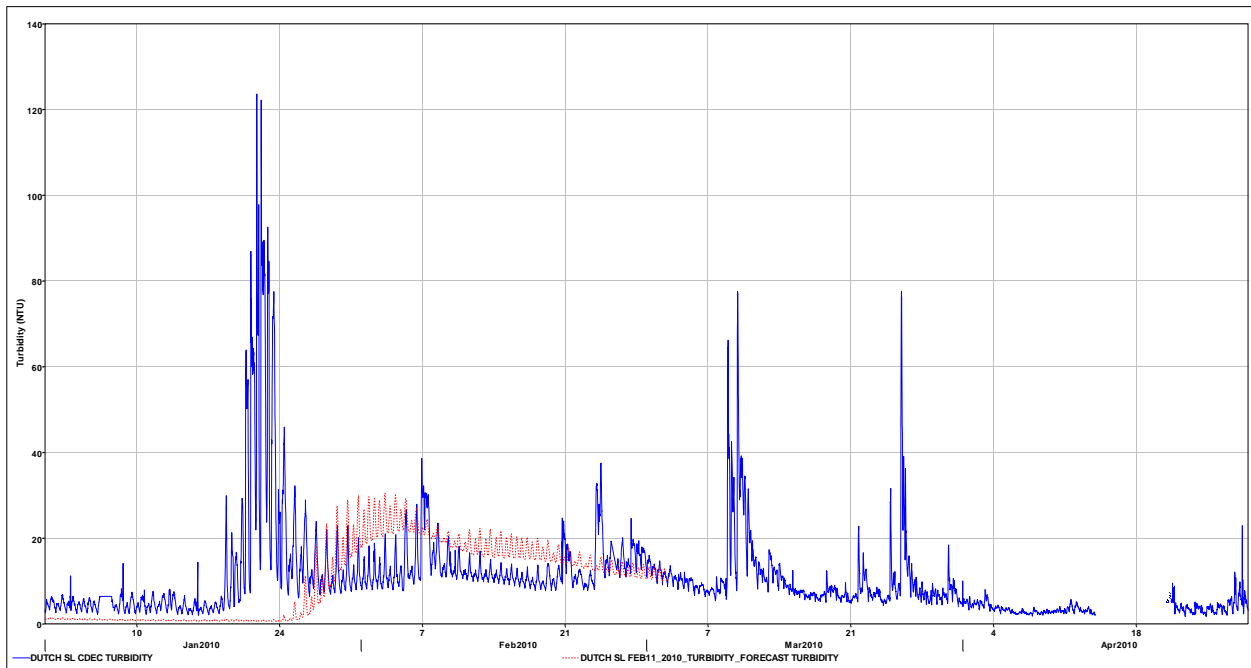


Figure 13-14 Turbidity data (blue line) and Feb 11th model forecast (red dash) at Dutch Sl.

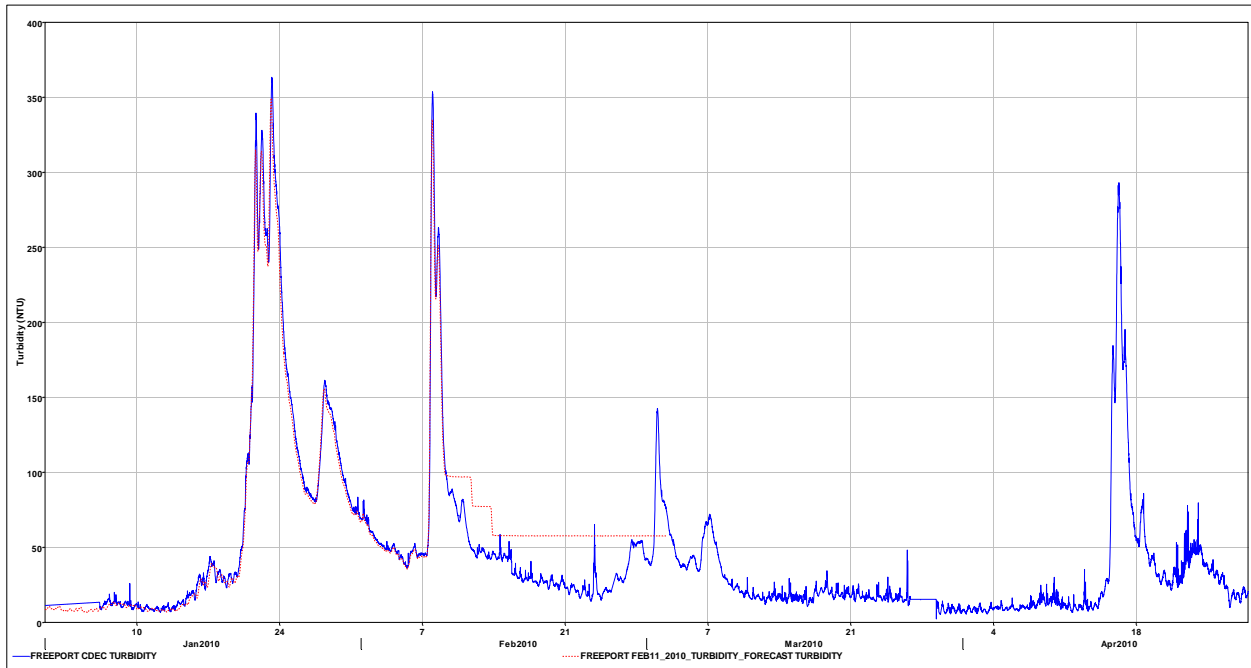


Figure 13-15 Turbidity data (blue line) and Feb 11th model forecast (red dash) at Freepoint.

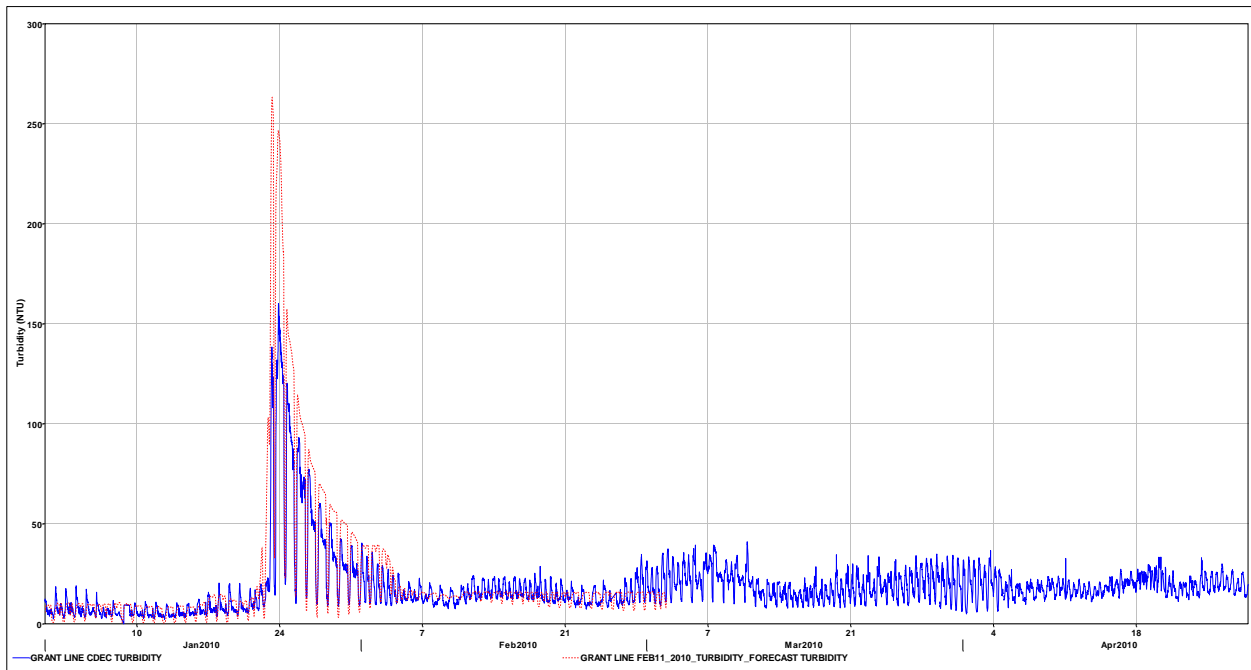


Figure 13-16 Turbidity data (blue line) and Feb 11th model forecast (red dash) at Grant Line.

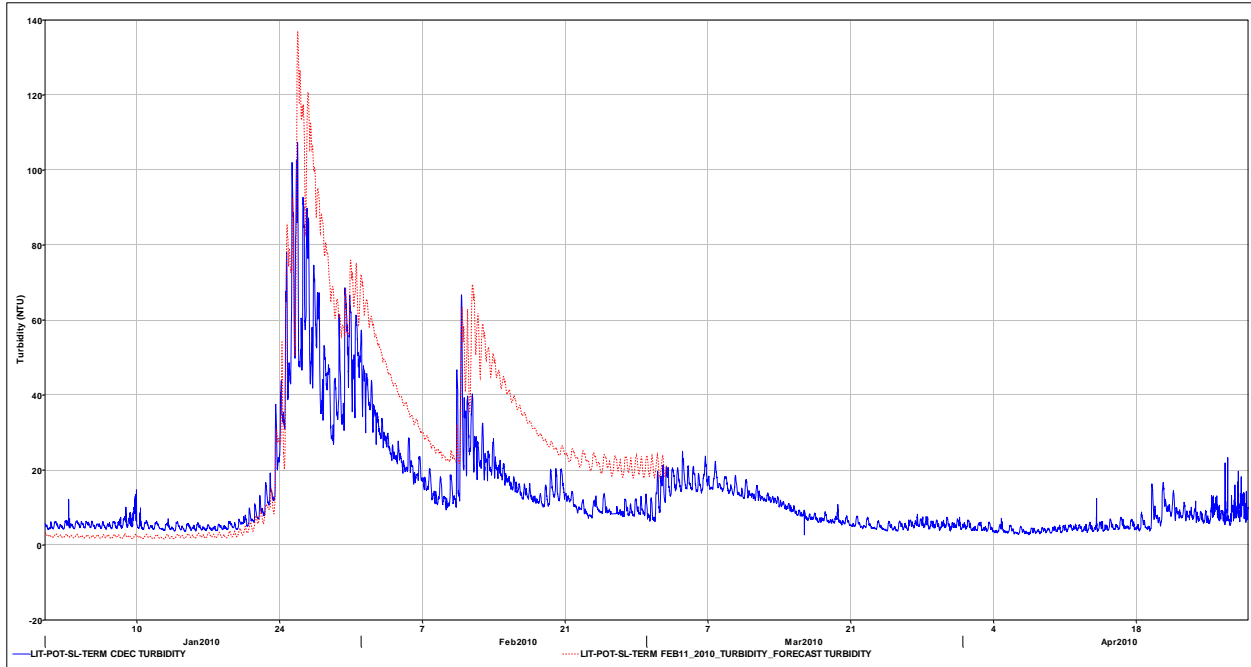


Figure 13-17 Turbidity data (blue line) and Feb 11th model forecast (red dash) at LIT-POT-SL-TERM.

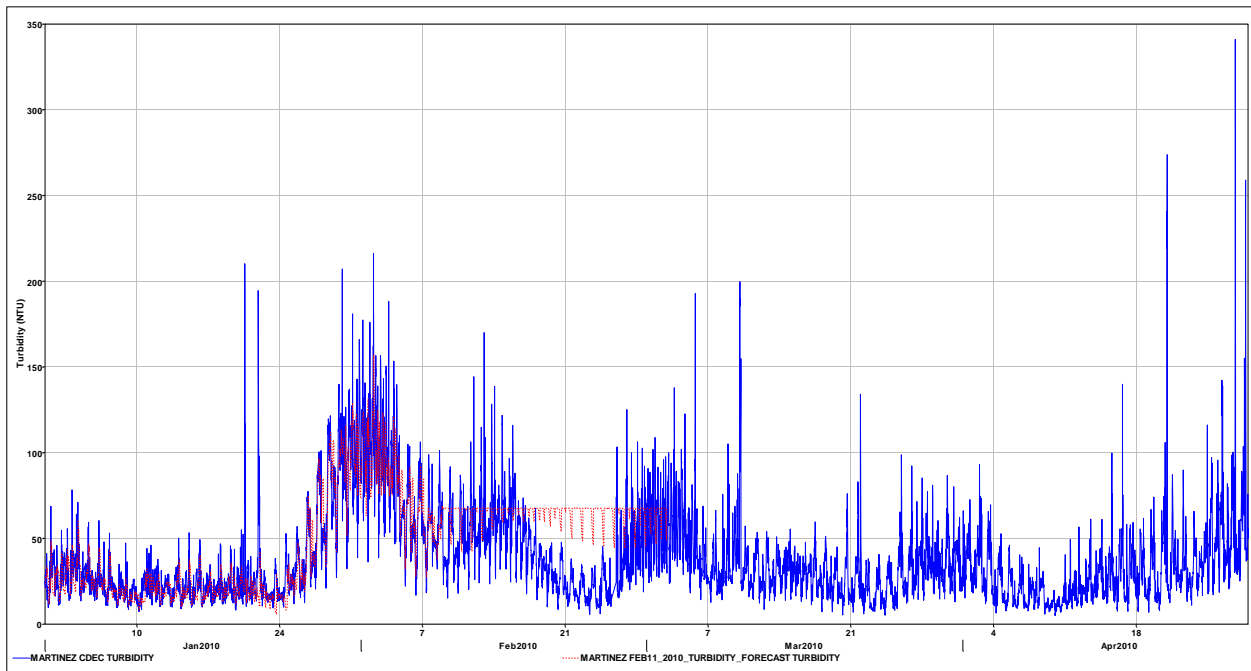


Figure 13-18 Turbidity data (blue line) and Feb 11th model forecast (red dash) at Martinez.

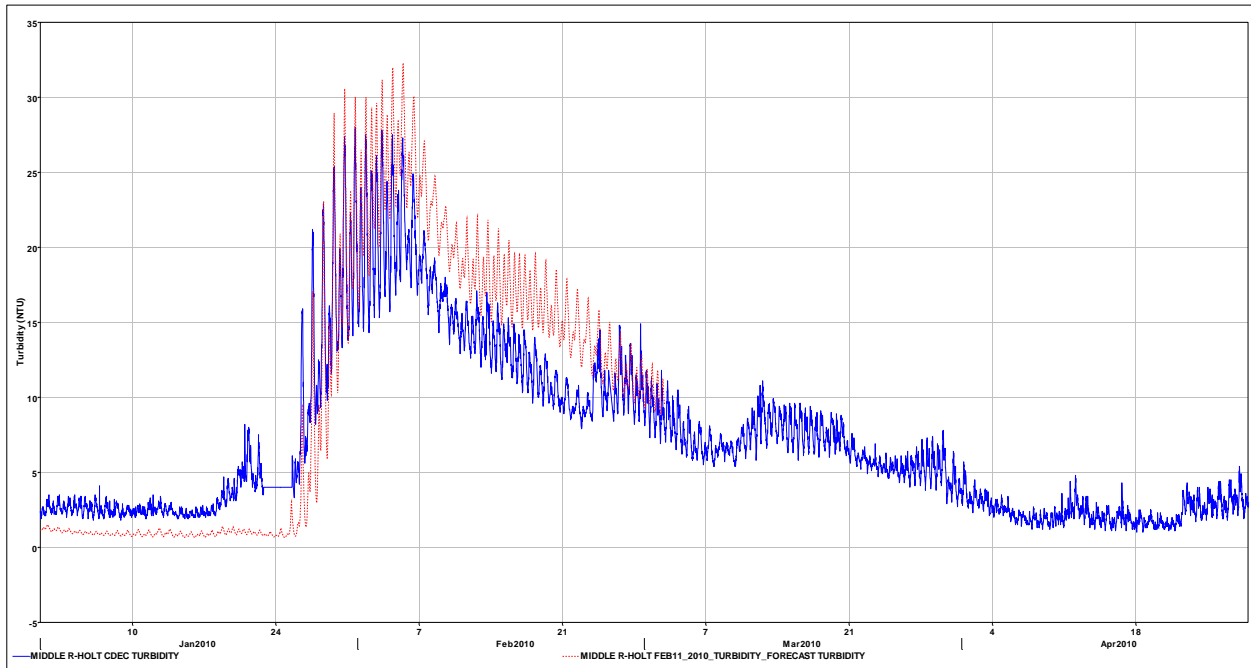


Figure 13-19 Turbidity data (blue line) and Feb 11th model forecast (red dash) at Middle R-Holt.

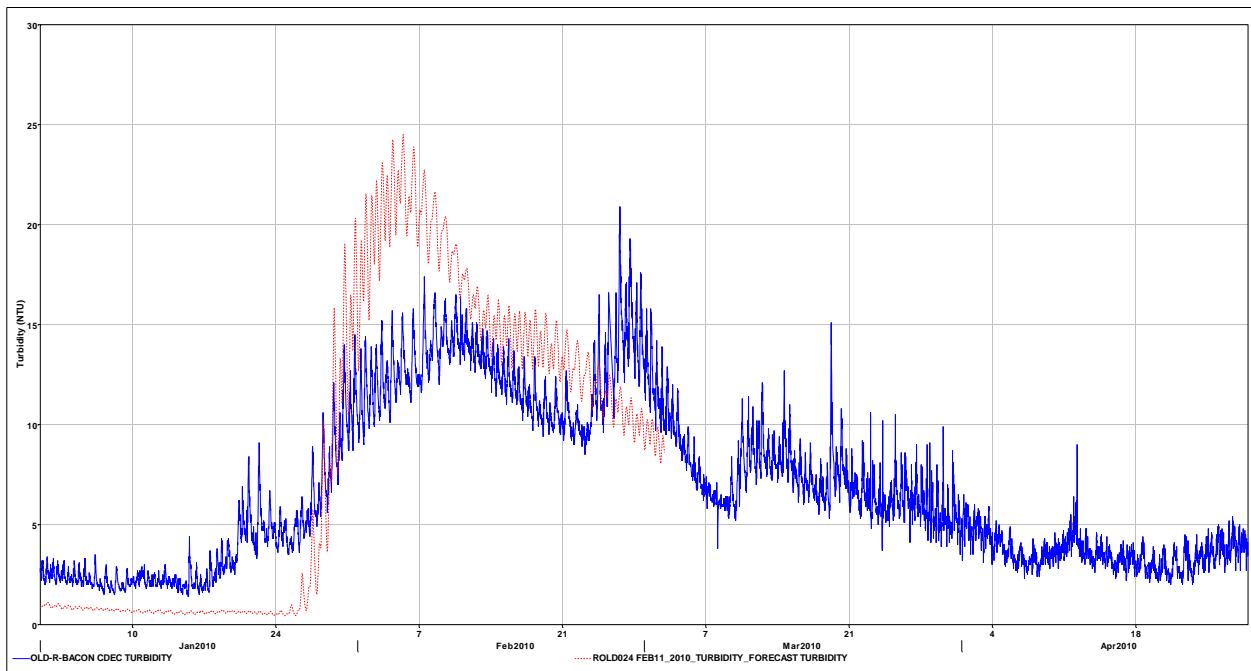


Figure 13-20 Turbidity data (blue line) and Feb 11th model forecast (red dash) at Old R- Bacon.

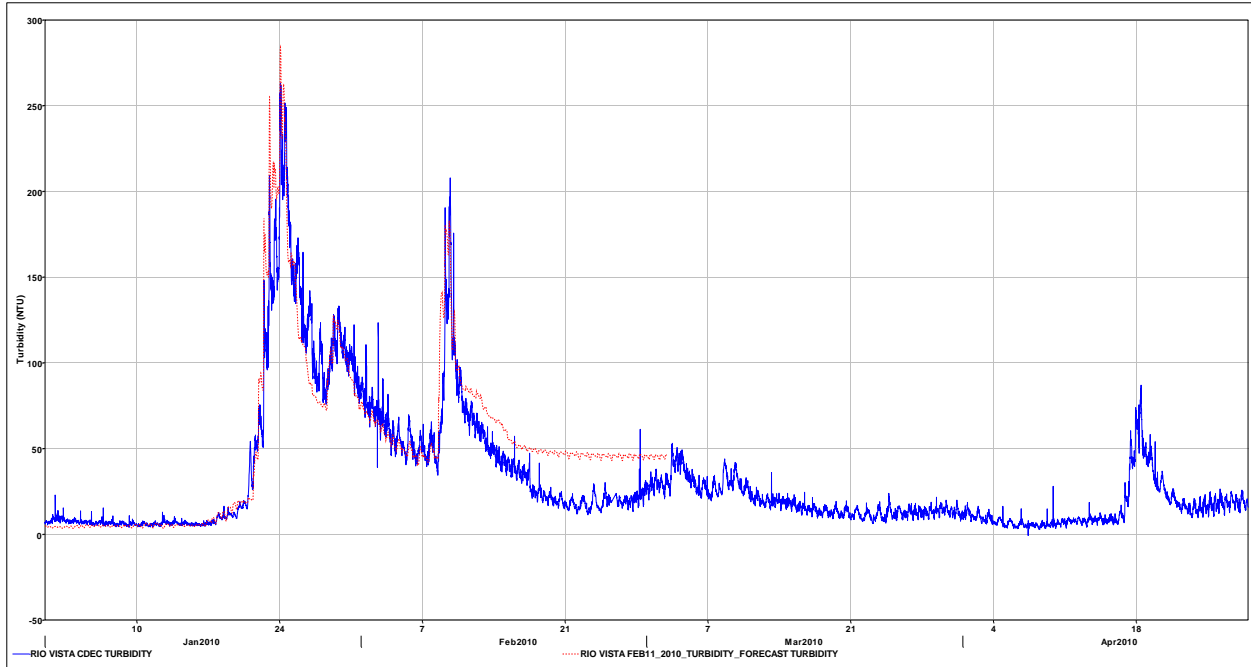


Figure 13-21 Turbidity data (blue line) and Feb 11th model forecast (red dash) at Rio Vista.

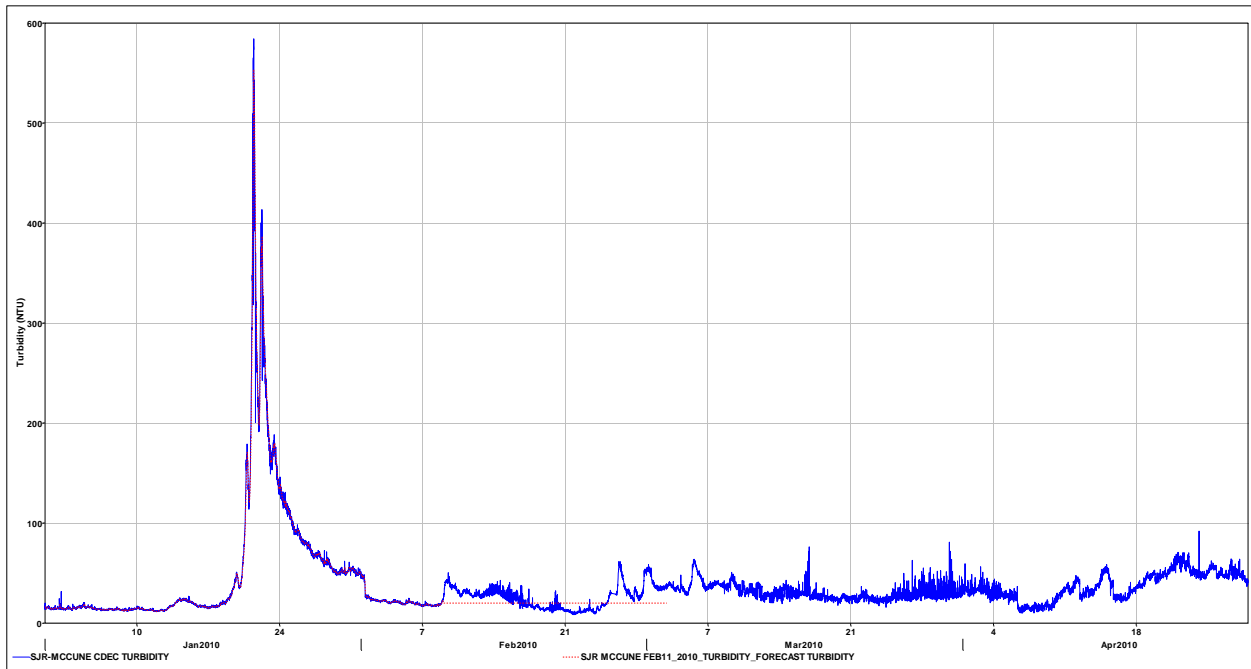


Figure 13-22 Turbidity data (blue line) and Feb 11th model forecast (red dash) at SJR McCune.

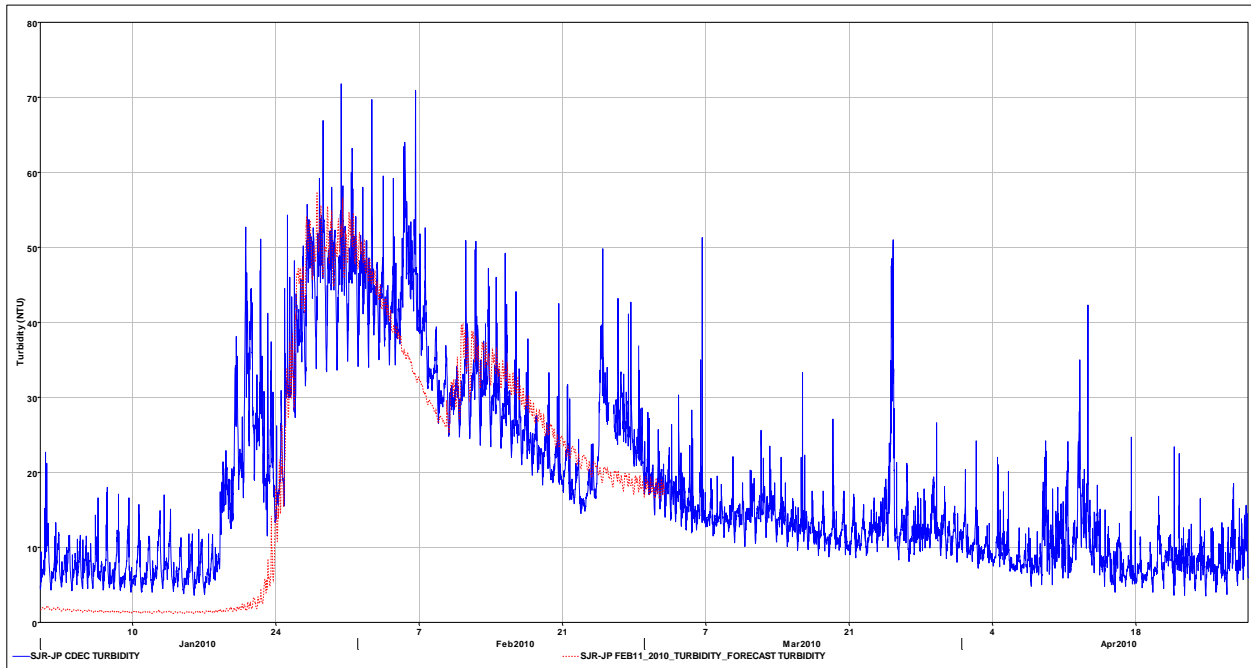


Figure 13-23 Turbidity data (blue line) and Feb 11th model forecast (red dash) at SJR-JP.

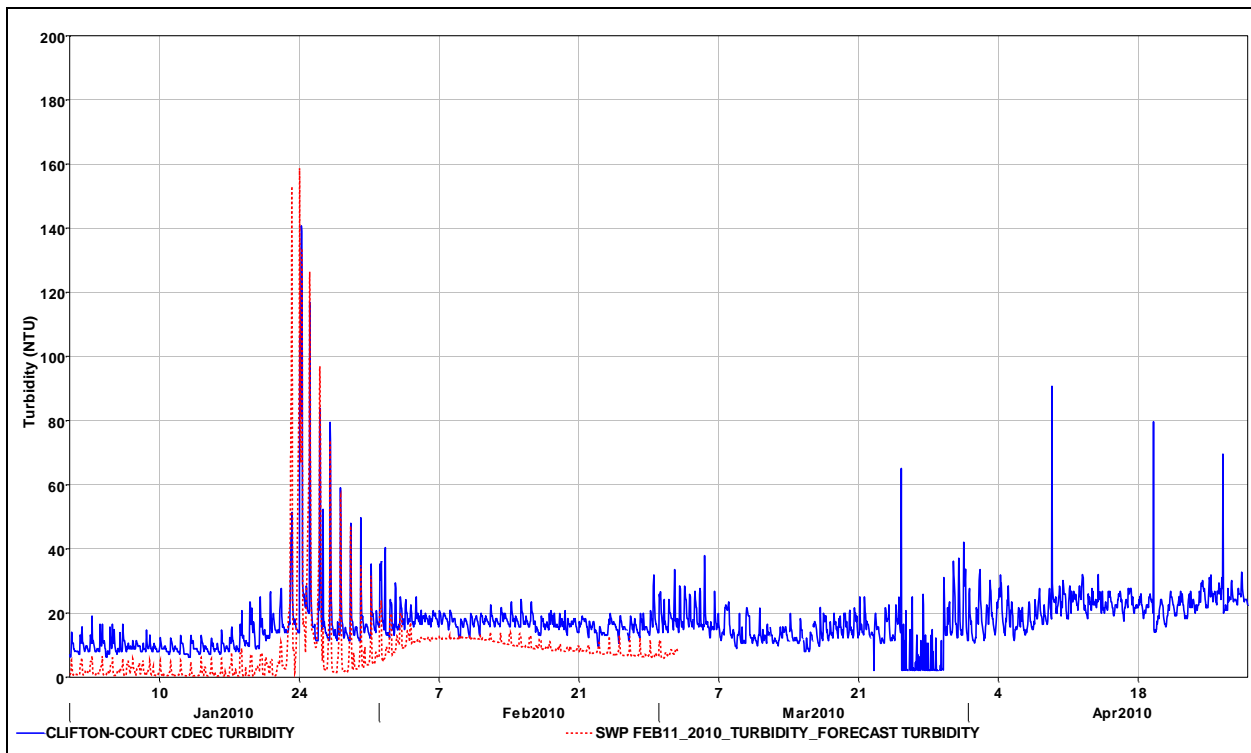


Figure 13-24 Turbidity data at CCFB (blue line) and Feb. 11th model forecast (red dash) at the SWP Intake.

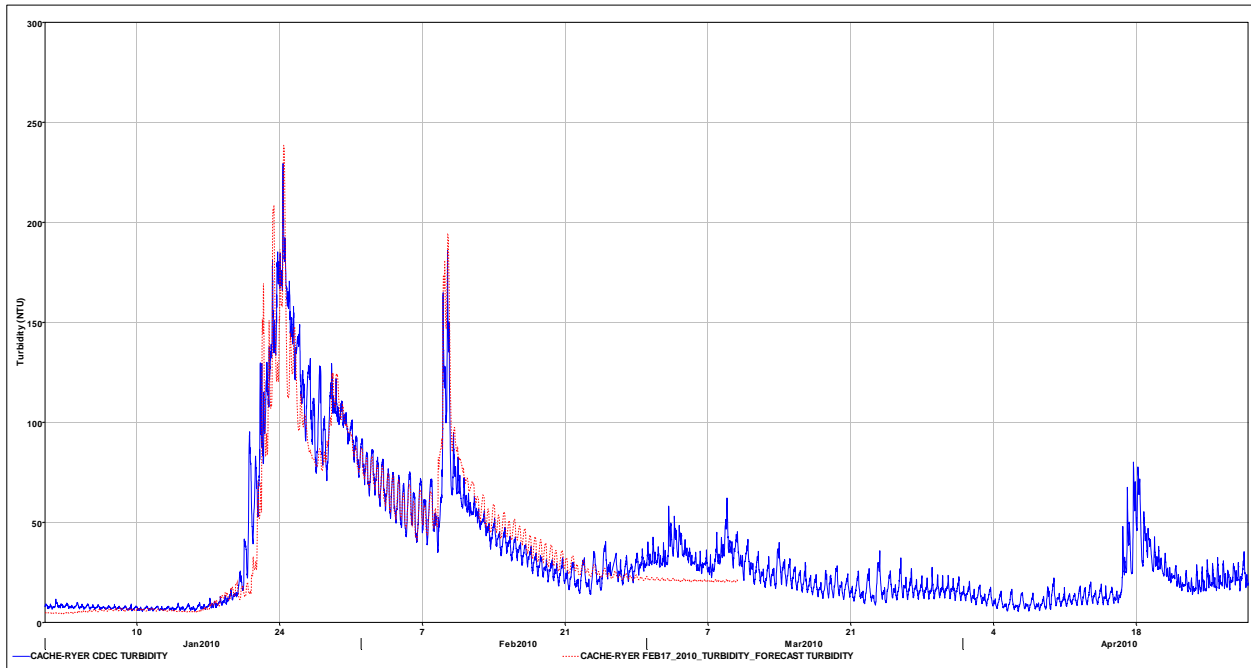


Figure 13-25 Turbidity data (blue line) and Feb 17th model forecast (red dash) at Cache-Ryer.

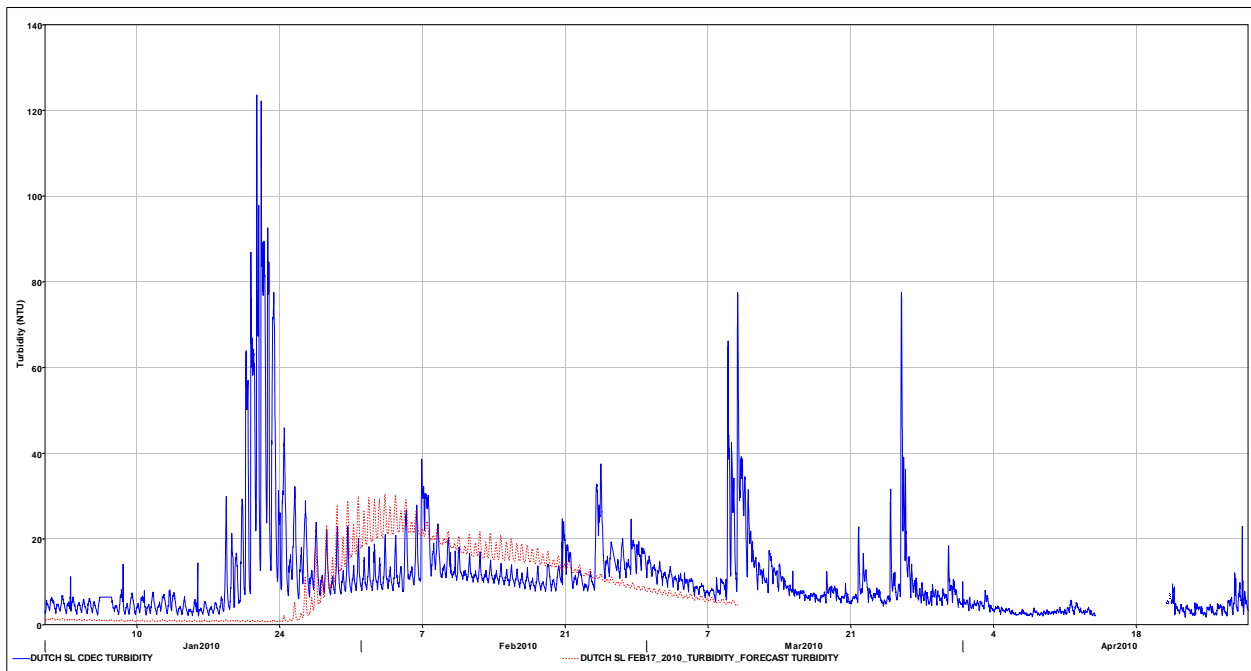


Figure 13-26 Turbidity data (blue line) and Feb 17th model forecast (red dash) at Dutch SL.

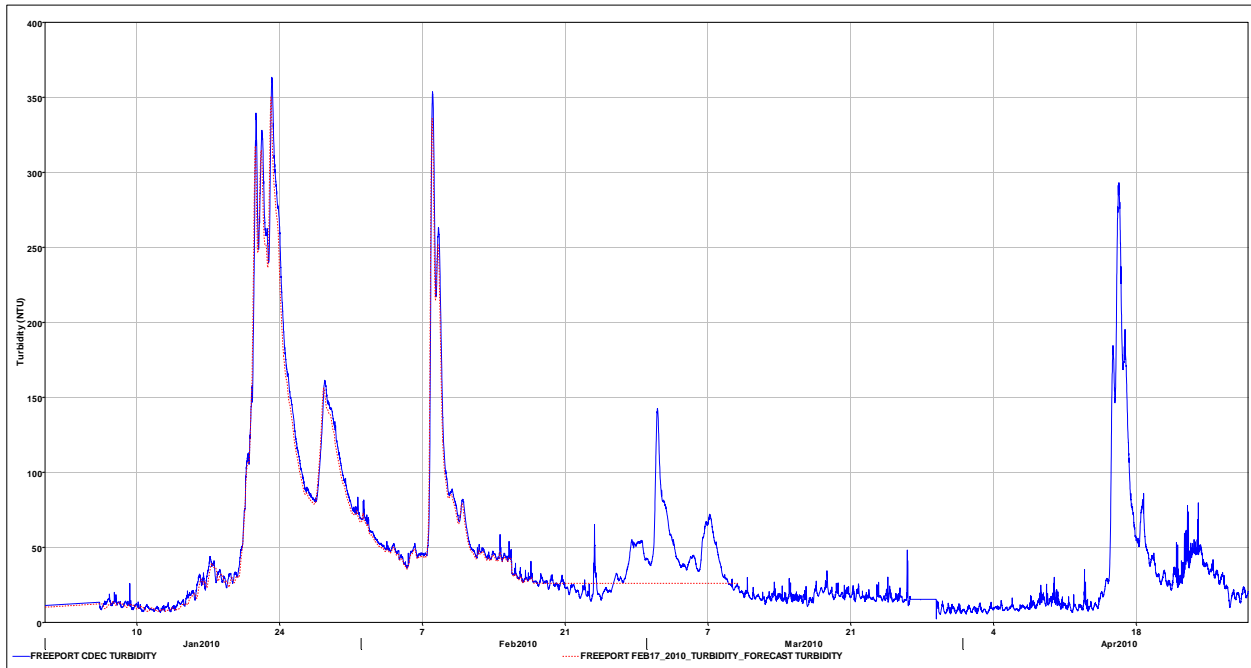


Figure 13-27 Turbidity data (blue line) and Feb 17th model forecast (red dash) at Freepoint.

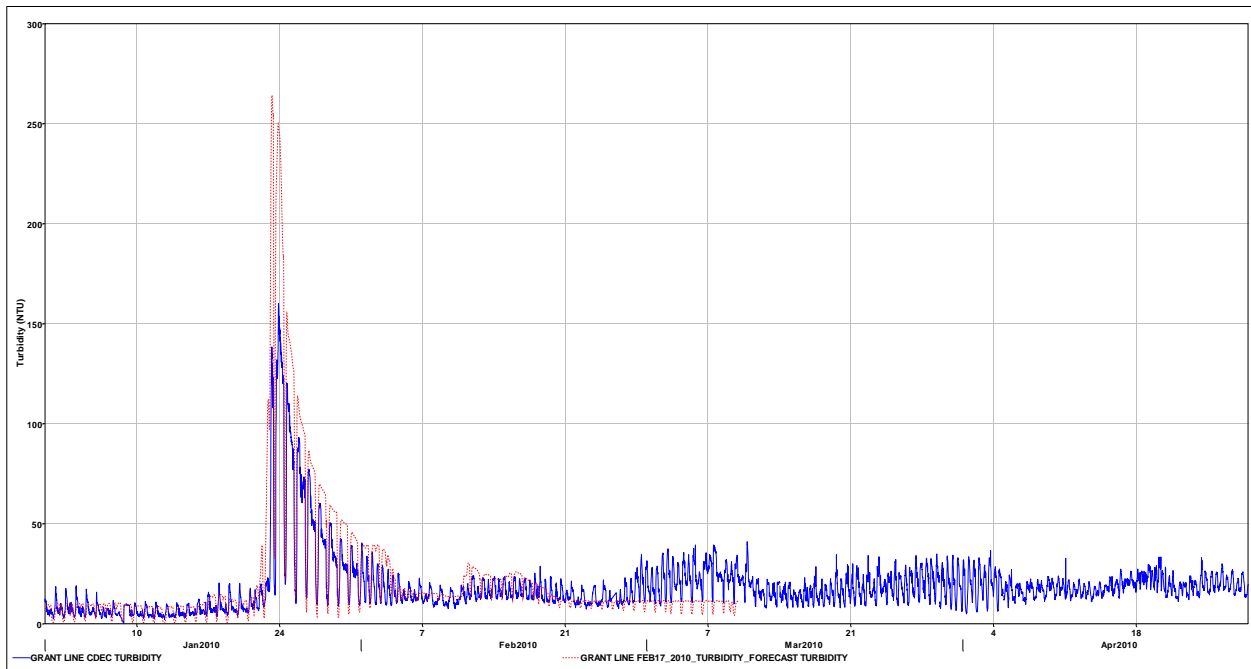


Figure 13-28 Turbidity data (blue line) and Feb 17th model forecast (red dash) at Grant Line.

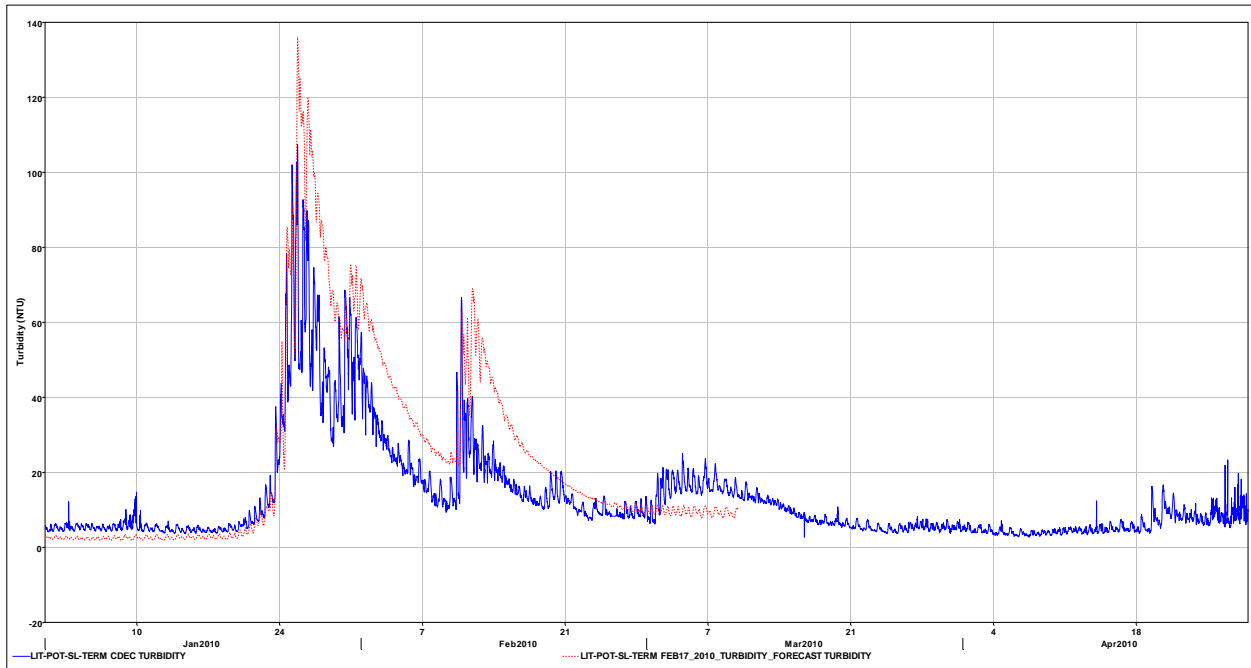


Figure 13-29 Turbidity data (blue line) and Feb 17th model forecast (red dash) at LIT-POT-SL-TERM.

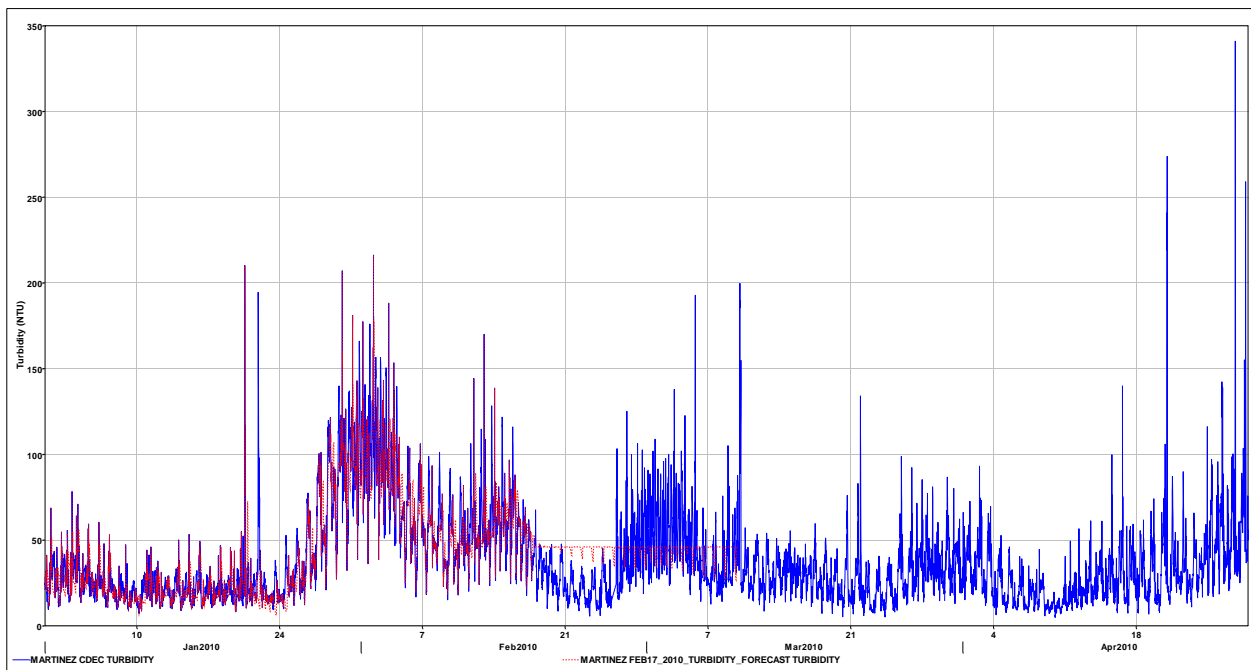


Figure 13-30 Turbidity data (blue line) and Feb 17th model forecast (red dash) at Martinez.

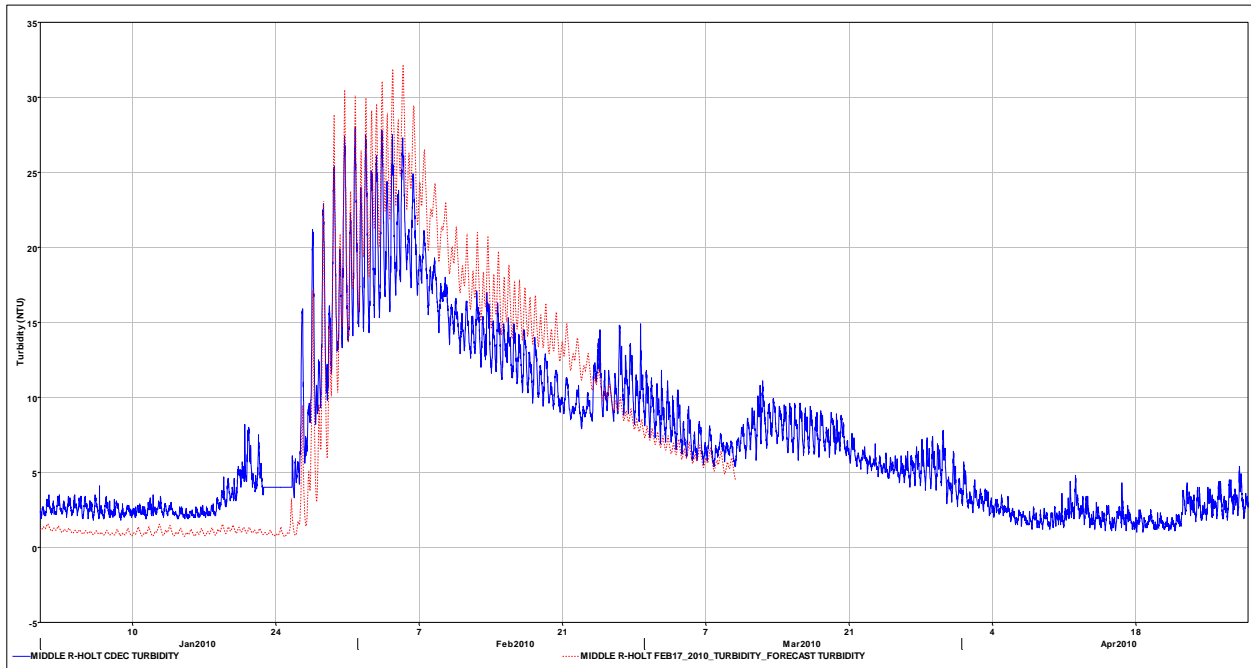


Figure 13-31 Turbidity data (blue line) and Feb 17th model forecast (red dash) at Middle R-Holt.

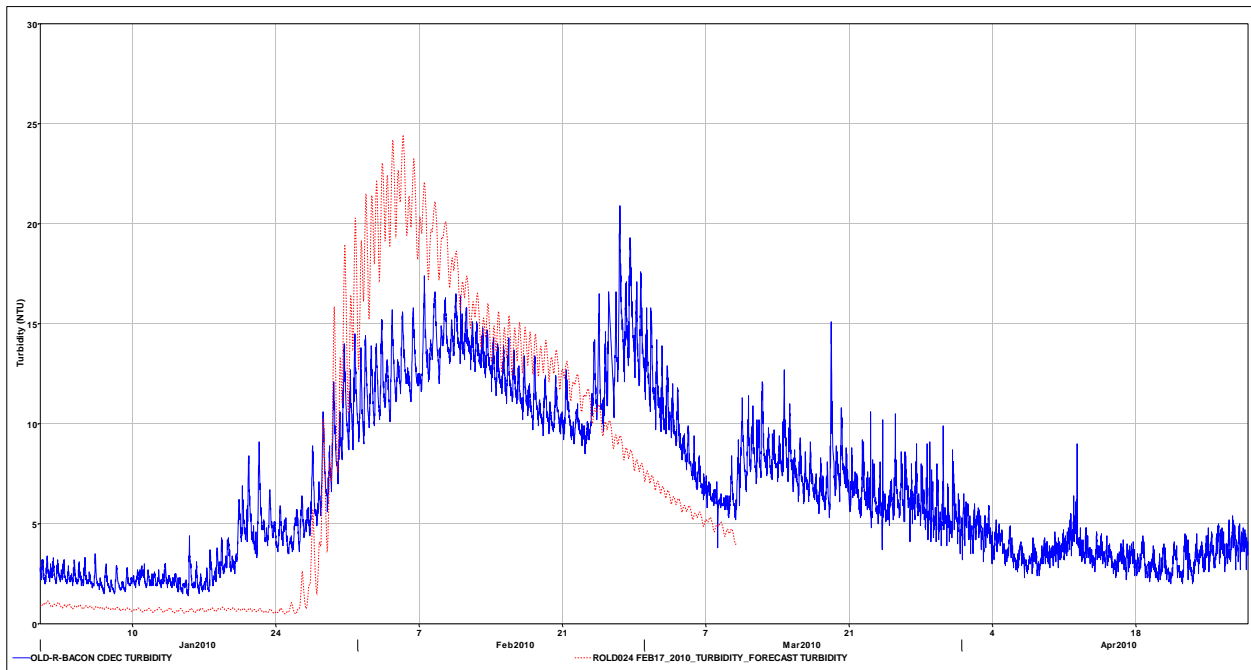


Figure 13-32 Turbidity data (blue line) and Feb 17th model forecast (red dash) at Old R-Bacon.

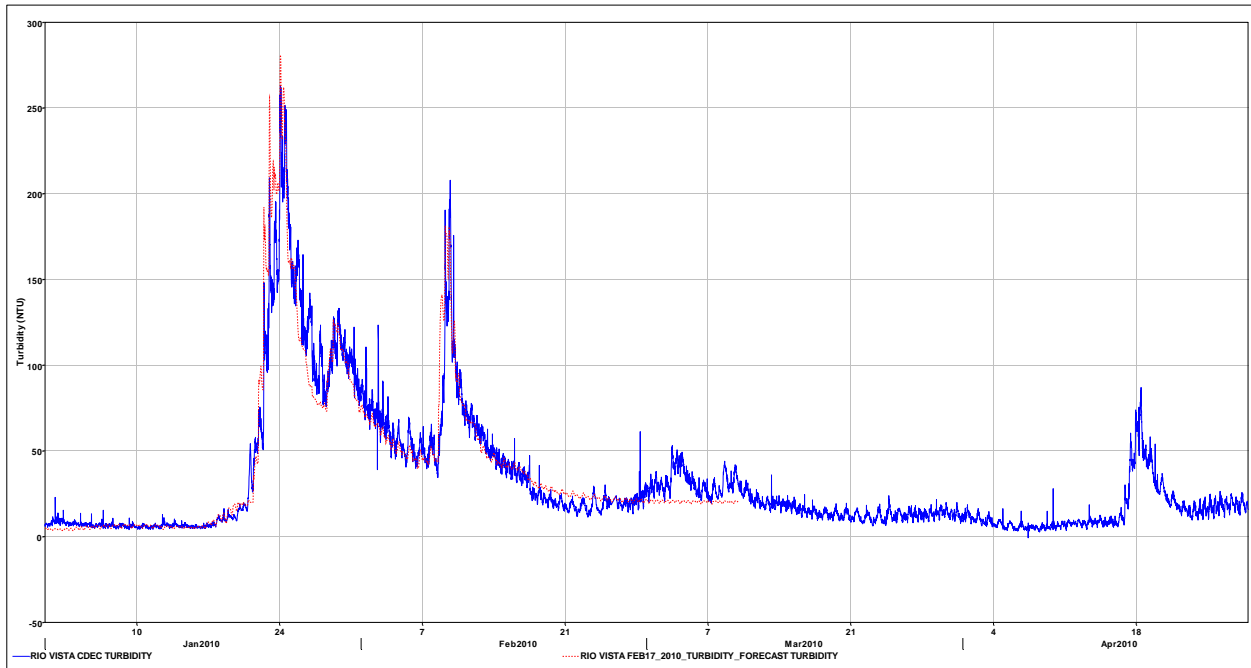


Figure 13-33 Turbidity data (blue line) and Feb 17th model forecast (red dash) at Rio-Vista.

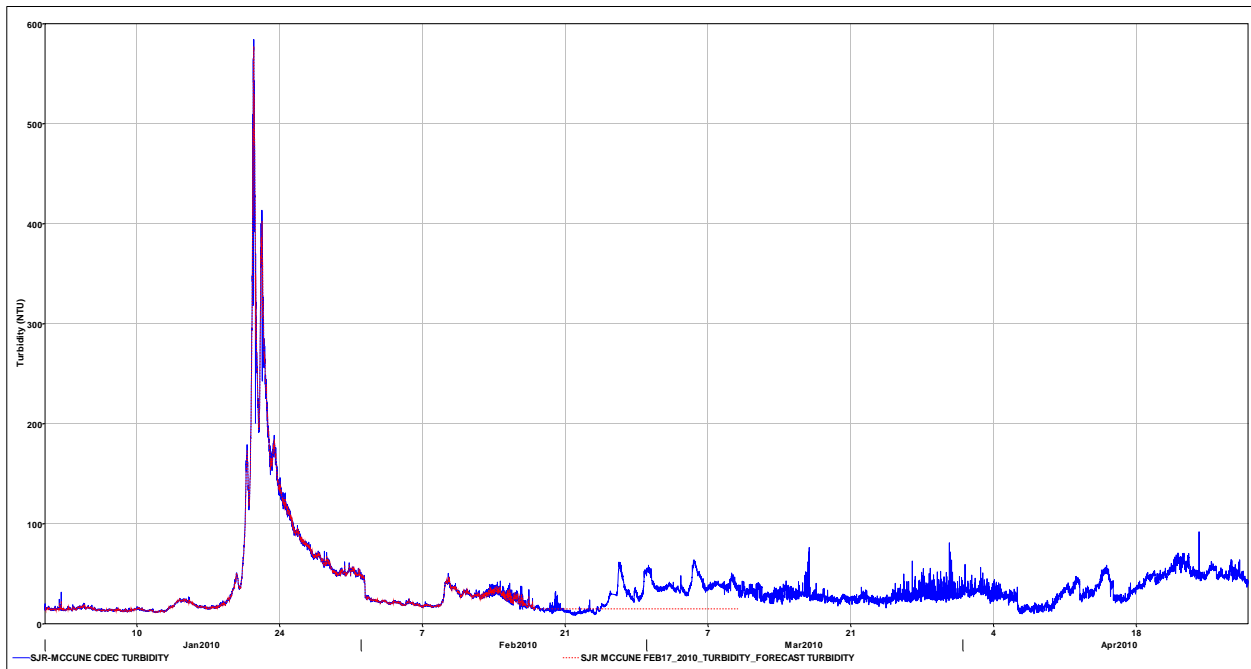


Figure 13-34 Turbidity data (blue line) and Feb 17th model forecast (red dash) at SJR McCune.

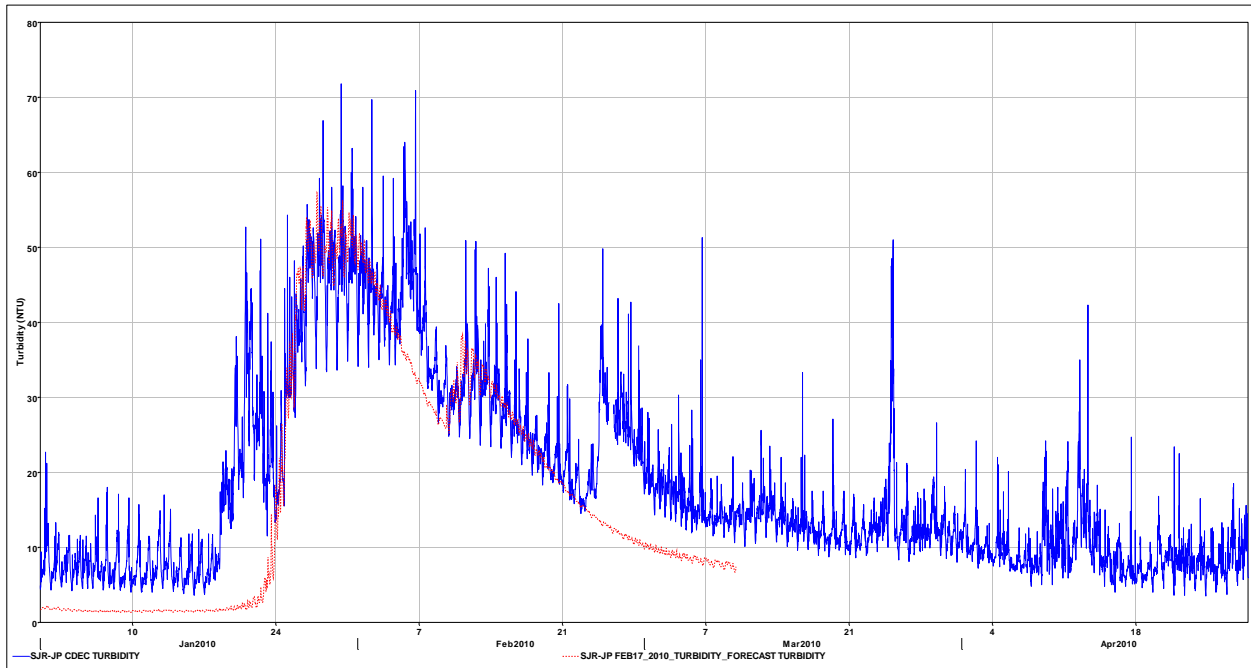


Figure 13-35 Turbidity data (blue line) and Feb 17th model forecast (red dash) at SJR-JP.

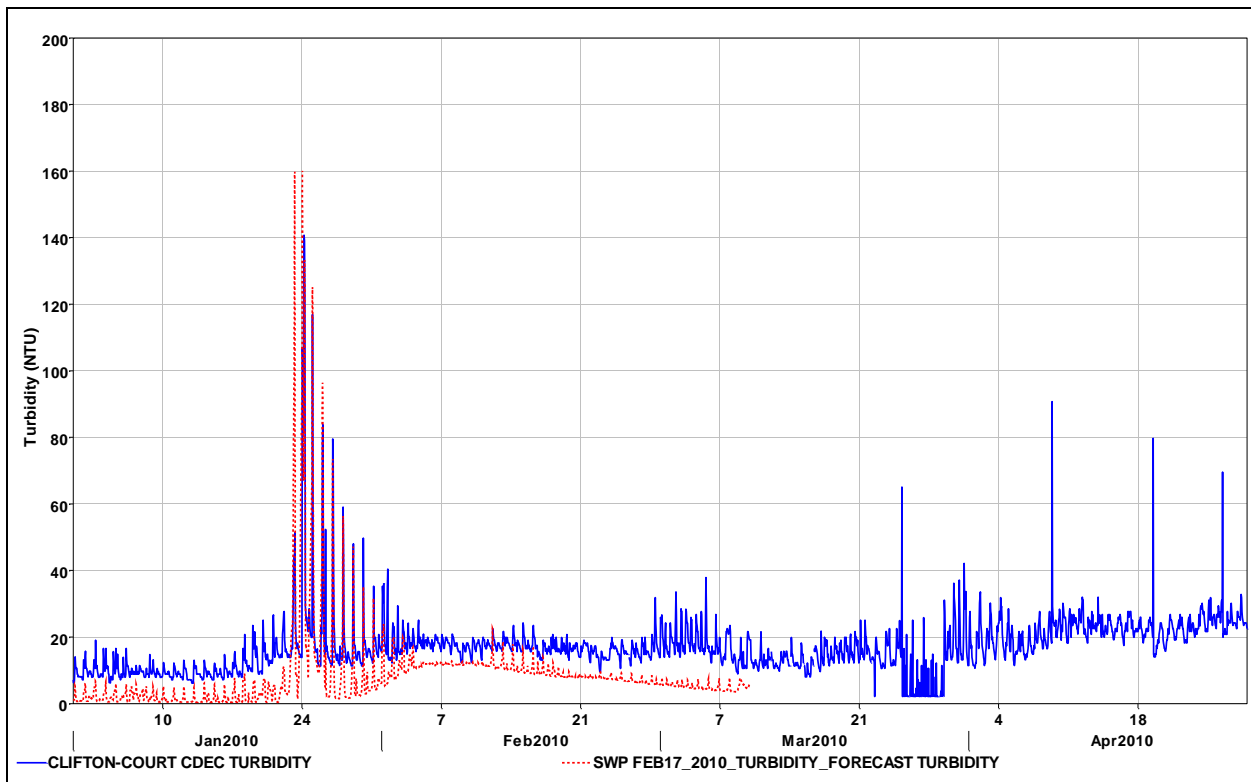


Figure 13-36 Turbidity data at CCFB (blue line) and Feb. 17th model forecast (red dash) at the SWP Intake.

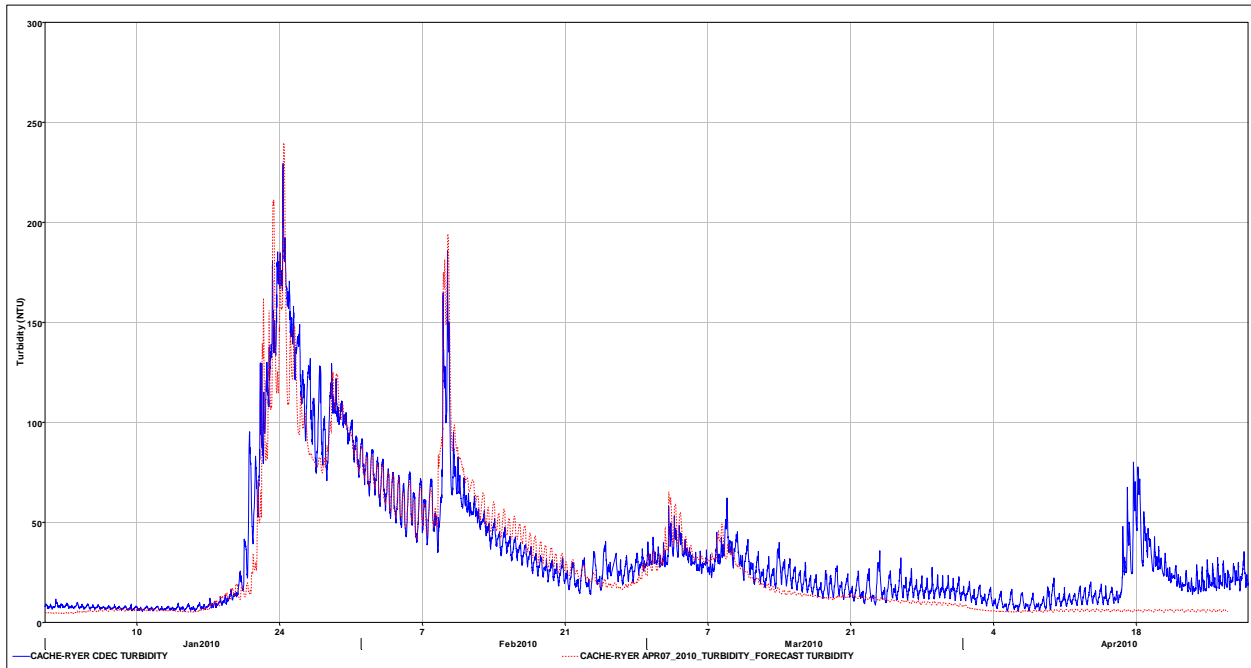


Figure 13-37 Turbidity data (blue line) and April 7th model forecast (red dash) at Cache-Ryer.

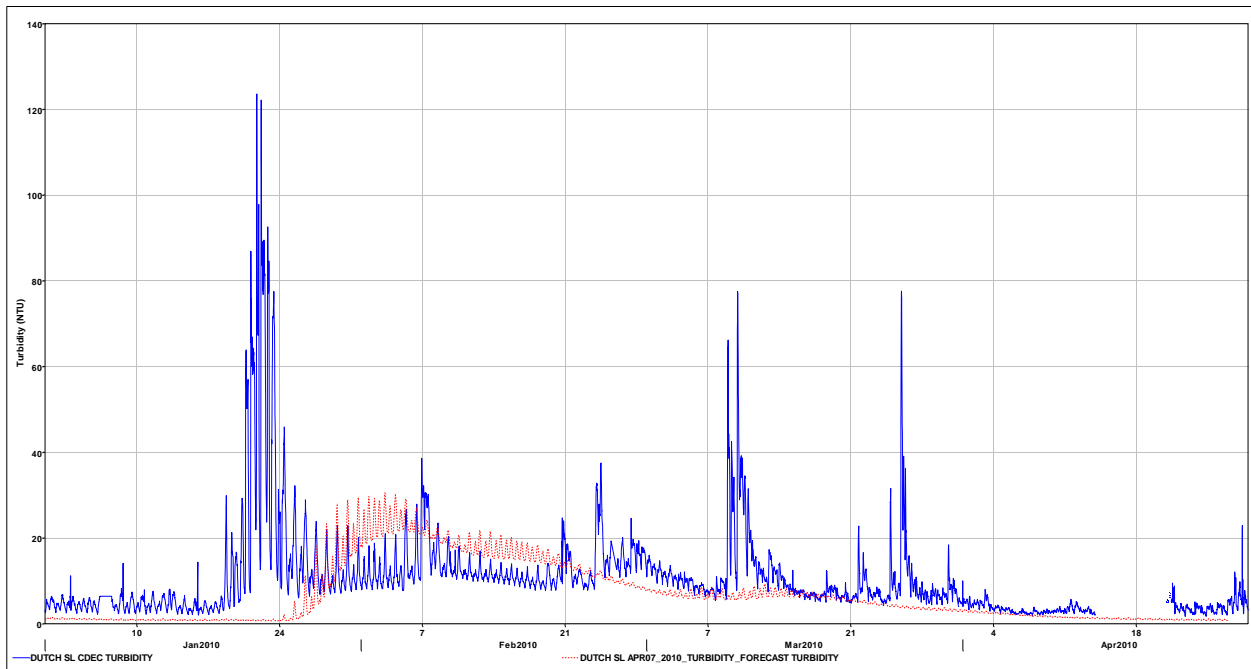


Figure 13-38 Turbidity data (blue line) and April 7th model forecast (red dash) at Dutch SL.

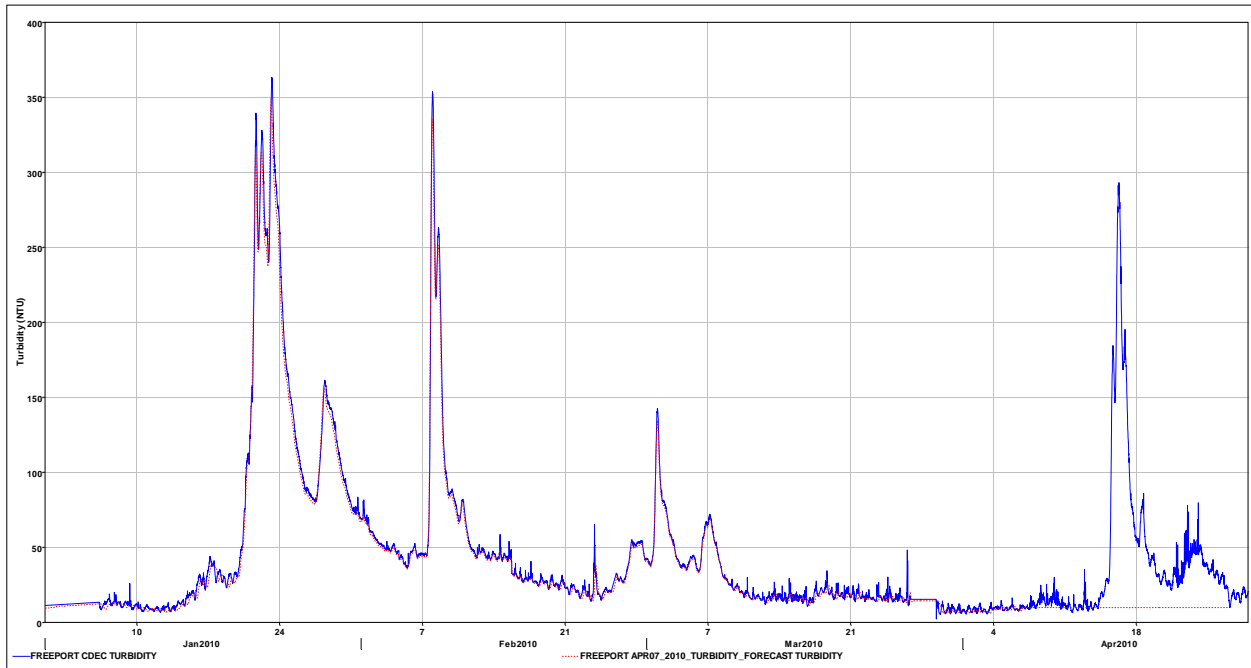


Figure 13-39 Turbidity data (blue line) and April 7th model forecast (red dash) at Freeport.

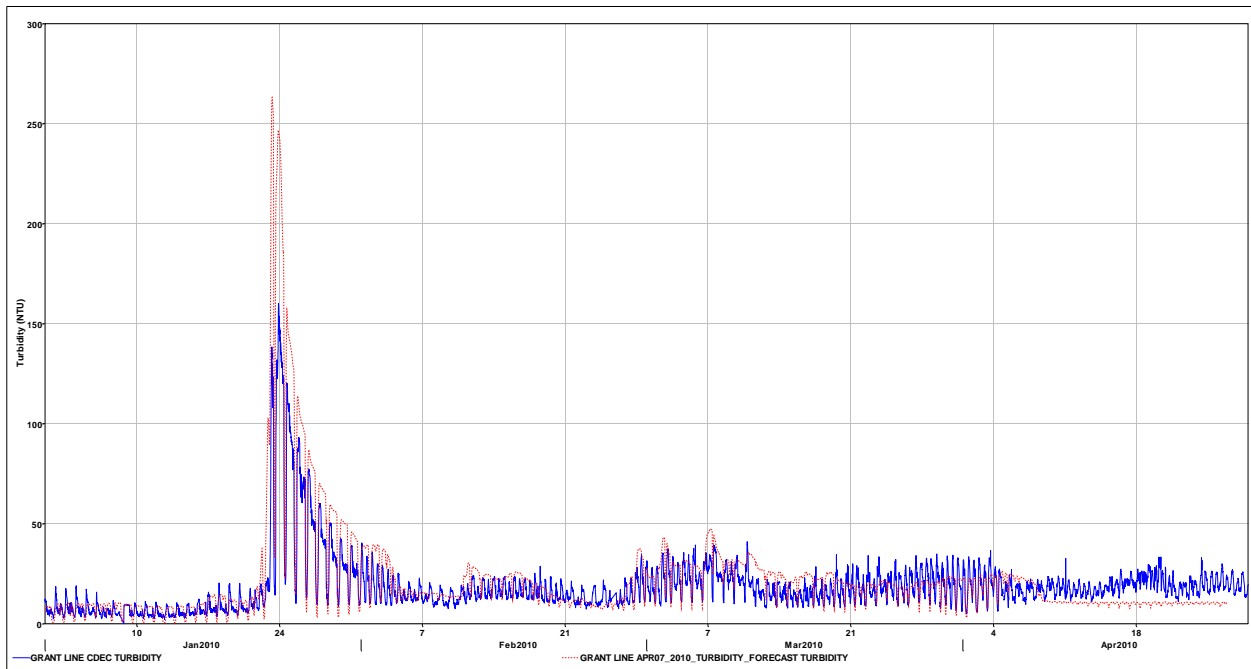


Figure 13-40 Turbidity data (blue line) and April 7th model forecast (red dash) at Grant Line.

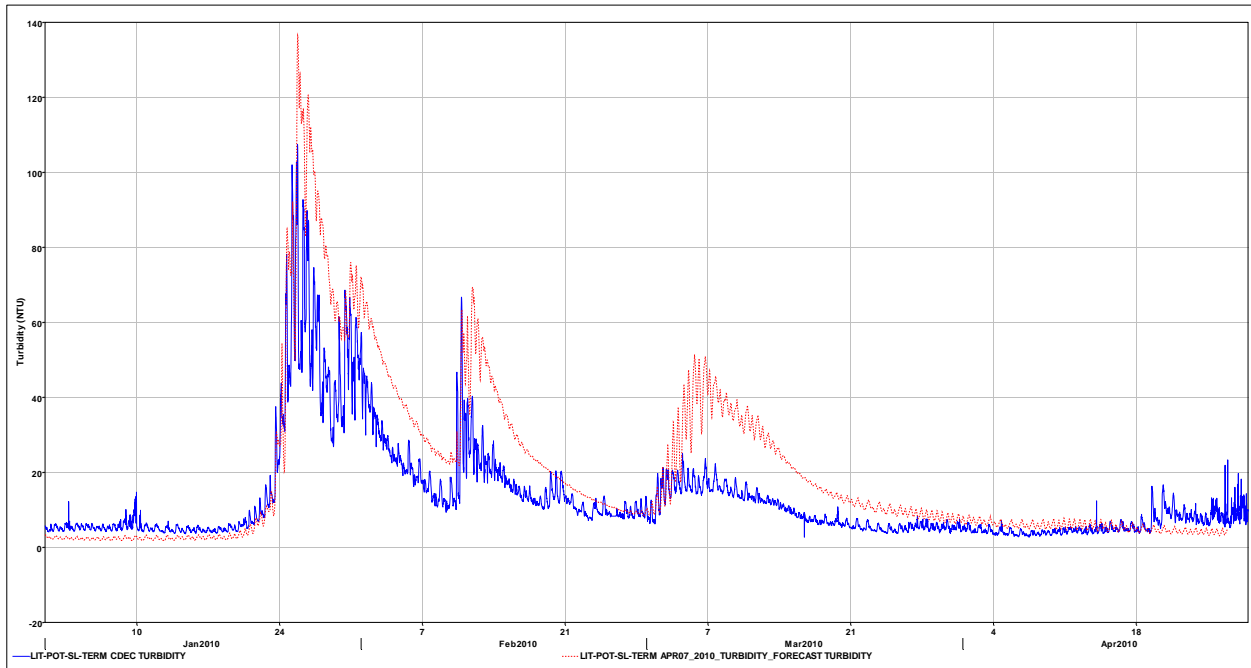


Figure 13-41 Turbidity data (blue line) and April 7th model forecast (red dash) at LIT-POT-SL-TERM.

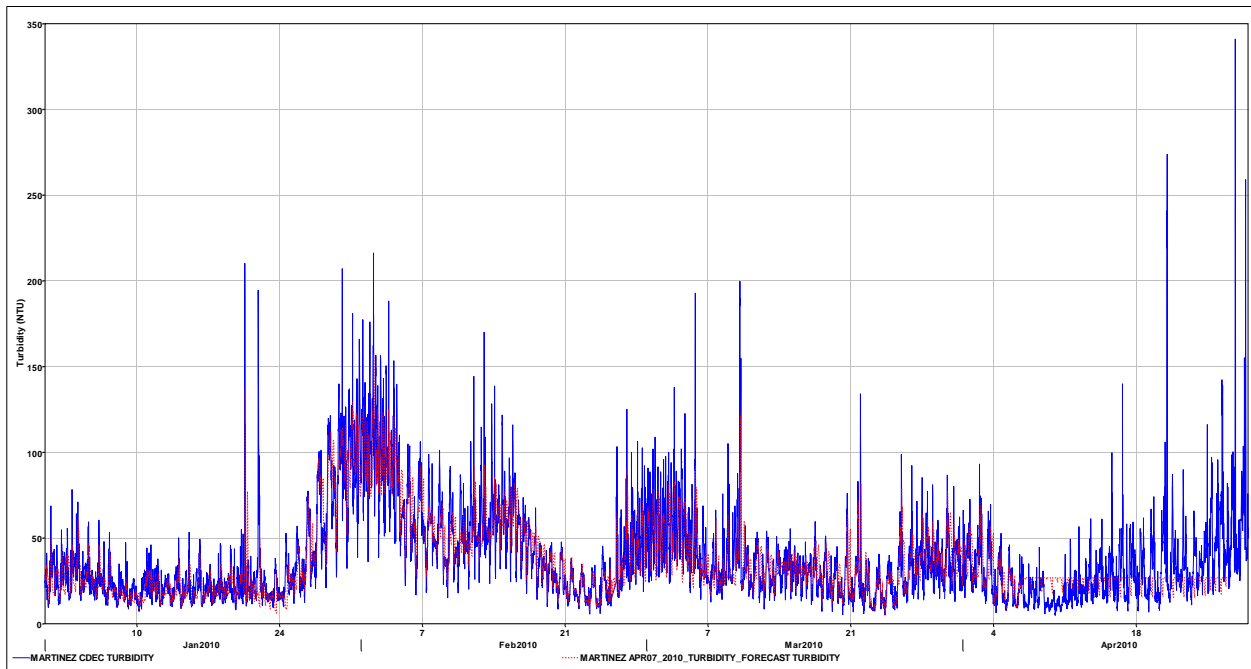


Figure 13-42 Turbidity data (blue line) and April 7th model forecast (red dash) at Martinez.

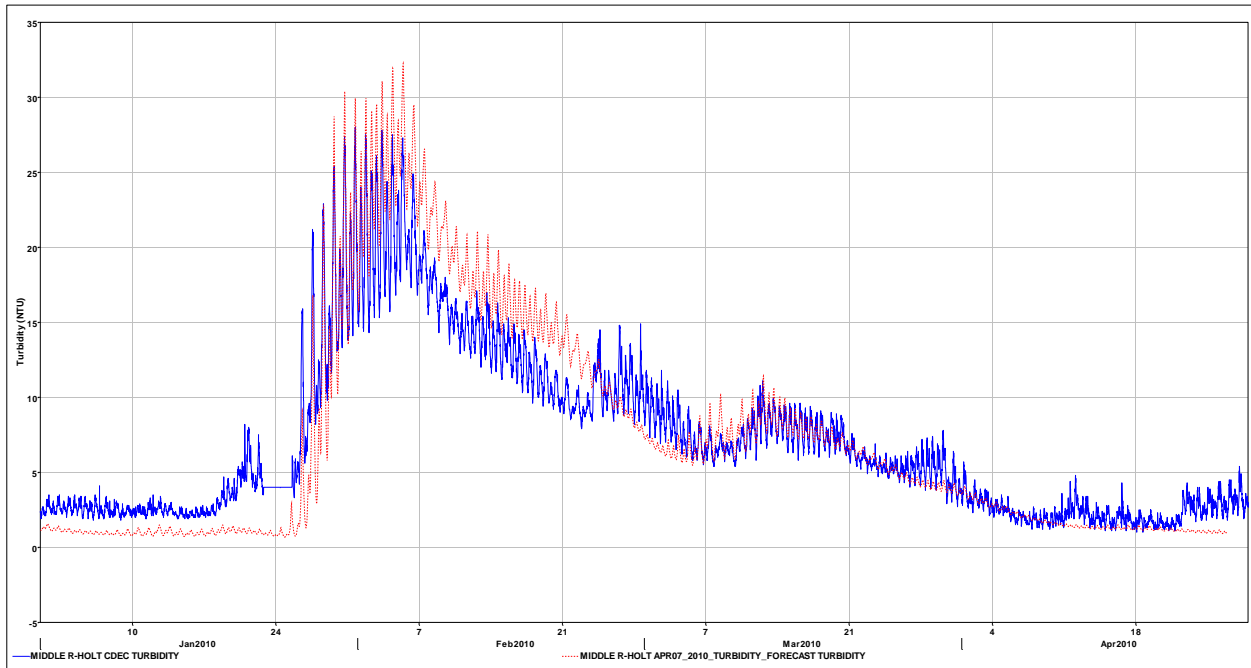


Figure 13-43 Turbidity data (blue line) and April 7th model forecast (red dash) at Middle R-Holt.

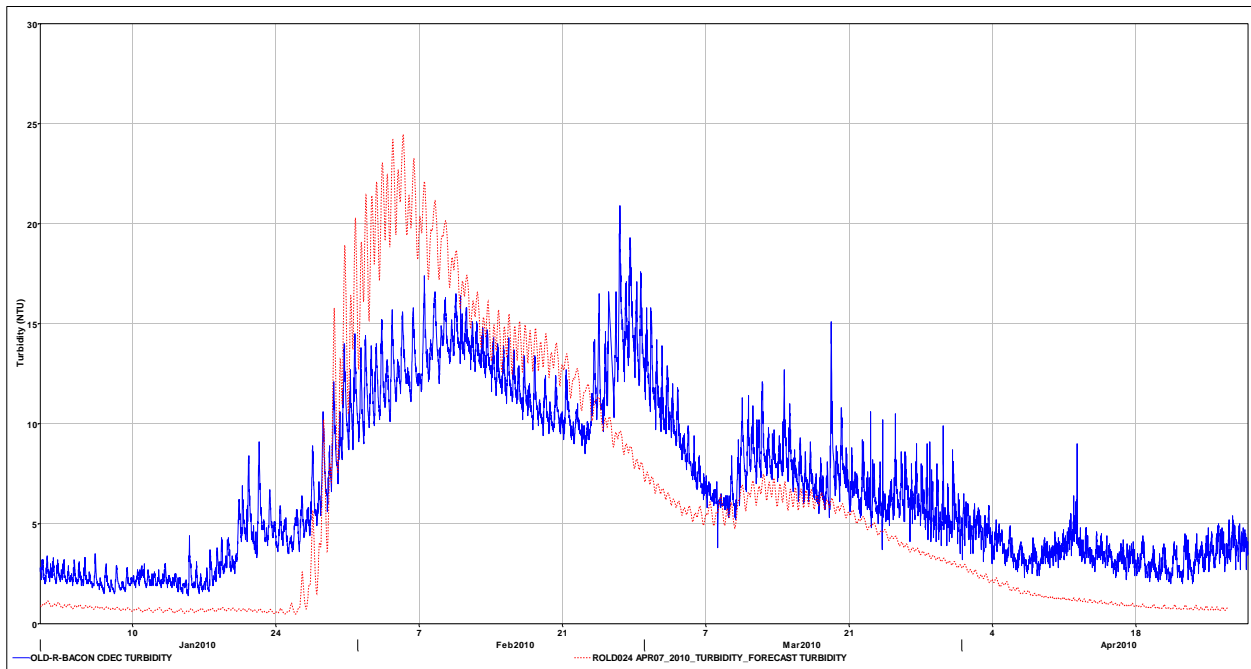


Figure 13-44 Turbidity data (blue line) and April 7th model forecast (red dash) at Old R-Bacon.

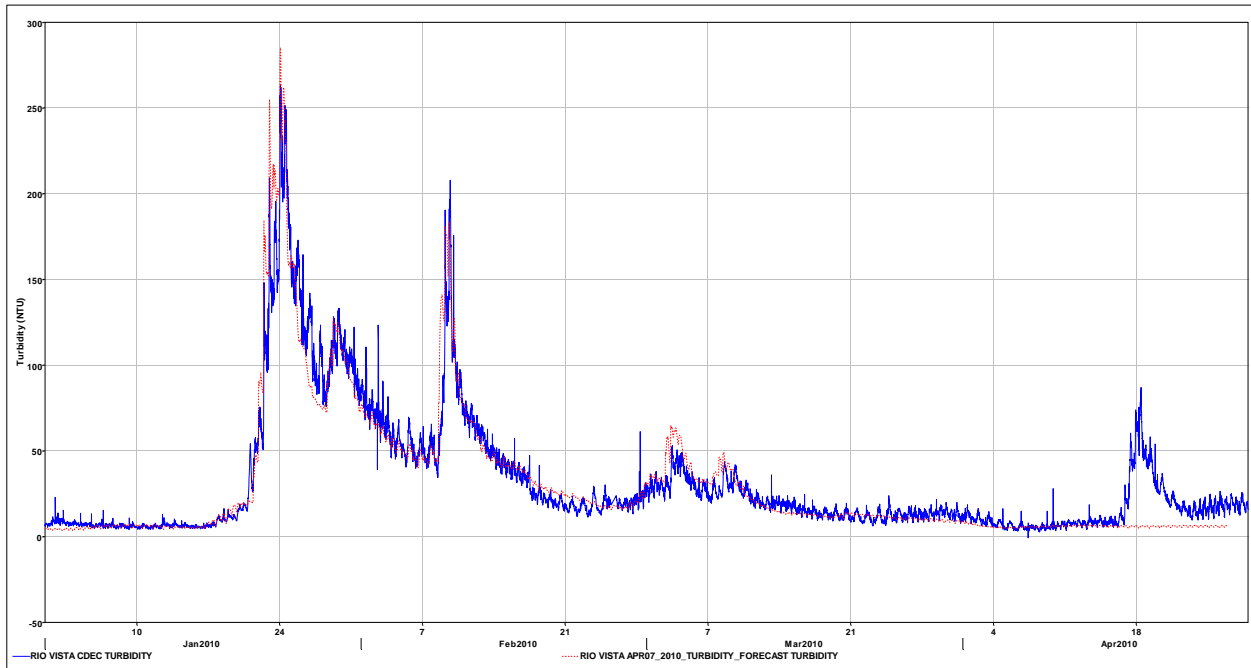


Figure 13-45 Turbidity data (blue line) and April 7th model forecast (red dash) at Rio Vista.

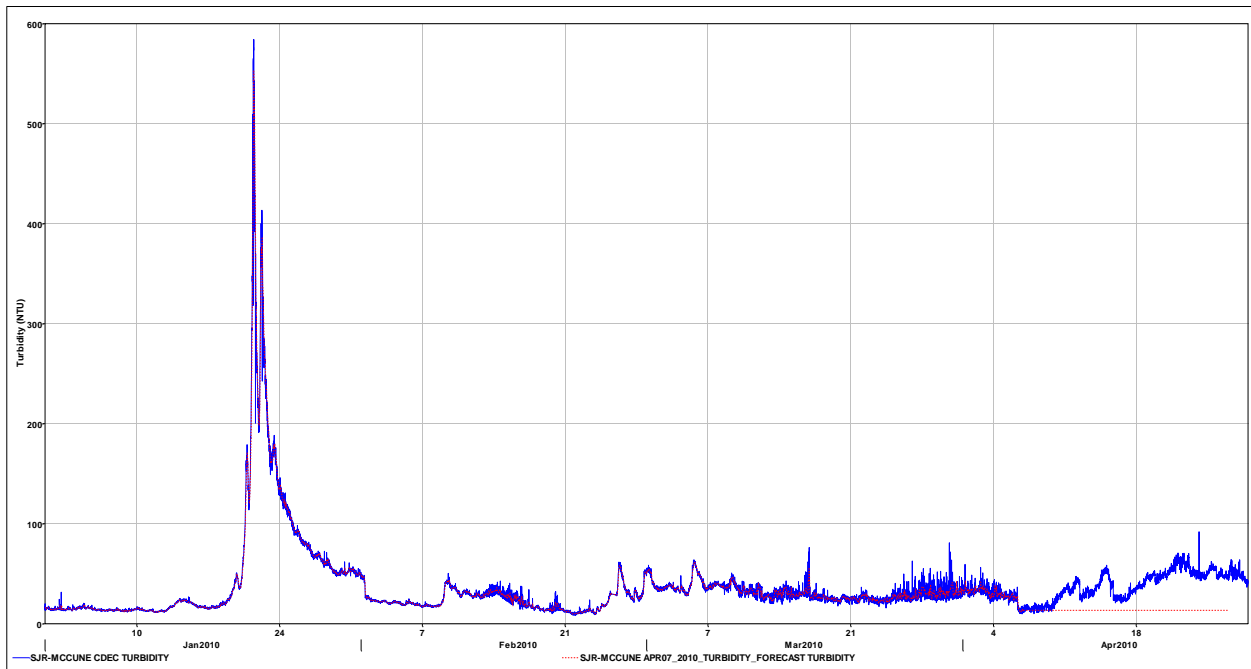


Figure 13-46 Turbidity data (blue line) and April 7th model forecast (red dash) at SJR McCune.

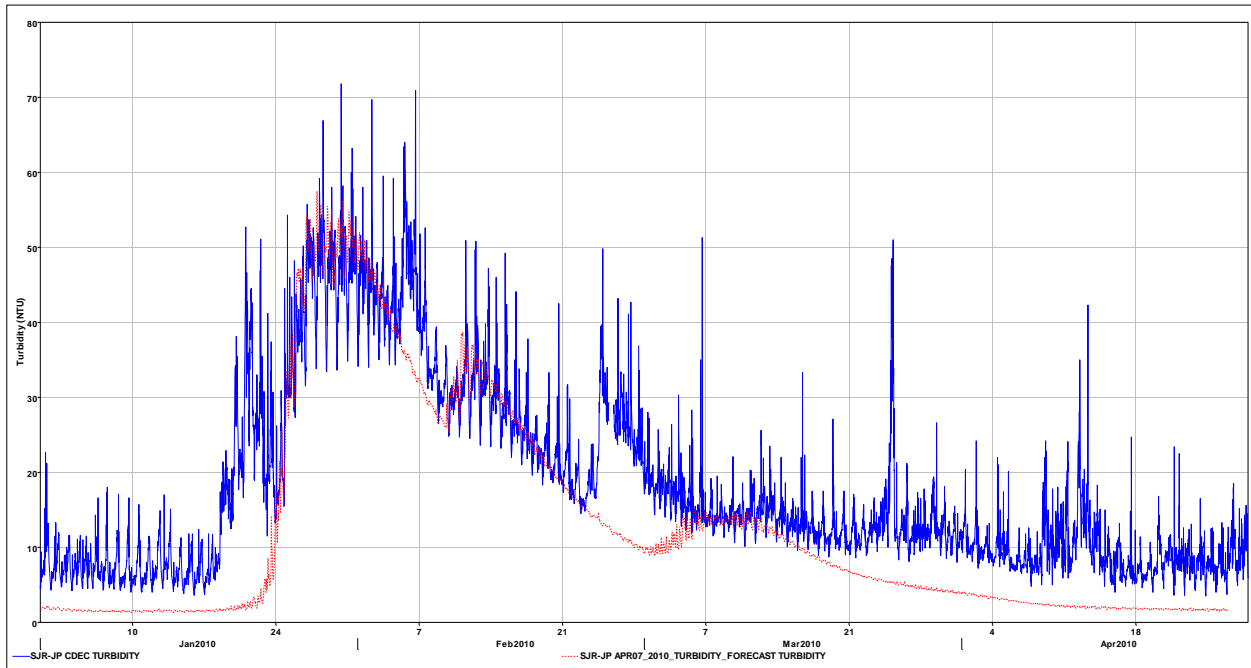


Figure 13-47 Turbidity data (blue line) and April 7th model forecast (red dash) at SJR-JP.

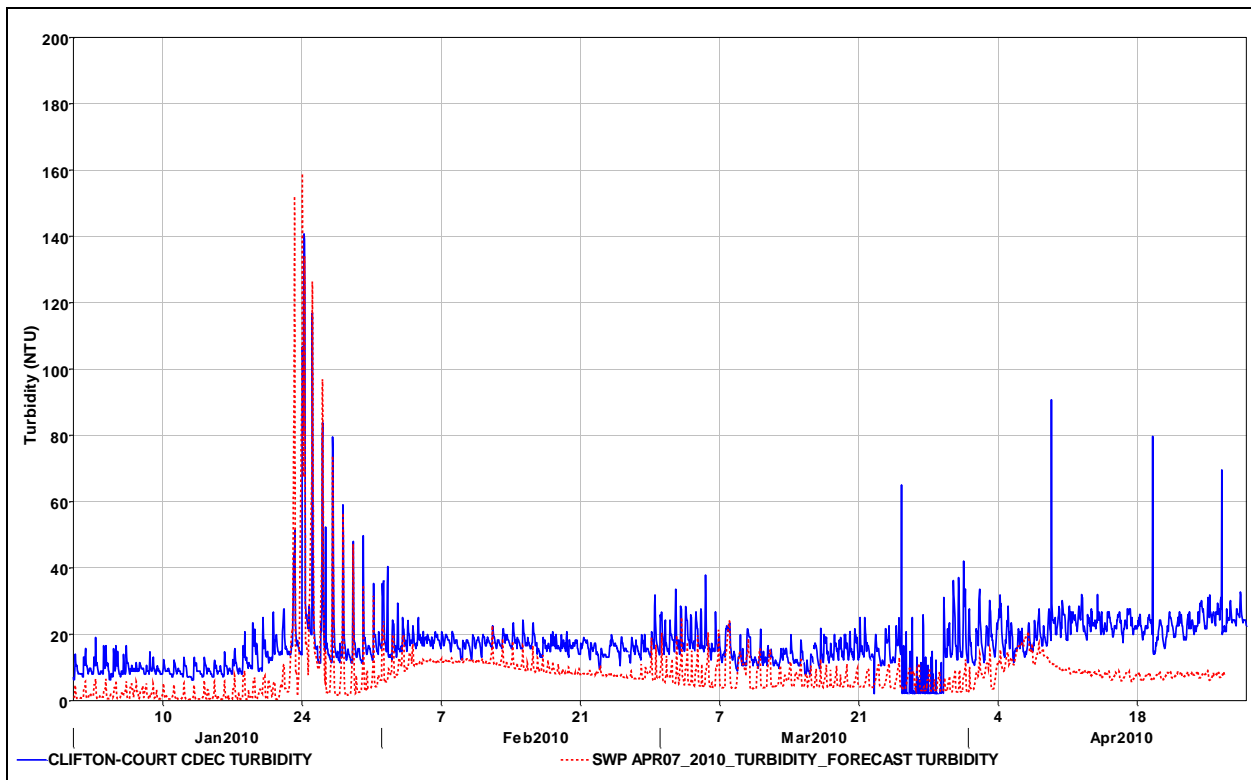


Figure 13-48 Turbidity data at CCFB (blue line) and Apr. 7th model forecast (red dash) at the SWP Intake.